DISTRIBUTED NETWORKS: NEW OUTLOOKS ON CEREBELLAR FUNCTION

EDITED BY: Thomas C. Watson, Stella Koutsikou, Richard Apps and Matthew W. Jones

PUBLISHED IN: Frontiers in Systems Neuroscience

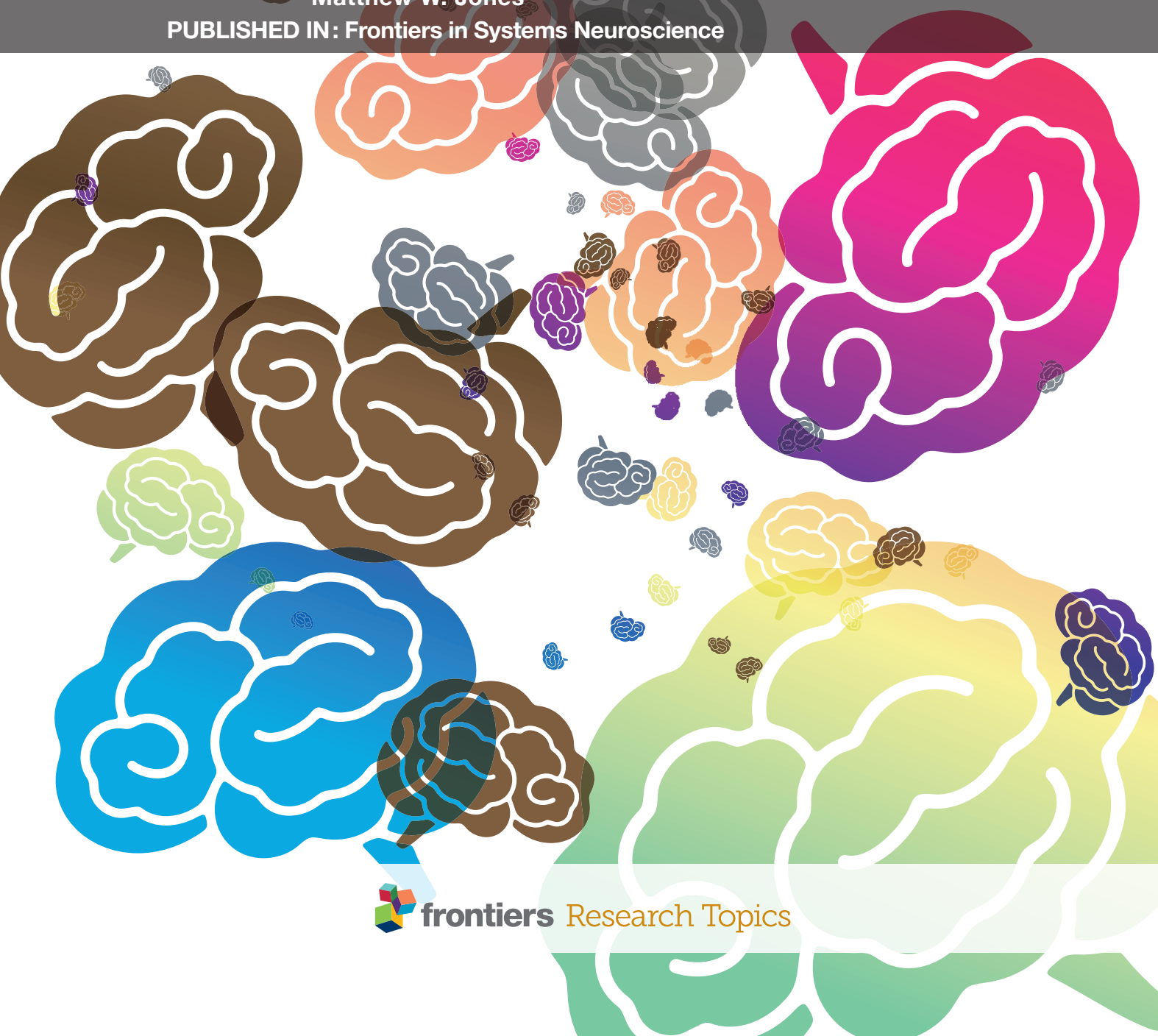

frontiers Research Topics

frontiers

ISSN 1664-8714
ISBN 978-2-88919-626-5
DOI 10.3389/978-2-88919-626-5

About Frontiers

Frontiers is more than just an open-access publisher of scholarly articles: it is a pioneering approach to the world of academia, radically improving the way scholarly research is managed. The grand vision of Frontiers is a world where all people have an equal opportunity to seek, share and generate knowledge. Frontiers provides immediate and permanent online open access to all its publications, but this alone is not enough to realize our grand goals.

Frontiers Journal Series

The Frontiers Journal Series is a multi-tier and interdisciplinary set of open-access, online journals, promising a paradigm shift from the current review, selection and dissemination processes in academic publishing. All Frontiers journals are driven by researchers for researchers; therefore, they constitute a service to the scholarly community. At the same time, the Frontiers Journal Series operates on a revolutionary invention, the tiered publishing system, initially addressing specific communities of scholars, and gradually climbing up to broader public understanding, thus serving the interests of the lay society, too.

Dedication to Quality

Each Frontiers article is a landmark of the highest quality, thanks to genuinely collaborative interactions between authors and review editors, who include some of the world's best academicians. Research must be certified by peers before entering a stream of knowledge that may eventually reach the public - and shape society; therefore, Frontiers only applies the most rigorous and unbiased reviews.
Frontiers revolutionizes research publishing by freely delivering the most outstanding research, evaluated with no bias from both the academic and social point of view.
By applying the most advanced information technologies, Frontiers is catapulting scholarly publishing into a new generation.

What are Frontiers Research Topics?

Frontiers Research Topics are very popular trademarks of the Frontiers Journals Series: they are collections of at least ten articles, all centered on a particular subject. With their unique mix of varied contributions from Original Research to Review Articles, Frontiers Research Topics unify the most influential researchers, the latest key findings and historical advances in a hot research area! Find out more on how to host your own Frontiers Research Topic or contribute to one as an author by contacting the Frontiers Editorial Office: **researchtopics@frontiersin.org**

DISTRIBUTED NETWORKS: NEW OUTLOOKS ON CEREBELLAR FUNCTION

Topic Editors:
Thomas C. Watson, University of Bristol, UK; Neuroscience Paris Seine, UMR CNRS 8246, INSERM 1130, Institut de Biologie Paris Seine, Sorbonne Universites, UPMC Univ Paris 06, F-75005, France
Stella Koutsikou, University of Bristol, UK
Richard Apps, University of Bristol, UK
Matthew W. Jones, University of Bristol, UK

Accumulating evidence suggests that the cerebellum subserves functions beyond the sensorimotor realm. This possibility has received considerable attention during the past quarter century, with recent findings revealing putative cerebellar roles in cognition, emotion and spatial navigation. These functions are potentially underpinned by the behaviour-dependent formation of functional networks in which the cerebellum forms one node of distributed circuits spanning thalamic, limbic and neocortical regions.

However, these views are not universally accepted.

Therefore, the over-arching aim of this Research Topic was to provide a forum through which the debate on the role of cerebellar interactions with motor and "non-motor" structures can be pursued in a rigorous manner. In particular, we aimed to bring together findings from the clinical, animal, theoretical and neuroimaging fields.

Citation: Watson, T. C., Koutsikou, S., Apps, R., Jones, M. W., eds. (2015). Distributed Networks: New Outlooks on Cerebellar Function. Lausanne: Frontiers Media.
doi: 10.3389/978-2-88919-626-5

Table of Contents

frontiers in Systems Neuroscience

EDITORIAL
published: 15 May 2015
doi: 10.3389/fnsys.2015.00078

"And the little brain said to the big brain…" Editorial: Distributed networks: new outlooks on cerebellar function

Thomas C. Watson [1, 2]*

[1] School of Physiology and Pharmacology, University of Bristol, Bristol, UK, [2] Sorbonne Universites, UPMC Univ Paris 06, Neuroscience Paris Seine, UMR CNRS 8246, INSERM 1130, Institut de Biologie Paris Seine, Cerebellum Navigation and Memory Team, Paris, France

Keywords: cerebellum, networks, purkinje cell, autism spectrum disorders, internal model, navigation, oscillations, cerebellar nuclei

The purpose of this research topic is to showcase recent anatomical, physiological, and clinical studies revealing how the cerebellum is embedded within distributed neural networks recruited during both direct motor functions plus cognitive and other domains. The topic comprises a total of 15 articles that together span experimental, theoretical, methodological approaches, and reviews of the literature.

In recent decades, converging lines of evidence indicate that the roles of the cerebellum extend beyond direct motor control to include interactions with higher centers associated with cognition. Identifying the functional roles of the cerebellum within these wider brain networks is therefore of critical importance when developing methods to alleviate symptoms of both motor and non-motor disorders (as recently exemplified by Chen et al., 2014 in a mouse model of rapid onset dystonia).

The papers in this research topic highlight several themes relevant to deciphering the cerebellar position within the wider brain-web. Voogd (2014), through his detailed review, emphasizes the importance of understanding structure to help understand function. Indeed, he describes numerous ascending pathways linking discrete cerebellar zones/modules to cerebral regions. The article also serves as a reminder that, despite best efforts, we still understand cerebellar systems rather superficially.

Anatomical studies are fundamental to shedding light on this problem and Ruigrok and Teune (2014) demonstrate how the use of intricate retrograde neural tracing techniques can help chart the route of the all-important "modular" cerebellar output via the deep cerebellar nuclei. They identify two ascending cerebellar pathways in which cerebellar output to premotor areas such as the red nucleus can supply simultaneous feedback to both the mossy and climbing fiber systems, and can act in concert with a designated GABAergic nucleo-olivary circuit. How these findings extend to cerebellar connectivity with non-motor brain regions will be of great interest and ultimately, discrete manipulations of these specific pathways will allow us to understand their importance in controlling cerebellar processes. Watson et al. (2014) employed electrophysiological techniques to map out physiological interactions between the cerebellar fastigial nuclei and the prelimbic cortex in anaesthetized and awake rats. This study demonstrates clear physiological coupling between the structures: local field potential (LFP) oscillations in the theta frequency range (5–10 Hz) in both the prefrontal cortex and cerebellar fastigius nucleus are synchronized according to behavioral demands. Along similar lines, Frederick et al. (2014) have demonstrated the presence of a cerebello-striatal interaction linked to circadian rhythms and dopamine levels. Like Watson et al. (2014) they have also used coherence analysis of LFPs but in this case recorded in dorsal striatum

Edited and reviewed by:
Maria V. Sanchez-Vives, Institució Catalana de Recerca i Estudis Avançats-Institut d'Investigacions Biomèdiques August Pi i Sunyer, Spain

***Correspondence:**
Thomas C. Watson, thomas.watson203@gmail.com

Received: *13 March 2015*
Accepted: *01 May 2015*
Published: *15 May 2015*

Citation:
Watson TC (2015) "And the little brain said to the big brain…" Editorial: Distributed networks: new outlooks on cerebellar function Front. Syst. Neurosci. 9:78. doi: 10.3389/fnsys.2015.00078

and Crus 1 of the cerebellar hemisphere. The authors reveal correlated low (0–3 Hz) and theta (3–8 Hz) frequency rhythmic oscillations within both regions in anaesthetized rats that vary depending upon time of day and dopamine levels. Together, these two papers highlight the utility of LFP recording in rodent models in understanding distributed networks that involve the cerebellum.

In keeping with these results, Parker et al. (2014) have suggested an experimental methodology to test the importance of cingulate-cerebellar connectivity in rat models of schizophrenia. By combining optogenetic and anatomical tracing techniques they suggest a strategy to selectively modulate cerebello-cingulate pathways in an attempt to alleviate abnormal behavior. The outcomes of future rodent studies adopting this approach will prove especially valuable when viewed in a translational context alongside human neuroimaging and clinical studies.

In this respect, the review paper of Reeber et al. (2013) usefully summarizes the multitude of non-motor human disorders associated with disrupted cerebellar function and outlines their genetic, electrophysiological, and behavioral bases. Amongst others, they highlight a recent landmark study in which the loss of the Tsc1 gene from mouse cerebellar Purkinje cells (Tsai et al., 2012) is sufficient to cause social impairments, cognitive defects and abnormal vocalizations –core features of autism spectrum disorder (ASD). These behaviors were successfully blocked in mutants treated with the mTOR inhibitor rapamycin. Such rodent models will be essential to understanding cerebellar circuit function in disorders that encompass symptoms beyond direct motor abnormalities, particularly developmental disorders that may compromise the strict patterns of cerebellar connectivity laid down during development. Furthermore, as Stoodley (2014) has demonstrated in this research topic, fMRI experiments in humans identify that clearly localized disruption of distinct cerebellar anatomical clusters, and the networks they connect to, exists in disorders such as ASD, dyslexia, and ADHD. The importance of appropriately controlled analysis of fMRI data is also described here by Michael et al. (2014). Alongside the contribution of Ordek et al. (2014), who describe the effect of percussive damage to cerebellar cortical processing of sensory information, these studies collectively emphasize the vulnerability of the cerebellar cortex and the diverse symptoms its dysfunction can trigger.

The organization of the cerebellum is often described as a uniform circuit, but this belies the complexity of its rich molecular architecture. Our understanding of the functional significance of these expression patterns is still in its infancy. One of the best known examples is the parasagittal striping that results from the non-uniform expression of zebrin II/aldolase C in Purkinje cells. Hawkes (2014) provides a review of the importance of this molecular architecture in long term depression (LTD) at the parallel fiber- Purkinje cell synapse. But many questions remain unresolved, including how the presence of specific molecular markers within select Purkinje cell populations might alter their firing patterns in response to afferent input.

Within this review topic this important question is beginning to be addressed. Physiological evidence suggests that Purkinje cell firing patterns are not homogenous across the cerebellar cortex (De Gruijl et al., 2014; Xiao et al., 2014) and the control of cerebellar population firing is indeed influenced by factors such as zebrin expression (Tsutsumi et al., 2015). Additionally, the pattern of complex spike waveform seen within Purkinje cells is modulated by the synchrony of firing within the inferior olive (Lang et al., 2014), which provides details of how afferent input, carried via olivo-cerebellar pathways, can influence cerebellar spiking. Whether this synchrony level is selectively gated or modified by olivary inputs remains to be seen, but this finding provides a potential route via which the activity in populations of Purkinje cells could vary depending upon upstream activity in non-cerebellar regions (see also Ros et al., 2009), and also possess the capacity to process motor and non-motor information in a differential manner. Future studies utilizing optogenetic manipulations restricted by zebrin markers should provide a method to probe the functional significance of these neuronal populations (e.g., Tsubota et al., 2013).

At a behavioral level, our understanding of cerebellar contributions remains far from complete. In their review, Rondi-Reig et al. (2014) describe the anatomical pathways through which the cerebellum may connect to known navigation centers (e.g., hippocampus) and highlight the contribution of cerebellar monitoring of sensory information to maintaining body position in space. They extend the work of Dean et al. (2010) to suggest that during navigation, the cerebellum may filter out predictable sensory signals and preferentially convey novel sensory information to hippocampal circuits to facilitate the maintenance of cognitive maps (as manifest in the activity of CA1 place cells). Such a cerebello-hippocampal network model may indeed rely upon the predictive nature of cerebellar processing. In relation to internal models, Popa et al. (2014) describe how Purkinje cell simple spike firing can accurately predict movements across a variable timescale while also detecting errors within the motor domain. They suggest that this capacity may extend to support associative learning, sequencing, working memory, and forward internal models in non-motor domains. Indeed, the ability to predict both the motor and non-motor consequence of movements is likely to be fundamental to the generation and execution of appropriate goal-directed behaviors. Cheron et al. (2014) build upon preliminary data from an Angelman syndrome mouse model to suggest that normal synaptic plasticity processes (specifically, LTD) in the cerebellar cortex modulate inhibition/excitation balance within cerebral cortical areas, thereby influencing plasticity in disparate regions such as the barrel cortex. By using transcranial cerebello-cerebral direct-current stimulation to relieve symptoms of spino-cerebellar ataxias, Grimaldi et al. (2014) have also demonstrated the importance of cerebro-cerebellar dialog in generating appropriate muscle control in upper limbs.

The wide-ranging contributions made to this research topic reinforce the view that the cerebellum plays a role in a variety of processes that are fundamental to the generation of appropriate behaviors. While we know a great deal about the intrinsic anatomy of the cerebellum, it is also clear that

we are still some way from gaining a full understanding of the functional significance of this intricate organization. Meanwhile, from a clinical perspective, much can be gained by further investigating cerebellar contributions to a variety of neuropsychiatric disorders. We are entering an exciting period in cerebellar research—the adoption of behavioral, genetic, and translational approaches (as often employed when deciphering other "big-brain" circuits) will surely lead to important advances in our understanding of cerebellar roles in health and disease.

Acknowledgments

We are very grateful to all of the contributors for their commitment to this project and for providing fresh insights into cerebellar systems neuroscience. We hope that this e-volume will not only serve as a useful point of reference to current work in the field but will also help promote further research and in particular attract interest from those outside the cerebellar community. Many thanks are also due to the reviewers and members of the Editorial team of Frontiers.

References

Chen, C. H., Fremont, R., Arteaga-Bracho, E. E., and Khodakhah, K. (2014). Short latency cerebellar modulation of the basal ganglia. *Nat. Neurosci.* 17, 1767–1775. doi: 10.1038/nn.3868

Cheron, G., Marquez-Ruiz, J., Kishino, T., and Dan, B. (2014). Disruption of the LTD dialogue between the cerebellum and the cortex in Angelman syndrome model: a timing hypothesis. *Front. Syst. Neurosci.* 8:221. doi: 10.3389/fnsys.2014.00221

Dean, P., Porrill, J., Ekerot, C. F., and Jorntell, H. (2010). The cerebellar microcircuit as an adaptive filter: experimental and computational evidence. *Nat. Rev. Neurosci.* 11, 30–43. doi: 10.1038/nrn2756

De Gruijl, J. R., Hoogland, T. M., and De Zeeuw, C. I. (2014). Behavioral correlates of complex spike synchrony in cerebellar microzones. *J. Neurosci.* 34, 8937–8947. doi: 10.1523/JNEUROSCI.5064-13.2014

Frederick, A., Bourget-Murray, J., Chapman, C. A., Amir, S., and Courtemanche, R. (2014). Diurnal influences on electrophysiological oscillations and coupling in the dorsal striatum and cerebellar cortex of the anesthetized rat. *Front. Syst. Neurosci.* 8:145. doi: 10.3389/fnsys.2014.00145

Grimaldi, G., Oulad Ben Taib, N., Manto, M., and Bodranghien, F. (2014). Marked reduction of cerebellar deficits in upper limbs following transcranial cerebello-cerebral DC stimulation: tremor reduction and re-programming of the timing of antagonist commands. *Front. Syst. Neurosci.* 8:9. doi: 10.3389/fnsys.2014.00009

Hawkes, R. (2014). Purkinje cell stripes and long-term depression at the parallel fiber-Purkinje cell synapse. *Front. Syst. Neurosci.* 8:41. doi: 10.3389/fnsys.2014.00041

Lang, E. J., Tang, T., Suh, C. Y., Xiao, J., Kotsurovskyy, Y., Blenkinsop, T. A., et al. (2014). Modulation of Purkinje cell complex spike waveform by synchrony levels in the olivocerebellar system. *Front. Syst. Neurosci.* 8:210. doi: 10.3389/fnsys.2014.00210

Michael, A. M., Anderson, M., Miller, R. L., Adali, T., and Calhoun, V. D. (2014). Preserving subject variability in group fMRI analysis: performance evaluation of GICA vs. IVA. *Front. Syst. Neurosci.* 8:106. doi: 10.3389/fnsys.2014.00106

Ordek, G., Proddutur, A., Santhakumar, V., Pfister, B. J., and Sahin, M. (2014). Electrophysiological monitoring of injury progression in the rat cerebellar cortex. *Front. Syst. Neurosci.* 8:197. doi: 10.3389/fnsys.2014.00197

Parker, K. L., Narayanan, N. S., and Andreasen, N. C. (2014). The therapeutic potential of the cerebellum in schizophrenia. *Front. Syst. Neurosci.* 8:163. doi: 10.3389/fnsys.2014.00163

Popa, L. S., Hewitt, A. L., and Ebner, T. J. (2014). The cerebellum for jocks and nerds alike. *Front. Syst. Neurosci.* 8:113. doi: 10.3389/fnsys.2014.00113

Reeber, S. L., Otis, T. S., and Sillitoe, R. V. (2013). New roles for the cerebellum in health and disease. *Front. Syst. Neurosci.* 7:83. doi: 10.3389/fnsys.2013.00083

Rondi-Reig, L., Paradis, A. L., Lefort, J. M., Babayan, B. M., and Tobin, C. (2014). How the cerebellum may monitor sensory information for spatial representation. *Front. Syst. Neurosci.* 8:205. doi: 10.3389/fnsys.2014.00205

Ros, H., Sachdev, R. N., Yu, Y., Sestan, N., and Mccormick, D. A. (2009). Neocortical networks entrain neuronal circuits in cerebellar cortex. *J. Neurosci.* 29, 10309–10320. doi: 10.1523/JNEUROSCI.2327-09.2009

Ruigrok, T. J., and Teune, T. M. (2014). Collateralization of cerebellar output to functionally distinct brainstem areas. A retrograde, non-fluorescent tracing study in the rat. *Front. Syst. Neurosci.* 8:23. doi: 10.3389/fnsys.2014.00023

Stoodley, C. J. (2014). Distinct regions of the cerebellum show gray matter decreases in autism, ADHD, and developmental dyslexia. *Front. Syst. Neurosci.* 8:92. doi: 10.3389/fnsys.2014.00092

Tsai, P. T., Hull, C., Chu, Y., Greene-Colozzi, E., Sadowski, A. R., Leech, J. M., et al. (2012). Autistic-like behaviour and cerebellar dysfunction in Purkinje cell Tsc1 mutant mice. *Nature* 488, 647–651. doi: 10.1038/nature11310

Tsubota, T., Ohashi, Y., and Tamura, K. (2013). Optogenetics in the cerebellum: purkinje cell-specific approaches for understanding local cerebellar functions. *Behav. Brain Res.* 255, 26–34. doi: 10.1016/j.bbr.2013.04.019

Tsutsumi, S., Yamazaki, M., Miyazaki, T., Watanabe, M., Sakimura, K., Kano, M., et al. (2015). Structure-function relationships between aldolase C/zebrin II expression and complex spike synchrony in the cerebellum. *J. Neurosci.* 35, 843–852. doi: 10.1523/JNEUROSCI.2170-14.2015

Voogd, J. (2014). What we do not know about cerebellar systems neuroscience. *Front. Syst. Neurosci.* 8:227. doi: 10.3389/fnsys.2014.00227

Watson, T. C., Becker, N., Apps, R., and Jones, M. W. (2014). Back to front: cerebellar connections and interactions with the prefrontal cortex. *Front. Syst. Neurosci.* 8:4. doi: 10.3389/fnsys.2014.00004

Xiao, J., Cerminara, N. L., Kotsurovskyy, Y., Aoki, H., Burroughs, A., Wise, A. K., et al. (2014). Systematic regional variations in Purkinje cell spiking patterns. *PLoS ONE* 9:e105633. doi: 10.1371/journal.pone.0105633

Conflict of Interest Statement: The author declares that the research was conducted in the absence of any commercial or financial relationships that could be construed as a potential conflict of interest.

frontiers in
SYSTEMS NEUROSCIENCE

REVIEW ARTICLE
published: 18 December 2014
doi: 10.3389/fnsys.2014.00227

What we do not know about cerebellar systems neuroscience

Jan Voogd*

Department of Neuroscience, Erasmus Medical Center Rotterdam, Rotterdam, Netherlands

Edited by:
Thomas C. Watson, University of Bristol, UK

Reviewed by:
José M. Delgado-García, University Pablo de Olavide, Spain
Richard Apps, University of Bristol, UK

****Correspondence:***
Jan Voogd, Department of Neuroscience, Erasmus Medical Center Rotterdam, Rhijngeesterstraatweg 1, 2342AN, Oegstgeest, Netherlands
e-mail: janvoogd@bart.nl

Our knowledge of the modular organization of the cerebellum and the sphere of influence of these modules still presents large gaps. Here I will review these gaps against our present anatomical and physiological knowledge of these systems.

Keywords: cerebellar modules, mossy fiber systems, climbing fiber systems, purkinje cell zones, cerebro-cerebellar relations

INTRODUCTION

Advances in our knowledge of the functional anatomy of the cerebellum have raised new questions. In this review I will draw attention to some of, what I consider, the main flaws in our knowledge of the anatomy and physiology of cerebellar modules and their connections.

My main questions are:

1. The anatomical organization of the cerebellum is based on modules, defined by their projection to a specific cerebellar or vestibular nucleus, their climbing fiber input and the physiological and neurochemical properties of their Purkinje cells. Why do the modules in motor regions of the cerebellum alternate between those connected with motor pathways and those connected with wide regions of the cerebral cortex?
2. The cerebello-rubral pathway, the cerebello-thalamo-cortical projections and the corticorubral-olivary climbing fiber system seem to be organized as closed loops. What is the function of these loops and of the convergence of cortical and cerebellar nuclear input to the parvocellular red nucleus and other intercallated nuclei at the meso-diencephalic junction?
3. Which are the tractable behaviors with which to evaluate the hypothesis that each Purkinje cell zone constitutes a basic functional unit of the cerebellum (Simpson, 2011)?
4. What are the topographical and functional relations between mossy and climbing fibers in the cerebellar cortex?
5. Are mossy and climbing fiber pathways organized according to the same anatomical principles?
6. What are the topographical interrelations of different mossy fiber system in the cerebellum?

THE MODULAR ORGANIZATION OF THE CEREBELLUM

The cerebellum is known to be organized in a modular fashion. Cerebellar modules consist of one or more Purkinje cell zones that project to a particular cerebellar or vestibular nucleus, their climbing fiber input from a subdivision of the contralateral inferior olive with a collateral projection to the cerebellar target nucleus and reciprocal connections of this target nucleus with the contralateral inferior olive. Seven to nine of these modules originally were distinguished on both sides of the cerebellum in carnivores, rodents and primates (**Figures 1A–C**).

In rodents Purkinje cells that react with a Purkinje cell-specific antibody known as Zebrin, are distributed in a pattern of alternating zebrin-positive bands separated ny zebrin-.negative bands (Hawkes and Leclerc, 1987). More recently it was found that the zebrin pattern is congruent with the zonal organization of its corticonuclear and afferent climbing fiber projections (compare **Figure 1**, panels **(A)** and **(D)**). Purkinje cell zones, therefore, are either zebrin-positive or negative (Voogd et al., 2003; Sugihara and Shinoda, 2004). The zebrin signature stands for the distribution in these neurons of many different neuroactive substances, such as glutamate transporters and cytochrome oxidase (Apps and Hawkes, 2009). Moreover, zebrin-positive and negative Purkinje cells differ in their development, their physiological properties and the organization of their climbing fiber input from the periphery or the cerebral cortex. Zebrin-negative Purkinje cells are born later than the zebrin-positive ones and, in monkeys at least, reach the meningeal surface at a later stage. The medio-lateral compartmentation of the Purkinje cells, therefore, is determined at a very early stage of cerebellar development (Namba et al., 2011; Voogd, 2012). Purkinje cells of the mouse and rat zebrin-positive modules fire at a lower rate than Purkinje

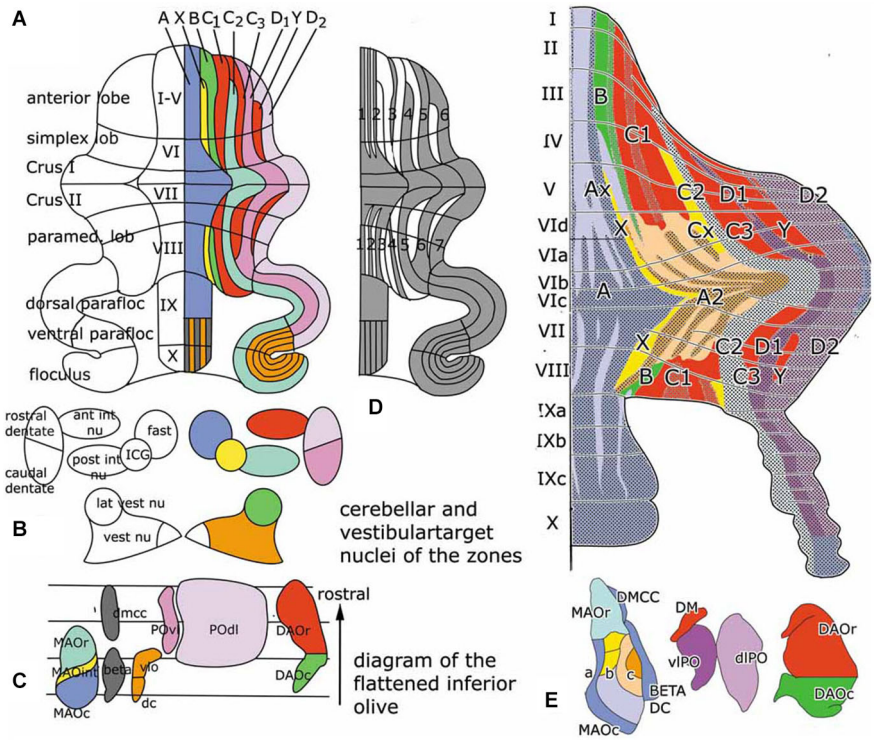

FIGURE 1 | (A) Diagram of the flattened cerebellum of the rat showing the Purkinje cell zones **(A–D)**. The same color-code is used for the Purkinje cell zones in panels **(A)** and **(E)**, for the target nuclei of the zones in panel **(B)** and in the flattened map of the inferior olive, with the subnuclei that give rise to climbing fibers innervating the different zones in panel **(C)**. **(D)** Diagram of the distribution of zebrin-positive and –negative Purkinje cells. Zebrin-positive bands are numbered 1–7. **(E)** Sugihara and Shinoda (2004) diagram of the zebrin-positive and negative Purkinje cell zones. The main zones are indicated with the same colors as in panel **(A)** Redrawn from Sugihara and Shinoda (2004). Abbreviations: ant int nu, anterior interposed nucleus; DAOc/r, caudal/rostral dorsal accessory olive; dc, dorsal cap; DMCC, dorsomedial cell column; a, b, c, subnuclei a,b,c of caudal medial accessory olive; fast, fastigial nucleus; ICG, interstitial cell groups; lat vest nu, lateral vestibular nucleus; MAOr/int/c, caudal/intermediate/rostral subnucleus of the medial accessory olive; POdl, dorsal lamina principal olive; post int nu, posterior interposed nucleus; POvl, ventral lamina principal olive; vest nu, vestibular nuclei; vlo, ventrolateral outgrowth.

cells of zebrin-negative modules (Xiao et al., 2014; Zhou et al., 2014).

Zebrin negative zones occur in anterior and posterior regions of the rodent cerebellar hemisphere, in the anterior lobe and the simplex lobule, and in the paramedian lobule. These regions are considered as the "motor" regions of the cerebellar hemisphere because they were found to receive input from the primary motor cortex and to be involved in movement in several fMRI studies (Stoodley and Scmahmann, 2009). In rodents the zebrin-negative zones C1, C3 and Y alternate with the zebrin-positive zones C2, D1 and D2 (**Figures 1A,D**). The circuitry of the zebrin-negative zones typically is part of the motor system (Voogd and Ruigrok, 2004). The zebrin-positive zones maintain connections with wide areas of the cerebral cortex.

Figure 2 is based on the situation in the cat, where the C1, C3 and Y zones receive topically organized somatosensory climbing fiber input from the rostral dorsal accessory olive (DAO). The C1 and C3 zones also receive short-latency somatotopically arranged climbing fiber input from the contralateral posterior sigmoid gyrus (area 4γ: the motor cortex), relayed by the dorsal column nuclei. Long-latency climbing fiber input to these zones and climbing fiber input from wide areas of the cerebral cortex, including parietal and sensory areas to the C2 and D1 zones is not relayed by the dorsal column nuclei (Andersson and Nyquist, 1983; Andersson, 1984). The parvocellar red nucleus and other nuclei at the mesodiencephalic border my serve as links in these cortico-cerebellar pathways (Saint-Cyr, 1987).

The C1, C3 and Y zones project to the anterior interposed nucleus, where their somatopical maps converge upon a single map (Apps and Garwicz, 2000). This nucleus projects to the magnocellular red nucleus (Gibson et al., 1987) and, via the thalamus, to the motor and possibly to the premotor areas of the cerebral cortex (Kievit, 1979; Jörntell and Ekerot, 1999). These cortical areas give rise to the pyramidal tract that emits collaterals to the magnocellular nucleus (Catsman-Berrevoets et al., 1979). Direct projections of the rubrospinal tract are present to C8-T1 motoneurons that innervate distal forelimb muscles (McCurdy et al., 1987). Connections of the pyramidal tract to motoneurons are mediated by spinal interneurons. In primates both the rubrospinal and corticospinal tracts connect with C8-T1 motoneurons that innervate distal forelimb muscles (Holstege

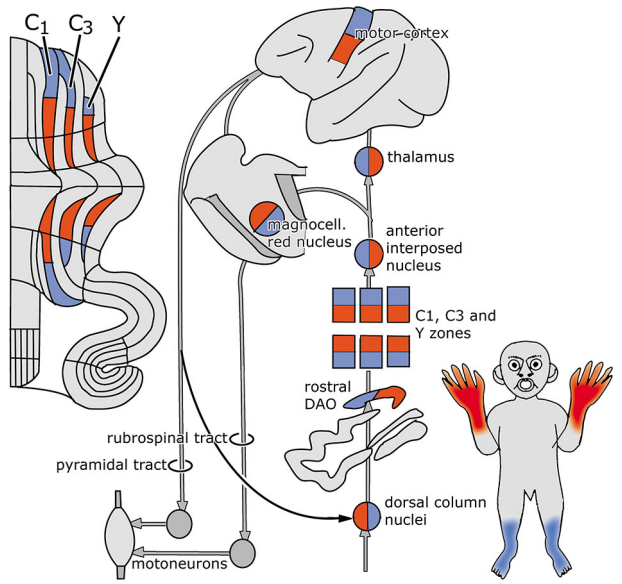

FIGURE 2 | Circuitry of the zebrin-negative C1, C3 and Y zones. Abbreviation: DAO, dorsal accessory olive.

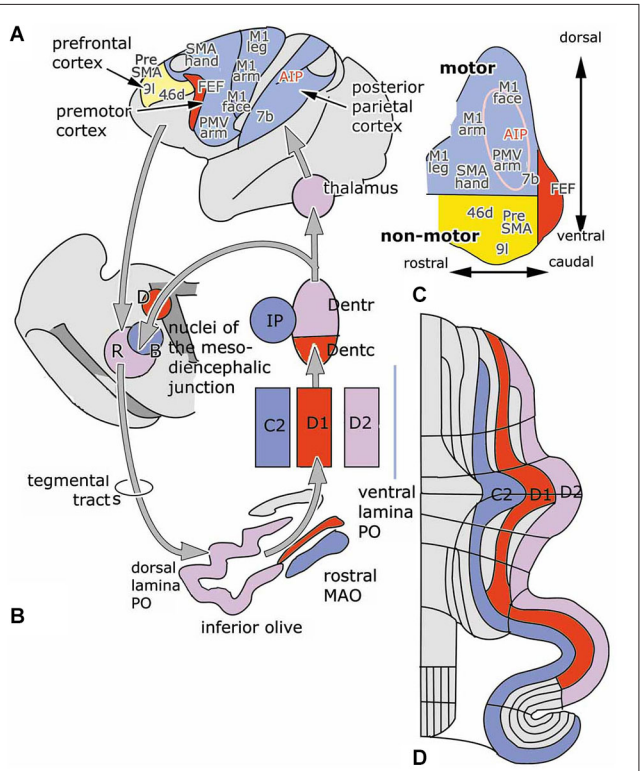

FIGURE 3 | (A) Diagram of the left cerebral hemisphere of a monkey. Areas receiving input from the rostral motor dentate (blue), the caudal non-motor dentate (yellow) and the caudal pole of the dentate (red), as indicated in panel **(C)**, a diagram of the functional division of the monkey dentate nucleus according to Strick et al. (2009), are indicated. **(B)** Circuitry of the C2, D1 and D2 zones. **(D)** Diagram of the flattened cerebellar cortex showing the position of the C2, D1 and D2 zones. Abbreviations: AIP, anterior intraparietal area; B, Bechterew's nucleus; D, Darkschewitsch nucleus; Dentc/r, caudal/rostral dentate nucleus; FEF, frontal eye field; IP, posterior interposed nucleus; MAO, medial accessory olive; PO, principal olive; R, parvocellular red nucleus; SMA, supplementary motor area; a, anterior; p, posterior.

et al., 1988; Bortov and Strick, 1993). The whole system is somatotopically organized (**Figure 2**).

The anterior vermis and the pyramis, posterior vermal lobule VIII, also are part of the motor system. The medial vermal A zone projects to the fastigial and vestibular nuclei, the X zone to the interstitial cell groups, the B zone to the lateral vestibular nucleus. These zones supervise the long descending brain stem pathways, with the interstitial cell groups giving rise to branching axons with spinal and thalamic targets. Sugihara and Shinoda (2004) found the A zone and the adjoining A2 zone (a zone that has only been identified in the rodent cerebellum) to be composed of a number of narrow alternating zebrin-positive and negative-subzones (**Figure 1E**). Each of these zones receives climbing fibers carrying somatosensory, vestibular or tectal information input from particular regions of the caudal medial accessory olive (MAO). The share of each of these subzones in the corticonuclear projections to the fastigial and vestibular nuclei, and their connections with the brain stem motor systems remains to be established. Although it has been shown in mice that the ipsilateral fastigiobulbar pathway is glycinergic (Bagnall et al., 2009), we do not know which Purkinje cells provide the input to these inhibitory neurons.

CEREBELLAR EFFERENT PATHWAYS AND CLIMBING FIBER PATHS TO THE C2, D1 AND D2 ZONES ARE ORGANIZED AS CLOSED LOOPS

The zebrin-positive zones C2, D1 and D2 that alternate with the zebrin-negative zones in the "motor" regions of the cerebellum extend beyond these regions in the hemisphere of the ansiform lobule and the paraflocculus. These lobules, lacking zebrin-negative zones are entirely zebrin-positive and the borders between the zones cannot be determined from the zebrin pattern.

With some exceptions, the cerebello-cerebral pathways were found to be crossed. Strick et al. (2009) distinguished a rostromedial "motor" area of the dentate that projects in a somatotopical manner to motor, premotor and parietal areas, and a more ventral and caudal "non-motor" part that is connected with prefrontal and parietal areas. The caudal pole of the dentate projects to the frontal eye field (**Figure 3**, inset). In this review, rostral and caudal portions of the dentate have been distinguished as target nuclei of the D2 and D1 zones, that are also distinguished by their climbing fiber projections from the dorsal and ventral lamina of the principal olive and their differential projection to the parvocellular red nucleus. It seems most likely, if not proved, that both Strick's rostral, "motor" and caudal "non-motor" divisions of the monkey dentate should be included in the target nucleus of the D2 zone, and that its caudal, visual pole serves as the target nucleus of the D1 zone. In accordance with this the circuitry of the D1 zone is shown in red in **Figure 3**. As a consequence, the D2 zone would consist of motor and non-motor segments. The motor segments would be located in the lateral hemisphere of the motor

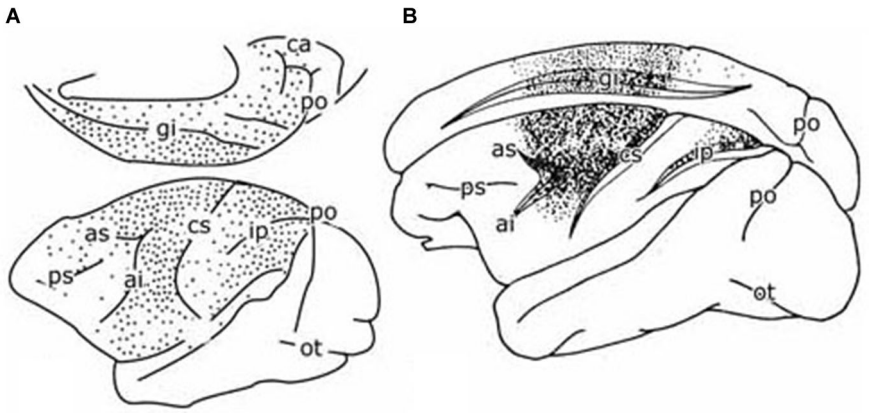

FIGURE 4 | (A) Diagram of the cerebral hemisphere of a monkey showing the distribution of retrogradely labeled cells from a large injection of a retrograde tracer in the pontine nuclei. Redrawn from Glickstein et al. (1985). **(B)** Diagram of the cerebral hemisphere of a monkey showing the distribution of retrogradely labeled cells from an injection of a retrograde tracer in the parvocellular red nucleus of a monkey. Redrawn from Humphrey et al. (1984). Abbreviations: ai, inferior limb arcuate fissure; as, superior limb of arcuate fissure; ca, calcerine fissure; ci, central fissure; gi, cingulate fissure; Ip, intraparietal fissure; ot, occipito-temporal fisure; po, parieto-occipital fissure; ps, principal fissure.

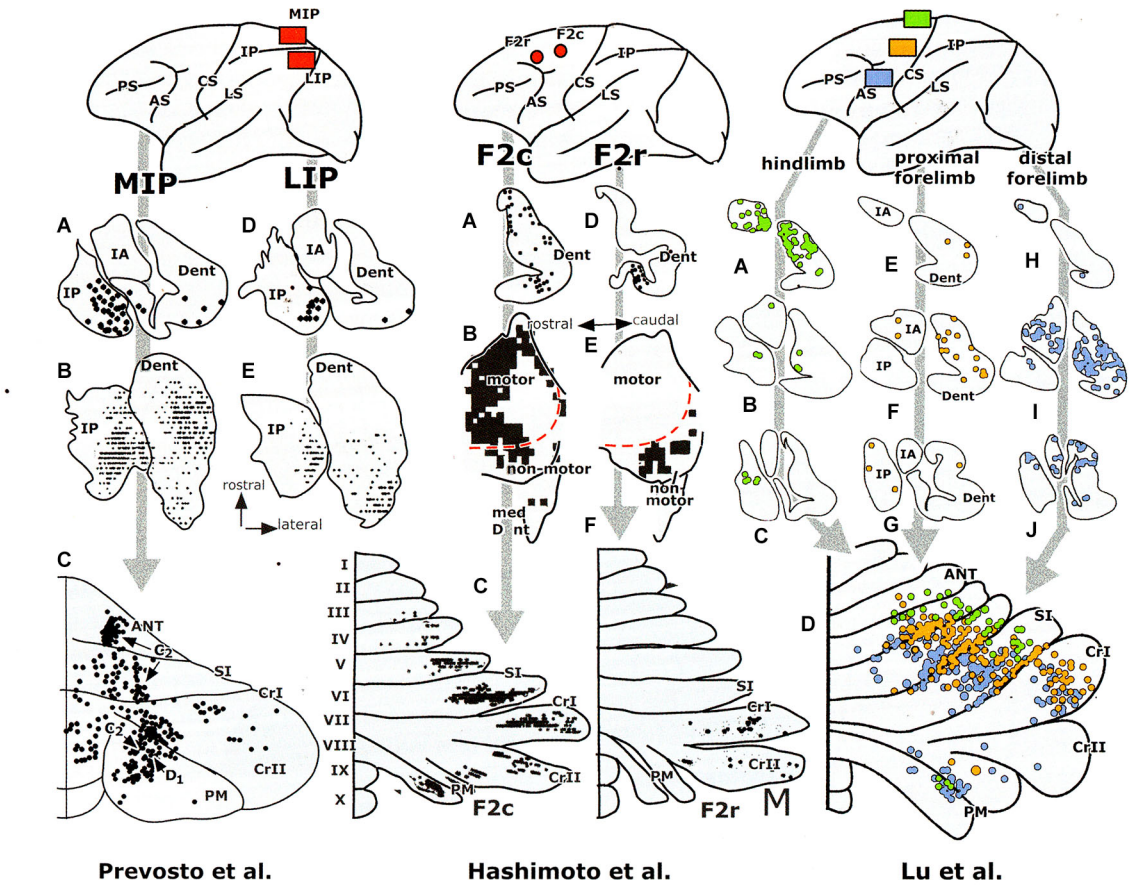

FIGURE 5 | Retrograde transneuronal labeling experiments with injections of the tracer in areas of the cerebral cortex of a monkey, showing labeling in the cerebellar nuclei (A–J) and of Purkinje cells in the diagrams of the cerebellar cortex (lower panels). Redrawn from Hashimoto et al. (2010) and Prevosto et al. (2010). Abbreviations: ANT, anterior lobe; AS, arcuate sulcus; CRI/II, Crus I /II; CS, central sulcus; Dent, dentate nucleus; F2c/r, caudal/rostral dorsal premotor area; IPAR, intraparietal sulcus; IP, posterior interposed nucleus; LS, lateral sulcus; IA, anterior interposed nucleus; MIP, medial intraparietal area; LIP, lateral intraparietal area; PM, paramedian lobule; PS, principal sulcus; SI, simplex lobule.

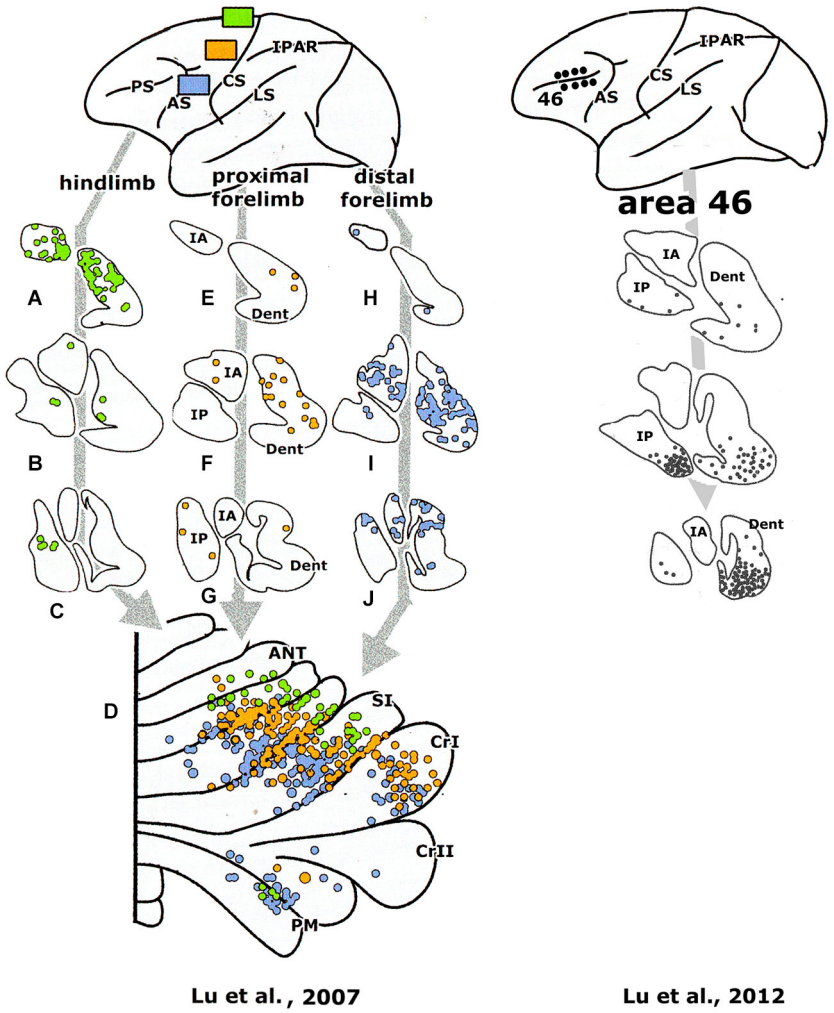

FIGURE 6 | Retrograde transneuronal labeling experiments with injections of the tracer in areas of the cerebral cortex of a monkey, showing labeling in the cerebellar nuclei (A–J) and of Purkinje cells in the diagrams of the cerebellar cortex (lower panels). Redrawn from Lu et al. (2007, 2012), For abbreviations see **Figure 5**.

divisions of the cerebellum. This localization is supported by the observations in transneuronal labeling experiments illustrated in **Figures 5–7**.

The climbing fiber circuitry of the zebrin-positive zones differs from the zebrin-negative zones (**Figure 4**). Their olivary subnuclei, the rostral (MAO) and the principal olive, receive their afferents from nuclei located at the meso-diencephalic border, the parvocellular red nucleus and the nuclei of Darkschewitsch and Bechterew (Onodera, 1984). Direct cortico-olivary projections appear to be few. The rostral MAO that innervates the C2 zone receives its afferents from Darkschewitsch nucleus, the ventral lamina of the principal olive that innervates D1 from Bechterew's nucleus, corresponding to the dorsomedial portion of the parvocellular red nucleus in primates, and the dorsal lamina of the principal olive, that innervates D2, from the main lateral portion of the parvocellular red nucleus (Strominger et al., 1979). These nuclei receive a double input, both from the target nuclei of the zebrin-positive zones, the posterior interposed and dentate nuclei, and from the cerebral cortex. The posterior interposed nucleus projects to Darkschewitsch nucleus (Voogd, 1964), the rostral dentate to the main lateral and caudal portion of the parvocellular red nucleus (Flumerfelt et al., 1973) and the caudal dentate to the dorsomedial subnucleus of the parvocellular red nucleus (van Kan et al., 1993, see Voogd and Ruigrok, 2004). These zebrin-positive zones, therefore, are included in large closed cerebello-mesencephalo-olivary circuits. The central tegmental tract, the pathway from the parvocellular red nucleus to the dorsal lamina of the inferior olive belongs to the largest systems in the human brain stem.

The question, whether the cerebello-thalamocortical and corticorubro-olivary loops are also reciprocally organized remains. In monkeys the target nucleus of the D2 zone, the rostral dentate, projects to the primary motor and several premotor areas,to parietal area7b, the medial (MIP) and lateral (LIP)

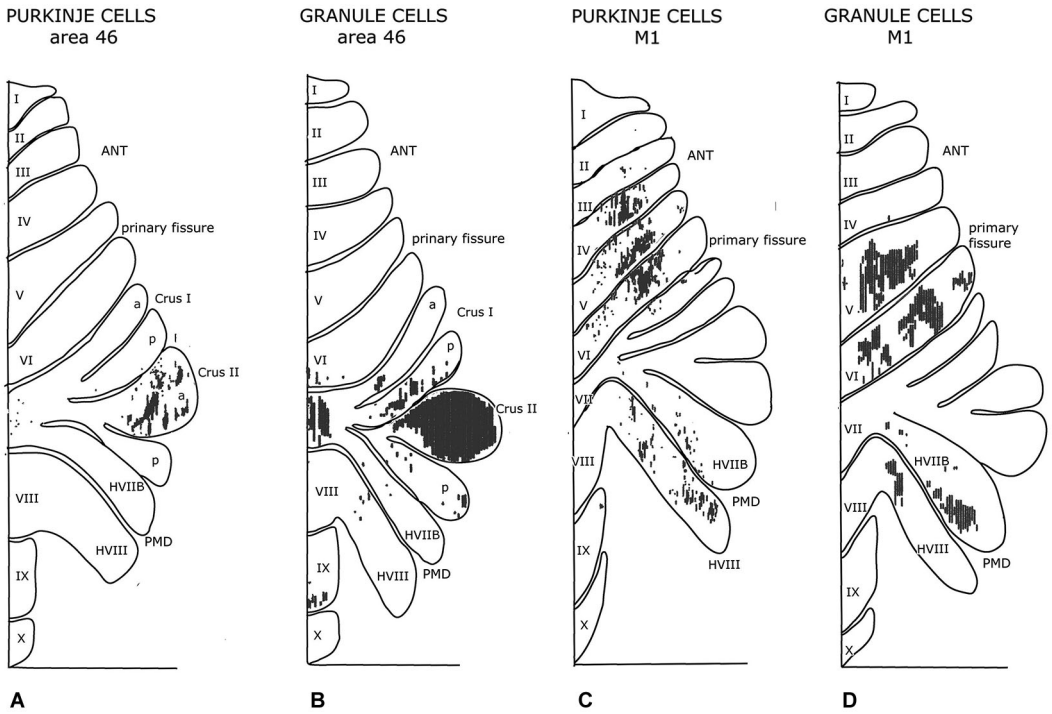

FIGURE 7 | Diagrams of the monkey cerebellum showing transneuronal retrograde labeling of Purkinje cells and transneuronal antegrade labeling of mossy fibers after injections of tracers in prefrontal area 46 and the primary motor cortex. Note similarity in the localization of Purkinje cells and granule cells labeled from the same cortical area. Redrawn from Kelly and Strick (2003). Abbreviations: ANT, anterior lobe; PMD, pramedian lobule.

intraparietal areas and prefrontal areas 9l, 46d, preSMA and the rostral dorsal premotor area (Strick et al., 2009, **Figure 3**; Hashimoto et al., 2010; Prevosto et al., 2010, **Figure 5**; Lu et al., 2007, **Figure 6**; Kelly and Strick, 2003, **Figure 7**; Kievit, 1979). Targets of the D1 zone and the caudal dentate are limited to the frontal eye field (Lynch et al., 1994, **Figure 3**). The posterior interposed nucleus, the target nucleus of the C2 zone, projects to tne primary motor and premotor areas, the intraparietal areas MIP and LIP, prefrontal area 46 and the frontal eye fields (Strick et al., 2009; Prevosto et al., 2010, **Figure 5**; Lu et al., 2012, **Figure 6**; Kievit, 1979; Lynch et al., 1994). Widespread projections of the posterior interposed nucleus to these cortical areas were confirmed by Sultan et al. (2012) using fMRI after electrically stimulating the cerebellar nuclei and/or the superior cerebellar peduncle. Their observation of bilateral blood-oxygenation-level dependent (BOLD) responses by these authors after stimulation of the posterior interposed nucleus or the peduncle remains unexplained.

For monkeys the presence of reciprocal projections from primary and premotor areas, the frontal eye field and the posterior parietal cortex to the parvocellular red nucleus is clear from the plot of Humphrey et al. (1984) of retrogradely labeled neurons from an injection of this nucleus (**Figure 4B**). Somatotopically organized projections from the primary motor and premotor areas are located in the laterocaudal red nucleus and thus target the D2 zone via the dorsal lamina of the principal olive (Kuypers and Lawrence, 1967; Hartmann von Monakow et al., 1979; Strominger et al., 1979; Orioli and Strick, 1989; Tokuno et al., 1995; Burman et al., 2000). Projections from the frontal eye fields are shunted through the dorsomedial parvocellular red nucleus and the ventral lamina of the principal olive to the D1 zone (Huerta et al., 1986; Stanton, 1988; Huerta and Kaas, 1990). The location of the posterior parietal projection to the parvocellular red nucleus is not known; a prefrontal projection to the dorsomedial red nucleus only has been substantiated for area 9 by Leichnetz (1982). Cortical afferents of Darkschewitsch nucleus, the link in the C2 circuitry, are mostly the same as for the parvocellular red nucleus: motor cortex, frontal eyefields, prefrontal cortex and the posterior parietal area (Faugier-Grimaud and Ventre, 1989; Leichnetz and Gonzalo-Ruiz, 1996). Caudal, motor and rostral, visual receiving, parts of the rostral MAO were distinguished by Porter et al. (1993) in the cat. These divisions, presumably, supply climbing fibers to the anterior and posterior motor divisions, and the hemisphere of the ansiform lobule and the paraflocculus, respectively. Similar laterocaudal visuomotor and rostromedial skeletomotor divisions also have been recognized in the posterior interposed nucleus (van Kan et al., 1993).

Evidence for the reciprocity in the cerebello-cortical climbing fiber loops is still incomplete, although more complete for the monkey than for the cat; studies with modern tracing methods on these connections have not yet been published. Cortical

afferents in the circuitry of the C2 and D2 zones appear to be very similar, the D2 zone and its tributaries, standing out as the largest system in primates. In cetacea the C2 zone occupies this prominent position (Korneliussen, 1968). Remarkably, the interaction of cerebellar and cortical afferents in the parvocellular red nucleus and the nucleus of Darkschewitsch, and the physiology of the recurrent climbing fiber loops has never been studied.

It should be remembered that the projections of the dentate and interposed nuclei are not limited to the thalamus and the cortex. Branching axons of the anterior interposed nucleus terminate in the contralateral magnocellular red nucleus and in the nucleus reticularis tegmenti pontis. The posterior interposed nucleus projects to parts of the reticular formation, to a medial ridge of cells along the red nucleus and to the tectum and pretectum. Apart from its projection to the parvocellular red nucleus the dentate is also connected with the pontine nuclei and the nucleus reticularis tegmenti pontis. The rostral dentate projects to the main, lateral and caudal parvocellular red nucleus, its caudal part to the dorsomedial subnucleus of the parvocellular red nucleus and to the tectum and the pretectum (Teune et al., 2000; Ruigrok and Teune, 2014).

Few studies have appeared on climbing fiber afferent systems using MRI. According to Diedrichsen et al. (2010) the BOLD signal in the cerebellum in fMRI mostly depends on the mossy fiber input and obscures the activity in the Purkinje cells and the climbing fibers. One study of the cortico-rubral relations in the human brain, using brain resting state functional connectivity, showed correlations of signal intensity of the red nucleus and insular, hippocampal, occipital and prefrontal cortices, but not with motor and premotor areas (Nioche et al., 2009). Jang et al. (2012), using diffusion tensor tractography, found direct projections to the inferior olive from the sensorimotor and posterior parietal cortex, in addition to the red nucleus and the pontine nuclei. Thus far the conclusions of these studies differ substantially from the experimental findings.

The picture that emerges of the motor regions of the cerebellum is that of an array of intercallated modules with peripheral motor and more extensive motor and non-motor cortical connections. The latter are part of a system of closed cerebello-rubral and cortical climbing fiber loops. Parallel fibers traverse Purkinje cells of these different modules and effectuate a cerebellar output serving adaptation or coordination of the motor system. These vague terms hide our lack of knowledge on what is actually happening at the brain stem and cortical targets of the modules.

IS EACH PURKINJE CELL ZONE A BASIC FUNCTIONAL UNIT?

Simpson (2011) pointed out that what is missing in the old postulate that each Purkinje cell zone constitutes a basic functional unit of the cerebellum, are tractable behaviors with which to evaluate hypothesis about the functions performed by the zones in relation to each other. This kind of behavior can be studied by stimulation or inactivation of a Purkinje cell zone, its cerebellar or vestibular target nucleus or its climbing fiber afferents.

Reaching and grasping were studied by Mason et al. (1998) in monkeys after inactivation of small parts of the cerebellar nuclei by the injection of muscimol. In accordance with the somatotopical localization in the anterior interposed and rostral dentate nuclei, discussed before, they found deficits in grasping with the hindlimb in the most anterior injections of these nuclei and with the forelimb with injections in their more caudal parts. Injections in the posterior interposed nucleus and the adjoining dentate resulted in deficits in aiming of reach and stability of the arm. These experiments suggest that the posterior interposed nucleus, with the C2 zone, and the dentate, with the D2 zone, are involved in motor functions of the cerebellum. But how? Mason et al. (1998) suggested that the medial strip of the magnocellular red nucleus, that receives a projection of the posterior interposed nucleus is involved. No such a brainstem relay is known for the rostral dentate.

Horn et al. (2010) defined functions of cerebellar modules by inactivating their olivary subnuclei in the cat. Deletion of the complex spikes causes an increase of the simple spikes, a high rate of the Purkinje cell discharge and inhibition of the output of the modules. They studied possible deficits in the reach-to-grasp where the cat grasps a handle on a tone cue to get a reward, and locomotion. Inactivation of the C1, C3 and Y modules from the rostral DAO caused contralateral deficits in gripping the handle with the paw, paw dragging during locomotion and maintaining limb position during stance. With inactivation of the C2 module from the rostral MAO there are less problems with grasping but, stance and reach trajectory and locomotion are seriously affected. These observations are very similar to those of Mason et al. (1998) on inactivation of the anterior and posterior interposed nuclei in the monkey.

Deficits similar to inactivation of the rostral DAO had been found with lesions of the anterior interposed nucleus or the contralateral red nucleus (Gibson et al., 1994). But the deficits caused by inactivation of the rostral MAO could not be reproduced by lesions of the contralateral red nucleus.

Martin et al. (2000) found under reaching in a reach to grasp task in cats after inactivation of the anterior interposed nucleus and overreaching when the posterior interposed nucleus was affected. Under- and overreaching were also found after inactivation of the projection areas of the anterior and posterior interposed nuclei in the rostromedial and rostrolateral motor cortex, respectively. However, undereaching rather than overreaching was found by Horn et al. (2010) after inactivation of the rostral MAO.

Pijpers et al. (2008) injected a neurotoxin in the hindlimb region of the C1 zone in the copula pyramidis of the rat. This caused local degeneration of mossy and climbing fibers. Climbing and mossy fiber collaterals that innervate rostral parts of the C1 and related zebrin-negative zones also are affected. Inactivation of hindlimb segments of the C1 and related zones did not affect skilled walking or the overall stepping pattern but reduced step-dependent modulation of cutaneous reflexes. Paw-dragging of the forelimb, as observed by Horn et al. (2010) in the cat could not observed in the rat because in Pijpers' experiments the hindlimb rather than the forelimb segments of the C1 zone were injected.

Seone et al. (2005) found greater control of axial muscles in rats treated with a toxin that preserves the caudal MAO than in animals treated with another toxin that preserves the rostral MAO. Reaching and grasping were not studied by these authors. In a critical review of these studies Cerminara (2010) pointed out that it is premature to conclude, as Horn et al. (2010) did, that "... each module has a specific and unique function in sensory-motor integration". True, restriction to a single module could not be guaranteed in any of the relevant studies. The injections of the toxin in the experiments of Horn et al. (2010) may have affected more than one subdivision of the olive, degeneration of climbing and mossy fiber collaterals with toxin injections of the caudal C1 zone in the experiments of Pijpers et al. (2008) deafferented other Purkinje cell zones in the rostral cerebellum, and the toxins used by Seone et al. (2005) preserved 47–59% of the neurons in other subdivisions of the olive apart from the rostral and caudal MAO. Still, in my opinion, involvement of the principal olive in the experiments of Horn et al. (2010) with injections of the rostral MAO or DAO is unlikely to have influenced their observations on the reach to grasp and locomotion (Milak et al., 1997; Martin et al., 2000). An extension of their rostral MAO injection into the caudal MAO was never observed by these authors. Even when other zones than the injected C1 zone in the experiments of Pijpers et al. (2008) would have been deafferented, they would belong to the same C1, C3, Y category. Other confusing factors mentioned by Cerminara (2010), such as the mutual inhibition of microzones or electrotonic coupling do not cross the spaces between the olivary subdivisions and, therefore, cannot have been involved.

In evaluating the function of Purkinje cell zones their composite nature has to be taken into account. The caudal MAO innervates at least 4 subzones both in the A zone and the A2 zone, the latter being present in rodents only. Specific regions in the C3 zone have been identified as the link in the conditioned eyeblink response (Jirenhed et al., 2007). Similar to the motor effects observed by Horn et al. (2010) eyeblink resposes of the C3 zone are relayed by the anterior interposed nucleus and the contralateral red nucleus (Morcuendo et al., 2002; Pacheco-Calderón et al., 2012). In the rat the relay is a separate population of neurons in the dorsolateral red nucleus and the adjoining pararubral area with projections to the facial motor nucleus (Ruigrok and Cella, 1995). In the cat two antagonistic groups of neurons occur in the anterior interposed nucleus. A-cells fire during the active contraction of the orbicularis oculi muscle, B-cells stop firing during downward displacement of the upper eyelid. A-cells project to the red nucleus, B-cells would project to the perioculomotor area, a projection that has not yet been verified anatomically (Sánchez-Campusano et al., 2012; Perciavalle et al., 2013). Visually dominated segments of the C2 zone do not participate in the initiation or storage of acquired memories in the conditioned eyeblink response, but play an enhancer role in the performance and the proper timing of the reflex (Jiménez-Díaz et al., 2004).

Behavioral studies of the D1 and D2 zones are available for its Crus I segments only; the anterior lobe, the paramedian lobules and the paraflocculus have not yet been studied. Purkinje cells of the Crus I D1 zone in the cat were found to encode the motion of a target, a moving tube in front of the animal, and the visual GO signal for the cat to reach for food in the tube (Miles et al., 2006). Purkinje cells in the adjoining Crus I D2 zone also encode target motion, but tonic spike activity was maintained during the transient disappearance of the target. This Purkinje cell activity may reflect the operation of an internal model based on memory of its previous motion (Cerminara et al., 2009; Cerminara and Apps, 2013). Whether such a model is also operative in the D1 zone is not known. Visual climbing fiber input has been documented for the D1 zone (Edge et al., 2003, see also section III) but not for D2. Visual mossy fiber input in the cat, relayed by the pontine nuclei, reaches the Crus I, but has not been studied in detail (Mower et al., 1980; Xiong et al., 2002).

Proville et al. (2014) found partially overlapping projections from the pontine whisker sensory and motor projections to the Crus I D2 zone in mice. Recurrent projections from these Purkinje cells excite neurons in lamina V of the whisker motor cortex and are responsible for the fine modulation of the whisker movement parameters observed in these experiments.

Transneuronal retrograde labeling in the caudal non-motor dentate and of Purkinje cells in the ansiform lobule (Hashimoto et al., 2010, **Figure 5**) or in the Crus II only (Kelly and Strick, 2003, **Figure 7**) was found with injections in the rostral dorsal premotor area (which is considered as a prefrontal area because it lacks connections with the primary motor cortex) and prefrontal area 46, respectively. This supports the notion of Crus II D2 zone being one of the main non-motor areas of the cerebellum.

Function is best-known for the Purkinje cell zones of the cerebellar flocculus that are part of the circuitry subserving compensatory eye movements in the planes of the horizontal and anterior semicircular canals (Van der Steen et al., 1994; Voogd et al., 2012). Behavioral paradigms for other Purkinje cell zones are still scarce, and the nature of the interactions of the cerebellum at brain stem motor centers or at the level of the cerebral cortex remain largely unknown.

TOPOGRAPHICAL RELATIONS BETWEEN MOSSY AND CLIMBING FIBERS IN THE CEREBELLAR CORTEX

Purkinje cell zones of the hemisphere receiving peripheral somatosensory climbing fiber input (C1, C3 and Y zones) can be subdivided into microzones. Microzones are narrow longitudinal strips of Purkinje cells that receive climbing fiber input sharing the same receptive field (Andersson and Oscarsson, 1978). Microzones were visualized by Sugihara et al. (2001) as longitudinal strips of branching olivocerebellar fibers (**Figure 8B**). This type of branching was observed in all parts of the cerebellum. A microzonal organization, therefore, appears to be a general property of the cerebellum.

Mossy fibers, initially, follow a transverse course through the cerebellar white matter (**Figure 8A**). At regular sites they emit thin collaterals that terminate in longitudinal aggregates of mossy fiber terminals (rosettes) in the granular layer (Scheibel, 1977; Wu et al., 1999). There is a special topographical relationship between the climbing fiber microzones and these mossy fiber terminal aggregates. Climbing and mossy fiber collateral projections were

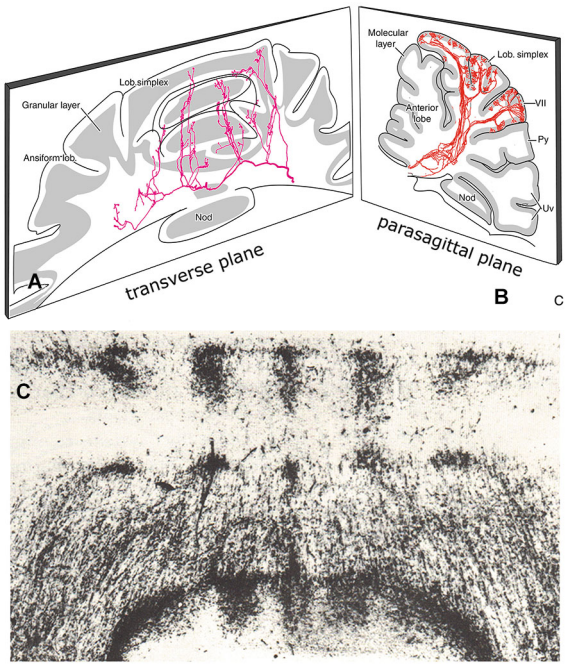

FIGURE 8 | (A) Transverse section through the cerebellum of the rat showing course and collateralization of a reticulocerebellar mossy fiber. The collaterals terminate as longitudinal aggregates of mossy fiber terminals. Redrawn from Wu et al. (1999). **(B)** Parasagittal section showing branching olivocerebellar fibers from a small injection of an antegrade tracer in the inferior olive. The branches terminate in a narrow longitudinal strip of climbing fibers in the molecular layer, Redrawn from Sugihara et al. (1999). **(C)** Transverse section through the anterior lobe of the cerebellum of the tree shrew (Tupaia glis) showing distribution of the spinocerebellar mossy fibers. Abbreviations: Nod, nodulus; Py, pyramis; Uv, uvula.

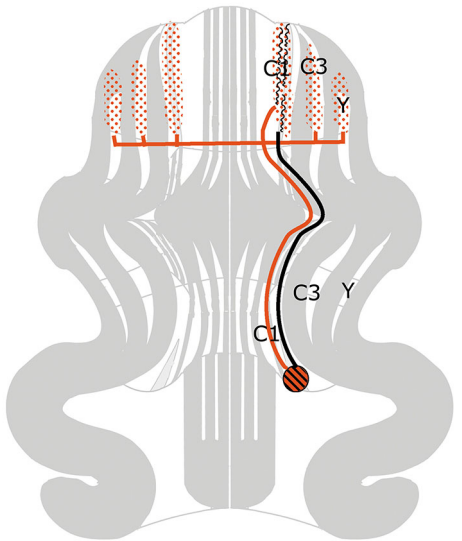

FIGURE 9 | Diagram of the flattened cerebellar cortex showing collateralization of climbing and mossy fibers from a small injection site of choleras toxin B subunit in the caudal C1 zone of the rat. Climbing collaterals remain in the same zone. Mossy fibers collateralize subjacent to the climbing fiber collaterals and in symmetrically disposed neighboring zones of the same zebrin-signature.

traced in the rat from small injections of cholera toxin B subunit in identified cortical zones, that included the molecular and granular layers. Climbing fiber collaterals were found to terminate in narrow strips within other segments of the same zone. Mossy fiber collaterals always terminate subjacent to the climbing fiber collaterals in the granular layer (Pijpers et al., 2006). In addition, mossy fiber collaterals terminate, bilaterally and symmetrically, as multiple longitudinal aggregates (**Figures 8A**, **9**). Mossy fiber collaterals remain restricted to zones of the same zebrin-type of the injected zone. The convergence of mossy and climbing fiber evoked potentials from stimulation of peripheral nerves or the somatosensory cortex onto a single somatotopical map in the anterior lobe was already known from Provini et al. (1968). In the cat C3 zone, both the climbing fibers of the dorsal column spine-olivary climbing fiber path and the mossy fibers of the exteroceptive component of the cuneocerebellar mossy fiber system were found to terminate according to the same detailed somatotopical pattern (Ekerot and Larson, 1980; Garwicz et al., 1998). Similar observations for somatotopically organized climbing fiber and mossy fiber input from the basilar pontine nuclei to the copula pyramidis of the rat were made by Cerminara et al. (2013).

In the studies of Voogd et al. (2003) and Pijpers et al. (2006) the topographical relationship of climbing fiber and mossy fiber microzones was found in all parts of the cerebellum. In regions without somatotopical input we do not know the nature of this relationship. Do mossy and climbing fibers share input from the same cortical regions? Or from similar functional networks? Or from the same axis in the vestibular coordinate system (Simpson and Graf, 1985)? We do not know.

Different ideas have been proposed for the functional relations of mossy fiber terminal aggregates and the climbing fiber microzones. Llinás (1982) hypothesized that ascending segments of granule cell axons preferentially terminate on the superjacent Purkinje cell dendrites. This idea received support from Brown and Bower (2001), who demonstrated that the receptive field for a Purkinje cell complex spike is similar to the receptive field of the granule cells immediately subjacent to that Purkinje cell. Ekerot and Jörntell (2003) confirmed the similarity in receptive field organization of climbing fiber microzones and the subjacent mossy fiber terminal aggregates. However, determining the receptive field organization of parallel fibers innervating the Purkinje cells and interneurons in these microzones, they found the receptive fields of interneurons to correspond to the mossy fiber terminal aggregate of the microzone, whereas the receptive fields of Purkinje cells corresponded to mossy fibers in neighboring microzones. Llinás (1982) hypothesis, therefore, may apply to interneurons but not to Purkinje cells.The properties of the parallel fibers cannot be explained without involving learning mechanisms. Barmack and Yakhanitsa (2011) found the optimal planes for complex and simple spikes of Purkinje cells in climbing fiber zones of the uvula-nodulus innervated by the vertical semicircular canals to be identical, but oppositely polarized. This observation

is not in accordance with the Llinás (1982) hypothesis.They proposed that the opposite polarization is due to inhibition of Purkinje cells by stellate cells. Stellate cells are modulated in phase with the complex spikes and out of phase with the simple spikes. Stellate cells can be excited by glutamate spillover from the discharge of adjacent climbing fibers. Golgi cells are modulated in phase with the simple spikes and, therefore, cannot be account for the modulation of simple spikes by complex spikes. The relations between mossy fiver aggregates and climbing fiber microzones, therefore, are complicated and involve interneurons and plastic changes in the circuitry.

SIMILARITIES IN THE ANATOMICAL ORGANIZATION OF MOSSY AND CLIMBING FIBER SYSTEMS

Gibson et al. (2004) and others emphasized the different properties of. mossy and climbing fibers. Climbing fibers have a strong influence on a small number of Purkinje cells, discharge at a low rate and signal externally imposed disturbances to particular regions of the body when the animal is not actively moving. Mossy fibers exert a relatively small effect on a large number of Purkinje cells via the parallel fibers; they discharge at high frequencies and carry detailed information about the external world as well as intended and actual body movement. Still, the topographical relationship of climbing fiber microzones and mossy fiber aggregates suggests similarities in the anatomical organization of both systems.

It has been suggested that the efferent thalamocortical and the cortico-ponto-cerebellar mossy fiber systems are organized as closed loops (Kelly and Strick, 2003, **Figure 7**), similar to the reciprocal circuitry of the climbing fiber system discussed in section III. Indeed, at the origin of these loops, as the cortico-rubral and corticopontine projections (**Figure 4**) and at their end, as the common somatotopical map in the anterior lobe, the two systems are very similar. Mossy fiber loops differ from climbing fiber loops because the latter are organized as a separate loop for each module **Figure 10A**), whereas mossy fiber loops always include multiple modules (**Figure 10B**). Moreover, the relays in recurrent mossy fiber loops are different from the climbing fiber loops. The projection of the anterior interposed nucleus to the magnocellular red nucleus is reciprocated by a collateral projection of the rubrospinal tract to this nucleus (Huisman et al., 1983). The circuitry through the nucleus reticularis tegmenti pontis and through the red nucleus and the lateral reticular nucleus was emphasized by Allen and Tsukahara (1974). Whether these connections are reciprocal at the level of the cerebellum is not known. Moreover, these systems are complicated by the presence of cortical input at the level of the reticular nucleus of the pons (Brodal and Brodal, 1971) and by the termination of the ipsilateral forelimb tract in the lateral reticular nucleus (Clendelin et al., 1974). The electrophysiology of these convergent inputs has not been studied.

Cerebellar-cortical connections and the cortico-cerebellar mossy fiber projections in monkeys have been found to be reciprocally organized (Kelly and Strick, 2003). Injections of a retrograde transneuronal tracer in the forelimb motor cortex labeled Purkinje cells in the anterior lobe hemisphere and in the paramedian lobule. Granule cells labeled from an injection of an antegrade transneuronal tracer were found in the same lobules. Injections in prefrontal area 46 labeled both types of neurons in the Crus II (**Figure 7**). Injections of the primary motor cortex would be expected to label Purkinje cells in the C1, C2, C3 and D2 zones, and injections of area 46 in the C2 and D2 zones, all of which project to these cortical area through their target nuclei (section III). Transneuronal labeling of granule cells from injection sites in the same areas would label mossy fibers from all precerebellar nuclei that receive cortical input: apart from the pontine nuclei these would include reticular, dorsal column and even spinocerebellar nuclei. Moreover retrogradely labeled mossy fibers would distribute widely, collateralizing to different Purkinje cell zones. True reciprocity, therefore, has not been demonstrated in this study.

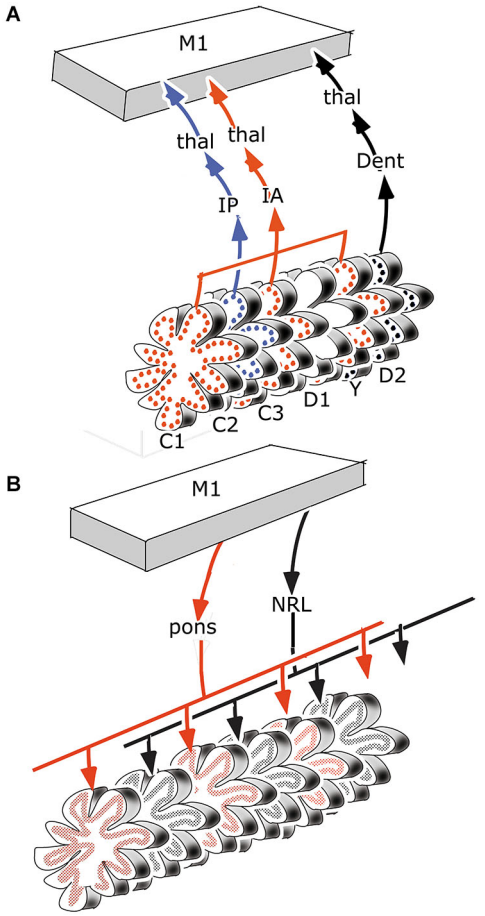

FIGURE 10 | (A) Retrograde transneuronal retrograde labeling of Purkinje cells from the primary motor cortex would affect all modules with thalamocortical to this area, in the case of motor regions of the cerebellum they would include the C1, C2, C3, Y and D2 modules. **(B)** Antegrade transneuronal labeling from the primary motor cortex of mossy fiber terminals in the granular layer would label all mossy fiber systems with intermediate stations that receive cortical input, such as the pontine nuclei and the lateral reticular nucleus. Each of these systems would distribute in multiple parallel strips of labeled mossy fiber rosettes. Abbreviations: Dent, dentate nucleus; IA, anterior interposed nucleus; IP, posterior interposed nucleus; NRL, lateral reticular nucleus; thal, thalamus.

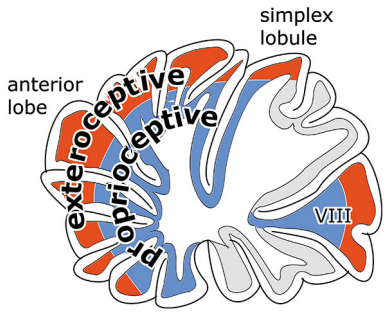

FIGURE 11 | Diagram illustrating concentric arrangement of exteroceptive components of mossy fiber systems and pontocerebellar mossy fibers to superficial and of proprioceptive and vestibular mossy fibers to the cortex in the bottom of the fissures.

TOPOGRAPHICAL RELATIONS OF DIFFERENT MOSSY FIBER SYSTEM IN THE CEREBELLUM

Where individual mossy fibers emit collaterals bilaterally at specific medio-lateral positions, entire mossy fiber systems all terminate in bilaterally distributed discrete aggregates of mossy fiber rosettes (**Figure 8C**). This parcellated distribution has been found for all mossy fiber systems, spinocerebellar, cuneocerebellar (Voogd, 1969), trigeminocerebellar (Ikeda and Matsushita, 1992), reticulocerebellar (Wu et al., 1999), vestibulocerebellar (Matsushita and Wang, 1987) and pontocerebellar systems (Serapide et al., 2001). Antegrade axonal tracing studies of different mossy fiber systems have been published for cats and rats, but scarcely any are available for primates. The last study on the spinocerebellar tracts in monkeys dates from the 19th century. Little is known of the interrelations of different mossy fiber systems in the cortex. The relation of mosssy fiber terminal fields to the zebrin-positive and -negative Purkinje cell zones was studied for the spino- and cuneocerebellar mossy fiber projection in the anterior vermis of the rat (Ji and Hawkes, 1994). In this case the two systems were found to interdigitate, an observation confirmed by Gebre et al. (2012). Similar information on other mossy fiber system is not available.

Another feature of the distribution of mossy fibers in motor regions of the cerebellum is their concentric arrangement (**Figure 11**). Corticopontine and exteroceptive components of mossy fiber systems terminate in apical parts of the lobules, proprioceptive components and vestibular mossy fibers in the bottom of the fissures (Ekerot and Larson, 1972; Voogd and Ruigrok, 2004). This configuration raises an interesting question on the convergence of Purkinje cell axons onto the cerebellar nuclei. Do superficial and deep Purkinje cells of a lobule converge upon the same nuclear neurons? In this case lobules would have an integrating function,apart from increasing the surface area of the cerebellar cortex.

Length and synaptic size of parallel fibers differ for the upper and lower molecular layer (see Van der Want et al. (1985) for references). A relation with differences in mossy fiber input, of spinocerebellar mossy fibers to deep and pontocerebellar mossy fibers to more superficial parts of the granular layer has been suggested (Eccles et al., 1967) but has not been studied since.

CONCLUSIONS

Repairing gaps in our knowledge on cerebellar systems asks for a collaborative effort of anatomists and physiologists. Noninvasive techniques for the tracing of axonal pathways will have to be developed to collect information in non-human primates. MRI technology will have to be improved to visualize climbing fiber paths and Purkinje cell activity. The alternation of Purkinje cell zones receiving peripheral and cortical climbing fiber input, and the contribution of the mutiple narrow Purkinje cell zones to cerebellar function should be evaluated in suitable animal models. But even when we know the precise interrelations of different cortical areas and brainstem centers with the cerebellum, the contribution of the cerebellum to the information processing in these structures remains incompletely known.

REFERENCES

Allen, G., and Tsukahara, N. (1974). Cerebrcerebellar communication systems. *Physiol. Rev.* 54, 957–1006.

Andersson, G. (1984). Demonstration of a cuneate relay in a cortico-olivocerebellar pathway in the cat. *Neurosci. Lett.* 46, 47–52. doi: 10.1016/0304-3940(84)90197-6

Andersson, G., and Nyquist, J. (1983). Origin and sagittal termination areas of cerebro-cerebellar climbing fibre paths. *J. Physiol.* 337, 257–285.

Andersson, G., and Oscarsson, O. (1978). Climbing fiber microzones in the cerebellar vermis and their projection to different groups of cells in the lateral vestibular nucleus. *Exp. Brain Res.* 32, 565–579. doi: 10.1007/bf00239553

Apps, R., and Garwicz, M. (2000). Precise matching of olivo-cortical divergence and cortico-nuclear convergence between somatotopically corresponding areas in the medial C1 and medial C3 zones of the paravermal cerebellum. *Eur. J. Neurosci.* 12, 205–214. doi: 10.1046/j.1460-9568.2000.00897.x

Apps, R., and Hawkes, R. (2009). Cerebellar cortical organization: a one map hypothesis. *Nat. Rev. Neurosci.* 10, 670–681. doi: 10.1038/nrn2698

Bagnall, M. W., Zingg, B., Sakatos, A., Moghadam, S. H., Zeilhofer, H. U., and du Lac, S. (2009). Glycinergic projection neurons of the cerebellum. *J. Neurosci.* 29, 10104–10110. doi: 10.1523/JNEUROSCI.2087-09.2009

Barmack, N. H., and Yakhanitsa, V. (2011). Topsy Turvy: functions of climbing and mossy fibers in the vestibulo-cerebellum. *Neuroscientist* 17, 221–236. doi: 10.1177/1073858410380251

Bortov, G. A., and Strick, P. L. (1993). Corticospinal terminations in two new-world primates: further evidence that corticomotoneuronal connections provide part of the neural substrate for manual dexterity. *J. Neurosci.* 13, 5105–5118.

Brodal, A., and Brodal, P. (1971). The organization of the nucleus reticularis tegmenti pontis in the cat in the light of experimental anatomical studies of its cerebral cortical afferents. *Exp. Brain Res.* 13, 90–110. doi: 10.1007/bf00236432

Brown, J. E., and Bower, J. M. (2001). Congruence of mossy fiber and climbing fiber tactile projections in the lateral hemisphere of the rat cerebellum. *J. Comp. Neurol.* 429, 59–70. doi: 10.1002/1096-9861(20000101)429:1<59::AID-CNE5>3.0.CO;2-3

Burman, K., Darian-Smith, C., and Darian-Smith, I. (2000). Macaque red nucleus: origins of spinal and olivary projections and terminations of cortical inputs. *J. Comp. Neurol.* 423, 179–196. doi: 10.1002/1096-9861(20000724)423:2<179::aid-cne1>3.0.co;2-#

Catsman-Berrevoets, C. E., Kuypers, H. H., and Lemon, R. N. (1979). Cells of origin of the frontal projection to magnocellular and parvocellular red nucleus and superior colliculus in cynomolgus monkey. An HRP study. *Neurosci. Lett.* 12, 41–46. doi: 10.1016/0304-3940(79)91477-0

Cerminara, N. L. (2010). Cerebellar modules: individual or composite entities?. *J. Neurosci.* 30, 16065–16067. doi: 10.1523/jneurosci.4823-10.2010

Cerminara, N. L., Aoki, H., Loft, M., Sugihara, I., and Apps, R. (2013). Structural basis of cerebellar micricircuits in the rat. *J. Neurosci.* 33, 16427–16442. doi: 10.1523/JNEUROSCI.0861-13.2013

Cerminara, N. L., and Apps, R. (2013). Behavioural significance of cerebellar modules. *Cerebellum* 10, 484–494. doi: 10.1007/s12311-010-0209-2

Cerminara, N. L., Apps, R., and Marple-Horvat, D. E. (2009). An internal model of a moving visual target in the lateral cerebellum. *J. Physiol.* 587, 429–442. doi: 10.1113/jphysiol.2008.163337

Clendelin, M., Ekerot, C. F., and Oscarsson, O. (1974). The laterql reticular nucleusin the cat. III. Organization of component activated from ipsilateral forelimb tract. *Exp. Brain Res.* 21, 501–513. doi: 10.1007/bf00237168

Diedrichsen, J., Verstynen, T., Schhlerf, J., and Wiestler, T. (2010). Advances in functional imaging of the human cerebellum. *Curr. Opin. Neurol.* 23, 382–387. doi: 10.1097/WCO.0B013e32833be837

Eccles, J. C., Ito, M., and Szentagothaii, J. (1967). *The Cerebellum as a Neuronal Machine.* Heidelberg, New York: Springer Verlag.

Edge, A. L., Marple-Horvat, E., and Apps, R. (2003). Lateral cerebellum: functional localization within crus I and correspondance to cortical zones. *Eur. J. Neurosci.* 18, 1468–1485. doi: 10.1046/j.1460-9568.2003.02873.x

Ekerot, C. F., and Jörntell, H. (2003). Parallel fiber receptive fields: a key to understanding cerebellar operation and learning. *Cerebellum* 2, 101–109. doi: 10.1080/14734220309411

Ekerot, C. F., and Larson, B. (1972). Differential termination of the exteroceptive and proprioceptive components of the cuneocerebellar tract. *Brain Res.* 36, 420–424. doi: 10.1016/0006-8993(72)90748-2

Ekerot, C. F., and Larson, B. (1980). Termination in overlapping sagittal zones in cerebellar anterior lobe of mossy and climbing fiber paths activated from dorsal funiculus. *Exp. Brain Res.* 38, 163–172. doi: 10.1007/bf00236737

Faugier-Grimaud, S., and Ventre, J. (1989). Anatomic connections of inferior parietal cortex (area 7) with subcortical structures related to vestibulo-ocular function in a monkey (Macaca fascicularis). *J. Comp. Neurol.* 280, 1–14. doi: 10.1002/cne.902800102

Flumerfelt, B. A., Otabe, S., and Courville, J. (1973). Distinct projections to the red nucleus from the dentate and interposed nuclei in the monkey. *Brain Res.* 50, 408–414. doi: 10.1016/0006-8993(73)90742-7

Garwicz, M., Jörntell, H., and Ekerot, C.-F. (1998). Cutaneous receptive fields and topography of mossy fibres and climbing fibres projecting to cat cerebellar C3 zone. *J. Physiol.* 512, 277–293. doi: 10.1111/j.1469-7793.1998.277bf.x

Gebre, S. A., Reeber, S. L., and Sillitoe, R. V. (2012). Parasagittal compartmentation of cerebellar mossy fibers as revealed by the patterned expression of vesicular glutamate transporters VGLUT1 and VGLUT2. *Brain Struct. Funct.* 217, 165–180. doi: 10.1007/s00429-011-0339-4

Gibson, A. R., Horn, K. M., and Pong, M. (2004). Activation of climbing fibers. *Cerebellum* 3, 212–221. doi: 10.1080/14734220410018995

Gibson, A. R., Horn, K. M., and van Kan, P. M. (1994). "Grasping cerebellar function," in *Insights in the Reach to Grasp*, eds K. M. B. Hennett and U. Castiello (Amsterdam: Elsevier), 85–108.

Gibson, A. R., Robinson, A. R., Alam, J., and Houk, J. C. (1987). Somatotopic alignment between climbing fiber input and nuclear output of the cat intermediate cerebellum. *J. Comp. Neurol.* 260, 362–377. doi: 10.1002/cne.902600304

Glickstein, M., May, J. G., and Mercier, B. E. (1985). Corticopontine projection in the macaque: the distribution of labeled cortical cells after large injections of horseradish peroxidase in the pontine nuclei. *J. Comp. Neurol.* 15, 235–259. doi: 10.1002/cne.902350306

Hartmann von Monakow, K., Akert, K., and Künzle, H. (1979). Projections of precentral and premotor cortex to the red nucleus and other midbrain areas in Macaca fascicularis. *Exp. Brain Res.* 34, 91–105. doi: 10.1007/bf00238343

Hashimoto, M., Takahara, D., Hirata, Y., Inoue, K., Miyachi, S., Nambu, A., et al. (2010). Motor and non-motor projections from the cerebellum to rostrocaudally distinct sectors of the dorsal premotor cortex in macaques. *Eur. J. Neurosci.* 31, 1402–1413. doi: 10.1111/j.1460-9568.2010.07151.x

Hawkes, R., and Leclerc, N. (1987). Antigenic map of the rat cerebellar cortex: the distribution of parasagittal bands as revealed by monoclonal anti-Purkinje cell antibody mapQ113. *J. Comp. Neurol.* 256, 29–41. doi: 10.1002/cne.902560104

Holstege, G., Blok, B. F., and Ralston, D. D. (1988). Anatomical evidence for red nucleus projections to motoneuronal cell groups in the spinal cord of the monkey. *Neurosci. Lett.* 95, 97–101. doi: 10.1016/0304-3940(88)90639-8

Horn, K. M., Pong, M., and Gibson, A. R. (2010). Functional relations of cerebellar modules of the cat. *J. Neurosci.* 30, 9411–9423. doi: 10.1523/JNEUROSCI.0440-10.2010

Huerta, M. F., and Kaas, J. H. (1990). Supplementary eye field as defined by intracortical microstimulation: connections in macaques. *J. Comp. Neurol.* 293, 299–330. doi: 10.1002/cne.902930211

Huerta, M. F., Krubitzer, L. A., and Kaas, J. H. (1986). Frontal eye field as defined by intracortical microstimulation in squirrel monkeys, owl monkeys and macaque monkeys: I. Subcortical connections. *J. Comp. Neurol.* 253, 415–439. doi: 10.1002/cne.902530402

Huisman, A. M., Kuypers, H. G., Condé, F., and Keizer, K. (1983). Collateral od rubrospinal neurons to the cerebellum in rat. A retrograde fluorescent double labelling study. *Brain Res.* 264, 181–196. doi: 10.1016/0006-8993(83)90816-8

Humphrey, D. R., Gold, R., and Reed, D. J. (1984). Sizes, laminar and topographical origins of cortical projections to the major divisions of the red nucleus in the monkey. *J. Comp. Neurol.* 225, 75–94. doi: 10.1002/cne.902250109

Ikeda, M., and Matsushita, M. (1992). Trigeminocerebellar projections to the posterior lobe in the cat as studied by antegrade transport of wheat germ agglutinin-horseradish peroxidase. *J. Comp. Neurol.* 316, 221–237. doi: 10.1002/cne.903160207

Jang, S. H., Chang, P. H., and Kwon, H. G. (2012). The neural connectivity of the inferior olivary nucleus in the human brain: diffusion tensor tractography study. *Neurosci. Lett.* 523, 67–70. doi: 10.1016/j.neulet.2012.06.043

Ji, Z., and Hawkes, R. (1994). Topography of Purkinje cell compartments and mossy fiber terminal fields in lobules II and III of the rat cerebellar cortex: spinocerebellar and cuneocerebellar projections. *Neuroscience* 61, 935–954. doi: 10.1016/0306-4522(94)90414-6

Jiménez-Díaz, L., Navarro-López Jde, D., Gruart, A., and Delgado-García, J. M. (2004). Role of cerebellar interpositus nucleus in the genesis and control of reflex and conditioned eyelid responses. *J. Neurosci.* 24, 9138–9145. doi: 10.1523/jneurosci.2025-04.2004

Jirenhed, D. A., Bengtsson, F., and Hesslow, G. (2007). Acquisition, extinction and reacquisition of a cerebellar cortical memory trace. *J. Neurosci.* 27, 2493–2502. doi: 10.1523/jneurosci.4202-06.2007

Jörntell, H., and Ekerot, C. G. (1999). Topographical organization of projections to cat motor cortex from nucleus interpositus anterior and forelimb skin. *J. Physiol.* 514, 551–566. doi: 10.1111/j.1469-7793.1999.551ae.x

Kelly, R. M., and Strick, P. L. (2003). Cerebellar loops with motor cortex and prefrontal cortex of a nonhuman primate. *J. Neurosci.* 23, 8432–8444.

Kievit, J. (1979). *Cerebello-Thalamische Projecties en de Efferente Verbindingen naar de Frontaalschors in de Rhesus Aap.* Thesis. Rotterdam: Bronder.

Korneliussen, H. K. (1968). Comments on the cerebellum and its division. *Brain Res.* 8, 229–236. doi: 10.1016/0006-8993(68)90044-9

Kuypers, H. G., and Lawrence, D. G. (1967). Cortical projections to the red nucleus and the brain stem in the Rhesus monkey. *Brain Res.* 4, 151–188. doi: 10.1016/0006-8993(67)90004-2

Leichnetz, G. R. (1982). The medial accessory nucleus of bechterew: a cell group within the anatomical limits of the rostral oculomotor complex receives a direct prefrontal projection in the monkey. *J. Comp. Neurol.* 210, 147–151. doi: 10.1002/cne.902100205

Leichnetz, G. R., and Gonzalo-Ruiz, A. (1996). Prearcuate cortex in the Cebus monkey has cortical and subcortical connections like the macaque frontal eye field and projects to fastigial-recipient oculomotor-related brainstem nuclei. *Brain Res. Bull.* 41, 1–29. doi: 10.1016/s0361-9230(96)00154-2

Llinás, R. (1982). General discussion: radial connectivity in the cerebellar cortex: a novel view regarding the functional organization of the molecular layer. *Exp. Brain Res. Suppl.* 6, 189–192. doi: 10.1007/978-3-642-68560-6_10

Lu, X., Miyachi, S., Ito, Y., Nambu, A., and Takada, M. (2007). Topopgraphical distribution of output neurons in cerebellar nuclei and cortex to somatotopic map of primary motor cortex. *Eur. J. Neurosci.* 25, 2374–2382. doi: 10.1111/j.1460-9568.2007.05482.x

Lu, X., Miyachi, S., and Takada, M. (2012). Anatomical evidence for the involvement of medial cerebellar output from the interpositus nuclei in cognitive functions. *Proc. Natl. Acad. Sci. U S A* 109, 18980–18984. doi: 10.1073/pnas.1211168109

Lynch, J. C., Hoover, J. E., and Strick, P. L. (1994). Input to the primate frontal eye field from the substantia nigra, superior colliculus and dentate nucleus demonstrated by transneuronal transport. *Exp. Brain Res.* 100, 181–186. doi: 10.1007/bf00227293

Martin, J. H., Cooper, S. E., Hacking, A., and Ghez, C. (2000). Differential effects of deep cerebellar nuclei inactivation on reaching and adaptive control. *J. Neurophysiol.* 83, 1886–1899.

Mason, C. R., Miller, L. E., Baker, J. F., and Houk, J. C. (1998). Organization of reaching and grasping movements in the primate cerebellar nuclei as revealed by focal muscimol inactivations. *J. Neurophysiol.* 79, 537–554.

Matsushita, M., and Wang, C. L. (1987). Projection pattern of vestibulocerebllar fibers in the anterior vermis of the cat: an antegrade wheat germ agglutinin-horseradish peroxidase study. *Neurosci. Lett.* 74, 25–30. doi: 10.1016/0304-3940(87)90045-0

McCurdy, M. L., Hansma, D. I., Houk, J. C., and Gibson, A. R. (1987). Selective projections from the cat red nucleus to digit motor neurons. *J. Comp. Neurol.* 265, 367–379. doi: 10.1002/cne.902650306

Milak, M. S., Shimansky, Y., Bracha, V., and Bloedel, J. R. (1997). Effects of inactivating individual cerebellar nuclei on the performance and retention of an operantly conditioned forelimb movement. *J. Neurophysiol.* 78, 939–959.

Miles, Ö. B., Cerminara, N. L., and Marple-Horvat, D. E. (2006). Purkinje cells in the lateral cerebellum of the cat encode visual events and target motion during visually guided reaching. *J. Physiol.* 571, 619–637. doi: 10.1113/jphysiol.2005.099382

Morcuendo, S., Delgado-Garcia, J.-M., and Ugolini, G. (2002). Neuronal premotor networks involved in eyelid responses: retrograde transneuronal tracing with rabies virus from the orbicularis oculi muscle in the rat. *J. Neurosci.* 22, 8808–8818.

Mower, G., Gibson, A., Robinson, F., Stein, J., and Glickstein, M. (1980). Visual pontocerebellar projections in the cat. *J. Neurophysiol.* 43, 355–366.

Namba, K., Sugihara, I., and Hahimoto, M. (2011). Close correlation between the birth date of Purkinje cells and the longitudinal compartmentalization of the mouse adult cerebellum. *J. Comp. Neurol.* 519, 2594–2614. doi: 10.1002/cne.22640

Nioche, C., Cabanis, E. A., and Habas, C. (2009). Functional connectivity of the human red nucleus in brain resting state at 3T. *AJNR Am. J. Neuroradiol.* 30, 396–403. doi: 10.3174/ajnr.A1375

Onodera, S. (1984). Olivary projections from the mesodiencephalic structures in the cat studied by means of axonal transport of horseradish peroxidase and tritiated amino acids. *J. Comp. Neurol.* 227, 37–49. doi: 10.1002/cne.902270106

Orioli, P. J., and Strick, P. L. (1989). Cerebellar connections with the motor cortex and the arcuate premotor area: an analysis employing retrograde transneuronal transport of WGA-HRP. *J. Comp. Neurol.* 288, 612–626. doi: 10.1002/cne.902880408

Pacheco-Calderón, R., Carretero-Guillén, A., Delgado-Garcia, J. M., and Gruart, A. (2012). Red nucleus neurons actively contribute to the acquisition of classically conditioned eyelid responses in rabbits. *J. Neurosci.* 32, 12129–12143. doi: 10.1523/JNEUROSCI.1782-12.2012

Perciavalle, V., Apps, R., Bracha, V., Delgado-Garcia, J. M., Gibson, A. R., Leggio, M., et al. (2013). Consensus paper; current views on the role of cerebellar interpositus nucleus in movement control and emotion. *Cerebellum* 12, 738–757. doi: 10.1007/s12311-013-0464-0

Pijpers, A., Apps, R., Pardoe, J., Voogd, J., and Ruigrok, T. J. (2006). Precise spatial relationships between mossy fibers and climbing fibers in rat cerebellar cortical zones. *J. Neurosci.* 26, 12057–12080. doi: 10.1523/jneurosci.2905-06.2006

Pijpers, A., Winkelman, B. H., Bronsing, R., and Ruigrok, T. J. (2008). Selective impairment of the cerebellar C1 module involved in rat hind limb control reduces step-dependent modulation of cutaneous reflexes. *J. Neurosci.* 28, 2179–2189. doi: 10.1523/JNEUROSCI.4668-07.2008

Porter, C. M., van Kan, P. L. E., Horn, K. M., Bloedel, J. R., and Gibson, A. R. (1993). Functional divisions of cat rMAO. *Soc. Neurosci. Abstr.* 499, 10.

Prevosto, V., Graf, W., and Ugolini, G. (2010). Cerebellar inputs to intraparietal cortex areas MIP and LIP: functional frameworks for adaptive control of eye movements, reaching and arm/eye/head movement coordination. *Cereb. Cortex* 20, 214–228. doi: 10.1093/cercor/bhp091

Proville, R. D., Spolidoro, M., Guyon, N., Duqué, G. P., Selimi, F., Isope, P., et al. (2014). Cerebellum involvement in cortical sensorimotor circuits for the control of voluntary movements. *Nat. Neurosci.* 17, 1233–1239. doi: 10.1038/nn.3773

Provini, L., Redman, S., and Strata, P. (1968). Mossy and climbing fibre organization on the anterior lobe of the cerebellum activated by forelimb and hindlimb reas of the sensorimotor cortex. *Exp. Brain Res.* 6, 216–233. doi: 10.1007/bf00235125

Ruigrok, T. J., and Cella, F. (1995). "Precerebellar nuclei and red nucleus," in *The Rat Nervous System*, ed G. Paxnos (San Diego: Academic Press), 277–308.

Ruigrok, T. J., and Teune, T. M. (2014). Collateralization of cerebellar output to functionally distinct brainstem areas. A retrograde, non-fluorescent tracing study in the rat. *Front. Syst. Neurosci.* 8:23. doi: 10.3389/fnsys.2014.00023

Saint-Cyr, J. A. (1987). Anatomical oraganization of cortico-mesencephalo-olivary pathways in the cat as demonstratted by axonal transport techniques. *J. Comp. Neurol.* 257, 39–59. doi: 10.1002/cne.902570105

Sánchez-Campusano, R., Gruart, A., Fernández-Mas, R., and Delgado-García, J. M. (2012). An agonist-antagonist cerebellar nuclear system controlling eyelid kinematics during motor learning. *Front. Neuroanat.* 6:8. doi: 10.3389/fnana.2012.00008

Scheibel, A. B. (1977). Sagittal organization of mossy fiber terminal systems in the cerebellum of the rat: a golgi study. *Exp. Neurol.* 57, 1067–1070. doi: 10.1016/0014-4886(77)90130-3

Seone, A., Apps, R., Balbuena, E., Herrero, L., and Liorens, J. (2005). Differential effects of trans-crotononitrile and 3-acetylpyridine on inferior olive integrity and behavioural performance in the rat. *Eur. J. Neurosci.* 22, 880–894. doi: 10.1111/j.1460-9568.2005.04230.x

Serapide, M. F., Panto, M. R., Parenti, A., Zappala, A., and Cicirata, F. (2001). Multiple zonal projections of the basilar pontine nuclei to the cerebellar cortex of the rat. *J. Comp. Neurol.* 430, 471–484. doi: 10.1002/1096-9861(20010219)430:4<471::aid-cne1044>3.0.co;2-g

Simpson, J. I. (2011). Crossing zones in the vestibulocerebellum: a commentary. *Cerebellum* 10, 515–522. doi: 10.1007/s12311-011-0305-y

Simpson, J. L., and Graf, W. (1985). The selection of reference frames by nature and its investigators. *Rev. Oculomot. Res.* 1, 3–16.

Stanton, G. B. (1988). Topographical organization of ascending cerebellar projections from the dentate and interposed nuclei in Macaca mulatta: an antergrade degeneration study. *J. Comp. Neurol.* 190, 699–731. doi: 10.1002/cne.901900406

Stoodley, C. J., and Scmahmann, J. D. (2009). Functional topography in the human cerebellum.: a metaanalysis of neuroimaging studies. *Neuroimage* 44, 489–501. doi: 10.1016/j.neuroimage.2008.08.039

Strick, P. L., Dum, R. P., and Fiez, J. A. (2009). Cerebellum and nonmotor function. *Ann. Rev. Neurosci.* 32, 413–434. doi: 10.1146/annurev.neuro.31.060407.125606

Strominger, N. L., Truscott, T. C., Miller, R. A., and Royce, G. J. (1979). An autoradiographic study of the rubroolivary tract in the rhesus monkey. *J. Comp. Neurol.* 183, 33–45. doi: 10.1002/cne.901830104

Sugihara, I., and Shinoda, Y. (2004). Molecular, topographic and functional organization of the cerebellar cortex: a study with combined aldolase C and olivocerebellar labeling. *J. Neurosci.* 24, 8771–8785. doi: 10.1523/jneurosci.1961-04.2004

Sugihara, I., Wu, H. S., and Shinoda, Y. (2001). The entire trajectories of single olivocerebellar axons in the cerebellar cortex and their contribution to cerebellar compartmentalization. *J. Neurosci.* 21, 7715–7723.

Sultan, F., Augath, A., Hamodeh, S., Murayama, Y., Oeltermann, A., Rauch, A., et al. (2012). Unravelling cerebellar pathways with high temporal precision targeting motor and extensive sensory and parietal networks. *Nat. Commun.* 3:924. doi: 10.1038/ncomms1912

Teune, T. M., van der Burg, J., van der Moer, J., Voogd, J., and Ruigrok, T. J. H. (2000). Topography of cerebellar nuclear projections to the brain stem in the rat. *Prog. Brain Res.* 124, 141–172. doi: 10.1016/s0079-6123(00)24014-4

Tokuno, H., Takada, M., Nambu, A., and Inase, M. (1995). Somatotopical projections from the supplementary motor area to the red nucleus in the macaque monkey. *Exp. Brain Res.* 106, 351–355. doi: 10.1007/BF00241130

Van der Steen, J., Simpson, J. I., and Tan, J. (1994). Fubctional and anatomoic organization of three-dimensional eye movements in rabbit cerebellar flocculus. *J. Neurophysiol.* 72, 31–46.

Van der Want, J. J., Vrensen, G. F., and Voogd, J. (1985). Differences in synaptic size in the superficial and deep layers of the molecular layer of the cerebellar cortex of the cat. An electronmicroscopic and autoradiographic study. *Anat. Embryol. (Berl)* 172, 303–309. doi: 10.1007/bf00318978

van Kan, P. L. E., Hou, J. C., and Gibson, A. R. (1993). Output organization of intermediate cerebellum of the monkey. *J. Neurophysiol.* 69, 57–73.

Voogd, J. (1964). *The Cerebellum of the Cat.* Thesis Leiden. Assen: van Gorcum & Co.

Voogd, J. (1969). "The importance of fiber connections in the comparative anatomy of the mammalian cerebellum," in *Neurobiology of Cerebellar Evolution and Development*, ed R. Llinas (Chicago: AMA), 493–514.

Voogd, J. (2012). A note on the definition and the development of cerebellar Purkinje cell zones. *Cerebellum* 11, 422–425. doi: 10.1007/s12311-012-0367-5

Voogd, J., Pardoe, J., Ruigrok, T. J., and Apps, R. (2003). The distribution of climbing and mossy fiber collateral branches from the copula pyramidis and the paramedian lobule: congruence of climbing fiber cortical zones and the pattern of zebrin banding within the rat cerebellum. *J. Neurosci.* 23, 4645–4656.

Voogd, J., and Ruigrok, T. J. (2004). "Cerebellum and precerebellar nuclei," in *The Human Nervous System*, eds G. Paxinos and J. K. Mai (Amsterdam: Elsevier), 321–392.

Voogd, J., Schraa-Tam, C. K., van der Geest, J. N., and De Zeeuw, C. I. (2012). Visuomotor cerebellum in human and nonhuman primates. *Cerebellum* 11, 392–410. doi: 10.1007/s12311-010-0204-7

Wu, H. S., Sugihara, I., and Shinoda, Y. (1999). Projection patterns of single mossy fibers originating from the lateral reticular nucleus in the rat cerebellar cortex and nuclei. *J. Comp. Neurol.* 411, 97–118. doi: 10.1002/(sici)1096-9861(19990816)411:1<97::aid-cne8>3.0.co;2-o

Xiao, J., Cerminara, N. L., Kotssurovskyy, Y., Aoki, H., Burroughs, A., Wise, K. A., et al. (2014). Systematic regional variaions in Purkinje cell spiking patterns. *PLoS One* 9:e105633. doi: 10.1371/journal.pone.0105633

Xiong, G., Hiramatsu, T., and Nagao, S. (2002). Corticopontocerebellar pathway from the prearcrcuate region to hemispheric lobule VII of the cerebellum: an antegrade and retrograde tracing study in the monkey. *Neurosci. Lett.* 322, 173–176. doi: 10.1016/s0304-3940(02)00108-8

Zhou, H., Lin, Z., Voges, K., Ju, C., Gao, Z., Bosman, L. W. J., et al. (2014). Cerebellar modules operate at different frequencies. *Elife* 3:e02536. doi: 10.7554/eLife.02536

Conflict of Interest Statement: The author declares that the research was conducted in the absence of any commercial or financial relationships that could be construed as a potential conflict of interest.

Received: 28 July 2014; accepted: 12 November 2014; published online: 18 December 2014.

Citation: Voogd J (2014) What we do not know about cerebellar systems neuroscience. Front. Syst. Neurosci. ***8****:227. doi: 10.3389/fnsys.2014.00227*

This article was submitted to the journal Frontiers in Systems Neuroscience.

frontiers in
SYSTEMS NEUROSCIENCE

ORIGINAL RESEARCH ARTICLE
published: 21 February 2014
doi: 10.3389/fnsys.2014.00023

Collateralization of cerebellar output to functionally distinct brainstem areas. A retrograde, non-fluorescent tracing study in the rat

Tom J. H. Ruigrok* and Thea M. Teune†

Department of Neuroscience, Erasmus MC Rotterdam, Rotterdam, Netherlands

Edited by:
Richard Apps, University of Bristol, UK

Reviewed by:
Izumi Sugihara, Tokyo Medical and Dental University, Japan
José M. Delgado-García, University Pablo de Olavide, Seville, Spain

****Correspondence:***
Tom J. H. Ruigrok, Department of Neuroscience, Erasmus MC Rotterdam, PO Box 2040, 3000 DR Rotterdam, Netherlands
e-mail: t.ruigrok@erasmusmc.nl

† Present address:
Thea M. Teune, Laboratory of Pathology, Dordrecht, Netherlands

The organization of the cerebellum is characterized by a number of longitudinally organized connection patterns that consist of matching olivo-cortico-nuclear zones. These entities, referred to as modules, have been suggested to act as functional units. The various parts of the cerebellar nuclei (CN) constitute the output of these modules. We have studied to what extent divergent and convergent patterns in the output of the modules to four, functionally distinct brain areas can be recognized. Two retrograde tracers were injected in various combinations of the following nuclei: the red nucleus (RN), as a main premotor nucleus; the prerubral area, as a main supplier of afferents to the inferior olive (IO); the nucleus reticularis tegmenti pontis (NRTP), as a main source of cerebellar mossy fibers; and the IO, as the source of climbing fibers. For all six potential combinations three cases were examined. All nine cases with combinations that involved the IO did not, or hardly, resulted in double labeled neurons. In contrast, all other combinations resulted in at least 10% and up to 67% of double labeled neurons in cerebellar nuclear areas where both tracers were found. These results show that the cerebellar nuclear neurons that terminate within the studied areas represent basically two intermingled populations of projection cells. One population corresponds to the small nucleo-olivary neurons whereas the other consists of medium- to large-sized neurons which are likely to distribute their axons to several other areas. Despite some consistent differences between the output patterns of individual modules we propose that modular cerebellar output to premotor areas such as the RN provides simultaneous feedback to both the mossy fiber and the climbing fiber system and acts in concert with a designated GABAergic nucleo-olivary circuit. These features seem to form a basic characteristic of cerebellar operation.

Keywords: cerebellar nuclei, red nucleus, inferior olive, nucleus reticularis tegmenti pontis, nucleus of Darkschewitsch

INTRODUCTION

The cerebellum provides its regulatory influence on many aspects of the central nervous system through its cerebellar nuclear output. It has become abundantly clear that cerebellar nuclear efferents terminate, mostly contralaterally, in a great variety of brain stem regions. Ramón y Cajal (1911) already described that, immediately after its decussation in the midbrain, the superior cerebellar peduncle (scp) branches into ascending and descending bundles (also see Voogd and Van Baarsen, 2014). The descending branch is located in the ventromedial tegmentum and mainly terminates in the nucleus reticularis tegmenti pontis (NRTP), the basilar pontine nuclei, the pontine, and medullary reticular formation and in the inferior olive (IO). The ascending branch terminates in many areas such as the red nucleus (RN), periaqueductal gray, the prerubral area (including the area surrounding the fasciculus retroflexus, PreRN), the accessory oculomotor nuclei, the superior colliculus, zona incerta, and the thalamus (Chan-Palay, 1977; Faull, 1978; Faull and Carman, 1978; Teune et al., 2000). Since the cerebellar nuclei (CN) serve as the output stations of the cerebellar modules as defined by the organization of their cortico-nuclear and olivo-cortical connections (Voogd and Bigaré, 1980; Buisseret-Delmas and Angaut, 1993; Apps and Garwicz, 2005; Ruigrok, 2011), it has become a point of interest to investigate in what way this modular organization becomes implemented within the brain stem circuitry. More detailed knowledge on the distribution of information processed by cerebellar modules has become even more pressing since behavioral studies indeed suggest that cerebellar modules may represent functional entities (Godschalk et al., 1994; Van Der Steen et al., 1994; Apps and Garwicz, 2005; Pijpers et al., 2008; Cerminara and Apps, 2011).

Within the CN, at least two types of projection cells can be distinguished. One type consists of relatively small cells that are GABAergic and predominantly, if not exclusively, project to the IO (Chan-Palay, 1977; Bentivoglio and Kuypers, 1982; Buisseret-Delmas and Angaut, 1989; De Zeeuw et al., 1989; Fredette and Mugnaini, 1991; Teune et al., 1995) whereas the other group consists of large- and medium-sized cells that are mostly excitatory (Toyama et al., 1968) although recently a separate glycinergic group of large projection neurons has been distinguished

in the medial cerebellar nucleus (MCN) (Bagnall et al., 2009). Neurons that belong to the population of large projection cells may collateralize to a wide array of target sites as has been shown with fluorescent retrograde double-labeling techniques. In the rat, collateralization has been demonstrated for combinations involving the medullary and pontine reticular formation (or the spinal cord), the thalamus, the superior colliculus, the accessory oculomotor nuclei or the basilar pontine nuclei (Bentivoglio and Kuypers, 1982; Gonzalo-Ruiz and Leichnetz, 1987; Lee et al., 1989). The group of medium- and large-sized relay cells does not appear to terminate within the IO (Bentivoglio and Kuypers, 1982; Lee et al., 1989; Teune et al., 1995). Also, although electrophysiological data, performed in the cat, have suggested otherwise (Ban and Ohno, 1977; McCrea et al., 1978; Tolbert et al., 1978), it seems unlikely that in the rat the nucleo-olivary pathway contributes to the crossed ascending branch of the scp. Indeed, double-labeling experiments with combinations of the RN and IO (Teune et al., 1995) or of thalamus or superior colliculus and the caudal ventral medulla (Bentivoglio and Kuypers, 1982) failed to show double-labeled small neurons in the CN.

In the present study, we make use of small, confined injections of highly selective and permanently visible, retrogradely transported tracers (Ruigrok and Apps, 2007) in order to further investigate the degree of collateralization of individual neurons within the CN. Since, as outlined above, the output of individual CN may reflect functional characteristics, particular interest was paid to the potential divergence of this output to four well-known, but functionally rather different cerebellar target sites. We have selected the RN as an example of a premotor area (Ruigrok, 2004); the IO as the sole source of cerebellar climbing fibers (Desclin, 1974); the NRTP as an important mossy fiber source which also collateralizes to the CN (Mihailoff, 1993; Ruigrok, 2004), and the prerubral area (PreRN), here defined as including the region surrounding the fasciculus retroflexus from which a major projection to the IO originates (De Zeeuw and Ruigrok, 1994; Ruigrok, 2004; Onodera and Hicks, 2009). The results will be discussed in relation to the coupling of the motor output of the cerebellum with recurrent mossy fiber and climbing fiber paths. Differences in collateralization between different parts of the CN will be discussed in relation to the modular organization of the cerebellum (Ruigrok, 2011).

MATERIALS AND METHODS

SURGICAL PROCEDURES AND TRACER APPLICATION

All experiments were performed on purpose-bred male Wistar rats. The experimental procedure fully adhered to EC guidelines and was accorded by a national ethical committee overseeing animal experiments (DEC). A total of 18 rats, weighing 250–300 grams, were anesthetized by an intraperitoneal injection with a cocktail of ketamine (80 mg/kg) and xylazine (5 mg/kg) and were subsequently mounted in a stereotactic device according to Paxinos and Watson (2005). Additional dosages of anesthetics were given when needed.

Access to the cerebellum and lower brain stem was gained by partially removing the squamosal part of the occipital bone after partition of the covering skin and muscles through a midline incision over the skull and neck area. The IO was reached by penetrating the medulla oblongata at obex level dorsally, at an angle of 45° with the horizontal plane. The RN and PreRN were approached through a small hole drilled in the parietal bone directly overlying these areas (between 3.0 and 5.0 mm rostral to the interaural line, laterality: 0.8–1.0 mm). The NRTP was approached stereotactically through the caudal cerebellum (entering between lobule IXb and IXc) at an angle of 34° with the horizontal plane. In this way, the electrode would pass ventrally to the CN, avoiding possible spread of tracer into the CN and/or IO.

All injections were made at the left side of the brainstem using double barrel glass micro pipettes (overall tip diameter: 12–18 μm). One barrel contained the tracer, whereas the other was filled with 4 M NaCl and was connected to standard electrophysiological equipment. In this way, and prior to the actual application of tracers, electrophysiological recordings were made in order to verify the location of the glass electrode tip. The RN and IO both demonstrate a spontaneous and characteristic firing pattern (Gellman et al., 1983; Ruigrok and Voogd, 1995). The location of the NRTP was inferred by identifying the medial lemniscus, which demonstrated increased firing rates in response to tapping or touching the animal's contralateral body, and positioning the electrode tip slightly dorsal to this region.

As retrograde tracers, cholera toxin ß subunit (CTb: 1% w/v in 0.1 M phosphate buffer, pH 7.2; List Biol. Lab. Inc. Campbell, CA) was used in combination with a gold-lectin conjugate, wheat-germ agglutinin coupled to bovine serum albumin and 10 nm gold sol particles (Ruigrok and Apps, 2007). CTb was delivered iontophoretically by means of a 4 μA positive current for 10–15 min., with a 7 s on/off cycle. The gold-lectin injections were delivered using a home-made pressure device and comprised approximately 30 nl for PreRN and RN, 50 nl for the NRTP and up to around 100 nl using several tracks for the IO (Ruigrok and Apps, 2007).

In order to reduce potential inadvertent labeling of fibers of passage (Chen and Aston-Jones, 1995), CTb was preferentially injected into the more distal of the injection sites, whereas gold-lectin, which has not been reported to be taken up by passing fibers (Menetrey, 1985; Llewellyn-Smith et al., 1992; Ruigrok and Apps, 2007) was predominantly selected for injections more proximal to the CN. However, when occasionally tracer injections were reversed this did not appear to influence the resulting labeling (**Table 1**).

After injection, all wounds were sutured and the animals recovered uneventfully and survived for 4 or 5 days during which they did not demonstrate signs of stress and/or discomfort.

PERFUSION AND IMMUNOHISTOCHEMISTRY

Before perfusion, the animals were deeply re-anaesthetized with an overdose of sodium pentobarbital (120 mg/kg i.p.), and transcardially perfusion-fixed by first clearing the cardiovascular system with a rinsing solution (300 ml of a 0.8% NaCl, 0.8% sucrose, 0.4% d-glucose solution in 0.05 M phosphate buffer, PB, pH 7.2, at room temperature: RT), followed by fixative (1000 ml of a freshly prepared solution containing 4% paraformaldehyde, 4% sucrose, 0.1% glutaraldehyde in 0.05 M PB, pH 7.2, at RT).

Brains were extracted, blocked and post-fixed for 4 h. The blocked brains were stored overnight in 10% sucrose in 0.05 M

Table 1 | Numbers of single and double-labeled neurons plotted in 5 equidistant sections of the CN of all studied cases.

Exp. #	Combination		Total # of cells plotted in CN			# of plotted cells in overlapping areas		
	Injected	Tracer	# cells labeled from 1	# cells labeled from 2	# cells labeled from 1 and 2	# cells labeled from 1	# cells labeled from 2	# cells labeled from 1 and 2
	1: IO	**2: RN**						
T45	Gold-lectin	CTb	527	463	2	501	340	2
T42	Gold-lectin	CTb	698	423	0	460	380	0
T39	Gold-lectin	CTb	491	379	1	433	208	1
	1: IO	**2: PreRN**						
T53	CTb	Gold-lectin	474	240	0	336	217	0
T54	CTb	Gold-lectin	503	282	0	338	247	0
T55	Gold-lectin	CTb	827	237	1	584	217	1
	1: IO	**2: NRTP**						
T61	CTb	Gold-lectin	511	293	3	196	187	3
T58	CTb	Gold-lectin	229	161	2	70	99	2
T68	CTb	Gold-lectin	167	513	2	149	213	2
	1: NRTP	**2: RN**						
T56	Gold-lectin	CTb	615	460	225	568	407	225
T60	Gold-lectin	CTb	375	493	78	250	341	78
T64	Gold-lectin	CTb	399	779	180	392	557	180
	1: NRTP	**2: PreRN**						
T63	Gold-lectin	CTb	521	425	126	508	387	126
T65	Gold-lectin	CTb	315	862	140	482	298	140
T69	Gold-lectin	CTb	322	149	33	312	99	33
	1: RN	**2: PreRN**						
T118	Gold-lectin	CTb	967	106	71	679	105	71
R746	Gold-lectin	CTb	543	287	86	495	233	86
R747	Gold-lectin	CTb	582	452	176	582	350	176

The total number (#) of plotted neurons is given as well as the number of labeled neurons that were located in the same (i.e., "overlapping") area.

PB for cryoprotection at 4°C. Next, the brains were gelatin-embedded (10% gelatine, 10% sucrose in distilled water), hardened in 10% formaldehyde with 30% sucrose for 3 h (RT) and stored until sectioning in 30% sucrose in 0.05 M PB at 4°C.

With a freezing microtome, 40 μm transverse sections were cut and serially collected in 0.1 M PB, pH 7.2 in eight glass vials. Free floating sections were processed for CTb immunohistochemistry as follows. First, sections were thoroughly rinsed in TBS+ (0.05 M Tris, 0.5 M NaCl, 0.5% Triton X-100, pH 8.6), and were subsequently incubated for 48 h in the dark at 4°C under constant agitation with anti-CTb (1:15,000 in TBS+, List Lab.). Hereafter, sections were thoroughly rinsed with TBS+, and incubated with biotinylated donkey-anti-goat antibodies (List Biological Lab.; 1: 2000 in TBS+) for 2 h at RT. Then, rinsed sections were incubated with the avidine-biotine complex (ABC Elite Kit, 1:100 in TBS+, Vector Lab., Burlingame, CA) for 2 h (RT). Following a subsequent rinses in 0.05 M Tris-HCl, pH 7.3, sections were reacted with diaminobenzidine (37.5 mg DAB per 150 ml Tris-HCl with 25 μl 30% H_2O_2) for 20–30 min. This reaction was stopped by rinsing the sections in 0.1 M PB (pH 7.2). Finally, the gold-lectin labeling was intensified by a silver-enhancement procedure (Aurion, Wageningen, Netherlands: Ruigrok and Apps, 2007). Sections within a vial were mounted serially, air dried, counterstained with thionine and coverslipped with Permount™ (Fisher Scientific).

ANALYSIS OF SECTIONS

Sections were analyzed with a motorized Olympus BH-2 light microscope equipped with a Lucivid™ miniature camera and a plotting system using Neurolucida™ software (MicroBrightfield, Inc., Colchester, VT). Using this system the resulting CN labeling contralateral to the injection site was plotted indicating every labeled neuron in the CN in a one out of eight series of sections. In this way five representative sections throughout the rostrocaudal length of the CN and separated by 320 micron were analyzed using a 40× objective. The resulting plots were subsequently compiled into a standardized diagram of the flattened, stretched-out CN as based on transverse sections (**Figure 1**). The lateral vestibular nucleus (LVN) was not included in the analysis. Injection sites were indicated on standardized diagrams.

In order to obtain an estimate of the degree of collateralization, the percentage of double-labeled cells was calculated based on the number of labeled cells in an overlapping area. To do this, a contour enveloping the area in which both types of labeled neurons were found was made. Labeled neurons were defined as positioned within an overlapping areas if they were separated by less than 300 micron. the surface of the areas indicating labeling of

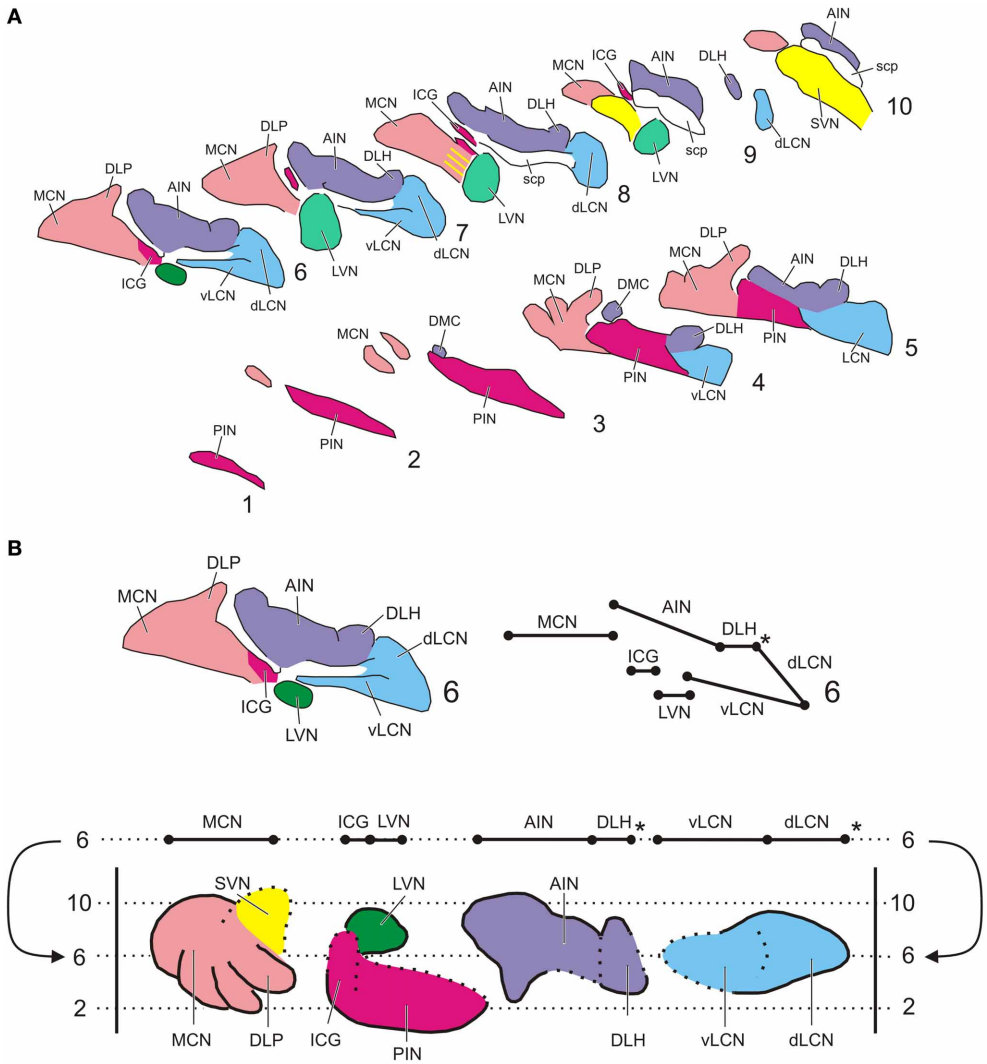

FIGURE 1 | Standardized diagrams of the right hand cerebellar nuclear complex of the rat. (A) Series of transverse sections from caudal (1) to rostral (10) separated by 160 micron (adapted after Ruigrok and Voogd, 2000). Medial is to the left. **(B)** Construction of the standardized diagram of a dorsal view of the separated cerebellar nuclei (adapted after Ruigrok and Voogd, 2000). Upper diagrams show how level 6 of the transverse diagrams is transposed into the bottom diagram. Note that the dorsal and ventral parts of the LCN are unfolded. *Denotes a break in the cellular chain from dorsal LCN to the lateral aspect of the DLH. Abbreviations: AIN, anterior interposed nucleus; dLCN, dorsolateral part of LCN; DLH, dorsolateral hump; DLP, dorsolateral protuberance; DMC, dorsomedial crest; ICG, interstitial cell groups; LCN, lateral cerebellar nucleus; LVN, lateral vestibular nucleus; MCN, medial cerebellar nucleus; PIN, posterior interposed nucleus; scp, superior cerebellar nucleus; SVN, superior vestibular nucleus; vLCN, ventromedial part of LCN.

either type in the flattened CN diagrams was determined as well as the surface of the overlapping area. Subsequently, the number of labeled cells of either type (single or double labeled) was determined (**Table 1**).

Selected sections were photographed with a Leica DMR microscope equipped with a digital camera (Leica DC300) and the photopanel (**Figure 2**) was constructed with CorelDraw™ 11.0 after some correction for brightness and contrast in CorelPhotopaint™ 11.0.

NOMENCLATURE AND DEFINITION OF AREAS

Identification and nomenclature of the subdivisions of the IO and of the CN (**Figure 1**) was based on Ruigrok (2004) and Voogd (2004), respectively. Outlines of the NRTP were based on Mihailoff et al. (1981). The delineation of the RN and adjacent prerubral area were based on descriptions by Reid et al. (1975) and Ruigrok (2004).

RESULTS

GENERAL ASPECTS OF INJECTION SITES AND RESULTING LABELING

The iontophoretic CTb injection sites appeared as globular shaped concentrations of a brownish, fine granular substance, with centrally the darkest coloring and the highest concentration of granules, gradually fading toward the edges but with well outlined borders (**Figure 2A**). Gold-lectin injections consisted of an

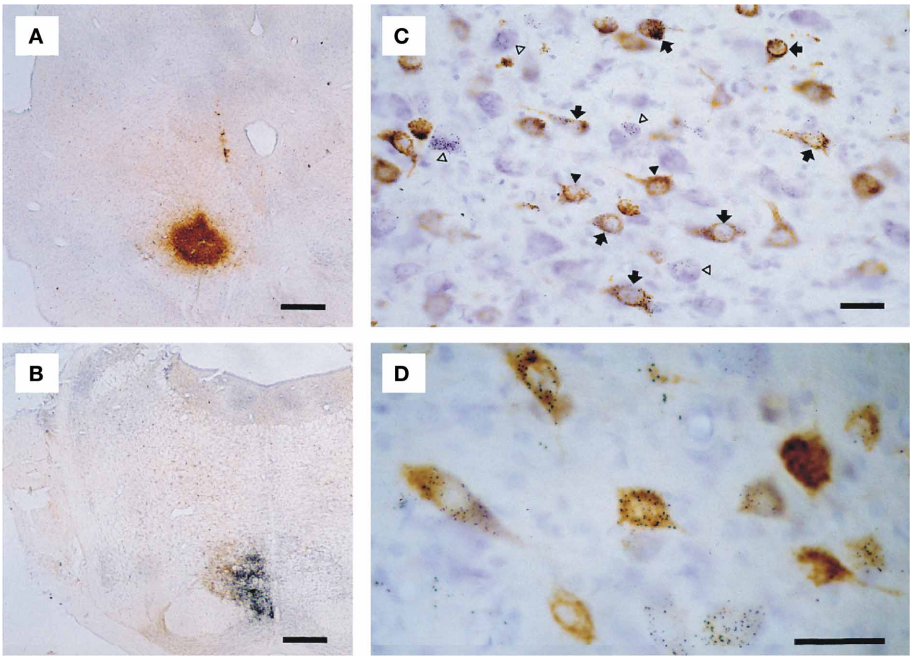

FIGURE 2 | Microphotographs showing examples of double labeling experiment T64. (A) Iontophoretic injection with CTb centered on the RN. **(B)** Pressure injection with gold-lectin injection centered on the ipsilateral NRTP. **(C)** Detail of resultant labeling in the contralateral lateral cerebellar nucleus; neurons only labeled with gold-lectin are indicated by open arrow heads, neurons only labeled with CTb are indicated by black arrow heads, arrows depict neurons that contain both labels. **(D)** Higher magnification of single and double-labeled cells within the anterior interposed nucleus. Scale bars equal 500 μm in **(A,B)** and 25 μm in **(C,D)**.

irregularly shaped, but usually well-outlined aggregate of small black particles (**Figure 2B**).

All injections resulted in labeling of somatic neuronal contours in the CN. CTb labeled neurons were readily identified in thionine counterstained sections by their content of brown granules in the somata and proximal dendrites (**Figures 2C,D**), which frequently gave the soma a solidly brown appearance. Silver-intensified gold-lectin containing neurons were readily identified and discriminated from unlabeled or CTb labeled neurons by their content of small, intensely black particles in the cytoplasm (**Figures 2C,D**). Gold-particles were evenly distributed through the somata and proximal-most parts of dendrites. Double-labeled neurons were identified by the simultaneous occurrence of coarse brown granules and fine black particles in the same neuronal contour (**Figures 2C,D**). No indications were found that the resultant retrograde labeling was biased by the choice of tracer (Koekkoek and Ruigrok, 1995; Ruigrok et al., 1995b; Ruigrok and Apps, 2007).

COLLATERALIZATION OF NUCLEO-BULBAR PROJECTIONS

All injections resulted in labeled neurons that were distributed throughout several of the main CN. Indeed, it would appear to be a rule that projections from a particular CN subnucleus are distributed to at least several of the investigated areas. This would imply that individual neurons located within such an area could collateralize to all these regions, or, when collateralization is absent, that every type of projection stems from a distinct, but intermingled, population of cells within such a CN subnucleus. Details of the distribution of single and double labeled neurons resulting from the six different combinations of injections will be presented below (also see **Table 1**).

Combinations involving the inferior olive

Inferior olive and red nucleus. **Figures 3A,B** shows the injection sites and resultant retrograde labeling in the contralateral CN of case T45. The olivary injection with gold-lectin covered large areas of the principal olive (PO), central part of the medial accessory olive (MAO) and dorsal accessory olive (DAO) and resulted in concomitant labeling within large areas of the lateral cerebellar nucleus (LCN), posterior interposed nucleus (PIN), and anterior interposed nucleus (AIN). Only a few labeled cells were observed in the rostromedial part of the MCN. The CTb injection was centered on the medial aspect of the rostral halve of the RN. Retrogradely labeled cells were mostly confined to the LCN, sparing its ventromedial-most part. More sparsely distributed neurons were located within both interposed nuclei. Large areas of overlap are noted, especially when the labeled areas are indicated in the flattened and stretched-out diagrams of the CN (**Figure 3C**). Within overlapping areas, gold-lectin labeled neurons were completely intermingled with the CTb labeled neurons (also see Teune et al., 1995). However, out of a total of 990 labeled neurons only two double-labeled cells were found (**Table 1**). Obviously, not all retrogradely labeled cells were located in regions were both types of cells are encountered (i.e., in an "overlapping" area). Therefore, in order to obtain a better estimate of the chance that a CN neuron can collateralize to both

injected areas, the percentage of double-labeled cells was calculated based on the number of labeled cells in an overlapping area (see Materials and Methods). Thus, for case T45, the two double-labeled neurons were located in an overlapping area where 501 gold-lectin-labeled neurons and 340 CTb-labeled neurons were found in the analyzed sections. This would indicate that in the overlapping areas (i.e., central PIN, lateral AIN, and rostral LCN) 0.40% of the gold-lectin-labeled neurons were double-labeled and 0.59% of the neurons that were labeled from the RN injection (**Table 1**).

In two additional cases (T39 and T42, for injection sites see **Figure 3A**) overlapping areas were also found in PIN, AIN and in a relatively small area of the LCN (**Figure 3C**). Similar to case T45 virtually no double-labeled cells were encountered (0 out of a total of 1121 and 1 out of 870 labeled neurons in T 42 and T 39, respectively, see also **Table 1**).

Inferior olive and prerubral area. Case T53 was chosen as a typical example of an IO-PreRN injection combination (**Figures 4A,B**). Here, gold-lectin was injected in the prerubral region but also involved the medial part of the parvicellular part of the RN (RNp). CTb had been injected in the central and medial aspects of the inferior olivary complex. Although within the overlapping regions of the CN, i.e., the medial part of the PIN, central part of the AIN and most of the LCN, 336 CTb-labeled and 217 gold-lectin-labeled neurons were counted in the analyzed sections, no double-labeled cells were observed (**Table 1**). A similar picture emerged in two additional cases (**Figures 4A,B**: T54 and T55). Again, despite extensive CN areas where both cell types were intermingled not a single (T54) and only one (T55) double-labeled neuron was found (**Table 1**, **Figure 9**).

Inferior olive and nucleus reticularis tegmenti pontis. Three examples of cases with injections in the IO and NRTP are shown in **Figure 5**. Case T61 received a gold-lectin injection in the medial half of the NRTP and two iontophoretic CTb injections were centered on the central MAO and DAO, respectively, but also involved parts of the PO. CN regions that contained both types of retrogradely labeled neurons were located in the lateral part of the AIN and within the ventrolateral part of the LCN. These overlapping regions contained 187 gold-lectin and 196 CTb labeled neurons. Three of these neurons, which were all small-sized, contained both labels and were located in the caudal half of the dorsolateral hump (DLH: 2 cells) and lateral AIN (1 cell). In case T58 (CTb injections in IO centered on lateral bend in PO and involving adjacent DAO and an additional injection centered on central MAO, and gold-lectin centered on the rostroventral aspect of the medial NRTP and involving the dorsomedial part of the basilar pontine nuclei, **Figure 5A**), the overlapping area was mainly restricted to the LCN where 2 out of 99 gold-lectin and 70 CTb-labeled neurons were double-labeled. The CN of case T68 harbored only two double labeled neurons (out of a total plotted number of 680 labeled neurons), which were both located in the rostroventral aspect of the PIN, directly bordering the roof of the 4th ventricle (**Figures 5**, **9** and **Table 1**).

Remaining combinations that involve the nucleus reticularis tegmenti pontis

Nucleus reticularis tegmenti pontis and the red nucleus. **Figures 6A,B** displays the results of case T56 with a CTb injection that was centered on the RNp but also incorporated part of the magnocellular division of the RN (RNm), and a gold-lectin injection in the NRTP that only just encroached upon the dorsal part of the basilar pontine nuclei. CN regions where both types of retrogradely labeled cells were found encompassed most of the LCN and AIN, a small strip of cells in the rostroventral PIN and to some degree within the rostralateral part of the MCN. Double-labeled neurons were present in all areas of the CN where the two populations overlapped. Of 407 CTb-labeled cells that were located in these areas, 225 (55%) were also labeled with gold-lectin. The plotted number of cells projecting to the NRTP (gold-lectin labeled) in these overlapping areas was 568, implying that approximately 40% of these neurons collateralize to the RN. Two additional cases, T60 and T64, had CTb injections that centered on most of the RNm and RNp and gold-lectin injections into the medial NRTP (**Figures 2A,D**, **6A,C**). As in T56, many double-labeled neurons were encountered in the LCN, lateral half of the AIN, and in the rostral part of the interstitial cell groups (ICG) and rostroventral part of the PIN (also see **Figure 9** and **Table 1**).

Nucleus reticularis tegmenti pontis and the prerubral area. T63 serves as a typical example of a case with a combination of injections in the NRTP (with gold-lectin) and in the prerubral area (**Figures 7A,B**). Gold-lectin labeling in the CN, as in the other cases where the NRTP was injected, was found in many areas but was essentially absent in the dorsomedial MCN and within the PIN. CTb-labeling was prominent within the LCN and PIN, whereas more scattered cells were encountered in the AIN/DLH and the caudal MCN. Thus, most of the LCN, the lateral AIN/DLH, caudal MCN and the rostroventral PIN/rostral ICG constitute regions where both cell types were intermingled. Indeed, in all these areas double-labeled cells were encountered, contributing to about 25% of the number of gold-lectin labeled cells (projecting to the NRTP) and to 30% of the CTb labeled cells (**Table 1**, **Figure 9**). Basically similar results were obtained in two additional cases (cases T65 and T69, see **Figures 7A,C**). Note that in all cases the number of double-labeled cells appears highest in the LCN.

Combination of red nucleus and prerubral area

In this combination gold-lectin injections were made that were centered on the RN while the CTb injections were centered on the PreRN. Care was taken that in these selected cases the injection sites were not overlapping. The three selected cases are presented in **Figure 8**. The PreRN injection of case T118 did not incorporate the confines of the RNp (**Figure 8A**) and resulted in many CTb-labeled neurons in the rostrodorsal LCN, medial AIN, and, more sparsely, in the rostral PIN. Neurons labeled from a rather large gold-lectin injection into the RN were observed throughout most of the cerebellar nuclear complex except the rostral

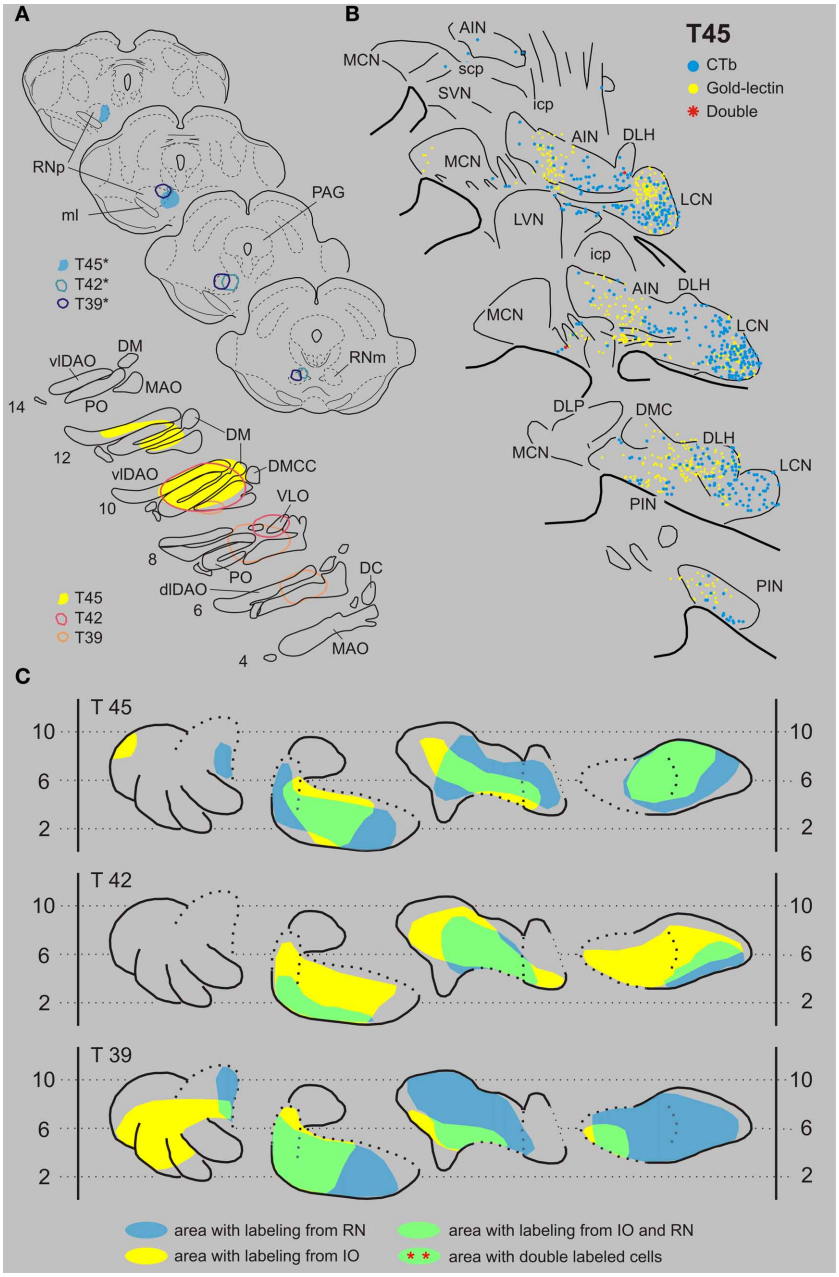

FIGURE 3 | Diagrams depicting results of the combination IO and RN. **(A)** Injection sites of all three analyzed cases. Upper left hand panels show the injection sites within transverse diagrams of the midbrain. Bottom panels show the related injection sites as placed in the left inferior olivary complex, depicted in standardized diagrams (adapted after Ruigrok and Voogd, 2000). In this combination all CTb injection sites (case number indicated with*) were made in the RN, while gold-lectin was injected in the IO. **(B)** Resultant plots of 5 equidistant (320 micron) sections (from caudal, bottom, to rostral, top) showing labeled neurons within the contralateral CN of case T45. Every symbol indicates a single labeled neuron. **(C)** Single and double-labeling of case T45 as well as from the other two cases (T42 and T39) indicated in standardized diagrams shown in **Figure 1B**. Areas containing retrograde labeling from the RN are indicated in blue, whereas labeling from the IO are indicated in yellow. Areas containing cells with either label are indicated in green. However, in all cases virtually no double labeled neurons were encountered (**Table 1**). Abbreviations: AIN, anterior interposed nucleus; DC, dorsal cap; dfDAO, dorsal fold of dorsal accessory olive; dLCN, dorsolateral part of LCN; DLH, dorsolateral hump; DLP, dorsolateral protuberance; DM, dorsomedial group; DMC, dorsomedial crest; DMCC, dorsomedial cell column; ICG, interstitial cell groups; icp, inferior cerebellar peduncle; LCN, lateral cerebellar nucleus; LVN, lateral vestibular nucleus; MAO, medial accessory olive; MCN, medial cerebellar nucleus; ml, medial lemniscus; PAG, periaqueductal gray; PIN, posterior interposed nucleus; PO, principal olive; RN, red nucleus; RNm, magnocellular red nucleus; RNp, parvicellular red nucleus; scp, superior cerebellar nucleus; SVN, superior vestibular nucleus; vLCN, ventromedial part of LCN; vlDAO, ventral fold of dorsal accessory olive; VLO, ventrolateral outgrowth.

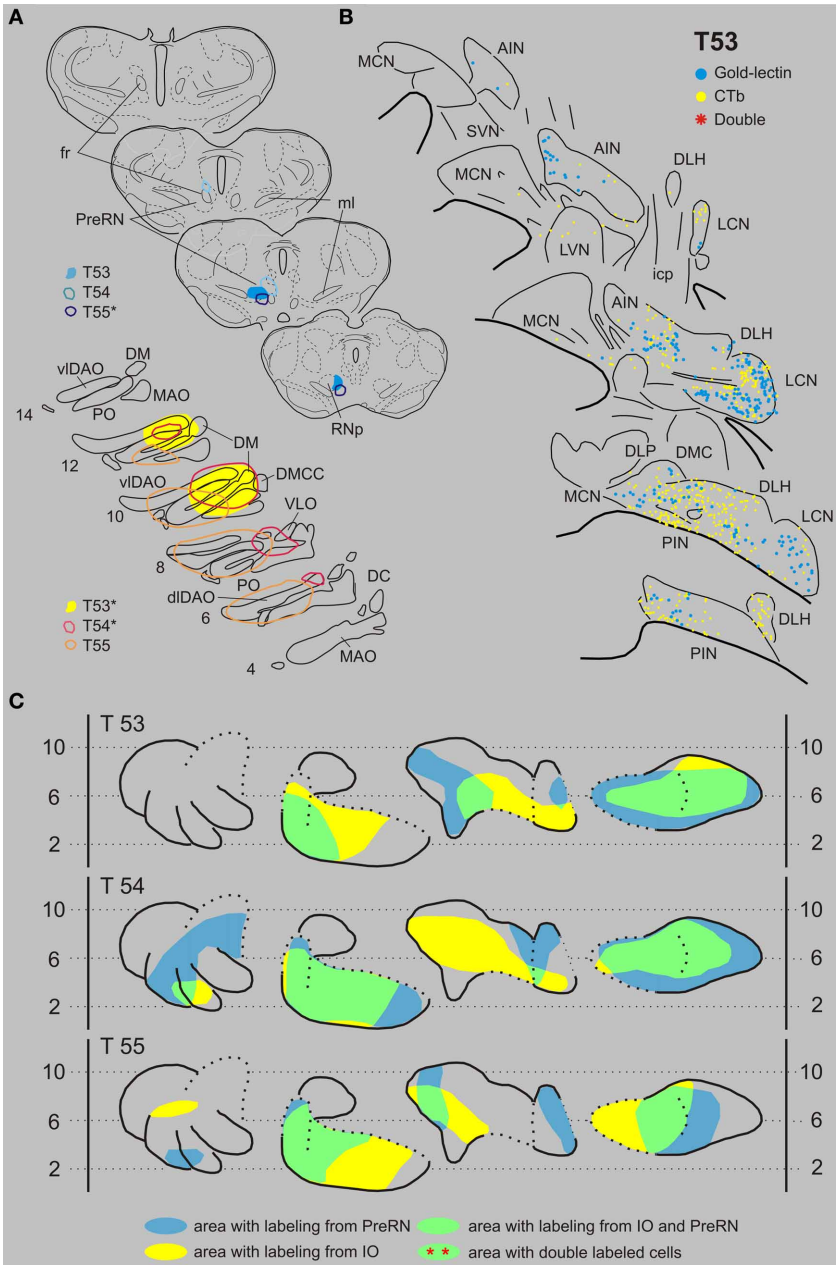

FIGURE 4 | Diagrams depicting results of the combination IO and the PreRN. (A) Injection sites of all three analyzed cases. Upper left hand panels show the injection sites within transverse diagrams of the mesodiencephalon. Bottom panels show the related injections sites in the IO. CTb injections (case number indicated with*) were made in the IO in cases T53 and T54, but in the PreRN in case T55. **(B)** Plots of 5 equidistant (320 micron) sections showing labeled neurons within the contralateral CN of case T53. **(C)** Overview of the distribution of retrogradely labeled neurons of case T53 and of the two additional cases (T54 and T55) in standardized diagrams of the CN. Areas containing labeled neurons from the PreRN and IO are indicated in blue and yellow, respectively. In all cases virtually no double-labeled neurons were encountered (**Table 1**). Abbreviations: PreRN, prerubral area; fr, fasciculus retroflexus; SN, substantia nigra. Conventions and other abbreviations as in **Figure 3**.

MCN and ventromedial LCN (**Figures 8B,C**). In all overlapping areas, i.e., dorsal LCN, medial AIN en rostral PIN, double-labeled neurons were encountered, amounting to about 10% of the gold-labeled cells but to almost 70% of the CTb labeled neurons (**Figures 8**, **9**, **Table 1**). In two additional cases, the PreRN injections were centered just between the medial lemniscus and the retroflex bundle in case R746, and slightly more dorsomedially in case R747 (**Figure 8A**). The gold-lectin injections were both centered on the caudal aspect of the RNm. In both cases overlapping areas and many double-labeled neurons were observed in the medial halves of the AIN and PIN/ICG and, more sparsely, in the LCN (**Figures 8**, **9**, **Table 1**).

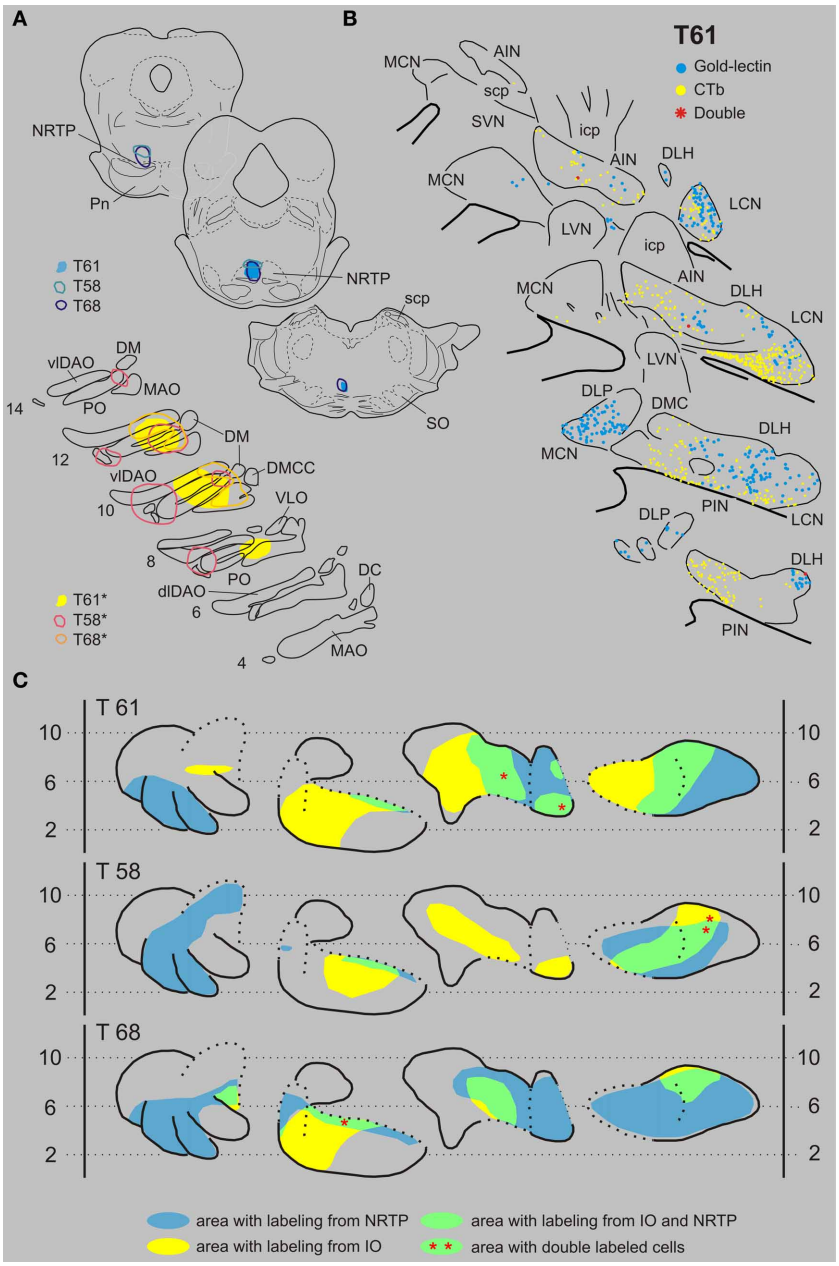

FIGURE 5 | Diagrams depicting results of the combination IO and the NRTP. (A) Injection sites of all three analyzed cases. Upper left hand panels show the injection sites within transverse diagrams of the pontine region. Bottom panels show the related injections sites in the IO. CTb injections (case number indicated with*) were made in the IO of all three cases. **(B)** Plots of 5 equidistant (320 micron) sections showing labeled neurons within the contralateral CN of case T61. **(C)** Overview of the distribution of retrogradely labeled neurons of case T61 and of the two additional cases (T58 and T68) in standardized diagrams of the CN. Areas containing labeled neurons from the NRTP and IO are indicated in blue and yellow, respectively. Only a few double-labeled neurons were encountered (**Table 1**). Abbreviations: NRTP, nucleus reticularis tegmenti pontis; Pn, basilar pontine nuclei; SO, superior olivary complex. Conventions and other abbreviations as in **Figure 3**.

DISCUSSION

OBJECTIVE OF THIS STUDY

This study was prompted by mounting evidence that the basis for cerebellar functioning may be found in its modular organization (Voogd and Bigaré, 1980; Apps and Garwicz, 2005; Apps and Hawkes, 2009; Ruigrok, 2011). As such, the distribution of the output of these modules by way of the cerebellar or vestibular target nuclei became a point of interest (Teune et al., 2000). In addition, it is evident that further identification of the level of collateralization of individual neurons would be necessary in order to evaluate the impact of cerebellar output. Here, we have selected four areas in the brainstem, which are known to receive

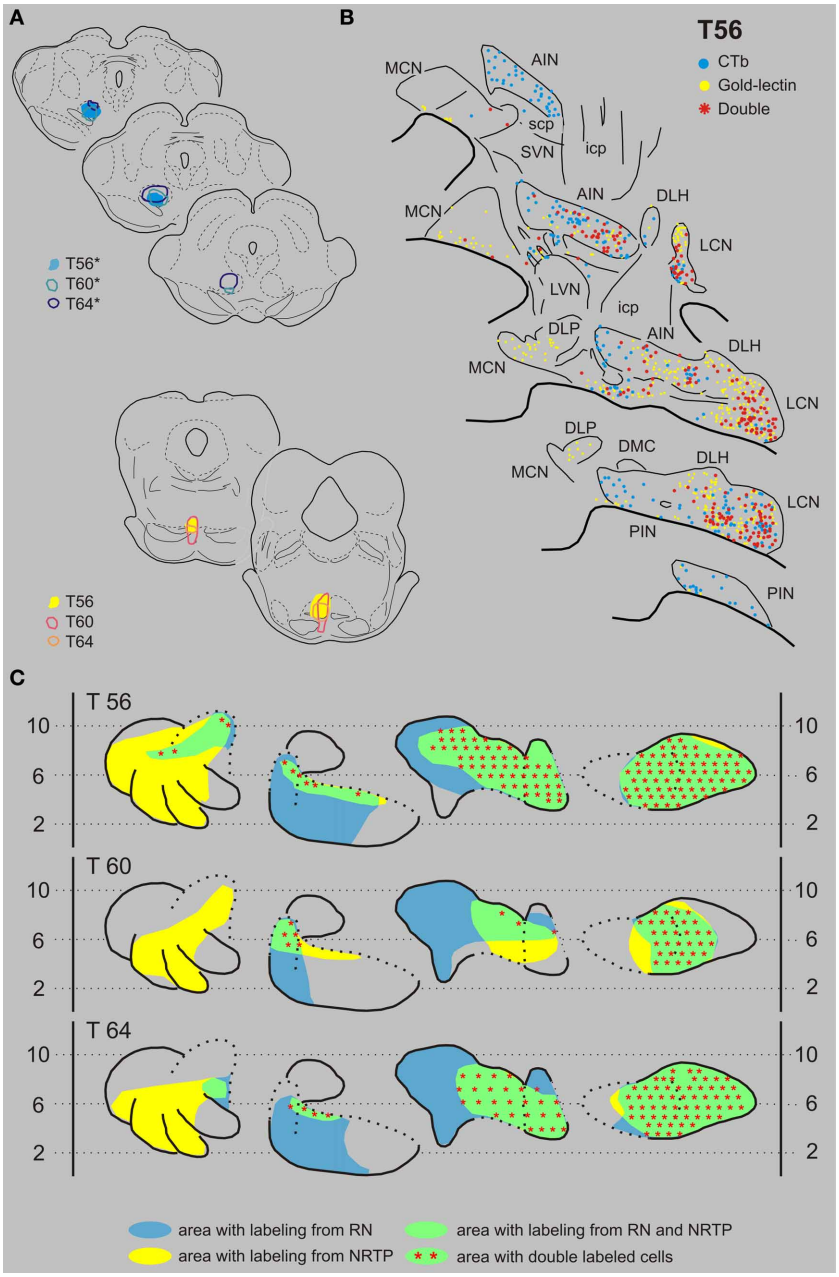

FIGURE 6 | Diagrams depicting results of the combination NRTP and the RN. (A) Injection sites of all three analyzed cases. Upper left hand panels show the injection sites within transverse diagrams of the midbrain. Bottom panels show the related injections sites in the NRTP. CTb injections (case number indicated with*) were made in the RN of all three cases. **(B)** Plots of 5 equidistant (320 micron) sections showing labeled neurons within the contralateral CN of case T56. **(C)** Overview of the distribution of retrogradely labeled neurons of case T56 and of the two additional cases (T60 and T64) in standardized diagrams of the CN. Areas containing labeled neurons from the RN and NRTP are indicated in blue and yellow, respectively. Note that all overlapping areas (green) contain double labeled neurons (red symbols). Conventions and abbreviations as in **Figures 3–5**.

cerebellar input but, as based on their own output characteristics, are very different in their function. The RN was chosen as a premotor nucleus since most of its neurons will enter the rubrospinal (or rubrobulbar) tract (Ruigrok, 2013) and because it is a compact and well delineated area. Other CN target areas with a premotor function that could have been selected would be e.g., the "motor" thalamus, the medial reticular formation, or the superior colliculus (Ruigrok, 2013). Many of the remaining projections appear to enter either directly or indirectly the cerebellar circuitry. Cerebellar projections to the NRTP but also to the basilar pontine nuclei (Mihailoff et al., 1989; Ruigrok, 2004), will influence cerebellar mossy fiber activity, whereas the

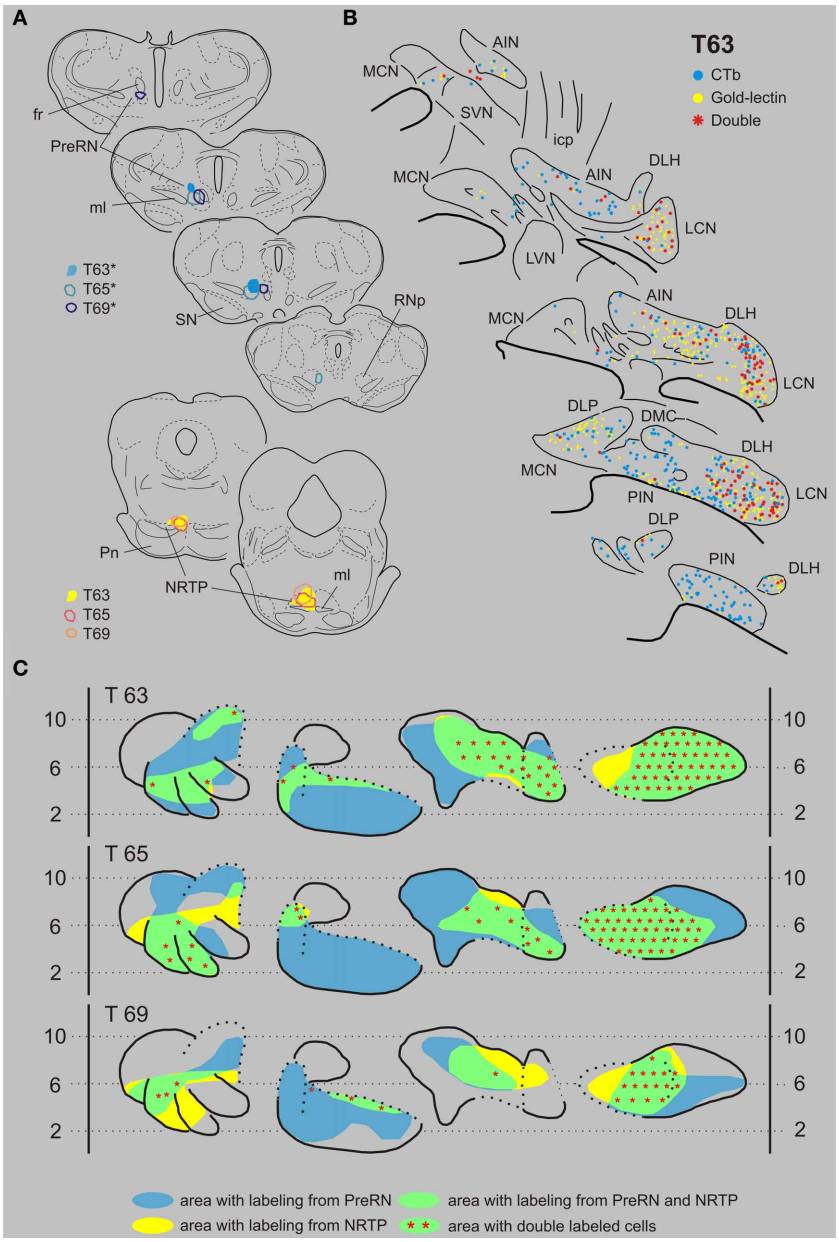

FIGURE 7 | Diagrams depicting results of the combination NRTP and the PreRN. (A) Injection sites of all three analyzed cases. Upper left hand panels show the injection sites within transverse diagrams of the mesodiencephalon. Bottom panels show the related injections sites in the NRTP. CTb injections (case number indicated with*) were made in the PreRN of all three cases. **(B)** Plots of 5 equidistant (320 micron) sections showing labeled neurons within the contralateral CN of case T63. **(C)** Overview of the distribution of retrogradely labeled neurons of case T63 and of the two additional cases (T65 and T69) in standardized diagrams of the CN. Areas containing labeled neurons from the PreRN and NRTP are indicated in blue and yellow, respectively. Note that all overlapping areas (green) contain double labeled neurons (red symbols). Conventions and abbreviations as in **Figures 3–5**.

source of climbing fibers, the IO, also receives a direct and prominent cerebellar nuclear projection. However, the IO is also heavily afferented by areas located at the mesodiencephalic junction such as the nucleus of Darkschewitsch, the prerubral area, the accessory oculomotor nucleus and the interstitial nucleus of the medial longitudinal fascicle (for review see Ruigrok, 2004). These areas are known to receive cerebellar input (Berretta et al., 1993; De Zeeuw and Ruigrok, 1994; Ruigrok and Voogd, 1995). Indeed, stimulation of the brachium conjunctivum in cat can result in disynaptic activation of olivary cells (Ruigrok and Voogd, 1995; Bazzigaluppi et al., 2012). Hence, as an excitatory pre-olivary area, the prerubral area was included in our study on the degree of convergence and divergence of cerebellar nuclear projections.

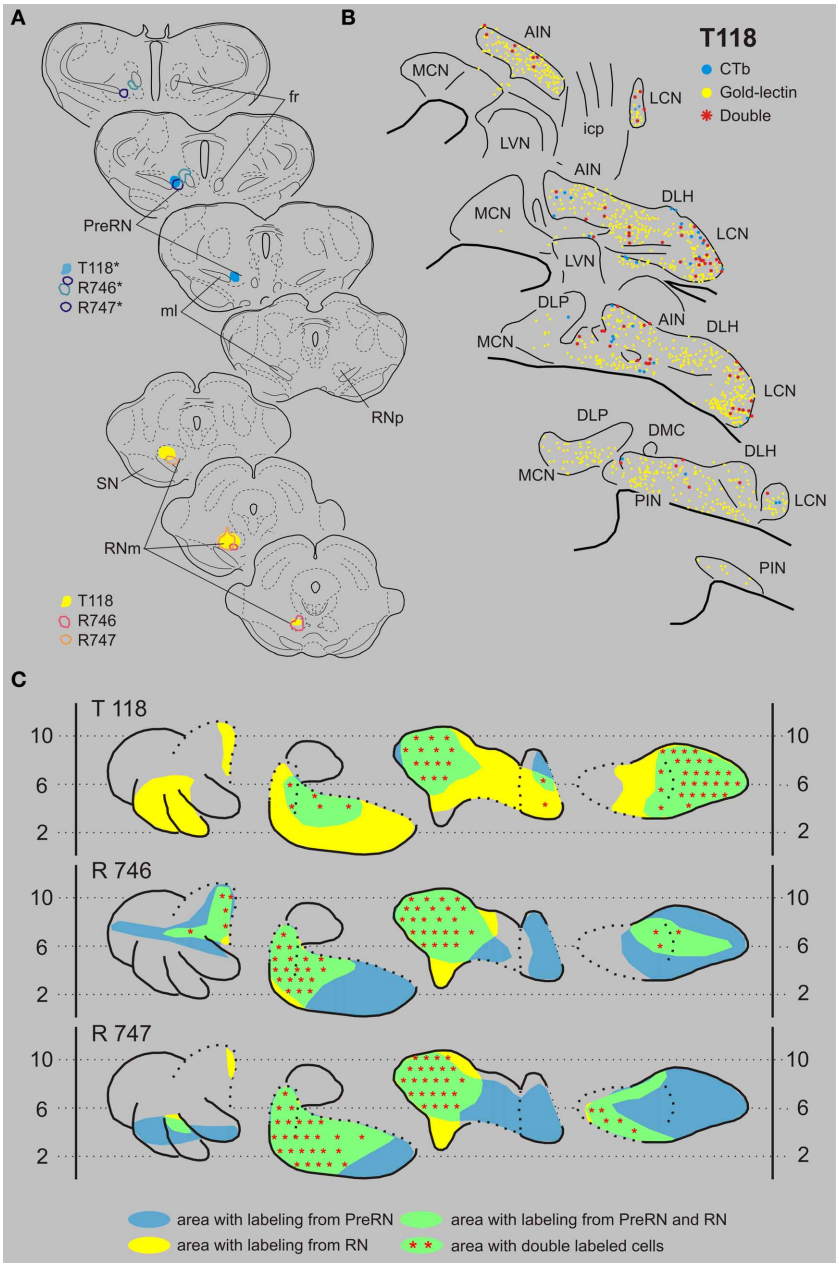

FIGURE 8 | Diagrams depicting results of the combination RN and the PreRN. (A) Injection sites of all three analyzed cases. Upper left hand panels show the injection sites within transverse diagrams of the mesodiencephalon. Bottom panels show the related injections sites in the RN. CTb injections (case number indicated with*) were made in the PreRN of all three cases. **(B)** Plots of 5 equidistant (320 micron) sections showing labeled neurons within the contralateral CN of case T118. **(C)** Overview of the distribution of retrogradely labeled neurons of case T118 and of the two additional cases (R746 and R747) in standardized diagrams of the CN. Areas containing labeled neurons from the RN and PreRN are indicated in blue and yellow, respectively. Note that all overlapping areas (green) contain double labeled neurons (red symbols). Conventions and abbreviations as in **Figures 3–5**.

The results show that cerebellar nuclear neurons collateralize extensively to the NRTP, innervated by the crossed descending branch of the scp, and to the RN and prerubral area (PreRN), both provided by its crossed ascending branch. Moreover, a large proportion of the CN neurons projecting to RN also have terminations in the prerubral area. Neurons that provide an input to the IO, however, do not collateralize to these areas.

GENERAL ASPECTS OF CN PROJECTIONS TO IO, NRTP, RN, AND PRERUBRAL AREA

Inferior olive

Nucleo-olivary neurons in general can be distinguished from other cerebellar nuclear relay neurons by their size and immunoreactive characteristics. They are small-sized, spindle shaped neurons and contain GABA as their main

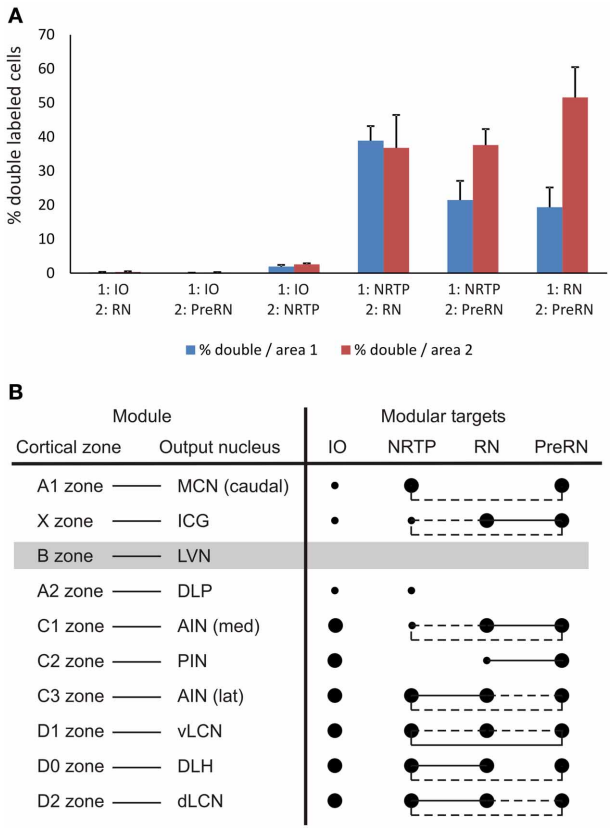

FIGURE 9 | (A) Diagram depicting the average percentage (+SEM) of double-labeled neurons found in overlapping areas for all six combinations, based on the data of **Table 1**. Blue bars refer to the percentage of double labeled cells that project to the first mentioned area of the injection combination but containing both labels. Red bars refer to the percentage of double-labeled cells that project to the other injection site. **(B)** Overview of projection and collateralization patterns from different parts of the CN to the four investigated brainstem areas and related to the modular organization of the rat cerebellum. Filled large and small circles indicate major and minor projections, respectively, as noted between the listed CN areas and the investigated brainstem areas. Circles linked by pulled or hatched lines indicate that many or some double-labeled neurons, respectively, were encountered in the part of the CN of the same row. The lateral vestibular nucleus (LVN), output nucleus of the B zone, was not specifically studied in the present study (gray bar).

neurotransmitter (Chan-Palay, 1977; De Zeeuw et al., 1989; Fredette and Mugnaini, 1991). Since virtually all injections were made in the center of the IO complex (in order to maximize the amount of retrograde labeled cells without risk of tracer spillage to extraolivary regions), not much information is available on the results of injections into the caudal- and rostral-most aspects of the olivary complex. Nevertheless, the pattern of retrograde labeling following these injections was completely compatible with a detailed report by Ruigrok and Voogd (1990), which was based on anterograde tracing studies. In brief, injection sites involving the PO resulted in labeling in the LCN. Labeled neurons in the PIN were found after an injection involving the rostral MAO; the AIN contained labeled cells when the injection incorporated the DAO (excluding its dorsal fold). Injections involving the dorsomedial group resulted in labeling in the DLH. The organization of the nucleo-olivary projections appears to be neatly reciprocated by a matching olivonuclear projection by the climbing fiber collaterals (Ruigrok, 1997; Ruigrok and Voogd, 2000; Sugihara and Shinoda, 2007).

Nucleus reticularis tegmenti pontis

In all cases, most of the retrogradely labeled neurons were observed in the LCN. In agreement with an anterograde tracing study by Angaut et al. (1985) we noted that injections that were centered on the caudal part of the NRTP tended to result in labeling of neurons in the rostrodorsal part of the LCN, whereas labeling in caudomedial LCN resulted from more rostrally placed injections. Within the interposed nuclei most labeling was observed within the DLH and lateral part of the AIN. Virtually no projections to the NRTP originate from the PIN as was already noted by Torigoe et al. (1986). In our material, however, there was some, but consistent, retrograde labeling of neurons located directly dorsal to the roof of the 4th ventricle, a transition area that is continuous with labeling in the rostral part of the ICG located between the medial part of the AIN and the MCN.

The projections from the MCN onto the NRTP have been described as relatively sparse and to terminate mainly in a dorsomedial column throughout the NRTP (Cicirata et al., 1982; Watt and Mihailoff, 1983). In our retrograde study we have noted that the NRTP injections, which all involved the medial part of the NRTP, resulted in labeled neurons that were usually confined to the caudal pole of the MCN, but sometimes included the base of the DLP and the rostrolateral MCN.

Red nucleus

The organization of cerebellar nuclear projections to the RN in the rat has been investigated using anterograde and retrograde tracing techniques (for review see Ruigrok, 2004). Basically, the results presented here are in agreement with earlier studies. The medial part of the AIN projects to the ventrolateral RNm, the lateral AIN projects to the dorsomedial RNm and the medial part of the PIN contains labeled neurons when the medial border of the RN was included in the injection site. Although our injections that were centered on the RNp never resulted in exclusive labeling of the LCN, we concur with other authors that most cerebellar terminals to this part of the RN originate from the LCN (Flumerfelt, 1978; Angaut and Cicirata, 1988). The MCN is usually devoid of labeling with exception of some neurons in the rostrolateral MCN. In some cases (e.g., T118, **Figure 8**) additional labeling within the MCN may have been caused by inadvertent spread of the tracer to overlying accessory oculomotor areas (Gonzalo-Ruiz and Leichnetz, 1987).

When the injection extended into the area directly lateral to the RNm (pararubral area: Paxinos and Watson, 2005), retrograde labeling involved a small area in the caudal part of the ventromedial LCN (Ruigrok and Cella, 1995; Teune et al., 2000). It is not known to what extent this pararubral region should be considered as a premotor or a preolivary region (Newman, 1985).

Prerubral area

The medial part of the mesodiencephalic junction has received attention as an area from which a prominent projection to the IO originates (for review see Ruigrok, 2004). This region includes the prerubral field (medial to the medial lemniscus and dorsal and lateral to the fasciculus retroflexus), the medial accessory oculomotor nucleus, the rostral part of the nucleus of Darkschewitsch, the subparafascicular nucleus and the rostral interstitial nucleus of the medial longitudinal fascicle. Here, this area is collectively referred to as prerubral area (PreRN). The rat PreRN, rather than the RNp, has been considered as a homolog of the primate parvicellular RN (Ruigrok, 2004; Onodera and Hicks, 2009).

Cerebellar projections to the mesodiencephalic junction have been mainly investigated in cat and appear to originate predominantly from the LCN and PIN, but projections to the nucleus of Darkschewitsch have also been shown to arise from AIN and MCN (Kawamura et al., 1982; Sugimoto et al., 1982; Onodera and Hicks, 1995; Teune et al., 2000). In accordance with these studies, injection with retrograde tracers in the PreRN mostly result in retrograde labeling in the LCN and PIN, but also involves the AIN including the DLH. LCN labeling included its ventromedial (parvicellular) part. In the PIN, labeling incorporated the ICG but also extended into the lateral and caudal pole of the nucleus. In some cases labeled cells were present in the rostrolateral MCN as well as in the caudal pole of this nucleus. We propose, as indeed demonstrated in the cat, that neurons in the PreRN mediate a major disynaptic excitatory pathway between the CN and the IO (De Zeeuw and Ruigrok, 1994; Ruigrok and Voogd, 1995).

COLLATERALIZATION OF CEREBELLAR NUCLEAR OUTPUT

Our experiments are in agreement with and extend the generally held concept that the CN harbor at least two different populations of projection neurons. One group, the nucleo-olivary neurons, consists of small-sized neurons which are distributed throughout the CN and reportedly all contain GABA as neurotransmitter (Angaut and Sotelo, 1989; De Zeeuw et al., 1989; Fredette and Mugnaini, 1991). The question remains, however, to what extent the nucleo-olivary neurons may collateralize to other cerebellar projection areas such as the bulbar reticular formation (Buisseret-Delmas et al., 1989), the thalamus or the basilar pontine nuclei and/or NRTP (Border et al., 1986; Aas and Brodal, 1990; Verveer et al., 1997).

The second group of projection neurons consists of medium- to large-sized cells which may show a rather extensive collateralization to these latter areas, while observing regional differences in their projection pattern. These neurons, apart from a group of glycinergic neurons in the rostral MCN (Bagnall et al., 2009), most likely, are all excitatory (Giuffrida et al., 1993; De Zeeuw and Ruigrok, 1994; Uusisaari and Knopfel, 2011). Below, we will discuss our observations in relation to these two main populations of cerebellar projection neurons.

Nucleo-olivary neurons

The collateralization of nucleo-olivary neurons to other brainstem regions has been investigated with both anatomical and electrophysiological techniques. The fluorescent double-labeling studies by Bentivoglio and Kuypers (1982), investigating cerebellar nuclear collateralization to the cervical cord, the caudal medulla, the mesencephalon (superior colliculus and RN) and the thalamus, were already suggestive of a non-collateralizing projection from small-sized neurons to the IO. However, definite conclusions were hampered by the large injection sites that covered sizable parts of the caudal medulla. In the cat, and in line with an unique nucleo-olivary projection, Legendre and Courville (1987) and Bharos et al. (1981) were unable to find nucleo-olivary neurons that project to the thalamus. Lee et al. (1989), on the other hand, found evidence of a small, collateral projection of nucleo-olivary neurons to the contralateral basilar pontine nuclei in the rat. This would be in line with observations in both the rat and the cat of a cerebellar derived GABAergic projection to the basilar pontine nuclei and including NRTP (Border et al., 1986; Aas and Brodal, 1990). Electrophysiologically obtained data in the rat (Berretta et al., 1991) appears to collaborate this notion but contrasts a similar study in the cat where only excitatory monosynaptic responses could be elicited in NRTP neurons after stimulation of the LCN (Kitai et al., 1976). Our own data indicate that only a very small portion of the nucleo-olivary fibers may collateralize to the NRTP. At best only 2 out of 70 labeled neurons in an overlapping region (case T 58) was double-labeled in a combination involving the NRTP and IO. It should be realized, however, that, although specifically for this reason gold-lectin was used as the injected tracer, the interpretation of a potential collateralization of nucleo-olivary fibers to the NRTP may be hampered by the risk of false positive double-labeling which may result from inadvertent uptake by damaged axons of the crossed descending limb of the scp that runs directly dorsal to and through the NRPT and which contains most of the nucleo-olivary fibers (Legendre and Courville, 1987; Ruigrok and Voogd, 1990). Indeed in the cat, an ultrastructural study failed to establish a GABAergic projection originating from the CN to the NRTP in the cat (Verveer et al., 1997). Nevertheless, especially since Lee et al. (1989) made use of a ventral approach to the BPN, thus minimizing the risk of false positive labeling, it would seem possible that a very small number of nucleo-olivary neurons truly may have collaterals to the basilar pontine nuclei and/or NRTP.

In the cat, several studies, mostly based on electrophysiological techniques have suggested that at least part of the nucleo-olivary neurons possess ascending collaterals to the thalamus (Ban and Ohno, 1977; McCrea et al., 1978; Tolbert et al., 1978). This conclusion was mainly based on electrophysiological studies of recordings in the interpositus nuclei and employing antidromic stimulation and collision experiments from thalamus and IO. However, it should be noted that some PIN neurons, especially located in its medial part and within the ICG, project to the contralateral upper cervical cord and course just dorsal to the IO (Bharos et al., 1981; Buisseret-Delmas et al., 1998; Teune et al., 2000). In addition, a major projection from the LCN to the contralateral ventromedial medulla may, in addition, provide projections to the thalamus (Tolbert et al., 1980; Bharos et al., 1981; Teune et al., 2000).

In conclusion, despite the possibility that a very small proportion of the nucleo-olivary neurons may collateralize to the NRTP, we propose that this population of, GABAergic, cerebellar nuclear projection neurons is unique in its projection to the IO. Yet, a

definite evaluation of this assertion has to await cell type specific tracing or reconstruction of individual axons.

Other nucleo-bulbar projection neurons

Several anatomical studies, including the present data, have shown that many of the medium- and large-sized, excitatory projection cells of the CN project to two or more different brain stem areas (Bentivoglio and Kuypers, 1982; Bentivoglio and Molinari, 1986; Gonzalo-Ruiz and Leichnetz, 1987; Lee et al., 1989). CN axons may bifurctate and follow both the crossed descending limb of the scp toward the caudal medulla and upper cervical cord as well as the crossed ascending limb toward the superior colliculus and thalamus (Bentivoglio and Kuypers, 1982). In addition, individual neurons of the lateral AIN and DLH can both enter the crossed ascending limb but also send one or more collaterals to the ipsilateral bulbar reticular formation (Bentivoglio and Molinari, 1986). Collateralization of many neurons located in the LCN and of a few in the AIN to the basilar pontine nuclei and thalamus were demonstrated by Lee et al. (1989). The same authors also describe a collateral projection to the basilar pontine nuclei and the superior colliculus arising from several LCN neurons. Finally, Gonzalo-Ruiz and Leichnetz (1987) observed double-labeled neurons predominantly in the MCN but also in the LCN after double fluorescent tracer injections in combinations of several areas involved in eye movement control such as the superior colliculus, the paraoculomotor region, and the medial pontine reticular formation.

In our study, we found that all CN regions that contained neurons that project to the NRTP as well as regions that project to either RN or PreRN also contain neurons that were double labeled. However, double-labeled neurons were rather sparse within the medial AIN and within the meager overlapping areas within the PIN. In addition, our data indicate that many CN neurons that project to the RN also provide terminals to the PreRN. The occurrence of double-labeled neurons varied between experiments but, in some instances, could amount to more than 50% of the total number of labeled cells in an area where both types of labeling were found (**Table 1**). For this reason, it seems quite probable that some neurons, especially in the LCN, will project to more than two of these areas. This would be in line with the observation by Shinoda et al. (1988) who noted that cerebellar nuclear axons with terminals within the RN all continued toward the thalamus. It is remarkable, however, that cells that project to the PreRN are more likely to be double labeled from the RN than vice versa. This would imply that many neurons that project to the RN (and/or directly surrounding area such as the pararubral area) will not consider the PreRN area as a target, whereas neurons that project to the PreRN are likely to also target the RN (**Table 1**, **Figure 9**). As yet, it seems feasible to suggest that most cerebellar nuclear cells with an axon in the crossed ascending limb of the scp will ultimately project to the thalamus and may or may not have collaterals to one or several other brain stem areas.

OUTPUT PROFILES OF CEREBELLAR MODULES

The present data should be discussed in relation to the modular organization of the CN, which is based on the strict organizational pattern of longitudinal strips of Purkinje cells which terminate upon a specific part of the CN and which is mimicked by climbing fibers that originate from particular subdivisions of the IO to the same longitudinal strips or zones of Purkinje cells and that, simultaneously, provide a collateral projection to the CN target nucleus of these strips (Voogd and Bigaré, 1980; Sugihara and Shinoda, 2004, 2007; Ruigrok, 2011; Voogd et al., 2013). In this way, the output of the cerebellar cortex is organized as a series of discrete, parallel olivo-cortico-nuclear modules. As such, the MCN is considered the output nucleus of the A1 module, whereas the lateral extension of the A zone, representing the cortical constituent of the A2 module, specifically outputs by way of the DLP. The B module, mostly present in the lateral vermis of the anterior lobe, targets the LVN. The thin vermal X zone, interspersed between the A1 and B zones targets to the ICG, while the medial PIN is considered to be the output station of the CX zone. The C1, C2, and C3 zones of the intermediate cortex target AIN, PIN, and AIN, respectively. Projections of the D1 and D2 zones are directed to the vLCN and the dLCN, respectively. Finally, the D0 zone, intercalated between D1 and D2, selects the DLH as output station (for review see Voogd et al., 2013).

Figure 9B summarizes the results with respect to the modular organization of the rat cerebellum. Basically, the MCN in the rat can be divided into a caudal, a rostromedial and a rostrolateral subdivisions. The DLP, in addition, may be considered as a distinct MCN subnucleus. The difference in brainstem projections originating from these four MCN target areas is remarkable (Teune et al., 2000) and may be related to the presence of subzones restricted to certain cerebellar lobules (Voogd et al., 1996; Sugihara and Shinoda, 2004). Here, due to the virtual absent retrograde labeling in the rostral parts of the MCN, the rostromedial and rostrolateral parts will not be further considered. The caudal part of the MCN, which receives Purkinje cell axons from vermal lobules VIb,c—IX, including the vermal visual area (Voogd and Barmack, 2006; Voogd et al., 2013), contains many neurons with projections to the NRTP but also targets the prerubral area. In addition, neurons in this MCN subdivision have been shown to project to the thalamus, the superior colliculus, the basilar pontine nuclei, the medullary reticular formation and the cord and to several preoculomotor nuclei (Bentivoglio and Kuypers, 1982; Gonzalo-Ruiz and Leichnetz, 1987; Lee et al., 1989). Many of these projections arise as branches of the same neurons. Finally, the DLP gives rise to a major, crossed, projection to the bulbar reticular formation, which partly branches to the thalamus (Bentivoglio and Kuypers, 1982), but not to the areas investigated in this study (cf. Teune et al., 2000).

The ICG (X-module) possesses diverging projections to the RN, PreRN and, to a lesser degree, NRTP regions. However, its most typical feature is found in its projections to the medial medullary reticular formation and, especially, to the spinal cord with collateralizations to the thalamus (Bentivoglio and Kuypers, 1982; Buisseret-Delmas et al., 1998; Teune et al., 2000).

The LVN (B-module) was not included in our analysis as it at the origin of the lateral vestibulospinal tract and does not seem to participate in any of the ascending projections (Ruigrok, 2013). However, it does contain a population of small cells that project to the dorsal fold of the DAO (Ruigrok and Voogd, 1990).

The zonal targeting of the interposed nuclei in the rat has been subject of some controversy. Here, we essentially adhere to the description offered by Voogd et al. (2013). The medial AIN (receiving mostly input from the C1 and, to a lesser degree, from the C3 zones), apart from the non-collateralizing projections to the IO, targets both RN and PreRN with many neurons collateralizing to both regions. More scant projections are directed to the NRTP. The lateral AIN (also receiving input from the C1 and C3 zones) targets all investigated areas. Collateralization is especially prominent between NRTP and RN. Also within the PIN, classically designated as target of the C2 zone, a division between its rostromedial and caudolateral aspect seems to be relevant. The rostromedial part possesses features similar to the neurons of the ICG with respect to their projections to the cervical cord and thalamus (Bentivoglio and Kuypers, 1982). This part of the PIN is now regarded as target area of the CX zone, which is interspersed between C1 and C2 proper (Sugihara and Shinoda, 2007). However, the rostromedial PIN also gives rise to projections to the RN and, to a lesser extent, the PreRN. These projections also arise from the caudolateral PIN, with many neurons collateralizing to both areas. In addition, collateralizing projections from the lateral PIN have been described to the contralateral thalamus and superior colliculus (Bentivoglio and Kuypers, 1982). Both PIN regions, however, do not provide a significant projection to the NRTP.

The DLH, interspersed between lateral AIN and dLCN, functions as the output nucleus of D0 zone (referred to as Y-zone in Voogd et al., 2013). Like the lateral AIN, the DLH is characterized by branched projections to the ipsilateral lateral medulla oblongata and the thalamus (Bentivoglio and Molinari, 1986). However, neurons in this area may also collateralize to RN and NRTP, and, more sparsely, to the PreRN. In addition, the DLH also issues projections to oculomotor related areas (Gonzalo-Ruiz and Leichnetz, 1987).

The output of the vLCN (D1-module) and the dLCN (D2-module) is directed to all four studied areas. Apart from the projections to the IO, prominent collateralization was observed to the RN (pararubral and parvicellular parts), PreRN and NRTP regions. Collateralizing projections from the LCN were also noted to the superior colliculus, the thalamus, the medial reticular formation, the basilar pontine nuclei and several oculomotor related nuclei (Bentivoglio and Kuypers, 1982; Gonzalo-Ruiz and Leichnetz, 1987; Lee et al., 1989). Indeed, it would appear that extensive collateralization to large variety of brainstem structures is a specific feature of the output nucleus of the D-zone.

FUNCTIONAL CONSIDERATIONS

The cerebellum is suggested to be involved in a great variety of functions which effect the coordination, adaptation, timing, and learning of motor programs as well as of cognitive, emotional and visceral functions (Nisimaru et al., 1991, 2013; Schmahmann and Caplan, 2006; Watson et al., 2013). Nevertheless, cerebellar function is thought to involve a characteristic operation that is performed across various, structurally homogeneous components (Bloedel, 1992; Apps and Garwicz, 2005; Ito, 2006). Our study provides information on the level and organization of cerebellar control on motor behavior, through the RN, the PreRN, the NRTP, and the IO. The observation that from a particular cerebellar nuclear region projections to several brainstem regions may originate, indicates that a particular cerebellar module influences these various brainstem areas simultaneously. Although the influence on the IO originates from a distinct neuronal population, we show that these neurons are completely intermingled with the medium- and large-sized relay cells of the CN (Teune et al., 1995) and are likely to be influenced simultaneously the same Purkinje cells (De Zeeuw and Berrebi, 1995; Teune et al., 1998). However, as yet, it is not known to what extent they respond differently to their input in a physiological situation (e.g., see Hoebeek et al., 2011; Uusisaari and De Schutter, 2011).

The projections to the NRTP should be viewed with respect to its role as major supplier of cerebellar mossy fibers with a distinct collateral input to the CN. The classic electrophysiological studies of Tsukahara et al. (1983) showed that a two-neuron excitatory loop exists between the nucleus interpositus of the cat cerebellum and the NRTP. Our findings on the occurrence of neurons with projections to the RN or PreRN to the NRTP in parts of the CN, both extend and qualify the existence of these two-neuron excitatory loops in the rat. When our retrograde labeling experiments are compared to the results of an anterograde tracing study of the projections from the NRTP and basilar pontine nuclei (Mihailoff, 1993), it appears that closed loops may be present between the NRTP and the lateral portion of the AIN, the LCN, and the caudal MCN (excluding DLP). It is interesting to note that the NRTP loop is absent in medial AIN, a region that has been implicated in the control of the ipsilateral hindlimb (Atkins and Apps, 1997). In contrast, the PIN receives input from the NRTP but does not reciprocate it. The obvious absence of major afferent and efferent connections between the medial AIN and medial PIN with the NRTP, may be compensated by a three neuron-loop, between the RN, lateral reticular nucleus and the medial parts of the interposed nuclei (Tsukahara et al., 1983; Ruigrok and Cella, 1995; Ruigrok et al., 1995a). The lateral reticular nucleus may also be involved in reciprocal connections to the MCN (Ruigrok et al., 1995a), while reciprocal projections also seem to exist between the interposed nuclei and the RN (Huisman et al., 1983). The collateral projections of the loops to the RN and the prerubral area are likely to proceed to the thalamus (Shinoda et al., 1988). Presently, no information seems to be available to determine whether or not the ascending collaterals from these loops also terminate in other target CN areas, such as the superior colliculus, oculomotor-related areas and the reticular formation.

The prerubral area may be particularly involved in establishing a 3-neuron excitatory loop between the CN and the IO. Excitatory connections between the interposed nuclei, the nucleus of Darkschewitsch (one of the nuclei in the prerubral area), and the inferior olivary nuclei have been established in the cat with both anatomical and electrophysiological techniques (Ruigrok et al., 1990; De Zeeuw and Ruigrok, 1994; Ruigrok and Voogd, 1995). The olivary nuclei, in particular the principal and MAOs, are involved in cerebello-midbrain-olivo-cerebellar circuitry, which, in man, is known as the triangle of Guillain-Mollaret (Sarnat et al., 2013). As climbing fiber collaterals provide an excitatory collateral projection to the PIN and LCN (Kitai et al., 1977; Ruigrok, 1997; Hoebeek et al., 2011). The function of these

excitatory, CN-prerubral-IO-CN circuits, which in primates is more substantiated in a CN-parvicellular RN-IO-CN circuit, is not well understood (Hoebeek et al., 2011). Interactions of the corticospinal system and cerebellar output at the level of the parvicellular RN/PreRN (Pardoe et al., 2004) may be essential for motor learning.

At the level of the IO the excitatory cerebello-midbrain-olivary-cerebellar circuit interacts with the GABAergic nucleo-olivary pathway (Ruigrok and Voogd, 1995; Best and Regehr, 2009; Bazzigaluppi et al., 2012). Since this projection to the IO does not appear to possess major diverging projections (if any at all) to extra-olivary regions, the information carried by this pathway may be completely independent from the information to other brainstem areas. However, as single Purkinje cells may simultaneously influence nucleo-olivary as well as other CN relay neurons (De Zeeuw and Berrebi, 1995; Teune et al., 1998), activity patterns in both CN cell types may be well correlated and explain why, during movement, the excitability of the IO appears to be reduced (e.g., Horn et al., 1996). In addition, the nucleo-olivary pathway appears to be involved in regulation of the electrotonic coupling between olivary cells, thus regulating its oscillatory properties which may be important for synchronicity and timing of olivary activity (Best and Regehr, 2009; Bazzigaluppi et al., 2012). This may be an important feature for selection, timing and learning of motor functions executed by the cerebellum (Welsh et al., 1995; Van Der Giessen et al., 2008; Llinas, 2009).

ACKNOWLEDGMENTS

The authors would like to thank Erika Sabel-Goedknegt for expert technical assistance. This research was supported by NWO grant 903-47-005 to Thea M. Teune and by the Dutch Ministry of Health, Welfare and Sports to Tom J. H. Ruigrok.

REFERENCES

Aas, J.-E., and Brodal, P. (1990). GABA and glycine as putative transmitters in subcortical pathways to the pontine nuclei. A combined immunochemical and retrograde tracing study in the cat with some observations in the rat. *Neuroscience* 34, 149–162. doi: 10.1016/0306-4522(90)90309-R

Angaut, P., and Cicirata, F. (1988). The dentatorubral projection in the rat: an autoradiographic study. *Behav. Brain Res.* 28, 71–73. doi: 10.1016/0166-4328(88)90079-4

Angaut, P., Cicirata, F., and Pantò, M.-R. (1985). An autoradiographic study of the cerebellopontine projections from the interposed and lateral cerebellar nuclei in the rat. *J. Hirnforsch.* 26, 463–470.

Angaut, P., and Sotelo, C. (1989). Synaptology of the cerebello-olivary pathway. Double labelling with anterograde axonal tracing and GABA immunocytochemistry in the rat. *Brain Res.* 479, 361–365. doi: 10.1016/0006-8993(89)91641-7

Apps, R., and Garwicz, M. (2005). Anatomical and physiological foundations of cerebellar information processing. *Nat. Rev. Neurosci.* 6, 297–311. doi: 10.1038/nrn1646

Apps, R., and Hawkes, R. (2009). Cerebellar cortical organization: a one-map hypothesis. *Nat. Rev. Neurosci.* 10, 670–681. doi: 10.1038/nrn2698

Atkins, M. J., and Apps, R. (1997). Somatotopical organisation within the climbing fibre projection to the paramedian lobule and copula pyramidis of the rat cerebellum. *J. Comp. Neurol.* 389, 249–263. doi: 10.1002/(SICI)1096-9861(19971215)389:2<249::AID-CNE5>3.0.CO;2-1

Bagnall, M. W., Zingg, B., Sakatos, A., Moghadam, S. H., Zeilhofer, H. U., and Du Lac, S. (2009). Glycinergic projection neurons of the cerebellum. *J. Neurosci.* 29, 10104–10110. doi: 10.1523/JNEUROSCI.2087-09.2009

Ban, M., and Ohno, T. (1977). Projection of cerebellar nuclear neurones to the inferior olive by descending collaterals of ascending fibers. *Brain Res.* 133, 156–161. doi: 10.1016/0006-8993(77)90057-9

Bazzigaluppi, P., Ruigrok, T., Saisan, P., De Zeeuw, C. I., and De Jeu, M. (2012). Properties of the nucleo-olivary pathway: an *in vivo* whole-cell patch clamp study. *PLoS ONE* 7:e46360. doi: 10.1371/journal.pone.0046360

Bentivoglio, M., and Kuypers, H. G. J. M. (1982). Divergent axon colaterals from rat cerebellar nuclei to diencephalon, mesencephalon, medulla oblongata and cervical cord. *Exp. Brain Res.* 46, 339–356. doi: 10.1007/BF00238629

Bentivoglio, M., and Molinari, M. (1986). Crossed divergent axon collaterals from cerebellar nuclei to thalamus and lateral medulla oblongata in the rat. *Brain Res.* 362, 180–184. doi: 10.1016/0006-8993(86)91414-9

Berretta, S., Bosco, G., Giaquinta, G., Smecca, G., and Perciavalle, V. (1993). Cerebellar influences on accessory oculomotor nuclei of the rat: a neuroanatomical, immunohistochemical, and electrophysiological study. *J. Comp. Neurol.* 338, 50–66. doi: 10.1002/cne.903380105

Berretta, S., Bosco, G., Smecca, G., and Perciavalle, V. (1991). The cerebellopontine system: an electrophysiological study in the rat. *Brain Res.* 568, 178–184. doi: 10.1016/0006-8993(91)91395-H

Best, A. R., and Regehr, W. G. (2009). Inhibitory regulation of electrically coupled neurons in the inferior olive is mediated by asynchronous release of GABA. *Neuron* 62, 555–565. doi: 10.1016/j.neuron.2009.04.018

Bharos, T. B., Kuypers, H. G. J. M., Lemon, R. N., and Muir, R. B. (1981). Divergent collaterals from deep cerebellar neurons to thalamus and tectum, and to the medulla oblongata and spinal cord: retrograde fluorescent and electrophysiological studies. *Exp. Brain Res.* 42, 399–410.

Bloedel, J. R. (1992). Functional heterogeneity with structural homogeneity: How does the cerebellum operate? *Behav. Brain Sci.* 15, 666–678.

Border, B. G., Kosinski, R. J., Azizi, S. A., and Mihailoff, G. A. (1986). Certain basilar pontine afferent systems are GABA-ergic: combined HRP and immunocytochemical studies in the rat. *Brain Res. Bull.* 17, 169–179. doi: 10.1016/0361-9230(86)90113-9

Buisseret-Delmas, C., and Angaut, P. (1989). Anatomical mapping of the cerebellar nucleocortical projections in the rat: a retrograde labeling study. *J. Comp. Neurol.* 288, 297–310. doi: 10.1002/cne.902880208

Buisseret-Delmas, C., and Angaut, P. (1993). The cerebellar olivo-cortico-nuclear connections in the rat. *Progr. Neurobiol.* 40, 63–87. doi: 10.1016/0301-0082(93)90048-W

Buisseret-Delmas, C., Angaut, P., Compoint, C., Diagne, M., and Buisseret, P. (1998). Brainstem efferents from the interface between the nucleus medialis and the nucleus interpositus in the rat. *J. Comp. Neurol.* 402, 264–275.

Buisseret-Delmas, C., Batini, C., Compoint, C., Daniel, H., and Menetrey, D. (1989). The GABAergic neurones of the cerebellar nuclei: projection to the caudal inferior olive and to the bulbar reticular formation. *Exp.Brain Res.* 17, 108–110.

Cerminara, N. L., and Apps, R. (2011). Behavioural significance of cerebellar modules. *Cerebellum* 10, 484–494. doi: 10.1007/s12311-010-0209-2

Chan-Palay, V. (1977). *Cerebellar Dentate Nucleus: Organization, Cytology and Transmitters*. Berlin: Springer-Verlag. doi: 10.1007/978-3-642-66498-4

Chen, S., and Aston-Jones, G. (1995). Evidence that cholera toxin B subunit (CTb) can be avidly taken up and transported by fibers of passage. *Brain Res.* 674, 107–111. doi: 10.1016/0006-8993(95)00020-Q

Cicirata, F., Panto, M. R., and Angaut, P. (1982). An autoradiographic study of the cerebellopontine projections in the rat. I. Projections from the medial cerebellar nucleus. *Brain Res.* 253, 303–308. doi: 10.1016/0006-8993(82)90697-7

Desclin, J. C. (1974). Histological evidence supporting the inferior olive as the major source of cerebellar climbing fibers in the rat. *Brain Res.* 77, 365–388. doi: 10.1016/0006-8993(74)90628-3

De Zeeuw, C. I., and Berrebi, A. S. (1995). Individual Purkinje cell axons terminate on both inhibitory and excitatory neurons in the cerebellar and vestibular nuclei. *Ann. N.Y. Acad. Sci.* 781, 607–610. doi: 10.1111/j.1749-6632.1996.tb15736.x

De Zeeuw, C. I., Holstege, J. C., Ruigrok, T. J., and Voogd, J. (1989). Ultrastructural study of the GABAergic, cerebellar, and mesodiencephalic innervation of the cat medial accessory olive: anterograde tracing combined with immunocytochemistry. *J. Comp. Neurol.* 284, 12–35. doi: 10.1002/cne.902840103

De Zeeuw, C. I., and Ruigrok, T. J. H. (1994). Olivary projecting neurons in the nucleus of Darkschewitsch in the cat receive excitatory monosynaptic

input from the cerebellar nuclei. *Brain Res.* 653, 345–350. doi: 10.1016/0006-8993(94)90411-1

Faull, R. L. (1978). The cerebellofugal projections in the brachium conjunctivum of the rat. II. The ipsilateral and contralateral descending pathways. *J. Comp. Neurol.* 178, 519–535. doi: 10.1002/cne.901780307

Faull, R. L., and Carman, J. B. (1978). The cerebellofugal projections in the brachium conjunctivum of the rat I. The contralateral ascending pathway. *J. Comp. Neurol.* 178, 495–517. doi: 10.1002/cne.901780307

Flumerfelt, B. A. (1978). Organization of the mammalian red nucleus and its interconnections wiht the cerebellum. *Experientia* 34, 1178–1180. doi: 10.1007/BF01922943

Fredette, B. J., and Mugnaini, E. (1991). The GABAergic cerebello-olivary projection in the rat. *Anat. Embryol. (Berl.)* 184, 225–243. doi: 10.1007/BF01673258

Gellman, R., Houk, J. C., and Gibson, A. R. (1983). Somatosensory properties of the inferior olive of the cat. *J. Comp. Neurol.* 215, 228–243. doi: 10.1002/cne.902150210

Giuffrida, R., Aicardi, G., Canedi, A., and Rapisarda, C. (1993). Excitatory amino acids as neurotransmitters of cortical and cerebellar projections to the red nucleus: an immunocytochemical study in the guinea pig. *Somatosens. Motor Res.* 10, 365–376. doi: 10.3109/08990229309028844

Godschalk, M., Van Der Burg, J., Van Duin, B., and De Zeeuw, C. I. (1994). Topography of saccadic eye movements evoked by microstimulation in rabbit cerebellar vermis. *J. Physiol.* 480(Pt 1), 147–153.

Gonzalo-Ruiz, A., and Leichnetz, G. R. (1987). Collateralization of cerebellar efferent projections to the paraoculomotor region, superior colliculus, and medial pontine reticular formation in the rat: a fluorescent double labeling study. *Exp.Brain Res.* 68, 365–378. doi: 10.1007/BF00248802

Hoebeek, F. E., Witter, L., Ruigrok, T. J., and De Zeeuw, C. I. (2011). Differential olivo-cerebellar cortical control of rebound activity in the cerebellar nuclei. *Proc. Natl. Acad. Sci. U.S.A.* 107, 8410–8415. doi: 10.1073/pnas.0907118107

Horn, K. M., Vankan, P. L. E., and Gibson, A. R. (1996). Reduction of rostral dorsal accessory olive responses during reaching. *J. Neurophysiol.* 76, 4140–4151.

Huisman, A. M., Kuypers, H. G. J. M., Conde, F., and Keizer, K. (1983). Collaterals of rubrospinal neurons to the cerebellum in rat. A retrograde fluorescent double labeling study. *Brain Res.* 264, 181–196. doi: 10.1016/0006-8993(83)90816-8

Ito, M. (2006). Cerebellar circuitry as a neuronal machine. *Prog. Neurobiol.* 78, 272–303. doi: 10.1016/j.pneurobio.2006.02.006

Kawamura, S., Hattori, S., Higo, S., and Matsuyama, T. (1982). The cerebellar projections to the superior colliculus and pretectum in the cat: an autoradiographic and horseradish peroxidase study. *Neuroscience* 7, 1673–1689. doi: 10.1016/0306-4522(82)90026-4

Kitai, S. T., Kocsis, J. D., and Kiyohara, T. (1976). Electrophysiological properties of nucleus reticularis tegmenti pontis cells: antidromic and synaptic activation. *Exp. Brain Res.* 24, 295–309. doi: 10.1007/BF00235017

Kitai, S. T., McCrea, R. A., Preston, R. J., and Bishop, G. A. (1977). Electrophysiological and horseradish peroxidase studies of precerebellar afferents to the nucleus interpositus anterior. I. Climbing fiber system. *Brain Res.* 122, 197–214. doi: 10.1016/0006-8993(77)90289-X

Koekkoek, S. K. E., and Ruigrok, T. J. H. (1995). Lack of bilateral projection of individual spinal neurons to the lateral reticular nucleus in the rat: a retrograde, non-fluorescent, double labeling study. *Neurosci. Lett.* 200, 13–16. doi: 10.1016/0304-3940(95)12077-H

Lee, H. S., Kosinski, R. J., and Mihailoff, G. A. (1989). Collateral branches of cerebellopontine axons reach the thalamus, superior colliculus or inferior olive: a double-fluorescence and combined fluorescence -horseradish peroxidase study in the rat. *Neuroscience* 28, 725–735. doi: 10.1016/0306-4522(89)90017-1

Legendre, A., and Courville, J. (1987). Origin and trajectory of the cerebello-olivary projection: an experimental study with radioactive and fluorescent tracers in the cat. *Neurosci.* 21, 877–891. doi: 10.1016/0306-4522(87)90044-3

Llewellyn-Smith, I. J., Pilowsky, P., and Minson, J. B. (1992). "Retrograde tracers for light and electron microscopy," in *Experimental Neuroanatomy. A practical approach,* ed. J. P. Bolam (Oxford: Oxford University Press), 31–59.

Llinas, R. R. (2009). Inferior olive oscillation as the temporal basis for motricity and oscillatory reset as the basis for motor error correction. *Neuroscience* 162, 797–804. doi: 10.1016/j.neuroscience.2009.04.045

McCrea, R. A., Bishop, G. A., and Kitai, S. T. (1978). Morphological and electrophysiological characteristics of projection neurons in the nucleus interpositus of the cat cerebellum. *J. Comp. Neurol.* 181, 397–420. doi: 10.1002/cne.901810210

Menetrey, D. (1985). Retrograde tracing of neural pathways with a protein-gold complex. I. Light microscopic detection after silver intensification. *Histochemistry* 83, 391–395. doi: 10.1007/BF00509197

Mihailoff, G. (1993). Cerebellar nuclear projections from the basilar pontine nuclei and nucleus reticularis tegmenti pontis as demonstrated with PHA-L tracing in the rat. *J. Comp. Neurol.* 330, 130–146. doi: 10.1002/cne.903300111

Mihailoff, G. A., Kosinski, R. J., Azizi, S. A., and Border, B. G. (1989). Survey of noncortical afferent projections to the basilar pontine nuclei: a retrograde tracing study in the rat. *J. Comp. Neurol.* 282, 617–643. doi: 10.1002/cne.902820411

Mihailoff, G. A., McArdle, C. B., and Adams, C. E. (1981). The cytoarchitecture, cytology, and synaptic organization of the basilar pontine nuclei in the rat. I. Nissl and Golgi studies. *J. Comp. Neurol.* 195, 181–201. doi: 10.1002/cne.901950202

Newman, D. B. (1985). Distinguishing rat brainstem reticulospinal nuclei by their neuronal morphology. II. Pontine and mesencephalic nuclei. *J. Hirnforsch.* 26, 385–418.

Nisimaru, N., Mittal, C., Shirai, Y., Sooksawate, T., Anandaraj, P., Hashikawa, T., et al. (2013). Orexin-neuromodulated cerebellar circuit controls redistribution of arterial blood flows for defense behavior in rabbits. *Proc. Natl. Acad. Sci. U.S.A.* 110, 14124–14131. doi: 10.1073/pnas.1312804110

Nisimaru, N., Okahara, K., and Nagao, S. (1991). Olivocerebellar projection to the cardiovascular zone of rabbit cerebellum. *Neurosci. Res.* 12, 240–250. doi: 10.1016/0168-0102(91)90114-E

Onodera, S., and Hicks, T. P. (1995). Patterns of transmitter labelling and connectivity of the cat's nucleus of Darkschewitsch: a wheat germ agglutinin-horseradish peroxidase and immunocytochemical study at light and electron microscopical levels. *J. Comp. Neurol.* 361, 553–573. doi: 10.1002/cne.903610402

Onodera, S., and Hicks, T. P. (2009). A comparative neuroanatomical study of the red nucleus of the cat, macaque and human. *PLoS ONE* 4:e6623. doi: 10.1371/journal.pone.0006623

Pardoe, J., Edgley, S. A., Drew, T., and Apps, R. (2004). Changes in excitability of ascending and descending inputs to cerebellar climbing fibers during locomotion. *J. Neurosci.* 24, 2656–2666. doi: 10.1523/JNEUROSCI.1659-03.2004

Paxinos, G., and Watson, C. (2005). *The Rat Brain in Stereotaxic Coordinates.* San Diego, CA: Elsevier Academic Press.

Pijpers, A., Winkelman, B. H., Bronsing, R., and Ruigrok, T. J. (2008). Selective impairment of the cerebellar C1 module involved in rat hind limb control reduces step-dependent modulation of cutaneous reflexes. *J. Neurosci.* 28, 2179–2189. doi: 10.1523/JNEUROSCI.4668-07.2008

Ramón y Cajal, S. (1911). *Histologie du Système Nerveux de l'homme et des Vertébrés.* Paris: Maloine.

Reid, J. M., Gwyn, D. G., and Flumerfelt, B. A. (1975). A cytoarchitectonic and Golgi study of the red nucleus in the rat. *J. Comp. Neurol.* 162, 337–362. doi: 10.1002/cne.901620305

Ruigrok, T. J. (2011). Ins and outs of cerebellar modules. *Cerebellum* 10, 464–474. doi: 10.1007/s12311-010-0164-y

Ruigrok, T. J., and Apps, R. (2007). A light microscope-based double retrograde tracer strategy to chart central neuronal connections. *Nat. Protoc.* 2, 1869–1878. doi: 10.1038/nprot.2007.264

Ruigrok, T. J., and Voogd, J. (2000). Organization of projections from the inferior olive to the cerebellar nuclei in the rat. *J. Comp. Neurol.* 426, 209–228. doi: 10.1002/1096-9861(20001016)426:2%3C209::AID-CNE4%3E3.0.CO;2-0

Ruigrok, T. J. H. (1997). "Cerebellar nuclei: the olivary connection," in *The Cerebellum: from Structure to Control,* eds C. I. De Zeeuw, P. Strata, and J. Voogd. (Amsterdam: Elsevier Science B.V.), 162–197.

Ruigrok, T. J. H. (2004). "Precerebellar nuclei and red nucleus," in *The Rat Nervous System, 3rd Edn.,* ed G. Paxinos. (San Diego, CA: Elsevier Academic Press), 167–204.

Ruigrok, T. J. H. (2013). "Cerebellar influences on descending spinal motor systems," in *Handbook of the cerebellum and cerebellum disorders,* eds M. Manto, J. D. Gruol, N. Schmahmann, N. Koibuchi, and F. Rossi (Dordrecht: Springer), 497–528. doi: 10.1007/978-94-007-1333-8_23

Ruigrok, T. J. H., and Cella, F. (1995). "Precerebellar nuclei and red nucleus," in *The Rat Nervous System, 2nd Edn.,* ed G. Paxinos (Sydney, NSW: Academic Press), 277–308.

Ruigrok, T. J. H., Cella, F., and Voogd, J. (1995a). Connections of the lateral reticular nucleus to the lateral vestibular nucleus in the rat. An anterograde tracer

study with Phaseolus vulgaris leucoagglutinin. *Eur. J. Neurosci.* 7, 1410–1413. doi: 10.1111/j.1460-9568.1995.tb01133.x

Ruigrok, T. J. H., De Zeeuw, C. I., Van Der Burg, J., and Voogd, J. (1990). Intracellular labeling of neurons in the medial accessory olive of the cat. I. Physiology and light microscopy. *J. Comp. Neurol.* 300, 462–477. doi: 10.1002/cne.903000403

Ruigrok, T. J. H., Teune, T. M., Van Der Burg, J., and Sabel-Goedknegt, H. (1995b). A retrograde double labeling technique for light microscopy. A combination of axonal transport of cholera toxin B-subunit and a gold-lectin conjugate. *J. Neurosci. Meth.* 61, 127–138. doi: 10.1016/0165-0270(94)00034-E

Ruigrok, T. J. H., and Voogd, J. (1990). Cerebellar nucleo-olivary projections in rat. An anterograde tracing study with Phaseolus vulgaris-leucoagglutinin (PHA-L). *J. Comp. Neurol.* 298, 315–333. doi: 10.1002/cne.902980305

Ruigrok, T. J. H., and Voogd, J. (1995). Cerebellar influence on olivary excitability in the cat. *Eur. J. Neurosci.* 7, 679–693. doi: 10.1111/j.1460-9568.1995.tb00672.x

Sarnat, H. B., Flores-Sarnat, L., and Auer, R. N. (2013). Synaptogenesis in the foetal and neonatal cerebellar system. 2. Pontine nuclei and cerebellar cortex. *Dev. Neurosci.* 35, 317–325. doi: 10.1159/000351031

Schmahmann, J. D., and Caplan, D. (2006). Cognition, emotion and the cerebellum. *Brain* 129, 290–292. doi: 10.1093/brain/awh729

Shinoda, Y., Futami, T., Mitoma, H., and Yokota, J. (1988). Morphology of single neurones in the cerebello-rubrospinal system. *Behav. Brain Res.* 28, 59–64. doi: 10.1016/0166-4328(88)90076-9

Sugihara, I., and Shinoda, Y. (2004). Molecular, topographic, and functional organization of the cerebellar cortex: a study with combined aldolase C and olivocerebellar labeling. *J. Neurosci.* 24, 8771–8785. doi: 10.1523/JNEUROSCI.1961-04.2004

Sugihara, I., and Shinoda, Y. (2007). Molecular, topographic, and functional organization of the cerebellar nuclei: analysis by three-dimensional mapping of the olivonuclear projection and aldolase C labeling. *J. Neurosci.* 27, 9696–9710. doi: 10.1523/JNEUROSCI.1579-07.2007

Sugimoto, T., Mizuno, N., and Uchida, K. (1982). Distribution of cerebellar fiber terminals in the midbrain visuomotor areas: an autoradiographic study in the cat. *Brain Res.* 238, 353–370. doi: 10.1016/0006-8993(82)90110-X

Teune, T. M., Van Der Burg, J., De Zeeuw, C. I., Voogd, J., and Ruigrok, T. J. H. (1998). Single Purkinje cell can innervate multiple classes of projection neurons in the cerebellar nuclei of the rat: a light microscopic and ultrastructural triple-tracer study in the rat. *J. Comp. Neurol.* 392, 164–178. doi: 10.1002/(SICI)1096-9861(19980309)392:2<164::AID-CNE2>3.0.CO;2-0

Teune, T. M., Van Der Burg, J., and Ruigrok, T. J. (1995). Cerebellar projections to the red nucleus and inferior olive originate from separate populations of neurons in the rat: a non-fluorescent double labeling study. *Brain Res.* 673, 313–319. doi: 10.1016/0006-8993(94)01431-G

Teune, T. M., Van Der Burg, J., Van Der Moer, J., Voogd, J., and Ruigrok, T. J. H. (2000). "Topography of cerebellar nuclear projections to the brain stem in the rat," in *Cerebellar Modules: Molecules, Morphology and Function,* eds N. M. Gerrits, T. J. H. Ruigrok, and C. I. De Zeeuw (Amsterdam: Elsevier Science B.V.), 141–172. doi: 10.1016/S0079-6123(00)24014-4

Tolbert, D. L., Bantli, H., and Bloedel, J. R. (1978). Multiple branching of cerebellar efferent projections in cats. *Exp. Brain Res.* 31, 305–316. doi: 10.1007/BF00237291

Tolbert, D. L., Bantli, H., Hames, E. G., Ebner, T. J., McMullen, T. A., and Bloedel, J. R. (1980). A demonstration of the dentato-reticulospinal projection in the cat. *Neuroscience* 5, 1479–1488. doi: 10.1016/0306-4522(80)90010-X

Torigoe, Y., Blanks, R. H., and Precht, W. (1986). Anatomical studies on the nucleus reticularis tegmenti pontis in the pigmented rat. II. Subcortical afferents demonstrated by the retrograde transport of horseradish peroxidase. *J. Comp. Neurol.* 243, 88–105. doi: 10.1002/cne.902430108

Toyama, K., Tsukahara, N., and Udo, M. (1968). Nature of the cerebellar influences upon the red nucleus neurones. *Exp. Brain Res.* 4, 292–309. doi: 10.1007/BF00235697

Tsukahara, N., Bando, T., Murakami, F., and Oda, Y. (1983). Properties of cerebello-precerebellar reverberating circuits. *Brain Res.* 274, 249–259. doi: 10.1016/0006-8993(83)90702-3

Uusisaari, M., and De Schutter, E. (2011). The mysterious microcircuitry of the cerebellar nuclei. *J. Physiol.* 589, 3441–3457. doi: 10.1113/jphysiol.2010.201582

Uusisaari, M., and Knopfel, T. (2011). Functional classification of neurons in the mouse lateral cerebellar nuclei. *Cerebellum* 10, 637–646. doi: 10.1007/s12311-010-0240-3

Van Der Giessen, R. S., Koekkoek, S. K., Van Dorp, S., De Gruijl, J. R., Cupido, A., Khosrovani, S., et al. (2008). Role of olivary electrical coupling in cerebellar motor learning. *Neuron* 58, 599–612. doi: 10.1016/j.neuron.2008.03.016

Van Der Steen, J., Simpson, J. I., and Tan, J. (1994). Functional and anatomic organization of three-dimensional eye movements in rabbit cerebellar flocculus. *J. Neurophysiol.* 72, 31–46.

Verveer, C., Hawkins, R. K., Ruigrok, T. J. H., and De Zeeuw, C. I. (1997). Ultrastructural study of the GABAergic and cerebellar input t o the nucleus reticularis tegmenti pontis. *Brain Res.* 766, 289–296. doi: 10.1016/S0006-8993(97)00774-9

Voogd, J. (2004). "Cerebellum," in *The Rat Nervous System, 3rd Edn.,* ed G. Paxinos (San diego, CA: Elsevier Academic Press), 205–242.

Voogd, J., and Barmack, N. H. (2006). Oculomotor cerebellum. *Prog. Brain Res.* 151, 231–268. doi: 10.1016/S0079-6123(05)51008-2

Voogd, J., and Bigaré, F. (1980). "Topographical distribution of olivary and cortico nuclear fibers in the cerebellum: a review," in *The Inferior Olivary Nucleus. Anatomy and Physiology,* eds. J. Courville, C. De Montigny, and Y. Lamarre (New York, NY: Raven Press), 207–234.

Voogd, J., Gerrits, N. M., and Ruigrok, T. J. H. (1996). Organization of the vestibulocerebellum. *Ann. N.Y. Acad. Sci.* 781, 553–579. doi: 10.1111/j.1749-6632.1996.tb15728.x

Voogd, J., Shinoda, Y., Ruigrok, T., and Sugihara, I. (2013). "Cerebellar nuclei and the inferior olivary nuclei: organization and connections," in *Handbook of the Cerebellum and Cerebellar Disorders*, eds M. Manto, J. D. Gruol, N. Schmahmann, N. Koibuchi, and F. Rossi (Dordreclht: Springer Science), 377–436. doi: 10.1007/978-94-007-1333-8_19

Voogd, J., and Van Baarsen, K. (2014). The horseshoe-shaped commissure of Wernekinck or the decussation of the brachium conjunctivum methodological changes in the 1840s. *Cerebellum* 13, 113–120. doi: 10.1007/s12311-013-0520-9

Watson, T. C., Koutsikou, S., Cerminara, N. L., Flavell, C. R., Crook, J. J., Lumb, B. M., et al. (2013). The olivo-cerebellar system and its relationship to survival circuits. *Front. Neural Circuits* 7:72. doi: 10.3389/fncir.2013.00072

Watt, C. B., and Mihailoff, G. A. (1983). The cerebello-pontine system in the rat. I. Autoradiographic studies. *J. Comp. Neurol.* 215, 312–330. doi: 10.1002/cne.902150307

Welsh, J. P., Lang, E. J., Sugihara, I., and Llinas, R. (1995). Dynamic organization of motor control within the olivocerebellar system. *Nature* 374, 453–457. doi: 10.1038/374453a0

Conflict of Interest Statement: The authors declare that the research was conducted in the absence of any commercial or financial relationships that could be construed as a potential conflict of interest.

Received: 29 December 2013; accepted: 01 February 2014; published online: 21 February 2014.

Citation: Ruigrok TJH and Teune TM (2014) Collateralization of cerebellar output to functionally distinct brainstem areas. A retrograde, non-fluorescent tracing study in the rat. Front. Syst. Neurosci. ***8****:23. doi: 10.3389/fnsys.2014.00023*

This article was submitted to the journal Frontiers in Systems Neuroscience.

frontiers in
SYSTEMS NEUROSCIENCE

ORIGINAL RESEARCH ARTICLE
published: 04 February 2014
doi: 10.3389/fnsys.2014.00004

Back to front: cerebellar connections and interactions with the prefrontal cortex

Thomas C. Watson†, Nadine Becker, Richard Apps* and Matthew W. Jones*

School of Physiology and Pharmacology, University of Bristol, Bristol, UK

Edited by:
Neeraj Jain, National Brain Research Centre, India

Reviewed by:
Huo Lu, Philadelphia College of Osteopathic Medicine, USA
Laurens Witter, Harvard Medical School, USA

****Correspondence:***
Richard Apps and Matthew W. Jones, School of Physiology and Pharmacology, University of Bristol, Medical Sciences Building, Bristol BS8 1TD, UK
e-mail: r.apps@bristol.ac.uk; matt.jones@bristol.ac.uk

†Present address:
Thomas C. Watson, Sorbonne Universités, UPMC Univ Paris 06, UMR-S 8246, Neuroscience Paris Seine, Navigation Memory and Aging Team, F-75005, Paris, France; INSERM, UMR-S 1130, Neuroscience Paris Seine, Navigation Memory and Aging Team, F-75005, Paris, France; CNRS, UMR 8246, Neuroscience Paris Seine, Navigation Memory and Aging Team, F-75005, Paris, France

Although recent neuroanatomical evidence has demonstrated closed-loop connectivity between prefrontal cortex and the cerebellum, the physiology of cerebello-cerebral circuits and the extent to which cerebellar output modulates neuronal activity in neocortex during behavior remain relatively unexplored. We show that electrical stimulation of the contralateral cerebellar fastigial nucleus (FN) in awake, behaving rats evokes distinct local field potential (LFP) responses (onset latency ∼13 ms) in the prelimbic (PrL) subdivision of the medial prefrontal cortex. Trains of FN stimulation evoke heterogeneous patterns of response in putative pyramidal cells in frontal and prefrontal regions in both urethane-anesthetized and awake, behaving rats. However, the majority of cells showed decreased firing rates during stimulation and subsequent rebound increases; more than 90% of cells showed significant changes in response. Simultaneous recording of on-going LFP activity from FN and PrL while rats were at rest or actively exploring an open field arena revealed significant network coherence restricted to the theta frequency range (5–10 Hz). Granger causality analysis indicated that this coherence was significantly directed from cerebellum to PrL during active locomotion. Our results demonstrate the presence of a cerebello-prefrontal pathway in rat and reveal behaviorally dependent coordinated network activity between the two structures, which could facilitate transfer of sensorimotor information into ongoing neocortical processing during goal directed behaviors.

Keywords: cerebellum, fastigial nucleus, prefrontal cortex, prelimbic cortex, theta, coherence

INTRODUCTION

An increasing number of studies advocate the view that cerebellar contributions to behavior are not confined to motor control but also extend to cognitive function (e.g., Stoodley and Schmahmann, 2010). Consistent with this, convergent evidence from clinical, neuroimaging and anatomical tracing studies in primates suggests that the cerebellum forms "closed-loop" connections with neocortical brain regions including the prefrontal cortex (Middleton and Strick, 1994, 2001; Kelly and Strick, 2003; Schmahmann, 2004; Allen et al., 2005; Krienen and Buckner, 2009; Strick et al., 2009; O'Reilly et al., 2010; Stoodley and Schmahmann, 2010; Buckner et al., 2011; Stoodley, 2012). These anatomical connections provide the neural basis through which cerebellar contributions to neocortical processing may occur, enabling integration of sensorimotor information across hind- and fore-brain.

The understanding of such distributed networks may be especially pertinent given that abnormal prefrontal-cerebellar interactions are implicated in disorders such as autism and schizophrenia (Andreasen et al., 1996; Andreasen and Pierson, 2008; Fatemi et al., 2012). In particular, imaging studies frequently report abnormalities of the cerebellar vermis in schizophrenia (e.g., Okugawa et al., 2007; Lawyer et al., 2009; Henze et al., 2011) and direct electrical and transcranial magnetic stimulation of the vermis has shown some efficacy in treating the cognitive and emotional symptoms of the disease (Heath, 1977; Demirtas-Tatlidede et al., 2010).

Although the presence of a cerebello-cortical reciprocal network has not been demonstrated in non-primates, electrophysiological and amperometric studies have highlighted, respectively, the existence of a prefrontal-olivo-cerebellar pathway in anesthetized rats (specifically to vermal lobule VII; Watson et al., 2009), and modulation of prefrontal dopamine release following cerebellar stimulation in anesthetized mice (Mittleman et al., 2008). Anatomical data also suggest the existence of disynaptic fronto-cerebellar connectivity in rat (Suzuki et al., 2012) and preliminary data obtained in mouse suggest a neural connection exists between the cerebellar nuclei and prefrontal cortex (Arguello et al., 2012). Recent evidence has also highlighted the importance of cerebellar plasticity in goal-directed behavior and spatial navigation in mice (Burguière et al., 2010; Rochefort et al., 2011). Together, these studies suggest the basis of a rodent prefrontal-cerebellar network reminiscent of that described anatomically in primates (Middleton and Strick, 2001; Kelly and Strick, 2003).

While the neuroanatomical basis of non-human primate prefrontal-cerebellar networks is relatively well established, and becoming clearer in rodents (see above), scant information is available on the dynamic physiological interactions between the two structures, particularly during behavior. This is of importance given that temporally organized, large-scale, distributed networks are thought to be fundamental to information processing as reflected in frequency specific, coherent local field potential (LFP) oscillations (Gray, 1994; Varela et al., 2001; Fries, 2005). Indeed, coherent cerebro-cerebellar oscillations have been previously observed, across frequencies ranging from 1 to 40 Hz, in both anesthetized and awake, behaving animals (O'Connor et al., 2002; Courtemanche and Lamarre, 2005; Soteropoulos and Baker, 2006; Ros et al., 2009; Rowland et al., 2010). Nevertheless, it remains unknown whether prefrontal cortical activity also synchronizes with the cerebellum.

We therefore sought to address the basis and nature of cerebello-prefrontal interactions in rat by: (a) using electrophysiological mapping techniques to study connectivity between the cerebellar vermal output nucleus, fastigius and neocortical regions, including the PrL; (b) exploring the possibility that cerebellar stimulation may modulate ongoing firing patterns in neocortical regions; and (c) examining the coordination of LFP activity within this network.

METHODS

All experimental procedures were carried out in accordance with the UK Animals (Scientific Procedures) Act 1986 and were approved by the University of Bristol institutional animal licence advisory group. A total of 13 adult rats were used in two experimental groups: non-recovery electrophysiology (8 Wistar rats, weight 280–380 g, Harlan, UK) and chronic, recovery electrophysiology (4 Long-Evans and 1 Wistar, weight 340–440 g, Harlan, UK). Strain-related differences were not apparent in any of the results.

ELECTROPHYSIOLOGY IN ANESTHETIZED RATS

Rats were anesthetized with urethane (1.5 g/kg intraperitoneal injection) then placed in a stereotaxic frame (David Kopf instruments, Tujunga, CA) and secured with atraumatic ear bars coated with a topical local anesthetic (Xylocaine, Astra Pharmaceuticals, Kings Langley, UK). Occasionally a supplementary dose of urethane was given (10 % of original dose) to maintain surgical levels of anesthesia, as evidenced by the absence of limb withdrawal and corneal reflexes and lack of whisking. Core body temperature was maintained at 36–38°C through the use of a homoeothermic blanket (Harvard apparatus, Massachusetts, USA). Craniotomies were made over the frontal cortex (+3.2 mm, +0.6 mm from bregma) and cerebellum (−11.5 mm, +0.8 mm from bregma).

Cortical recordings were made using a Cheetah 32 system (Neuralynx, Montana, USA), with extracellular action potentials (sampled at 32 kHz and filtered between 0.6–6 kHz) recorded differentially using a local reference placed in a proximal cortical region in which spiking activity was absent. Typically, arrays of six extracellular tetrode recording electrodes were positioned on the surface of secondary motor cortex (M2) whilst a bipolar stimulating electrode (SNE-100X, interpolar distance of 0.5 mm, Rhodes Electromedical) was targeted toward the contralateral cerebellar fastigial nucleus (FN, 4.5 mm from surface of brain) and used to deliver trains of stimuli at 0.03 Hz (intensity of 100 μA and frequency of 100 Hz; cf. Mittleman et al., 2008). Extracellular responses to the cerebellar stimulation were recorded at two depths within the frontal cortex: firstly in superficial regions (M2/anterior cingulate border; 1.3–2 mm ventral from brain surface) and once again when the tetrodes had been lowered to their final position in the PrL region (2.6–3 mm ventral from brain surface). On average, we recorded 2.4 ± 0.2 well-isolated units per tetrode in anesthetized animals; continuous LFP was not recorded in these anesthetized preparations.

ELECTROPHYSIOLOGY IN CHRONICALLY IMPLANTED RATS

Rats were implanted with up to 8 tetrode recording electrodes into the left frontal cortex (+3.2 mm, +0.6 mm from bregma) and 1 bipolar stimulating/recording electrode into the contralateral FN (−11.5 mm, +0.8 mm from bregma; interpolar distance of 0.5 mm) under sodium pentobarbital recovery anesthesia. In one animal, tetrodes were implanted in both cerebellum and frontal cortex at the same coordinates as given above. Following surgery, the independently moveable tetrodes were lowered into the PrL subdivision of the prefrontal cortex (∼2.6–3 mm ventral from brain surface) over the course of 1 week. Differential recordings were made using a Digital Lynx system (Neuralynx, Montana, USA) with a local reference placed in a proximal cortical region without spiking activity (2.4–2.7 mm below the pial surface for prefrontal recordings). On average we recorded 2.2 ± 0.6 units per tetrode in the chronically implanted rats.

Cerebellar LFP recordings were made through either previously implanted bipolar electrodes positioned in the cerebellum, with overlying skull screws serving as the reference point or in one case with tetrodes, which were referenced locally to a tetrode without spiking activity. LFP signals were sampled at 2 KHz and filtered between 0.1 and 475 Hz. Extracellular action potentials were sampled and filtered as for the acute, non-recovery experiments and recording channels were grounded to two screws in the skull overlying the cerebellum. In some cases electrodes were coated in DiI (1,1′-dioctadecyl-3,3,3′,3′-tetramethylindocarbocyanine perchlorate; Molecular Probes, Invitrogen, UK) prior to implantation, which, in addition to electrolytic lesioning, was used to help establish electrode tip positions at the end of each experiment (see **Figure 1**).

CHRONIC RECORDING AND STIMULATION PROTOCOLS

Evoked field potentials and single unit responses were recorded in the M2/anterior cingulate (Cg1) and PrL regions whilst animals were in a rest box, which consisted of an elevated platform (20 cm diameter) inside a wooden box (45 × 45 × 100 cm). In all rest box experiments animal movement was monitored continuously by video. For field potential experiments, stimulation parameters consisted of a triplet burst of 3 pulses (0.1 ms pulse duration, 3 ms inter-pulse interval) delivered once every 2 s. The mean stimulation intensity required to evoke reliably detectable field potentials was 300 ± 115 μA (range 100 μA to 500 μA; $n = 4$). For single unit experiments, trains of stimuli (100 Hz, 100 stimuli, 1 s duration, mean stimulus intensity 80 ± 20 μA, range 40 μA to 100 μA; $n = 3$) were delivered to FN every 5 s. These stimulus parameters have previously been shown to drive cerebellar nuclear output

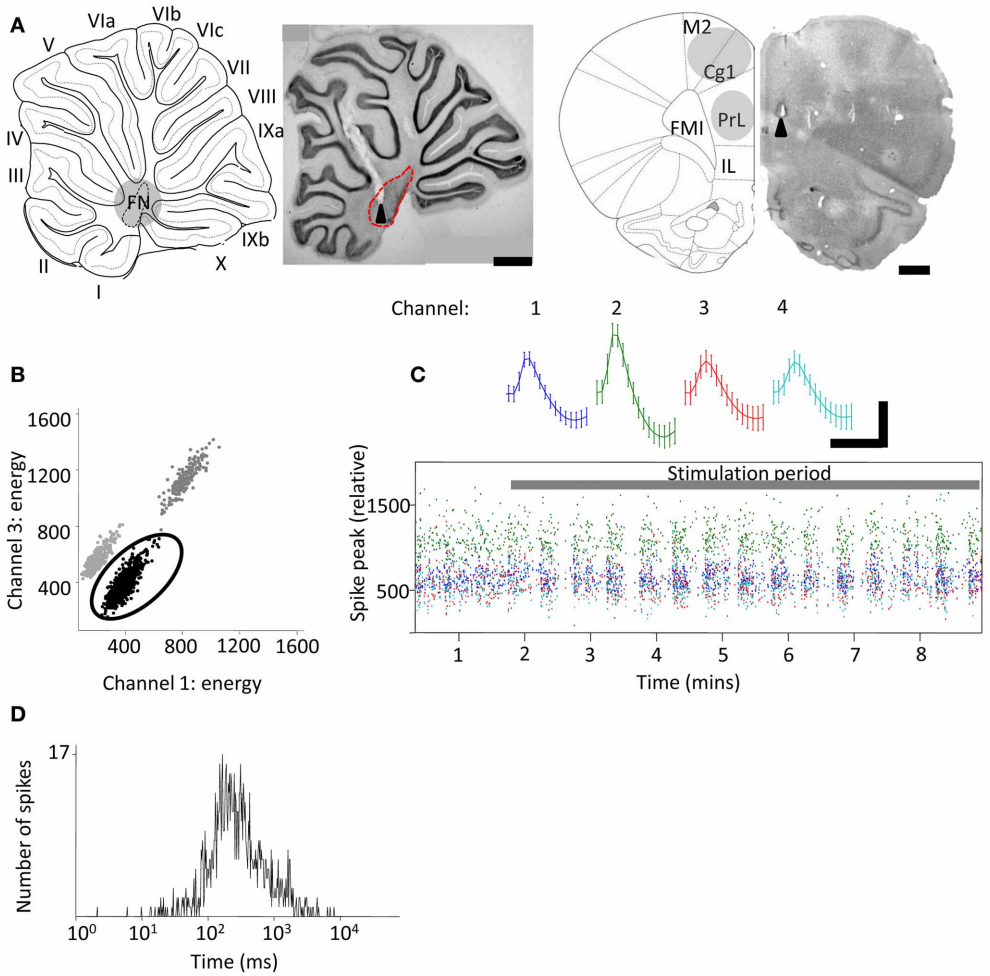

FIGURE 1 | Extracellular tetrode recordings of single-unit PrL activity during cerebellar stimulation. (A) Grouped schematic (shaded gray areas, adapted from Paxinos and Watson, 2006) and representative micrographs of neutral red-stained 50 μm saggital and transverse brain slices showing respectively the sites of electrolytic lesions (arrowheads) in the cerebellum (left,) and PrL, right). Dashed lines indicate outline of fastigial nucleus and overlying cerebellar cortical lobules are numbered; scale bars, 1 mm. M2, supplementary motor cortex; Cg1, cingulate cortex; IL, infralimbic cortex. FMI, forceps minor of the corpus callosum. **(B)** Three clusters of action potentials spread along the axes of relative energy recorded on two channels of a tetrode in PrL. The properties of the black cluster (circled) are shown in **(C,D)**. **(C)** Mean waveform recorded on color-coded channels of the tetrode (top) showing stable relative spike amplitudes throughout one experiment (bottom) (scale bar, 0.05 mV; 0.7 ms). **(D)**, Distribution of interspike intervals (ISI) for all spikes fired by the unit in the experimental session.

(Bagnall et al., 2009). For experiments in which recordings were made from both cerebellum and frontal cortex ($n = 5$), rat location was video tracked in the open field (a 1 m diameter circular arena) via light-emitting diodes attached to a powered headstage (Cheetah software; Neuralynx, Montana, USA).

DATA ANALYSIS

All data were processed in Matlab (Mathworks, USA) unless stated otherwise. LFP and single unit data were sorted based upon running speed (derived from video tracking data). For open field, a thresholding algorithm extracted stretches of LFP that fell within periods of active locomotion, defined as a z-score normalized running speed of greater than 0. These LFP sections were then used for subsequent analysis. For rest box recordings, LFP was selected when the rats were in a state of quiet wakefulness characterized by minimal locomotion and absence of frontal cortical sleep-spindle activity. Multitaper spectral analyses were performed using the Chronux toolbox (Bokil et al., 2010). Directed coherence—which uses autoregressive models of two LFP signals to estimate which signal best predicts the other—was calculated using custom scripts described and published elsewhere (e.g., Baker et al., 2006; Williams et al., 2009). Single units were manually isolated off-line (**Figures 1B,C**) using clustering software (MClust3.5; A.D.Redish, available at http://redishlab.neuroscience.umn.edu/MClust/MClust.html); inclusion criteria were set to isolation distance >15.0 and L-ratio <0.35 (cf. Harris et al., 2001). Putative pyramidal cells were classified on the basis of spike width, waveform and mean firing rate (Jung et al., 1998). Cross-correlograms were computed in Matlab and spike trains shuffle-corrected across trials then normalized by the number of spikes. Autocorrelograms were constructed in the same manner and normalized by the number of spikes.

Peri-stimulus histogram (PSTH) plots were calculated for 2 s pre- and 5 s post-stimulation epochs with mean baseline firing rate calculated from the pre-stimulus period. Firing rates were computed in 100 ms bins ± bootstrapped error estimate. Trial-averaged rate was calculated and smoothed by a Gaussian kernel. The standard deviation of the kernel was set to 0.1 s. Significance in firing rates was determined with a random permutation test performed with a minimum of 10,000 randomizations (cf. Hagan et al., 2012). Significance was assumed when mean ± bootstrapped error estimate was above/below the pre-stimulation baseline firing rate. Cell response characteristics were calculated using automated Matlab scripts and compared using χ^2-tests and One-Way ANOVA with *post-hoc* Tukey's Multiple Comparison Test.

Evoked field potential data were taken from a single tetrode channel and averages created in Spike2 software (Cambridge Electronic Design, UK). Evoked field potential onset latencies were measured from the time of the third and final stimulus of stimulation bursts to avoid contamination by stimulus artefacts (since total burst duration was 6 ms; see **Figure 2A**). Since absolute field potential amplitudes varied between animals, results were normalized and expressed as a percentage of the maximal response size. Response averages were then compared using One-Way ANOVA with *post-hoc* Tukey's Multiple Comparison Test. Data are presented as mean ± s.e.m. unless stated otherwise.

RESULTS

CEREBELLO-PREFRONTAL CONNECTIVITY DURING QUIET REST

We first examined the effects of FN stimulation on LFP in the frontal cortex in rats during quiet rest. In three out of four experiments FN stimulation evoked the largest field potentials at depths of 2.6–3 mm from the cortical surface. This depth range corresponds to PrL (see **Figure 2**). The evoked field potentials had an average onset latency of 13.1 ± 1.1 ms and peak-to-trough amplitude of 0.23 ± 0.12 mV. By comparison, superficially positioned tetrodes recorded evoked field potentials that were ∼60% smaller in size (0.09 ± 0.03 mV; onset latency of 13.2 ± 1.5 ms **Figure 2B**). Recordings from ventral PrL (depth 3.1–3.5 mm) revealed evoked field potentials that were ∼30% smaller than those recorded at 2.6–3 mm (0.16 ± 0.04 mV; onset latency of 13.2 ± 1.6 ms). Although changes in size of LFPs in the cerebral cortex should be interpreted with caution because current source-sink relationships are complex, nonetheless, the systematic variation in field potential amplitude found in the present study raises the possibility that this reflects a preferential physiological connectivity between FN and PrL compared to other areas of frontal cortex that were sampled.

MODULATION OF PREFRONTAL FIRING FOLLOWING FN STIMULATION

Following the discovery of cerebellar-prefrontal connectivity at the field potential level, we next sought to examine whether FN stimulation could modulate the ongoing firing patterns of individual frontal cortical neurons.

The large projection neurons in the cerebellar nuclei can be driven to fire at >100 Hz in slice preparations (Bagnall et al., 2009). Therefore, as an initial step we examined the effect of high frequency FN stimulation (100 Hz, 100 stimuli, 1 s duration, 100 μA) on PrL cell firing rates in the awake, behaving rat. Recordings were made from 20 cells in 3 animals as they sat quietly on an elevated rest platform (see methods for further details) whilst the contralateral FN was stimulated. Of the cells recorded, 50% (10 cells) displayed a decreased firing rate compared to baseline activity (mean baseline firing rate = 5.8 ± 1.2 Hz, see **Table 1**), 5% (1 cell) showed a significant increase, whereas 40% (8 cells) displayed a biphasic response (see **Figure 3**). Only 5% of the sample (1 cell) exhibited no change in firing rate following stimulation.

Consistently rhythmic cell firing was not detected in the awake animal, and FN stimulation did not modulate either auto- or cross-correlations (data not shown), most likely due to stochastic, behavior-dependent PrL firing in the awake, behaving rat (Jung et al., 1998). Therefore, in order to examine the influence of cerebellar stimulation on more stationary frontal cortical firing, we

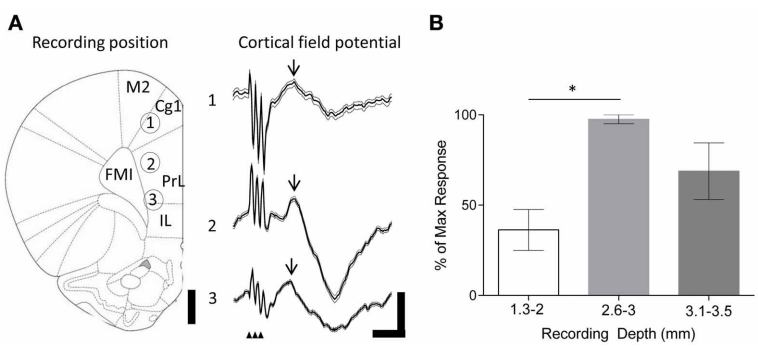

FIGURE 2 | Evoked field potentials in the frontal cortex following FN stimulation in behaving rats. (A) Example experiment illustrating averaged (thick black line) field potentials (72 trials) recorded from tetrodes at different depths in the frontal cortex following stimulation of the FN (recording positions indicated by numbers on rat brain schematic adapted from Paxinos and Watson (2006); small arrowheads indicate timing of FN stimulation artefacts; M2, supplementary motor cortex; Cg1, cingulate cortex; IL, infralimbic cortex. FMI, forceps minor of the corpus callosum); scale bars, 1 mm and 0.1 mV, 20 ms, respectively. Thin gray lines idicates s.e.m. Arrow indicates field potential peak. **(B)** Grouped field potential peak-to-trough amplitudes expressed as a percentage of the maximal reponse size at superficial (1.3–2 mm) and intermediate (2.6–3 mm) and ventral (3.1–3.5 mm) recording positions (* $P < 0.05$; One-Way ANOVA with Tukey's multiple comparison test; $n = 4$; each data point calculated from 72 trials per animal).

Table 1 | Frontal cortex cell responses following FN stimulation.

Cell recording depth/ anaesthetic	# cells	Baseline firing rate (Hz)	% of cells increasing firing only	Max firing rate (%)	Time of max firing rate (s)	% cells decreasing firing only	Minimum firing rate (%)	Time of minimum firing rate (s)	% cells showing biphasic response	% unresponsive cells
<2.5mm (urethane)	55	1.58 ± 0.20	28	460.3 ± 60.8	0.66 ± 0.07s	17	29.3 ± 1.8	1.85 ± 0.15	55	0
2.6-3mm (urethane)	69	1.10 ± 0.12	18	497.4 ± 47.9	1.28 ± 0.15	42	12.4 ± 2.3	1.62 ± 0.13	33	7
2.6-3mm (awake)	20	5.8 ± 1.2	5	148.8 ±12.0	1.63 ± 0.33	50	50 ± 6.4	0.94 ± 0.2	40	5

*P-values between data pairs marked by brackets. One-Way ANOVA with Tukey's multiple comparison test between cells recorded at <2.5 mm depth and those at 2.6–3 mm under anesthesia, and cells recorded between 2.6 and 3 mm in anesthesia and awake states. *P < 0.05; **P < 0.01; ***P < 0.001.*

next examined the result of FN stimulation on putative pyramidal cell firing rates in rats anesthetized with urethane, which induces dominant slow-wave oscillations (cf. Clement et al., 2008) that have been suggested to play an important role in neocortical-cerebellar communication (Ros et al., 2009; Rowland et al., 2010).

Using the same parameters as for awake rats (100 Hz, 100 stimuli, 1 s duration, 100 μA), we found that stimulation of the contralateral FN resulted in a robust but heterogeneous modulation of frontal cortex putative pyramidal cell firing (see **Figure 3** and **Table 1** for comparison of response characteristics). From a total of 55 cells recorded ($n = 5$ rats) in M2 and Cg1 regions of frontal cortex under urethane anesthesia, 27.3% (15 cells) displayed a significant increase in firing rate compared to pre-stimulation baseline activity, whereas 16.4% (9 cells) showed a significant firing rate decrease. A third category of cells (56.3%; 31 cells) showed a biphasic response that generally consisted of a significant firing rate decrease and subsequent increase (see **Table 1**). Cells recorded from tetrodes positioned at depths corresponding to PrL ($n = 8$ rats; 69 cells) were also heterogeneously modulated by the FN stimulation but the overall pattern of responses observed in PrL cells was significantly different to those recorded in M2/Cg1 (PrL cells: 12/69 (17.4%) displayed an increase in firing rate, 29/69 (42 %) displayed a decrease in firing rate, 23/69 (33.3%) showed a biphasic pattern, and 5/69 (7.3%) showed no response (**Figure 3C**, when the proportion of cells in these different categories were compared to those found in M2/Cg1 $\chi^2 = 15.66$, $df = 3$, $^{**}P < 0.01$; see **Table 1**).

Of the cells that responded to FN stimulation with decreases in firing rates, PrL cells showed more profound firing rate reductions than M2/Cg1 cells (to 29.3 ± 1.8% and 12.4 ± 2.3% of baseline respectively; $^{***}P < 0.001$, One-Way ANOVA with Tukey's multiple comparison test; see **Table 1**). Of cells responding with increased firing rates, relative increases were similar in PrL and M2/Cg1 populations (to 497 ± 47.9% and 460 ± 60.8% respectively), though FN stimulation-induced firing peaked more rapidly in M2/Cg1 than in PrL (0.66 ± 0.07 s following stimulation compared to 1.28 ± 0.15 s $^{**}P < 0.01$, One-Way ANOVA with Tukey's multiple comparison test). Overall, these data therefore reflect a complex pattern of modulation, with M2/Cg1 cells tending to respond with a rapid biphasic response and PrL cells typically displaying an initial reduction in firing rate following cerebellar stimulation.

This overall pattern of response did not differ significantly from the equivalent recordings made in awake rats ($\chi^2 = 2.2$, $df = 3$, $P > 0.05$; see **Table 1**). However, compared to recordings made in awake rats, PrL cell firing rate increases/decreases in anesthetized animals were significantly more pronounced following FN stimulation (See **Figure 3** and **Table 1**).

Next, by using auto- and cross- correlogram analyses, we investigated the effect of FN stimulation on the average, coordinated network rhythmicity within the PrL in urethane anesthetized rats. Despite the heterogeneity in PrL cell responses shown in **Figure 3** and **Table 1**, cerebellar stimulation resulted in modulation of ongoing population PrL network activity, as observed in the disruption of slow wave oscillations, and broadening of the central peak in both auto- and cross-correlations (see **Figure 4**). This finding highlights the potential of the cerebellum to influence ongoing network processing in the neocortex and provides further evidence of functional connectivity between the regions.

CEREBELLO- PREFRONTAL COMMUNICATION IN AWAKE RATS

As a first step to understanding cerebello-prefrontal network activity and interactions in behaving animals, we examined

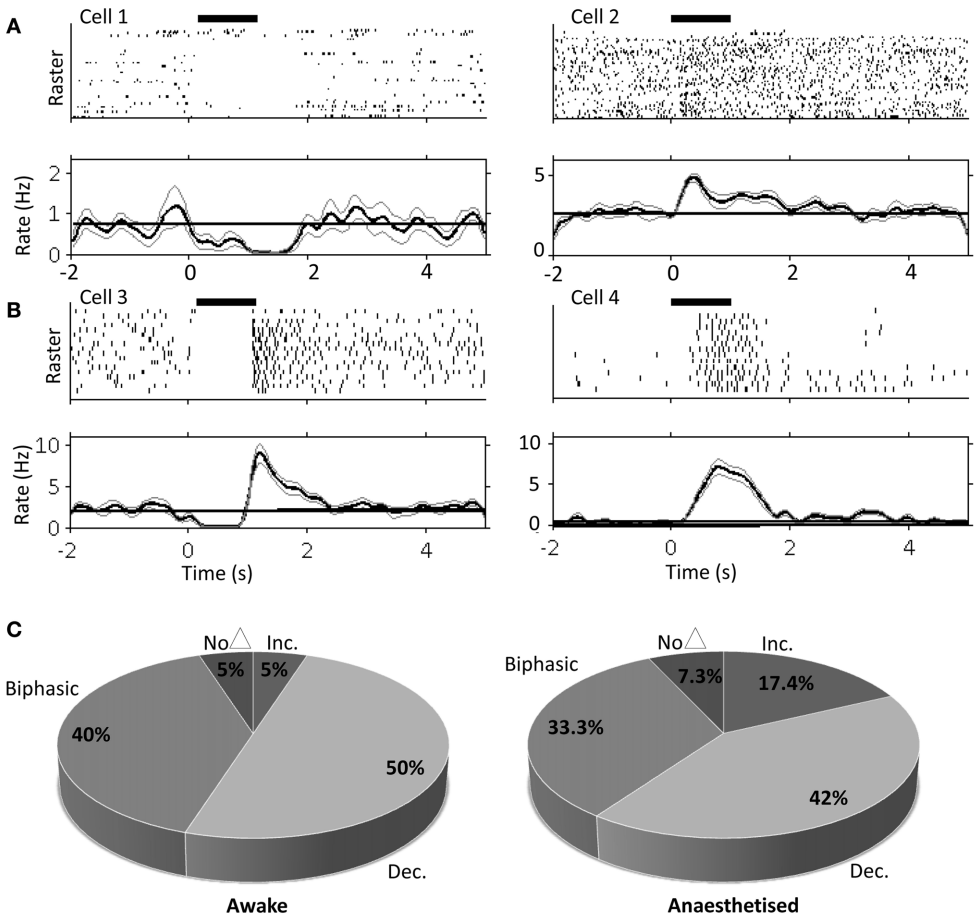

FIGURE 3 | Single unit PrL responses following FN stimulation in awake and urethane anesthetized rats. Raster and peri-stimulus rate plots for example cells recorded in PrL in the awake animal, cells 1 and 2 **(A)** and urethane anesthetized animal, cells 3 and 4 **(B)**. Horizontal black bar indicates duration of stimulation (100 μA; 100 Hz; 1s duration); bold line indicates instantaneous mean firing rate; gray lines indicate bootstrapped error estimate; horizontal line indicates mean baseline firing rate prestimulation; bin size, 100 ms; 17 trials for anesthetized and 33 trials for awake experiments. **(C)** Quantification of PrL cell firing patterns following FN stimulation in awake ($n = 20$ putative pyramidal cells from 3 animals) and anesthetized rats ($n = 69$ putative pyramidal cells from 8 animals).

the covariance of prelimbic cortical and fastigial nucleus LFP signals using Fourier coherence analysis (see methods for further details) during active locomotion in a 1 m diameter open field arena vs. quiet restfulness on a 20 cm platform.

Cerebellar theta power (5–10 Hz) showed a slight increase during active locomotion relative to rest (**Figure 5A** top; FN theta power during rest, 17 ± 1.6 dB; active locomotion, 25 ± 2.3 dB; $P < 0.05$, Wilcoxon rank sum test; $n = 4$ for open field and 5 for rest box recordings), whilst PrL theta power was similar in the two behavioral states (PrL theta during rest, 30 ± 4.8 dB; active locomotion, 29 ± 6.0 dB; $P > 0.05$). Despite these limited power changes, the FN LFP signal was significantly and selectively coherent with PrL oscillations in the theta range (5–10 Hz) only during active locomotion in the open field ($P < 0.05$, arrow in **Figure 5B**), but not while rats were at rest (**Figure 5A**). Consequently, the proportion of total coherence carried at theta frequency (a ratio between 5–10 Hz coherence and coherence at all other frequencies up to 45 Hz) was significantly higher during locomotion (ratio 1.85 ± 0.21) than rest (0.97 ± 0.01; $P < 0.05$, Wilcoxon rank sum).

Since coherence is a measure of consistent phase relationships and does not quantify the direction of interaction between two signals, we also used Granger causality (directed coherence; see methods for details) to infer directionality from the simultaneous FN and PrL LFP recordings (**Figure 5**). Unidirectional theta coherence was significantly weighted in the FN-PrL direction when animals were actively moving in the open field (see **Figure 5B** lower panel; $P < 0.05$ FN-PrL vs. PrL-FN, Wilcoxon rank sum test; $n = 4$). In contrast, theta coherence was no longer significantly directional (FN-PrL and PrL-FN comparision $P > 0.05$) and was significantly lower during rest ($P < 0.05$ vs. active locomotion, Wilcoxon rank sum test).

These coherence analyses provide evidence to suggest that the cerebellar-prefrontal connectivity exemplified by FN stimulation-evoked responses in PFC could subserve cross-structural, network interactions that preferentially manifest at theta frequencies during active behavior.

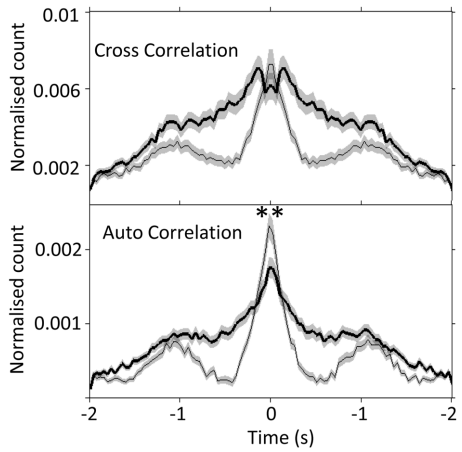

FIGURE 4 | Slow-wave modulation of PrL activity is disrupted by FN stimulation in urethane anesthetized rats. Cross- and auto-correlogram plots (40 ms bins, calculated over 2 s pre/post-stimulation) of all possible PrL cell pair combinations ($n = 69$ cells, 8 rats) during non-stimulated (thin line) and FN stimulation (thick black line) states in urethane anesthetized rats. $^{**}P < 0.01$, paired *t*-test. Note attenuation of slow-wave periodicity during FN stimulation also reported in anesthetized cat (Steriade, 1995).

DISCUSSION

The key findings of the current study are that: (1) stimulation of the FN evokes short latency (∼13 ms) field potentials in PrL alongside changes in frontal cortical neuronal firing rates and rhythmicity and (2) FN and PrL LFP are coherent in the theta (5–10 Hz) frequency range during active locomotion, an effect preferentially driven in the FN-PrL direction. These findings demonstrate physiological interactions between vermal cerebellum and prelimbic cortex in rat and provide insights into the neural dynamics of the reciprocally connected networks underpinning cerebellar-cerebro communication.

CEREBELLAR-PREFRONTAL CONNECTIVITY

Recent physiological evidence from rats indicates the presence of a prefrontal-olivo-cerebellar projection specifically to vermal lobule VII (Watson et al., 2009). In the current study we targeted the fastigial nucleus, the output of vermal lobule VII known to integrate signals from the cerebellar cortical A-zone (e.g., Voogd and Ruigrok, 2004), to examine reciprocal cerebellofugal influence on the prefrontal cortex. Our finding that fastigial stimulation can evoke discrete field potentials in the PrL (**Figure 2**) corroborates previous electrophysiological studies: fastigial nucleus projects to widespread cerebral cortical areas via the ventromedial thalamic nuclei in cat (∼10 ms latency; Steriade, 1995), plus cerebellar dentate nucleus stimulation results in short latency field potential responses in the prefrontal association areas of monkeys (2–4.5 ms latency; Sasaki et al., 1979).

Although we cannot categorically rule out incidental stimulation of neighboring cerebellar nuclei, our histological verification of stimulation sites, inter-animal consistency of LFP and

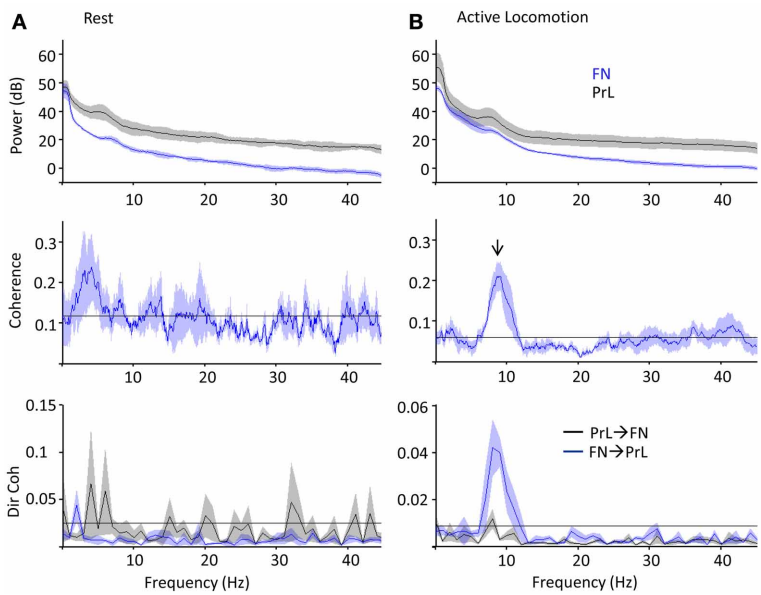

FIGURE 5 | PrL-FN LFP network activity during rest and open field exploration. Grouped power spectra (top panel; cerebellum/FN in blue, prelimbic cortex/PrL in black), coherence (middle panel) and directed coherence (Dir coh, bottom panel; FN-PrL direction in blue, PrL-FN in black) as rats sat quietly on rest platform (**A**, $n = 5$) or actively moved in the open field arena (**B**, 1 Hz bandwidth; $n = 4$). Confidence level at $P = 0.05$ marked by horizontal black lines, shading indicates jack-knife error bars. Arrow indicates significant coherence peak at theta frequency, which was only during active locomotion and preferentially driven in the FN-PrL direction.

comparable results in cat lend weight to the fastigial nucleus constituting a key relay in cerebello-cerebral interactions. The latency observed in the current study (∼13 ms) suggests that the cerebello-prefrontal pathway in rat is relatively slow conducting and/or polysynaptic, presumably involving at least one synaptic relay (most likely within the thalamus), though it is possible that a direct pathway to a frontal subregion other than M2/Cg1/PrL does exist. Alternatively, the shorter latency and faster conduction of the cerebello-prefrontal pathway in non-human primate could reflect evolution of a more rapid, direct line of communication in line with the increasing importance of this pathway in cerebellar contributions to cognitive functions (Ramnani, 2006).

CEREBELLAR MODULATION OF PREFRONTAL FIRING

Electrical stimulation of the fastigial nuclei drives heterogeneous modulation of prefrontal cell firing in both anesthetized and behaving rats. Preliminary findings in awake mice have reported similar frontal responses to cerebellar cortical stimulation, showing reductions in synchronized firing and pauses in cortical cell firing (Liu et al., 2012). Steriade (1995) showed that fastigial stimulation can modulate gamma frequency (∼20–40 Hz) EEG rhythms in the frontal cortex of anesthetized cats (with effects outlasting the duration of stimulus by ∼4–5 s) and cerebellar cortical stimulation has recently been shown to modulate EEG activity recorded over the motor cortex of awake mice (M1, Witter et al., 2013), thus highlighting the presence of multiple cerebello-cortical pathways.

Mittleman et al. (2008) described long lasting (7–8 s) dopamine efflux in the PrL of mice following cerebellar dentate nuclear stimulation and dopamine release may contribute to the effects on PrL found in the present experiments. Primate dorsolateral prefrontal cortex pyramidal neurons express mixed dopamine receptor distributions (Lidow et al., 1991; Muly et al., 1998), and *in vitro* experiments have highlighted the opposing effects that D1 and D2 receptor types exert on prefrontal neuron spiking (Seamans et al., 2001). The heterogeneous effects of fastigial nuclear stimulation on individual pyramidal cell responses summarized in **Table 1** may therefore reflect mixed dopamine receptor subtype expression and/or targeting by dopaminergic afferents.

The pathway(s) through which cerebellar stimulation can influence prefrontal dopamine release are unknown but one potential route includes projections via the thalamic nuclei, which send glutamatergic afferents to the cerebral cortex (Hoover and Vertes, 2007) that in turn form presynaptic inputs to dopamine varicosities within the prefrontal cortex (leading to a slow, neuromodulatory response, Blaha et al., 1997). Alternatively, fastigial stimulation could influence the release of dopamine in the prefrontal cortex via activation of the ventral tegmental area (VTA) through cerebello-VTA or cerebello-thalamo-VTA projections (Kehr et al., 1976; Snider and Maiti, 1976; Snider et al., 1976). The cerebellum may also influence prefrontal firing via the basal ganglia. For example, electrical stimulation of the cerebellar output nuclei (dentate in particular) alters neuronal firing rates (Li and Parker, 1969; Ratcheson and Li, 1969) and dopamine levels in the substantia nigra and caudate nucleus (Nieoullon et al., 1978). Anatomical studies demonstrate disynaptic projections from the cerebellum (dentate) to the basal ganglia in both rat and monkey (Ichinohe et al., 2000; Hoshi et al., 2005). In turn, basal ganglia projections influence prefrontal cortex (e.g., Middleton and Strick, 1994; Maurice et al., 1999; Middleton and Strick, 2002), thus highlighting the basal ganglia as a potential relay between hind- and forebrain.

COHERENT PREFRONTAL-CEREBELLAR LFP DURING BEHAVIOR

Neurobiological oscillations organize activity within and across different brain regions (e.g., Singer, 1999; Varela et al., 2001; Fries, 2005), creating coherent cell assemblies (Harris et al., 2003) and enabling plasticity processes dependent on the precise timing of pre- and post-synaptic activity (Markram et al., 1997; Bi and Poo, 1998; Cassenaer and Laurent, 2007). Coordinated oscillations may therefore support information transfer in cerebro-cerebellar pathways and have been reported across a range of frequencies: cerebellar oscillations phase-lock to neocortical slow waves (0–4 Hz; Ros et al., 2009; Rowland et al., 2010; Schwarz, 2010) and beta oscillations (∼10–25 Hz) bind cerebellar cortical LFP and nuclear cell firing with the somatosensory and motor cortices of primates (Courtemanche and Lamarre, 2005; Soteropoulos and Baker, 2006).

Of particular relevance to the current study are (1) the demonstration by Steriade (1995) that stimulation of cat FN disrupts slow wave activity, a result corroborated by our findings (**Figure 2**) and (2) the additional finding that cerebellar circuits have been shown to support oscillation frequencies within the theta bandwidth (Hartmann and Bower, 1998; D'Angelo et al., 2001; Solinas et al., 2007; Dugué et al., 2009), which could be driven by pacemaker theta rhythmicity within precerebellar nuclei including the inferior olive (Lang et al., 2006; Chorev et al., 2007; Van Der Giessen et al., 2008). Theta rhythmicity in the cerebellar fastigial nuclei may therefore reflect synchronous activation or inhibition in either the olivo-nuclear or olivo-cerebello-nuclear circuitry, and there is evidence that such oscillations synchronize activity within cerebellar hemispheres as well as between cerebellar and cortical/limbic regions (Hartmann and Bower, 1998; O'Connor et al., 2002; Hoffmann and Berry, 2009; Wikgren et al., 2010).

O'Connor et al. (2002) found that LFP activity in whisker-related areas of rat cerebellar cortex and neocortex are coherent at 5–20 Hz during periods of active whisking, and whisker- and eye-movement related activity is found in the rat prefrontal region (Brecht et al., 2004). Coherent cerebellar-cerebro activity may therefore reflect mechanisms through which sensory information can be integrated into ongoing neocortical processes (cf. Bland and Oddie, 2001; O'Connor et al., 2002; Bland, 2004). Our finding that coherence is significantly weighted in the cerebellum-to-PrL direction during epochs of active locomotion (**Figure 5B**) suggests the interaction derives from more than simple co-modulation of cerebellum and PrL during theta-frequency behaviors (e.g., whisking). The directed nature of this coupling may reflect the increased need for sensorimotor input to the neocortex during goal-directed behaviors including active locomotion. In particular, as vestibular information is combined with proprioceptive inputs in the FN to generate appropriate internal estimates of the animal's self motion (Brooks and Cullen,

2009), the cerebellum (FN in particular) may provide functionally relevant proprioceptive/egocentric information that can be integrated into decision making processes recruiting higher order structures such as the PrL.

CONCLUDING COMMENTS

Cerebellar vermal abnormalities are found in a host of psychiatric diseases (Heath et al., 1979, 1982; Okugawa et al., 2007; Lawyer et al., 2009) and can occur concomitantly with changes in the prefrontal cortex of autistic patients (Carper and Courchesne, 2000). Also, chronic cerebellar vermal stimulation in the theta frequency range has been reported to ameliorate the emotional and cognitive symptoms of intractable neurological disorders such as schizophrenia and epilepsy (Cooper, 1973; Cooper et al., 1976; Correa et al., 1980). Abnormalities of the cerebellum, and particularly its vermal region, may therefore contribute to neuro-psychiatric diseases that are typically associated with neocortical malfunction and aberrant dopamine neuromodulation. The present results provide evidence for a physiological framework whose dysfunction could underlie cerebellar contributions to such disorders.

Further work monitoring and manipulating cerebello-cerebral network activity with higher resolution during a range of behavioral states (e.g., with and without explicit cognitive load) is required before we fully appreciate the functional importance of activity in cerebello-prefrontal circuits. However, the current study provides initial evidence that the regions co-participate in distributed network activity and also offers novel insights into the dynamic interaction that occurs between the two structures during exploratory behavior. The potential mechanisms subserving these interactions include synchronized oscillations in the theta frequency, which may be important for sensory acquisition/integration (Bower, 1997; Bland and Oddie, 2001) and/or general cerebellar contributions to goal directed behaviors (Burguière et al., 2010).

AUTHOR CONTRIBUTIONS

T. C. Watson, Richard Apps, and Matthew W. Jones designed research; T. C. Watson performed research; T. C. Watson, N. Becker, and Matthew W. Jones analyzed data; T. C. Watson, Richard Apps, and Matthew W. Jones. wrote the paper.

ACKNOWLEDGMENTS

This work was supported by a Biotechnology and Biological Sciences Research Council (BBSRC) studentship awarded to T. C. Watson and BBSRC grant number BB/G006687/1 to Matthew W. Jones. We thank Rachel Bissett for expert assistance with histology and Professor Stuart Baker (Newcastle University) for kindly providing the Granger Causality analysis script.

REFERENCES

Allen, G., McColl, R., Barnard, H., Ringe, W. K., Fleckenstein, J., and Cullum, C. M. (2005). Magnetic resonance imaging of cerebellar-prefrontal and cerebellar-parietal functional connectivity. *Neuroimage* 28, 39–48. doi: 10.1016/j.neuroimage.2005.06.013

Andreasen, N. C., O'Leary, D. S., Cizadlo, T., Arndt, S., Rezai, K., Ponto, L. L., et al. (1996). Schizophrenia and cognitive dysmetria: a positron-emission tomography study of dysfunctional prefrontal-thalamic-cerebellar circuitry. *Proc. Natl. Acad. Sci. U.S.A.* 93, 9985–9990. doi: 10.1073/pnas.93.18.9985

Andreasen, N. C., and Pierson, R. (2008). The role of the cerebellum in schizophrenia. *Biol. Psychiatry* 64, 81–88. doi: 10.1016/j.biopsych.2008.01.003

Arguello, P. A., Enquist, L. W., and Wang, S. S.-H. (2012). "Long-distance connectivity between prefrontal cortex and cerebellum in mouse," in *Society for Neuroscience* (New Orleans).

Bagnall, M. W., Zingg, B., Sakatos, A., Moghadam, S. H., Zeilhofer, H. U., and du Lac, S. (2009). Glycinergic projection neurons of the cerebellum. *J. Neurosci.* 29, 10104–10110. doi: 10.1523/JNEUROSCI.2087-09.2009

Baker, S. N., Chiu, M., and Fetz, E. E. (2006). Afferent encoding of central oscillations in the monkey arm. *J. Neurophysiol.* 95, 3904–3910. doi: 10.1152/jn.01106.2005

Bi, G. Q., and Poo, M. M. (1998). Synaptic modifications in cultured hippocampal neurons: dependence on spike timing, synaptic strength, and postsynaptic cell type. *J. Neurosci.* 18, 10464–10472.

Blaha, C. D., Yang, C. R., Floresco, S. B., Barr, A. M., and Phillips, A. G. (1997). Stimulation of the ventral subiculum of the hippocampus evokes glutamate receptor-mediated changes in dopamine efflux in the rat nucleus accumbens. *Eur. J. Neurosci.* 9, 902–911. doi: 10.1111/j.1460-9568.1997.tb01441.x

Bland, B. H. (2004). The power of theta: providing insights into the role of the hippocampal formation in sensorimotor integration. *Hippocampus* 14, 537–538. doi: 10.1002/hipo.20027

Bland, B. H., and Oddie, S. D. (2001). Theta band oscillation and synchrony in the hippocampal formation and associated structures: the case for its role in sensorimotor integration. *Behav. Brain Res.* 127, 119–136. doi: 10.1016/S0166-4328(01)00358-8

Bokil, H., Andrews, P., Kulkarni, J. E., Mehta, S., and Mitra, P. P. (2010). Chronux: a platform for analyzing neural signals. *J. Neurosci. Methods* 192, 146–151. doi: 10.1016/j.jneumeth.2010.06.020

Bower, J. M. (1997). Is the cerebellum sensory for motor's sake, or motor for sensory's sake: the view from the whiskers of a rat? *Prog. Brain Res.* 114, 463–496. doi: 10.1016/S0079-6123(08)63381-6

Brecht, M., Krauss, A., Muhammad, S., Sinai-Esfahani, L., Bellanca, S., and Margrie, T. W. (2004). Organization of rat vibrissa motor cortex and adjacent areas according to cytoarchitectonics, microstimulation, and intracellular stimulation of identified cells. *J. Comp. Neurol.* 479, 360–373. doi: 10.1002/cne.20306

Brooks, J. X., and Cullen, K. E. (2009). Multimodal integration in rostral fastigial nucleus provides an estimate of body movement. *J. Neurosci.* 29, 10499–10511. doi: 10.1523/JNEUROSCI.1937-09.2009

Buckner, R. L., Krienen, F. M., Castellanos, A., Diaz, J. C., and Yeo, B. T. (2011). The organization of the human cerebellum estimated by intrinsic functional connectivity. *J. Neurophysiol.* 106, 2322–2345. doi: 10.1152/jn.00339.2011

Burguière, E., Arabo, A., Jarlier, F., De Zeeuw, C. I., and Rondi-Reig, L. (2010). Role of the cerebellar cortex in conditioned goal-directed behavior. *J. Neurosci.* 30, 13265–13271. doi: 10.1523/JNEUROSCI.2190-10.2010

Carper, R. A., and Courchesne, E. (2000). Inverse correlation between frontal lobe and cerebellum sizes in children with autism. *Brain* 123(Pt 4), 836–844. doi: 10.1093/brain/123.4.836

Cassenaer, S., and Laurent, G. (2007). Hebbian STDP in mushroom bodies facilitates the synchronous flow of olfactory information in locusts. *Nature* 448, 709–713. doi: 10.1038/nature05973

Chorev, E., Yarom, Y., and Lampl, I. (2007). Rhythmic episodes of subthreshold membrane potential oscillations in the rat inferior olive nuclei *in vivo*. *J. Neurosci.* 27, 5043–5052. doi: 10.1523/JNEUROSCI.5187-06.2007

Clement, E. A., Richard, A., Thwaites, M., Ailon, J., Peters, S., and Dickson, C. T. (2008). Cyclic and sleep-like spontaneous alternations of brain state under urethane anaesthesia. *PLoS ONE* 3:e2004. doi: 10.1371/journal.pone.0002004

Cooper, I. S. (1973). Effect of chronic stimulation of anterior cerebellum on neurological disease. *Lancet* 1, 206. doi: 10.1016/S0140-6736(73)90042-1

Cooper, I. S., Amin, I., Riklan, M., Waltz, J. M., and Poon, T. P. (1976). Chronic cerebellar stimulation in epilepsy. Clinical and anatomical studies. *Arch. Neurol.* 33, 559–570. doi: 10.1001/archneur.1976.00500080037006

Correa, A. J., Llewellyn, R. C., Epps, J., Jarrott, D., Eiswirth, C., and Heath, R. G. (1980). Chronic cerebellar stimulation in the modulation of behavior. *Acta Neurol. Latinoam.* 26, 143–153.

Courtemanche, R., and Lamarre, Y. (2005). Local field potential oscillations in primate cerebellar cortex: synchronization with cerebral cortex during active and passive expectancy. *J. Neurophysiol.* 93, 2039–2052. doi: 10.1152/jn.00080.2004

D'Angelo, E., Nieus, T., Maffei, A., Armano, S., Rossi, P., Taglietti, V., et al. (2001). Theta-frequency bursting and resonance in cerebellar granule cells:

experimental evidence and modeling of a slow k+-dependent mechanism. *J. Neurosci.* 21, 759–770.

Demirtas-Tatlidede, A., Freitas, C., Cromer, J. R., Safar, L., Ongur, D., Stone, W. S., et al. (2010). Safety and proof of principle study of cerebellar vermal theta burst stimulation in refractory schizophrenia. *Schizophr. Res.* 124, 91–100. doi: 10.1016/j.schres.2010.08.015

Dugué, G. P., Brunel, N., Hakim, V., Schwartz, E., Chat, M., Lévesque, M., et al. (2009). Electrical coupling mediates tunable low-frequency oscillations and resonance in the cerebellar Golgi cell network. *Neuron* 61, 126–139. doi: 10.1016/j.neuron.2008.11.028

Fatemi, S. H., Aldinger, K. A., Ashwood, P., Bauman, M. L., Blaha, C. D., Blatt, G. J., et al. (2012). Consensus paper: pathological role of the cerebellum in autism. *Cerebellum* 11, 777–807. doi: 10.1007/s12311-012-0355-9

Fries, P. (2005). A mechanism for cognitive dynamics: neuronal communication through neuronal coherence. *Trends Cogn. Sci.* 9, 474–480. doi: 10.1016/j.tics.2005.08.011

Gray, C. M. (1994). Synchronous oscillations in neuronal systems: mechanisms and functions. *J. Comput. Neurosci.* 1, 11–38. doi: 10.1007/BF00962716

Hagan, M. A., Dean, H. L., and Pesaran, B. (2012). Spike-field activity in parietal area LIP during coordinated reach and saccade movements. *J. Neurophysiol.* 107, 1275–90. doi: 10.1152/jn.00867.2011

Harris, K. D., Csicsvari, J., Hirase, H., Dragoi, G., and Buzsáki, G. (2003). Organization of cell assemblies in the hippocampus. *Nature* 424, 552–556. doi: 10.1038/nature01834

Harris, K. D., Hirase, H., Leinekugel, X., Henze, D. A., and Buzsáki, G. (2001). Temporal interaction between single spikes and complex spike bursts in hippocampal pyramidal cells. *Neuron* 32, 141–149. doi: 10.1016/S0896-6273(01)00447-0

Hartmann, M. J., and Bower, J. M. (1998). Oscillatory activity in the cerebellar hemispheres of unrestrained rats. *J. Neurophysiol.* 80, 1598–1604.

Heath, R. G. (1977). Modulation of emotion with a brain pacemamer. Treatment for intractable psychiatric illness. *J. Nerv. Ment. Dis.* 165, 300–317. doi: 10.1097/00005053-197711000-00002

Heath, R. G., Franklin, D. E., and Shraberg, D. (1979). Gross pathology of the cerebellum in patients diagnosed and treated as functional psychiatric disorders. *J. Nerv. Ment. Dis.* 167, 585–592. doi: 10.1097/00005053-197910000-00001

Heath, R. G., Franklin, D. E., Walker, C. F., and Keating, J. W. (1982). Cerebellar vermal atrophy in psychiatric patients. *Biol. Psychiatry* 17, 569–583.

Henze, R., Brunner, R., Thiemann, U., Parzer, P., Richterich, A., Essig, M., et al. (2011). Gray matter alterations in first-admission adolescents with schizophrenia. *J. Neuroimaging* 21, 241–246. doi: 10.1111/j.1552-6569.2010.00504.x

Hoffmann, L. C., and Berry, S. D. (2009). Cerebellar theta oscillations are synchronized during hippocampal theta-contingent trace conditioning. *Proc. Natl. Acad. Sci. U.S.A.* 106, 21371–21376. doi: 10.1073/pnas.0908403106

Hoover, W. B., and Vertes, R. P. (2007). Anatomical analysis of afferent projections to the medial prefrontal cortex in the rat. *Brain Struct. Funct.* 212, 149–179. doi: 10.1007/s00429-007-0150-4

Hoshi, E., Tremblay, L., Feger, J., Carras, P. L., and Strick, P. L. (2005). The cerebellum communicates with the basal ganglia. *Nat. Neurosci.* 8, 1491–1493. doi: 10.1038/nn1544

Ichinohe, N., Mori, F., and Shoumura, K. (2000). A di-synaptic projection from the lateral cerebellar nucleus to the laterodorsal part of the striatum via the central lateral nucleus of the thalamus in the rat. *Brain Res.* 880, 191–197. doi: 10.1016/S0006-8993(00)02744-X

Jung, M. W., Qin, Y., McNaughton, B. L., and Barnes, C. A. (1998). Firing characteristics of deep layer neurons in prefrontal cortex in rats performing spatial working memory tasks. *Cereb. Cortex* 8, 437–450. doi: 10.1093/cercor/8.5.437

Kehr, W., Lindqvist, M., and Carlsson, A. (1976). Distribution of dopamine in the rat cerebral cortex. *J. Neural Transm.* 38, 173–180. doi: 10.1007/BF01249437

Kelly, R. M., and Strick, P. L. (2003). Cerebellar loops with motor cortex and prefrontal cortex of a nonhuman primate. *J. Neurosci.* 23, 8432–8444.

Krienen, F. M., and Buckner, R. L. (2009). Segregated fronto-cerebellar circuits revealed by intrinsic functional connectivity. *Cereb. Cortex* 19, 2485–2497. doi: 10.1093/cercor/bhp135

Lang, E. J., Sugihara, I., and Llinás, R. (2006). Olivocerebellar modulation of motor cortex ability to generate vibrissal movements in rat. *J. Physiol.* 571, 101–120. doi: 10.1113/jphysiol.2005.102764

Lawyer, G., Nesvåg, R., Varnäs, K., Okugawa, G., and Agartz, I. (2009). Grey and white matter proportional relationships in the cerebellar vermis altered in schizophrenia. *Cerebellum* 8, 52–60. doi: 10.1007/s12311-008-0071-7

Li, C. L., and Parker, L. O. (1969). Effect of dentate stimulation on neuronal activity in the globus pallidus. *Exp. Neurol.* 24, 298–309. doi: 10.1016/0014-4886(69)90023-5

Lidow, M. S., Goldman-Rakic, P. S., Gallager, D. W., and Rakic, P. (1991). Distribution of dopaminergic receptors in the primate cerebral cortex: quantitative autoradiographic analysis using [3H]raclopride, [3H]spiperone and [3H]SCH23390. *Neuroscience* 40, 657–671. doi: 10.1016/0306-4522(91)90003-7

Liu, Y., Blaha, C. D., Mittleman, G., Goldowitz, D., and Heck, D. H. (2012). "Cerebellar modulation of neuronal activity in mouse prefrontal cortex," in *Society For Neuroscience* (New Orleans).

Markram, H., Lübke, J., Frotscher, M., and Sakmann, B. (1997). Regulation of synaptic efficacy by coincidence of postsynaptic APs and EPSPs. *Science* 275, 213–215. doi: 10.1126/science.275.5297.213

Maurice, N., Deniau, J. M., Glowinski, J., and Thierry, A. M. (1999). Relationships between the prefrontal cortex and the basal ganglia in the rat: physiology of the cortico-nigral circuits. *J. Neurosci.* 19, 4674–81.

Middleton, F. A., and Strick, P.L. (2002). Basal ganglia 'projections' to the prefrontal cortex of the primate. *Cereb. Cortex.* 12, 926–35. doi: 10.1093/cercor/12.9.926

Middleton, F. A., and Strick, P. L. (1994). Anatomical evidence for cerebellar and basal ganglia involvement in higher cognitive function. *Science* 266, 456–61. doi: 10.1126/science.7939688

Middleton, F. A., and Strick, P. L. (2001). Cerebellar projections to the prefrontal cortex of the primate. *J. Neurosci.* 21, 700–712.

Mittleman, G., Goldowitz, D., Heck, D. H., and Blaha, C. D. (2008). Cerebellar modulation of frontal cortex dopamine efflux in mice: relevance to autism and schizophrenia. *Synapse* 62, 544–550. doi: 10.1002/syn.20525

Muly, E. C., Szigeti, K., and Goldman-Rakic, P. S. (1998). D1 receptor in interneurons of macaque prefrontal cortex: distribution and subcellular localization. *J. Neurosci.* 18, 10553–10565.

Nieoullon, A., Cheramy, A., and Glowinski, J. (1978). Release of dopamine in both caudate nuclei and both substantia nigrae in response to unilateral stimulation of cerebellar nuclei in the cat. *Brain Res.* 148, 143–152. doi: 10.1016/0006-8993(78)90384-0

O'Connor, S. M., Berg, R. W., and Kleinfeld, D. (2002). Coherent electrical activity between vibrissa sensory areas of cerebellum and neocortex is enhanced during free whisking. *J. Neurophysiol.* 87, 2137–2148. doi: 10.1152/jn.00229.2001

Okugawa, G., Nobuhara, K., Takase, K., and Kinoshita, T. (2007). Cerebellar posterior superior vermis and cognitive cluster scores in drug-naive patients with first-episode schizophrenia. *Neuropsychobiology* 56, 216–219. doi: 10.1159/000122268

O'Reilly, J. X., Beckmann, C. F., Tomassini, V., Ramnani, N., and Johansen-Berg, H. (2010). Distinct and overlapping functional zones in the cerebellum defined by resting state functional connectivity. *Cereb. Cortex* 20, 953–965. doi: 10.1093/cercor/bhp157

Paxinos, G., and Watson, C. (2006). *The Rat Brain in Stereotaxic Coordinates, 6th Edn.* New York, NY: Academic.

Ramnani, N. (2006). The primate cortico-cerebellar system: anatomy and function. *Nat. Rev. Neurosci.* 7, 511–522. doi: 10.1038/nrn1953

Ratcheson, R. A., and Li, C. L. (1969). Effect of dentate stimulation on neuronal activity in the caudate nucleus. *Exp. Neurol.* 25, 268–281. doi: 10.1016/0014-4886(69)90050-8

Rochefort, C., Arabo, A., André, M., Poucet, B., Save, E., and Rondi-Reig, L. (2011). Cerebellum shapes hippocampal spatial code. *Science* 334, 385–389. doi: 10.1126/science.1207403

Ros, H., Sachdev, R. N., Yu, Y., Sestan, N., and McCormick, D. A. (2009). Neocortical networks entrain neuronal circuits in cerebellar cortex. *J. Neurosci.* 29, 10309–10320. doi: 10.1523/JNEUROSCI.2327-09.2009

Rowland, N. C., Goldberg, J. A., and Jaeger, D. (2010). Cortico-cerebellar coherence and causal connectivity during slow-wave activity. *Neuroscience* 166, 698–711. doi: 10.1016/j.neuroscience.2009.12.048

Sasaki, K., Jinnai, K., Gemba, H., Hashimoto, S., and Mizuno, N. (1979). Projection of the cerebellar dentate nucleus onto the frontal association cortex in monkeys. *Exp. Brain Res.* 37, 193–198. doi: 10.1007/BF01474266

Schmahmann, J. D. (2004). Disorders of the cerebellum: ataxia, dysmetria of thought, and the cerebellar cognitive affective syndrome. *J. Neuropsychiatry Clin. Neurosci.* 16, 367–378. doi: 10.1176/appi.neuropsych.16.3.367

Schwarz, C. (2010). The fate of spontaneous synchronous rhythms on the cerebro-cerebellar loop. *Cerebellum* 9, 77–87. doi: 10.1007/s12311-009-0143-3

Seamans, J. K., Gorelova, N., Durstewitz, D., and Yang, C. R. (2001). Bidirectional dopamine modulation of GABAergic inhibition in prefrontal cortical pyramidal neurons. *J. Neurosci.* 21, 3628–3638.

Singer, W. (1999). Neuronal synchrony: a versatile code for the definition of relations? *Neuron* 24, 49–65, 111–125. doi: 10.1016/S0896-6273(00)80821-1

Snider, R. S., and Maiti, A. (1976). Cerebellar contributions to the Papez circuit. *J. Neurosci. Res.* 2, 133–146. doi: 10.1002/jnr.490020204

Snider, R. S., Maiti, A., and Snider, S. R. (1976). Cerebellar pathways to ventral midbrain and nigra. *Exp. Neurol.* 53, 714–728. doi: 10.1016/0014-4886(76)90150-3

Solinas, S., Forti, L., Cesana, E., Mapelli, J., De Schutter, E., and D'Angelo, E. (2007). Fast-reset of pacemaking and theta-frequency resonance patterns in cerebellar golgi cells: simulations of their impact *in vivo*. *Front. Cell Neurosci.* 1:4. doi: 10.3389/neuro.03.004.2007

Soteropoulos, D. S., and Baker, S. N. (2006). Cortico-cerebellar coherence during a precision grip task in the monkey. *J. Neurophysiol.* 95, 1194–1206. doi: 10.1152/jn.00935.2005

Steriade, M. (1995). Two channels in the cerebellothalamocortical system. *J. Comp. Neurol.* 354, 57–70. doi: 10.1002/cne.903540106

Stoodley, C. J. (2012). The cerebellum and cognition: evidence from functional imaging studies. *Cerebellum* 11, 352–365. doi: 10.1007/s12311-011-0260-7

Stoodley, C. J., and Schmahmann, J. D. (2010). Evidence for topographic organization in the cerebellum of motor control versus cognitive and affective processing. *Cortex* 46, 831–844. doi: 10.1016/j.cortex.2009.11.008

Strick, P. L., Dum, R. P., and Fiez, J. A. (2009). Cerebellum and nonmotor function. *Annu. Rev. Neurosci.* 32, 413–434. doi: 10.1146/annurev.neuro.31.060407.125606

Suzuki, L., Coulon, P., Sabel-Goedknegt, E. H., and Ruigrok, T. J. (2012). Organization of cerebral projections to identified cerebellar zones in the posterior cerebellum of the rat. *J. Neurosci.* 32, 10854–10869. doi: 10.1523/JNEUROSCI.0857-12.2012

Van Der Giessen, R. S., Koekkoek, S. K., van Dorp, S., De Gruijl, J. R., Cupido, A., Khosrovani, S., et al. (2008). Role of olivary electrical coupling in cerebellar motor learning. *Neuron* 58, 599–612. doi: 10.1016/j.neuron.2008.03.016

Varela, F., Lachaux, J. P., Rodriguez, E., and Martinerie, J. (2001). The brainweb: phase synchronization and large-scale integration. *Nat. Rev. Neurosci.* 2, 229–239. doi: 10.1038/35067550

Voogd, J., and Ruigrok, T. J. (2004). The organization of the corticonuclear and olivocerebellar climbing fiber projections to the rat cerebellar vermis: the congruence of projection zones and the zebrin pattern. *J. Neurocytol.* 33, 5–21. doi: 10.1023/B:NEUR.0000029645.72074.2b

Watson, T. C., Jones, M. W., and Apps, R. (2009). Electrophysiological mapping of novel prefrontal—cerebellar pathways. *Front. Integr. Neurosci.* 3:18. doi: 10.3389/neuro.07.018.2009

Wikgren, J., Nokia, M. S., and Penttonen, M. (2010). Hippocampo-cerebellar theta band phase synchrony in rabbits. *Neuroscience* 165, 1538–1545. doi: 10.1016/j.neuroscience.2009.11.044

Williams, E. R., Soteropoulos, D. S., and Baker, S. N. (2009). Coherence between motor cortical activity and peripheral discontinuities during slow finger movements. *J. Neurophysiol.* 102, 1296–1309. doi: 10.1152/jn.90996.2008

Witter, L., Canto, C. B., Hoogland, T. M., de Gruijl, J. R., and De Zeeuw, C. I. (2013). Strength and timing of motor responses mediated by rebound firing in the cerebellar nuclei after Purkinje cell activation. *Front. Neural Circuits* 7:133. doi: 10.3389/fncir.2013.00133

Conflict of Interest Statement: The authors declare that the research was conducted in the absence of any commercial or financial relationships that could be construed as a potential conflict of interest.

Received: 30 October 2013; accepted: 08 January 2014; published online: 04 February 2014.

Citation: Watson TC, Becker N, Apps R and Jones MW (2014) Back to front: cerebellar connections and interactions with the prefrontal cortex. Front. Syst. Neurosci. ***8****:4. doi: 10.3389/fnsys.2014.00004*

This article was submitted to the journal Frontiers in Systems Neuroscience.

frontiers in
SYSTEMS NEUROSCIENCE

ORIGINAL RESEARCH ARTICLE
published: 15 September 2014
doi: 10.3389/fnsys.2014.00145

Diurnal influences on electrophysiological oscillations and coupling in the dorsal striatum and cerebellar cortex of the anesthetized rat

Ariana Frederick[1,2], Jonathan Bourget-Murray[1,3], C. Andrew Chapman[1,4], Shimon Amir[1,4] and Richard Courtemanche[1,5]*

[1] *Center for Studies in Behavioral Neurobiology/FRQS Groupe de Recherche en Neurobiologie Comportementale, Concordia University, Montreal, QC, Canada*
[2] *Department of Biology, Concordia University, Montreal, QC, Canada*
[3] *M.D., C.M. Program, Faculty of Medicine, McGill University, Montreal, QC, Canada*
[4] *Department of Psychology, Concordia University, Montreal, QC, Canada*
[5] *Department of Exercise Science, Concordia University, Montreal, QC, Canada*

Edited by:
Thomas C. Watson, University of Bristol, UK

Reviewed by:
Nadia Cerminara, University of Bristol, UK
Daniela Popa, Institut de Biologie de l'Ecole Normale Supérieure, France

****Correspondence:***
Richard Courtemanche, Center for Studies in Behavioral Neurobiology/FRQS Groupe de Recherche en Neurobiologie Comportementale, Concordia University, SP-165-03, 7141 Sherbrooke Street West, Montréal, QC H4B 1R6, Canada
e-mail: richard.courtemanche@concordia.ca

Circadian rhythms modulate behavioral processes over a 24 h period through clock gene expression. What is largely unknown is how these molecular influences shape neural activity in different brain areas. The clock gene *Per2* is rhythmically expressed in the striatum and the cerebellum and its expression is linked with daily fluctuations in extracellular dopamine levels and D2 receptor activity. Electrophysiologically, dopamine depletion enhances striatal local field potential (LFP) oscillations. We investigated if LFP oscillations and synchrony were influenced by time of day, potentially via dopamine mechanisms. To assess the presence of a diurnal effect, oscillatory power and coherence were examined in the striatum and cerebellum of rats under urethane anesthesia at four different times of day zeitgeber time (ZT1, 7, 13 and 19—indicating number of hours after lights turned on in a 12:12 h light-dark cycle). We also investigated the diurnal response to systemic raclopride, a D2 receptor antagonist. Time of day affected the proportion of LFP oscillations within the 0–3 Hz band and the 3–8 Hz band. In both the striatum and the cerebellum, slow oscillations were strongest at ZT1 and weakest at ZT13. A 3–8 Hz oscillation was present when the slow oscillation was lowest, with peak 3–8 Hz activity occurring at ZT13. Raclopride enhanced the slow oscillations, and had the greatest effect at ZT13. Within the striatum and with the cerebellum, 0–3 Hz coherence was greatest at ZT1, when the slow oscillations were strongest. Coherence was also affected the most by raclopride at ZT13. Our results suggest that neural oscillations in the cerebellum and striatum, and the synchrony between these areas, are modulated by time of day, and that these changes are influenced by dopamine manipulation. This may provide insight into how circadian gene transcription patterns influence network electrophysiology. Future experiments will address how these network alterations are linked with behavior.

Keywords: local field potential oscillation, coherence, dopamine, circadian, urethane

INTRODUCTION

Local field potential (LFP) oscillations are recorded when rhythmic fluctuations in membrane potentials synchronize within a nearby group of cells. These oscillations can provide a mechanism for the storage and transfer of information by coordinating the neuronal activity between distant networks (Başar et al., 2001; Buehlmann and Deco, 2010; Uhlhaas et al., 2010). The many ion channels involved in maintaining the membrane potential and in generating post-synaptic potentials, along with neurotransmitter modulation, influence the dominant oscillatory parameters within neural networks (Hutcheon and Yarom, 2000; Buzsáki and Draguhn, 2004). In the suprachiasmatic nucleus (SCN), a strong influence on many of these cellular processes is the circadian expression of proteins that regulate neuron function and local neural network connections (Herzog, 2007; Colwell, 2011). Circadian protein expression shows distinct phase relationships throughout widespread areas of the brain, including the striatum and cerebellum (Namihira et al., 1999; Rath et al., 2012; Harbour et al., 2013), however, little is known about the role of circadian protein expression in regulating neuron function in these areas. In this paper, we examine how striatal and cerebellar networks may be under the influence of circadian rhythms. The role of the cerebellum in the context of circadian rhythms has scarcely been studied, however it has been shown to share a role with the dorsal striatum in regulating locomotor activity patterns under restricted feeding, a behavior that is modified by circadian genes

(Mendoza et al., 2010; Verwey and Amir, 2012). Furthermore, there is an interest in the subcortical connectivity between these two areas and their cooperative contributions to motor control (Middleton and Strick, 2000; Bostan and Strick, 2010). In order to understand the neurophysiological changes associated with the circadian modulation influencing the striatum and cerebellum, we simultaneously recorded LFPs in these two areas and examined concurrent oscillations and their coherence.

Within the striatal networks, and the granule cell layer of the posterior lobe of the cerebellum of rats and primates, LFP oscillations around 5–30 Hz are present during a variety of tasks (Courtemanche et al., 2002, 2013; Berke et al., 2004; DeCoteau et al., 2007b). These oscillations, and their synchrony with more distant brain areas, are modulated under behavioral conditions such as sensorimotor associations, learning, reward expectancy and sleep (Destexhe et al., 1999; Steriade, 2003; Buzsáki, 2006; Thorn and Graybiel, 2014). Anesthetics, such as urethane, shape the LFPs of cortical and subcortical structures into predominant slow wave activity, inducing a sleep-like state in the LFP that shows widespread synchrony across many brain areas (Magill et al., 2004; Clement et al., 2008; Ros et al., 2009; Sharma et al., 2010). In this study, we used this oscillation-permissive state to evaluate the circadian expression of oscillatory network activity.

Both under anesthesia and in awake behaving animals, dopamine changes can induce important modifications to striatal oscillations (Walters et al., 2007; Lemaire et al., 2012). Dopamine depletion causes an increase in the power of oscillations below 30 Hz and an increase in coherence of these oscillations with the cerebral cortex and throughout the basal ganglia (Brown et al., 2001; Sharott et al., 2005). This is accompanied by a decrease in power of the oscillations above 70 Hz. Results from animal models that use dopamine antagonists or midbrain dopaminergic lesions are consistent with the findings in Parkinson's disease in humans, where abnormal oscillations can be normalized with dopamine agonists or dopamine-related treatments such as L-DOPA (Brown et al., 2001; Rivlin-Etzion et al., 2006; Ballion et al., 2009), further demonstrating the specific role of dopamine in modulating striatal oscillations.

The dopaminergic system is under the influence of circadian rhythmicity. Endogenous extracellular dopamine levels show cyclic fluctuations throughout the day and peak during the middle of the dark phase in rodents (Owasoyo et al., 1979; Hood et al., 2010; Ferris et al., 2014). Furthermore, activation of D2 dopamine receptors has been linked with normal expression of *Per*2, one of the core circadian genes, in the rat dorsal striatum (Hood et al., 2010; Gravotta et al., 2011). *Per2* is involved in regulating daily physiological and behavioral cycles and is found in most tissues throughout the body (Albrecht et al., 2007). However, it is unclear how its rhythmic expression leads to such behavioral changes. Vesicle transporter activity throughout the brain (Darna et al., 2009) and changes in hippocampal synaptic plasticity (Chaudhury et al., 2005) exhibit diurnal variations; similarly, modulation of neurotransmitter function by the circadian clock provide potential ways through which circadian molecular mechanisms may be translated into diurnal electrophysiological and behavioral changes.

A limited number of studies have assessed the electrophysiological correlates of the circadian cycle downstream of the SCN, the master circadian clock, or its direct connections (Guilding and Piggins, 2007). Mordel et al. (2013) assessed diurnal variations of *in vitro* Purkinje cell firing and spontaneous inhibitory post-synaptic potentials, but they found that these measures were not modulated in a circadian manner. Restrictive feeding influences the rhythm of *Per*2 expression in the Purkinje and granule cell layers (Mendoza et al., 2010). There is limited evidence that dopamine levels are also rhythmic in the cerebellum (Owasoyo et al., 1979) but little more is known about circadian modulation of cerebellar physiology; including the functional role of clock genes or their regulatory mechanisms. Clock gene expression may help to organize the activity of striatal and cerebellar networks through mechanisms that affect the generation and synchronization of LFP oscillations. Such oscillations, recorded under urethane anesthesia, can provide information about the local activity and the neural synchronization between distant brain structures.

The purpose of this study was to determine if there are diurnal changes in LFP oscillations and coherence in the rat dorsal striatum and cerebellar cortex. Furthermore, since *Per*2 rhythms in the striatum are responsive to D2 receptor antagonists and not D1 antagonists (Hood et al., 2010), we also explored the effects of raclopride, a D2 antagonist, at different times of day. Given the endogenous rhythm of dopamine in the striatum, we hypothesized that circadian electrophysiological correlates would be expressed through diurnal changes. These changes could be seen in the potency of the LFP oscillations in each area, and in their synchrony. The basal ganglia and cerebellum show a cooperative role in sensorimotor control (Doya, 2000), and in their regulation of locomotor activity patterns related to circadian timing. These areas can interact through the cerebral cortex (Middleton and Strick, 2000) and via subcortical pathways (Ichinohe et al., 2000; Hoshi et al., 2005; Bostan et al., 2010; Bostan and Strick, 2010). In order to identify their network interactions, we thus measured the LFP coherence between distant electrodes (DeCoteau et al., 2007a; Thorn et al., 2010; Frederick et al., 2013). The variables thus sought were the diurnal effects in (1) the power of LFP oscillations; (2) the LFP coherence within and across the striatum and cerebellar cortex; and also (3) if raclopride would induce an alteration in the circadian pattern of oscillations or coherence.

MATERIALS AND METHODS

ANIMALS

Sixteen Sprague-Dawley male rats (Charles River, St-Constant, QC) 300–400 g in size were used for the experiment. Rats were housed separately in cages equipped with running wheels and kept in individual lightproof and sound-attenuated cabinets. Prior to electrophysiological recordings, rats were maintained on a 12:12 h light-dark cycle for a minimum of 2 weeks. Rats were assigned randomly to groups designated by four different target experimental times, corresponding to zeitgeber time (ZT) 1, 7, 13 and 19, where ZT0 represents when lights were turned on and ZT12 when lights were turned off. Light cycles were

adjusted for each animal so that the target experimental time occurred at 1:30 pm for all animals. Environmental conditions were maintained at a constant temperature and rats were provided *ad libitum* access to tap water and laboratory chow throughout the entire entrainment period. To confirm that rats had adjusted to their light cycles, wheel-running activity was monitored continuously using the VitalView software (Mini Mitter, Bend, OR). All experimental procedures followed the guidelines of the Canadian Council on Animal Care and were approved by the Concordia University Animal Research Ethics Committee.

DRUG TREATMENT AND RECORDINGS

Surgical preparation for each animal was scheduled such that the animal's targeted circadian time occurred mid-way through the electrophysiological recording session. LFP recordings were obtained both before and after administration of raclopride. At the start of the recording procedures (ZT time − ∼4 h) the rats were anesthetized with a 5% isoflurane and 95% oxygen mixture until placement of a catheter into the jugular vein. They were then transferred to urethane anesthesia (0.8 g/ml), introduced through the jugular catheter in 1.0 ml boluses as needed. Verification of depth of anesthesia was monitored throughout the experiment by lack of a foot-pinch reflex. In 11 animals, transcardial heartbeat signals were also recorded along with LFPs using subdermal electrodes inserted at the level of the axillar forelimb fossa. Rats were placed in a stereotaxic apparatus and body temperature was maintained at 37°C, monitored by a rectal thermometer. Throughout the experiment, the eyes of the animal were covered to prevent light exposure from influencing changes in the SCN.

Four pairs of tungsten microelectrodes (1.0–1.2 MΩ; FHC, Bowdoin, ME) were used, and the difference in depth within each pair of electrodes was set to 0.5 mm. Electrodes were attached to microdrives, held by 2 modified head stages one for the striatal electrodes and one for the cerebellar electrodes, which were anchored to the stereotaxic apparatus by custom built arms. Two pairs of striatal electrodes were used, one placed in the medial dorsal striatum [0.48 mm AP, 1.40 mm ML, 4.70 mm DV; (Paxinos and Watson, 1998)] and another placed in the lateral dorsal striatum (0.48 mm AP, 5.40 mm ML, 5.00 mm DV). Two pairs of electrodes were also inserted into the cerebellar cortex, separated by approximately 2 mm, in the contralateral Crus2 or Paramedian lobule of the cerebellar cortex. Access to Crus2/Paramedian lobule was gained through a craniotomy roughly 2.5 mm in diameter in the occipital bone, located 2–3 mm lateral from the midline. Crus2 was then identified visually and electrodes were inserted at a 45° angle to a depth of about 0.5 mm. The electrode position was adjusted until the granule cell layer was identified by characteristic multiunit activity and LFP oscillatory activity was identified on an oscilloscope. The 0.5 mm distance between electrodes within a pair suggests that both electrodes were not necessarily in the granule cell layer; this distance allowed for a comparison of nearby circuit activity with a strong granule cell layer influence, given the density of the granule cell layer and the electrode impedance. The nearby comparison could then be contrasted with the 2 mm distance of the second pair. All signals were grounded to stainless steel screws anchored to the skull on the contralateral side and referenced to a 16 gauge circular steel wire placed either in the cerebral cortex approximately 5 mm posterior to the striatal electrodes or on the unrecorded side of the cerebellum.

Electrophysiological signals were collected with a Neuralynx Cheetah system (Neuralynx, Bozeman, MT) at a sampling rate of 30,300 Hz and band-pass filtered between 0.1 and 9000 Hz. LFPs were then extracted from this signal with a 300-Hz low-pass filter. A typical recording session began with a first set of recordings, including 5 samples of 120 s separated by an interval of 90 s without recording, following which raclopride tartrate (Sigma-Aldrich, Oakville, ON) was administered via intraperitoneal injection (1 mg/kg dissolved in distilled water at 1 μg/ml). After a 15 min waiting period, 5 additional 120 s samples were recorded. Raclopride was administered at a dosage shown to induce akinesia and prevent operant conditioning, and to have effects on neural activity in the striatum as early as 5 min following intraperitoneal injection (Fowler and Liou, 1998; Dejean et al., 2011). Even though the animals were heated between recordings, a drop in body temperature sometimes occurred in the later recording periods; therefore, the second recording periods both before and after raclopride administration were used for analysis, since these showed stability across all subjects.

TISSUE STAINING

Following recordings, the brain was lesioned using a lesion maker (Grass Products, Warwick, RI) to mark electrode placement (300 μA for 30 s). Rats were then perfused with 300 ml cold 0.9% saline followed by 300 ml cold 4% paraformaldehyde in 0.1M phosphate buffer. Brains were extracted and kept overnight at 4°C in a 4% paraformaldehyde solution then dehydrated in phosphate buffered saline (PBS) with 30% sucrose. The cerebrum was sliced coronally and the cerebellum was sliced horizontally into 50 μm sections on a cryostat and mounted directly onto slides. Sections were stained using cresyl violet and lesions were located using light microscopy.

ELECTROPHYSIOLOGICAL DATA PROCESSING

Raw microelectrode data was downsampled to 2020 Hz using Neuralynx software and off-line analysis of recorded data was conducted using custom Matlab (MathWorks, Natick, MA) functions and scripts. Once in Matlab, the data was low-pass filtered at 300 Hz and structured into 2-s windows. To analyze the rhythmicity content of the low-passed signal, Fast Fourier Transform (FFT) was calculated on each 2-s window. The following bands were used for analysis: (1) (0.1–3 Hz, delta); (2) (3–8 Hz, theta); (3) (8–13 Hz, alpha); (4) (13–30 Hz, beta); and (5) (30–55 Hz, gamma). The power spectrum was integrated within those bands, and then averaged for the 60 windows, providing one value per recording period. Coherence between LFP pairs was also calculated on each 2-s window and values within the same frequency bands were also averaged per recording period. The average FFT and coherence of each period was entered into the statistical analyses.

In order to establish the percentage of time where slow (0–3 Hz) vs. 3–8 Hz oscillations predominate, the integrated FFT power for each band was compared for each 2-s time window. Plotting those values in time for each recording period, we identified the power level around which the dominant power

between 0–3 Hz and 3–8 Hz was alternating. To compute this, we calculated the difference between the 0–3 and 3–8 Hz integrated power and took the mean of the values where this difference equaled 0 ± 10 of the total percent FFT power. This difference maintained a narrow range while still including enough data points to normalize, thus providing a baseline for each recording session, from which a threshold could be calculated. This mean +20% value determined if a window had strong 0–3 Hz activity, while the mean –15% determined if a window had strong 3–8 Hz activity. These thresholds were chosen empirically as the most conservative levels where the 0–3 Hz or 3–8 Hz oscillations could be detected across multiple recording sessions. The number of windows that fell above the threshold was calculated for each band, and then divided by the total number of windows to get a value expressed as a percentage.

To avoid duplication of data, spindles were analyzed for one electrode in each of the MStr and LStr pairs of electrodes and for one electrode placed in the cerebellum. The average of the number of spindles detected from the two striatal electrodes was then used for statistical analysis. A detectable spindle was defined as an oscillation within 8–20 Hz that occurred at the peak of the slow wave. Spindles were identified by first band-pass filtering the LFP signal between 0–3 Hz to identify the slow oscillation phase. The LFP was also filtered between 8–20 Hz, and this filtered signal was rectified, and convolved with a 14-Hz (71 ms) window. These 8–20 Hz filtered and rectified product-values were Z-scored and a threshold was set at 2 standard deviations. Spindles were detected when the 8–20 Hz signal reached above this threshold value within ±0.25 s of the peak of a slow wave oscillation. An example is shown in **Figure 5A**.

NEOCORTICAL RECORDINGS

In order to verify if coherence between the striatum and cerebellar cortex under urethane anesthesia involves neocortical connections, four additional recording sessions were done with neocortical electrodes added, one at each time of day (ZT1, 7, 13 and 19). The same electrophysiological set-up was used as described above, but instead of placing two pairs of electrodes in the striatum, one electrode from each pair was stopped in the overlying neocortex, corresponding to the sensorimotor cortex. These recordings were pooled together with the rest of the dataset to provide an overall description of synchrony between the neocortex, the striatum and the cerebellum. Coherence within each frequency band was analyzed as above, however the trend was similar across all bands, so we report below the 0.1–8 Hz and overall coherence from 0.1 to 55 Hz.

STATISTICAL ANALYSIS

Statistical tests were performed using Statistica 10 (StatSoft, Tulsa, OK) or in Matlab. All results are presented as the mean ± the standard error of the mean (SEM). The second recording period before and after raclopride showed the most stability with body temperature; so all further analysis was performed on these two periods. The dependent variables of oscillatory power and coherence (for each frequency band) were statistically assessed for two different analyses. Circadian effect on baseline recordings was assessed by one-way repeated measures ANOVA, with time-of-day as the independent variable. The circadian effects of raclopride assessed the interaction between pre-post raclopride conditions and time-of day using two-way repeated-measures ANOVAs. Results were considered significant at $p < 0.05$. *Post-hoc* comparisons used Tukey tests. For identifying the relationship between 0–3 Hz and 3–8 Hz power across windows, linear correlation ($p < 0.05$) was used.

RESULTS

IN VIVO RECORDINGS

LFP recordings were obtained from 16 urethane-anesthetized animals (4 animals × 4 ZT). There was no effect of either time-of-day or pre-post raclopride on the heart rate (ZT, $F_{(3,7)} = 0.14$, $p = 0.93$, pre-post, $F_{(1,7)} = 0.14$, $p = 0.72$). This confirms that at least from the heart rate marker, the depth of anesthesia was consistent across ZT and pre-post conditions. One additional (17th) animal from the ZT13 group failed to maintain normal body temperature during the experiment and was excluded from the analysis. Each of the remaining recordings included simultaneous medial and lateral striatal (MStr and LStr) recordings and cerebellar Crus2/Paramedian lobule (CB) recordings. As explained above, in 4 of these animals, one electrode from each pair aimed at the MStr and LStr was instead placed in the overlying neocortex. Electrode locations determined from electrolytic lesion sites confirmed the location of microelectrode tips in the striatum and granule cell layer of the cerebellum or close vicinity. Placement of 17 of the 32 cerebellar pairs, 10 of the 16 MStr and LStr pairs and all of the neocortical electrode tips are shown in **Figure 1**, providing a representative spread of recording location for each brain area.

Both the striatal and cerebellar LFPs showed predominant large amplitude slow wave activity between 0.8–2 Hz with intermittent smaller amplitude oscillations around 4–5 Hz (**Figure 2A**). The slow wave activity is consistent with other findings in which urethane anesthesia induces widespread cortical synchrony resulting in oscillations at ∼1 Hz that are intermittently interrupted by a desynchronized state (Destexhe et al., 1999; Clement et al., 2008). Slow wave activity tended to co-occur in the striatum and cerebellum, consistent with findings that anesthesia induces coherent slow-wave oscillations between the neocortex and striatum (Tseng et al., 2001; Mallet et al., 2005) and between the neocortex and cerebellum (Ros et al., 2009). We also observed transient spindle-like 8–20 Hz oscillations that were nested within the slow-wave activity. These spindles were most evident in the striatal LFPs, but similar electrophysiological events also occurred in the cerebellar LFPs (**Figure 2B**).

DIURNAL MODULATION OF LFP OSCILLATIONS

To determine the effects of time of day on both slow-wave and 3–8 Hz oscillations, the power of the FFT within each band recorded at baseline, was compared across the four times of day (**Figure 3A**). The MStr and LStr recordings showed the same variations by time of day and were thus combined for statistical analysis. In both striatal and cerebellar LFPs, slow-wave power showed a large diurnal rhythm in which power was the greatest at ZT1 and the lowest at ZT13 (Str, $F_{(3,52)} = 11.80$, $p < 0.001$; CB, $F_{(3,60)} = 14.75$, $p < 0.001$). There was an inverse diurnal pattern

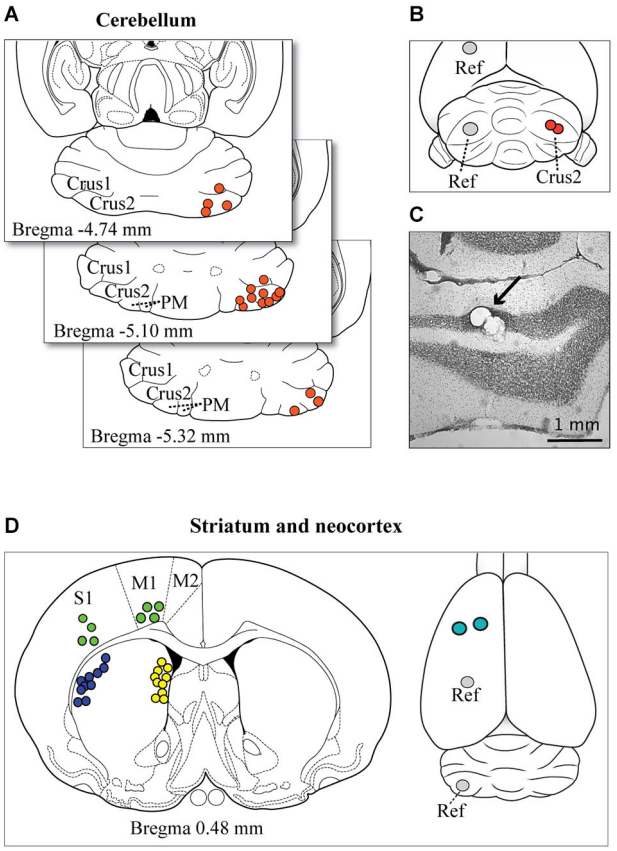

FIGURE 1 | Microelectrode tip localizations and reconstructions. **(A)** The representative spread of identified electrode tip locations in the cerebellum are shown (filled circles) on horizontal sections taken from the atlas of Paxinos and Watson (1998). **(B)** Example of the target location of the two insertion points of the microelectrodes on the surface of the exposed cerebellar cortex (red circles). Cerebellar recordings were obtained on the right side of the brain, and the reference wire (Ref) was positioned in the opposite hemisphere in either the left cerebellar cortex or more rostrally in the parietal cortex. **(C)** A photomicrograph shows the location of microelectrode tip lesions in the granule cell layer of Crus2 (arrow). Most electrode tips were located in the granule cell layer or within close proximity. **(D)** The panel at left shows a representative spread of the location, based on atlas reconstructions, of identified microelectrode tips in the striatum (dorsolateral, blue circles; medial, yellow circles) and neocortex (green circles). The panel at right shows the optional locations of the reference wires (Ref) and the insertion points for cortical and striatal electrodes (teal circles).

in the power of 3–8 Hz oscillations, in which power was highest at ZT13 (Str, $F_{(3,52)} = 5.78$, $p < 0.01$; CB, $F_{(3,60)} = 11.56$, $p < 0.001$). No diurnal effect was found in frequency bands above 8 Hz for either region (not shown).

Because the overall FFT power at 0–3 Hz and 3–8 Hz were inversely related to each other by time of day, we also sought to determine the relationship between the two frequency bands within each 2-s window, and to quantify differences in time spent in slow oscillations vs. 3–8 Hz oscillations. The relationship between the power of slow waves vs. 3–8 Hz oscillations was assessed by plotting the percent power of the FFT within the 0–3 Hz band vs. the 3–8 Hz band for each of the 180 2-s windows sampled in baseline recordings (**Figure 3B**). There was a strong negative correlation between power in the two bands for all recording sessions (**Figure 3B** shows two examples of this negative correlation). The inverse relationship of the power at 0–3 Hz vs. 3–8 Hz within each 2-s window indicated that the two oscillatory modes did not co-occur. This was then used to create the threshold to detect the duration of 0–3 Hz or 3–8 Hz activity within each recording session. Since no diurnal effect was observed in bands above 8 Hz, these bands were excluded from this detection analysis.

EFFECTS OF RACLOPRIDE ON DIURNAL VARIATIONS IN THE OCCURRENCE OF LFP OSCILLATIONS

Diurnal rhythms in the power of the LFP were highly associated to the proportion of time spent within each oscillatory mode, and raclopride influenced this distribution in a time-of-day-dependent manner (**Figure 4**). The percentage of time spent preferentially in slow wave oscillations vs. 3–8 Hz oscillations was calculated for each recording period, and both cerebellar and striatal LFPs showed robust, inverse diurnal rhythms for the proportion of time spent in each band (see **Figures 4C,D**, closed symbols; 0–3 Hz: Str, $F_{(3,52)} = 6.63$, $p < 0.001$, CB, $F_{(3,60)} = 11.85$, $p < 0.001$; 3–8 Hz: Str, $F_{(3,52)} = 7.78$, $p < 0.001$, CB, $F_{(3,60)} = 13.86$, $p < 0.001$). At ZT1, a large proportion of time was spent in slow wave oscillations (86.9 ± 5.9% of the time for cerebellum and 94.2 ± 5.7% for striatum) and at ZT13 there was a much greater prevalence of 3–8 Hz oscillations in both the striatum and cerebellar cortex (57.7 ± 5.2% of the time for cerebellum and 40.0 ± 4.3% for striatum). Overall, both cerebellar and striatal LFPs showed similar diurnal effects in the proportion of time spent in each of the two frequency bands.

Since circadian PER2 rhythms in the striatum are dependent upon dopamine and D2 receptor activation (Hood et al., 2010), we assessed the effects of raclopride on LFP oscillations as a function of time of day. For both striatal and cerebellar LFPs, systemic raclopride administration resulted in an increase in slow oscillations a decrease in in 3–8 Hz oscillations (**Figures 4A,B**). This effect was only significant at ZT13, except the 3–8 Hz band in the striatum, where only a trend was observed (**Figures 4C,D**; 0–3 Hz: Str, $F_{(3,52)} = 3.00$, $p < 0.05$; CB, $F_{(3,60)} = 4.67$, $p < 0.01$; 3–8 Hz: Str, $F_{(3,52)} = 2.37$, $p = 0.08$, CB, $F_{(3,60)} = 11.91$, $p < 0.001$). The raclopride-induced increase in the occurrence of 0–3 Hz oscillations at ZT13 was also mirrored in the overall power of the FFT (not shown). Typically, the changes in oscillatory activity were complementary between the bands, such that raclopride induced an approximate 15% increase in time spent in the 0–3 Hz band and an approximate 15% decrease in time spent in the 3–8 Hz band for both the striatal and cerebellar LFPs.

DIURNAL VARIATION IN THE INCIDENCE OF SPINDLES

Spindles occur during slow wave oscillations during sleep and under urethane anesthesia, and can be modulated by distinct thalamic mechanisms (Valencia et al., 2013). We sought to determine if the incidence of spindles varies in a diurnal manner. The incidence of spindles was determined for striatal and cerebellar recording sites for each animal, and then compared between ZT and before and after raclopride administration. The occurrence

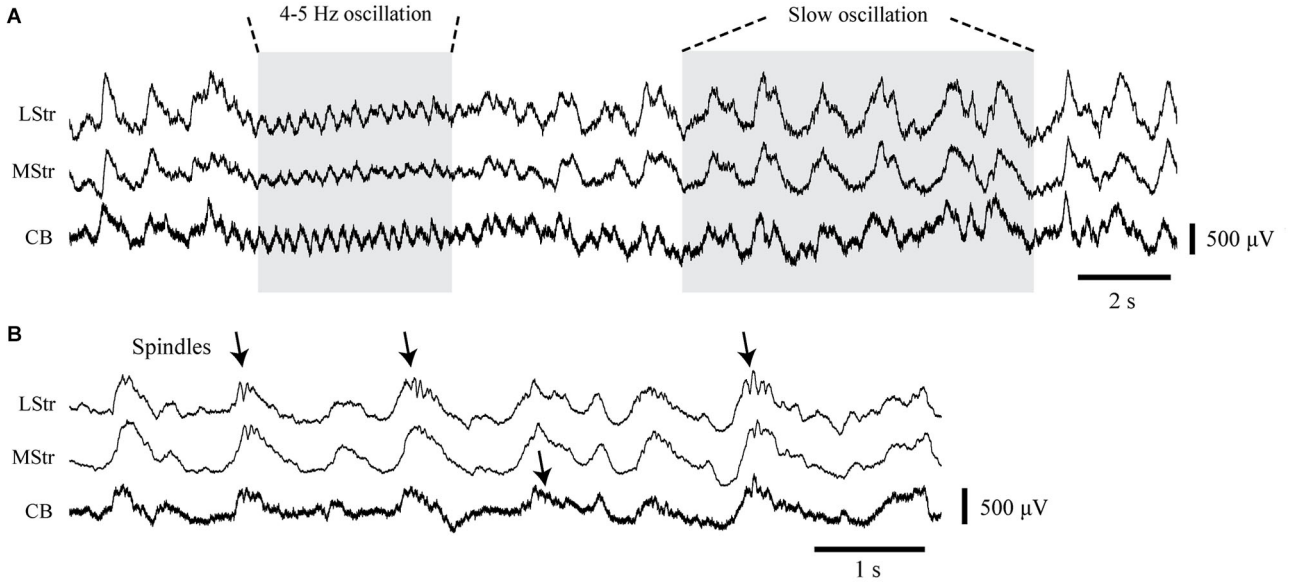

FIGURE 2 | LFP activity in the striatum and cerebellum under urethane anesthesia. **(A)** Simultaneously recorded LFPs from the dorsolateral striatum (LStr), medial striatum (MStr), and cerebellar cortex (CB) containing concurrent periods of 4–5 Hz oscillations and slow 1 Hz oscillations. **(B)** Recordings at an expanded time scale obtained from another recording period show spindle-like activity in association with slow waves (arrows).

of spindles in the LFP showed a similar pattern to that of slow waves, with a significant diurnal effect for striatal ($F_{(3,28)} = 4.93$, $p < 0.01$), but not cerebellar recordings ($F_{(3,12)} = 2.12$, $p = 0.15$) (**Figure 5B**). The diurnal pattern of spindles was dependent upon the occurrence of slow waves, such that when normalized to the amount of time spent in 0–3 Hz oscillations there was no diurnal variation in spindle incidence (Str, $F_{(3,28)} = 1.16$, $p = 0.34$; CB, $F_{(3,12)} = 1.54$, $p = 0.25$) (**Figure 5C**). In addition, raclopride did not have an effect on the incidence of spindles (Str, $F_{(3,28)} = 1.17$, $p = 0.34$; CB, $F_{(3,12)} = 1.88$, $p = 0.20$; data not shown). Therefore, diurnal variations in the incidence of spindles are dependent on the presence of slow wave oscillations under our urethane anesthesia preparation, and are not significantly affected by D2 receptor antagonism.

EFFECTS OF RACLOPRIDE ON DIURNAL VARIATIONS IN COHERENCE

To assess the overall interregional differences in the synchrony of LFP oscillations recorded in the striatum and cerebellum, coherence within and between these structures was evaluated. Within the 0–3 Hz and 3–8 Hz bands, coherence showed similar levels and were therefore combined. There was also no difference between the following comparisons, so this data was combined: MStr and LStr within pair, the MStr-CB and LStr-CB, the two cortical locations with the CB, and the two off-set cortico-striatal comparisons. 0–8 Hz coherence followed a similar pattern as 8–55 Hz coherence, but was consistently higher (see **Figure 6A**, 0–8 Hz vs. 0–55 Hz). Coherence was higher for recordings obtained from adjacent tips within each of the striatal electrode pairs (Within Pair) as compared to recordings obtained between electrode pairs (Btwn Pair) in the MStr vs. LStr ($p < 0.01$) or across electrode pairs in the cerebellum ($p < 0.001$). This demonstrates enhanced coherence of LFPs with spatial proximity in both the striatum and the cerebellar cortex (**Figure 6A**, Within Pair vs. Btwn Pair comparisons). Four additional recording sessions were performed to evaluate the contribution of the neocortex to the striato-cerebellar coherence and included simultaneous recordings from two striatal electrodes, two electrodes in the overlying neocortex, and four electrodes in the cerebellar cortex. Cortico-striatal coherence was greatest between electrodes in the same sagittal plane and was comparable to the striatal-within pair comparisons (**Figure 6A**, 0–8 Hz: Str-within pair = 0.92 ± 0.024; Ctx-Str vertical = 0.90 ± 0.042). Cortico-striatal coherence was reduced for comparisons in different medial vs. lateral positions, showing a similar coherence as the striatal-between pair comparisons (Str-between pair = 0.82 ± 0.016; Ctx-Str off-set = 0.79 ± 0.042). The levels of Str-CB or Ctx-CB coherence (Str-CB = 0.53 ± 0.008; Ctx-CB = 0.54 ± 0.021) were substantially lower than levels of coherence obtained from more nearby electrodes pairs within the striatum or cerebellum. However, levels of both Str-CB and Ctx-CB coherence had similar values. This is consistent with the neocortex playing a role in coordinating oscillations in the striatum and cerebellum under urethane anesthesia.

The presence of diurnal effects on mean coherence for each recording session was assessed for the 0–3 Hz and 3–8 Hz bands within striatal, cerebellar and striato-cerebellar comparisons. CB within pair and between pair along with CB-MStr and CB-LStr comparisons showed the same modulation by time-of-day and pre-post raclopride, so these data were combined. Coherence of striatal LFPs showed a significant main effect for time-of-day for slow oscillations between medial and lateral recording sites (Str-between pair $F_{(3,48)} = 7.24$, $p < 0.001$) but not with closer electrode pairs (Str-within pair, $F_{(3,20)} = 0.38$, $p = 0.77$)

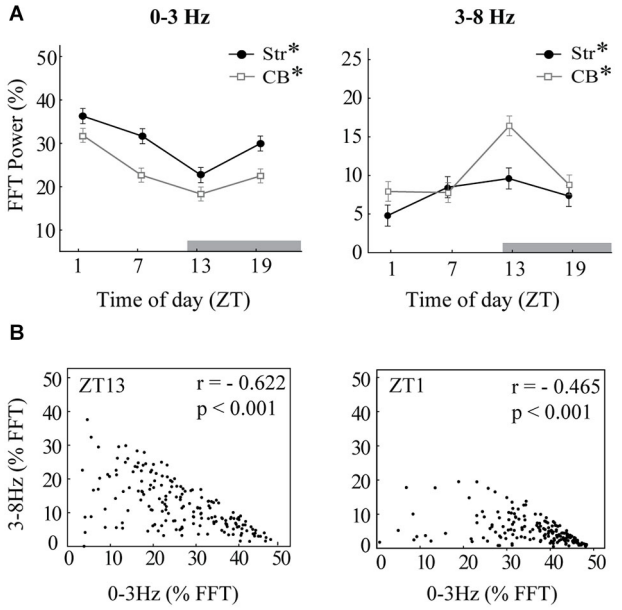

FIGURE 3 | Diurnal variation in oscillations. (A) The mean integrated power of 0–3 Hz oscillations (left) and 3–8 Hz oscillations (right) is shown for each time of day at baseline, before raclopride administration, expressed as a percentage of the total power spectrum (0–55 Hz). Time of day (ZT) is expressed in hours after onset of light. Note that the dark period began at ZT12 (gray bar). Asterisks indicate significant effects of ZT ($p < 0.05$). **(B)** Scatterplots indicate strong negative correlations between the power of 0–3 Hz oscillations and 3–8 Hz oscillations. Each dot represents the integrated power within each of the 2-s windows that compose the baseline recordings. The panel at left shows an example from ZT13 that includes both 1 Hz oscillations and 4–5 Hz oscillations. The panel at right shows an example from ZT1 that contains mainly 1 Hz oscillations. Both examples are from striatal LFPs, though cerebellar LFPs showed a similar correlation.

demonstrating higher levels at ZT1 and lower levels at ZT13 (**Figures 6B,C**, closed symbols). However, there was no diurnal effect on coherence of 3–8 Hz oscillations (**Figures 6F,G**; Str-Within pair, $F_{(3,20)} = 0.59$, $p = 0.63$, Str-between pair $F_{(3,48)} = 1.75$, $p = 0.17$). Similar to the coherence of striatal slow waves, both cerebellar coherence and striato-cerebellar coherence within 0-3 Hz demonstrated a significant peak at ZT1 (**Figures 6D,E**; CB, $F_{(3,92)} = 4.20$, $p < 0.01$; Str-CB, $F_{(3,220)} = 27.86$, $p < 0.001$) which is consistent with the prevalence of slow oscillations in these structures at ZT1. Similarly, within the 3–8 Hz band, there was a strong diurnal pattern in cerebellar and striato-cerebellar coherence with increased coherence at ZT13 (**Figures 6H,I**; CB-CB, $F_{(3,92)} = 5.54$, $p < 0.01$; Str-CB, $F_{(3,220)} = 16.54$, $p < 0.001$) when both structures show predominant 3–8 Hz oscillations (**Figure 4C**). These comparisons also showed a secondary increase at ZT1, suggesting a biphasic pattern of coherence in the 3–8 Hz band.

To assess the effect of D2 receptor antagonism on striatal and cerebellar coherence, the mean coherence before and after raclopride administration was compared for each of the four times of day. Raclopride had the effect of increasing coherence of slow oscillations at ZT13 between the MStr and LStr only (Str-between pair, $F_{(3,44)} = 7.52$, $p < 0.001$). Raclopride minimally affected 3–8 Hz coherence, where it induced a decrease only in the striato-cerebellar comparisons at ZT1 and ZT13 ($F_{(3,220)} = 11.291$, $p < 0.001$, **Figures 6F–I**). In general, changes in coherence in 0–3 Hz oscillations followed a diurnal pattern that is similar to the overall FFT power within these bands (compare **Figures 4C** and **6**). This implies that D2 receptor antagonism has the effect of enhancing both the power and coherence of slow oscillations, in a manner that is more potent at ZT13.

DISCUSSION

This study was aimed at determining if the neural network activity of the basal ganglia and the cerebellum, and their coupling, are influenced by time-of-day, and how raclopride, a D2 dopamine receptor antagonist, affects those relationships. A marked diurnal change in the rhythmicity of the striatal and cerebellar cortex networks was observed, with slow oscillatory activity decreasing at the beginning of the dark phase (when the rat would usually be more active), and 3–8 Hz activity increasing in the same period. The diurnal patterns of oscillations in the slow vs. 3–8 Hz bands were generally inversed, particularly in the cerebellum where 3–8 Hz oscillations were more prominent. This diurnal variation was also seen in the incidence of spindle activity, which was strongly influenced by the presence of the slow wave component. In addition, the shifting of activity from slow to 3–8 Hz at ZT13 was decreased by the administration of raclopride, which promoted slow band activity. Lastly, LFP coherence showed that cerebellar, striatal between-pair and striato-cerebellar slow wave coherence showed a strong diurnal pattern of modulation. Raclopride administration also influenced striatal coherence in a time-of-day dependent manner that was consistent with the shifts in oscillatory activity occurring in this area, such that coherence was enhanced when slow wave activity increased. These results show a clear diurnal modulation of striatal and cerebellar network activities and their coupling, and a time-specific effect of dopamine transmission that may serve to sculpt the activity of these networks.

OSCILLATORY ACTIVITY AND COUPLING UNDER URETHANE ANESTHESIA

Our experimental preparation, using urethane anesthesia, was chosen in order to minimize the chance of LFP signal contamination by behavioral artifacts such as neural movement-related LFP signal changes. Using the conventional parameters of heart rate and foot-pinch reflex, depth of anesthesia was stable across conditions. Urethane anesthesia is only minimally depressive, and thus permissive to neural oscillations (Maggi and Meli, 1986; Steriade, 2003; Clement et al., 2008). As such, urethane could be used for studying circadian effects on oscillations and communication between networks. This preparation favors slow wave oscillations and widespread synchrony (circa 1 Hz), while permitting transient oscillations in the 3–8 Hz range. In the context of sleep and urethane anesthesia, these slow oscillations have sculpting features in the neocortex (Steriade, 2003; Clement et al., 2008) whereby cortical "up" and "down" states greatly influence larger scale networks (Wilson and Kawaguchi, 1996; Stern et al., 1998; Ros et al., 2009). This cortical influence helps local

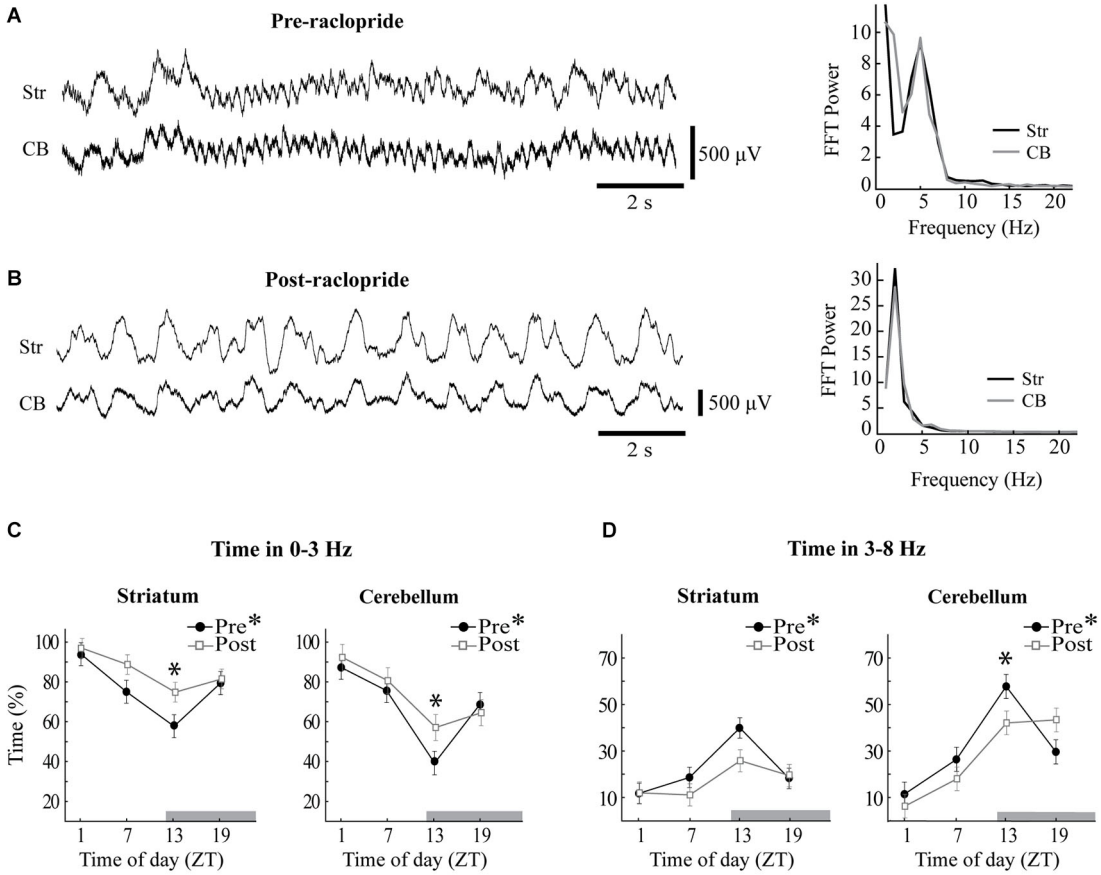

FIGURE 4 | Raclopride enhances slow oscillations and reduces 3–8 Hz oscillations at ZT13. Sample LFPs obtained from the striatum (Str) and the cerebellum (CB) before **(A)** and after **(B)** systemic administration of raclopride. The baseline recording shows extended periods of 5 Hz oscillations in both sites, which were replaced by a strong 2 Hz oscillation following raclopride. Power spectra at right correspond to the LFPs displayed at left and reflect similar spectral content in striatal and cerebellar recordings. **(C,D)** The percentage of time that each recording site spent within 0–3 Hz **(C)** or 3–8 Hz **(D)** oscillations was calculated before (filled circles) and after (open squares) raclopride administration. Asterisks in the figure legend indicates a main effect of ZT at baseline (pre-raclopride), asterisks above the data points indicate significant effects of raclopride in the Tukey *post hoc* analysis, $p < 0.05$.

circuits maintain synchronized activity during sleep, or sleep-like states (Sanchez-Vives and McCormick, 2000). We observed that cortical LFPs had a close relationship with striatal LFPs, and were more dissimilar with the cerebellar LFPs (**Figure 6**). Still, Ctx-CB coherence between 0–3 Hz could reach above 0.7, potentially indicating a strong cortical influence. In both structures, cortical slow oscillations can influence the cell membrane potential and firing pattern: slow oscillations are indeed related to granule and Golgi firing, and Purkinje cell complex spikes (Ros et al., 2009). Slow oscillations also have a strong influence on neuronal excitability in the striatum (Wilson and Kawaguchi, 1996; Sharott et al., 2012). The slow oscillations that we observed, synchronized in the striatum and cerebellar cortex, are therefore likely to arise from a common contribution of the neocortex, which may drive activity in both regions. Spindles recorded under urethane anesthesia are under the influence of thalamic pacemakers, particularly the reticular thalamic nucleus (Steriade, 2003). They occur during cortical "up" states and are dependent on the corticothalamic inputs. From our results, it appears that the diurnal modulation was more driven by the presence of the slow oscillations, further confirming the potential extrinsic influence on the local striatal and cerebellar cortex networks.

Oscillatory interactions between the striatum and cerebellum could, however, involve a variety of reverberating circuits. The faster 3–8 Hz oscillations appear less uniform in their expression across recording sites and may be generated by more local processes that could be differentially organized in the cerebellum and striatum (Schnitzler and Gross, 2005). In the cerebellar cortex, the granule and Golgi cells seem to follow 5–30 Hz oscillations in a steady manner (Courtemanche et al., 2002; Dugué et al., 2009). However, faster 10–25 Hz oscillations occur in the awake primate and are stopped by movement (Pellerin and Lamarre, 1997; Courtemanche et al., 2002); they can also be synchronized with the neocortex under specific behavioral conditions (Courtemanche and Lamarre, 2005). These oscillations follow a parasagittal modulatory pattern (Courtemanche et al., 2009),

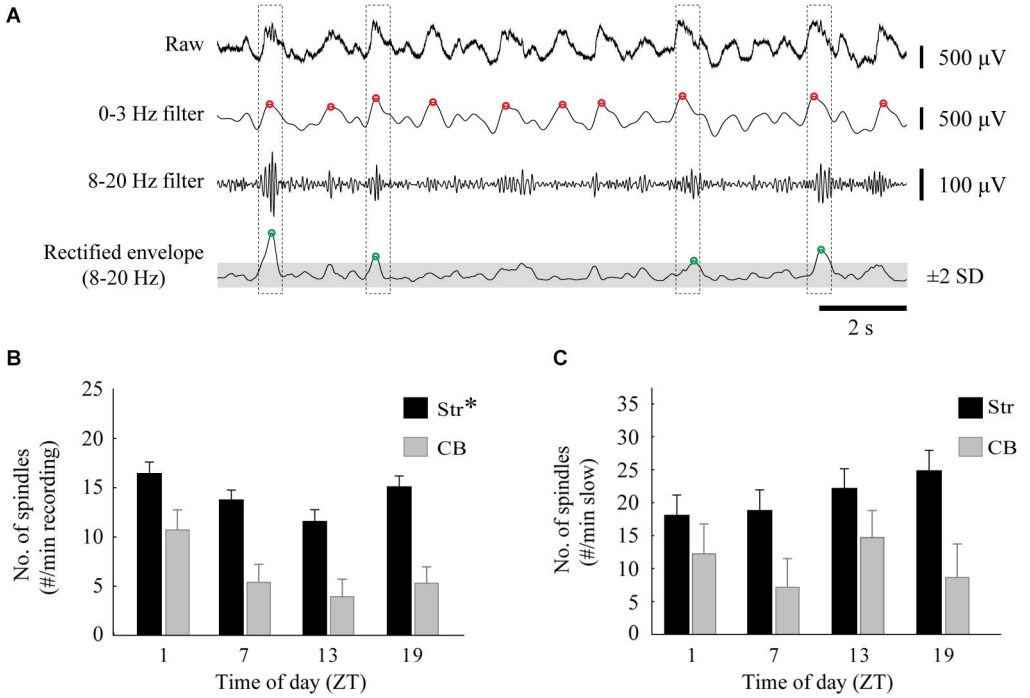

FIGURE 5 | Diurnal variation in spindles. **(A)** An example of the spindle detection method on a striatal recording. Spindles were identified by low-pass filtering the raw signal at 0–3 Hz to locate the peaks of slow oscillations (red circles), and also band-pass filtered at 8–20 Hz. The 8–20 Hz signal was rectified and peaks 2 standard deviations above the mean (gray area) of the smoothed envelope were located (green circles). A spindle was identified when the peaks of the slow oscillations and 8–20 Hz activity occurred within 0.5 s of each other (dashed boxes). **(B)** The average number of spindles per minute, calculated from two striatal (one MStr, one LStr) and one cerebellar LFP, for each time of day (asterisk indicates a main effect of ZT, $p < 0.05$). **(C)** The average number of spindles, normalized to the percentage of time that the signal spent in slow-wave activity.

adapting to the demands of the movement being performed. As for the striatum, both 4–12 Hz oscillations in rodents, and 10–30 Hz oscillations in primates also adapt to the task demands (Courtemanche et al., 2003; DeCoteau et al., 2007a; Thorn et al., 2010). This provides evidence of a capacity of the faster oscillations, and their synchrony, to adapt to behavioral conditions, organizing the networks in a task-dependent manner with a potentially more local organization than the slow oscillations.

DIURNAL AND DOPAMINE MODULATION OF LFP OSCILLATIONS

Many biological processes and daily changes in behavior are influenced by circadian gene expression patterns, yet little is known about the neural mechanisms that may be driving these changes. The striatum and the cerebellum are important subcortical structures for a number of functions subserving behavior, including motivation, adaptability of motor control, sequencing, and elaboration of cognitive and mental programs (Ito, 2006; Graybiel, 2008). To the best of our knowledge, this study is the first time subcortical LFP network activity has been analyzed in a circadian context. Our findings are consistent with the diurnal modulation of EEG oscillations observed in other brain sites (Grasing and Szeto, 1992), even though in this latter study, both sleep and awake states were included in their analysis. When states of sleep vs. wakefulness are compared, an increase in slow wave activity and inter-regional synchrony is expected early in the light phase (ZT1) when the rat would be falling asleep and, conversely, the slow oscillations should give way to faster oscillations in the transition into the dark phase (ZT13), when the animals become more active (Buzsáki and Draguhn, 2004). We found here that, even under urethane anesthesia, in both the striatum and the cerebellum, slow wave oscillations showed a clear diurnal variation that was consistent with this sleep-wake cycle. This indicates that the circadian mechanisms are robust enough to control network oscillations under anesthesia, suggesting that circadian clocks may influence how signal transmission occurs between local networks and play a role in establishing neural conditions that allow behavioral states to change throughout the day. The acceleration of the LFP oscillations and the shifts in coherence at the beginning of the dark period, at a time when the animal would normally be transitioning into its active phase, could be establishing optimal neural conditions that create a permissive state for networks to perform their awake activities.

Changes in neurotransmitter availability influence neuronal excitability and can contribute to the switching between oscillatory modes (McCormick, 2004), where different neuromodulators can promote shifts in frequencies in a manner that is anatomically specific (Roopun et al., 2010). Dopamine is known to promote wakefulness, but has scarcely been studied in its effect on cortical excitability during slow wave activity and our results seem similar to the neuromodulatory effects of dopamine in the

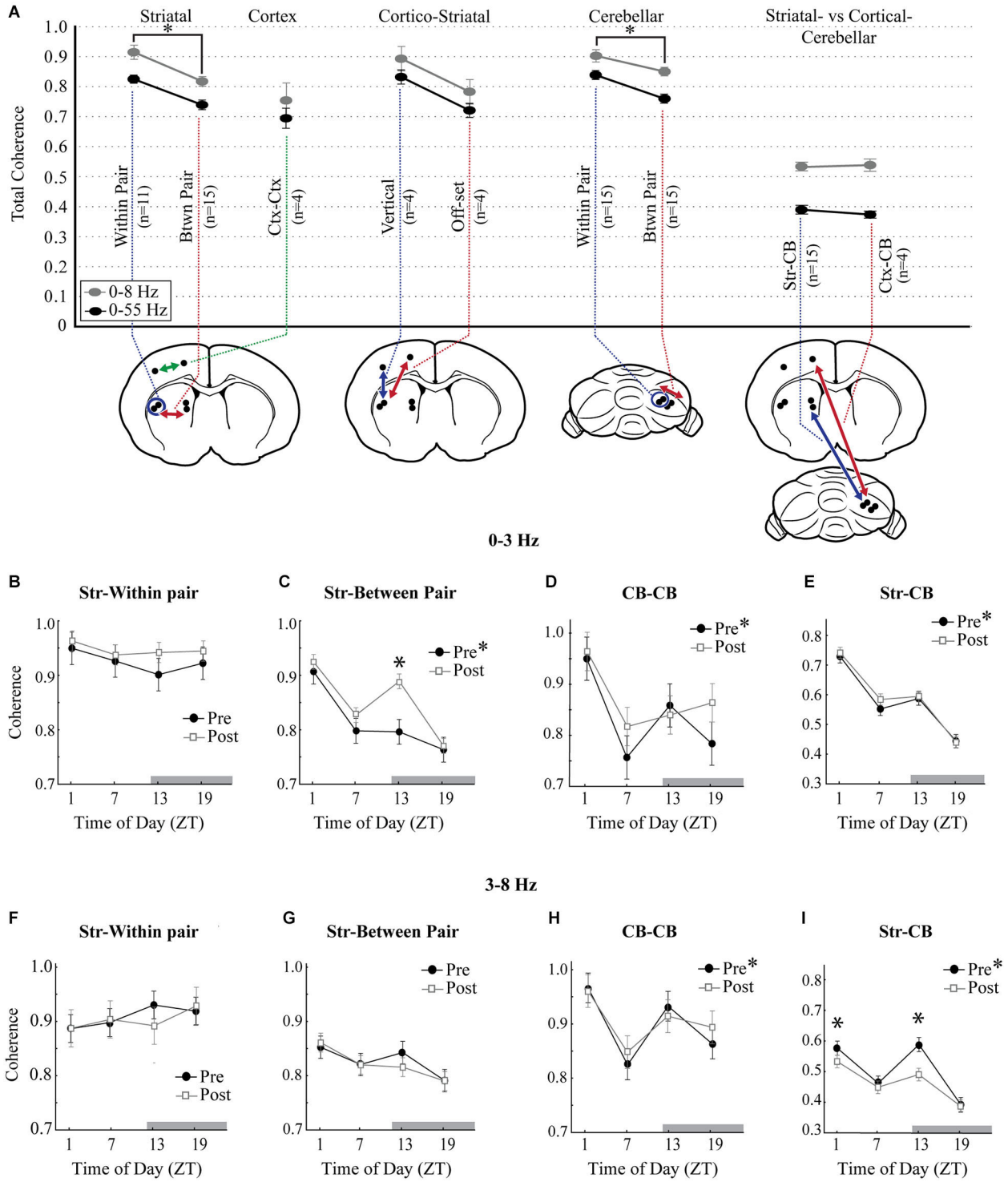

FIGURE 6 | Diurnal variation in measures of coherence. **(A)** Overall total coherence of oscillations (0–8 Hz, gray circles; 0–55 Hz, black circles), averaged across all times of day and all animals. Coherence comparisons are indicated by arrows in the schematic diagrams (*n*, number of animals). "Within Pair" indicates comparisons within the electrode pairs, "Btwn Pair" indicates comparisons between more distant electrodes. Coherence comparisons indicated with different colors. Asterisks signify significance in the Tukey *post hoc* analysis, $p < 0.05$. **(B–E)** 0–3 Hz coherence measured across each of the striatal and cerebellar comparisons showing diurnal variations at baseline (filled circles) and the effects of raclopride (open squares). **(F–I)** Coherence measures at baseline and after raclopride in the 3–8 Hz band, across each of the striatal and cerebellar comparisons. Asterisks in the figure legend indicates a main effect of ZT at baseline (pre-raclopride), asterisks above the data points indicate significant effects of raclopride in the Tukey *post hoc* analysis, $p < 0.05$.

entorhinal cortex (Mayne et al., 2013; Zeitzer, 2013). We found here that blocking D2 receptors could increase the slow oscillatory content of the LFP signal. Raclopride injections enhanced slow striatal and cerebellar oscillations, particularly at ZT13. This is the time of day that has the greatest reduction on the slow oscillations. This result points to a role of dopamine as a neuromodulator of the slow oscillations.

Dopamine itself has a strong influence on striatal oscillatory properties (Costa et al., 2006). Under urethane anesthesia, dopamine depletion increases basal ganglia entrainment to cortical slow oscillations (Tseng et al., 2001; Walters et al., 2007). Lesion to substantia nigra dopamine neurons causes depolarization of striatal medium spiny neurons and increases their spontaneous burst firing at frequencies coherent with the neocortex (Tseng et al., 2001; Sharott et al., 2012). This results in a decrease in the striatal filtering of the slow components from the neocortex, consequently increasing slow wave activity throughout the basal ganglia. Therefore, in our experiments, the decrease in slow wave activity in the striatum at ZT13 could be due to an increase in dopamine transmission. This is supported by raclopride having the largest effects at this time. In contrast, peak extracellular dopamine concentrations occur in the striatum somewhat later in the dark phase, around ZT18 (Owasoyo et al., 1979; Hood et al., 2010; Ferris et al., 2014). This suggests that oscillatory activity is being affected by factors in addition to dopamine availability, such as membrane receptor activation. Diurnal variations in the striatal LFP are likely dependent, in part, on alteration of dopamine function, which may help to provide an oscillatory state in the striatum which is more "disconnected" from the neocortex during awake conditions, thus enhancing the occurrence of higher frequency oscillations.

NETWORK INTERACTIONS

In the cerebellar LFPs, we found slow oscillations that are thought to have a neocortical origin (Ros et al., 2009), and 3–8 Hz oscillations, which are likely dependent on reverberating properties in the cerebellar granule cell layer (Dugué et al., 2009; Courtemanche et al., 2013). The cerebellum followed a similar diurnal pattern in oscillations as the striatum (mostly slow oscillations at ZT1; fewer slow oscillations and more 3–8 Hz at ZT1) and its oscillatory profile was similarly affected by raclopride. While the oscillations recorded could in part come from local cerebellar circuit resonance (Dugué et al., 2009), it is quite possible that there are contributions from larger circuit interactions, including the subcortical connections between the basal ganglia and the cerebellum and the neocortico-ponto-cerebellar circuits.

Addressing the local circuits, it is unclear exactly how dopamine can affect cerebellar cortex circuitry. Even if not traditionally considered as a prominent cerebellar neuromodulator, there is evidence for dopaminergic transmission in the cerebellum (Takada et al., 1993; Hurley et al., 2003; Delis et al., 2004; Schweighofer et al., 2004; Giompres and Delis, 2005) There is also some evidence that dopamine levels in the cerebellum follow a circadian cycle (Owasoyo et al., 1979). However, the role of dopamine in the cerebellum remains poorly understood (Schweighofer et al., 2004). D2 and D3 type dopamine receptors have primarily been reported in the molecular cell layer of the vermis (Bouthenet et al., 1987), however raclopride does show low levels of binding to the cerebellar hemispheres *in vivo* (Kiss et al., 2011). Dopamine projections from the ventral tegmental area (VTA) to the cerebellar cortex have been reported to terminate in the granule and Purkinje cell layers in the posterior lobe (Ikai et al., 1992) and alterations of activity in the VTA both acutely and chronically induce changes in *cFOS* expression in the granule cell layer in multiple cerebellar regions, including Crus1 and 2 (Herrera-Meza et al., 2014). It may be that these VTA projections were affected by the systemic raclopride injections, altering neural activity in the areas we recorded, however the effects of dopamine on neural activity in the cerebellar cortex is also not well described. It is unknown if dopamine affects the resonance aspect in the cerebellar circuits, enhancing the 3–8 Hz resonance that appears optimal in those circuits, reducing the capacity to entrain local circuits to the 0–3 Hz inputs arriving from the cortex via the pontine nuclei. We have seen interactions between the GCL and the Purkinje cell layers in monkey ∼15 Hz resonance, so faster oscillations could be partially affected by this local connectivity (Courtemanche et al., 2013). A potential mechanism could be the Lugaro connection affecting the Golgi cells, but at this point, since sufficient studies have not addressed this, these effects remains speculative.

A more probable action of dopamine in the cerebellar cortex however is its indirect effects through cerebellar interactions with other brain areas. The cerebellum is likely to interact with the striatum through the neocortex and subcortical connections. Interconnections between the neocortex and striatum as well as those between the neocortex and cerebellum are strong and numerous. Cortico-striatal connections are important inputs to the striatum (Graybiel, 2010), and these interactions are affected in disease models known to afflict the basal ganglia (Crittenden and Graybiel, 2011). In addition, cortico-pontocerebellar connections have an important effect on cerebellar processing (Morissette and Bower, 1996). This pathway constitutes one of the fastest central pathway in the CNS (Allen and Tsukahara, 1974). Overall, the potential avenue of communication between the striatum and cerebellar cortex taking advantage of the neocortical loops is a definite possibility. In addition, this interconnection is supplemented by the more recent finding of a plurisynaptic subcortical route between the cerebellum and basal ganglia (Hoshi et al., 2005; Bostan et al., 2010). In these papers and in their review, Bostan and Strick (2010) identify that these pathways permit bidirectional information transfer from the basal ganglia to the cerebellum (via a connection from the subthalamic nucleus to the pontine nuclei), or vice-versa (via a connection from the dentate nucleus to the thalamus—specifically, the thalamic central lateral nucleus (Ichinohe et al., 2000)), without requiring the passage through cerebral cortex connections. This anatomical connectivity is supported both by molecular and behavioral studies reporting alterations in either the basal ganglia or the cerebellum inducing rapid changes in the other area (Koch et al., 2009; Calderon et al., 2011; Moers-Hornikx et al., 2011). Since functional changes appear to be bidirectional, one would also assume changes in neural activity to have a similar bidirectional influence. Electrical stimulation of the dentate nucleus can increase firing in the basal ganglia

(Li and Parker, 1969; Ratcheson and Li, 1969), suggesting that altered firing in the cerebellar cortex could also be produced by modifying the neural activity in the striatum.

Dopamine may also affect circadian changes in oscillatory activity by altering more widespread circuit properties, such as thalamocortical circuits, which could then cascade down an effect on both the cerebellar and striatal oscillations. This is consistent with findings that systemic D2 antagonism reduces wakefulness and increases slow wave sleep, where it is believed to act through the nuclei responsible for regulating sleep and wakefulness in the brainstem, hypothalamus, and basal forebrain (Monti and Monti, 2007). With our particular LFP patterns showing widespread synchrony ∼1 Hz, and this oscillation having a strong link with the neocortex in the cerebellum (Ros et al., 2009) and striatum (Stern et al., 1998), it seems most likely that the coordination of the signals we recorded implicates neocortical activity. This would also support the appearance of spindles in the cerebellar LFPs. Spindles originate in the reticular thalamic and neocortical loops under conditions of slow wave oscillations, once appearing in the neocortex they could be transmit to the cerebellar cortex via the cortico-pontocerebellar pathway. It is possible that the neocortex circuits are also involved in the transmission of the 4–12 Hz activity between sites; many cortical areas do exhibit this 4–12 Hz activity, including the hippocampus (Buzsáki, 2006; Buzsáki and Moser, 2013), the cerebral somatosensory cortex (Nicolelis et al., 1995; Ahissar et al., 1997), and also the prefrontal cortex (Watson et al., 2014). However, this activity is better controlled locally, and less driven by large cortico-thalamic interactions that synchronize highly converging neocortical structures, as seems to be the case for slow rhythms during urethane anesthesia or sleep (Steriade, 2003).

The diurnal alterations between slow and 3–8 Hz oscillations are therefore likely influenced by the balance between widespread synchrony from the thalamocortical networks driving the slow oscillations and mechanisms underlying more locally generated oscillations. This is partly evidenced by the fact that when placing the electrodes, the cerebellum consistently showed weaker slow oscillations and stronger 3–8 Hz oscillations as compared to the striatum, reflective of a potentially more distant connection to the neocortex and stronger local resonance of this 3–8 Hz frequency range. This regional aspect would provide some rationale for the favoring of subcortical connections in the synchronization of theta-like activity patterns. A limitation of this study however, is that cortical activity can only be inferred in its role for driving these oscillations in both areas and to decipher regional connectivity will necessitate a more direct approach on the connectivity.

FUNCTIONAL AND CLINICAL IMPLICATIONS

This study uncovered a diurnal modulation that emphasizes the capacity of the striatal and cerebellar circuits to reorganize during the course of the day. The electrophysiological evidence presented here, with oscillations and synchrony alternating between ∼1 Hz or ∼4 Hz rhythms, shows that neural properties are being modulated in order to switch the underlying network states. This could allow the networks to optimally engage in various behaviors throughout the day. The drive in the diurnal modulation of these signals likely comes from the SCN, the central circadian pacemaker, and the subsidiary clocks that exist in a hierarchical network throughout the brain, including the striatum and the cerebellum (Namihira et al., 1999; Shieh, 2003; Imbesi et al., 2009; Rath et al., 2012; Harbour et al., 2013). Both latter areas are involved in locomotor activities driven by circadian gene expression (Masubuchi et al., 2000; Hood et al., 2010; Mendoza et al., 2010) and the diurnal modulation of LFP activity described here is likely to reflect network processes that promote these locomotor/movement activities and may further be important for fine-tuning sensorimotor performance and learning throughout the day. Future directions will include making the link between daily changes in neural network activity and behavioral processes that are driven by circadian genes.

There are a few neurological clinical conditions that affect both the basal ganglia and the cerebellum, and which display diurnal variations in symptoms or in response to pharmacological treatments. For example, Parkinson's disease patients with motor symptom fluctuations generally experience the least amount of impairment in the morning, with symptoms increasing throughout the day (Nutt et al., 1997; Bruguerolle and Simon, 2002). In addition, Parkinson's patients receiving dopamine treatments such as levodopa also experience a diurnal worsening of symptoms. Similarly, spinocerebellar type 3 ataxic symptoms also appear to show diurnal variations in symptoms (Wilder-Smith et al., 2003), though this seems to interact with a dyskinesia that is also levodopa responsive. The link could be direct with core function in these networks, as the ATX2 (ATAXIN-2) protein, which is implicated in the expression of spinocerebellar ataxia type 2 (or an increased risk of amyotrophic lateral sclerosis and Parkinsonism), is involved in the activation of the rate-limiting circadian clock component PERIOD in *Drosophila* (Lim and Allada, 2013) and their daily locomotor behavior (Zhang et al., 2013). In terms of circuit mechanisms, Nutt et al. (1997) report that circadian fluctuations in motor symptoms are independent of plasma levels of levodopa. Even when administering constant-rate infusions, symptoms still worsen despite plasma levels increasing throughout the day. This suggests that dopamine availability is not the only factor that is determining variations in motor behavior, but other factors such as receptor activation and interactions with other neuromodulators also likely play a role. Our results suggest that membrane targets responsible for changes in circuit properties change throughout the day, rather than simply availability of dopamine at the synapse. These daily alterations in circuit properties, both dopamine-related and otherwise, could underlie the diurnal symptomatology in basal ganglia and cerebellar patients.

AUTHOR CONTRIBUTIONS

Ariana Frederick, Jonathan Bourget-Murray, C. Andrew Chapman, Shimon Amir and Richard Courtemanche conceived the project design. Shimon Amir and Richard Courtemanche supervised the project. Ariana Frederick and Richard Courtemanche collected all electrophysiology data. Ariana Frederick, Jonathan Bourget-Murray, and Richard Courtemanche analyzed and interpreted data. Ariana Frederick, Jonathan Bourget-Murray, C. Andrew Chapman, Shimon Amir and Richard Courtemanche contributed to the preparation of the manuscript.

ACKNOWLEDGMENTS

The authors wish to thank Barry Robinson for technical help. This work was supported by grants from the Natural Sciences and Engineering Research Council (NSERC) of Canada to C. Andrew Chapman and Shimon Amir, a grant from CIHR to Shimon Amir, and by a Concordia grant to Richard Courtemanche. The study was undertaken at the Centre for Studies in Behavioral Neurobiology, which is group-funded by the Fonds de Recherche du Québec -Santé (FRQS).

REFERENCES

Ahissar, E., Haidarliu, S., and Zacksenhouse, M. (1997). Decoding temporally encoded sensory input by cortical oscillations and thalamic phase comparators. *Proc. Natl. Acad. Sci. U S A* 94, 11633–11638. doi: 10.1073/pnas.94.21.11633

Albrecht, U., Bordon, A., Schmutz, I., and Ripperger, J. (2007). The multiple facets of Per2. *Cold Spring Harb. Symp. Quant. Biol.* 72, 95–104. doi: 10.1101/sqb.2007.72.001

Allen, G. I., and Tsukahara, N. (1974). Cerebrocerebellar communication systems. *Physiol. Rev.* 54, 957–1006.

Ballion, B., Frenois, F., Zold, C. L., Chetrit, J., Murer, M. G., and Gonon, F. (2009). D2 receptor stimulation, but not D1, restores striatal equilibrium in a rat model of Parkinsonism. *Neurobiol. Dis.* 35, 376–384. doi: 10.1016/j.nbd.2009.05.019

Başar, E., Başar-Eroglu, C., Karakaş, S., and Schürmann, M. (2001). Gamma, alpha, delta and theta oscillations govern cognitive processes. *Int. J. Psychophysiol.* 39, 241–248. doi: 10.1016/s0167-8760(00)00145-8

Berke, J. D., Okatan, M., Skurski, J., and Eichenbaum, H. B. (2004). Oscillatory entrainment of striatal neurons in freely moving rats. *Neuron* 43, 883–896. doi: 10.1016/j.neuron.2004.08.035

Bostan, A. C., Dum, R. P., and Strick, P. L. (2010). The basal ganglia communicate with the cerebellum. *Proc. Natl. Acad. Sci. U S A* 107, 8452–8456. doi: 10.1073/pnas.1000496107

Bostan, A. C., and Strick, P. L. (2010). The cerebellum and basal ganglia are interconnected. *Neuropsychol. Rev.* 20, 261–270. doi: 10.1007/s11065-010-9143-9

Bouthenet, M. L., Martres, M. P., Sales, N., and Schwartz, J. C. (1987). A detailed mapping of dopamine D-2 receptors in rat central nervous system by autoradiography with [125I]iodosulpride. *Neuroscience* 20, 117–155. doi: 10.1016/0306-4522(87)90008-x

Brown, P., Oliviero, A., Mazzone, P., Insola, A., Tonali, P., and Di Lazzaro, V. (2001). Dopamine dependency of oscillations between subthalamic nucleus and pallidum in Parkinson's disease. *J. Neurosci.* 21, 1033–1038.

Bruguerolle, B., and Simon, N. (2002). Biologic rhythms and Parkinson's disease: a chronopharmacologic approach to considering fluctuations in function. *Clin. Neuropharmacol.* 25, 194–201. doi: 10.1097/00002826-200207000-00002

Buehlmann, A., and Deco, G. (2010). Optimal information transfer in the cortex through synchronization. *PLoS Comput. Biol.* 6:e1000934. doi: 10.1371/journal.pcbi.1000934

Buzsáki, G. (2006). *Rhythms of the Brain.* New York: Oxford University Press.

Buzsáki, G., and Draguhn, A. (2004). Neuronal oscillations in cortical networks. *Science* 304, 1926–1929. doi: 10.1126/science.1099745

Buzsáki, G., and Moser, E. I. (2013). Memory, navigation and theta rhythm in the hippocampal-entorhinal system. *Nat. Neurosci.* 16, 130–138. doi: 10.1038/nn.3304

Calderon, D. P., Fremont, R., Kraenzlin, F., and Khodakhah, K. (2011). The neural substrates of rapid-onset Dystonia-Parkinsonism. *Nat. Neurosci.* 14, 357–365. doi: 10.1038/nn.2753

Chaudhury, D., Wang, L. M., and Colwell, C. S. (2005). Circadian regulation of hippocampal long-term potentiation. *J. Biol. Rhythms* 20, 225–236. doi: 10.1177/0748730405276352

Clement, E. A., Richard, A., Thwaites, M., Ailon, J., Peters, S., and Dickson, C. T. (2008). Cyclic and sleep-like spontaneous alternations of brain state under urethane anaesthesia. *PLoS One* 3:e2004. doi: 10.1371/journal.pone.0002004

Colwell, C. S. (2011). Linking neural activity and molecular oscillations in the SCN. *Nat. Rev. Neurosci.* 12, 553–569. doi: 10.1038/nrn3086

Costa, R. M., Lin, S. C., Sotnikova, T. D., Cyr, M., Gainetdinov, R. R., Caron, M. G., et al. (2006). Rapid alterations in corticostriatal ensemble coordination during acute dopamine-dependent motor dysfunction. *Neuron* 52, 359–369. doi: 10.1016/j.neuron.2006.07.030

Courtemanche, R., Chabaud, P., and Lamarre, Y. (2009). Synchronization in primate cerebellar granule cell layer local field potentials: basic anisotropy and dynamic changes during active expectancy. *Front. Cell. Neurosci.* 3:6. doi: 10.3389/neuro.03.006.2009

Courtemanche, R., Fujii, N., and Graybiel, A. M. (2003). Synchronous, focally modulated beta-band oscillations characterize local field potential activity in the striatum of awake behaving monkeys. *J. Neurosci.* 23, 11741–11752. doi: 10.3410/f.1002999.201447

Courtemanche, R., and Lamarre, Y. (2005). Local field potential oscillations in primate cerebellar cortex: synchronization with cerebral cortex during active and passive expectancy. *J. Neurophysiol.* 93, 2039–2052. doi: 10.1152/jn.00080.2004

Courtemanche, R., Pellerin, J. P., and Lamarre, Y. (2002). Local field potential oscillations in primate cerebellar cortex: modulation during active and passive expectancy. *J. Neurophysiol.* 88, 771–782. doi: 10.1152/jn.00718.2001

Courtemanche, R., Robinson, J. C., and Aponte, D. I. (2013). Linking oscillations in cerebellar circuits. *Front. Neural Circuits* 7:125. doi: 10.3389/fncir.2013.00125

Crittenden, J. R., and Graybiel, A. M. (2011). Basal ganglia disorders associated with imbalances in the striatal striosome and matrix compartments. *Front. Neuroanat.* 5:59. doi: 10.3389/fnana.2011.00059

Darna, M., Schmutz, I., Richter, K., Yelamanchili, S. V., Pendyala, G., Holtje, M., et al. (2009). Time of day-dependent sorting of the vesicular glutamate transporter to the plasma membrane. *J. Biol. Chem.* 284, 4300–4307. doi: 10.1074/jbc.m805480200

DeCoteau, W. E., Thorn, C., Gibson, D. J., Courtemanche, R., Mitra, P., Kubota, Y., et al. (2007a). Learning-related coordination of striatal and hippocampal theta rhythms during acquisition of a procedural maze task. *Proc. Natl. Acad. Sci. U S A* 104, 5644–5649. doi: 10.1073/pnas.0700818104

DeCoteau, W. E., Thorn, C., Gibson, D. J., Courtemanche, R., Mitra, P., Kubota, Y., et al. (2007b). Oscillations of local field potentials in the rat dorsal striatum during spontaneous and instructed behaviors. *J. Neurophysiol.* 97, 3800–3805. doi: 10.1152/jn.00108.2007

Dejean, C., Arbuthnott, G., Wickens, J. R., Le Moine, C., Boraud, T., and Hyland, B. I. (2011). Power fluctuations in beta and gamma frequencies in rat globus pallidus: association with specific phases of slow oscillations and differential modulation by dopamine D1 and D2 receptors. *J. Neurosci.* 31, 6098–6107. doi: 10.1523/JNEUROSCI.3311-09.2011

Delis, F., Mitsacos, A., and Giompres, P. (2004). Dopamine receptor and transporter levels are altered in the brain of Purkinje cell degeneration mutant mice. *Neuroscience* 125, 255–268. doi: 10.1016/j.neuroscience.2004.01.020

Destexhe, A., Contreras, D., and Steriade, M. (1999). Spatiotemporal analysis of local field potentials and unit discharges in cat cerebral cortex during natural wake and sleep states. *J. Neurosci.* 19, 4595–4608.

Doya, K. (2000). Complementary roles of basal ganglia and cerebellum in learning and motor control. *Curr. Opin. Neurobiol.* 10, 732–739. doi: 10.1016/s0959-4388(00)00153-7

Dugué, G. P., Brunel, N., Hakim, V., Schwartz, E. J., Chat, M., Lévesque, M., et al. (2009). Electrical coupling mediates tunable low-frequency oscillations and resonance in the cerebellar Golgi cell network. *Neuron* 61, 126–139. doi: 10.1016/j.neuron.2008.11.028

Ferris, M. J., Espana, R. A., Locke, J. L., Konstantopoulos, J. K., Rose, J. H., Chen, R., et al. (2014). Dopamine transporters govern diurnal variation in extracellular dopamine tone. *Proc. Natl. Acad. Sci. U S A* 111, E2751–E2759. doi: 10.1073/pnas.1407935111

Fowler, S. C., and Liou, J. R. (1998). Haloperidol, raclopride and eticlopride induce microcatalepsy during operant performance in rats, but clozapine and SCH 23390 do not. *Psychopharmacology (Berl)* 140, 81–90. doi: 10.1007/s002130050742

Frederick, A., Bourget-Murray, J., and Courtemanche, R. (2013). "Local field potential, synchrony of," in *Encyclopedia of Computational Neuroscience: Springer Reference*, eds D. Jaeger and R. Jung (Berlin Heidelberg: Springer-Verlag). Available online at: http://www.springerreference.com

Giompres, P., and Delis, F. (2005). Dopamine transporters in the cerebellum of mutant mice. *Cerebellum* 4, 105–111. doi: 10.1080/14734220510007851

Grasing, K., and Szeto, H. (1992). Diurnal variation in continuous measures of the rat EEG power spectra. *Physiol. Behav.* 51, 249–254. doi: 10.1016/0031-9384(92)90138-r

Gravotta, L., Gavrila, A. M., Hood, S., and Amir, S. (2011). Global depletion of dopamine using intracerebroventricular 6-hydroxydopamine injection disrupts normal circadian wheel-running patterns and PERIOD2 expression in the rat forebrain. *J. Mol. Neurosci.* 45, 162–171. doi: 10.1007/s12031-011-9520-8

Graybiel, A. M. (2008). Habits, rituals and the evaluative brain. *Annu. Rev. Neurosci.* 31, 359–387. doi: 10.1146/annurev.neuro.29.051605.112851

Graybiel, A. M. (2010). "Templates for neural dynamics in the striatum: striosomes and matrisomes," in *Handbook of Brain Microcircuits*, eds G. M. Shepherd and S. Grillner (New York, NY: Oxford University Press), 120–126.

Guilding, C., and Piggins, H. D. (2007). Challenging the omnipotence of the suprachiasmatic timekeeper: are circadian oscillators present throughout the mammalian brain? *Eur. J. Neurosci.* 25, 3195–3216. doi: 10.1111/j.1460-9568.2007.05581.x

Harbour, V. L., Weigl, Y., Robinson, B., and Amir, S. (2013). Comprehensive mapping of regional expression of the clock protein PERIOD2 in rat forebrain across the 24-h day. *PLoS One* 8:e76391. doi: 10.1371/journal.pone.0076391

Herrera-Meza, G., Aguirre-Manzo, L., Coria-Avila, G. A., Lopez-Meraz, M. L., Toledo-Cárdenas, R., Manzo, J., et al. (2014). Beyond the basal ganglia: cFOS expression in the cerebellum in response to acute and chronic dopaminergic alterations. *Neuroscience* 267, 219–231. doi: 10.1016/j.neuroscience.2014.02.046

Herzog, E. D. (2007). Neurons and networks in daily rhythms. *Nat. Rev. Neurosci.* 8, 790–802. doi: 10.1038/nrn2215

Hood, S., Cassidy, P., Cossette, M. P., Weigl, Y., Verwey, M., Robinson, B., et al. (2010). Endogenous dopamine regulates the rhythm of expression of the clock protein PER2 in the rat dorsal striatum via daily activation of D2 dopamine receptors. *J. Neurosci.* 30, 14046–14058. doi: 10.1523/JNEUROSCI.2128-10.2010

Hoshi, E., Tremblay, L., Feger, J., Carras, P. L., and Strick, P. L. (2005). The cerebellum communicates with the basal ganglia. *Nat. Neurosci.* 8, 1491–1493. doi: 10.1038/nn1544

Hurley, M. J., Mash, D. C., and Jenner, P. (2003). Markers for dopaminergic neurotransmission in the cerebellum in normal individuals and patients with Parkinson's disease examined by RT-PCR. *Eur. J. Neurosci.* 18, 2668–2672. doi: 10.1046/j.1460-9568.2003.02963.x

Hutcheon, B., and Yarom, Y. (2000). Resonance, oscillation and the intrinsic frequency preferences of neurons. *Trends Neurosci.* 23, 216–222. doi: 10.1016/s0166-2236(00)01547-2

Ichinohe, N., Mori, F., and Shoumura, K. (2000). A di-synaptic projection from the lateral cerebellar nucleus to the laterodorsal part of the striatum via the central lateral nucleus of the thalamus in the rat. *Brain Res.* 880, 191–197. doi: 10.1016/s0006-8993(00)02744-x

Ikai, Y., Takada, M., Shinonaga, Y., and Mizuno, N. (1992). Dopaminergic and non-dopaminergic neurons in the ventral tegmental area of the rat project, respectively, to the cerebellar cortex and deep cerebellar nuclei. *Neuroscience* 51, 719–728. doi: 10.1016/0306-4522(92)90310-x

Imbesi, M., Yildiz, S., Dirim Arslan, A., Sharma, R., Manev, H., and Uz, T. (2009). Dopamine receptor-mediated regulation of neuronal "clock" gene expression. *Neuroscience* 158, 537–544. doi: 10.1016/j.neuroscience.2008.10.044

Ito, M. (2006). Cerebellar circuitry as a neuronal machine. *Prog. Neurobiol.* 78, 272–303. doi: 10.1016/j.pneurobio.2006.02.006

Kiss, B., Horti, F., and Bobok, A. (2011). In vitro and in vivo comparison of [^{3}H](+)-PHNO and [^{3}H]raclopride binding to rat striatum and lobes 9 and 10 of the cerebellum: a method to distinguish dopamine D(3) from D(2) receptor sites. *Synapse* 65, 467–478. doi: 10.1002/syn.20867

Koch, G., Brusa, L., Carrillo, F., Lo Gerfo, E., Torriero, S., Oliveri, M., et al. (2009). Cerebellar magnetic stimulation decreases levodopa-induced dyskinesias in Parkinson disease. *Neurology* 73, 113–119. doi: 10.1212/WNL.0b013e3181ad5387

Lemaire, N., Hernandez, L. F., Hu, D., Kubota, Y., Howe, M. W., and Graybiel, A. M. (2012). Effects of dopamine depletion on LFP oscillations in striatum are task- and learning-dependent and selectively reversed by L-DOPA. *Proc. Natl. Acad. Sci. U S A* 109, 18126–18131. doi: 10.1073/pnas.1216403109

Li, C. L., and Parker, L. O. (1969). Effect of dentate stimulation on neuronal activity in the globus pallidus. *Exp. Neurol.* 24, 298–309. doi: 10.1016/0014-4886(69)90023-5

Lim, C., and Allada, R. (2013). ATAXIN-2 activates PERIOD translation to sustain circadian rhythms in Drosophila. *Science* 340, 875–879. doi: 10.1126/science.1234785

Maggi, C. A., and Meli, A. (1986). Suitability of urethane anesthesia for physiopharmacological investigations in various systems. Part 1: general considerations. *Experientia* 42, 109–114. doi: 10.1007/bf01952426

Magill, P. J., Sharott, A., Bolam, J. P., and Brown, P. (2004). Brain state-dependency of coherent oscillatory activity in the cerebral cortex and basal ganglia of the rat. *J. Neurophysiol.* 92, 2122–2136. doi: 10.1152/jn.00333.2004

Mallet, N., Le Moine, C., Charpier, S., and Gonon, F. (2005). Feedforward inhibition of projection neurons by fast-spiking GABA interneurons in the rat striatum in vivo. *J. Neurosci.* 25, 3857–3869. doi: 10.1523/jneurosci.5027-04.2005

Masubuchi, S., Honma, S., Abe, H., Ishizaki, K., Namihira, M., Ikeda, M., et al. (2000). Clock genes outside the suprachiasmatic nucleus involved in manifestation of locomotor activity rhythm in rats. *Eur. J. Neurosci.* 12, 4206–4214. doi: 10.1111/j.1460-9568.2000.01313.x

Mayne, E. W., Craig, M. T., McBain, C. J., and Paulsen, O. (2013). Dopamine suppresses persistent network activity via D(1) -like dopamine receptors in rat medial entorhinal cortex. *Eur. J. Neurosci.* 37, 1242–1247. doi: 10.1111/ejn.12125

McCormick, D. A. (2004). "Membrane properties and neurotransmitter actions," in *The Synaptic Organization of the Brain*, ed G. M. Shepherd (New York, NY: Oxford University Press), 39–77.

Mendoza, J., Pevet, P., Felder-Schmittbuhl, M. P., Bailly, Y., and Challet, E. (2010). The cerebellum harbors a circadian oscillator involved in food anticipation. *J. Neurosci.* 30, 1894–1904. doi: 10.1523/JNEUROSCI.5855-09.2010

Middleton, F. A., and Strick, P. L. (2000). Basal ganglia and cerebellar loops: motor and cognitive circuits. *Brain Res. Brain Res. Rev.* 31, 236–250. doi: 10.1016/s0165-0173(99)00040-5

Moers-Hornikx, V. M., Vles, J. S., Tan, S. K., Cox, K., Hoogland, G., Steinbusch, W. M., et al. (2011). Cerebellar nuclei are activated by high-frequency stimulation of the subthalamic nucleus. *Neurosci. Lett.* 496, 111–115. doi: 10.1016/j.neulet.2011.03.094

Monti, J. M., and Monti, D. (2007). The involvement of dopamine in the modulation of sleep and waking. *Sleep Med. Rev.* 11, 113–133. doi: 10.1016/j.smrv.2006.08.003

Mordel, J., Karnas, D., Pevet, P., Isope, P., Challet, E., and Meissl, H. (2013). The output signal of Purkinje cells of the cerebellum and circadian rhythmicity. *PLoS One* 8:e58457. doi: 10.1371/journal.pone.0058457

Morissette, J., and Bower, J. M. (1996). Contribution of somatosensory cortex to responses in the rat cerebellar granule cell layer following peripheral tactile stimulation. *Exp. Brain Res.* 109, 240–250. doi: 10.1007/bf00231784

Namihira, M., Honma, S., Abe, H., Tanahashi, Y., Ikeda, M., and Honma, K. (1999). Daily variation and light responsiveness of mammalian clock gene, Clock and BMAL1, transcripts in the pineal body and different areas of brain in rats. *Neurosci. Lett.* 267, 69–72. doi: 10.1016/s0304-3940(99)00324-9

Nicolelis, M. A. L., Baccala, L. A., Lin, R. C. S., and Chapin, J. K. (1995). Sensorimotor encoding by synchronous neural ensemble activity at multiple levels of the somatosensory system. *Science* 268, 1353–1358. doi: 10.1126/science.7761855

Nutt, J. G., Carter, J. H., Lea, E. S., and Woodward, W. R. (1997). Motor fluctuations during continuous levodopa infusions in patients with Parkinson's disease. *Mov. Disord.* 12, 285–292. doi: 10.1002/mds.870120304

Owasoyo, J. O., Walker, C. A., and Whitworth, U. G. (1979). Diurnal variation in the dopamine level of rat brain areas: effect of sodium phenobarbital. *Life Sci.* 25, 119–122. doi: 10.1016/0024-3205(79)90382-5

Paxinos, G., and Watson, C. (1998). *The Rat Brain in Stereotaxic Coordinates.* SanDiego, CA: Academic Press.

Pellerin, J. P., and Lamarre, Y. (1997). Local field potential oscillations in primate cerebellar cortex during voluntary movement. *J. Neurophysiol.* 78, 3502–3507.

Ratcheson, R. A., and Li, C. L. (1969). Effect of dentate stimulation on neuronal activity in the caudate nucleus. *Exp. Neurol.* 25, 268–281. doi: 10.1016/0014-4886(69)90050-8

Rath, M. F., Rohde, K., and Moller, M. (2012). Circadian oscillations of molecular clock components in the cerebellar cortex of the rat. *Chronobiol. Int.* 29, 1289–1299. doi: 10.3109/07420528.2012.728660

Rivlin-Etzion, M., Marmor, O., Heimer, G., Raz, A., Nini, A., and Bergman, H. (2006). Basal ganglia oscillations and pathophysiology of movement disorders. *Curr. Opin. Neurobiol.* 16, 629–637. doi: 10.1016/j.conb.2006.10.002

Roopun, A. K., Lebeau, F. E., Rammell, J., Cunningham, M. O., Traub, R. D., and Whittington, M. A. (2010). Cholinergic neuromodulation controls directed temporal communication in neocortex in vitro. *Front. Neural Circuits* 4:8. doi: 10.3389/fncir.2010.00008

Ros, H., Sachdev, R. N., Yu, Y., Sestan, N., and McCormick, D. A. (2009). Neocortical networks entrain neuronal circuits in cerebellar cortex. *J. Neurosci.* 29, 10309–10320. doi: 10.1523/JNEUROSCI.2327-09.2009

Sanchez-Vives, M. V., and McCormick, D. A. (2000). Cellular and network mechanisms of rhythmic recurrent activity in neocortex. *Nat. Neurosci.* 3, 1027–1034. doi: 10.1038/79848

Schnitzler, A., and Gross, J. (2005). Normal and pathological oscillatory communication in the brain. *Nat. Rev. Neurosci.* 6, 285–296. doi: 10.1038/nrn1650

Schweighofer, N., Doya, K., and Kuroda, S. (2004). Cerebellar aminergic neuromodulation: towards a functional understanding. *Brain Res. Brain Res. Rev.* 44, 103–116. doi: 10.1016/j.brainresrev.2003.10.004

Sharma, A. V., Wolansky, T., and Dickson, C. T. (2010). A comparison of sleeplike slow oscillations in the hippocampus under ketamine and urethane anesthesia. *J. Neurophysiol.* 104, 932–939. doi: 10.1152/jn.01065.2009

Sharott, A., Doig, N. M., Mallet, N., and Magill, P. J. (2012). Relationships between the firing of identified striatal interneurons and spontaneous and driven cortical activities in vivo. *J. Neurosci.* 32, 13221–13236. doi: 10.1523/jneurosci.2440-12.2012

Sharott, A., Magill, P. J., Harnack, D., Kupsch, A., Meissner, W., and Brown, P. (2005). Dopamine depletion increases the power and coherence of beta-oscillations in the cerebral cortex and subthalamic nucleus of the awake rat. *Eur. J. Neurosci.* 21, 1413–1422. doi: 10.1111/j.1460-9568.2005.03973.x

Shieh, K. R. (2003). Distribution of the rhythm-related genes rPERIOD1, rPERIOD2 and rCLOCK, in the rat brain. *Neuroscience* 118, 831–843. doi: 10.1016/s0306-4522(03)00004-6

Steriade, M. (2003). *Neuronal Substrates of Sleep and Epilepsy.* Cambridge, UK: Cambridge University Press.

Stern, E. A., Jaeger, D., and Wilson, C. J. (1998). Membrane potential synchrony of simultaneously recorded striatal spiny neurons in vivo. *Nature* 394, 475–478. doi: 10.1038/28848

Takada, M., Sugimoto, T., and Hattori, T. (1993). MPTP neurotoxicity to cerebellar Purkinje cells in mice. *Neurosci. Lett.* 150, 49–52. doi: 10.1016/0304-3940(93)90105-t

Thorn, C. A., Atallah, H., Howe, M., and Graybiel, A. M. (2010). Differential dynamics of activity changes in dorsolateral and dorsomedial striatal loops during learning. *Neuron* 66, 781–795. doi: 10.1016/j.neuron.2010.04.036

Thorn, C. A., and Graybiel, A. M. (2014). Differential entrainment and learning-related dynamics of spike and local field potential activity in the sensorimotor and associative striatum. *J. Neurosci.* 34, 2845–2859. doi: 10.1523/jneurosci.1782-13.2014

Tseng, K. Y., Kasanetz, F., Kargieman, L., Riquelme, L. A., and Murer, M. G. (2001). Cortical slow oscillatory activity is reflected in the membrane potential and spike trains of striatal neurons in rats with chronic nigrostriatal lesions. *J. Neurosci.* 21, 6430–6439.

Uhlhaas, P. J., Roux, F., Rodriguez, E., Rotarska-Jagiela, A., and Singer, W. (2010). Neural synchrony and the development of cortical networks. *Trends Cogn. Sci.* 14, 72–80. doi: 10.1016/j.tics.2009.12.002

Valencia, M., Artieda, J., Bolam, J. P., and Mena-Segovia, J. (2013). Dynamic interaction of spindles and gamma activity during cortical slow oscillations and its modulation by subcortical afferents. *PLoS One* 8:e67540. doi: 10.1371/journal.pone.0067540

Verwey, M., and Amir, S. (2012). Variable restricted feeding disrupts the daily oscillations of Period2 expression in the limbic forebrain and dorsal striatum in rats. *J. Mol. Neurosci.* 46, 258–264. doi: 10.1007/s12031-011ds-9529-z

Walters, J. R., Hu, D., Itoga, C. A., Parr-Brownlie, L. C., and Bergstrom, D. A. (2007). Phase relationships support a role for coordinated activity in the indirect pathway in organizing slow oscillations in basal ganglia output after loss of dopamine. *Neuroscience* 144, 762–776. doi: 10.1016/j.neuroscience.2006.10.006

Watson, T. C., Becker, N., Apps, R., and Jones, M. W. (2014). Back to front: cerebellar connections and interactions with the prefrontal cortex. *Front. Syst. Neurosci.* 8:4. doi: 10.3389/fnsys.2014.00004

Wilder-Smith, E., Tan, E. K., Law, H. Y., Zhao, Y., Ng, I., and Wong, M. C. (2003). Spinocerebellar ataxia type 3 presenting as an L-DOPA responsive dystonia phenotype in a Chinese family. *J. Neurol. Sci.* 213, 25–28. doi: 10.1016/s0022-510x(03)00129-1

Wilson, C. J., and Kawaguchi, Y. (1996). The origins of two-state spontaneous membrane potential fluctuations of neostriatal spiny neurons. *J. Neurosci.* 16, 2397–2410.

Zeitzer, J. M. (2013). Control of sleep and wakefulness in health and disease. *Prog. Mol. Biol. Transl. Sci.* 119, 137–154. doi: 10.1016/B978-0-12-396971-2.00006-3

Zhang, Y., Ling, J., Yuan, C., Dubruille, R., and Emery, P. (2013). A role for Drosophila ATX2 in activation of PER translation and circadian behavior. *Science* 340, 879–882. doi: 10.1126/science.1234746

Conflict of Interest Statement: The authors declare no external commercial or financial relationships that could be perceived as a conflict of interest.

Received: 02 April 2014; accepted: 24 July 2014; published online: 15 September 2014.
*Citation: Frederick A, Bourget-Murray J, Chapman CA, Amir S and Courtemanche R (2014) Diurnal influences on electrophysiological oscillations and coupling in the dorsal striatum and cerebellar cortex of the anesthetized rat. Front. Syst. Neurosci. **8**:145. doi: 10.3389/fnsys.2014.00145*
This article was submitted to the journal Frontiers in Systems Neuroscience.

frontiers in
SYSTEMS NEUROSCIENCE

HYPOTHESIS AND THEORY ARTICLE
published: 15 September 2014
doi: 10.3389/fnsys.2014.00163

The therapeutic potential of the cerebellum in schizophrenia

Krystal L. Parker[1]*, Nandakumar S. Narayanan[1] and Nancy C. Andreasen[2]

[1] *Department of Neurology, University of Iowa, Iowa City, IA, USA*
[2] *Department of Psychiatry, University of Iowa, Iowa City, IA, USA*

Edited by:
Thomas C. Watson, University of Bristol, UK

Reviewed by:
Detlef H. Heck, University of Tennessee Health Science Center, USA
Pauline Yvanne Obiang, Centre national de la recherche scientifique, France

****Correspondence:***
Krystal L. Parker, Department of Neurology, University of Iowa, 2110 MedLabs, Iowa City, IA 52242, USA
e-mail: Krystallynn.parker@gmail.com

The cognitive role of the cerebellum is critically tied to its distributed connections throughout the brain. Accumulating evidence from anatomical, structural and functional imaging, and lesion studies advocate a cognitive network involving indirect connections between the cerebellum and non-motor areas in the prefrontal cortex. Cerebellar stimulation dynamically influences activity in several regions of the frontal cortex and effectively improves cognition in schizophrenia. In this manuscript, we summarize current literature on the cingulocerebellar circuit and we introduce a method to interrogate this circuit combining opotogenetics, neuropharmacology, and electrophysiology in awake-behaving animals while minimizing incidental stimulation of neighboring cerebellar nuclei. We propose the novel hypothesis that optogenetic cerebellar stimulation can restore aberrant frontal activity and rescue impaired cognition in schizophrenia. We focus on how a known cognitive region in the frontal cortex, the anterior cingulate, is influenced by the cerebellum. This circuit is of particular interest because it has been confirmed using tracing studies, neuroimaging reveals its role in cognitive tasks, it is conserved from rodents to humans, and diseases such as schizophrenia and autism appear in its aberrancy. Novel tract tracing results presented here provide support for how these two areas communicate. The primary pathway involves a disynaptic connection between the cerebellar dentate nuclei (DN) and the anterior cingulate cortex. Secondarily, the pathway from cerebellar fastigial nuclei (FN) to the ventral tegmental area, which supplies dopamine to the prefrontal cortex, may play a role as schizophrenia characteristically involves dopamine deficiencies. We hope that the hypothesis described here will inspire new therapeutic strategies targeting currently untreatable cognitive impairments in schizophrenia.

Keywords: schizophrenia, cerebellum, anterior cingulate, cognitive symptoms, optogenetic stimulation

INTRODUCTION

The purpose of this theory and hypothesis manuscript is two fold. First, we review the role of the cerebellum in cognition and schizophrenia, the anatomy of cerebellar projections to frontal cortex, and the available evidence indicating that the cerebellum influences the frontal cortex. Second, we introduce the novel hypothesis that optogenetic cerebellar stimulation may ameliorate cognitive symptoms of schizophrenia by normalizing frontal activity, and we propose testable animal and translational experiments to probe this hypothesis. Studies have shown that connections exist between the frontal cortex and cerebellum and that cerebellar stimulation improves cognitive symptoms of schizophrenia; to our knowledge, this manuscript is the first to propose a method to pharmacologically disrupt frontal function in rodents to mimic abnormalities in schizophrenia, document cognitive dysfunction similar to that reported in schizophrenia, and use cerebellar stimulation to restore frontal activity and rescue cognition. Specifically, we will evaluate the therapeutic potential of the cerebellum by introducing a technique to interrogate cerebellar connections to the frontal cortex using combined opotogenetics, neuropharmacology, and electrophysiology in awake-behaving animals while minimizing incidental stimulation of neighboring cerebellar nuclei.

The cerebellum is a critical component in tasks of both motor and cognitive origin. Thalamic connections between the cerebellum and frontal cortex create the potential for the cerebellum to powerfully influence cognition. In schizophrenia, there are abnormalities in all three regions, which led to the hypothesis that a distributed network involving the cerebellum contributes to cognitive deficits. We, and many of our colleagues, have been investigating this circuit for almost two decades (Leiner et al., 1994; Andreasen et al., 1998; Schmahmann, 1998, 2010; Andreasen and Pierson, 2008). Although studies of functional neuroimaging, anatomy, positron emission tomography (PET), and structural and functional magnetic resonance imaging are extensive, it is unclear how this circuitry is influenced by schizophrenia (Alphs, 2006). The advent of molecular tools and imaging technology such as tractography and diffusion tensor imaging (DTI) that can be used in psychiatric disorders have provided additional clarity to this issue (White et al., 2008).

Cognitive impairments in schizophrenia including executive dysfunctions in working and episodic memory, (Andreasen et al., 1999; Ragland et al., 2009), attention, reasoning, and timing (Carroll et al., 2009), remain untreatable (Alphs, 2006). These impairments have been described as cognitive dysmetrias, or disruptions in the synchronous coordination of cognitive capacities (Andreasen et al., 1998; Schmahmann, 1998). Recently, Demirtas-Tatlidede et al. reported that cerebellar vermal theta burst stimulation (TBS) has been effective at relieving some cognitive symptoms in treatment-resistant schizophrenia patients (Demirtas-Tatlidede et al., 2010). Specifically, eight schizophrenia patients were evaluated using comprehensive neuropsychological testing, Positive and Negative symptoms subscale (PANSS), Clinical Global Impression (CGI), Calgary Depression Scale for schizophrenics (CDSS), Profile of Mood States (POMS), and Visual Analogue Mood Scale (VAS) for dimensions of mood (Happiness, Sadness, Calmness, Anxiety, Wellbeing, Anger, Self-confidence, Fear, Alertness, and Energy). Subjects received cerebellar vermal TBS twice daily on 5 consecutive days for a total of 10 stimulation sessions. Baseline ratings were compared with ratings immediately following stimulation and 1 week later. The results showed significant improvement in negative symptoms reported by the PANSS both following treatment and at follow-up, and there was a significant elevation in mood. Cognition also improved as the subject had fewer working memory omissions with no worsening of other measures.

The mechanism underlying the efficacy of cerebellar stimulation in schizophrenia is unknown. Studies have shown that electrically stimulating the cerebellum produces downstream changes in the prefrontal cortex and anterior cingulate cortex (Mittleman et al., 2008; Rogers et al., 2011, 2013; Watson et al., 2014). Connections between the cerebellum and anterior cingulate, comprising a cingulocerebellar circuit, are of particular interest because they have been confirmed to exist by tracing studies, they are conserved between species including humans, primates, and rodents, and structural and functional abnormalities are present in schizophrenia. Here, we present empirical evidence that (1) the deep cerebellar nuclei and anterior cingulate cortex are disynaptically connected via two separate pathways (the thalamus and the ventral tegemental area—VTA) allowing the cerebellum access to the frontal cortex; and (2) the cerebellum may modulate frontal neuron ensembles. This cerebellar modulatory mechanism has the potential to be harnessed to rescue abnormalities in the anterior cingulate, typically associated with schizophrenia. The mechanism underlying the efficacy of cerebellar stimulation needs to be illuminated if cerebellar stimulation is to become a therapeutic treatment strategy for the negative and cognitive symptoms of schizophrenia (Demirtas-Tatlidede et al., 2013).

CINGULOCEREBELLAR INTERACTIONS IN SCHIZOPHRENIA

FUNCTIONAL NEUROIMAGING

Cognitive dysmetria has been probed in patients with schizophrenia (Andreasen and Pierson, 2008) concurrently undergoing neuroimaging using tasks such as recall of complex narratives (Andreasen et al., 1995a), episodic memory (Andreasen et al., 1999; Ragland et al., 2009), memory for word lists (Andreasen et al., 1995b; Paradiso et al., 1997; Crespo-Facorro et al., 1999), recognition memory (Crespo-Facorro et al., 2001), dichotic listening (O'Leary et al., 1996), eyeblink conditioning (Parker et al., 2013b; **Figure 1**), and timing (Volz et al., 2001). These data consistently indicate lower blood flow in the cerebellum and frontal cortex (Andreasen et al., 1997) including medial frontal regions such as the anterior cingulate (Adams and David, 2007).

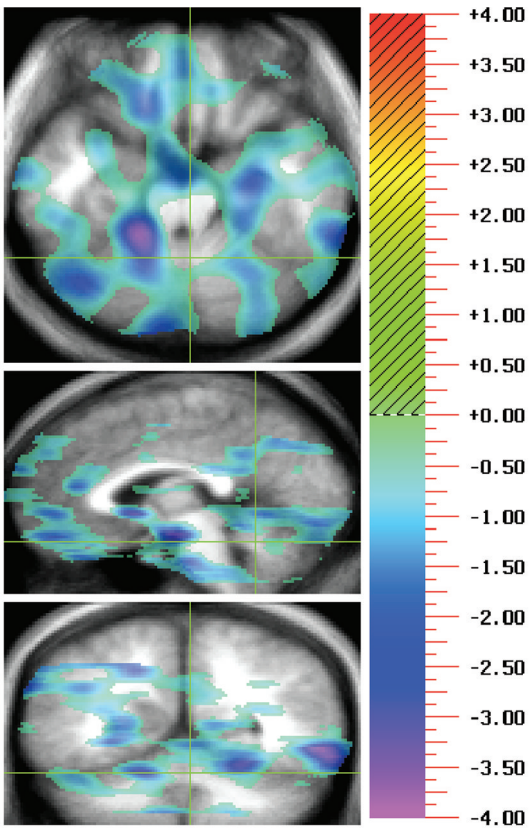

FIGURE 1 | During positron emissions tomography (PET) imaging of a task typically thought to be cerebellum dependent, eyeblink conditioning, hypofunction was revealed in the cingulocerebellar circuit. A double subtraction method where the baseline pseudoconditioning phase of unpaired tones and airpuffs was first subtracted and then the rCBF for patients with schizophrenia was subtracted from that of controls, show negative peaks indicating patients with schizophrenia have less rCBF than controls. This representative image shows hypofunction of the anterior cingulate (Talairach coordinates: −1, 30, 14) and cerebellar lobules IV/V, and IX (Talairach coordinates: −3, −67, −17) in patients with schizophrenia in comparison to healthy controls. For each illustration there are three orthogonal views per row with transaxial on the top, sagittal in the middle, and coronal on the bottom. Green crosshairs are used to show the location of the slice. Images follow radiological convention and show location as if facing the patient where the left side of the image represents the patient's right side. The statistical maps of the PET, showing the regions where the two groups differed significantly at the 0.005 level, are superimposed on a composite magnetic resonance image (MRI) derived by averaging the MR scans from the subjects. Regions in red/yellow tones indicate positive peaks (greater activation in patients than in controls) and regions with blue/purple indicate negative peaks (less activity in patients than controls). The statistical results are portrayed using the value of the associated *t*-statistic, which is shown on the color bar on the right. The images are referred to as "*t* maps" showing all voxels in the image which exceed a display threshold.

The correlation of these cognitive deficits with abnormal regional cerebral blood flow, led to the mechanistic explanation that abnormalities in a distributed cerebellar neural circuit may underlie cognitive impairments in schizophrenia (Andreasen et al., 1998). Aberrant connections from the cerebellum to the cerebral cortex may influence misconnections between percepts and their meanings, in turn causing errors in perceptual binding and misinterpretations of many kinds (e.g., delusions, hallucinations); they may also lead to inefficient or inaccurate information processing, forming the basis for the multiple types of cognitive impairments observed in schizophrenia (Andreasen et al., 1998; Wiser et al., 1998; Schmahmann, 2004).

The precise networks that are dysfunctional in schizophrenia remain elusive. Of particular interest is the anterior cingulate (Brodmann Areas 24/32) for its involvement in normal cognition and executive functioning including working memory, attention, emotional processing, response inhibition, performance monitoring, and timing (Devinsky et al., 1995; Narayanan et al., 2005, 2013; Picton et al., 2006; Cavanagh et al., 2009; Prabhakaran et al., 2011; Gasquoine, 2013). In addition, the anterior cingulate is consistently hypoactive in schizophrenia during cognitive tasks (Adams and David, 2007) such as random number generation (Artiges et al., 2000; Meyer-Lindenberg et al., 2001), error detection (Carter et al., 2001), monitoring self-performance (Carter et al., 1998, 2001), Stoop Tasks (Yücel et al., 2002; Minzenberg et al., 2009), continuous performance (Honey et al., 2005), and timing (Volz et al., 2001). Many of these studies found correlated cerebellar functional abnormalities (Honey et al., 2005; Koziol et al., 2013). These data provide evidence that cognitive impairments in schizophrenia may result from abnormalities in the cingulocerebellar circuit.

STRUCTURAL ABNORMALITIES

In addition to hypofunction, studies report structural abnormalities in the anterior cingulate, thalamus, and cerebellum in schizophrenia. Specifically, voxel based morphometry (Mouchet-Mages et al., 2011) and DTI (Wiser et al., 1998) reveal abnormalities in white matter connectivity between the nodes of the cingulocerebellar circuit in schizophrenia. The presence of structural abnormalities in these structures supports abnormalities in the distributed cerebellar network.

The cingulum bundle, including the anterior cingulate, has consistently shown abnormalities in schizophrenia (White et al., 2008). Patients with schizophrenia have an overall reduction of gray matter in the anterior cingulate (Brodmann Area 32) (Glahn et al., 2008; Takayanagi et al., 2013; Salgado-Pineda et al., 2014). Post mortem studies revealed a reduction in laminar thickness in the anterior cingulate (dorsal and subcullosal regions) (Fornito et al., 2009). Mitelman et al. report that schizophrenia patients with better outcomes have correspondingly higher fractional anisotropy (FA) than normal in frontal white matter areas including bilateral cingulate gyri; emphasizing the integral role of the anterior cingulate, he proposed that this increased FA in cingulate white matter may serve a neuroprotective role as indicated by a better outcome for patients (Mitelman et al., 2006). Our data support this hypothesis, as our patients with larger anterior cingulate volumes reported greater psychotic symptom improvement overtime (McCormick et al., 2005). In addition, functional and structural imaging data found convergent abnormalities in the medial frontal cortex including the anterior cingulate (Fornito et al., 2009; Pomarol-Clotet et al., 2010).

Structural abnormalities have also been revealed in thalamic nuclei and their projections in schizophrenia (Andreasen et al., 1994; Magnotta et al., 2008). Specifically, the thalamus has been shown to be reduced in size in schizophrenia (Andreasen et al., 1994; Buschman and Miller, 2007). In addition, FA was decreased in the internal capsule connecting the thalamus to the anterior cingulate (Oh et al., 2009). DTI reveals reduced FA in the white matter fiber tracts located between the thalamus and cerebellum in patients with schizophrenia compared to normal controls. Specifically, there was reduced FA within the superior cerebellar peduncle but not along the tract from the cerebellum to the thalamus (Magnotta et al., 2008). Little is known about whether the thalamus is essentially involved in schizophrenia or whether it is simply a convergence point and relay station for signals from other parts of the brain (Saalmann and Kastner, 2011). However, medial thalamic nuclei have been shown to project to the anterior cingulate cortex and inactivating these projections impairs working memory (Hsu and Shyu, 1997; Parnaudeau et al., 2013).

We have also reported that our schizophrenia patients have decreased overall cerebellar volume and, more specifically, decreased volume of the anterior lobe of the cerebellar vermis. Decreased cerebellar volume correlated with longer duration of psychotic and negative symptoms, and greater psychosocial impairment (Nopoulos et al., 1999; Wassink et al., 1999). Post mortem morphometric analyses of patients with schizophrenia confirm decreased anterior cerebellar vermis volume (Weinberger et al., 1980). A reduction of gray matter in Crus I and II of lobule VII has also been reported (Kühn et al., 2012). There may also be reduced FA in the vermis and middle cerebellar peduncles of schizophrenia patients (Okugawa et al., 2003, 2005).

Human lesion studies provide support for cingulocerebellar involvement in cognition. Although cerebellar lesions predominantly reveal motor impairments (Groiss and Ugawa, 2013), patients also suffer from comorbid cognitive impairments (Gottwald et al., 2004; Grimaldi and Manto, 2012). These dysfunctions include impaired timing, attention, memory, and language, all of which classically rely on the frontal lobes (Akshoomoff and Courchesne, 1992; Fiez et al., 1992; Grafman et al., 1992; Courchesne et al., 1994; Stoodley and Schmahmann, 2009). Schmahmann's cerebellar cognitive affective syndrome has shown that human cerebellar lesions cause cognitive impairments (Schmahmann, 2004). Inducing transient impairments using repetitive transcranial cerebellar stimulation has recently been shown to impair cognitive tasks such as language, emotion, learning, memory, perception, and timing (Fierro et al., 2007; Koch et al., 2007; Oliveri et al., 2007; Grube et al., 2010; Bijsterbosch et al., 2011; Boehringer et al., 2013; Tomlinson et al., 2013; Grimaldi et al., 2014). Similar deficits are reported following lesions to the anterior cingulate (Devinsky et al., 1995). Specifically, timing on the go-nogo task, which probes response inhibition, has been shown to be impaired (Picton et al., 2006).

ANATOMICAL CONNECTIONS

Neuronal tract-tracing has made giant strides to link the cerebellum to prefrontal networks, but many have focused exclusively on the dorsal lateral prefrontal cortex, which rodents lack (Uylings et al., 2003). The dorsal lateral prefrontal cortex (Brodmann Areas 9/46) has been the subject of extensive tracing studies in primates, which establish a "closed-loop" linking cerebellar nuclei (specifically the dentate) and the dorsal lateral prefrontal cortex via the contralateral thalamus. Retrograde tracer infusions in the dorsolateral prefrontal cortex and DTI reveal projections back to the deep cerebellar nuclei and cerebellar cortex via the pontine nuclei (PN; Middleton and Strick, 2001; Kamali et al., 2010; Schulz et al., 2014; **Figure 2**). These studies establish the potential for cerebellar-prefrontal interactions in primates but additional research is necessary (Uylings et al., 2003).

As we have argued, the anterior cingulate cortex is essential for normal cognition and shows impairments in schizophrenia. In humans, the anterior cingulate is also known as Brodmann areas 24/32 or the prelimbic cortices. Although homogenous in rodents, nomenclature is inconsistent. In rodents, the anterior cingulate cortex (Cg3/prelimbic) is commonly known as the medial prefrontal cortex and is described based on four cytoarchitecturally unique regions, Cg1, Cg2, Cg3/prelimbic, and infralimbic (Bostan et al., 2013; Vogt et al., 2013; Vogt and Paxinos, 2014). Although it remains unclear if a similar "closed-loop" exists in the cingulocerebellar circuit, we hope to elucidate these connections.

The cerebellar afferent pathway in the cingulocerebellar circuit involves direct anterior cingulate projections to the PN (Vilensky and Van Hoesen, 1981; Glickstein et al., 1985; Legg et al., 1989; Dembrow et al., 2010). Specifically, Vilensky et al. report that the rostral cingulate projects to the medial PN while the caudal cingulate regions project more laterally (Vilensky and Van Hoesen, 1981). These corticopontine fibers form the middle cerebellar peduncle and project to the deep cerebellar nuclei and cerebellar cortex.

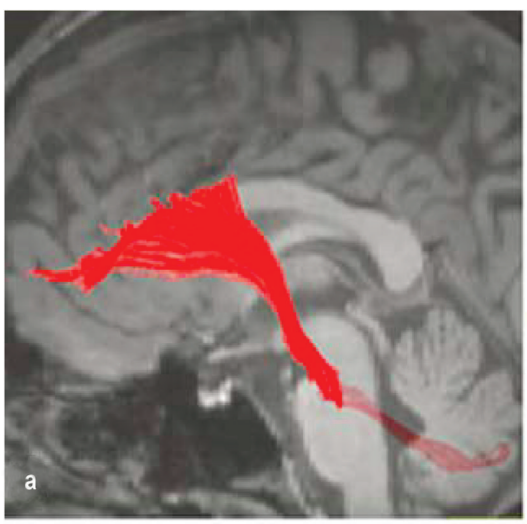

FIGURE 2 | Fronto-ponto-cerebellar tractography reconstructed on a 3D T1- weighted image (Kamali et al., 2010).

There is evidence for two efferent pathways through which deep cerebellar nuclei communicate with the anterior cingulate. The first efferent pathway involves a disynaptic connection between the deep cerebellar nuclei and contralateral thalamus (Magnotta et al., 2008; Strick et al., 2009). Medial thalamic nuclei have been shown to project to the anterior cingulate cortex (Hsu and Shyu, 1997; Parnaudeau et al., 2013) although there is evidence for projections from all thalamic nuclei depending on the precise location of the anterior cingulate/prelimbic area in question (Condé et al., 1990). Therefore, it is likely that cerebellar projections to the thalamus are capable of transmitting information to broad regions of the anterior cingulate cortex. These connections are highly topographic and the labeled neurons are highly dependent on the precise location of the tracer injection.

The second efferent pathway includes deep cerebellar nuclei (fastigial) projections to the VTA (Snider et al., 1976). The VTA is known to supply dopaminergic input to the anterior cingulate and is able to affect neuronal activity when pharmacologically manipulated (Williams and Goldman-Rakic, 1998). Studies have corroborated this efferent pathway by showing that electrically stimulating cerebellar dentate nuclei (DN; Mittleman et al., 2008) and fastigial nuclei (FN; Watson et al., 2009) influences medial prefrontal dopamine signaling, which is impaired in schizophrenia (Hadley et al., 2014). Conversely, electrically stimulating the medial prefrontal cortex elicited neuronal firing in cerebellar lobule VII which projects back to the deep nuclei (Watson et al., 2009). A similar pathway and mechanistic approach to target the dento-VTA-PFC tract has been suggested by Rogers et al. in autism (Rogers et al., 2013) (see section on applications for neuropsychiatric illnesses). One challenge of electrical stimulation in mapping these circuits is that the influence of fibers of passage and indirect stimulation of neighboring nuclei confounds the results. Future studies using optogenetics may achieve greater specificity.

Although these studies show connections exist, the precise projections remain elusive. To illuminate the cingulocerebellar circuit, we infused retrograde tracer (RetroBeads, Lumaflour) in the left anterior cingulate/medial frontal cortex and anterograde tracer (Phaseolus vulgaris leucoagglutinin, Life Technologies) in the right cerebellar dentate deep nuclei of Long Evans rats and found these structures to be disynaptically connected via two distinct routes as previously reported. Single synapse red prefrontal beads and green cerebellar tracer colocalized on left ventrolateral thalamic nuclei and on VTA neurons nuclei (**Figures 3A,B**). Convergence of information in these networks provides two avenues through which the cerebellum may influence neurons in the anterior cingulate cortex. However, the cerebellum may influence cortical function indirectly through other thalamic inputs. More analyses are needed to identify or rule out colocalization in other thalamic nuclei.

This anatomical connection opens up an avenue for the cerebellum to modulate aberrant prefrontal networks in schizophrenia. We are currently analyzing longitudinal DTI and tractography data from patients at intake and throughout the disease course, which will allow us to choose regions of interest in the anterior cingulate and the deep cerebellar nuclei to more precisely document abnormalities in the cingulocerebellar circuit.

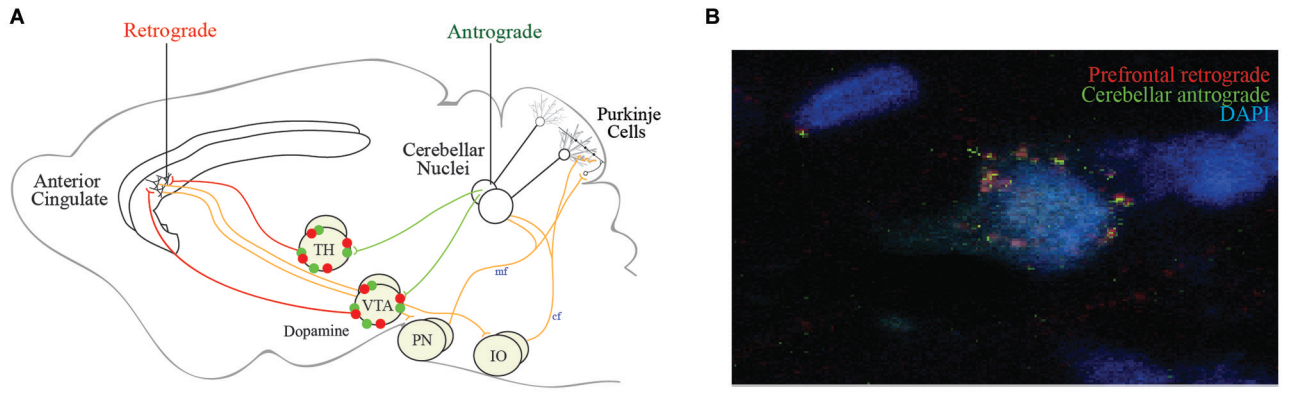

FIGURE 3 | Proposed efferent cingulocerellar circuitry. **(A)** Schematic representation of the efferent cerebellar projections enabling cerebellar access to the medial prefrontal cortex/anterior cingulate via the ventrolateral thalamus and VTA. Two efferent pathways are thought to connect the cerebellum and prefrontal cortex (1) Cerebellar projections originating from dentate (DN) or fastigial nuclei (FN) to the contralateral thalamus and anterior cingulate cortex; and (2) Cerebellar projections originating from DN or FN to the contralateral ventral tegmental area (VTA) which send dopaminergic projections to the anterior cingulate cortex. The afferent pathways from the anterior cingulate back to the cerebellum via the pontine nuclei (PN) and inferior olive (IO). **(B)** Our tract tracing data following anterograde tracer (green) in the right dentate nuclei and retrograde tracer (red) in the contralateral (left) medial prefrontal cortex revealed tracer colocalization of both red and green beads on a single contralateral ventrolateral thalamic (VLTh) neuron **(B)**.

It is important to note that as deep cerebellar nuclei are the sole output of the cerebellum, abnormalities in any area of the cerebellum have the potential to influence frontal function through the cinglocerebellar circuit.

A testable hypothesis: cerebellar stimulation restores prefrontal function and rescues cognition in schizophrenia

It is through the convergence of cerebellar deep nuclei and anterior cingulate projections on thalamic neurons that we propose the cerebellum can be harnessed to rescue aberrant prefrontal circuits in schizophrenia. The implications of this efferent, disynaptic pathway are numerous. Cerebellar stimulation may have the ability to restore prefrontal neuronal activity and firing patterns, allowing relief from some of the cognitive symptoms of schizophrenia.

Several studies provide support for the efficacy of cerebellar stimulation in neuropsychiatry (Grimaldi et al., 2014). A classic study electrically stimulated the cerebellum and reported improved cognition based on increased alertness, improvement in thinking, and fluency of speech in addition to many enriched emotional characteristics in patients with epilepsy (Cooper et al., 1976). Recently, cerebellar vermal TBS has been effective at relieving some cognitive symptoms in treatment-resistant schizophrenia patients (Demirtas-Tatlidede et al., 2010). In addition, Schutter et al. showed that cerebellar vermal TBS produced downstream changes in neuronal activity in the frontal cortex (Schutter et al., 2003). The exact cerebellar circuitry needs to be explicitly mapped prior to pursuing translational research.

How the cerebellum normally influences the prefrontal cortex and anterior cingulate is an important question that can be investigated using neuronal ensemble recordings of these areas in animals exhibiting phenotypes of schizophrenia. The cingulocerebellar circuit is likely essential for a variety of cognitive tasks as is documented by the previously described neuroimaging results. Correlating neuronal recordings will provide clarity as to how the cerebellum and prefrontal cortex work in synchrony during cognitive tasks such as learning, timing, and attention. Task-specific modulation will indicate if these areas are necessary.

Several groups have made progress deciphering the role of nodes in the cingulocerebellar circuit using electrical stimulation (Mittleman et al., 2008; Watson et al., 2009; Rogers et al., 2011, 2013). However, results from these studies are limited due to the unwanted spread of electrical stimulation. To circumvent this issue, we propose using optogenetic stimulation of select, isolated pools of neurons in the cingulocerebellar circuit. Optogenetic stimulation of Purkinje cells has been shown to be an effective way to modulate cerebellar output (Tsubota et al., 2011). Using our tract-tracing results to target specific deep nuclear projections in the cingluocerebellar circuit, channelrhodopsin, a light-activated channel, can be infused into cerebellar neurons. Once expressed, these proteins render their projections photoexcitable. Optical fibers can be placed in the thalamus to selectively stimulate the cerebellar neuronal projections to the anterior cingulate while not affecting other cerebellar neuronal populations. Optogenetically stimulating cerebellar dentate projections in the thalamus could influence the prefrontal cortex (**Figure 4**). This optogenetic paradigm could be combined with neuronal ensemble recordings to probe the dynamic relationship between the prefrontal cortex and cerebellum while analyzing task-dependent modulation. Based on evidence from cerebellar stimulation studies, cerebellar optogenetic stimulation has the potential to enhance prefrontal neuronal modulation and show correlates of behavioral improvement.

Another way to investigate the cingulocerebellar circuit is to induce abnormalities similar to those reported during schizophrenia and attempt to rescue impairments using cerebellar stimulation. Targeting neurotransmitter cascades such as

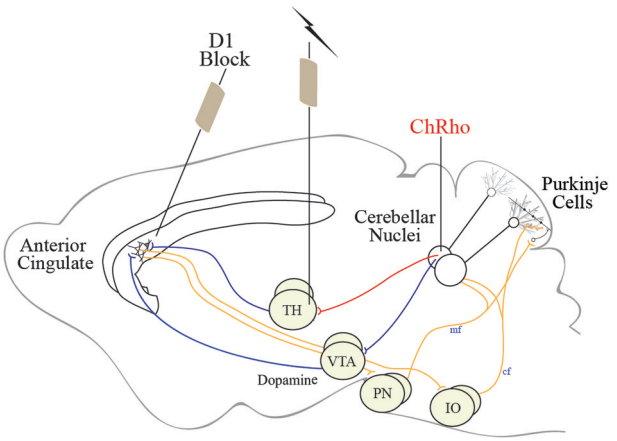

FIGURE 4 | Schematic representation of the cingulocerebellar pathways allowing the cerebellum access to the prefrontal cortex. We propose using optogenetic stimulation of cerebellar projection neurons in the thalamus to recover activity in aberrant prefrontal neuronal ensembles in schizophrenia. Channelrhodopsin, a light-activated channel, can be infused into cerebellar neurons rendering cerebellar projections photoexcitable. Stimulating thalamic (or VTA) optical fibers can selectively stimulate the cerebellar neuronal projections to the anterior cingulate while not affecting other cerebellar neuronal populations. This optogenetic paradigm can be used in animals exhibiting phenotypes of schizophrenia and other neuropsychiatric illnesses in combination with elementary cognitive tasks impaired in schizophrenia to recover cognitive function and probe the cingluocerebellar circuit.

dopamine (Abi-Dargham et al., 2002; Goldman-Rakic et al., 2004), glutamate (Olney and Farber, 1995; Chaki and Hikichi, 2011; Moghaddam and Javitt, 2012; Anticevic et al., 2013), and GABA in prefrontal pyramidal neurons, it is possible to mimic schizophrenia phenotypes by direct pharmacological microinjections (Jones et al., 2011). These manipulations may induce changes in neuronal activity that resemble abnormalities in schizophrenia and can be correlated with behavioral abnormalities. For example, frontal dopamine has been implicated in schizophrenia (Abi-Dargham et al., 2002; Goldman-Rakic et al., 2004; Stahl and Buckley, 2007). The level of frontal dopamine determines the type and severity of associated symptoms (Goldman-Rakic et al., 2004; Kuepper et al., 2012). Excess dopamine contributes to positive symptoms such as hallucinations and delusions, while depleted dopamine is responsible for negative symptoms such as anhedonia, avolition, and cognitive deficits such as impaired timing (Andreasen and Olsen, 1982; Seeman, 1987; Kuepper et al., 2012).

We, and others, have shown that temporal processing depends on the cerebellum for short, sub-second intervals (Ivry and Spencer, 2004; Buhusi and Meck, 2005; Bracha et al., 2009; Parker et al., 2009) while D1 dopamine signaling in the anterior cingulate of the prefrontal cortex is essential for longer intervals (Deutch, 1993; Narayanan et al., 2012; Parker et al., 2013a,c). In schizophrenia, the prefrontal cortex shows abnormal D1 dopamine (Weinberger et al., 1986; Okubo et al., 1997; Goldman-Rakic et al., 2004) and patients inaccurately estimate a discrete interval of time (Elvevåg et al., 2003; Bonnot et al., 2011). In animals, it is possible to model these concepts by locally infusing pharmacological agents into the frontal cortex to disrupt prefrontal D1 dopamine signaling and mimic impaired timing (Narayanan et al., 2012). If the cingulocerebellar circuit is necessary for temporal processing and is sensitive to levels of prefrontal dopamine, pharmacologically manipulating prefrontal dopamine will disrupt neuronal activity and impair timing. Mittleman et al. report efflux of dopamine in the prelimibic cortex (anterior cingulate) following electrical stimulation of the dentate nuclei (Mittleman et al., 2008). Therefore, optogenetically stimulating cerebellar nuclei has the potential to rescue aberrant contralateral prefrontal neuronal ensembles, recovering elementary cognitive tasks (Boyden et al., 2005; Narayanan et al., 2012).

An example of a task that has been used to probe the role of the cingulocerebellar circuit is eyeblink conditioning as it is abnormal in schizophrenia (Brown et al., 2005; Bolbecker et al., 2009; Forsyth et al., 2012; Parker et al., 2013b). Specifically, trace eyeblink conditioning, where a conditioning stimulus and an unconditioned stimulus are separated by a trace interval, requires integration of the cerebellum and frontal cortex (Weiss and Disterhoft, 1996). Siegel et al. have explored this afferent pathway and the influence of the dorsal anterior cingulate in layers V and VII (secondary motor cortices) in rabbits (Siegel et al., 2012). They found direct projections to the ipsilateral rostral PN via the corticospinal pyramidal tract. It has also been reported that prefrontal neurons are consistently active in the trace interstimulus interval, likely encoding the elapsed time between the stimulus and providing the cerebellum with the timing information necessary to accurately execute the eyeblink response (Siegel et al., 2012; Chen et al., 2014). It is possible to pharmacologically mimic psychiatric abnormalities by inactivating various areas of the prefrontal cortex to produce disruptions in trace eyeblink conditioning. Following expression of channelrhodopsin infusions in deep cerebellar nuclei, optogenetic stimulation of cerebellar projections to the thalamus have the potential to recover prefrontal neuronal activity and rescue eyeblink conditioning.

Optogenetic stimulation of the cingulocerebellar pathway can also be explored in genetically modified animals exhibiting schizophrenia phenotypes. Currently, several animals exist that exhibit some phenotypes of schizophrenia such as G72/G30, Df(16)A KO model, and Disrupted in Schizophrenia 1 (DISC1; Shevelkin et al., 2014). Each of these animals has cerebellar abnormalities similar to those consistently detected in schizophrenia making them ideal models to study the cingulocerebellar circuit (Shevelkin et al., 2014).

There are many additional aspects of this circuit that can be explored. Although we have focused on a very specific circuit involving the anterior cingulate and cerebellum, it is possible that a more widespread activity is sufficient for normal functioning. There are known connections throughout frontal lobes and normalized neuronal firing throughout the brain may prove essential rather than the firing patterns of one particular structure. This theory is supported by the more diffuse type of stimulation used by transcranial magnetic stimulation (Grimaldi et al., 2014) and thalamic stimulation (Klein et al., 2013).

CEREBELLAR STIMULATION IN PARKINSON'S DISEASE AND AUTISM

Although schizophrenia is not considered to be a motor disease, many indicators of motor dysfunction are present, suggesting that the basic abnormality in the disorder could be a brain system that mediates both motor and cognitive functions. Kraepelin described a variety of motor abnormalities in schizophrenia in his classic textbook (1919). Slowed reaction time is one of the oldest and most robust tests showing differences between schizophrenic patients and normal controls. More recent studies of premorbid indicators and neurological soft signs also implicate the motor system (Walker and Shaye, 1982; Gupta et al., 1995; Flashman et al., 1996; Mouchet-Mages et al., 2011). These mild indicators of poor coordination provide a clue that the underlying mechanism may reflect an abnormality in a basic process that regulates the synchrony of both thought and motor activity. Therefore, schizophrenia may be conceptualized as a disease that is characterized by poor coordination, or dysmetria, in all domains of functioning, including movement and cognition. In addition to its role in cognition, the cerebellum has traditionally been associated with movement and gait. Therefore, the circuit between the prefrontal cortex and cerebellum may facilitate the smooth execution, or synchrony of both motor and cognitive function. As we have proposed optogenetic stimulation of cerebellar projections for the treatment of the cognitive symptoms of schizophrenia, the motor impairments may actually benefit as well.

Parkinson's disease (PD) also causes impaired gait and cognition and involves abnormalities in the cerebellum, prefrontal cortex, and the basal ganglia. Cerebellar circuitry involves efferent connections with the basal ganglia which project back to the cerebellum via the PN (similar to the anterior cingulate projections) (Bostan and Strick, 2010; Bostan et al., 2010). However, similar to schizophrenia, the role of the cerebellum in PD is unknown. Recently, Wu et al. published a thorough review of the role of the cerebellum in PD (Wu and Hallett, 2013). They speculated that the cerebellum plays either a compensatory role or a pathological role (Wu and Hallett, 2013). Using optogenetic stimulation of cerebellar projections in the striatum, it may be possible to modulate cerebellar activity and repair movement, gait, and cognition in PD patients. How cerebellar circuitry interacts with the anterior cingulate via the dopaminergic VTA projections should be pursued, as cerebellar stimulation could represent novel therapeutic opportunities for both the cognitive and motor impairments in PD.

Courchesne et al. have documented cerebellar abnormalities in autism. In addition to decrease in cerebellar vermal volume, there appears to be aberrancies in cerebellar-prefrontal interactions (Carper and Courchesne, 2000; Pierce and Courchesne, 2001; Courchesne et al., 2011). Recently, Purkinje cell abnormalities have been linked to behavioral deficits similar to those exhibited in autism (Sudarov, 2013). The middle cerebellar peduncle has also shown structural impairments in autism and as the output pathway for cerebellar projections, this altered microstructure could have dire consequences for cerebellar-frontal lobe communications (Sivaswamy et al., 2010; Hanaie et al., 2013). More research needs to be done to understand the behavioral and cognitive symptoms in autism which depend on the cingulocerebellar pathway (Heck and Howell, 2013). Using optogenetics, this circuit should be parsed out and pursued to repair brain circuitry in autism. There are currently several animal models that exhibit phenotypes of autism, which are ripe for investigation.

CONCLUSIONS

The ideas described here have the potential to map the influence of cerebellar circuitry on the frontal cortex and lead to new insights about cingulocerebellar interactions. Through the cingulocerebellar circuit, cerebellar stimulation may recover aberrancies in the anterior cingulate cortex, rescuing cognition in schizophrenia. To our knowledge, this idea has not been proposed before, and we hope systematically applying the techniques described here to the many cognitive tasks impaired in schizophrenia such as attention and working memory, will encourage the development of new, targeted treatments for treatment-resistant patients.

ACKNOWLEDGMENTS

Grand funding was provided by Brain & Behavior Research Foundation NARSAD grant, Lieber Investigators, and Nellie Ball Trust Research Grant.

REFERENCES

Abi-Dargham, A., Mawlawi, O., Lombardo, I., Gil, R., Martinez, D., Huang, Y., et al. (2002). Prefrontal dopamine D1 receptors and working memory in schizophrenia. *J. Neurosci.* 22, 3708–3719.

Adams, R., and David, A. S. (2007). Patterns of anterior cingulate activation in schizophrenia: a selective review. *Neuropsychiatr. Dis. Treat.* 3, 87–101. doi: 10.2147/nedt.2007.3.1.87

Akshoomoff, N. A., and Courchesne, E. (1992). A new role for the cerebellum in cognitive operations. *Behav. Neurosci.* 106, 731–738. doi: 10.1037/0735-7044.106.5.731

Alphs, L. (2006). An industry perspective on the NIMH consensus statement on negative symptoms. *Schizophr. Bull.* 32, 225–230. doi: 10.1093/schbul/sbj056

Andreasen, N. C., Arndt, S., Swayze, V. 2nd, Cizadlo, T., Flaum, M., O'Leary, D., et al. (1994). Thalamic abnormalities in schizophrenia visualized through magnetic resonance image averaging. *Science* 266, 294–298. doi: 10.1126/science.7939669

Andreasen, N. C., O'Leary, D. S., Arndt, S., Cizadlo, T., Rezai, K., Watkins, G. L., et al. (1995a). I. PET studies of memory: novel and practiced free recall of complex narratives. *Neuroimage* 2, 284–295. doi: 10.1006/nimg.1995.1036

Andreasen, N. C., O'Leary, D. S., Cizadlo, T., Arndt, S., Rezai, K., Watkins, G. L., et al. (1995b). II. PET studies of memory: novel versus practiced free recall of word lists. *Neuroimage* 2, 296–305. doi: 10.1006/nimg.1995.1037

Andreasen, N. C., O'Leary, D. S., Flaum, M., Nopoulos, P., Watkins, G. L., Boles Ponto, L. L., et al. (1997). Hypofrontality in schizophrenia: distributed dysfunctional circuits in neuroleptic-naïve patients. *Lancet* 349, 1730–1734. doi: 10.1016/s0140-6736(96)08258-x

Andreasen, N. C., O'Leary, D. S., Paradiso, S., Cizadlo, T., Arndt, S., Watkins, G. L., et al. (1999). The cerebellum plays a role in conscious episodic memory retrieval. *Hum. Brain Mapp.* 8, 226–234. doi: 10.1002/(sici)1097-0193(1999)8:4<226::aid-hbm6>3.0.co;2-4

Andreasen, N. C., and Olsen, S. (1982). Negative v positive schizophrenia: definition and validation. *Arch. Gen. Psychiatry* 39, 789–794. doi: 10.1001/archpsyc.1982.04290070025006

Andreasen, N. C., Paradiso, S., and O'Leary, D. S. (1998). "Cognitive Dysmetria" as an integrative theory of schizophrenia. *Schizophr. Bull.* 24, 203–218. doi: 10.1093/oxfordjournals.schbul.a033321

Andreasen, N. C., and Pierson, R. (2008). The role of the cerebellum in schizophrenia. *Biol. Psychiatry* 64, 81–88. doi: 10.1016/j.biopsych.2008.01.003

Anticevic, A., Cole, M. W., Repovs, G., Savic, A., Driesen, N. R., Yang, G., et al. (2013). Connectivity, pharmacology and computation: toward a mechanistic understanding of neural system dysfunction in schizophrenia. *Front. Psychiatry* 4:169. doi: 10.3389/fpsyt.2013.00169

Artiges, E., Salamé, P., Recasens, C., Poline, J. B., Attar-Levy, D., De La Raillère, A., et al. (2000). Working memory control in patients with schizophrenia: a PET study during a random number generation task. *Am. J. Psychiatry* 157, 1517–1519. doi: 10.1176/appi.ajp.157.9.1517

Bijsterbosch, J. D., Lee, K.-H., Hunter, M. D., Tsoi, D. T., Lankappa, S., Wilkinson, I. D., et al. (2011). The role of the cerebellum in sub- and supraliminal error correction during sensorimotor synchronization: evidence from fMRI and TMS. *J. Cogn. Neurosci.* 23, 1100–1112. doi: 10.1162/jocn.2010.21506

Boehringer, A., Macher, K., Dukart, J., Villringer, A., and Pleger, B. (2013). Cerebellar transcranial direct current stimulation modulates verbal working memory. *Brain Stimul.* 6, 649–653. doi: 10.1016/j.brs.2012.10.001

Bolbecker, A. R., Mehta, C. S., Edwards, C. R., Steinmetz, J. E., O'Donnell, B. F., and Hetrick, W. P. (2009). Eye-blink conditioning deficits indicate temporal processing abnormalities in schizophrenia. *Schizophr. Res.* 111, 182–191. doi: 10.1016/j.schres.2009.03.016

Bonnot, O., de Montalembert, M., Kermarrec, S., Botbol, M., Walter, M., and Coulon, N. (2011). Are impairments of time perception in schizophrenia a neglected phenomenon? *J. Physiol. Paris* 105, 164–169. doi: 10.1016/j.jphysparis.2011.07.006

Bostan, A. C., Dum, R. P., and Strick, P. L. (2010). The basal ganglia communicate with the cerebellum. *Proc. Natl. Acad. Sci. U S A* 107, 8452–8456. doi: 10.1073/pnas.1000496107

Bostan, A. C., Dum, R. P., and Strick, P. L. (2013). Cerebellar networks with the cerebral cortex and basal ganglia. *Trends Cogn. Sci.* 17, 241–254. doi: 10.1016/j.tics.2013.03.003

Bostan, A. C., and Strick, P. L. (2010). The cerebellum and basal ganglia are interconnected. *Neuropsychol. Rev.* 20, 261–270. doi: 10.1007/s11065-010-9143-9

Boyden, E. S., Zhang, F., Bamberg, E., Nagel, G., and Deisseroth, K. (2005). Millisecond-timescale, genetically targeted optical control of neural activity. *Nat. Neurosci.* 8, 1263–1268. doi: 10.1038/nn1525

Bracha, V., Zbarska, S., Parker, K., Carrel, A., Zenitsky, G., and Bloedel, J. R. (2009). The cerebellum and eye-blink conditioning: learning versus network performance hypotheses. *Neuroscience* 162, 787–796. doi: 10.1016/j.neuroscience.2008.12.042

Brown, S. M., Kieffaber, P. D., Carroll, C. A., Vohs, J. L., Tracy, J. A., Shekhar, A., et al. (2005). Eyeblink conditioning deficits indicate timing and cerebellar abnormalities in schizophrenia. *Brain Cogn.* 58, 94–108. doi: 10.1016/j.bandc.2004.09.011

Buhusi, C. V., and Meck, W. H. (2005). What makes us tick? Functional and neural mechanisms of interval timing. *Nat. Rev. Neurosci.* 6, 755–765. doi: 10.1038/nrn1764

Buschman, T. J., and Miller, E. K. (2007). Top-down versus bottom-up control of attention in the prefrontal and posterior parietal cortices. *Science* 315, 1860–1862. doi: 10.1126/science.1138071

Carper, R. A., and Courchesne, E. (2000). Inverse correlation between frontal lobe and cerebellum sizes in children with autism. *Brain* 123(Pt. 4), 836–844. doi: 10.1093/brain/123.4.836

Carroll, C. A., O'Donnell, B. F., Shekhar, A., and Hetrick, W. P. (2009). Timing dysfunctions in schizophrenia as measured by a repetitive finger tapping task. *Brain Cogn.* 71, 345–353. doi: 10.1016/j.bandc.2009.06.009

Carter, C. S., Braver, T. S., Barch, D. M., Botvinick, M. M., Noll, D., and Cohen, J. D. (1998). Anterior cingulate cortex, error detection and the online monitoring of performance. *Science* 280, 747–749. doi: 10.1126/science.280.5364.747

Carter, C. S., MacDonald, A. W. 3rd, Ross, L. L., and Stenger, V. A. (2001). Anterior cingulate cortex activity and impaired self-monitoring of performance in patients with schizophrenia: an event-related fMRI study. *Am. J. Psychiatry* 158, 1423–1428. doi: 10.1176/appi.ajp.158.9.1423

Cavanagh, J. F., Cohen, M. X., and Allen, J. J. B. (2009). Prelude to and resolution of an error: EEG phase synchrony reveals cognitive control dynamics during action monitoring. *J. Neurosci.* 29, 98–105. doi: 10.1523/jneurosci.4137-08.2009

Chaki, S., and Hikichi, H. (2011). Targeting of metabotropic glutamate receptors for the treatment of schizophrenia. *Curr. Pharm. Des.* 17, 94–102. doi: 10.2174/138161211795049570

Chen, H., Yang, L., Xu, Y., Wu, G., Yao, J., Zhang, J., et al. (2014). Prefrontal control of cerebellum-dependent associative motor learning. *Cerebellum* 13, 64–78. doi: 10.1007/s12311-013-0517-4

Condé, F., Audinat, E., Maire-Lepoivre, E., and Crépel, F. (1990). Afferent connections of the medial frontal cortex of the rat. A study using retrograde transport of fluorescent dyes. I. Thalamic afferents. *Brain Res. Bull.* 24, 341–354. doi: 10.1016/0361-9230(90)90088-h

Cooper, I. S., Amin, I., Riklan, M., Waltz, J. M., and Poon, T. P. (1976). Chronic cerebellar stimulation in epilepsy. Clinical and anatomical studies. *Arch. Neurol.* 33, 559–570. doi: 10.1001/archneur.1976.00500080037006

Courchesne, E., Mouton, P. R., Calhoun, M. E., Semendeferi, K., Ahrens-Barbeau, C., Hallet, M. J., et al. (2011). Neuron number and size in prefrontal cortex of children with autism. *JAMA* 306, 2001–2010. doi: 10.1001/jama.2011.1638

Courchesne, E., Townsend, J., Akshoomoff, N. A., Saitoh, O., Yeung-Courchesne, R., Lincoln, A. J., et al. (1994). Impairment in shifting attention in autistic and cerebellar patients. *Behav. Neurosci.* 108, 848–865. doi: 10.1037/0735-7044.108.5.848

Crespo-Facorro, B., Paradiso, S., Andreasen, N. C., O'Leary, D. S., Watkins, G. L., Boles Ponto, L. L., et al. (1999). Recalling word lists reveals "cognitive dysmetria" in schizophrenia: a positron emission tomography study. *Am. J. Psychiatry* 156, 386–392.

Crespo-Facorro, B., Wiser, A. K., Andreasen, N. C., O'Leary, D. S., Watkins, G. L., Boles Ponto, L. L., et al. (2001). Neural basis of novel and well-learned recognition memory in schizophrenia: a positron emission tomography study. *Hum. Brain Mapp.* 12, 219–231. doi: 10.1002/1097-0193(200104)12:4<219::aid-hbm1017>3.0.co;2-l

Dembrow, N. C., Chitwood, R. A., and Johnston, D. (2010). Projection-specific neuromodulation of medial prefrontal cortex neurons. *J. Neurosci.* 30, 16922–16937. doi: 10.1523/jneurosci.3644-10.2010

Demirtas-Tatlidede, A., Freitas, C., Cromer, J. R., Safar, L., Ongur, D., Stone, W. S., et al. (2010). Safety and proof of principle study of cerebellar vermal theta burst stimulation in refractory schizophrenia. *Schizophr. Res.* 124, 91–100. doi: 10.1016/j.schres.2010.08.015

Demirtas-Tatlidede, A., Vahabzadeh-Hagh, A. M., and Pascual-Leone, A. (2013). Can noninvasive brain stimulation enhance cognition in neuropsychiatric disorders? *Neuropharmacology* 64, 566–578. doi: 10.1016/j.neuropharm.2012.06.020

Deutch, A. Y. (1993). Prefrontal cortical dopamine systems and the elaboration of functional corticostriatal circuits: implications for schizophrenia and Parkinson's disease. *J. Neural Transm. Gen. Sect.* 91, 197–221. doi: 10.1007/bf01245232

Devinsky, O., Morrell, M. J., and Vogt, B. A. (1995). Contributions of anterior cingulate cortex to behaviour. *Brain* 118(Pt. 1), 279–306. doi: 10.1093/brain/118.1.279

Elvevåg, B., McCormack, T., Gilbert, A., Brown, G. D. A., Weinberger, D. R., and Goldberg, T. E. (2003). Duration judgements in patients with schizophrenia. *Psychol. Med.* 33, 1249–1261. doi: 10.1017/s0033291703008122

Fierro, B., Palermo, A., Puma, A., Francolini, M., Panetta, M. L., Daniele, O., et al. (2007). Role of the cerebellum in time perception: a TMS study in normal subjects. *J. Neurol. Sci.* 263, 107–112. doi: 10.1016/j.jns.2007.06.033

Fiez, J. A., Petersen, S. E., Cheney, M. K., and Raichle, M. E. (1992). Impaired nonmotor learning and error detection associated with cerebellar damage. A single case study. *Brain* 115(Pt. 1), 155–178. doi: 10.1093/brain/115.1.155

Flashman, L. A., Flaum, M., Gupta, S., and Andreasen, N. C. (1996). Soft signs and neuropsychological performance in schizophrenia. *Am. J. Psychiatry* 153, 526–532.

Fornito, A., Yücel, M., Dean, B., Wood, S. J., and Pantelis, C. (2009). Anatomical abnormalities of the anterior cingulate cortex in schizophrenia: bridging the gap between neuroimaging and neuropathology. *Schizophr. Bull.* 35, 973–993. doi: 10.1093/schbul/sbn025

Forsyth, J. K., Bolbecker, A. R., Mehta, C. S., Klaunig, M. J., Steinmetz, J. E., O'Donnell, B. F., et al. (2012). Cerebellar-dependent eyeblink conditioning deficits in schizophrenia spectrum disorders. *Schizophr. Bull.* 38, 751–759. doi: 10.1093/schbul/sbQ128

Gasquoine, P. G. (2013). Localization of function in anterior cingulate cortex: from psychosurgery to functional neuroimaging. *Neurosci. Biobehav. Rev.* 37, 340–348. doi: 10.1016/j.neubiorev.2013.01.002

Glahn, D. C., Laird, A. R., Ellison-Wright, I., Thelen, S. M., Robinson, J. L., Lancaster, J. L., et al. (2008). Meta-analysis of gray matter anomalies in schizophrenia: application of anatomic likelihood estimation and network analysis. *Biol. Psychiatry* 64, 774–781. doi: 10.1016/j.biopsych.2008.03.031

Glickstein, M., May, J. G. 3rd, and Mercier, B. E. (1985). Corticopontine projection in the macaque: the distribution of labelled cortical cells after large injections

of horseradish peroxidase in the pontine nuclei. *J. Comp. Neurol.* 235, 343–359. doi: 10.1002/cne.902350306

Goldman-Rakic, P. S., Castner, S. A., Svensson, T. H., Siever, L. J., and Williams, G. V. (2004). Targeting the dopamine D1 receptor in schizophrenia: insights for cognitive dysfunction. *Psychopharmacology (Berl)* 174, 3–16. doi: 10.1007/s00213-004-1793-y

Gottwald, B., Wilde, B., Mihajlovic, Z., and Mehdorn, H. M. (2004). Evidence for distinct cognitive deficits after focal cerebellar lesions. *J. Neurol. Neurosurg. Psychiatry* 75, 1524–1531. doi: 10.1136/jnnp.2003.018093

Grafman, J., Litvan, I., Massaquoi, S., Stewart, M., Sirigu, A., and Hallett, M. (1992). Cognitive planning deficit in patients with cerebellar atrophy. *Neurology* 42, 1493–1496. doi: 10.1212/wnl.42.8.1493

Grimaldi, G., Argyropoulos, G. P., Boehringer, A., Celnik, P., Edwards, M. J., Ferrucci, R., et al. (2014). Non-invasive cerebellar stimulation-a consensus paper. *Cerebellum* 13, 121–138. doi: 10.1007/s12311-013-0514-7

Grimaldi, G., and Manto, M. (2012). Topography of cerebellar deficits in humans. *Cerebellum* 11, 336–351. doi: 10.1007/s12311-011-0247-4

Groiss, S. J., and Ugawa, Y. (2013). "Chapter 51—Cerebellum," in *Handbook of Clinical Neurology. Brain Stimulation*, eds A. M. Lozano, M. Hallett (Elsevier), 643–653. Available online at: http://www.sciencedirect.com/science/article/pii/B9780444534972000516. Accessed on February 21, 2014.

Grube, M., Lee, K.-H., Griffiths, T. D., Barker, A. T., and Woodruff, P. W. (2010). Transcranial magnetic theta-burst stimulation of the human cerebellum distinguishes absolute, duration-based from relative, beat-based perception of subsecond time intervals. *Front. Psychol.* 1:171. doi: 10.3389/fpsyg.2010.00171

Gupta, S., Andreasen, N. C., Arndt, S., Flaum, M., Schultz, S. K., Hubbard, W. C., et al. (1995). Neurological soft signs in neuroleptic-naive and neuroleptic-treated schizophrenic patients and in normal comparison subjects. *Am. J. Psychiatry* 152, 191–196.

Hadley, J. A., Nenert, R., Kraguljac, N. V., Bolding, M. S., White, D. M., Skidmore, F. M., et al. (2014). Ventral tegmental area/midbrain functional connectivity and response to antipsychotic medication in schizophrenia. *Neuropsychopharmacology* 39, 1020–1030. doi: 10.1038/npp.2013.305

Hanaie, R., Mohri, I., Kagitani-Shimono, K., Tachibana, M., Azuma, J., Matsuzaki, J., et al. (2013). Altered microstructural connectivity of the superior cerebellar peduncle is related to motor dysfunction in children with autistic spectrum disorders. *Cerebellum* 12, 645–656. doi: 10.1007/s12311-013-0475-x

Heck, D. H., and Howell, J. W. (2013). Prefrontal cortical-cerebellar interaction deficits in autism spectrum disorders. *Autism* S4:001. doi: 10.4172/2165-7890.S4-001

Honey, G. D., Pomarol-Clotet, E., Corlett, P. R., Honey, R. A. E., McKenna, P. J., Bullmore, E. T., et al. (2005). Functional dysconnectivity in schizophrenia associated with attentional modulation of motor function. *Brain* 128, 2597–2611. doi: 10.1093/brain/awh632

Hsu, M. M., and Shyu, B. C. (1997). Electrophysiological study of the connection between medial thalamus and anterior cingulate cortex in the rat. *Neuroreport* 8, 2701–2707. doi: 10.1097/00001756-199708180-00013

Ivry, R. B., and Spencer, R. M. (2004). Evaluating the role of the cerebellum in temporal processing: beware of the null hypothesis. *Brain* 127, E13–E14. doi: 10.1093/brain/awh227

Jones, C., Watson, D., and Fone, K. (2011). Animal models of schizophrenia. *Br. J. Pharmacol.* 164, 1162–1194. doi: 10.1111/j.1476-5381.2011.01386.x

Kamali, A., Kramer, L. A., Frye, R. E., Butler, I. J., and Hasan, K. M. (2010). Diffusion tensor tractography of the human brain cortico-ponto-cerebellar pathways: a quantitative preliminary study. *J. Magn. Reson. Imaging* 32, 809–817. doi: 10.1002/jmri.22330

Klein, J., Hadar, R., Götz, T., Männer, A., Eberhardt, C., Baldassarri, J., et al. (2013). Mapping brain regions in which deep brain stimulation affects schizophrenia-like behavior in two rat models of schizophrenia. *Brain Stimul.* 6, 490–499. doi: 10.1016/j.brs.2012.09.004

Koch, G., Oliveri, M., Torriero, S., Salerno, S., Lo Gerfo, E., and Caltagirone, C. (2007). Repetitive TMS of cerebellum interferes with millisecond time processing. *Exp. Brain Res.* 179, 291–299. doi: 10.1007/s00221-006-0791-1

Koziol, L. F., Budding, D., Andreasen, N., D'Arrigo, S., Bulgheroni, S., Imamizu, H., et al. (2013). Consensus paper: the cerebellum's role in movement and cognition. *Cerebellum* 13, 151–177. doi: 10.1007/s12311-013-0511-x

Kuepper, R., Skinbjerg, M., and Abi-Dargham, A. (2012). The dopamine dysfunction in schizophrenia revisited: new insights into topography and course. *Handb. Exp. Pharmacol.* 212, 1–26. doi: 10.1007/978-3-642-25761-2_1

Kühn, S., Romanowski, A., Schubert, F., and Gallinat, J. (2012). Reduction of cerebellar grey matter in Crus I and II in schizophrenia. *Brain Struct. Funct.* 217, 523–529. doi: 10.1007/s00429-011-0365-2

Legg, C. R., Mercier, B., and Glickstein, M. (1989). Corticopontine projection in the rat: the distribution of labelled cortical cells after large injections of horseradish peroxidase in the pontine nuclei. *J. Comp. Neurol.* 286, 427–441. doi: 10.1002/cne.902860403

Leiner, H. C., Leiner, A. L., and Dow, R. S. (1994). The underestimated cerebellum. *Hum. Brain Mapp.* 2, 244–254. doi: 10.1002/hbm.460020406

Magnotta, V. A., Adix, M. L., Caprahan, A., Lim, K., Gollub, R., and Andreasen, N. C. (2008). Investigating connectivity between the cerebellum and thalamus in schizophrenia using diffusion tensor tractography: a pilot study. *Psychiatry Res.* 163, 193–200. doi: 10.1016/j.pscychresns.2007.10.005

McCormick, L., Decker, L., Nopoulos, P., Ho, B.-C., and Andreasen, N. (2005). Effects of atypical and typical neuroleptics on anterior cingulate volume in schizophrenia. *Schizophr. Res.* 80, 73–84. doi: 10.1016/j.schres.2005.06.022

Meyer-Lindenberg, A., Poline, J. B., Kohn, P. D., Holt, J. L., Egan, M. F., Weinberger, D. R., et al. (2001). Evidence for abnormal cortical functional connectivity during working memory in schizophrenia. *Am. J. Psychiatry* 158, 1809–1817. doi: 10.1176/appi.ajp.158.11.1809

Middleton, F. A., and Strick, P. L. (2001). Cerebellar projections to the prefrontal cortex of the primate. *J. Neurosci.* 21, 700–712.

Minzenberg, M. J., Laird, A. R., Thelen, S., Carter, C. S., and Glahn, D. C. (2009). Meta-analysis of 41 functional neuroimaging studies of executive function in schizophrenia. *Arch. Gen. Psychiatry* 66, 811–822. doi: 10.1001/archgenpsychiatry.2009.91

Mitelman, S. A., Newmark, R. E., Torosjan, Y., Chu, K.-W., Brickman, A. M., Haznedar, M. M., et al. (2006). White matter fractional anisotropy and outcome in schizophrenia. *Schizophr. Res.* 87, 138–159. doi: 10.1016/j.schres.2006.06.016

Mittleman, G., Goldowitz, D., Heck, D. H., and Blaha, C. D. (2008). Cerebellar modulation of frontal cortex dopamine efflux in mice: relevance to autism and schizophrenia. *Synapse* 62, 544–550. doi: 10.1002/syn.20525

Moghaddam, B., and Javitt, D. (2012). From revolution to evolution: the glutamate hypothesis of schizophrenia and its implication for treatment. *Neuropsychopharmacology* 37, 4–15. doi: 10.1038/npp.2011.181

Mouchet-Mages, S., Rodrigo, S., Cachia, A., Mouaffak, F., Olie, J. P., Meder, J. F., et al. (2011). Correlations of cerebello-thalamo-prefrontal structure and neurological soft signs in patients with first-episode psychosis. *Acta Psychiatr. Scand.* 123, 451–458. doi: 10.1111/j.1600-0447.2010.01667.x

Narayanan, N. S., Cavanagh, J. F., Frank, M. J., and Laubach, M. (2013). Common medial frontal mechanisms of adaptive control in humans and rodents. *Nat. Neurosci.* 16, 1888–1895. doi: 10.1038/nn.3549

Narayanan, N. S., Land, B. B., Solder, J. E., Deisseroth, K., and Dileone, R. J. (2012). Prefrontal D1 dopamine signaling is required for temporal control. *Proc. Natl. Acad. Sci. U S A* 109, 20726–20731. doi: 10.1073/pnas.1211258109

Narayanan, N. S., Prabhakaran, V., Bunge, S. A., Christoff, K., Fine, E. M., and Gabrieli, J. D. E. (2005). The role of the prefrontal cortex in the maintenance of verbal working memory: an event-related FMRI analysis. *Neuropsychology* 19, 223–232. doi: 10.1037/0894-4105.19.2.223

Nopoulos, P. C., Ceilley, J. W., Gailis, E. A., and Andreasen, N. C. (1999). An MRI study of cerebellar vermis morphology in patients with schizophrenia: evidence in support of the cognitive dysmetria concept. *Biol. Psychiatry* 46, 703–711. doi: 10.1016/s0006-3223(99)00093-1

Oh, J. S., Kubicki, M., Rosenberger, G., Bouix, S., Levitt, J. J., McCarley, R. W., et al. (2009). Thalamo-frontal white matter alterations in chronic schizophrenia: a quantitative diffusion tractography study. *Hum. Brain Mapp.* 30, 3812–3825. doi: 10.1002/hbm.20809

Okubo, Y., Suhara, T., Suzuki, K., Kobayashi, K., Inoue, O., Terasaki, O., et al. (1997). Decreased prefrontal dopamine D1 receptors in schizophrenia revealed by PET. *Nature* 385, 634–636. doi: 10.1038/385634a0

Okugawa, G., Nobuhara, K., Sugimoto, T., and Kinoshita, T. (2005). Diffusion tensor imaging study of the middle cerebellar peduncles in patients with schizophrenia. *Cerebellum* 4, 123–127. doi: 10.1080/14734220510007879

Okugawa, G., Sedvall, G. C., and Agartz, I. (2003). Smaller cerebellar vermis but not hemisphere volumes in patients with chronic schizophrenia. *Am. J. Psychiatry* 160, 1614–1617. doi: 10.1176/appi.ajp.160.9.1614

O'Leary, D. S., Andreason, N. C., Hurtig, R. R., Hichwa, R. D., Watkins, G. L., Ponto, L. L., et al. (1996). A positron emission tomography study of binaurally and dichotically presented stimuli: effects of level of language and directed attention. *Brain Lang.* 53, 20–39. doi: 10.1006/brln.1996.0034

Oliveri, M., Torriero, S., Koch, G., Salerno, S., Petrosini, L., and Caltagirone, C. (2007). The role of transcranial magnetic stimulation in the study of cerebellar cognitive function. *Cerebellum* 6, 95–101. doi: 10.1080/14734220701213421

Olney, J. W., and Farber, N. B. (1995). Glutamate receptor dysfunction and schizophrenia. *Arch. Gen. Psychiatry* 52, 998–1007. doi: 10.1001/archpsyc.1995.03950240016004

Paradiso, S., Crespo Facorro, B., Andreasen, N. C., O'Leary, D. S., Watkins, L. G., Boles Ponto, L., et al. (1997). Brain activity assessed with PET during recall of word lists and narratives. *Neuroreport* 8, 3091–3096. doi: 10.1097/00001756-199709290-00017

Parker, K. L., Alberico, S. L., Miller, A. D., and Narayanan, N. S. (2013a). Prefrontal D1 dopamine signaling is necessary for temporal expectation during reaction time performance. *Neuroscience* 255, 246–254. doi: 10.1016/j.neuroscience.2013.09.057

Parker, K. L., Andreasen, N. C., Liu, D., Freeman, J. H., and O'Leary, D. S. (2013b). Eyeblink conditioning in unmedicated schizophrenia patients: a positron emission tomography study. *Psychiatry Res.* 214, 402–409. doi: 10.1016/j.pscychresns.2013.07.006

Parker, K. L., Lamichhane, D., Caetano, M. S., and Narayanan, N. S. (2013c). Executive dysfunction in Parkinson's disease and timing deficits. *Front. Integr. Neurosci.* 7:75. doi: 10.3389/fnint.2013.00075

Parker, K. L., Zbarska, S., Carrel, A. J., and Bracha, V. (2009). Blocking GABAA neurotransmission in the interposed nuclei: effects on conditioned and unconditioned eyeblinks. *Brain Res.* 1292, 25–37. doi: 10.1016/j.brainres.2009.07.053

Parnaudeau, S., O'Neill, P.-K., Bolkan, S. S., Ward, R. D., Abbas, A. I., Roth, B. L., et al. (2013). Inhibition of mediodorsal thalamus disrupts thalamofrontal connectivity and cognition. *Neuron* 77, 1151–1162. doi: 10.1016/j.neuron.2013.01.038

Picton, T. W., Stuss, D. T., Alexander, M. P., Shallice, T., Binns, M. A., and Gillingham, S. (2006). Effects of focal frontal lesions on response inhibition. *Cereb. Cortex* 17, 826–838. doi: 10.1093/cercor/bhk031

Pierce, K., and Courchesne, E. (2001). Evidence for a cerebellar role in reduced exploration and stereotyped behavior in autism. *Biol. Psychiatry* 49, 655–664. doi: 10.1016/s0006-3223(00)01008-8

Pomarol-Clotet, E., Canales-Rodríguez, E. J., Salvador, R., Sarró, S., Gomar, J. J., Vila, F., et al. (2010). Medial prefrontal cortex pathology in schizophrenia as revealed by convergent findings from multimodal imaging. *Mol. Psychiatry* 15, 823–830. doi: 10.1038/mp.2009.146

Prabhakaran, V., Rypma, B., Narayanan, N. S., Meier, T. B., Austin, B. P., Nair, V. A., et al. (2011). Capacity-speed relationships in prefrontal cortex. *PLoS One* 6:e27504. doi: 10.1371/journal.pone.0027504

Ragland, J. D., Laird, A. R., Ranganath, C., Blumenfeld, R. S., Gonzales, S. M., and Glahn, D. C. (2009). Prefrontal activation deficits during episodic memory in schizophrenia. *Am. J. Psychiatry* 166, 863–874. doi: 10.1176/appi.ajp.2009.08091307

Rogers, T. D., Dickson, P. E., Heck, D. H., Goldowitz, D., Mittleman, G., and Blaha, C. D. (2011). Connecting the dots of the cerebro-cerebellar role in cognitive function: neuronal pathways for cerebellar modulation of dopamine release in the prefrontal cortex. *Synapse* 65, 1204–1212. doi: 10.1002/syn.20960

Rogers, T. D., Dickson, P. E., McKimm, E., Heck, D. H., Goldowitz, D., Blaha, C. D., et al. (2013). Reorganization of circuits underlying cerebellar modulation of prefrontal cortical dopamine in mouse models of autism spectrum disorder. *Cerebellum* 12, 547–556. doi: 10.1007/s12311-013-0462-2

Saalmann, Y. B., and Kastner, S. (2011). Cognitive and perceptual functions of the visual thalamus. *Neuron* 71, 209–223. doi: 10.1016/j.neuron.2011.06.027

Salgado-Pineda, P., Landin-Romero, R., Fakra, E., Delaveau, P., Amann, B. L., and Blin, O. (2014). Structural abnormalities in schizophrenia: further evidence on the key role of the anterior cingulate cortex. *Neuropsychobiology* 69, 52–58. doi: 10.1159/000356972

Schmahmann, J. D. (1998). Dysmetria of thought: clinical consequences of cerebellar dysfunction on cognition and affect. *Trends Cogn. Sci.* 2, 362–371. doi: 10.1016/s1364-6613(98)01218-2

Schmahmann, J. D. (2004). Disorders of the cerebellum: ataxia, dysmetria of thought and the cerebellar cognitive affective syndrome. *J. Neuropsychiatry Clin. Neurosci.* 16, 367–378. doi: 10.1176/appi.neuropsych.16.3.367

Schmahmann, J. D. (2010). The role of the cerebellum in cognition and emotion: personal reflections since 1982 on the dysmetria of thought hypothesis and its historical evolution from theory to therapy. *Neuropsychol. Rev.* 20, 236–260. doi: 10.1007/s11065-010-9142-x

Schulz, R., Wessel, M. J., Zimerman, M., Timmerman, J., Gerloff, C., and Hummel, F. C. (2014). White matter integrity of specific dentato-thalamo-cortical pathways is associated with learning gains in precise movement timing. *Cereb. Cortex* doi: 10.1093/cercor/bht356. [Epub ahead of print].

Schutter, D. J. L. G., van Honk, J., d' Alfonso, A. A. L., Peper, J. S., and Panksepp, J. (2003). High frequency repetitive transcranial magnetic over the medial cerebellum induces a shift in the prefrontal electroencephalography gamma spectrum: a pilot study in humans. *Neurosci. Lett.* 336, 73–76. doi: 10.1016/s0304-3940(02)01077-7

Seeman, P. (1987). Dopamine receptors and the dopamine hypothesis of schizophrenia. *Synapse* 1, 133–152. doi: 10.1002/syn.890010203

Shevelkin, A. V., Ihenatu, C., and Pletnikov, M. V. (2014). Pre-clinical models of neurodevelopmental disorders: focus on the cerebellum. *Rev. Neurosci.* 25, 177–194. doi: 10.1515/revneuro-2013-0049

Siegel, J. J., Kalmbach, B., Chitwood, R. A., and Mauk, M. D. (2012). Persistent activity in a cortical-to-subcortical circuit: bridging the temporal gap in trace eyelid conditioning. *J. Neurophysiol.* 107, 50–64. doi: 10.1152/jn.00689.2011

Sivaswamy, L., Kumar, A., Rajan, D., Behen, M., Muzik, O., Chugani, D., et al. (2010). A diffusion tensor imaging study of the cerebellar pathways in children with autism spectrum disorder. *J. Child Neurol.* 25, 1223–1231. doi: 10.1177/0883073809358765

Snider, R. S., Maiti, A., and Snider, S. R. (1976). Cerebellar pathways to ventral midbrain and nigra. *Exp. Neurol.* 53, 714–728. doi: 10.1016/0014-4886(76)90150-3

Stahl, S. M., and Buckley, P. F. (2007). Negative symptoms of schizophrenia: a problem that will not go away. *Acta Psychiatr. Scand.* 115, 4–11. doi: 10.1111/j.1600-0447.2006.00947.x

Stoodley, C. J., and Schmahmann, J. D. (2009). The cerebellum and language: evidence from patients with cerebellar degeneration. *Brain Lang.* 110, 149–153. doi: 10.1016/j.bandl.2009.07.006

Strick, P. L., Dum, R. P., and Fiez, J. A. (2009). Cerebellum and nonmotor function. *Annu. Rev. Neurosci.* 32, 413–434. doi: 10.1146/annurev.neuro.31.060407.125606

Sudarov, A. (2013). Defining the role of cerebellar Purkinje cells in autism spectrum disorders. *Cerebellum* 12, 950–955. doi: 10.1007/s12311-013-0490-y

Takayanagi, M., Wentz, J., Takayanagi, Y., Schretlen, D. J., Ceyhan, E., Wang, L., et al. (2013). Reduced anterior cingulate gray matter volume and thickness in subjects with deficit schizophrenia. *Schizophr. Res.* 150, 484–490. doi: 10.1016/j.schres.2013.07.036

Tomlinson, S. P., Davis, N. J., and Bracewell, R. M. (2013). Brain stimulation studies of non-motor cerebellar function: a systematic review. *Neurosci. Biobehav. Rev.* 37, 766–789. doi: 10.1016/j.neubiorev.2013.03.001

Tsubota, T., Ohashi, Y., Tamura, K., Sato, A., and Miyashita, Y. (2011). Optogenetic manipulation of cerebellar purkinje cell activity in vivo. *PLoS One* 6:e22400. doi: 10.1371/journal.pone.0022400

Uylings, H. B. M., Groenewegen, H. J., and Kolb, B. (2003). Do rats have a prefrontal cortex? *Behav. Brain Res.* 146, 3–17. doi: 10.1016/j.bbr.2003.09.028

Vilensky, J. A., and Van Hoesen, G. W. (1981). Corticopontine projections from the cingulate cortex in the rhesus monkey. *Brain Res.* 205, 391–395. doi: 10.1016/0006-8993(81)90348-6

Vogt, B. A., Hof, P. R., Zilles, K., Vogt, L. J., Herold, C., and Palomero-Gallagher, N. (2013). Cingulate area 32 homologies in mouse, rat, macaque and human: cytoarchitecture and receptor architecture. *J. Comp. Neurol.* 521, 4189–4204. doi: 10.1002/cne.23409

Vogt, B. A., and Paxinos, G. (2014). Cytoarchitecture of mouse and rat cingulate cortex with human homologies. *Brain Struct. Funct.* 219, 185–192. doi: 10.1007/s00429-012-0493-3

Volz, H.-P., Nenadic, I., Gaser, C., Rammsayer, T., Häger, F., and Sauer, H. (2001). Time estimation in schizophrenia: an fMRI study at adjusted levels of difficulty. *Neuroreport* 12, 313–316. doi: 10.1097/00001756-200102120-00026

Walker, E., and Shaye, J. (1982). Familial schizophrenia. A predictor of neuromotor and attentional abnormalities in schizophrenia. *Arch. Gen. Psychiatry* 39, 1153–1156. doi: 10.1001/archpsyc.1982.04290100027005

Wassink, T. H., Andreasen, N. C., Nopoulos, P., and Flaum, M. (1999). Cerebellar morphology as a predictor of symptom and psychosocial outcome in schizophrenia. *Biol. Psychiatry* 45, 41–48. doi: 10.1016/s0006-3223(98)00175-9

Watson, T. C., Becker, N., Apps, R., and Jones, M. W. (2014). Back to front: cerebellar connections and interactions with the prefrontal cortex. *Front. Syst. Neurosci.* 8:4. doi: 10.3389/fnsys.2014.00004

Watson, T. C., Jones, M. W., and Apps, R. (2009). Electrophysiological mapping of novel prefrontal - cerebellar pathways. *Front. Integr. Neurosci.* 3:18. doi: 10.3389/neuro.07.018.2009

Weinberger, D. R., Berman, K. F., and Zec, R. F. (1986). Physiologic dysfunction of dorsolateral prefrontal cortex in schizophrenia. I. Regional cerebral blood flow evidence. *Arch. Gen. Psychiatry* 43, 114–124. doi: 10.1001/archpsyc.1986.01800020020004

Weinberger, D. R., Kleinman, J. E., Luchins, D. J., Bigelow, L. B., and Wyatt, R. J. (1980). Cerebellar pathology in schizophrenia: a controlled postmortem study. *Am. J. Psychiatry* 137, 359–361.

Weiss, C., and Disterhoft, J. F. (1996). Eyeblink conditioning, motor control and the analysis of limbic-cerebellar interactions. *Behav. Brain Sci.* 19, 479–481. doi: 10.1017/s0140525x00081929

White, T., Nelson, M., and Lim, K. O. (2008). Diffusion tensor imaging in psychiatric disorders. *Top. Magn. Reson. Imaging* 19, 97–109. doi: 10.1097/rmr.0b013e3181809f1e

Williams, S. M., and Goldman-Rakic, P. S. (1998). Widespread origin of the primate mesofrontal dopamine system. *Cereb. Cortex* 8, 321–345. doi: 10.1093/cercor/8.4.321

Wiser, A. K., Andreasen, N. C., O'Leary, D. S., Watkins, G. L., Boles Ponto, L. L., and Hichwa, R. D. (1998). Dysfunctional cortico-cerebellar circuits cause "cognitive dysmetria" in schizophrenia. *Neuroreport* 9, 1895–1899. doi: 10.1097/00001756-199806010-00042

Wu, T., and Hallett, M. (2013). The cerebellum in Parkinson's disease. *Brain* 136, 696–709. doi: 10.1093/brain/aws360

Yücel, M., Pantelis, C., Stuart, G. W., Wood, S. J., Maruff, P., Velakoulis, D., et al. (2002). Anterior cingulate activation during Stroop task performance: a PET to MRI coregistration study of individual patients with schizophrenia. *Am. J. Psychiatry* 159, 251–254. doi: 10.1176/appi.ajp.159.2.251

Conflict of Interest Statement: The authors declare that the research was conducted in the absence of any commercial or financial relationships that could be construed as a potential conflict of interest.

Received: 01 March 2014; accepted: 22 August 2014; published online: 15 September 2014.

Citation: Parker KL, Narayanan NS and Andreasen NC (2014) The therapeutic potential of the cerebellum in schizophrenia. Front. Syst. Neurosci. ***8****:163. doi: 10.3389/fnsys.2014.00163*

This article was submitted to the journal Frontiers in Systems Neuroscience.

frontiers in
SYSTEMS NEUROSCIENCE

REVIEW ARTICLE
published: 14 November 2013
doi: 10.3389/fnsys.2013.00083

New roles for the cerebellum in health and disease

Stacey L. Reeber[1], Tom S. Otis[2]* and Roy V. Sillitoe[1]*

[1] *Department of Pathology and Immunology, Department of Neuroscience, Baylor College of Medicine, Jan and Dan Duncan Neurological Research Institute of Texas Children's Hospital, Houston, TX, USA*
[2] *Department of Neurobiology, Geffen School of Medicine at University of California, Los Angeles, Los Angeles, CA, USA*

Edited by:
Thomas C. Watson, University of Bristol, UK

Reviewed by:
Charles R. Watson, Curtin University, Australia
Mario U. Manto, Fonds de la Recherche Scientifique, Belgium

****Correspondence:***
Tom S. Otis, Department of Neurobiology, Geffen School of Medicine at University of California, Los Angeles, 650 Charles Young Dr. South, Room 63-251, Los Angeles, CA 90095, USA
e-mail: otist@ucla.edu;
Roy V. Sillitoe, Department of Pathology and Immunology, Department of Neuroscience, Baylor College of Medicine, Jan and Dan Duncan Neurological Research Institute of Texas Children's Hospital, 1250 Moursund Street, Suite 1325, Houston, TX 77030, USA
e-mail: sillitoe@ bcm.edu

The cerebellum has a well-established role in maintaining motor coordination and studies of cerebellar learning suggest that it does this by recognizing neural patterns, which it uses to predict optimal movements. Serious damage to the cerebellum impairs this learning and results in a set of motor disturbances called ataxia. However, recent work implicates the cerebellum in cognition and emotion, and it has been argued that cerebellar dysfunction contributes to non-motor conditions such as autism spectrum disorders (ASD). Based on human and animal model studies, two major questions arise. *Does* the cerebellum contribute to non-motor as well as motor diseases, and if so, *how* does altering its function contribute to such diverse symptoms? The architecture and connectivity of cerebellar circuits may hold the answers to these questions. An emerging view is that cerebellar defects can trigger motor and non-motor neurological conditions by globally influencing brain function. Furthermore, during development cerebellar circuits may play a role in wiring events necessary for higher cognitive functions such as social behavior and language. We discuss genetic, electrophysiological, and behavioral evidence that implicates Purkinje cell dysfunction as a major culprit in several diseases and offer a hypothesis as to how canonical cerebellar functions might be at fault in non-motor as well as motor diseases.

Keywords: neurological disorders, genetics, circuitry, neural activity, brain behavior

INTRODUCTION

The cerebellum is essential for smooth, purposeful movement. Recently, human neuroimaging and animal behavior studies have implicated the cerebellum in the processing of signals for perception, cognition, and emotion (Schmahmann, 2010; Bastian, 2011; D'Angelo and Casali, 2012), particularly in circumstances involving predictions or timing. Participation of the cerebellum in higher order brain function is likely mediated by extensive connections with cortical and sub-cortical centers. These anatomical connections raise the intriguing possibility that cerebellar dysfunction may lead not only to motor impairments, but also to non-motor deficits in complex neurological conditions. Furthermore, the implication that cerebellar circuits malfunction in certain neurodevelopmental disorders suggests that cerebellar processing could be required during development for proper wiring in other brain areas (Kuemerle et al., 2007). We discuss the etiology of cerebellar disease in the context of how circuits are organized, and present evidence that cerebellar connectivity may be altered in ataxia, dystonia, and autism spectrum disorders ASD.

ALTHOUGH CEREBELLAR CIRCUITS ARE STRUCTURALLY "SIMPLE," THEY CONTAIN MILLIONS OF CONNECTIONS

To appreciate how the cerebellum works, it is useful to first recall the major cell types, and revisit the relationships between them (**Figure 1**). Purkinje cells are the corner stone of all cerebellar circuits; during development they orchestrate morphogenesis, and in the adult each one computes hundreds of thousands of signals (**Figure 1B**). The elaborate dendrite of each Purkinje cell is directly innervated by a single excitatory climbing fiber that comes from the inferior olive in the brainstem (**Figures 1**, **2A**). Purkinje cells also receive excitatory input indirectly from mossy fibers, which originate from over two-dozen brain and spinal cord nuclei. Approximately 25 million mossy fibers enter the cerebellum and synapse on ∼50 billion granule cells (Palkovits et al., 1972; Andersen et al., 1992). Granule cells then converge massively (100,000 to 1) onto the dendrites of Purkinje cells. This striking expansion from mossy fibers to granule cells and equally striking contraction from granule cells onto the Purkinje cell dendrite is believed to provide a computational benefit, namely the ability of the cerebellum to discriminate a large number of different patterns (Marr, 1969; Albus, 1971; Brunel et al., 2004). Various inhibitory interneurons regulate the excitatory inputs onto Purkinje cells (**Figure 1**), and specialized astrocytes called Bergmann glia maintain efficient synaptic signaling. The Purkinje cells send exclusively inhibitory signals to the cerebellar nuclei, which control the final output of the cerebellum (White and Sillitoe, 2013). An excitatory feedback projection terminating in mossy fiber-like endings exists between the cerebellar nuclei and granule cell layer, and an inhibitory feedback connection is made from the cerebellar nuclei to the inferior olive. These two connections form parts of the nucleo-cortical (Tolbert et al., 1976; Hess,

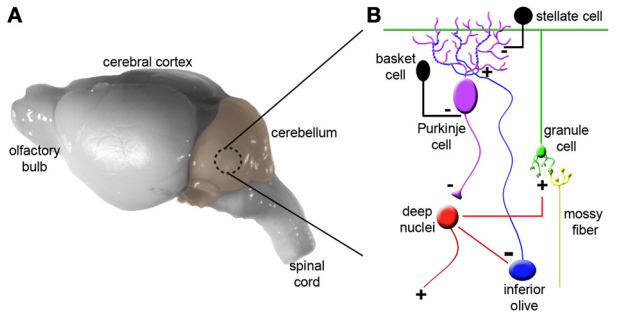

FIGURE 1 | Cytoarchitecture and connectivity in the cerebellum. **(A)** Mouse brain shown from a lateral view with the cerebellum highlighted in color. **(B)** The basic cerebellar circuit is comprised of granule cells, Purkinje cells, stellate and basket cell interneurons, and deep nuclei. Afferent information is delivered to the cerebellum as climbing fibers or mossy fibers. The plus and minus signs indicate whether each synapse is excitatory or inhibitory. Note that inhibitory connections between the cerebellar nuclei and inferior olive complete the olivo-cortico-nuclear loop and excitatory projections from the cerebellar nuclei loop back to the cerebellar cortex. Panel **(B)** was modified from (Reeber et al., 2012). For simplicity we have not shown Golgi cells, unipolar brush cells, Lugaro cells, and candelabrum cells.

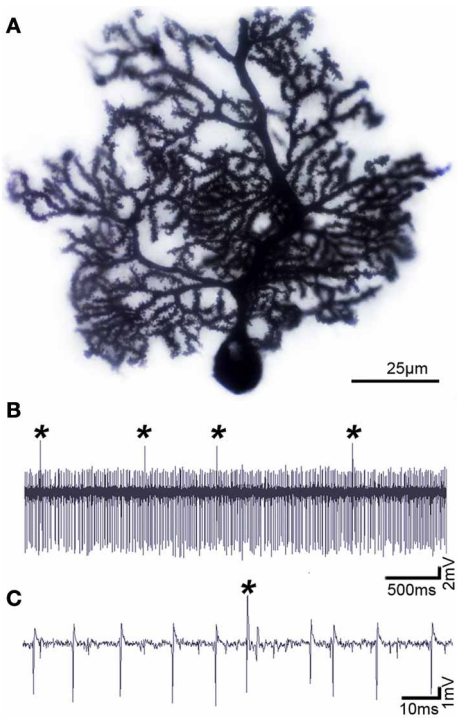

FIGURE 2 | Purkinje cells have a distinct morphology and electrophysiological profile. **(A)** Purkinje cell labeled using the classic Golgi-Cox staining method, demonstrating the exquisite morphology and extensive dendritic branching of the Purkinje cell. **(B)** Purkinje cells can be identified by their unique activity: each one fires complex spikes that are triggered by climbing fibers (asterisks) and simples spikes that are driven either by intrinsic activity or by mossy fiber-granule cell inputs. **(C)** Higher power image of the Purkinje cell recording shown in panel **(B)**. Defects in Purkinje cell morphology and/or firing are thought to instigate motor and non-motor neurological conditions.

1982) and olivo-cortico-nuclear loops (Angaut and Sotelo, 1987; Chaumont et al., 2013), respectively. This canonical cerebellar circuit, which was once thought to be simple and synonymous with motor signaling, is now thought to have underlying complexities that also mediate non-motor brain behaviors.

CEREBELLAR CONNECTIONS ARE INTEGRATED INTO MULTIPLE BRAIN NETWORKS

The classic view that cerebellar function is restricted to controlling motor coordination has been challenged by recent imaging studies in humans that suggest cerebellar contributions to cognition (language), emotional behavior (fear), sleep, and even non-somatic, visceral responses (Demirtas-Tatlidede et al., 2011; Baumann and Mattingley, 2012; D'Angelo and Casali, 2012). Anatomical studies performed in non-human primates and rodents strongly support the imaging data. Extensive mono- and poly-synaptic pathways connect the cerebellum to the cerebral cortex, hippocampus, amygdala, hypothalamus, periaqueductal gray, basal ganglia, thalamus, brain stem, and spinal cord (Dietrichs and Haines, 1989; Middleton and Strick, 2001; Hoshi et al., 2005; Cerminara et al., 2009; Buckner et al., 2011; Dum and Strick, 2012). Considering such widespread connections between the cerebellum and the forebrain, dozens of brainstem nuclei, and with several major autonomic centers (**Figure 3**), it seems difficult to imagine that cerebellar circuit dysfunction would interfere only with the ability to perform motor tasks. Still, valid arguments against non-motor contributions of the cerebellum have been presented (Glickstein, 2007), and recent data demonstrates that caution should be taken when interpreting for cerebellar non-motor behavior in experimental preparations (Galliano et al., 2013). Keeping in mind that a lively debate continues as to whether the cerebellum is involved in non-motor function (Lemon and Edgley, 2010), in the following sections we present recent evidence that has unveiled unexpected roles for the cerebellum in conditions that are historically "non-cerebellar" (**Table 1**).

Diseases of the cerebellum: significantly more than just uncoordinated locomotion

Cerebellar damage causes a number of motor symptoms including dysmetria (in which patients overshoot (hypermetria) or undershoot (hypometria) a target during voluntary goal-directed tasks), hypotonia, tremor, and dysarthic speech. These symptoms, and the interpretations of what they mean to brain function date back to the pioneering neurological examinations of Sir Gordon Holmes (Holmes, 1939). However, descriptions of cerebellar diseases, and in particular those that affect Purkinje cell development and/or function, typically disrupt the accuracy and coordination of movement, conditions which are often cumulatively referred to as "ataxia."

ATAXIA, THE CLASSIC CASE OF CEREBELLAR DYSFUNCTION

As a symptom, ataxia refers to uncoordinated movement and as a disorder it refers to a family of neurological diseases that typically involve neurodegeneration. Ataxia-related defects can also

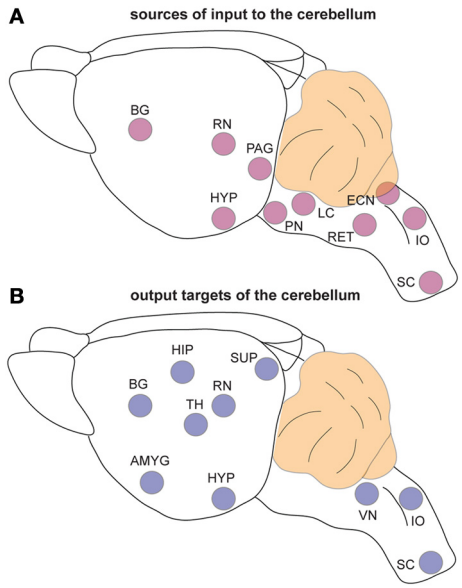

FIGURE 3 | The cerebellum is extensively connected to the brain and spinal cord. (A) Schematic representation of brain regions that send input to the cerebellum. **(B)** Schematic representation of the regions that receive information from the cerebellum. Note that the TH is a major relay station for cerebellar input to the cortex while the PN is the primary gateway for cerebral cortical input to the cerebellum. Abbreviations: AMG, amygdala; BG, basal ganglia; ECN, external cuneate nucleus; HIP, hippocampus; HYP; hypothalamus; IO, inferior olive; LC, locus coeruleus; PAG, periaqueductal gray; PN, pontine nuclei; RET, reticular nucleus; RN, red nucleus; SC, spinal cord; SUP, superior colliculi; TH, thalamus; VN, vestibular nuclei.

Table 1 | Cerebellar dysfunction contributes to motor and non-motor diseases.

MOTOR DISEASES
Ataxia
Dystonia
Huntington's
Multiple sclerosis
Parkinson's
Tourette's (and other "tic"-related disorders)
Tremor
NON-MOTOR DISEASES
Autism spectrum disorders
Dyslexia
Fetal alcohol syndrome
Medulloblastoma
Obsessive-compulsive disorder
Schizophrenia
Sleep apnea
Vertigo

The list is by no means exhaustive, although it does include some major conditions with either known (e.g., ataxia) or heavily suspected (e.g., autism spectrum disorders) cerebellar involvement. Note that in each section the different diseases are listed in alphabetical order. And, some motor disorders may have additional complex non-motor symptoms (e.g., mental retardation in ataxia) and vice versa, some patients with non-motor disorders have problems making day-to-day movements (e.g., motor abnormalities in autism spectrum disorders).

be acquired, and develop as a result of stroke, multiple sclerosis, tumors, alcoholism, peripheral neuropathy, metabolic disorders, and vitamin deficiencies (Klockgether, 2010). Ataxia can also arise sporadically (Klockgether, 2010). Patients with ataxia have poor muscle control, and when they have limb movement problems the lack of balance and coordination ultimately disturbs their gait, a symptom often associated with cerebellar defects.

Cerebellar ataxia is the most common form of ataxia. There are over 60 forms of inherited cerebellar-based ataxia, with more than half of them classified as either spinocerebellar ataxias, Friedreich's ataxia, episodic ataxia, or fragile X tremor/ataxia syndrome (Durr, 2010; Klockgether, 2010). Recapitulating disease mechanisms in engineered animal models has allowed major breakthroughs in our understanding of the pathogenesis of the cerebellar ataxias (Burright et al., 1995; Hamilton et al., 1996; Serra et al., 2006). A unifying cellular phenotype observed in the nervous system of ataxic mice and humans, regardless of the type of ataxia, is extensive Purkinje cell degeneration. However, while neuronal degeneration may be essential for the severe pathophysiological features of ataxia (Chen et al., 2008; Liu et al., 2009), electrophysiological and calcium imaging data show that Purkinje cells and their major inputs are dysfunctional prior to degeneration in ataxia mouse models coinciding with milder ataxic phenotypes (Barnes et al., 2011; Hourez et al., 2011; Shakkottai et al., 2011; Kasumu et al., 2012; Hansen et al., 2013). This prompts two considerations regarding disease etiology in any disorder that alters the brain at the level of circuits: (1) neuronal function can be affected in the absence of pathological defects, and (2) neuronal circuit dysfunction may be the primary cause of behavioral symptoms. A case in point is dystonia, where no clear or consistent pathology is evident, yet brain dysfunction can cause overt behaviors that are obstructive to daily life.

DYSTONIA PATHOGENESIS PROVIDES NEW INSIGHTS INTO CEREBELLAR (DYS)CONNECTIVITY

Dystonia is a complex movement disorder that causes involuntary, sustained muscle contractions that result in postural twisting and repetitive movements (Hallett, 2009; Shamim et al., 2011). Symptoms can be mild and transient, appearing only under conditions of exertion or fatigue, or severe and constant enough to make even simple day-to-day movements impossible. The involuntary painful muscle contractions can affect virtually any muscle in the body, causing blepharospams in the eyelids [a frequent result of anti-psychotic drugs; (Hallett, 2009)], to the common writer's cramp (Shamim et al., 2011), to inherited torsion dystonia that blocks the normal execution of trunk and limbs movements (Muller, 2009; Shamim et al., 2011). It can be acquired as a hereditary disorder, or spontaneously arise as an idiopathic condition. Although it is considered the third most common motor disease, the true prevalence of dystonia is difficult to estimate because it can be comorbid with other disorders such as Parkinson's disease, Huntington's disease, stroke, or ataxia, and many milder cases do not get reported (Muller, 2009; Asmus and Gasser, 2010). Despite the wide range of its manifestations and causes, dystonia consistently involves erroneous communication

along circuits that link the cerebral cortex, basal ganglia, thalamus, and brainstem (Hendrix and Vitek, 2012). Recently, several groups have considerably deepened our understanding of dystonia by confirming that the cerebellum can play a role in the disorder (Argyelan et al., 2009; Calderon et al., 2011; LeDoux, 2011; **Table 2**). Now, the general consensus in field is that in dystonia, communication is disrupted along two primary pathways: the cerebello-thalamo-striatial (CTS) circuit and cerebello-thalamocortical (CTC) circuit (Niethammer et al., 2011). Moreover, a recent elegant study demonstrated using a model of rapid onset dystonia-parkinsonism that defects in either the basal ganglia or the cerebellum could instigate disease onset (Calderon et al., 2011; **Table 2**).

Functional imaging studies have revealed abnormal cerebellar activity in *DYT1* dystonia (Eidelberg et al., 1998), hemi-dystonia (Ceballos-Baumann et al., 1995), exercise-induced paroxysmal dystonia (Kluge et al., 1998), writer's cramp (Odergren et al., 1998; Preibisch et al., 2001), cervical dystonia (Galardi et al., 1996) and blepharospasm (Hutchinson et al., 2000). Consistent with these human data, abnormal cerebellar activity is observed in several genetic models of dystonia, including dystonic (*dt*) rats, both transgenic and knock-in *Dyt1* mice, and spontaneous mutant mice such as *tottering* (Brown and Lorden, 1989; Campbell and Hess, 1998; Calderon et al., 2011; Ulug et al., 2011; Zhao et al., 2011). *In vivo* electrophysiology recording in these rodent models reveals that Purkinje cells lose their regular firing patterns (**Figures 2B,C**) and instead fire in erratic "burst" patterns (LeDoux, 2011). Interestingly, in mice with ataxia it has been suggested that irregular firing of Purkinje cells is the primary alteration that causes motor defects (Walter et al., 2006). Surgical removal of the cerebellum terminates the dystonic attacks in rodents, supporting the notion that the cerebellum can drive dystonia (Neychev et al., 2008; LeDoux, 2011; Neychev et al., 2011). At the cellular level, Ellen Hess and colleagues have pioneered the view that cerebellar Purkinje cells may be the source of dystonia (Campbell et al., 1999). In their initial experiments they

Table 2 | Animal models and human data that implicate the cerebellum in dystonia.

A. ANIMAL MODELS			
Model	**Mode of induction**	**Contribution**	**Reference**
Genetically *dystonic rat (dt)*	Spontaneous mutation in the *Atcay* gene	Purkinje cell and cerebellar nuclei "burst" firing	LeDoux et al., 1993, 1998; LeDoux and Lorden, 2002
tottering mice	Spontaneous mutation in the gene encoding the alpha subunit of the Cacna1a P/Q-type calcium channel	Purkinje cells might contribute to dystonia	Campbell et al., 1999; Neychev et al., 2008
Purkinje specific deletion of Cacna1a	Conditional mouse genetics	Regional Purkinje cell dysfunction initiates dystonia	Raike et al., 2012
Dyt1 mutant mice	Genetically engineered knock-in into *Tor1a*	Gene dysfunction in cerebellum may cause dystonia	Ulug et al., 2011; Yokoi et al., 2012
Kainic acid (glutamate receptor agonist)	Injection into cerebellum	Abnormal cerebellar activity can induce dystonia	Pizoli et al., 2002
Ouabain (binds and inhibits the Na^+/K^+-ATPase sodium pump)	Micro-pump infusion into cerebellum	Cerebellum (presumably Purkinje cells) instigates dystonia	Calderon et al., 2011
B. HUMAN PHYSIOLOGY AND NEUROPATHOLOGY			
Approach	**Measurement**	**Contribution**	**Reference**
Eye blink conditioning (cervical dystonia)	Function of the olivo-cerebellar pathway	Functional defects in the cerebellar circuit in dystonia	Teo et al., 2009
DTI imaging (DYT1 and DYT6 carriers)	Tractography	Cerebello-thalamic pathway is defective in dystonia patients	Argyelan et al., 2009
[(18)F]-fluorodeoxyglucose PET (DYT11 myoclonus-dystonia patients)	Metabolic changes	Metabolic changes in the cerebellum and inferior olive of dystonia patients	Carbon et al., 2013
Neuropathology (cervical dystonia)	Purkinje cell density	Purkinje cell loss is "patchy" in dystonia	Prudente et al., 2013

This table lists some recent publications that demonstrate a potentially critically role for the cerebellum is various forms of dystonia. For clarity we have only listed a few pertinent examples.

removed Purkinje cells by cross-breeding dystonic *tottering* mice with mutants that exhibit Purkinje cell degeneration (Campbell et al., 1999). Remarkably, doing so alleviated dystonia. In their recent studies, Hess' group showed using an elegant conditional genetic approach that selectively eliminating the Cacna1a calcium channel in Purkinje cells is sufficient to evoke widespread dystonic movements (Raike et al., 2012). Moreover, this conditional approach was further used to show that stress, caffeine, and alcohol can operate through shared mechanisms to trigger severe episodic dystonia attacks (Raike et al., 2013). While Purkinje cell defects induce dystonia, extra-cerebellar synapses may be targeted to block dystonia. Micro-lesions made in the central-lateral thalamus, which connects the cerebellum to the basal ganglia (Ichinohe et al., 2000), alleviated motor defects in mice with rapid-onset dystonia-parkinsonism (Calderon et al., 2011).

On the one hand, genetically altering Purkinje cells has revealed an unexpected requirement for the cerebellum in dystonia, yet on the other hand, it may not be entirely surprising that altering Purkinje cell function would produce complex motor deficits. In fact, one has to wonder whether defective Purkinje cell communication could also, and perhaps simultaneously, influence non-motor behavior. This logic was recently put to the test in experiments that sought to determine whether the cerebellum is linked to ASD.

AUTISM SPECTRUM DISORDERS MAY BE LINKED TO CEREBELLAR DEVELOPMENT AND FUNCTION

The ASD's are developmental disorders characterized by impaired social communication, repetitive stereotypic behaviors, and delayed language development (Association, 1994). Individuals with ASD can also display dysfunction in both fine and gross motor skills (Fatemi et al., 2012). Although the signs and symptoms of ASD have become well appreciated, an ongoing debate has been centered on one important question: what regions of the brain are defective in ASD? Not so appreciated is that the cerebellum exhibits consistent neuropathological abnormalities in ASD (Ritvo et al., 1986; Bauman, 1991). In postmortem brain tissue from ASD patients, regardless of age, sex, and cognitive ability, a significant decrease in the number of Purkinje cells is reported (Bauman and Kemper, 2005; Whitney et al., 2008; Fatemi et al., 2012). In addition, functional neuroimaging demonstrates abnormal cerebellar activation in patients with ASD (Allen et al., 2004). Although controversial, in part due to co-morbidity with other developmental deficits, magnetic resonance imaging has also revealed hypoplasia of the cerebellum in some ASD patients (Courchesne et al., 1994; Stanfield et al., 2008; Scott et al., 2009).

Genetic studies also support a role for the cerebellum in ASD (Fatemi et al., 2012). For example, trinucleotide repeat expansions that cause fragile X syndrome by disrupting the function of the gene *FMR1* lead to cerebellar vermis abnormalities. In both global and Purkinje cell-specific fragile X knockout mice, Purkinje cell spine morphology, synaptic plasticity, and cerebellar behaviors are impaired. Moreover, in humans, cerebellar learning is deficient as fragile X patients show abnormal eye blink conditioning (Koekkoek et al., 2005; Smit et al., 2008; Tobia and Woodruff-Pak, 2009). There is also a Fragile X associated ataxia/tremor syndrome exhibited by parents of Fragile X patients (Hagerman et al., 2001; Hall and O'Keefe, 2012). This syndrome is linked to "premutation" expansions in the fragile X gene and presents with classic cerebellar deficits of gait ataxia and tremor. Imaging studies show clear atrophy of the cerebellum.

Other genes highly expressed in cerebellum such as *EN2, MET*, and *GABRB3* may also be associated with non-syndromic ASD. Each of these genes exhibits specific roles during cerebellar development. In mice, *En2* is required for cell proliferation, tissue patterning, regional morphogenesis, and circuit formation in the cerebellum (White and Sillitoe, 2013). Importantly, two intronic polymorphisms in human *EN2* have been reported to be associated with the risk of developing ASD (Gharani et al., 2004; Wang et al., 2008; Banerjee-Basu and Packer, 2010; Sen et al., 2010; Yang et al., 2010). Loss of *En2* in mice results in altered aggressiveness and excessive grooming, which are hallmark ASD-like behaviors (Cheh et al., 2006; Brielmaier et al., 2012). Several studies have demonstrated an association between three *MET* single nucleotide polymorphisms and ASD (Campbell et al., 2008; Hedrick et al., 2012). MET is expressed in proliferating granule cell precursors and disrupting its function results in cerebellar hypoplasia (Ieraci et al., 2002; Fatemi et al., 2012). Positive associations with ASD have also been reported for both common and rare variants of the *GABRB3* gene (Banerjee-Basu and Packer, 2010), and *GABRB3* expression is reduced in the cerebellum of affected individuals. Importantly, *GABRB3* is located within chromosome 15q11–13, a site linked to duplications that are associated with ASD (Fatemi et al., 2012). *GABRB3* null mice display hypoplasia of the cerebellar vermis (DeLorey et al., 2008; Fatemi et al., 2009, 2012). Despite the potential links between cerebellar dysfunction and ASD pathogenesis, no clear view has emerged about *why* the cerebellum might be involved in ASD (genetic and cellular mechanisms?) or *how* it might be involved (specific brain connections or neural circuits?). However, recent landmark studies strongly support the idea that Purkinje cell dysfunction can result in ASD.

Tuberous sclerosis (TSC1, TSC2) is a rare disorder associated with ASD, and is characterized by benign tumors (harmartomas) that form in the brain, skin, eyes, kidneys, and heart (Curatolo et al., 2008). Interestingly, tuberous sclerosis patients with cerebellar lesions have more severe ASD symptoms than patients with lesions in only other brain regions (Eluvathingal et al., 2006). In a recent paper, Sahin and co-workers showed that loss of *Tsc1* from cerebellar Purkinje cells is sufficient to cause social impairments, cognitive defects, abnormal vocalizations, and a number of motor problems (Tsai et al., 2012). The mutant mice also exhibited a reduction in the number of Purkinje cells, and an increase in the expression of endoplasmic reticulum and oxidative stress response markers. The study further showed that Purkinje cell excitability was altered in both heterozygous and homozygous *Tsc1* mutants (Tsai et al., 2012) in a very similar manner as has been described in spinocerebellar ataxia models (Hourez et al., 2011; Shakkottai et al., 2011; Kasumu et al., 2012; Hansen et al., 2013). Both the pathology and abnormal ASD-like behaviors were successfully blocked in mutants treated with the mTOR inhibitor rapamycin. Together, these *Tsc1* conditional mutants recapitulated several core features of human ASD and using their model the authors demonstrate that pharmacological treatments

that target Purkinje cell function can alleviate multiple ASD-associated features (Tsai et al., 2012). In a different study, loss of *Tsc2* in Purkinje cells resulted in neurodegeneration, increased repetitive behavior, and social interaction deficits (Reith et al., 2013). Cumulatively, the impressive body of data from these two studies suggests that Purkinje cell dysfunction can cause ASD-like behaviors, and that defects in specific cerebellar circuits might be sufficient to trigger downstream neuronal network alterations that contribute to severe abnormalities in motor and non-motor behaviors.

Might the cerebellum be performing a common computational task in its motor and non-motor functions?

Although the identification of the Purkinje cell as a major player in motor and non-motor disease has opened new avenues for understanding complex brain disorders (**Table 3**), one question that immediately arises is how could a single cell type with seemingly unique and specialized functions encode such diverse disease-related information? One can speculate that some of the basic computational capacities of the cerebellum that have been studied with respect to motor behavior, such as the ability to discriminate patterns and the capacity to use these patterns to learn to make context-dependent predictions (Bastian, 2011), are useful to non-motor areas of the brain. For example, it is intriguing to consider whether cerebellar output may be required during a critical period of development so that cortical circuits responsible for complex social behavior and language can be properly wired. This may not be confined to cortical circuitry. Interestingly, Herrup and colleagues observed that loss of *En2* resulted in defects in the position of the amygdala, a brain region regularly altered in individuals with ASD (Kuemerle et al., 2007). These findings suggest that a gene (*En2*) expressed exclusively in the mid/hindbrain region can affect distant cerebral cortex structures such as the amygdala. Herrup and colleagues hypothesized that disrupting the location of neurons relative to their efferent and afferent partners may have detrimental effects on cognition. In this scenario, cerebellar dysfunction during development could result in ASD-like symptoms (Kuemerle et al., 2007). In adults who suffer cerebellar damage, cognitive impairments may result from a loss of cerebellar processing power contributing to tasks involving prediction or complex sensory discrimination (Bastian, 2011). Such hypotheses derive support from the parallel anatomical substrates that connect the cerebellum to motor areas and non-motor areas. Progress on these fascinating questions is likely to emerge from studies of the remarkable patterning of the cerebellum into a complex array of topographic "zonal" circuits that are thought to shape cellular function during behavior (**Figure 4**).

Table 3 | Animal models of cerebellar dysfunction.

Model	Phenotype	Relationship to disease
ATXN1[82Q]	ataxia	Spinocerebellar ataxia type 1
ATXN2[Q127]	ataxia	Spinocerebellar ataxia type 2
Genetically *dystonic rat (dt)*	Cerebellar functional defects and severe co-contractions of the muscles	Dystonia
tottering mice	Baseline locomotor dysfunction with stress induced increase	Episodic ataxia and dystonia
Purkinje specific deletion of Cacna1a	Ataxia and dystonic-like postures	Dystonia and ataxia
Dyt1 mutant mice	Generalized motor dysfunction	Hereditary dystonia
Kainic acid (glutamate receptor agonist)	Dystonic postures of the limbs and trunk	Generalized dystonia
Ouabain (binds and inhibits the Na^+/K^+-ATPase sodium pump)	Ataxia and dystonic-like postures (hyperextended limbs)	Rapid onset dystonia-Parkinsonism
En2 null mice	Motor coordination, motor learning, and social behavior deficits	Autism spectrum disorders
Met knock-in mutant mice	Cerebellar development defects	Autism spectrum disorders
Gabrb3 null mice	Cerebellar morphogenesis defects and social behavior impairments	Autism spectrum disorders
Purkinje cell deletion of *Tsc1*	Purkinje cell electrophysiological dysfunction, repetitive behaviors, social behavior abnormalities	Autism spectrum disorders
Purkinje cell deletion of *Tsc2*	Social behavior defects and repetitive behaviors	Autism spectrum disorders

This table lists the animal models we have discussed and their utility in understanding specific cerebellar diseases. Note that for clarity only two spinocerebellar ataxia (SCA) models are mentioned—SCA has been extensively studied using different models.

Toward a circuit topography hypothesis for understanding cerebellar disease

Natural selection has adorned the animal kingdom with a rich collection of exquisite patterns. We revel in admiration of butterfly wing spots, peacock feathers and zebra stripes. Beyond their beauty, these precise patterns are essential for sexual selection and evading predators. In humans, our own body parts such as ribs, vertebrae, and digits develop into patterns that permit the execution of essential day-to-day functions. The human brain, arguably the most complicated structure in nature, is no exception to the hypothesis that patterns are inherent to all forms, regardless of their simplicity or complexity. Much like the developing wings and body segments of an insect, the mammalian

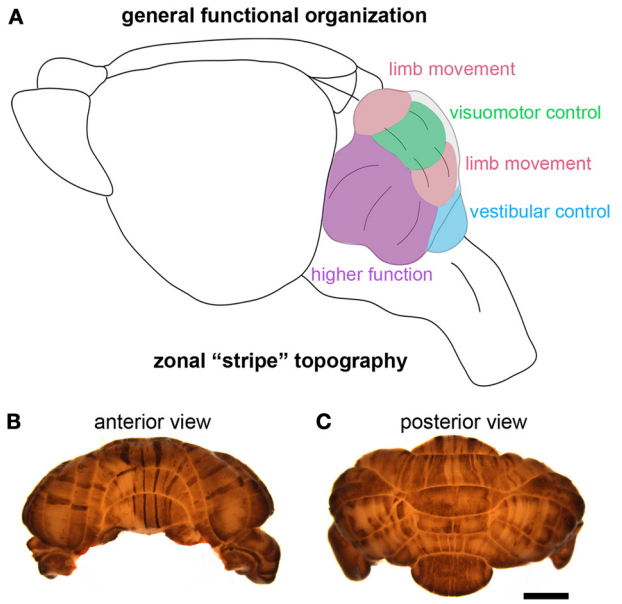

FIGURE 4 | The cerebellum is highly compartmentalized into functional regions. (A) Schematic illustrating the division of the cerebellum into behaviorally relevant domains. The cartoon is a simplified model of the functional cerebellum and is based on functional imaging, human and animal lesions, afferent connectivity, electrophysiology, and animal behavior studies. **(B,C)** Wholemount immunohistochemical staining of the mouse cerebellum—zebrin II expression reveals the intricate patterning of the cerebellum into zones. The scale bar in **(C)** = 2 mm (also applies to **(B)**.

brain contains a striking array of patterns. Each of the billions of neurons in the human brain is decorated with a specific pattern of connections that drive brain function. Although many regions of the brain have patterned neural circuits (Reeber et al., 2012), the cerebellum arguably contains the most exquisitely patterned circuits of all central nervous system structures. This high level of patterning may be essential for packaging a large number of functionally distinct circuits into a logical network for seamless communication during behavior.

Cerebellar circuits are patterned into a topographic map of genetically determined "zones" (White and Sillitoe, 2013). Zones are best revealed by molecular expression patterns in Purkinje cells. The most comprehensively studied zonal marker is zebrin II (Brochu et al., 1990) (**Figures 4B,C**), also known as aldolase C. Zebrin II is expressed by a subset of Purkinje cells (zebrin II +) that alternate with Purkinje cells that do not express zebrin II (zebrin II −), thus forming complementary rows of biochemically distinct Purkinje cells. The zonal organization of zebrin II is symmetrical about the midline, highly reproducible between individuals, and conserved across species (Sillitoe et al., 2005). Molecular tools such as zebrin II expression have been used to show that zonal compartments divide the cerebellar cortex into thousands of reproducible units, with each one containing several hundred Purkinje cells (Apps and Hawkes, 2009). The Purkinje cell zonal plan has a predictable and well-defined relationship to its thousands of incoming afferent projections [**Figure 3**; (Reeber et al., 2012)]. Moreover, each cerebellar cortical region has a defined and strict relationship to specific cells within the cerebellar nuclei, which send topographic projections out of the cerebellum to unique regions within the brain and spinal cord [(Uusisaari and De Schutter, 2011); **Figure 3**]. Together, Purkinje cell zones and their associated synapses organize cerebellar function into a spatial map that encodes multiple behaviors (Wadiche and Jahr, 2005; Horn et al., 2010; Cerminara and Apps, 2011). It is intriguing to speculate that this zonal plan may extend beyond cerebellar circuits into connected regions such as the thalamus and cerebral cortex. Indeed, cerebellar efferent projections to the inferior olive and the basal ganglia are highly topographic, and because of bi-directional connectivity projections between these structures forms closed loop circuits (Middleton and Strick, 2000; Bazzigaluppi et al., 2012).

With such a high level of organization it seems plausible that certain circuits, and therefore certain zones, may be more affected by some diseases and not others. That is, could disrupting one set of zones cause ataxia while disrupting an adjacent set cause dystonia? Perhaps. However, given that each zone likely encodes multiple behaviors (Cerminara and Apps, 2011), manipulating the function of any given set would almost certainly result in a "mixed" disease outcome. The phenotypes of several animal models of episodic movement disorders support this idea. For instance, in *Cacna1a* mutant mice [*tottering*; (Alvina and Khodakhah, 2010)], loss of the Cav2.1 voltage dependent calcium channel not only causes ataxic episodes, but severe dystonia can also be induced in the same mice. Similarly, in *Tsc1*, *Tsc2*, and *En2* mouse models of ASD, loss of cerebellar function triggers circuit defects that disrupt both motor and non-motor behaviors. And, *En2* mutant mice exhibit severe alterations in Purkinje cell patterning and consequently, at least three functionally distinct classes of afferent fibers are mis-targeted into ectopic positions within the cerebellar cortex (White and Sillitoe, 2013). It is therefore intriguing that Purkinje cell loss may be patterned in dystonia and ASD since the cell loss has been described as "patchy" in both conditions (Carper et al., 2006; Prudente et al., 2013). The burning question that we must now tackle is does zonal function directly control disease related behaviors? The answer may lie within the operational units of the zones, which are referred to as cerebellar modules (Ruigrok, 2011). Each module is comprised of topographically organized afferent fibers, Purkinje cell stripe gene expression (e.g., zebrin II), and the zonally organized Purkinje cell efferent projections to the cerebellar nuclei. Systematic analyses will have to be conducted in existing mutant mouse models in order to determine how each module, or subsets of functionally related modules, operates during the expression of disease-related behaviors. In addition, however, powerful inducible approaches such as channelrhodopsin or CreER genetics should be used to target specific modules (or specific circuits within them) to ask whether defective connectivity in select pathways can recapitulate the disease phenotypes. Such models would be invaluable for therapeutic design and testing. In parallel, further studies in humans should be conducted. Recent likelihood meta-analysis of neuroimaging data demonstrated a precise functional topography in different lobules; subsets of lobules are apparently associated with specific functions (e.g., lobule V = sensorimotor function and lobule VII = cognitive function;

(Stoodley and Schmahmann, 2009). Each set of lobules was also linked to specific cerebello-cerebral cortical loops (Stoodley and Schmahmann, 2010), which include connections with somatomotor, premotor and association cortices (Buckner et al., 2011). In general, these functional and anatomic topographies are remarkably reminiscent of the transverse divisions that were delineated by mouse developmental and genetic analyses of zones (Ozol et al., 1999; Sgaier et al., 2007). For more than 60 years zonal cerebellar circuits have been invaluable for understanding basic neuroanatomy, development, cellular function, and behavior. Now, the time is right to apply this wealth of knowledge toward understanding the cellular and molecular mechanisms of neurological disease using animal models and also human pathophysiology. Purkinje cell zones are highly attractive candidates for mediating cerebellar disease (Tolbert et al., 1995; Sarna and Hawkes, 2003). In this context, the expression of calcium associated proteins such as mGluR, EAAT4, and IP3R1 may render certain zones more vulnerable to particular insults (Welsh et al., 2002; Wadiche and Jahr, 2005; Schorge et al., 2010). Although, why particular zones are so susceptible to specific conditions whereas others are resistant, remains an intriguing mystery.

Summary

Despite the remarkable strides that have been made in understanding the role of the cerebellum in normal brain behavior and disease, we still do not have a consensus on either issue. We are far from fully understanding what the cerebellum does or what happens if it fails to work properly. Moreover, with only five major neuronal types, one wonders how diverse information from regions ranging from the spinal cord and brainstem to the hypothalamus and basal ganglia converge within functionally coherent circuits in the cerebellum. Even after more than 100 years since the seminal work of Cajal, the cerebellum remains one of the most intriguing structures in the body: despite its simple structure it has the computing power to process more information than any other brain region, and changes to its normal state translate into devastating conditions that apparently reverberate throughout the brains major circuits. While the precise mechanisms that mediate cerebellar (dys)function remain a mystery, powerful new genetic and circuit physiology approaches hold great promise for improving our understanding of this fascinating brain region.

ACKNOWLEDGMENTS

Roy V. Sillitoe is supported by the Caroline Wiess Law Fund for Research in Molecular Medicine, a BCM IDDRC Project Development Award, and start-up funds from Baylor College of Medicine and Texas Children's Hospital (Houston, TX). This work was also supported by BCM IDDRC Grant Number 5P30HD024064 from the Eunice Kennedy Shriver National Institute Of Child Health & Human Development. Tom S. Otis is supported by NIH grants NS086429, NS033123 and by the McKnight Foundation.

REFERENCES

Albus. (1971). A theory of cerebellar function. *Math. Biosci.* 10, 25–61. doi: 10.1016/0025-5564(71)90051-4

Allen, G., Muller, R. A., and Courchesne, E. (2004). Cerebellar function in autism: functional magnetic resonance image activation during a simple motor task. *Biol. Psychiatry* 56, 269–278. doi: 10.1016/j.biopsych.2004.06.005

Alvina, K., and Khodakhah, K. (2010). KCa channels as therapeutic targets in episodic ataxia type-2. *J. Neurosci.* 30, 7249–7257. doi: 10.1523/JNEUROSCI.6341-09.2010

Andersen, B. B., Korbo, L., and Pakkenberg, B. (1992). A quantitative study of the human cerebellum with unbiased stereological techniques. *J. Comp. Neurol.* 326, 549–560. doi: 10.1002/cne.903260405

Angaut, P., and Sotelo, C. (1987). The dentato-olivary projection in the rat as a presumptive GABAergic link in the olivo-cerebello-olivary loop. An ultrastructural study. *Neurosci. Lett.* 83, 227–231. doi: 10.1016/0304-3940(87)90090-5

Apps, R., and Hawkes, R. (2009). Cerebellar cortical organization: a one-map hypothesis. *Nat. Rev. Neurosci.* 10, 670–681. doi: 10.1038/nrn2698

Argyelan, M., Carbon, M., Niethammer, M., Ulug, A. M., Voss, H. U., Bressman, S. B., et al. (2009). Cerebellothalamocortical connectivity regulates penetrance in dystonia. *J. Neurosci.* 29, 9740–9747. doi: 10.1523/JNEUROSCI.2300-09.2009

Asmus, F., and Gasser, T. (2010). Dystonia-plus syndromes. *Eur. J. Neurol.* 17(Suppl. 1), 37–45. doi: 10.1111/j.1468-1331.2010.03049.x

Association, A. P. (1994). *Diagnostic and Statistical Manual of Mental Disorders (DSM-4), 4th Edn*. Washington, DC: APA.

Banerjee-Basu, S., and Packer, A. (2010). SFARI Gene: an evolving database for the autism research community. *Dis. Model. Mech.* 3, 133–135. doi: 10.1242/dmm.005439

Barnes, J. A., Ebner, B. A., Duvick, L. A., Gao, W., Chen, G., Orr, H. T., et al. (2011). Abnormalities in the climbing fiber-Purkinje cell circuitry contribute to neuronal dysfunction in ATXN1[82Q] mice. *J. Neurosci.* 31, 12778–12789. doi: 10.1523/JNEUROSCI.2579-11.2011

Bastian, A. J. (2011). Moving, sensing and learning with cerebellar damage. *Curr. Opin. Neurobiol.* 21, 596–601. doi: 10.1016/j.conb.2011.06.007

Bauman, M. L. (1991). Microscopic neuroanatomic abnormalities in autism. *Pediatrics* 87, 791–796.

Bauman, M. L., and Kemper, T. L. (2005). Neuroanatomic observations of the brain in autism: a review and future directions. *Int. J. Dev. Neurosci.* 23, 183–187. doi: 10.1016/j.ijdevneu.2004.09.006

Baumann, O., and Mattingley, J. B. (2012). Functional topography of primary emotion processing in the human cerebellum. *Neuroimage* 61, 805–811. doi: 10.1016/j.neuroimage.2012.03.044

Bazzigaluppi, P., Ruigrok, T., Saisan, P., De Zeeuw, C. I., and de Jeu, M. (2012). Properties of the nucleo-olivary pathway: an *in vivo* whole-cell patch clamp study. *PloS ONE* 7:e46360. doi: 10.1371/journal.pone.0046360

Brielmaier, J., Matteson, P. G., Silverman, J. L., Senerth, J. M., Kelly, S., Genestine, M., et al. (2012). Autism-relevant social abnormalities and cognitive deficits in engrailed-2 knockout mice. *PloS ONE* 7:e40914. doi: 10.1371/journal.pone.0040914

Brochu, G., Maler, L., and Hawkes, R. (1990). Zebrin II: a polypeptide antigen expressed selectively by Purkinje cells reveals compartments in rat and fish cerebellum. *J. Comp. Neurol.* 291, 538–552. doi: 10.1002/cne.902910405

Brown, L. L., and Lorden, J. F. (1989). Regional cerebral glucose utilization reveals widespread abnormalities in the motor system of the rat mutant dystonic. *J. Neurosci.* 9, 4033–4041.

Brunel, N., Hakim, V., Isope, P., Nadal, J. P., and Barbour, B. (2004). Optimal information storage and the distribution of synaptic weights: perceptron versus Purkinje cell. *Neuron* 43, 745–757.

Buckner, R. L., Krienen, F. M., Castellanos, A., Diaz, J. C., and Yeo, B. T. (2011). The organization of the human cerebellum estimated by intrinsic functional connectivity. *J. Neurophysiol.* 106, 2322–2345. doi: 10.1152/jn.00339.2011

Burright, E. N., Clark, H. B., Servadio, A., Matilla, T., Feddersen, R. M., Yunis, W. S., et al. (1995). SCA1 transgenic mice: a model for neurodegeneration caused by an expanded CAG trinucleotide repeat. *Cell* 82, 937–948. doi: 10.1016/0092-8674(95)90273-2

Calderon, D. P., Fremont, R., Kraenzlin, F., and Khodakhah, K. (2011). The neural substrates of rapid-onset Dystonia-Parkinsonism. *Nat. Neurosci.* 14, 357–365. doi: 10.1038/nn.2753

Campbell, D. B., and Hess, E. J. (1998). Cerebellar circuitry is activated during convulsive episodes in the tottering (tg/tg) mutant mouse. *Neuroscience* 85, 773–783. doi: 10.1016/S0306-4522(97)00672-6

Campbell, D. B., Li, C., Sutcliffe, J. S., Persico, A. M., and Levitt, P. (2008). Genetic evidence implicating multiple genes in the MET receptor tyrosine

kinase pathway in autism spectrum disorder. *Autism Res.* 1, 159–168. doi: 10.1002/aur.27

Campbell, D. B., North, J. B., and Hess, E. J. (1999). Tottering mouse motor dysfunction is abolished on the Purkinje cell degeneration (pcd) mutant background. *Exp. Neurol.* 160, 268–278. doi: 10.1006/exnr.1999.7171

Carbon, M., Raymond, D., Ozelius, L., Saunders-Pullman, R., Frucht, S., Dhawan, V., et al. (2013). Metabolic changes in DYT11 myoclonus-dystonia. *Neurology* 80, 385–391. doi: 10.1212/WNL.0b013e31827f0798

Carper, R. A., Wideman, G. M., and Courchesne, E. (2006). "Understanding autism from basic neuroscience to treatment," in *Structural Neuroimaging*, eds Steve, O. Moldin and John, L. R. Rubenstein (Boca Raton, FL: CRC Press Taylor and Francis), 347–377.

Ceballos-Baumann, A. O., Passingham, R. E., Marsden, C. D., and Brooks, D. J. (1995). Motor reorganization in acquired hemidystonia. *Ann. Neurol.* 37, 746–757. doi: 10.1002/ana.410370608

Cerminara, N. L., and Apps, R. (2011). Behavioural significance of cerebellar modules. *Cerebellum* 10, 484–494. doi: 10.1007/s12311-010-0209-2

Cerminara, N. L., Koutsikou, S., Lumb, B. M., and Apps, R. (2009). The periaqueductal grey modulates sensory input to the cerebellum: a role in coping behaviour. *Eur. J. Neurosci.* 29, 2197–2206. doi: 10.1111/j.1460-9568.2009.06760.x

Chaumont, J., Guyon, N., Valera, A. M., Dugue, G. P., Popa, D., Marcaggi, P., et al. (2013). Clusters of cerebellar Purkinje cells control their afferent climbing fiber discharge. *Proc. Natl. Acad. Sci. U.S.A.* 110, 16223–16228. doi: 10.1073/pnas.1302310110

Cheh, M. A., Millonig, J. H., Roselli, L. M., Ming, X., Jacobsen, E., Kamdar, S., et al. (2006). En2 knockout mice display neurobehavioral and neurochemical alterations relevant to autism spectrum disorder. *Brain Res.* 1116, 166–176. doi: 10.1016/j.brainres.2006.07.086

Chen, X., Tang, T. S., Tu, H., Nelson, O., Pook, M., Hammer, R., et al. (2008). Deranged calcium signaling and neurodegeneration in spinocerebellar ataxia type 3. *J. Neurosci.* 28, 12713–12724. doi: 10.1523/JNEUROSCI.3909-08.2008

Courchesne, E., Saitoh, O., Yeung-Courchesne, R., Press, G. A., Lincoln, A. J., Haas, R. H., et al. (1994). Abnormality of cerebellar vermian lobules VI and VII in patients with infantile autism: identification of hypoplastic and hyperplastic subgroups with MR imaging. *AJR. Am. J. Roentgenol.* 162, 123–130. doi: 10.2214/ajr.162.1.8273650

Curatolo, P., Bombardieri, R., and Jozwiak, S. (2008). Tuberous sclerosis. *Lancet* 372, 657–668. doi: 10.1016/S0140-6736(08)61279-9

D'Angelo, E., and Casali, S. (2012). Seeking a unified framework for cerebellar function and dysfunction: from circuit operations to cognition. *Front. Neural Circuits* 6:116. doi: 10.3389/fncir.2012.00116

DeLorey, T. M., Sahbaie, P., Hashemi, E., Homanics, G. E., and Clark, J. D. (2008). Gabrb3 gene deficient mice exhibit impaired social and exploratory behaviors, deficits in non-selective attention and hypoplasia of cerebellar vermal lobules: a potential model of autism spectrum disorder. *Behav. Brain Res.* 187, 207–220. doi: 10.1016/j.bbr.2007.09.009

Demirtas-Tatlidede, A., Freitas, C., Pascual-Leone, A., and Schmahmann, J. D. (2011). Modulatory effects of theta burst stimulation on cerebellar nonsomatic functions. *Cerebellum* 10, 495–503. doi: 10.1007/s12311-010-0230-5

Dietrichs, E., and Haines, D. E. (1989). Interconnections between hypothalamus and cerebellum. *Anat. Embryol.* 179, 207–220. doi: 10.1007/BF00326585

Dum, R. P., and Strick, P. L. (2012). Transneuronal tracing with neurotropic viruses reveals network macroarchitecture. *Curr. Opin. Neurobiol.* 23, 245–249. doi: 10.1016/j.conb.2012.12.002

Durr, A. (2010). Autosomal dominant cerebellar ataxias: polyglutamine expansions and beyond. *Lancet Neurol.* 9, 885–894. doi: 10.1016/S1474-4422(10)70183-6

Eidelberg, D., Moeller, J. R., Antonini, A., Kazumata, K., Nakamura, T., Dhawan, V., et al. (1998). Functional brain networks in DYT1 dystonia. *Ann. Neurol.* 44, 303–312. doi: 10.1002/ana.410440304

Eluvathingal, T. J., Behen, M. E., Chugani, H. T., Janisse, J., Bernardi, B., Chakraborty, P., et al. (2006). Cerebellar lesions in tuberous sclerosis complex: neurobehavioral and neuroimaging correlates. *J. Child Neurol.* 21, 846–851. doi: 10.1177/08830738060210100301

Fatemi, S. H., Aldinger, K. A., Ashwood, P., Bauman, M. L., Blaha, C. D., Blatt, G. J., et al. (2012). Consensus paper: pathological role of the cerebellum in autism. *Cerebellum* 11, 777–807. doi: 10.1007/s12311-012-0355-9

Fatemi, S. H., Reutiman, T. J., Folsom, T. D., and Thuras, P. D. (2009). GABA(A) receptor downregulation in brains of subjects with autism. *J. Autism Dev. Disord.* 39, 223–230. doi: 10.1007/s10803-008-0646-7

Galardi, G., Perani, D., Grassi, F., Bressi, S., Amadio, S., Antoni, M., et al. (1996). Basal ganglia and thalamo-cortical hypermetabolism in patients with spasmodic torticollis. *Acta Neurol. Scand.* 94, 172–176. doi: 10.1111/j.1600-0404.1996.tb07049.x

Galliano, E., Potters, J. W., Elgersma, Y., Wisden, W., Kushner, S. A., De Zeeuw, C. I., et al. (2013). Synaptic transmission and plasticity at inputs to murine cerebellar Purkinje cells are largely dispensable for standard nonmotor tasks. *J. Neurosci.* 33, 12599–12618. doi: 10.1523/JNEUROSCI.1642-13.2013

Gharani, N., Benayed, R., Mancuso, V., Brzustowicz, L. M., and Millonig, J. H. (2004). Association of the homeobox transcription factor, ENGRAILED 2 3, with autism spectrum disorder. *Mol. Psychiatry* 9, 474–484. doi: 10.1038/sj.mp.4001498

Glickstein, M. (2007). What does the cerebellum really do. *Curr. Biol.* 17, R824–R827. doi: 10.1016/j.cub.2007.08.009

Hagerman, R. J., Leehey, M., Heinrichs, W., Tassone, F., Wilson, R., Hills, J., et al. (2001). Intention tremor, parkinsonism, and generalized brain atrophy in male carriers of fragile X. *Neurology* 57, 127–130. doi: 10.1212/WNL.57.1.127

Hall, D. A., and O'Keefe, J. A. (2012). Fragile x-associated tremor ataxia syndrome: the expanding clinical picture, pathophysiology, epidemiology, and update on treatment. *Tremor Other Hyperkinet Mov. (N.Y.)* 2, 1–11. pii: tre-02-56-352-1

Hallett, M. (2009). Dystonia: a sensory and motor disorder of short latency inhibition. *Ann. Neurol.* 66, 125–127. doi: 10.1002/ana.21762

Hamilton, B. A., Frankel, W. N., Kerrebrock, A. W., Hawkins, T. L., FitzHugh, W., Kusumi, K., et al. (1996). Disruption of the nuclear hormone receptor RORalpha in staggerer mice. *Nature* 379, 736–739. doi: 10.1038/379736a0

Hansen, S. T., Meera, P., Otis, T. S., and Pulst, S. M. (2013). Changes in Purkinje cell firing and gene expression precede behavioral pathology in a mouse model of SCA2. *Hum. Mol. Genet.* 22, 271–283. doi: 10.1093/hmg/dds427

Hedrick, A., Lee, Y., Wallace, G. L., Greenstein, D., Clasen, L., Giedd, J. N., et al. (2012). Autism risk gene MET variation and cortical thickness in typically developing children and adolescents. *Autism Res.* 5, 434–439. doi: 10.1002/aur.1256

Hendrix, C. M., and Vitek, J. L. (2012). Toward a network model of dystonia. *Ann. N.Y. Acad. Sci.* 1265, 46–55. doi: 10.1111/j.1749-6632.2012.06692.x

Hess, D. T. (1982). Cerebellar nucleo-cortical neurons projecting to the vermis of lobule VII in the rat. *Brain Res.* 248, 361–366. doi: 10.1016/0006-8993(82)90595-9

Holmes, G. (1939). The cerebellum of man. *Brain* 62, 2–30. doi: 10.1093/brain/62.1.1

Horn, K. M., Pong, M., and Gibson, A. R. (2010). Functional relations of cerebellar modules of the cat. *J. Neurosci.* 30, 9411–9423. doi: 10.1523/JNEUROSCI.0440-10.2010

Hoshi, E., Tremblay, L., Feger, J., Carras, P. L., and Strick, P. L. (2005). The cerebellum communicates with the basal ganglia. *Nat. Neurosci.* 8, 1491–1493. doi: 10.1038/nn1544

Hourez, R., Servais, L., Orduz, D., Gall, D., Millard, I., de Kerchove D'Exaerde, A., et al. (2011). Aminopyridines correct early dysfunction and delay neurodegeneration in a mouse model of spinocerebellar ataxia type 1. *J. Neurosci.* 31, 11795–11807. doi: 10.1523/JNEUROSCI.0905-11.2011

Hutchinson, M., Nakamura, T., Moeller, J. R., Antonini, A., Belakhlef, A., Dhawan, V., et al. (2000). The metabolic topography of essential blepharospasm: a focal dystonia with general implications. *Neurology* 55, 673–677. doi: 10.1212/WNL.55.5.673

Ichinohe, N., Mori, F., and Shoumura, K. (2000). A di-synaptic projection from the lateral cerebellar nucleus to the laterodorsal part of the striatum via the central lateral nucleus of the thalamus in the rat. *Brain Res.* 880, 191–197. doi: 10.1016/S0006-8993(00)02744-X

Ieraci, A., Forni, P. E., and Ponzetto, C. (2002). Viable hypomorphic signaling mutant of the Met receptor reveals a role for hepatocyte growth factor in postnatal cerebellar development. *Proc. Natl. Acad. Sci. U.S.A.* 99, 15200–15205. doi: 10.1073/pnas.222362099

Kasumu, A. W., Liang, X., Egorova, P., Vorontsova, D., and Bezprozvanny, I. (2012). Chronic suppression of inositol 1 4, 5-triphosphate receptor-mediated calcium signaling in cerebellar purkinje cells alleviates pathological phenotype in spinocerebellar ataxia 2 mice. *J. Neurosci.* 32, 12786–12796. doi: 10.1523/JNEUROSCI.1643-12.2012

Klockgether, T. (2010). Sporadic ataxia with adult onset: classification and diagnostic criteria. *Lancet Neurol.* 9, 94–104. doi: 10.1016/S1474-4422(09)70305-9

Kluge, A., Kettner, B., Zschenderlein, R., Sandrock, D., Munz, D. L., Hesse, S., et al. (1998). Changes in perfusion pattern using ECD-SPECT indicate frontal lobe and cerebellar involvement in exercise-induced paroxysmal dystonia. *Mov. Disord.* 13, 125–134. doi: 10.1002/mds.870130124

Koekkoek, S. K., Yamaguchi, K., Milojkovic, B. A., Dortland, B. R., Ruigrok, T. J., Maex, R., et al. (2005). Deletion of FMR1 in Purkinje cells enhances parallel fiber LTD, enlarges spines, and attenuates cerebellar eyelid conditioning in Fragile X syndrome. *Neuron* 47, 339–352. doi: 10.1016/j.neuron.2005.07.005

Kuemerle, B., Gulden, F., Cherosky, N., Williams, E., and Herrup, K. (2007). The mouse Engrailed genes: a window into autism. *Behav. Brain Res.* 176, 121–132. doi: 10.1016/j.bbr.2006.09.009

LeDoux, M. S. (2011). Animal models of dystonia: lessons from a mutant rat. *Neurobiol. Dis.* 42, 152–161. doi: 10.1016/j.nbd.2010.11.006

LeDoux, M. S., Hurst, D. C., and Lorden, J. F. (1998). Single-unit activity of cerebellar nuclear cells in the awake genetically dystonic rat. *Neuroscience* 86, 533–545. doi: 10.1016/S0306-4522(98)00007-4

LeDoux, M. S., and Lorden, J. F. (2002). Abnormal spontaneous and harmaline-stimulated Purkinje cell activity in the awake genetically dystonic rat. *Exp. Brain Res.* 145, 457–467. doi: 10.1007/s00221-002-1127-4

LeDoux, M. S., Lorden, J. F., and Ervin, J. M. (1993). Cerebellectomy eliminates the motor syndrome of the genetically dystonic rat. *Exp. Neurol.* 120, 302–310. doi: 10.1006/exnr.1993.1064

Lemon, R. N., and Edgley, S. A. (2010). Life without a cerebellum. *Brain* 133, 652–654. doi: 10.1093/brain/awq030

Liu, J., Tang, T. S., Tu, H., Nelson, O., Herndon, E., Huynh, D. P., et al. (2009). Deranged calcium signaling and neurodegeneration in spinocerebellar ataxia type 2. *J. Neurosci.* 29, 9148–9162. doi: 10.1523/JNEUROSCI.0660-09.2009

Marr, D. (1969). A theory of cerebellar cortex. *J. Physiol.* 202, 437–470.

Middleton, F. A., and Strick, P. L. (2000). Basal ganglia and cerebellar loops: motor and cognitive circuits. *Brain Res. Brain Res. Rev.* 31, 236–250. doi: 10.1016/S0165-0173(99)00040-5

Middleton, F. A., and Strick, P. L. (2001). Cerebellar projections to the prefrontal cortex of the primate. *J. Neurosci.* 21, 700–712.

Muller, U. (2009). The monogenic primary dystonias. *Brain* 132, 2005–2025. doi: 10.1093/brain/awp172

Neychev, V. K., Fan, X., Mitev, V. I., Hess, E. J., and Jinnah, H. A. (2008). The basal ganglia and cerebellum interact in the expression of dystonic movement. *Brain* 131, 2499–2509. doi: 10.1093/brain/awn168

Neychev, V. K., Gross, R. E., Lehericy, S., Hess, E. J., and Jinnah, H. A. (2011). The functional neuroanatomy of dystonia. *Neurobiol. Dis.* 42, 185–201. doi: 10.1016/j.nbd.2011.01.026

Niethammer, M., Carbon, M., Argyelan, M., and Eidelberg, D. (2011). Hereditary dystonia as a neurodevelopmental circuit disorder: evidence from neuroimaging. *Neurobiol. Dis.* 42, 202–209. doi: 10.1016/j.nbd.2010.10.010

Odergren, T., Stone-Elander, S., and Ingvar, M. (1998). Cerebral and cerebellar activation in correlation to the action-induced dystonia in writer's cramp. *Mov. Disord.* 13, 497–508. doi: 10.1002/mds.870130321

Ozol, K., Hayden, J. M., Oberdick, J., and Hawkes, R. (1999). Transverse zones in the vermis of the mouse cerebellum. *J. Comp. Neurol.* 412, 95–111. doi: 10.1002/(SICI)1096-9861(19990913)412:1<95::AID-CNE7>3.3.CO;2-P

Palkovits, M., Magyar, P., and Szentagothai, J. (1972). Quantitative histological analysis of the cerebellar cortex in the cat. IV. Mossy fiber-Purkinje cell numerical transfer. *Brain Res.* 45, 15–29. doi: 10.1016/0006-8993(72)90213-2

Pizoli, C. E., Jinnah, H. A., Billingsley, M. L., and Hess, E. J. (2002). Abnormal cerebellar signaling induces dystonia in mice. *J. Neurosci.* 22, 7825–7833.

Preibisch, C., Berg, D., Hofmann, E., Solymosi, L., and Naumann, M. (2001). Cerebral activation patterns in patients with writer's cramp: a functional magnetic resonance imaging study. *J. Neurol.* 248, 10–17. doi: 10.1007/s004150170263

Prudente, C. N., Pardo, C. A., Xiao, J., Hanfelt, J., Hess, E. J., Ledoux, M. S., et al. (2013). Neuropathology of cervical dystonia. *Exp. Neurol.* 241, 95–104. doi: 10.1016/j.expneurol.2012.11.019

Raike, R. S., Pizoli, C. E., Weisz, C., van den Maagdenberg, A. M., Jinnah, H. A., and Hess, E. J. (2012). Limited regional cerebellar dysfunction induces focal dystonia in mice. *Neurobiol. Dis.* 49C, 200–210. doi: 10.1016/j.nbd.2012.07.019

Raike, R. S., Weisz, C., Hoebeek, F. E., Terzi, M. C., De Zeeuw, C. I., van den Maagdenberg, A. M., et al. (2013). Stress, caffeine and ethanol trigger transient neurological dysfunction through shared mechanisms in a mouse calcium channelopathy. *Neurobiol. Dis.* 50, 151–159. doi: 10.1016/j.nbd.2012.09.005

Reeber, S. L., White, J. J., George-Jones, N. A., and Sillitoe, R. V. (2012). Architecture and development of olivocerebellar circuit topography. *Front. Neural Circuits* 6:115. doi: 10.3389/fncir.2012.00115

Reith, R. M., McKenna, J., Wu, H., Hashmi, S. S., Cho, S. H., Dash, P. K., et al. (2013). Loss of Tsc2 in Purkinje cells is associated with autistic-like behavior in a mouse model of tuberous sclerosis complex. *Neurobiol. Dis.* 51, 93–103. doi: 10.1016/j.nbd.2012.10.014

Ritvo, E. R., Freeman, B. J., Scheibel, A. B., Duong, T., Robinson, H., Guthrie, D., et al. (1986). Lower Purkinje cell counts in the cerebella of four autistic subjects: initial findings of the UCLA-NSAC Autopsy Research Report. *Am. J. Psychiatry* 143, 862–866.

Ruigrok, T. J. (2011). Ins and outs of cerebellar modules. *Cerebellum* 10, 464–474. doi: 10.1007/s12311-010-0164-y

Sarna, J. R., and Hawkes, R. (2003). Patterned Purkinje cell death in the cerebellum. *Prog. Neurobiol.* 70, 473–507. doi: 10.1016/S0301-0082(03)00114-X

Schmahmann, J. D. (2010). The role of the cerebellum in cognition and emotion: personal reflections since 1982 on the dysmetria of thought hypothesis, and its historical evolution from theory to therapy. *Neuropsychol. Rev.* 20, 236–260. doi: 10.1007/s11065-010-9142-x

Schorge, S., van de Leemput, J., Singleton, A., Houlden, H., and Hardy, J. (2010). Human ataxias: a genetic dissection of inositol triphosphate receptor (ITPR1)-dependent signaling. *Trends Neurosci.* 33, 211–219. doi: 10.1016/j.tins.2010.02.005

Scott, J. A., Schumann, C. M., Goodlin-Jones, B. L., and Amaral, D. G. (2009). A comprehensive volumetric analysis of the cerebellum in children and adolescents with autism spectrum disorder. *Autism Res.* 2, 246–257. doi: 10.1002/aur.97

Sen, B., Singh, A. S., Sinha, S., Chatterjee, A., Ahmed, S., Ghosh, S., et al. (2010). Family-based studies indicate association of Engrailed 2 gene with autism in an Indian population. *Genes Brain Behav.* 9, 248–255. doi: 10.1111/j.1601-183X.2009.00556.x

Serra, H. G., Duvick, L., Zu, T., Carlson, K., Stevens, S., Jorgensen, N., et al. (2006). RORalpha-mediated Purkinje cell development determines disease severity in adult SCA1 mice. *Cell* 127, 697–708. doi: 10.1016/j.cell.2006.09.036

Sgaier, S. K., Lao, Z., Villanueva, M. P., Berenshteyn, F., Stephen, D., Turnbull, R. K., et al. (2007). Genetic subdivision of the tectum and cerebellum into functionally related regions based on differential sensitivity to engrailed proteins. *Development* 134, 2325–2335. doi: 10.1242/dev.000620

Shakkottai, V. G., do Carmo Costa, M., Dell'Orco, J. M., Sankaranarayanan, A., Wulff, H., and Paulson, H. L. (2011). Early changes in cerebellar physiology accompany motor dysfunction in the polyglutamine disease spinocerebellar ataxia type 3. *J. Neurosci.* 31, 13002–13014. doi: 10.1523/JNEUROSCI.2789-11.2011

Shamim, E. A., Chu, J., Scheider, L. H., Savitt, J., Jinnah, H. A., and Hallett, M. (2011). Extreme task specificity in writer's cramp. *Mov. Disord.* 26, 2107–2109. doi: 10.1002/mds.23827

Sillitoe, R. V., Marzban, H., Larouche, M., Zahedi, S., Affanni, J., and Hawkes, R. (2005). Conservation of the architecture of the anterior lobe vermis of the cerebellum across mammalian species. *Prog. Brain Res.* 148, 283–297. doi: 10.1016/S0079-6123(04)48022-4

Smit, A. E., van der Geest, J. N., Vellema, M., Koekkoek, S. K., Willemsen, R., Govaerts, L. C., et al. (2008). Savings and extinction of conditioned eyeblink responses in fragile X syndrome. *Genes Brain Behav.* 7, 770–777. doi: 10.1111/j.1601-183X.2008.00417.x

Stanfield, A. C., McIntosh, A. M., Spencer, M. D., Philip, R., Gaur, S., and Lawrie, S. M. (2008). Towards a neuroanatomy of autism: a systematic review and meta-analysis of structural magnetic resonance imaging studies. *Eur. Psychiatry* 23, 289–299. doi: 10.1016/j.eurpsy.2007.05.006

Stoodley, C. J., and Schmahmann, J. D. (2009). Functional topography in the human cerebellum: a meta-analysis of neuroimaging studies. *Neuroimage* 44, 489–501. doi: 10.1016/j.neuroimage.2008.08.039

Stoodley, C. J., and Schmahmann, J. D. (2010). Evidence for topographic organization in the cerebellum of motor control versus cognitive and affective processing. *Cortex* 46, 831–844. doi: 10.1016/j.cortex.2009.11.008

Teo, J. T., van de Warrenburg, B. P., Schneider, S. A., Rothwell, J. C., and Bhatia, K. P. (2009). Neurophysiological evidence for cerebellar dysfunction in primary

focal dystonia. *J. Neurol. Neurosurg. Psychiatry.* 80, 80–83. doi: 10.1136/jnnp.2008.144626

Tobia, M. J., and Woodruff-Pak, D. S. (2009). Delay eyeblink classical conditioning is impaired in Fragile X syndrome. *Behav. Neurosci.* 123, 665–676. doi: 10.1037/a0015662

Tolbert, D. L., Bantli, H., and Bloedel, J. R. (1976). Anatomical and physiological evidence for a cerebellar nucleo-cortical projection in the cat. *Neuroscience* 1, 205–217. doi: 10.1016/0306-4522(76)90078-6

Tolbert, D. L., Ewald, M., Gutting, J., and La Regina, M. C. (1995). Spatial and temporal pattern of Purkinje cell degeneration in shaker mutant rats with hereditary cerebellar ataxia. *J. Comp. Neurol.* 355, 490–507. doi: 10.1002/cne.903550403

Tsai, P. T., Hull, C., Chu, Y., Greene-Colozzi, E., Sadowski, A. R., Leech, J. M., et al. (2012). Autistic-like behaviour and cerebellar dysfunction in Purkinje cell Tsc1 mutant mice. *Nature* 488, 647–651. doi: 10.1038/nature11310

Ulug, A. M., Vo, A., Argyelan, M., Tanabe, L., Schiffer, W. K., Dewey, S., et al. (2011). Cerebellothalamocortical pathway abnormalities in torsinA DYT1 knock-in mice. *Proc. Natl. Acad. Sci. U.S.A.* 108, 6638–6643. doi: 10.1073/pnas.1016445108

Uusisaari, M., and De Schutter, E. (2011). The mysterious microcircuitry of the cerebellar nuclei. *J. Physiol.* 589, 3441–3457. doi: 10.1113/jphysiol.2010.201582

Wadiche, J. I., and Jahr, C. E. (2005). Patterned expression of Purkinje cell glutamate transporters controls synaptic plasticity. *Nat. Neurosci.* 8, 1329–1334. doi: 10.1038/nn1539

Walter, J. T., Alvina, K., Womack, M. D., Chevez, C., and Khodakhah, K. (2006). Decreases in the precision of Purkinje cell pacemaking cause cerebellar dysfunction and ataxia. *Nat. Neurosci.* 9, 389–397. doi: 10.1038/nn1648

Wang, L., Jia, M., Yue, W., Tang, F., Qu, M., Ruan, Y., et al. (2008). Association of the ENGRAILED 2 (EN2) gene with autism in Chinese Han population. *Am. J. Med.l Genet. B Neuropsychiatr. Genet.* 147B, 434–438. doi: 10.1002/ajmg.b.30623

Welsh, J. P., Yuen, G., Placantonakis, D. G., Vu, T. Q., Haiss, F., O'Hearn, E., et al. (2002). Why do Purkinje cells die so easily after global brain ischemia? Aldolase, C, EAAT4, and the cerebellar contribution to posthypoxic myoclonus. *Adv. Neurol.* 89, 331–359.

White, J., and Sillitoe, R. V. (2013). Development of the cerebellum: from gene expression patterns to circuit maps. *WIREs Dev. Biol.* 2, 149–164. doi: 10.1002/wdev.65

Whitney, E. R., Kemper, T. L., Bauman, M. L., Rosene, D. L., and Blatt, G. J. (2008). Cerebellar Purkinje cells are reduced in a subpopulation of autistic brains: a stereological experiment using calbindin-D28k. *Cerebellum* 7, 406–416. doi: 10.1007/s12311-008-0043-y

Yang, P., Shu, B. C., Hallmayer, J. F., and Lung, F. W. (2010). Intronic single nucleotide polymorphisms of engrailed homeobox 2 modulate the disease vulnerability of autism in a han chinese population. *Neuropsychobiology* 62, 104–115. doi: 10.1159/000315441

Yokoi, F., Dang, M. T., and Li, Y. (2012). Improved motor performance in Dyt1 ΔGAG heterozygous knock-in mice by cerebellar Purkinje-cell specific Dyt1 conditional knocking-out. *Behav. Brain Res.* 230, 389–398. doi: 10.1016/j.bbr.2012.02.029

Zhao, Y., Sharma, N., and LeDoux, M. S. (2011). The DYT1 carrier state increases energy demand in the olivocerebellar network. *Neuroscience* 177, 183–194. doi: 10.1016/j.neuroscience.2011.01.015

Conflict of Interest Statement: The authors declare that the research was conducted in the absence of any commercial or financial relationships that could be construed as a potential conflict of interest.

Received: 29 August 2013; accepted: 25 October 2013; published online: 14 November 2013.

Citation: Reeber SL, Otis TS and Sillitoe RV (2013) New roles for the cerebellum in health and disease. Front. Syst. Neurosci. 7:83. doi: 10.3389/fnsys.2013.00083

This article was submitted to the journal Frontiers in Systems Neuroscience.

frontiers in
SYSTEMS NEUROSCIENCE

ORIGINAL RESEARCH ARTICLE
published: 20 May 2014
doi: 10.3389/fnsys.2014.00092

Distinct regions of the cerebellum show gray matter decreases in autism, ADHD, and developmental dyslexia

Catherine J. Stoodley*

Department of Psychology, American University, Washington, DC, USA

Edited by:
Thomas C. Watson, University of Bristol, UK

Reviewed by:
Volker Steuber, University of Hertfordshire, UK
Roy Vincent Sillitoe, Baylor College of Medicine, USA

****Correspondence:***
Catherine J. Stoodley, Department of Psychology, American University, 4400 Massachusetts Ave., NW, Washington, DC 20016, USA
e-mail: stoodley@american.edu

Differences in cerebellar structure have been identified in autism spectrum disorder (ASD), attention deficit hyperactivity disorder (ADHD), and developmental dyslexia. However, it is not clear if different cerebellar regions are involved in each disorder, and thus whether cerebellar anatomical differences reflect a generic developmental vulnerability or disorder-specific characteristics. To clarify this, we conducted an anatomic likelihood estimate (ALE) meta-analysis on voxel-based morphometry (VBM) studies which compared ASD (17 studies), ADHD (10 studies), and dyslexic (10 studies) participants with age-matched typically-developing (TD) controls. A second ALE analysis included studies in which the cerebellum was a region of interest (ROI). There were no regions of significantly increased gray matter (GM) in the cerebellum in ASD, ADHD, or dyslexia. Data from ASD studies revealed reduced GM in the inferior cerebellar vermis (lobule IX), left lobule VIIIB, and right Crus I. In ADHD, significantly decreased GM was found bilaterally in lobule IX, whereas participants with developmental dyslexia showed GM decreases in left lobule VI. There was no overlap between the cerebellar clusters identified in each disorder. We evaluated the functional significance of the regions revealed in both whole-brain and cerebellar ROI ALE analyses using Buckner and colleagues' 7-network functional connectivity map available in the SUIT cerebellar atlas. The cerebellar regions identified in ASD showed functional connectivity with frontoparietal, default mode, somatomotor, and limbic networks; in ADHD, the clusters were part of dorsal and ventral attention networks; and in dyslexia, the clusters involved ventral attention, frontoparietal, and default mode networks. The results suggest that different cerebellar regions are affected in ASD, ADHD, and dyslexia, and these cerebellar regions participate in functional networks that are consistent with the characteristic symptoms of each disorder.

Keywords: cerebellum, autism spectrum disorder, attention deficit hyperactivity disorder, developmental dyslexia, meta-analysis

INTRODUCTION

Our understanding of the human cerebellum has undergone substantial revision in the past 20 years. Traditionally considered a motor structure, anatomical, clinical, and neuroimaging data have converged to suggest that the cerebellum has a role in modulation of cerebro-cerebellar circuits involved in cognition and emotion as well as motor control (for reviews, see Strick et al., 2009; Stoodley and Schmahmann, 2010). The cerebellum forms closed-loop circuits with the majority of the cerebral cortex, with the cerebellar hemispheres projecting to the contralateral cerebral cortex. This closed-loop circuitry, together with the crystalline structure of the cerebellar cortex, suggests that the cerebellum contains repeating modules (Apps and Garwicz, 2005), such that the function of a given region of the cerebellum depends on its inputs and outputs (for review, Ramnani, 2006). Supporting this concept, within the cerebellum different regions are involved in overt motor control vs. cognitive and emotional processing (Stoodley and Schmahmann, 2009). This functional topography of the human cerebellum is based on its anatomical connections with the cerebral cortex and spinal cord (Stoodley and Schmahmann, 2010): briefly, lobules I–V and lobule VIII are predominantly sensorimotor; lobules VI and VII form circuits with frontal and parietal association cortices; lobule IX may participate in multiple cortical networks, including the default mode network; and lobule X comprises the vestibulocerebellum. Resting-state functional connectivity studies also support this topography, and indicate that the regions of the cerebellum showing correlated activity with sensorimotor cortices differ from those that are functionally related to prefrontal and parietal association areas (e.g., Habas et al., 2009; Buckner et al., 2011). **Figure 1** shows cerebellar lobular anatomy, and cerebellar functional topography as revealed by task-based neuroimaging (**Figure 1B**) and resting state functional connectivity (**Figure 1C**).

Cerebellar functional topography is of importance when considering the role of the cerebellum in developmental disorders. As early as 1990, Levinson suggested that cerebellar-vestibular testing could potentially be used in the diagnosis of learning disabilities (such as developmental dyslexia) and attention deficit hyperactivity disorder (ADHD; Levinson, 1990). Since then, neuroimaging studies have reported cerebellar structural and functional differences in autism spectrum disorder (ASD), ADHD, and developmental dyslexia (hereafter "dyslexia"). However, it is

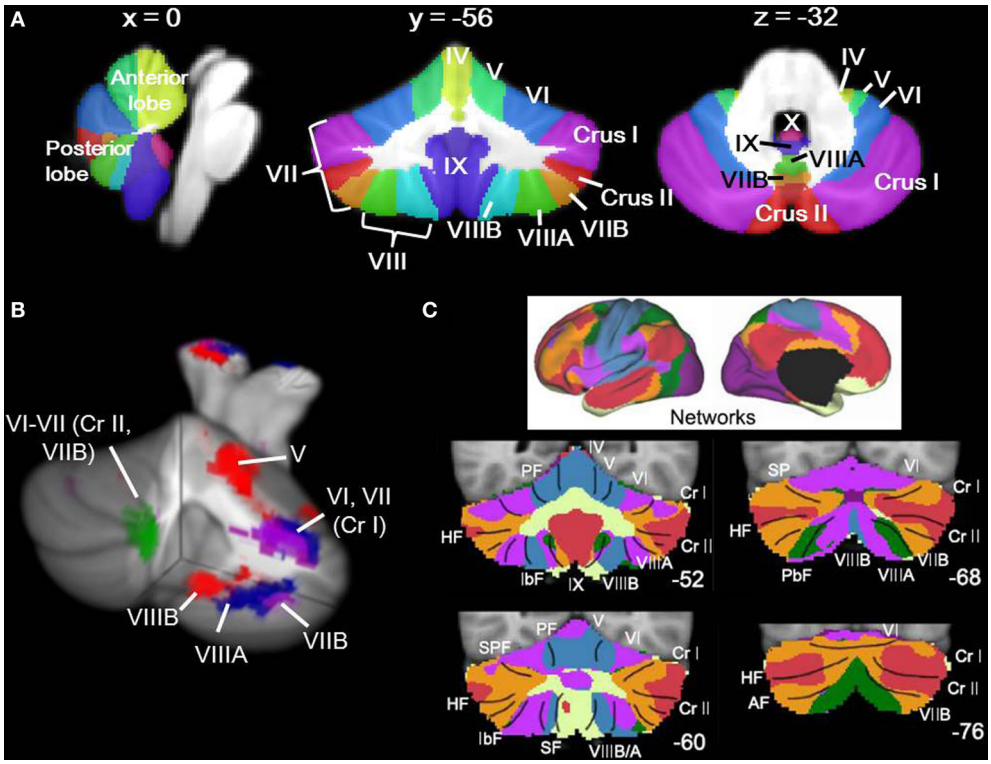

FIGURE 1 | Cerebellar anatomy and functional topography. **(A)** Cerebellar anatomy shown on coronal, sagittal, and axial slices through the Spatially Unbiased Infratentorial (SUIT) atlas (Diedrichsen, 2006; Diedrichsen et al., 2009). The cerebellum is subdivided into three lobes (anterior, posterior, and flocculonodular [lobule X]) and 10 lobules (I-X). In humans, lobule VII is subdivided into Crus I, Crus II, and VIIB, and lobule VIII is divided into VIIIA and VIIIB. Yellow, lobules I–IV; light green, lobule V; blue, lobule VI; purple, lobule VII (Crus I); red, lobule VII (Crus II); orange, lobule VII (VIIB); green, lobule VIIIA; aqua, lobule VIIIB; dark purple, lobule IX; pink-purple, X. **(B)** Functional topography revealed by task-based neuroimaging (Stoodley et al., 2012b). Activation related to right-handed finger tapping (red), language tasks (blue), working memory (violet), and spatial (green) tasks is shown. **(C)** Functional connectivity of the cerebellum based on correlations with cortical networks (adapted with permission from Buckner et al., 2011). Dark purple, visual; blue, somatomotor; green, dorsal attention; violet, ventral attention; cream, limbic; orange, frontoparietal; red, default network.

not clear whether the same or different cerebellar regions are affected in these disorders. Understanding the convergence and divergence of cerebellar structural differences in ASD, ADHD and dyslexia can clarify whether the role of the cerebellum in these disorders is specific to particular cerebro-cerebellar circuits or represents a more general characteristic of a developmental disorder.

ASD is characterized by deficits in communication and social interaction, and repetitive and restrictive behaviors and interests (American Psychiatric Association, 2013). Mounting evidence from early postmortem (Bauman and Kemper, 1985; Ritvo et al., 1986; Bailey et al., 1998) and imaging studies (Courchesne et al., 1988) and more recent genetic, clinical, and imaging findings (for more comprehensive review on the cerebellum and ASD, see Becker and Stoodley, 2013) suggest the cerebellum is part of the distributed neural circuits that are dysfunctional in ASD. Decreased bilateral cerebellar cortical volume has been reported as one of the most important biomarkers for classification of ASD brains (Ecker et al., 2010), and reduction in the posterior midline vermis has been widely shown (e.g., Courchesne et al., 1988, 2011; Kaufmann et al., 2003; Allen et al., 2005). Reduced integrity of the superior cerebellar peduncle (through which output fibers exit the cerebellum) in ASD has also been reported (Sivaswamy et al., 2010) and was associated with degree of social impairment (Catani et al., 2008). Both increases and decreases in cerebellar gray matter (GM) and white matter (WM) have been described in voxel-based morphometry (VBM) studies. Decreased GM is consistently found in midline lobule IX, right Crus I, and lobule VIII in ASD; increased GM has been reported in lobule VI (Cauda et al., 2011; Yu et al., 2011; Duerden et al., 2012; Nickl-Jockschat et al., 2012). These structural differences correlate with scores on autism diagnostic measures: increased GM in lobule VI correlated with worse social and communication scores (Rojas et al., 2006), posterior vermal GM and bilateral Crus II GM correlated with communication scores (Riva et al., 2013), and reduced GM in Crus I was associated with increased repetitive and stereotyped behaviors (Rojas et al., 2006).

ADHD is characterized by behavioral patterns of inattention, hyperactivity, and impulsivity (American Psychiatric Association, 2013). Like ASD and developmental dyslexia, there are several neural systems implicated in ADHD, including frontal-striatal and frontal-cerebellar circuits (for a recent review, see Kasparek et al., 2013). Cerebellar differences are evident on structural, functional, and spectroscopy imaging (Valera et al., 2007), and

were the most significant finding in a recent VBM study in medication-naïve adults (Makris et al., 2013). From a pharmacological perspective, the cerebellum is one of the regions that shows altered activation following a single dose of methylphenidate (Czerniak et al., 2013), suggesting that the cerebellar differences are functionally significant in terms of the behavioral profile of ADHD. In the first quantitative study of brain morphometry in ADHD, Castellanos et al. (1996) reported smaller cerebellar volume in ADHD children and adolescents relative to their typically-developing (TD) counterparts. In one of the earliest longitudinal studies investigating neurobiological underpinnings of ADHD, overall cerebellar volume was significantly reduced in ADHD children, a difference that persisted throughout development and correlated with symptom severity (Castellanos et al., 2002). Reduced right cerebellar volume was reported in ADHD children but not their unaffected siblings, even though prefrontal regions showed decreases in both children with ADHD and their unaffected siblings (Durston et al., 2004). As in ASD, posterior vermal volumes (lobules VIII–X) were reduced in ADHD relative to TD comparison groups (with no significant reduction in lobules VI–VII; Berquin et al., 1998; Mostofsky et al., 1998; Castellanos et al., 2001), and the reduction in the posterior vermis correlated with severity of ADHD symptoms (Bledsoe et al., 2011; Ivanov et al., 2014). ADHD children treated with methylphenidate did not show the same decreased volume in the posterior vermis (lobules VIII–X) as untreated ADHD children (Bledsoe et al., 2009), consistent with the proposal that methylphenidate can normalize cerebellar differences in the ADHD brain (see review by Schweren et al., 2013). Though less often reported, Mackie et al. (2007) found that reduced superior cerebellar vermis volume was a stable difference in ADHD children that persisted over time; in the same study, smaller inferior posterior cerebellar hemisphere regions were associated with poorer outcome. VBM studies provide more detailed analyses of cerebellar structure than volumetric measures. Seidman et al. (2011) conducted a region-of-interest VBM study and found reduced GM in several regions in the cerebellum compared to the TD group, including left cerebellar lobules IV–VI, VIII, IX, and X and right cerebellar lobules IV, Crus I, VIII, and IX. Other studies have reported differences in right Crus I (Carmona et al., 2005; Montes et al., 2011), left Crus I (Carmona et al., 2005), and in the posterior vermis (McAlonan et al., 2007; Yang et al., 2008).

Diffusion tensor imaging studies investigating WM differences in ADHD have reported reduced fractional anisotropy in the middle cerebellar peduncles (on the right, Bechtel et al., 2009; on the left, Ashtari et al., 2005), and WM in the left cerebellum (Ashtari et al., 2005; van Ewijk et al., 2013). Functional connectivity studies also suggest differences in cerebellar connectivity in ADHD (Tomasi and Volkow, 2012), particularly in the inattentive subtype (Fair et al., 2013). Reduced cerebellar activation has been reported during working memory tasks in right Crus I (Kobel et al., 2009; Wolf et al., 2009) and left lobule VI (Valera et al., 2005), and reduced functional connectivity was reported in left Crus I and right IX (Wolf et al., 2009).

Developmental dyslexia is defined as deficient literacy skills in the context of normal intelligence and educational opportunity (American Psychiatric Association, 2000). In addition to reading difficulties, poorer performance on a variety of "cerebellar" measures have been reported in dyslexia, including poorer balance, motor skills, and abnormal eye movements (reviewed by Stoodley and Stein, 2011, 2013). The inability of dyslexic readers to achieve fast, fluent reading prompted Nicolson and Fawcett (Nicolson et al., 2001; Nicolson and Fawcett, 2011) to propose the cerebellar theory of dyslexia. They hypothesized that cerebellar dysfunction is a core aspect of the etiology of dyslexia and leads to a deficit in procedural learning, which could explain not only the reading difficulties but also other symptoms associated with dyslexia. Certainly, functional imaging studies show cerebellar engagement during reading tasks (e.g., Turkeltaub et al., 2002; reviewed in Stoodley and Stein, 2011) and a magnetoencephalography study by Kujala et al. (2007) indicated that the cerebellum was one of the forward-driving nodes in the reading network. Structural differences in the cerebellum have been reported in dyslexia (e.g., Eckert, 2004), including differences in symmetry (with dyslexic individuals showing less-asymmetric cerebella than their TD counterparts, who generally show a rightward cerebellar asymmetry; Rae et al., 2002; Kibby et al., 2008; Leonard et al., 2008). Pernet et al. (2009) reported that a region in right lobule VI was the most significant biomarker for classification of adult dyslexic brains.

How might these neural differences arise? Many of the genes implicated in developmental disorders affect brain development at its earliest stages. Of note, many of the candidate genes for these disorders are strongly expressed in the cerebellum; for example, KIAA0319 for dyslexia and CNTNAP2 in ASD (for reviews, see Abrahams and Geschwind, 2010; Carrion-Castillo et al., 2013). Multiple genes have been implicated in each disorder, and linking genetics with imaging data is a relatively new approach (see Durston, 2010). Genetics in ADHD have focused on the dopamine and serotonin systems (e.g., DAT, DRD4, 5-HTT; Faraone et al., 2005), whereas studies of dyslexia have identified several candidate genes that are thought to be involved in early brain development, particularly neuronal migration (e.g., DYX1C1, DCDC2, KIAA0319; for review, Carrion-Castillo et al., 2013). In ASD, a very heterogeneous genetic picture emerges, including multiple candidate genes and a potential significant role of rare copy number variants, with the cerebellum amongst the regions showing a relationship between genetic variants and structural differences in the brain (see Abrahams and Geschwind, 2010, for review). For example, in non-ASD individuals, those who were homozygous for a risk allele on the autism candidate gene CNTNAP2 showed significantly reduced GM in the cerebellum in left lobule VI, bilateral Crus I, and in vermis lobule IX (Tan et al., 2010). It has been hypothesized that shared endophenotypes in these disorders, particularly between ASD and ADHD (see Rommelse et al., 2011), may be due to shared genetic factors (e.g., Rommelse et al., 2010); CNTNAP2, which is expressed in the cerebellum and potentially impacts language function, has been linked to both ASD and dyslexia (Abrahams and Geschwind, 2010; Carrion-Castillo et al., 2013). It is possible that any shared differences in cerebellar structure might be related to some shared genetic factors amongst ASD, ADHD, and dyslexia.

Taken together, these data suggest that in developmental disorders merely stating that there are "cerebellar" findings is perhaps

too broad. It is important to consider the location *within* the cerebellum, and the potential for different cerebro-cerebellar circuits to be impacted in different disorders. In other words, are cerebellar findings a general sign of developmental disorder, or are they more specifically related to the etiology of each disorder? Although different regions seem to be involved in ASD, ADHD, and developmental dyslexia, no study has examined this directly. Here we conduct an anatomical likelihood estimate (ALE) meta-analysis of VBM studies of ASD, ADHD, and dyslexia (compared to TD groups). First, we conducted a whole-brain ALE meta-analysis to evaluate the significance of cerebellar differences in the context of the whole brain. Second, we included studies using cerebellar regions of interest for a cerebellar-only analysis in each disorder. Third, we evaluated the overlap of the ALE maps for ASD, ADHD, and dyslexia. Finally, we interpreted our findings in the context of the functional connectivity of the cerebellum with the cerebral cortex, using Buckner et al. (2011)'s 7-network map implemented as part of the Spatially Unbiased Infratentorial (SUIT) cerebellar atlas (Diedrichsen, 2006; Diedrichsen et al., 2009). The findings are discussed in the context of the diagnostic symptoms of each disorder.

MATERIALS AND METHODS

LITERATURE SEARCH

Articles were identified through a PubMed (http://www.ncbi.nlm.nih.gov/pubmed) search including "autism AND imaging," "autism AND MRI"; "attention deficit AND imaging," "attention deficit AND MRI," "ADHD AND imaging," "ADHD AND MRI"; and "dyslexia AND imaging," "dyslexia AND MRI" with the limit "English," completed in July 2013. Only studies utilizing whole-brain VBM that compared the clinical groups with TD age-matched comparison groups were included. Therefore, for the initial analysis we eliminated studies that reported the results of functional neuroimaging studies; those that reported non-VBM or region-of-interest analyses of structural MRI data; those that did not report the coordinates of the results in standard space (Montreal Neurological Institute, MNI; Collins et al., 1998 or Talairach and Tournoux, 1988); studies reporting incomplete coverage of the cerebellum; and studies that investigated clinical populations without reporting data from a TD comparison group. We also excluded studies whose primary focus was to investigate a comorbid disorder (e.g., individuals with ADHD who were also cocaine-dependent).

The 37 studies listed in **Table 1** met these criteria. There were 17 VBM studies studying ASD, 10 investigating ADHD, and 10 for developmental dyslexia. These analyses thus represent the data from a total of 363 ASD participants vs. 373 TD controls; 249 ADHD participants vs. 248 TD controls; and 173 dyslexic participants vs. 163 TD controls. Twenty-one studies investigated children and adolescents (8 ASD, 8 ADHD, and 5 dyslexia studies) and adults were the participants in 14 studies (7 ASD, 2 ADHD, and 5 dyslexia studies).

CEREBELLAR REGION OF INTEREST ANALYSIS

Since our goal was to focus on cerebellar structural differences in ASD, ADHD, and dyslexia, we also conducted a secondary analysis in which only cerebellar coordinates were included in the ALE analysis. Studies not reporting cerebellar differences were not included in this analysis, and therefore not all studies included in the whole-brain analysis were added to the cerebellum-only analysis. In this analysis, we also included studies which conducted voxel-based analyses in which cerebellar findings were reported as part of a region of interest (ROI) analysis. Five additional studies were included (2 for ASD, 2 for ADHD, 1 for dyslexia). All studies included in the ROI analysis are listed in **Table 2**. As with most ROI analyses, limiting the coordinates included in the analysis to the cerebellum increases statistical power for detecting voxel-level differences within the ROI.

CO-MORBID DISORDERS IN INCLUDED STUDIES

While we excluded studies which focused on co-morbid disorders, it is possible that within each sample there were participants with, for example, ADHD and developmental dyslexia. It is less likely that there would be a co-morbid group of ASD and ADHD participants, as the versions of the Diagnostic and Statistical Manual of Mental Disorders (DSM) that were employed in these studies excluded symptoms of inattention and hyperactivity "during the course of a pervasive developmental disorder," which by nature excludes ASD from the ADHD diagnosis (e.g., American Psychiatric Association, 2000).

In ADHD, the most commonly reported co-morbid disorders were anxiety disorder (Carmona et al., 2005; McAlonan et al., 2007; Yang et al., 2008; Kobel et al., 2010), major depressive disorder (Seidman et al., 2011), conduct disorder (Overmeyer et al., 2001; McAlonan et al., 2007; Kobel et al., 2010; Sasayama et al., 2010), oppositional defiant disorder (Overmeyer et al., 2001; Yang et al., 2008; Sasayama et al., 2010), and obsessive-compulsive disorder (McAlonan et al., 2007; Kobel et al., 2010). These disorders are commonly co-morbid with ADHD (Biederman, 2005). Only one study reported a participant with co-morbid dyslexia (Overmeyer et al., 2001; one participant in their clinical sample of 18). Two studies noted a subset of participants with learning disability. In Seidman et al. (2011) the diagnosis of co-morbid learning disability in their adult sample (9 adults of 74 ADHD participants) was based on scores on reading and/or arithmetic scores (Wide Range Achievement Test), and so could include participants with reading disorder; in Yang et al. (2008), 5 of the 57 ADHD children were diagnosed with learning disability. In each study, the number of participants with learning disability (which may or may not include reading disability) was relatively low.

In the ASD group, the vast majority of studies ruled out genetic syndromes such as Fragile X as part of their standard exclusion criteria. In the one study in which there was a Fragile X comparison group (Wilson et al., 2009), we only included the data from the ASD group without Fragile X. In the one study including both ASD and ADHD participants (Brieber et al., 2007), the individuals with ASD did not have symptoms of ADHD and *vice versa*. Three other ASD studies specifically noted that ADHD was an exclusion criterion (Salmond et al., 2005, 2007; McAlonan et al., 2008), though most studies more broadly excluded psychiatric disorders. In the dyslexia group, the diagnosis of reading disorder excludes reading difficulties that could be better attributed to another disorder. Several studies did specifically note that

Table 1 | Studies included in the analyses.

	Study by author	Total *N*	Clinical group *N* (gender)	TD group *N* (gender)	Age (years) clinical group	Age (years) TD group
ASD	Abell et al., 1999	30	15 (12 males)	15 (12 males)	28.8	25.3
	Boddaert et al., 2004	33	21 (16 males)	12 (7 males)	9.3	10.8
	Bonilha et al., 2008	28	12 (12 males)	16 (16 males)	12.4	13.2
	Brieber et al., 2007	30	15 (15 males)	15 (15 males)	Adults	Adults
	Craig et al., 2007	33	14 (0 males)	19 (0 males)	37.9	35
	Ecker et al., 2010*	44	22 (22 males)	22 (22 males)	27	28
	Ecker et al., 2012	178	89 (89 males)	89 (89 males)	26	28
	Hyde et al., 2010	30	15 (15 males)	15 (15 males)	22.7	19.2
	Ke et al., 2008	32	17 (14 males)	15 (12 males)	8.9	9.7
	Kwon et al., 2004	33	20 (20 males)	13 (13 males)	13.5	13.6
	McAlonan et al., 2005	34	17 (16 males)	17 (16 males)	11	12
	McAlonan et al., 2008	88	33 (27 males)	55 (47 males)	11.6	10.7
	Riva et al., 2011	42	21 (13 males)	21 (13 males)	6.5	6.8
	Rojas et al., 2006	47	24 (24 males)	23 (23 males)	20.8	21.4
	Schmitz et al., 2006	22	10 (10 males)	12 (12 males)	36.0	38.0
	Waiter et al., 2004	32	16 (16 males)	16 (16 males)	15.4	15.5
	Wilson et al., 2009	20	10 (8 males)	10 (7 males)	30.1	29.4
	Total ASD	736	363 (323 males)	373 (326 males)	19.0 years (10.1 *SD*)	18.7 years (9.2 *SD*)
ADHD	Ahrendts et al., 2010	40	31 (20 males)	31 (20 males)	31.2	31.5
	Brieber et al., 2007	30	15 (15 males)	15 (15 males)	13.1	13.3
	Carmona et al., 2005	50	25 (21 males)	25 (21 males)	10.8	11.2
	Kobel et al., 2010	26	14 (14 males)	12 (12 males)	10.4	10.9
	Lim et al., 2013	58	29 (29 males)	29 (29 males)	13.8	14.4
	McAlonan et al., 2007	59	28 (28 males)	31 (31 males)	9.9	9.6
	Overmeyer et al., 2001	34	18 (15 males)	16 (15 males)	10.4	10.3
	Sasayama et al., 2010	35	18 (13 males)	17 (12 males)	10.6	10.0
	van Wingen et al., 2013	29	14 (14 males)	15 (15 males)	32.0	37.0
	Yang et al., 2008	114	57 (35 males)	57 (34 males)	11.1	11.7
	Total ADHD	497	249 (204 males)	248 (204 males)	15.3 years (8.7 *SD*)	16.0 years (9.8 *SD*)
Dyslexia	Brambati et al., 2004	21	10 (5 males)	11 (5 males)	31.6	27.4
	Brown et al., 2001	30	16 (16 males)	14 (14 males)	24	24
	Eckert et al., 2005	26	13 (13 males)	13 (13 males)	11.4	11.3
	Hoeft et al., 2007	38	19 (10 males)	19 (10 males)	14.4	14.4
	Jednorog et al., 2013	81	46 (26 males)	35 (13 males)	10.3	10.3
	Kronbichler et al., 2008	28	13 (13 males)	15 (15 males)	15.9	15.5
	Silani et al., 2005	64	32 (32 males)	32 (32 males)	24.4	26.3
	Siok et al., 2008	32	16 (8 males)	16 (13 males)	11.0	11.0
	Steinbrink et al., 2008	16	8 (6 males)	8 (6 males)	20.1	23.7
	Vinckenbosch et al., 2005	23	13 (13 males)	10 (10 males)	Adults	Adults
	Total Dyslexia	336	173 (142 males)	163 (121 males)	18.1 (7.4 *SD*)	18.2 (7.1 *SD*)

**This study used support vector machine (SVM) analysis of VBM data.*

individuals with co-morbid ADHD were excluded (Brown et al., 2001; Vinckenbosch et al., 2005; Jednorog et al., 2013).

DATA EXTRACTION AND ANALYSIS

Anatomic likelihood estimate (ALE) meta-analysis

The ALE meta-analysis method for imaging studies was originally described by Turkeltaub et al. (2002). This method treats each focus as the center of a probability distribution, rather than a single point, and so is better able to deal with inevitable inter-study differences in scanning parameters and imaging analyses (Turkeltaub et al., 2002). Newer iterations of the program (GingerALE software 2.3, www.brainmap.org/ale; Eickhoff et al., 2009, 2012; Turkeltaub et al., 2012) incorporate random effects analysis and a modification to limit the effect of any single experiment on the ALE results (Turkeltaub et al., 2012).

Table 2 | Studies included in the cerebellar ROI analyses.

	Study by author	Total *N*	Clinical group *N* (gender)	TD group *N* (gender)	Age (years) clinical group	Age (years) TD group
ASD	Ecker et al., 2010	44	22 (22 males)	22 (22 males)	27	28
	Ecker et al., 2012	178	89 (89 males)	89 (89 males)	26	28
	McAlonan et al., 2005	34	17 (16 males)	17 (16 males)	11	12
	McAlonan et al., 2008	88	33 (27 males)	55 (47 males)	11.6	10.7
	Riva et al., 2011	42	21 (13 males)	21 (13 males)	6.5	6.8
	Rojas et al., 2006	47	24 (24 males)	23 (23 males)	20.8	21.4
	Salmond et al., 2005	27	14 (13 males)	13 (13 males)	12.9	12.1
	Salmond et al., 2007	44	22 (20 males)	22 (19 males)	11.8	12.1
	Wilson et al., 2009	20	10 (8 males)	10 (7 males)	30.1	29.4
ADHD	Carmona et al., 2005	50	25 (21 males)	25 (21 males)	10.8	11.2
	Lim et al., 2013	58	29 (29 males)	29 (29 males)	13.8	14.4
	McAlonan et al., 2007	59	28 (28 males)	31 (31 males)	9.9	9.6
	Montes et al., 2011*	23	11 (0 males)	12 (0 males)	7.2	7.8
	Montes et al., 2011*	18	8 (0 males)	10 (0 males)	14.9	14.9
	Montes et al., 2011*	20	10 (0 males)	10 (0 males)	27.9	26.5
	Seidman et al., 2011	128	74 (38 males)	54 (25 males)	37.3	34.3
	Yang et al., 2008	114	57 (35 males)	57 (34 males)	11.1	11.7
Dyslexia	Brambati et al., 2004	21	10 (5 males)	11 (5 males)	31.6	27.4
	Brown et al., 2001	30	16 (16 males)	14 (14 males)	24	24
	Eckert et al., 2005	26	13 (13 males)	13 (13 males)	11.4	11.3
	Kronbichler et al., 2008	28	13 (13 males)	15 (15 males)	15.9	15.5
	Pernet et al., 2009	77	38 (34 males)	39 (35 males)	27.2	27.8

**This study separately compared children, adolescents, and adults with ADHD vs. age-matched TD populations, and thus was entered as three separate comparisons in the ALE analysis.*

The meta-analysis procedure using GingerALE is summarized as follows. Text files for each clinical group (ASD, ADHD, dyslexia) were generated that contained the GM foci reported in each study for the clinical group vs. TD group comparison, with separate files for clinical group > TD and clinical group < TD. Foci in Talairach space were converted to MNI space using the icbm2tal transform (Lancaster et al., 2007) prior to analysis. Foci that were reported in Talairach space that had been transformed from MNI space using the Brett transform were converted back to MNI space using the Brett transform (mni2tal) rather than icbm2tal. The foci were blurred with a full-width half-maximum (FWHM) calculated based on the subject size of each study. GingerALE uses the foci from each study to create a Modeled Activation (MA) map for each study by taking the maximum across each focus' Gaussian (Turkeltaub et al., 2012). The union of all the MA maps creates the ALE image. The null distribution of the ALE statistic at each voxel was determined as described in Eickhoff et al. (2012). ALE maps were thresholded at $p < 0.001$ (uncorrected) with a minimum cluster size (k) of 50 for the whole-brain analyses and at false discovery rate (FDR)-corrected $p < 0.01$ ($k > 50$) for the cerebellum-only ROI analysis. The data were visualized using MRIcron (http://www.mccauslandcenter.sc.edu/mricro/mricron/) with the thresholded ALE maps as the overlay, and the SUIT (Diedrichsen, 2006; Diedrichsen et al., 2009) template as the underlay.

Anatomical localization of results

The GingerALE program outputs the size, extent, weighted center, peak coordinates, and ALE values for each cluster. We used the SUIT atlas (Diedrichsen, 2006; Diedrichsen et al., 2009) to localize the cluster peak coordinates to different lobules of the cerebellum.

Network analyses

In order to evaluate the cerebellar findings in the context of cerebro-cerebellar circuits, we utilized the Buckner et al. (2011) 7-network map available in MRIcron in conjunction with the SUIT cerebellar atlas. The 7-network map is the result of a winner-takes-all algorithm at each voxel in the cerebellum used to determine which of 7 cortical networks (defined by Yeo et al., 2011) showed the strongest functional correlation with that cerebellar region. These data resulted from functional connectivity analyses in 1000 healthy adults (500 in the discovery sample, 500 in the replication sample). **Figure 1C** shows the connectivity map and the corresponding 7 cortical networks, including the somatomotor, visual, limbic, frontoparietal, dorsal and ventral attention, and default mode networks. We overlaid our thresholded ALE maps on top of the cerebellar connectivity maps in order to estimate the functional connectivity of the cerebellar regions showing significant effects in each disorder.

RESULTS

ASD

The whole brain analysis revealed significant GM reduction in cerebellar clusters in right Crus I, left lobule VIIIB, and vermis lobule IX in ASD (**Figure 2**, **Table 3**; whole-brain results are available in Supplementary Table 1: the most significant cluster in the brain was in the left cuneus [BA 7], followed by the left cerebellar VIII cluster, the right Crus I cluster, and the midline IX cluster). No GM increases were found in the cerebellum. The cerebellar-only ALE analysis (**Figure 3**, **Table 3**), including the additional studies with cerebellar ROIs, revealed GM reduction again in right Crus I, midline IX, and left VIIIB, with more voxels reaching significance than in the whole-brain analysis. The cerebellar analysis of GM increases showed increased GM in the right dentate nucleus and bilaterally in lobule VIIB.

ADHD

In the ADHD group, significant ALE values indicating decreased GM were found in bilateral cerebellar lobule IX (**Figure 4**, **Table 4**; whole-brain results are reported in Supplementary Table 2). Clusters in the basal ganglia (putamen, caudate), medial frontal gyrus (BA 11), cuneus (BA 18), and amygdala had more significant ALE values than the cerebellar clusters (see Supplementary Table 2). There were no cerebellar regions in which increased GM was found relative to the TD groups. In the cerebellar ROI analysis, in addition to the bilateral IX clusters reported as part of the whole-brain analysis, significant GM differences (ADHD < TD) were found in right Crus I, left lobule X, and bilaterally in VIIIB.

DEVELOPMENTAL DYSLEXIA

ALE analysis of VBM studies in developmental dyslexia only revealed regions in which GM in dyslexia was reduced relative to TD groups (**Figure 5**, **Table 5**; whole-brain analyses are in Supplementary Table 3). In dyslexia, the most significant and largest ALE cluster in the whole brain was in the cerebellum (left lobule VI); a second significant cluster was found in right lobule VI. In addition to the bilateral lobule VI clusters, the cerebellar ROI analyses revealed regions of reduced GM in dyslexia in right lobule VI and right Crus II.

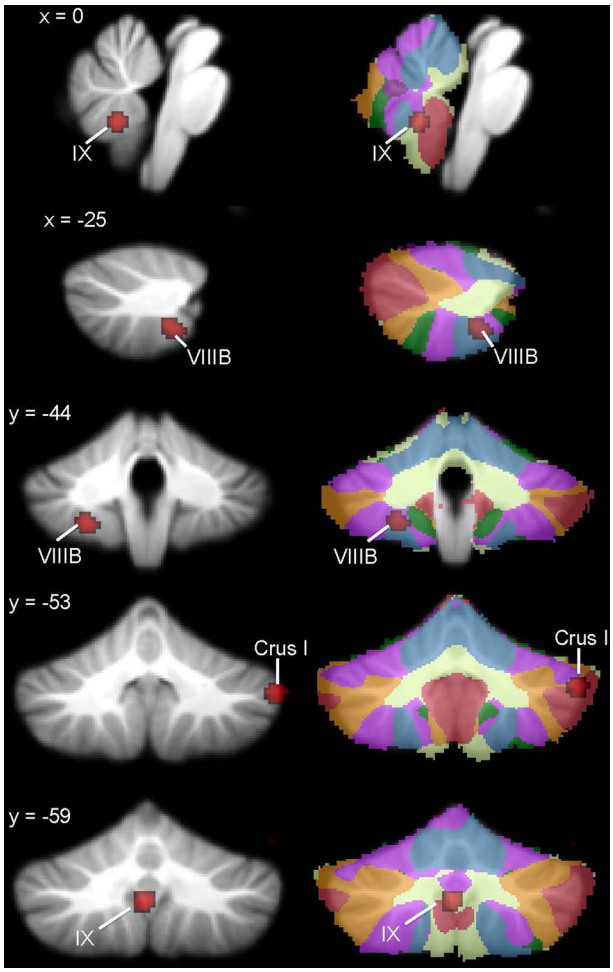

FIGURE 2 | Cerebellar GM differences in ASD. Left, regions in the whole-brain analysis showing significant ALE voxels where ASD < TD (red), thresholded at $p < 0.001$, $k > 50$. **Right**, corresponding slices showing functional connectivity maps of the cerebellum (Buckner et al., 2011). Networks are color-coded such that blue, somatomotor; green, dorsal attention; violet, ventral attention; cream, limbic; orange, frontoparietal; red, default network.

CONVERGENCE OR DIVERGENCE?

Figures 6, **7** show the ALE maps of the locations where the clinical groups have less GM than the TD groups for ASD, ADHD, and dyslexia. It is clear, based on the whole-brain analyses (**Figure 6**), that different regions of the cerebellum are impacted in each disorder. Even though the ROI analyses revealed additional significant cerebellar clusters within each group, there were no overlapping cerebellar regions affected (**Figure 7**).

NETWORK ANALYSIS

We estimated the functional significance of the cerebellar findings in ASD, ADHD, and dyslexia using Buckner et al.'s (2011) 7-network functional connectivity mapping of the cerebellum, available in conjunction with the SUIT cerebellar atlas. This functional connectivity map enables us to evaluate which of 7 broad cortical networks shows the strongest functional connectivity with each of our cerebellar clusters. The 7 cortical networks include the somatomotor, frontoparietal, dorsal and ventral attention, visual, limbic, and default mode networks (see Buckner et al., 2011 and Yeo et al., 2011, for more details).

In ASD, the right Crus I cluster fell within both the frontoparietal cortical network and the default mode network. The left lobule VIIIB cluster mapped to the somatomotor network, whereas the vermis lobule IX cluster mapped to the limbic network. **Figure 2** (right) shows these clusters in the context of the functional connectivity mapping of the cerebellum. Additional clusters from the ROI analysis were also in the limbic (additional IX cluster) and default (second right Crus I cluster) networks (**Figure 3**, right). In ADHD, the clusters were part of the dorsal attention network (**Figure 4**, right); the additional clusters emerging from the cerebellar ROI analysis involved the ventral attention network (additional bilateral VIIIB clusters), the somatomotor network (right anterior lobe), and the default

Table 3 | GM differences in ASD: whole brain and cerebellar-only analyses.

	Cluster number	Volume (mm^3)	ALE value × 10^{-3}	*x*	*y*	*z*	Location
WHOLE BRAIN ANALYSIS							
ASD < TD	1	368	11.50	−24	−44	−52	Left VIIIB
	2	352	13.98	54	−54	−36	Right Crus I
	3	328	12.85	−2	−60	−40	Midline IX
	4	56	10.41	30	−84	−24	Right Crus I
ASD>TD	No sig. clusters						
CEREBELLAR ROI ANALYSIS							
ASD < TD	1	416	13.98	54	−54	−36	Right Crus I
	2	400	13.13	0	−58	−40	Midline IX
	3	152	10.41	30	−84	−24	Right Crus I
	4	64	7.87	−4	−60	−58	Midline IX
	5	56	9.02	−26	−48	−48	Left VIIIB
ASD > TD	1	784	12.96	12	−68	−36	Right dentate
	2	72	8.41	26	−72	−50	Right VIIB
	3	64	8.35	−26	−72	−48	Left VIIB

ASD, Autism spectrum disorder; TD, typically-developing; ROI, region of interest; x, y, z, MNI coordinates.

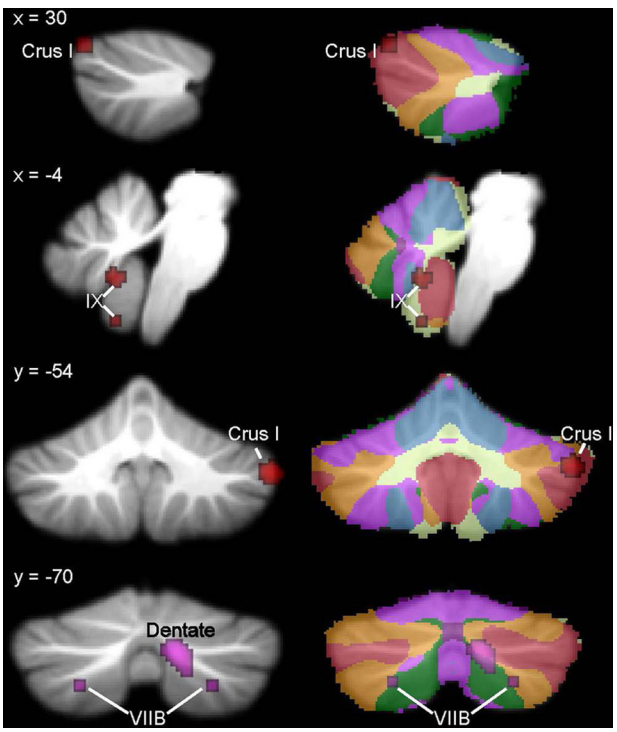

FIGURE 3 | ASD cerebellar ROI analysis. Left, ASD < TD in additional IX and right Crus I clusters (red) and regions where ASD > TD (violet) in the right dentate nucleus and bilaterally in VIIB. These ALE maps are thresholded at FDR-corrected $p < 0.05$, $k > 50$. Right, corresponding slices showing functional connectivity maps of the cerebellum (Buckner et al., 2011). Networks are color-coded such that blue, somatomotor; green, dorsal attention; violet, ventral attention; cream, limbic; orange, frontoparietal; red, default network.

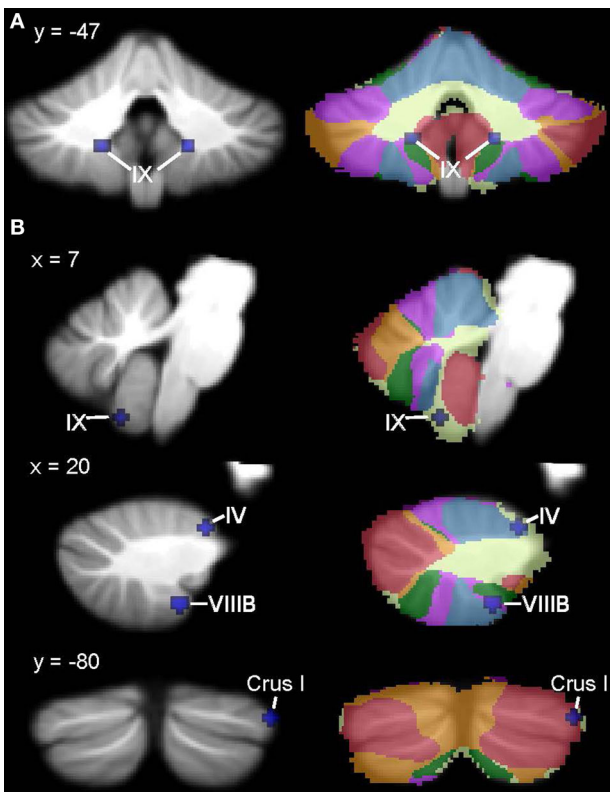

FIGURE 4 | ADHD < TD GM: whole-brain and ROI analyses. Left **(A)**, Regions in the whole-brain analysis showing significant ALE voxels where ADHD < TD (blue), thresholded at $p < 0.001$, $k > 50$. **(B)** Regions showing ADHD < TD in the ROI analysis. Right, corresponding slices showing functional connectivity maps of the cerebellum (Buckner et al., 2011). Networks are color-coded such that blue, somatomotor; green, dorsal attention; violet, ventral attention; cream, limbic; orange, frontoparietal; red, default network.

Table 4 | GM differences in ADHD: whole brain and cerebellar-only analyses.

	Cluster number	Volume (mm^3)	ALE value × 10^{-3}	x	y	z	Location
WHOLE-BRAIN ANALYSIS							
ADHD < TD	1	80	9.67	−16	−48	−45	Left lobule IX
	2	64	8.99	18	−48	−46	Right lobule IX
CEREBELLAR ROI ANALYSIS							
ADHD<TD	1	96	10.49	20	−44	−54	Right VIIIB
	2	80	9.80	−16	−48	−46	Left lobule IX
	3	72	9.75	18	−46	−46	Right lobule IX
	4	64	10.21	56	−68	−32	Right Crus I
	5	56	9.98	6	−60	−58	Right lobule IX
	6	56	10.03	−14	−44	−56	Left VIIIB
	7	56	9.99	−26	−32	−40	Left X
	8	56	9.98	44	−80	−30	Right Crus I
	9	56	9.98	20	−34	−24	Right I–IV

ADHD, attention deficit hyperactivity disorder; TD, typically-developing; ROI, region of interest; x, y, z, MNI coordinates.

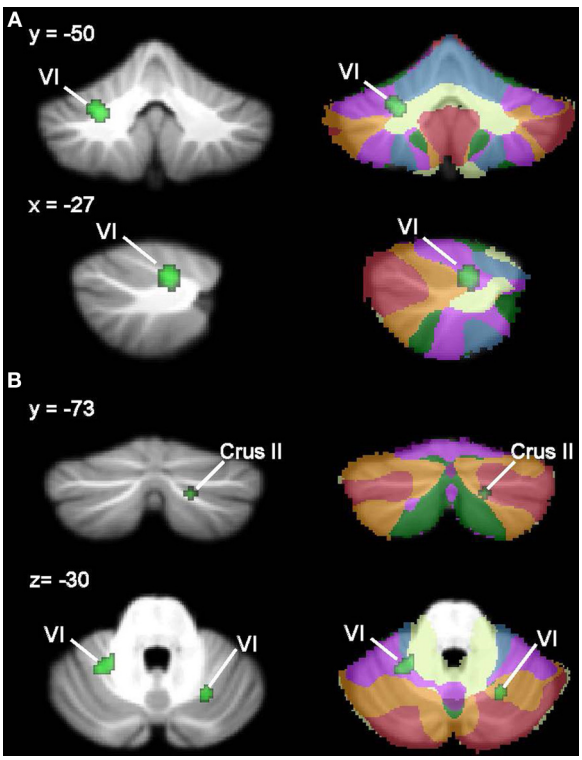

FIGURE 5 | Dyslexia < TD GM: whole-brain and ROI analyses. Left **(A)**, Regions in the whole-brain analysis showing significant ALE voxels where Dyslexia < TD (green), thresholded at $p < 0.001$, $k > 50$. **(B)** Regions showing Dyslexia < TD in the ROI analysis. Right, corresponding slices showing functional connectivity maps of the cerebellum (Buckner et al., 2011). Networks are color-coded such that blue, somatomotor; green, dorsal attention; violet, ventral attention; cream, limbic; orange, frontoparietal; red, default network.

network (right Crus I cluster). In dyslexia, the left VI cluster was located in the part of the cerebellum mapping to the ventral attention network (**Figure 5**, right); the clusters identified in the cerebellar ROI analysis mapped to the frontoparietal (right VI) and default mode networks (right Crus II). Therefore, while there were no regions of overlap within the cerebellum anatomically, there is some degree of overlap as to the potential cerebro-cerebellar networks affected in these disorders.

DISCUSSION

Our ALE meta-analysis of VBM studies revealed that different regions of the cerebellum show reduced GM in ASD, ADHD, and developmental dyslexia relative to TD age-matched individuals. The cerebellar findings were significant in the context of whole-brain analyses, and were supported and extended by the cerebellar ROI analyses. The network analyses also suggested that different cerebro-cerebellar networks are disrupted in these developmental disorders, and it is possible that, within each disorder, different core symptoms are mediated by unique cerebro-cerebellar circuits. This is consistent with the repeating, modular circuitry of the cerebellar cortex, such that discrete sub-regions within the cerebellum have different functions. In this context, cerebellar modulation could be applied to various cortical networks, including somatomotor, attention, frontoparietal, and default mode networks (see Ito, 2008). These findings indicate that the localization of regional differences in ASD, ADHD, and dyslexia and their functional significance should be considered in the context of the functional topography of the human cerebellum.

In ASD, three regions of reduced GM emerged from the analysis: midline lobule IX, right Crus I, and left lobule VIIIB; in functional connectivity analyses, these regions are associated with limbic, frontoparietal/default mode, and somatomotor networks, respectively (Buckner et al., 2011). Therefore, the structural and functional connectivity of these regions are consistent with the complex behavioral profile of ASD, which includes difficulties in social interaction and communication, as well as repetitive and stereotyped behaviors. Structurally, the midline lobule IX cluster is consistent with early anatomical reports of reduced volume of the inferior cerebellar vermis in ASD (e.g., Courchesne et al., 1988, 1994). In terms of the functional significance of this region, vermal damage in preterm infants has also been associated with ASD symptoms (Limperopoulos et al., 2008). Clinical studies

Table 5 | GM differences in dyslexia: whole brain and cerebellar-only analyses.

	Cluster number	Volume (mm^3)	ALE value × 10^{-3}	*x*	*y*	*z*	Location
WHOLE-BRAIN ANALYSIS							
Dyslexia < TD	1	392	10.18	−26	−50	−32	Left VI
	2	64	6.73	32	−52	−20	Right VI
CEREBELLAR ROI ANALYSIS							
Dyslexia < TD	1	304	8.98	−26	−50	−30	Left VI
	2	208	9.72	26	−64	−28	Right VI
	3	64	7.13	26	−54	−32	Right VI
	4	56	7.14	18	−74	−38	Right Crus II

TD, typically-developing; ROI, region of interest; x, y, z, MNI coordinates.

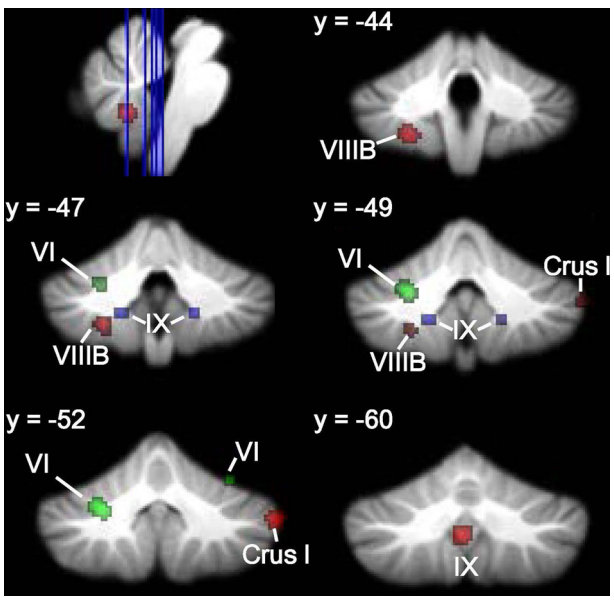

FIGURE 6 | Different cerebellar regions affected in ASD vs. ADHD vs. dyslexia. Coronal slices through the cerebellum show clusters of GM decreases in ASD (red), ADHD (blue), and dyslexia (green).

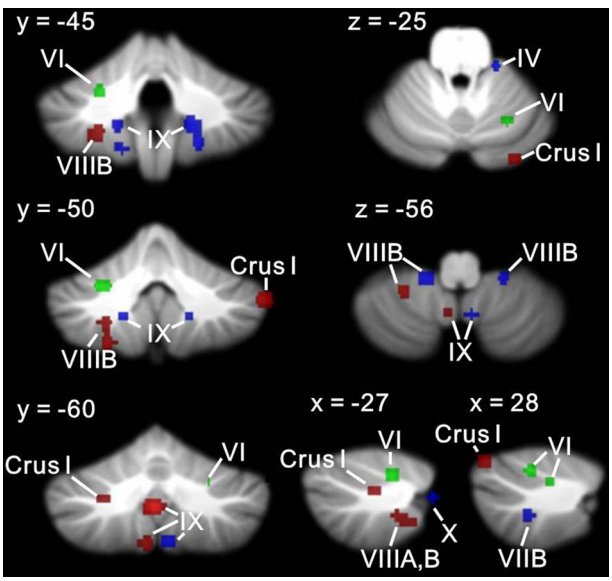

FIGURE 7 | Different cerebellar regions affected in ASD vs. ADHD vs. dyslexia in the cerebellar ROI analyses. Coronal, axial, and sagittal slices through the cerebellum show clusters of GM decreases in ASD (red), ADHD (blue), and dyslexia (green) resulting from the ROI analysis.

investigating the behavioral effects of cerebellar malformations also support a relationship between vermal malformations and positive ASD screens, whereas cerebellar hemisphere malformations are more often associated with selective deficits in executive function, language, or spatial cognition (Tavano et al., 2007; Bolduc et al., 2011, 2012). Right Crus I is active during cognitive tasks, including language and working memory paradigms (e.g., Stoodley and Schmahmann, 2009), and right posterolateral damage to the cerebellum has been associated with language deficits (e.g., Riva and Giorgi, 2000; Stoodley et al., 2012a). It is therefore possible that right Crus I differences could be related to communication deficits in ASD. The relationship between this right Crus I cluster and the frontoparietal association network supports this idea, as does a recent report showing reduced functional connectivity between right Crus I and cortical language regions including the supplementary motor area, inferior frontal gyrus, and dorsolateral prefrontal cortex in ASD (Verly et al., 2014). The right Crus I cluster also overlapped with cerebellar regions associated with the default mode network, which is thought to be dysfunctional in ASD (see review by Minshew and Keller, 2010) and is associated with various aspects of social processing (Li et al., 2014). Consistent with our structural finding, a large resting-state functional connectivity study reported reduced functional connectivity in the cerebellum and the default mode networks in ASD (Tomasi and Volkow, 2012). Crus I is also engaged during empathy and theory of mind tasks in TD individuals (Vollm et al., 2006), which suggests that structural differences in this region may contribute to the well-documented difficulties with empathy and theory of mind in ASD individuals. Finally, we found reduced GM in left lobule VIIIB in ASD, which may be related to impaired motor control (see Becker and Stoodley, 2013, for review of motor symptoms in ASD), since lobule VIIIB participates in somatomotor networks (Krienen and Buckner, 2009; Buckner et al., 2011) and is active during sensorimotor tasks (e.g., Stoodley and Schmahmann, 2009, for review). The finding that cerebellar differences in ASD map to different functional regions

of the cerebellum—including those that are involved in affective function, language, and motor control—suggests that GM reductions in midline lobule IX, right Crus I, and left VIIIB may make different contributions to the core symptoms of ASD.

In ADHD, the whole-brain analysis showed GM reduction bilaterally in lobule IX; notably, not the same regions of IX as were found in ASD. Instead, these clusters mapped to cerebellar regions associated with the dorsal attention network (Buckner et al., 2011), which is thought to modulate voluntary allocation of attention (see Corbetta and Shulman, 2002; Vossel et al., 2014, for review). In the ROI analysis, GM reductions were also found in VIIIB and right Crus I, in regions involving the ventral attention network and default mode network, respectively. A cluster was also found in the anterior lobe of the cerebellum, which shows structural and functional connectivity with sensorimotor areas of the cerebral cortex (see Krienen and Buckner, 2009; Stoodley and Schmahmann, 2010). Frontal-cerebellar circuits have been associated with timing functions that are hypothesized to be crucial to prediction and attention (Ghajar and Ivry, 2009), and timing is considered a critical impairment in ADHD (e.g., Sonuga-Barke et al., 2010). Consistent with this, Durston et al. (2011) have proposed that frontal-cerebellar circuits in ADHD are specifically related to timing, a concept which is supported by a range of neuroimaging studies reporting cerebellar dysfunction in ADHD during time duration judgments and violations of timing (e.g., Durston et al., 2007; Valera et al., 2010; Vloet et al., 2010). The functional connectivity of the cerebellar regions associated with ADHD with the dorsal and ventral attention networks and the default mode network make sense in the context of the networks thought to be affected in ADHD (Bush, 2010, for review). Consistent with the decreased GM in VIIIB found in the ROI analysis, Hoekzema et al. (2010, 2011) found that VIIIB showed GM and BOLD signal increases following cognitive training in children with ADHD, which was associated with improved performance on an attention task. These findings suggest that the cerebellum mediates attention-related circuitry that is relevant to the etiology of ADHD.

In participants with developmental dyslexia, reduced GM was located in lobule VI bilaterally; when the ROI analysis was performed, an additional cluster was found in right Crus II. These findings are consistent with other studies in dyslexia, including Pernet et al.'s (2009) report that a right lobule VI cluster was the best biomarker for differentiating adults with dyslexia. The left lobule VI cluster was associated with the ventral attention network, whereas the right VI cluster mapped to the frontoparietal network, and the right Crus II cluster to the default mode network. While the default mode network has not been explicitly investigated in dyslexia, dyslexia is thought to involve dysfunction in a left-lateralized reading network (for recent review, see Richlan, 2012), which involves regions associated with both the frontoparietal and ventral attention networks. Although the predominant causal theory of dyslexia proposes a core deficit in phonological processing (e.g., Bradley and Bryant, 1983)—which may be relevant to the right lobule VI cluster, which connects with left cerebral cortex—it has also been proposed that dyslexia results from deficient visual-spatial attention (Vidyasagar and Pammer, 2010), which could be related to the left lobule VI cluster, projecting to right-lateralized cortical regions. The idea that visual-spatial attention is important to reading development is supported by a recent study investigating predictors of reading achievement in preschoolers, which found that a visual attention task was a better predictor of later reading skills than naming and language tasks (Franceschini et al., 2012). The ventral attention network includes the right temporo-parietal junction (TPJ; Corbetta and Shulman, 2002), and neuroimaging evidence suggests significant overactivation of this area during both phonological (Simos et al., 2000; Richlan et al., 2009) and attention tasks (Goldfarb and Shaul, 2013) in dyslexic participants. Our finding that the most significant cerebellar ALE cluster in dyslexia was associated with the ventral attention network is consistent with these data. The right lobule VI cluster is consistent with right-lateralized activation in the cerebellum for language tasks (Stoodley and Schmahmann, 2009), and reduced GM here may be relevant to phonological processing difficulties in dyslexia. As to the specific contribution of the cerebellum to reading (see Stoodley and Stein, 2011, 2013, for reviews), the observation that dyslexic readers very rarely achieve fluent, automatic reading led to the proposal that an impairment in cerebellar procedural learning functions could lead to the range of symptoms seen in dyslexia (Nicolson et al., 2001; Nicolson and Fawcett, 2007, 2011). Consistent with the idea that modification of cerebellar circuits could improve skill acquisition, cerebellar GM in the right anterior lobe increased in response to successful remediation in dyslexia (Krafnick et al., 2011). The left VI cerebellar cluster identified here overlaps with regions of overactivation in dyslexia during functional imaging studies (Linkersdorfer et al., 2012). The authors suggest that the overactivation in this region reflects the increased effort or compensatory strategies of dyslexic readers during reading tasks. In summary, as in ASD, it is possible that the different cerebellar clusters showing GM alterations in dyslexia may make differential contributions to the behavioral manifestations of the disorder, such that the left lobule VI cluster is involved in visual-spatial attention difficulties and the right lobule VI cluster is related to phonological deficits. Consistent with this idea, left lobule VI was involved in spatial processing while right lobule VI was involved in language and working memory processing in a meta-analysis of task-based neuroimaging studies (Stoodley and Schmahmann, 2009).

DIVERGENT CEREBELLAR STRUCTURAL FINDINGS ACROSS DISORDERS AND CO-MORBIDITY

The results of this ALE meta-analysis suggest that different regions of the cerebellum show GM reductions in ASD, ADHD, and developmental dyslexia. Although there were no regions of overlap between the disorders, there were some commonalities in the putative cerebro-cerebellar networks affected, including the ventral attention network for ADHD and dyslexia, and the frontoparietal and default networks for ASD and dyslexia. This is not surprising, given the co-morbidities between these disorders: it is estimated that ∼40% of individuals with ADHD have reading difficulties (e.g., Willcutt et al., 2010), ∼30% of males with ADHD have elevated ASD traits (Reiersen et al., 2007), and ∼30% of individuals with ASD show clinically significant

signs of ADHD (e.g., Simonoff et al., 2008). Imaging studies have been attempting to establish the unique and shared neural substrates between ASD and ADHD, using both functional (task-based, Christakou et al., 2013; functional connectivity, Di Martino et al., 2013) and structural (Brieber et al., 2007) approaches. The only relevant cerebellar findings thus far revealed overactivation in ASD relative to ADHD and TD groups in the anterior left cerebellum during a sustained attention task (Christakou et al., 2013). In ADHD and dyslexia, structural imaging has focused on specific regions of interest (Hynd et al., 1990; Semrud-Clikeman et al., 1996; Kibby et al., 2009a) and overall cerebral volume (Kibby et al., 2009b), with no cerebellar findings to report. Future prospective structural and functional imaging studies will be required to examine the relationship between cerebellar structure and function in ASD, ADHD, and dyslexia and the overlapping symptoms among these disorders.

LIMITATIONS

In any meta-analysis of neuroimaging data, there are inherent limitations due to combining studies using different groups of participants (with different ages, diagnostic criteria, co-morbidities, medication status), imaging parameters and analytical approaches, including normalization methods and thresholding. The ALE approach attempts to accommodate issues related to imaging analyses and registration by treating each focus as the center of a Gaussian probability distribution, and foci are converted between Talairach and MNI space using algorithms that depend on the initial processing software (e.g., SPM vs. FSL). However, there are limitations to the ALE approach, such that it does not account for differences in cluster size between studies. We tried to limit the effect of these issues by restricting our analyses to whole-brain VBM studies which directly compared the patient groups with age-matched TD groups. The strength of this approach is that we were able to determine regions of the cerebellum which are consistently reported in such studies, pooling data from a larger number of participants. Another limitation is the use of the 7-network cerebellar map (Buckner et al., 2011) to interpret the predominant cerebral networks associated with our cerebellar clusters. As these maps only include 7 networks, and are based on a winner-takes-all algorithm, there are surely nuances in functional connectivity that will be missed with this approach. Therefore, the results of this study should be used as a basis for future prospective investigations of the role(s) of different cerebellar regions in ASD, ADHD, and developmental dyslexia.

Another limitation is that the results of VBM studies cannot determine the cellular alterations that produce the observed differences in GM (see Zatorre et al., 2012). That said, molecular analyses of animal models and post-mortem studies in ASD, ADHD, and dyslexia can provide some clues. The cerebellar cortex is comprised of three layers (the molecular layer, Purkinje cell layer, and the granule cell layer); inputs come in via the mossy fibers and climbing fibers, and the sole output neurons of the cerebellar cortex are the Purkinje cells, which are amongst the largest neurons in the brain with extensively branched dendritic trees. The most substantial body of post-mortem data comes from ASD, where smaller Purkinje cell size and reduced number and density of Purkinje cells have been reported (reviewed in Becker and Stoodley, 2013). These findings suggest that GM differences in ASD might be related to these alterations in Purkinje cells, although Kemper and Bauman (1993) also reported reduced numbers of granule cells in the cerebellum in ASD brains. There are very few, if any, post-mortem analyses evaluating the cerebellum for ADHD and developmental dyslexia. One study investigating a small sample of 4 dyslexic brains reported differences in Purkinje cell area (significantly larger in the posterior lobe) and cell density (a trend toward reduced cell density in the posterior lobe), consistent with our findings of reduced GM in the posterior lobe of the cerebellum in dyslexia. In a rodent model of ADHD, a reduced number of Purkinje cells in the cerebellar vermis was reported, which was not present in the ADHD rats treated with methylphenidate (Yun et al., 2014). Finally, a recent study investigating GAD65 antibodies in the serum of children with ASD and ADHD found that the serum of 60% of ASD and 53% of ADHD participants reacted with cerebellar Purkinje cells; in a smaller subset of ADHD participants (20%) the serum also reacted with cells in the molecular and granule cell layers (Rout et al., 2012). The authors suggest a potential relationship between the Purkinje cell loss reported in ASD and GAD65 reactivity in their ASD group (Rout et al., 2012); this relationship may also be present in ADHD. While only a small body of evidence, these data suggest that the differences in GM reported here may have a basis in cellular differences in the circuitry of the cerebellar cortex.

FUTURE DIRECTIONS

The results of this meta-analysis suggest that different cerebellar regions are affected in ASD, ADHD, and dyslexia. Further, the clusters where anatomical differences were found in the whole-brain analysis are associated with different functional circuits which are consistent with the behavioral profiles of each disorder: e.g., the default mode network in ASD, the dorsal attention network in ADHD. These findings indicate that the specific subregion of the cerebellum that is affected in a given developmental disorder should be considered in the context of cerebellar functional topography and cerebro-cerebellar connectivity. Future studies will aim to determine how and when these cerebellar differences arise in the context of neural development, and the specific contribution that cerebellar dysfunction makes to the behavioral manifestations of autism, ADHD, and developmental dyslexia.

ACKNOWLEDGMENTS

The author would like to acknowledge the contributions of Anila D'Mello, Alexa Desko, Rebecca Dawn Finzi, Joyce Oates, Edward Sawyer, Naomi Shakerdge, and Alexandra Thompson to this project. The author would like to thank Anila D'Mello and Lauren McGrath for helpful comments on the manuscript.

SUPPLEMENTARY MATERIAL

The Supplementary Material for this article can be found online at: http://www.frontiersin.org/journal/10.3389/fnsys.2014.00092/abstract

REFERENCES

Abell, F., Krams, M., Ashburner, J., Passingham, R., Friston, K., Frackowiak, R., et al. (1999). The neuroanatomy of autism: a voxel-based whole brain analysis of structural scans. *Neuroreport* 10, 1647–1651. doi: 10.1097/00001756-199906030-00005

Abrahams, B. S., and Geschwind, D. H. (2010). Connecting genes to brain in the autism spectrum disorders. *Arch. Neurol.* 67, 395–399. doi: 10.1001/archneurol.2010.47

Ahrendts, J., Rusch, N., Wilke, M., Philipsen, A., Eickhoff, S. B., Glauche, V., et al. (2010). Visual cortex abnormalities in adults with ADHD: a structural MRI study. *World J. Biol. Psychiatry* 12, 260–270. doi: 10.3109/15622975.2010.518624

Allen, G., McColl, R., Barnard, H., Ringe, W., Fleckenstein, J., and Cullum, C. (2005). Magnetic resonance imaging of cerebellar-prefrontal and cerebellar parietal functional connectivity. *Neuroimage* 28, 39–48. doi: 10.1016/j.neuroimage.2005.06.013

American Psychiatric Association. (2000). *Diagnostic and Statistical Manual of Mental Disorders, 4th Edn., Text revision*. Washington, DC: American Psychiatric Association. doi: 10.1176/appi.books.9780890423349

American Psychiatric Association. (2013). *Diagnostic and Statistical Manual of Mental Disorders, 5th Edn.* Arlington, VA: American Psychiatric Association, Inc.

Apps, R., and Garwicz, M. (2005). Anatomical and physiological foundations of cerebellar information processing. *Nat. Rev. Neurosci.* 6, 297–311. doi: 10.1038/nrn1646

Ashtari, M., Kumra, S., Bhaskar, S. L., Clarke, T., Thaden, E., Cervellione, K. L., et al. (2005). Attention-deficit/hyperactivity disorder: a preliminary diffusion tensor imaging study. *Biol. Psychiatry* 57, 448–455. doi: 10.1016/j.biopsych.2004.11.047

Bailey, A., Luthert, P., Dean, A., Harding, B., Janota, I., Montgomery, M., et al. (1998). A clinicopathological study of autism. *Brain* 121(Pt 5), 889–905. doi: 10.1093/brain/121.5.889

Bauman, M., and Kemper, T. (1985). Histoanatomic observations of the brain in early infantile autism. *Neurology* 35, 866–874. doi: 10.1212/WNL.35.6.866

Bechtel, N., Kobel, M., Penner, I. K., Klarhofer, M., Scheffler, K., Opwis, K., et al. (2009). Decreased fractional anisotropy in the middle cerebellar peduncle in children with epilepsy and/or attention deficit/hyperactivity disorder: a preliminary study. *Epilepsy Behav.* 15, 294–298. doi: 10.1016/j.yebeh.2009.04.005

Becker, E. B., and Stoodley, C. J. (2013). Autism spectrum disorder and the cerebellum. *Int. Rev. Neurobiol.* 113, 1–34. doi: 10.1016/B978-0-12-418700-9.00001-0

Berquin, P. C., Giedd, J. N., Jacobsen, L. K., Hamburger, S. D., Krain, A. L., Rapoport, J. L., et al. (1998). Cerebellum in attention-deficit hyperactivity disorder-A morphometric MRI study. *Neurology* 50, 1087–1093. doi: 10.1212/WNL.50.4.1087

Biederman, J. (2005). Attention-deficit/hyperactivity disorder: a selective overview. *Biol. Psychiatry* 57, 1215–1220. doi: 10.1016/j.biopsych.2004.10.020

Bledsoe, J., Semrud-Clikeman, M., and Pliszka, S. R. (2009). A magnetic resonance imaging study of the cerebellar vermis in chronically treated and treatment-naive children with attention-deficit/hyperactivity disorder combined type. *Biol. Psychiatry* 65, 620–624. doi: 10.1016/j.biopsych.2008.11.030

Bledsoe, J. C., Semrud-Clikeman, M., and Pliszka, S. R. (2011). Neuroanatomical and neuropsychological correlates of the cerebellum in children with attention-deficit/hyperactivity disorder–combined type. *J. Am. Acad. Child Adolesc. Psychiatry* 50, 593–601. doi: 10.1016/j.jaac.2011.02.014

Boddaert, N., Chabane, N., Gervais, H., Good, C. D., Bourgeois, M., Plumet, M. H., et al. (2004). Superior temporal sulcus anatomical abnormalities in childhood autism: a voxel-based morphometry MRI study. *Neuroimage* 23, 364–369. doi: 10.1016/j.neuroimage.2004.06.016

Bolduc, M. E., Du Plessis, A. J., Evans, A., Guizard, N., Zhang, X., Robertson, R. L., et al. (2011). Cerebellar malformations alter regional cerebral development. *Dev. Med. Child Neurol.* 53, 1128–1134. doi: 10.1111/j.1469-8749.2011.04090.x

Bolduc, M. E., du Plessis, A. J., Sullivan, N., Guizard, N., Zhang, X., Robertson, R. L., et al. (2012). Regional cerebellar volumes predict functional outcome in children with cerebellar malformations. *Cerebellum* 11, 531–542. doi: 10.1007/s12311-011-0312-z

Bonilha, L., Cendes, F., Rorden, C., Eckert, M., Dalgalarrondo, P., Li, L. M., et al. (2008). Gray and white matter imbalance–typical structural abnormality underlying classic autism? *Brain Dev.* 30, 396–401. doi: 10.1016/j.braindev.2007.11.006

Bradley, L., and Bryant, P. (1983). Categorising sounds and learning to read–a causal connection. *Nature* 301, 419–421. doi: 10.1038/301419a0

Brambati, S. M., Termine, C., Ruffino, M., Stella, G., Fazio, F., Cappa, S. F., et al. (2004). Regional reductions of gray matter volume in familial dyslexia. *Neurology* 63, 742–745. doi: 10.1212/01.WNL.0000134673.95020.EE

Brieber, S., Neufang, S., Bruning, N., Kamp-Becker, I., Remschmidt, H., Herpertz-Dahlmann, B., et al. (2007). Structural brain abnormalities in adolescents with autism spectrum disorder and patients with attention deficit/hyperactivity disorder. *J. Child Psychol. Psychiatry* 48, 1251–1258. doi: 10.1111/j.1469-7610.2007.01799.x

Brown, W., Eliez, S., Menon, V., Rumsey, J., White, C., and Reiss, A. (2001). Preliminary evidence of widespread morphological variations in the brain in dyslexia. *Neurology* 56, 781–783. doi: 10.1212/WNL.56.6.781

Buckner, R. L., Krienen, F. M., Castellanos, A., Diaz, J. C., and Yeo, B. T. (2011). The organization of the human cerebellum estimated by intrinsic functional connectivity. *J. Neurophysiol.* 106, 2322–2345. doi: 10.1152/jn.00339.2011

Bush, G. (2010). Attention-deficit/hyperactivity disorder and attention networks. *Neuropsychopharmacology* 35, 278–300. doi: 10.1038/npp.2009.120

Carmona, S., Vilarroya, O., Bielsa, A., Tremols, V., Soliva, J. C., Rovira, M., et al. (2005). Global and regional gray matter reductions in ADHD: a voxel-based morphometric study. *Neurosci. Lett.* 389, 88–93. doi: 10.1016/j.neulet.2005.07.020

Carrion-Castillo, A., Franke, B., and Fisher, S. E. (2013). Molecular genetics of dyslexia: an overview. *Dyslexia* 19, 214–240. doi: 10.1002/dys.1464

Castellanos, F., Lee, P., Sharp, W., Jeffries, N., Greenstein, D., Clasen, L., et al. (2002). Developmental trajectories of brain volume abnormalities in children and adolescents with attention-deficit/hyperactivity disorder. *JAMA* 288, 1740–1748. doi: 10.1001/jama.288.14.1740

Castellanos, F. X., Giedd, J. N., Berquin, P. C., Walter, J. M., Sharp, W., Tran, T., et al. (2001). Quantitative brain magnetic resonance imaging in girls with attention-deficit/hyperactivity disorder. *Arch. Gen. Psychiatry* 58, 289–295. doi: 10.1001/archpsyc.58.3.289

Castellanos, F. X., Giedd, J. N., Marsh, W. L., Hamburger, S. D., Vaituzis, A. C., Dickstein, D. P., et al. (1996). Quantitative brain magnetic resonance imaging in attention-deficit hyperactivity disorder. *Arch. Gen. Psychiatry* 53, 607–616. doi: 10.1001/archpsyc.1996.01830070053009

Catani, M., Jones, D., Daly, E., Embiricos, N., Deeley, Q., Pugliese, L., et al. (2008). Altered cerebellar feedback projections in Asperger syndrome. *Neuroimage* 41, 1184–1191. doi: 10.1016/j.neuroimage.2008.03.041

Cauda, F., Geda, E., Sacco, K., D'Agata, F., Duca, S., Geminiani, G., et al. (2011). Grey matter abnormality in autism spectrum disorder: an activation likelihood estimation meta-analysis study. *J. Neurol. Neurosurg. Psychiatry* 82, 1304–1313. doi: 10.1136/jnnp.2010.239111

Christakou, A., Murphy, C. M., Chantiluke, K., Cubillo, A. I., Smith, A. B., Giampietro, V., et al. (2013). Disorder-specific functional abnormalities during sustained attention in youth with Attention Deficit Hyperactivity Disorder (ADHD) and with autism. *Mol. Psychiatry* 18, 236–244. doi: 10.1038/mp.2011.185

Collins, D., Zijdenbos, A., Kollokian, V., Sled, J., Kabani, N., Holmes, C., et al. (1998). Design and construction of a realistic digital brain phantom. *IEEE Trans. Med. Imaging* 17, 463–468. doi: 10.1109/42.712135

Corbetta, M., and Shulman, G. L. (2002). Control of goal-directed and stimulus-driven attention in the brain. *Nat. Rev. Neurosci.* 3, 201–215. doi: 10.1038/nrn755

Courchesne, E., Campbell, K., and Solso, S. (2011). Brain growth across the life span in autism: age-specific changes in anatomical pathology. *Brain Res.* 1380, 138–145. doi: 10.1016/j.brainres.2010.09.101

Courchesne, E., Saitoh, O., Townsend, J. P., Yeung-Courchesne, R., Press, G. A., Lincoln, A. J., et al. (1994). Cerebellar hypoplasia and hyperplasia in infantile autism. *Lancet* 343, 63–64. doi: 10.1016/S0140-6736(94)90923-7

Courchesne, E., Yeung-Courchesne, R., Press, G., Hesselink, J., and Jernigan, T. (1988). Hypoplasia of cerebellar vermal lobules VI and VII in autism. *New Engl. J. Med.* 318, 1349–1354. doi: 10.1056/NEJM198805263182102

Craig, M. C., Zaman, S. H., Daly, E. M., Cutter, W. J., Robertson, D. M., Hallahan, B., et al. (2007). Women with autistic-spectrum disorder: magnetic resonance imaging study of brain anatomy. *Br. J. Psychiatry* 191, 224–228. doi: 10.1192/bjp.bp.106.034603

Czerniak, S. M., Sikoglu, E. M., King, J. A., Kennedy, D. N., Mick, E., Frazier, J., et al. (2013). Areas of the brain modulated by a single-dose methylphenidate treatment in youth with ADHD during task-based fMRI: a systematic review. *Harv. Rev. Psychiatry* 21, 151–162. doi: 10.1097/HRP.0b013e318293749e

Diedrichsen, J. (2006). A spatially unbiased atlas template of the human cerebellum. *Neuroimage* 33, 127–138. doi: 10.1016/j.neuroimage.2006.05.056

Diedrichsen, J., Balsters, J. H., Flavell, J., Cussans, E., and Ramnani, N. (2009). A probabilistic MR atlas of the human cerebellum. *Neuroimage* 46, 39–46. doi: 10.1016/j.neuroimage.2009.01.045

Di Martino, A., Zuo, X. N., Kelly, C., Grzadzinski, R., Mennes, M., Schvarcz, A., et al. (2013). Shared and distinct intrinsic functional network centrality in autism and attention-deficit/hyperactivity disorder. *Biol. Psychiatry* 74, 623–632. doi: 10.1016/j.biopsych.2013.02.011

Duerden, E. G., Mak-Fan, K. M., Taylor, M. J., and Roberts, S. W. (2012). Regional differences in grey and white matter in children and adults with autism spectrum disorders: an activation likelihood estimate (ALE) meta-analysis. *Autism Res.* 5, 49–66. doi: 10.1002/aur.235

Durston, S. (2010). Imaging genetics in ADHD. *Neuroimage* 52, 832–838. doi: 10.1016/j.neuroimage.2010.02.071

Durston, S., Davidson, M. C., Mulder, M. J., Spicer, J. A., Galvan, A., Tottenham, N., et al. (2007). Neural and behavioral correlates of expectancy violations in attention-deficit hyperactivity disorder. *J. Child Psychol. Psychiatry* 48, 881–889. doi: 10.1111/j.1469-7610.2007.01754.x

Durston, S., Hulshoff Pol, H. E., Schnack, H. G., Buitelaar, J. K., Steenhuis, M. P., Minderaa, R. B., et al. (2004). Magnetic resonance imaging of boys with attention-deficit/hyperactivity disorder and their unaffected siblings. *J. Am. Acad. Child Adolesc. Psychiatry* 43, 332–340. doi: 10.1097/00004583-200403000-00016

Durston, S., van Belle, J., and de Zeeuw, P. (2011). Differentiating frontostriatal and fronto-cerebellar circuits in attention-deficit/hyperactivity disorder. *Biol. Psychiatry* 69, 1178–1184. doi: 10.1016/j.biopsych.2010.07.037

Ecker, C., Rocha-Rego, V., Johnston, P., Mourao-Miranda, J., Marquand, A., Daly, E. M., et al. (2010). Investigating the predictive value of whole-brain structural MR scans in autism: a pattern classification approach. *Neuroimage* 49, 44–56. doi: 10.1016/j.neuroimage.2009.08.024

Ecker, C., Suckling, J., Deoni, S. C., Lombardo, M. V., Bullmore, E. T., Baron-Cohen, S., et al. (2012). Brain anatomy and its relationship to behavior in adults with autism spectrum disorder: a multicenter magnetic resonance imaging study. *Arch. Gen. Psychiatry* 69, 195–209. doi: 10.1001/archgenpsychiatry.2011.1251

Eckert, M. (2004). Neuroanatomical markers for dyslexia: a review of dyslexia structural imaging studies. *Neuroscientist* 10, 362–371. doi: 10.1177/1073858404263596

Eckert, M. A., Leonard, C. M., Wilke, M., Eckert, M., Richards, T., Richards, A., et al. (2005). Anatomical signatures of dyslexia in children: unique information from manual and voxel based morphometry brain measures. *Cortex* 41, 304–315. doi: 10.1016/S0010-9452(08)70268-5

Eickhoff, S. B., Bzdok, D., Laird, A. R., Kurth, F., and Fox, P. T. (2012). Activation likelihood estimation meta-analysis revisited. *Neuroimage* 59, 2349–2361. doi: 10.1016/j.neuroimage.2011.09.017

Eickhoff, S. B., Laird, A. R., Grefkes, C., Wang, L. E., Zilles, K., and Fox, P. T. (2009). Coordinate-based activation likelihood estimation meta-analysis of neuroimaging data: a random-effects approach based on empirical estimates of spatial uncertainty. *Hum. Brain Mapp.* 30, 2907–2926. doi: 10.1002/hbm.20718

Fair, D. A., Nigg, J. T., Iyer, S., Bathula, D., Mills, K. L., Dosenbach, N. U., et al. (2013). Distinct neural signatures detected for ADHD subtypes after controlling for micro-movements in resting state functional connectivity MRI data. *Front. Syst. Neurosci.* 6:80. doi: 10.3389/fnsys.2012.00080

Faraone, S. V., Perlis, R. H., Doyle, A. E., Smoller, J. W., Goralnick, J. J., Holmgren, M. A., et al. (2005). Molecular genetics of attention-deficit/hyperactivity disorder. *Biol. Psychiatry* 57, 1313–1323. doi: 10.1016/j.biopsych.2004.11.024

Franceschini, S., Gori, S., Ruffino, M., Pedrolli, K., and Facoetti, A. (2012). A causal link between visual spatial attention and reading acquisition. *Curr. Biol.* 22, 814–819. doi: 10.1016/j.cub.2012.03.013

Ghajar, J., and Ivry, R. B. (2009). The predictive brain state: asynchrony in disorders of attention? *Neuroscientist* 15, 232–242. doi: 10.1177/1073858408326429

Goldfarb, L., and Shaul, S. (2013). Abnormal attentional internetwork link in dyslexic readers. *Neuropsychology* 27, 725–729. doi: 10.1037/a0034422

Habas, C., Kamdar, N., Nguyen, D., Prater, K., Beckmann, C. F., Menon, V., et al. (2009). Distinct cerebellar contributions to intrinsic connectivity networks. *J. Neurosci.* 29, 8586–8594. doi: 10.1523/JNEUROSCI.1868-09.2009

Hoeft, F., Meyler, A., Hernandez, A., Juel, C., Taylor-Hill, H., Martindale, J. L., et al. (2007). Functional and morphometric brain dissociation between dyslexia and reading ability. *Proc. Natl. Acad. Sci. U.S.A.* 104, 4234–4239. doi: 10.1073/pnas.0609399104

Hoekzema, E., Carmona, S., Ramos-Quiroga, J. A., Barba, E., Bielsa, A., Tremols, V., et al. (2011). Training-induced neuroanatomical plasticity in ADHD: a tensor-based morphometric study. *Hum. Brain Mapp.* 32, 1741–1749. doi: 10.1002/hbm.21143

Hoekzema, E., Carmona, S., Tremols, V., Gispert, J. D., Guitart, M., Fauquet, J., et al. (2010). Enhanced neural activity in frontal and cerebellar circuits after cognitive training in children with attention-deficit/hyperactivity disorder. *Hum. Brain Mapp.* 31, 1942–1950. doi: 10.1002/hbm.20988

Hyde, K. L., Samson, F., Evans, A. C., and Mottron, L. (2010). Neuroanatomical differences in brain areas implicated in perceptual and other core features of autism revealed by cortical thickness analysis and voxel-based morphometry. *Hum. Brain Mapp.* 31, 556–566. doi: 10.1002/hbm.20887

Hynd, G. W., Semrud-Clikeman, M., Lorys, A. R., Novey, E. S., and Eliopulos, D. (1990). Brain morphology in developmental dyslexia and attention deficit disorder/hyperactivity. *Arch. Neurol.* 47, 919–926. doi: 10.1001/archneur.1990.00530080107018

Ito, M. (2008). Control of mental activities by internal models in the cerebellum. *Nat. Rev. Neurosci.* 9, 304–313. doi: 10.1038/nrn2332

Ivanov, I., Murrough, J. W., Bansal, R., Hao, X., and Peterson, B. S. (2014). Cerebellar morphology and the effects of stimulant medications in youths with attention deficit-hyperactivity disorder. *Neuropsychopharmacology* 39, 718–726. doi: 10.1038/npp.2013.257

Jednorog, K., Gawron, N., Marchewka, A., Heim, S., and Grabowska, A. (2013). Cognitive subtypes of dyslexia are characterized by distinct patterns of grey matter volume. *Brain Struct. Funct.* doi: 10.1007/s00429-013-0595-6. [Epub ahead of print].

Kasparek, T., Theiner, P., and Filova, A. (2013). Neurobiology of ADHD from childhood to adulthood: findings of imaging methods. *J. Atten. Disord.* doi: 10.1177/1087054713505322. [Epub ahead of print].

Kaufmann, W. E., Cooper, K. L., Mostofsky, S. H., Capone, G. T., Kates, W. R., Newschaffer, C. J., et al. (2003). Specificity of cerebellar vermian abnormalities in autism: a quantitative magnetic resonance imaging study. *J. Child Neurol.* 18, 463–470. doi: 10.1177/08830738030180070501

Ke, X., Hong, S., Tang, T., Zou, B., Li, H., Hang, Y., et al. (2008). Voxel-based morphometry study on brain structure in children with high-functioning autism. *Neuroreport* 19, 921–925. doi: 10.1097/WNR.0b013e328300edf3

Kemper, T. L., and Bauman, M. L. (1993). The contribution of neuropathologic studies to the understanding of autism. *Neurol. Clin.* 11, 175–187.

Kibby, M. Y., Fancher, J. B., Markanen, R., and Hynd, G. W. (2008). A quantitative magnetic resonance imaging analysis of the cerebellar deficit hypothesis of dyslexia. *J. Child Neurol.* 23, 368–380. doi: 10.1177/0883073807309235

Kibby, M. Y., Kroese, J. M., Krebbs, H., Hill, C. E., and Hynd, G. W. (2009a). The pars triangularis in dyslexia and ADHD: a comprehensive approach. *Brain Lang.* 111, 46–54. doi: 10.1016/j.bandl.2009.03.001

Kibby, M. Y., Pavawalla, S. P., Fancher, J. B., Naillon, A. J., and Hynd, G. W. (2009b). The relationship between cerebral hemisphere volume and receptive language functioning in dyslexia and attention-deficit hyperactivity disorder (ADHD). *J. Child Neurol.* 24, 438–448. doi: 10.1177/0883073808324772

Kobel, M., Bechtel, N., Specht, K., Klarhofer, M., Weber, P., Scheffler, K., et al. (2010). Structural and functional imaging approaches in attention deficit/hyperactivity disorder: does the temporal lobe play a key role? *Psychiatry Res.* 183, 230–236. doi: 10.1016/j.pscychresns.2010.03.010

Kobel, M., Bechtel, N., Weber, P., Specht, K., Klarhofer, M., Scheffler, K., et al. (2009). Effects of methylphenidate on working memory functioning in children with attention deficit/hyperactivity disorder. *Eur. J. Paediatr. Neurol.* 13, 516–523. doi: 10.1016/j.ejpn.2008.10.008

Krafnick, A. J., Flowers, D. L., Napoliello, E. M., and Eden, G. F. (2011). Gray matter volume changes following reading intervention in dyslexic children. *Neuroimage* 57, 733–741. doi: 10.1016/j.neuroimage.2010.10.062

Krienen, F. M., and Buckner, R. L. (2009). Segregated fronto-cerebellar circuits revealed by intrinsic functional connectivity. *Cereb. Cortex* 19, 2485–2497. doi: 10.1093/cercor/bhp135

Kronbichler, M., Wimmer, H., Staffen, W., Hutzler, F., Mair, A., and Ladurner, G. (2008). Developmental dyslexia: gray matter abnormalities in the occipitotemporal cortex. *Hum. Brain Mapp.* 29, 613–625. doi: 10.1002/hbm.20425

Kujala, J., Pammer, K., Cornelissen, P., Roebroeck, A., Formisano, E., and Salmelin, R. (2007). Phase coupling in a cerebro-cerebellar network at

8-13 Hz during reading. *Cereb. Cortex* 17, 1476–1485. doi: 10.1093/cercor/bhl059

Kwon, H., Ow, A. W., Pedatella, K. E., Lotspeich, L. J., and Reiss, A. L. (2004). Voxel-based morphometry elucidates structural neuroanatomy of high-functioning autism and Asperger syndrome. *Dev. Med. Child Neurol.* 46, 760–764. doi: 10.1111/j.1469-8749.2004.tb00996.x

Lancaster, J. L., Tordesillas-Gutierrez, D., Martinez, M., Salinas, F., Evans, A., Zilles, K., et al. (2007). Bias between MNI and Talairach coordinates analyzed using the ICBM-152 brain template. *Hum. Brain Mapp.* 28, 1194–1205. doi: 10.1002/hbm.20345

Leonard, C. M., Kuldau, J. M., Maron, L., Ricciuti, N., Mahoney, B., Bengtson, M., et al. (2008). Identical neural risk factors predict cognitive deficit in dyslexia and schizophrenia. *Neuropsychology* 22, 147–158. doi: 10.1037/0894-4105.22.2.147

Levinson, H. N. (1990). The diagnostic value of cerebellar-vestibular tests in detecting learning disabilities, dyslexia, and attention deficit disorder. *Percept. Mot. Skills* 71, 67–82. doi: 10.2466/pms.1990.71.1.67

Li, W., Mai, X., and Liu, C. (2014). The default mode network and social understanding of others: what do brain connectivity studies tell us. *Front. Hum. Neurosci.* 8:74. doi: 10.3389/fnhum.2014.00074

Lim, L., Marquand, A., Cubillo, A. A., Smith, A. B., Chantiluke, K., Simmons, A., et al. (2013). Disorder-specific predictive classification of adolescents with attention deficit hyperactivity disorder (ADHD) relative to autism using structural magnetic resonance imaging. *PLoS ONE* 8:e63660. doi: 10.1371/journal.pone.0063660

Limperopoulos, C., Bassan, H., Sullivan, N. R., Soul, J. S., Robertson, R. L. Jr., Moore, M., et al. (2008). Positive screening for autism in ex-preterm infants: prevalence and risk factors. *Pediatrics* 121, 758–765. doi: 10.1542/peds.2007-2158

Linkersdorfer, J., Lonnemann, J., Lindberg, S., Hasselhorn, M., and Fiebach, C. J. (2012). Grey matter alterations co-localize with functional abnormalities in developmental dyslexia: an ALE meta-analysis. *PLoS ONE* 7:e43122. doi: 10.1371/journal.pone.0043122

Mackie, S., Shaw, P., Lenroot, R., Pierson, R., Greenstein, D. K., Nugent, T. F., et al. (2007). Cerebellar development and clinical outcome in attention deficit hyperactivity disorder. *Am. J. Psychiatry* 164, 647–655. doi: 10.1176/appi.ajp.164.4.647

Makris, N., Liang, L., Biederman, J., Valera, E. M., Brown, A. B., Petty, C., et al. (2013). Toward defining the neural substrates of ADHD: a controlled structural MRI study in medication-naive adults. *J. Atten. Disord.* doi: 10.1177/1087054713506041. [Epub ahead of print].

McAlonan, G. M., Cheung, V., Cheung, C., Chua, S. E., Murphy, D. G., Suckling, J., et al. (2007). Mapping brain structure in attention deficit-hyperactivity disorder: a voxel-based MRI study of regional grey and white matter volume. *Psychiatry Res.* 154, 171–180. doi: 10.1016/j.pscychresns.2006.09.006

McAlonan, G. M., Cheung, V., Cheung, C., Suckling, J., Lam, G. Y., Tai, K. S., et al. (2005). Mapping the brain in autism: a voxel-based MRI study of volumetric differences and intercorrelations in autism. *Brain* 128, 268–276. doi: 10.1093/brain/awh332

McAlonan, G. M., Suckling, J., Wong, N., Cheung, V., Lienenkaemper, N., Cheung, C., et al. (2008). Distinct patterns of grey matter abnormality in high-functioning autism and Asperger's syndrome. *J. Child Psychol. Psychiatry* 49, 1287–1295. doi: 10.1111/j.1469-7610.2008.01933.x

Minshew, N. J., and Keller, T. A. (2010). The nature of brain dysfunction in autism: functional brain imaging studies. *Curr. Opin. Neurol.* 23, 124–130. doi: 10.1097/WCO.0b013e32833782d4

Montes, L. G., Ricardo-Garcell, J., De la Torre, L. B., Alcantara, H. P., Garcia, R. B., Acosta, D. A., et al. (2011). Cerebellar gray matter density in females with ADHD combined type: a cross-sectional voxel-based morphometry study. *J. Atten. Disord.* 15, 368–381. doi: 10.1177/1087054710366421

Mostofsky, S. H., Reiss, A. L., Lockhart, P., and Denckla, M. B. (1998). Evaluation of cerebellar size in attention-deficit hyperactivity disorder. *J. Child Neurol.* 13, 434–439. doi: 10.1177/088307389801300904

Nickl-Jockschat, T., Habel, U., Michel, T. M., Manning, J., Laird, A. R., Fox, P. T., et al. (2012). Brain structure anomalies in autism spectrum disorder–a meta-analysis of VBM studies using anatomic likelihood estimation. *Hum. Brain Mapp.* 33, 1470–1489. doi: 10.1002/hbm.21299

Nicolson, R., Fawcett, A., and Dean, P. (2001). Developmental dyslexia: the cerebellar deficit hypothesis. *Trends Neurosci.* 24, 508–511. doi: 10.1016/S0166-2236(00)01896-8

Nicolson, R. I., and Fawcett, A. J. (2007). Procedural learning difficulties: reuniting the developmental disorders? *Trends Neurosci.* 30, 135–141. doi: 10.1016/j.tins.2007.02.003

Nicolson, R. I., and Fawcett, A. J. (2011). Dyslexia, dysgraphia, procedural learning and the cerebellum. *Cortex* 47, 117–127. doi: 10.1016/j.cortex.2009.08.016

Overmeyer, S., Bullmore, E. T., Suckling, J., Simmons, A., Williams, S. C., Santosh, P. J., et al. (2001). Distributed grey and white matter deficits in hyperkinetic disorder: MRI evidence for anatomical abnormality in an attentional network. *Psychol. Med.* 31, 1425–1435. doi: 10.1017/S0033291701004706

Pernet, C. R., Poline, J. B., Demonet, J. F., and Rousselet, G. A. (2009). Brain classification reveals the right cerebellum as the best biomarker of dyslexia. *BMC Neurosci.* 10:67. doi: 10.1186/1471-2202-10-67

Rae, C., Harasty, J. A., Dzendrowskyj, T. E., Talcott, J. B., Simpson, J. M., Blamire, A. M., et al. (2002). Cerebellar morphology in developmental dyslexia. *Neuropsychologia* 40, 1285–1292. doi: 10.1016/S0028-3932(01)00216-0

Ramnani, N. (2006). The primate cortico-cerebellar system: anatomy and function. *Nat. Rev. Neurosci.* 7, 511–522. doi: 10.1038/nrn1953

Reiersen, A. M., Constantino, J. N., Volk, H. E., and Todd, R. D. (2007). Autistic traits in a population-based ADHD twin sample. *J. Child Psychol. Psychiatry* 48, 464–472. doi: 10.1111/j.1469-7610.2006.01720.x

Richlan, F. (2012). Developmental dyslexia: dysfunction of a left hemisphere reading network. *Front. Hum. Neurosci.* 6:120. doi: 10.3389/fnhum.2012.00120

Richlan, F., Kronbichler, M., and Wimmer, H. (2009). Functional abnormalities in the dyslexic brain: a quantitative meta-analysis of neuroimaging studies. *Hum. Brain Mapp.* 30, 3299–3308. doi: 10.1002/hbm.20752

Ritvo, E. R., Freeman, B. J., Scheibel, A. B., Duong, T., Robinson, H., Guthrie, D., et al. (1986). Lower Purkinje cell counts in the cerebella of four autistic subjects: initial findings of the UCLA-NSAC Autopsy Research Report. *Am. J. Psychiatry* 143, 862–866.

Riva, D., Annuziata, S., Contarino, V., Erbetta, A., Aquino, D., and Bulgheroni, S. (2013). Gray matter reduction in the vermis and CRUS-II is associated with social and interaction deficits in low-functioning children with autistic spectrum disorders: a VBM-DARTEL study. *Cerebellum* 12, 676–685. doi: 10.1007/s12311-013-0469-8

Riva, D., Bulgheroni, S., Aquino, D., Di Salle, F., Savoiardo, M., and Erbetta, A. (2011). Basal forebrain involvement in low-functioning autistic children: a voxel-based morphometry study. *AJNR Am. J. Neuroradiol.* 32, 1430–1435. doi: 10.3174/ajnr.A2527

Riva, D., and Giorgi, C. (2000). The cerebellum contributes to higher functions during development: evidence from a series of children surgically treated for posterior fossa tumours. *Brain* 123, 1051–1061. doi: 10.1093/brain/123.5.1051

Rojas, D. C., Peterson, E., Winterrowd, E., Reite, M. L., Rogers, S. J., and Tregellas, J. R. (2006). Regional gray matter volumetric changes in autism associated with social and repetitive behavior symptoms. *BMC Psychiatry* 6:56. doi: 10.1186/1471-244X-6-56

Rommelse, N. N., Franke, B., Geurts, H. M., Hartman, C. A., and Buitelaar, J. K. (2010). Shared heritability of attention-deficit/hyperactivity disorder and autism spectrum disorder. *Eur. Child Adolesc. Psychiatry* 19, 281–295. doi: 10.1007/s00787-010-0092-x

Rommelse, N. N. J., Geurts, H. M., Franke, B., Buitelaar, J. K., and Hartman, C. A. (2011). A review on cognitive and brain endophenotypes that may be common in autism spectrum disorder and attention-deficit/hyperactivity disorder and facilitate the search for pleiotropic genes. *Neurosci. Biobehav. Rev.* 35, 1363–1396. doi: 10.1016/j.neubiorev.2011.02.015

Rout, U. K., Mungan, N. K., and Dhossche, D. M. (2012). Presence of GAD65 autoantibodies in the serum of children with autism or ADHD. *Eur. Child Adolesc. Psychiatry* 21, 141–147. doi: 10.1007/s00787-012-0245-1

Salmond, C. H., Ashburner, J., Connelly, A., Friston, K. J., Gadian, D. G., and Vargha-Khadem, F. (2005). The role of the medial temporal lobe in autistic spectrum disorders. *Eur. J. Neurosci.* 22, 764–772. doi: 10.1111/j.1460-9568.2005.04217.x

Salmond, C. H., Vargha-Khadem, F., Gadian, D. G., de Haan, M., and Baldeweg, T. (2007). Heterogeneity in the patterns of neural abnormality in autistic spectrum disorders: evidence from ERP and MRI. *Cortex* 43, 686–699. doi: 10.1016/S0010-9452(08)70498-2

Sasayama, D., Hayashida, A., Yamasue, H., Harada, Y., Kaneko, T., Kasai, K., et al. (2010). Neuroanatomical correlates of attention-deficit-hyperactivity disorder accounting for comorbid oppositional defiant disorder and conduct disorder. *Psychiatry Clin. Neurosci.* 64, 394–402. doi: 10.1111/j.1440-1819.2010.02102.x

Schmitz, N., Rubia, K., Daly, E., Smith, A., Williams, S., and Murphy, D. G. (2006). Neural correlates of executive function in autistic spectrum disorders. *Biol. Psychiatry* 59, 7–16. doi: 10.1016/j.biopsych.2005.06.007

Schweren, L. J., de Zeeuw, P., and Durston, S. (2013). MR imaging of the effects of methylphenidate on brain structure and function in Attention-Deficit/Hyperactivity Disorder. *Eur. Neuropsychopharmacol.* 23, 1151–1164. doi: 10.1016/j.euroneuro.2012.10.014

Seidman, L. J., Biederman, J., Liang, L., Valera, E. M., Monuteaux, M. C., Brown, A., et al. (2011). Gray matter alterations in adults with attention-deficit/hyperactivity disorder identified by voxel based morphometry. *Biol. Psychiatry* 69, 857–866. doi: 10.1016/j.biopsych.2010.09.053

Semrud-Clikeman, M., Hooper, S. R., Hynd, G. W., Hern, K., Presley, R., and Watson, T. (1996). Prediction of group membership in developmental dyslexia, attention deficit hyperactivity disorder, and normal controls using brain morphometric analysis of magnetic resonance imaging. *Arch. Clin. Neuropsychol.* 11, 521–528. doi: 10.1093/arclin/11.6.521

Silani, G., Frith, U., Demonet, J., Fazio, F., Perani, D., Price, C., et al. (2005). Brain abnormalities underlying altered activation in dyslexia: a voxel based morphometry study. *Brain* 128, 2453–2461. doi: 10.1093/brain/awh579

Simonoff, E., Pickles, A., Charman, T., Chandler, S., Loucas, T., and Baird, G. (2008). Psychiatric disorders in children with autism spectrum disorders: prevalence, comorbidity, and associated factors in a population-derived sample. *J. Am. Acad. Child Adolesc. Psychiatry* 47, 921–929. doi: 10.1097/CHI.0b013e318179964f

Simos, P., Breier, J., Fletcher, J., Foorman, B., Bergman, E., Fishbeck, K., et al. (2000). Brain activation profiles in dyslexic children during non-word reading: a magnetic source imaging study. *Neurosci. Lett.* 290, 61–65. doi: 10.1016/S0304-3940(00)01322-7

Siok, W. T., Niu, Z., Jin, Z., Perfetti, C. A., and Tan, L. H. (2008). A structural-functional basis for dyslexia in the cortex of Chinese readers. *Proc. Natl. Acad. Sci. U.S.A.* 105, 5561–5566. doi: 10.1073/pnas.0801750105

Sivaswamy, L., Kumar, A., Rajan, D., Behen, M., Muzik, O., Chugani, D., et al. (2010). A diffusion tensor imaging study of the cerebellar pathways in children with autism spectrum disorder. *J. Child Neurol.* 25, 1223–1231. doi: 10.1177/0883073809358765

Sonuga-Barke, E., Bitsakou, P., and Thompson, M. (2010). Beyond the dual pathway model: evidence for the dissociation of timing, inhibitory, and delay-related impairments in attention-deficit/hyperactivity disorder. *J. Am. Acad. Child Adolesc. Psychiatry* 49, 345–355. doi: 10.1016/j.jaac.2009.12.018

Steinbrink, C., Vogt, K., Kastrup, A., Muller, H. P., Juengling, F. D., Kassubek, J., et al. (2008). The contribution of white and gray matter differences to developmental dyslexia: insights from DTI and VBM at 3.0 T. *Neuropsychologia* 46, 3170–3178. doi: 10.1016/j.neuropsychologia.2008.07.015

Stoodley, C. J., MacMore, J., Makris, N., Sherman, J. C., and Schmahmann, J. D. (2012a). "Preliminary voxel-based lesion-symptom mapping in cerebellar stroke patients: Motor vs. cognitive outcomes," in *Society for Neuroscience Annual Meeting* (New Orleans, LA).

Stoodley, C. J., and Schmahmann, J. D. (2009). Functional topography in the human cerebellum: a meta-analysis of neuroimaging studies. *Neuroimage* 44, 489–501. doi: 10.1016/j.neuroimage.2008.08.039

Stoodley, C. J., and Schmahmann, J. D. (2010). Evidence for topographic organization in the cerebellum of motor control versus cognitive and affective processing. *Cortex* 46, 831–844. doi: 10.1016/j.cortex.2009.11.008

Stoodley, C. J., and Stein, J. F. (2011). The cerebellum and dyslexia. *Cortex* 47, 101–116. doi: 10.1016/j.cortex.2009.10.005

Stoodley, C. J., and Stein, J. F. (2013). Cerebellar function in developmental dyslexia. *Cerebellum* 12, 267–276. doi: 10.1007/s12311-012-0407-1

Stoodley, C. J., Valera, E. M., and Schmahmann, J. D. (2012b). Functional topography of the cerebellum for motor and cognitive tasks: an fMRI study. *Neuroimage* 59, 1560–1570. doi: 10.1016/j.neuroimage.2011.08.065

Strick, P. L., Dum, R. P., and Fiez, J. A. (2009). Cerebellum and nonmotor function. *Annu. Rev. Neurosci.* 32, 413–434. doi: 10.1146/annurev.neuro.31.060407.125606

Talairach, J., and Tournoux, P. (1988). *Co-Planar Stereotaxic Atlas of the Human Brain. 3-Dimensional Proportional System: An Approach to Cerebral Imaging*. New York, NY: Thieme Medical Publishers, Inc.

Tan, G. C. Y., Doke, T. F., Ashburner, J., Wood, N. W., and Frackowiak, R. S. J. (2010). Normal variation in fronto-occipital circuitry and cerebellar structure with an autism-associated polymorphism of CNTNAP2. *Neuroimage* 53, 1030–1042. doi: 10.1016/j.neuroimage.2010.02.018

Tavano, A., Grasso, R., Gagliardi, C., Triulzi, F., Bresolin, N., Fabbro, F., et al. (2007). Disorders of cognitive and affective development in cerebellar malformations. *Brain* 130, 2646–2660. doi: 10.1093/brain/awm201

Tomasi, D., and Volkow, N. D. (2012). Abnormal functional connectivity in children with attention-deficit/hyperactivity disorder. *Biol. Psychiatry* 71, 443–450. doi: 10.1016/j.biopsych.2011.11.003

Turkeltaub, P. E., Eden, G. F., Jones, K. M., and Zeffiro, T. A. (2002). Meta-analysis of the functional neuroanatomy of single-word reading: method and validation. *Neuroimage* 16, 765–780. doi: 10.1006/nimg.2002.1131

Turkeltaub, P. E., Eickhoff, S. B., Laird, A. R., Fox, M., Wiener, M., and Fox, P. (2012). Minimizing within-experiment and within-group effects in Activation Likelihood Estimation meta-analyses. *Hum. Brain Mapp.* 33, 1–13. doi: 10.1002/hbm.21186

Valera, E., Faraone, S., Murray, K., and Seidman, L. (2007). Meta-analysis of structural imaging findings in Attention-Deficit/Hyperactivity Disorder. *Biol. Psychiatry* 61, 1361–1369. doi: 10.1016/j.biopsych.2006.06.011

Valera, E. M., Faraone, S. V., Biederman, J., Poldrack, R. A., and Seidman, L. J. (2005). Functional neuroanatomy of working memory in adults with attention-deficit/hyperactivity disorder. *Biol. Psychiatry* 57, 439–447. doi: 10.1016/j.biopsych.2004.11.034

Valera, E. M., Spencer, R. M., Zeffiro, T. A., Makris, N., Spencer, T. J., Faraone, S. V., et al. (2010). Neural substrates of impaired sensorimotor timing in adult attention-deficit/hyperactivity disorder. *Biol. Psychiatry* 68, 359–367. doi: 10.1016/j.biopsych.2010.05.012

van Ewijk, H., Heslenfeld, D. J., Zwiers, M. P., Buitelaar, J. K., and Oosterlaan, J. (2013). Diffusion tensor imaging in attention deficit/hyperactivity disorder: a systematic review and meta-analysis. *Neurosci. Biobehav. Rev.* 36, 1093–1106. doi: 10.1016/j.neubiorev.2012.01.003

van Wingen, G. A., van den Brink, W., Veltman, D. J., Schmaal, L., Dom, G., Booij, J., et al. (2013). Reduced striatal brain volumes in non-medicated adult ADHD patients with comorbid cocaine dependence. *Drug Alcohol. Depend.* 131, 198–203. doi: 10.1016/j.drugalcdep.2013.05.007

Verly, M., Verhoeven, J., Zink, I., Mantini, D., Peeters, R., Deprez, S., et al. (2014). Altered functional connectivity of the language network in ASD: role of classical language areas and cerebellum. *Neuroimage Clin.* 4, 374–382. doi: 10.1016/j.nicl.2014.01.008

Vidyasagar, T. R., and Pammer, K. (2010). Dyslexia: a deficit in visuo-spatial attention, not in phonological processing. *Trends Cogn. Sci.* 14, 57–63. doi: 10.1016/j.tics.2009.12.003

Vinckenbosch, E., Robichon, F., and Eliez, S. (2005). Gray matter alteration in dyslexia: converging evidence from volumetric and voxel-by-voxel MRI analyses. *Neuropsychologia* 43, 324–331. doi: 10.1016/j.neuropsychologia.2004.06.023

Vloet, T. D., Gilsbach, S., Neufang, S., Fink, G. R., Herpertz-Dahlmann, B., and Konrad, K. (2010). Neural mechanisms of interference control and time discrimination in attention-deficit/hyperactivity disorder. *J. Am. Acad. Child Adolesc. Psychiatry* 49, 356–367. doi: 10.1016/j.jaac.2010.01.004

Vollm, B. A., Taylor, A. N., Richardson, P., Corcoran, R., Stirling, J., McKie, S., et al. (2006). Neuronal correlates of theory of mind and empathy: a functional magnetic resonance imaging study in a nonverbal task. *Neuroimage* 29, 90–98. doi: 10.1016/j.neuroimage.2005.07.022

Vossel, S., Geng, J. J., and Fink, G. R. (2014). Dorsal and ventral attention systems: distinct neural circuits but collaborative roles. *Neuroscientist* 20, 150–159. doi: 10.1177/1073858413494269

Waiter, G. D., Williams, J. H., Murray, A. D., Gilchrist, A., Perrett, D. I., and Whiten, A. (2004). A voxel-based investigation of brain structure in male adolescents with autistic spectrum disorder. *Neuroimage* 22, 619–625. doi: 10.1016/j.neuroimage.2004.02.029

Willcutt, E. G., Betjemann, R. S., McGrath, L. M., Chhabildas, N. A., Olson, R. K., DeFries, J. C., et al. (2010). Etiology and neuropsychology of comorbidity between RD and ADHD: the case for multiple-deficit models. *Cortex* 46, 1345–1361. doi: 10.1016/j.cortex.2010.06.009

Wilson, L. B., Tregellas, J. R., Hagerman, R. J., Rogers, S. J., and Rojas, D. C. (2009). A voxel-based morphometry comparison of regional gray matter between fragile X syndrome and autism. *Psychiatry Res.* 174, 138–145. doi: 10.1016/j.pscychresns.2009.04.013

Wolf, R. C., Plichta, M. M., Sambataro, F., Fallgatter, A. J., Jacob, C., Lesch, K. P., et al. (2009). Regional brain activation changes and abnormal functional

connectivity of the ventrolateral prefrontal cortex during working memory processing in adults with attention-deficit/hyperactivity disorder. *Hum. Brain Mapp.* 30, 2252–2266. doi: 10.1002/hbm.20665

Yang, P., Wang, P. N., Chuang, K. H., Jong, Y. J., Chao, T. C., and Wu, M. T. (2008). Absence of gender effect on children with attention-deficit/hyperactivity disorder as assessed by optimized voxel-based morphometry. *Psychiatry Res.* 164, 245–253. doi: 10.1016/j.pscychresns.2007.12.013

Yeo, B. T., Krienen, F. M., Sepulcre, J., Sabuncu, M. R., Lashkari, D., Hollinshead, M., et al. (2011). The organization of the human cerebral cortex estimated by intrinsic functional connectivity. *J. Neurophysiol.* 106, 1125–1165. doi: 10.1152/jn.00338.2011

Yu, K. K., Cheung, C., Chua, S. E., and McAlonan, G. M. (2011). Can Asperger syndrome be distinguished from autism? An anatomic likelihood meta-analysis of MRI studies. *J. Psychiatry Neurosci.* 36, 412–421. doi: 10.1503/jpn.100138

Yun, H. S., Park, M. S., Ji, E. S., Kim, T. W., Ko, I. G., Kim, H. B., et al. (2014). Treadmill exercise ameliorates symptoms of attention deficit/hyperactivity disorder through reducing Purkinje cell loss and astrocytic reaction in spontaneous hypertensive rats. *J. Exerc. Rehabil.* 28, 22–30. doi: 10.12965/jer.140092

Zatorre, R. J., Fields, R. D., and Johansen-Berg, H. (2012). Plasticity in gray and white: neuroimaging changes in brain structure during learning. *Nat. Neurosci.* 15, 528–536. doi: 10.1038/nn.3045

Conflict of Interest Statement: The author declares that the research was conducted in the absence of any commercial or financial relationships that could be construed as a potential conflict of interest.

Received: 25 March 2014; accepted: 30 April 2014; published online: 20 May 2014.
Citation: Stoodley CJ (2014) Distinct regions of the cerebellum show gray matter decreases in autism, ADHD, and developmental dyslexia. Front. Syst. Neurosci. ***8****:92. doi: 10.3389/fnsys.2014.00092*
This article was submitted to the journal Frontiers in Systems Neuroscience.

frontiers in
SYSTEMS NEUROSCIENCE

METHODS ARTICLE
published: 26 June 2014
doi: 10.3389/fnsys.2014.00106

Preserving subject variability in group fMRI analysis: performance evaluation of GICA vs. IVA

Andrew M. Michael[1,2]*, Mathew Anderson[3], Robyn L. Miller[2], Tülay Adali[3] and Vince D. Calhoun[2,4]

[1] Autism and Developmental Medicine Institute, Geisinger Health System, Danville, PA, USA
[2] The Mind Research Network and LBERI, Albuquerque, NM, USA
[3] Department of Computer Science and Electrical Engineering, University of Maryland, Baltimore, MD, USA
[4] Department of Electrical and Computer Engineering, University of New Mexico, Albuquerque, NM, USA

Edited by:
Stella Koutsikou, University of Bristol, UK

Reviewed by:
Maarten De Vos, Oldenburg University, Germany
Kewei Chen, Banner Alzheimer's Institute, USA

***Correspondence:**
Andrew M. Michael, The Mind Research Network, 1101 Yale Blvd NE, Albuquerque, NM 87106, USA
e-mail: andru4u@gmail.com

Independent component analysis (ICA) is a widely applied technique to derive functionally connected brain networks from fMRI data. Group ICA (GICA) and Independent Vector Analysis (IVA) are extensions of ICA that enable users to perform group fMRI analyses; however a full comparison of the performance limits of GICA and IVA has not been investigated. Recent interest in resting state fMRI data with potentially higher degree of subject variability makes the evaluation of the above techniques important. In this paper we compare component estimation accuracies of GICA and an improved version of IVA using simulated fMRI datasets. We systematically change the degree of inter-subject spatial variability of components and evaluate estimation accuracy over all spatial maps (SMs) and time courses (TCs) of the decomposition. Our results indicate the following: (1) at low levels of SM variability or when just one SM is varied, both GICA and IVA perform well, (2) at higher levels of SM variability or when more than one SMs are varied, IVA continues to perform well but GICA yields SM estimates that are composites of other SMs with errors in TCs, (3) both GICA and IVA remove spatial correlations of overlapping SMs and introduce artificial correlations in their TCs, (4) if number of SMs is over estimated, IVA continues to perform well but GICA introduces artifacts in the varying and extra SMs with artificial correlations in the TCs of extra components, and (5) in the absence or presence of SMs unique to one subject, GICA produces errors in TCs and IVA estimates are accurate. In summary, our simulation experiments (both simplistic and realistic) and our holistic analyses approach indicate that IVA produces results that are closer to ground truth and thereby better preserves subject variability. The improved version of IVA is now packaged into the GIFT toolbox (http://mialab.mrn.org/software/gift).

Keywords: fMRI, group ICA method, brain network analysis, functional connectivity, independent vector analysis

INTRODUCTION

Investigating macro-level brain circuitry using functional magnetic resonance imaging (fMRI) is of great interest to the neuroimaging community. Functional brain connectivity maps are widely used to investigate healthy and diseased populations in order to identify aberrant networks patterns (Garrity et al., 2007; Greicius, 2008; Bassett and Bullmore, 2009). Recently there has been increased interest to identify brain networks of resting state fMRI (rsMRI); data acquired while a subject is not performing a particular task. Approaches used to analyze resting state data include seed-based correlation analyses (Cohen et al., 2008) and data-driven approaches such as independent component analysis (ICA) (McKeown et al., 1998). ICA can identify multiple coherent networks without the need for an *a priori* seed voxel, region of interest or model timecourse. Group ICA (GICA), a framework that includes ICA, is widely applied to group fMRI data (Calhoun et al., 2001; Calhoun and Adali, 2012). GICA provides a solution to the problem of permutation ambiguity of ICA by matching components across subjects; first estimating the group level components and then estimating single subject spatial maps (SM) and time courses (TC). GICA makes no assumption about the temporal consistency across subjects but does assume spatial stationarity. It can capture inter-subject spatial variability, but there are limits (Allen et al., 2012). Independent vector analysis (IVA), a multivariate extension of ICA, was introduced by Lee et al. as an alternate way of performing group fMRI analyses while avoiding the permutation ambiguity of ICA (Lee et al., 2007, 2008). Lee et al. indicated through their simplistic experiments that IVA can better capture subject variability; however, a full comparison of the limits of both GICA and IVA was not performed. In this paper, we compare component estimation accuracies of GICA and IVA using simulated fMRI data under varying types and degrees of inter-subject spatial variability. In addition we find several important characteristics of both methods and make recommendations to users. FMRI data were simulated using SimTB (http://mialab.mrn.org/software/), a recently developed toolbox that generates data under the spatio-temporal assumption of ICA and IVA (Erhardt et al., 2012).

Changes in brain morphology between subjects and even within the same subject over time are well reported (Giedd et al.,

1999). Variability among subjects in functional brain network patterns (distinct from anatomic patterns) was recently shown in Khullar et al. (2011). Spatial and temporal differences across subjects can exist in fMRI networks especially in resting state studies where subjects do not follow an assigned task. Effectively preserving subject specific activation patterns is critical to identify differences and potential biomarkers in patient populations. Subject variability in functional activity can occur in the amplitude of activation, spatial location/extent of activation and temporal variations. In the ICA/IVA domain, subject variability can be measured in terms of variations in the SMs and TCs.

ICA can be successfully applied to separate statistically independent SMs from fMRI data. ICA is particularly useful since *a priori* knowledge of these sources is not required. In the application of ICA to fMRI data, ICA assumes that the fMRI data is a linear mixture of SMs and TCs and decomposes the fMRI data to find temporally coherent SMs that are spatially independent (statistically). Application of ICA to individual subject fMRI data is relatively straightforward. FMRI data is separated into a user specified number of SMs and their corresponding TCs. When ICA is applied separately to multiple subjects on an individual basis, comparing SMs across subjects to make group level inferences becomes challenging due to inter-subject spatial variability of SMs. With such spatial variability, especially when the number of SMs is high, it is not easy to cluster similar SMs across subjects to perform statistical analyses at the group level. GICA provides a way to address this problem by estimating a decomposition from all subjects' data (Calhoun et al., 2001). In GICA subject data are first temporally concatenated, followed by a group level PCA reduction, and then application of ICA yielding group level components. Finally, a back-reconstruction step is applied to make subject specific SMs and TCs (Erhardt et al., 2011). The GICA framework has been applied extensively across many studies, in both healthy and patient populations, to make inferences about intrinsic networks (Sorg et al., 2007; Calhoun et al., 2009; Allen et al., 2011).

IVA was first introduced as a blind source separation technique to separate time delayed and convolved signals using higher order frequency dependencies. IVA uses a multivariate extension of the mutual information cost function used in ICA (Lee et al., 2007). In the original IVA application the source signal was made independent within each frequency bin while enforcing higher order dependencies across frequency bins. In a previous study IVA was applied to multi-subject fMRI data to construct individual SMs and TCs (Lee et al., 2008). In GICA the input matrix is the PCA reduced two dimensional group matrix, in contrast, in IVA subject data are not mixed together but kept separate along the 3rd dimension of the input matrix. IVA maximizes an objective function that considers both the independence of within subject SMs and the dependence of similar SMs across subjects. With this strategy the back reconstruction step needed in GICA to estimate subject specific SMs is avoided. Further, since IVA accounts for the dependence of similar components, component ordering across subjects is preserved making group analyses across subjects straightforward.

Studies have investigated the performance of GICA (Allen et al., 2012) and IVA (Lee et al., 2008). In Lee et al. (2008) a two trial based simulated dataset was used to test the performance of ICA and IVA under slight inter-subject variability and noise levels. Results of their experiment showed that, compared to GICA, IVA captured inter-subject variability better. Most of their results compare estimations from real fMRI data using GLM, GICA, and IVA. Although marginal variability to subject TCs and SMs were added to the task-related data, they did not evaluate the performance of IVA at high variability of SMs and TCs. Resting state fMRI data do not follow a task like TC and its activation patterns can have significant inter-subject variability.

Recent improvements (IVA-GL) have been made to the IVA algorithm to achieve reliable source separation for linearly dependent Gaussian and non-Gaussian sources and extend the application of IVA to separate sources with linear dependence (Anderson et al., 2010). In Dea et al. (2011) realistic fMRI datasets were simulated using SimTB to investigate the performance of two different IVA approaches, IVA-GL and IVA-GJD (Li et al., 2011). In Ma et al. (2013) it was shown that performance of IVA in capturing group difference improved as group variability increased and that GICA performed better at low variability. Using mutual information as a metric, they showed that the IVA algorithm outperforms GICA in capturing spatial inter-subject variability. The initial results of the above studies provide evidence that IVA can provide improved component estimations in datasets where there is SM variability. However, these studies did not evaluate the performance of GICA and IVA under different degrees of subject variability and other estimation parameters.

In this paper, we compare SM and TC estimation accuracies of GICA vs. IVA under spatial variation of SMs between subjects. In addition to comparing estimation accuracies of the component that is varied between subjects, we also inspect changes in all other components of the decomposition. In other words, we investigate all elements of the cross correlation matrices between the ground truth components (GND) and reconstructed or estimated components (EST) of all SMs and TCs. In our initial experiments (*Experiments 1–3*), we select a lower number of subjects and components to make result presentation easier. In *Experiment 4* we repeat with a larger number of subjects and components. We simulate several scenarios of inter-subject variability; *Experiment 1:* SM amplitude at different noise levels, *Experiment 2:* different types of spatial variability (translation, rotation, and size) in one SM, *Experiment 3:* combinations of different types of variability in two SMs, *Experiment 4:* all SMs in all subjects have a combination of spatial variability. Under each experiment, we perform several sub–experiments to address effects of different degrees of variability, slight spatial overlap of SMs, effects of overestimation of component, effects of presence or absence of components, effects of different noise levels and other variations.

METHODS

GICA vs. IVA

Main steps of GICA and IVA while applying these techniques to perform group analysis of fMRI data are briefly presented in this section.

Definitions of main notations used:

M: Total number of subjects in the group

V: Total number of in-brain voxels, V is common to all M subjects

T: Number of time points in the fMRI data, T is common to all M subjects

C: Number of spatially independent components (user defined parameter), C is common to all M subjects

$\mathbf{Y}_i$ $[T \times V]$: fMRI data matrix from the i^{th} subject, $i = 1$ to M. $\mathbf{Y}_i$ is formed after the three dimensional brain voxels are stacked along the columns of $\mathbf{Y}_i$ and time points along the rows

$\mathbf{X}$: Input matrix to ICA/IVA algorithm. For ICA dimensions of $\mathbf{X}$ are $[C \times V]$, for IVA dimensions of $\mathbf{X}$ are $[C \times V \times M]$.

$\dot{\mathbf{S}}_i$ $[C \times V]$: Contains the i^{th} subject's C independent spatial maps (SMs) estimated by the algorithm

$\dot{\mathbf{R}}_i$ $[T \times C]$: Contains the i^{th} subject's C independent timecourses (TCs) corresponding to the SMs

Main steps of Group GICA (see **Figure 1**).

(1) *Subject level principal component analysis (PCA):* Each subject's data matrix $(\mathbf{Y}_i)$ $[T \times V]$ is reduced along the time domain to retain T_1 principal components, where $T_1 < T$. Let $\mathbf{Y}_i^*$ $[T_1 \times V]$ be the subject level PCA reduced matrix of the i^{th} subject.

(2) *Temporal concatenation of subject data:* PCA reduced subject matrices $(\mathbf{Y}_i^*)$ are concatenated along the temporal domain (rows) to form the group fMRI matrix $\mathbf{Y}^* = \left[\mathbf{Y}_1^{*T}, \mathbf{Y}_2^{*T}, \ldots \mathbf{Y}_M^{*T}\right]^T$ of size $[MT_1 \times V]$.

(3) *Group level PCA:* Perform PCA reduction on the $\mathbf{Y}^*$ matrix and retain C principal components. Let $\mathbf{X}$ $[C \times V]$ be the group level PCA reduced matrix.

(4) *Independent Component Analysis (ICA):* Perform spatial ICA on the $\mathbf{X}$ matrix to decompose $\mathbf{X}$ into group level SMs given by $\mathbf{X} = \mathbf{AS}$, where $\mathbf{A}$ $[C \times C]$ is related to component TCs and $\mathbf{S}$ $[C \times V]$ contains group level SMs.

(5) *Subject level back-reconstruction:* There are several methods to back-project group level maps to subject data to obtain subject specific SMs $(\dot{\mathbf{S}}_i)$ and TCs $(\dot{\mathbf{R}}_i)$, as described in Erhardt et al. (2011) for a detailed explanation of the different techniques. In this work we used the spatio-temporal regression (STR) method to back-reconstruct subject specific SMs and TCs. $\dot{\mathbf{R}}_i$ is given by $\dot{\mathbf{R}}_i = \mathbf{Y}_i\mathbf{S}^-$, and $\dot{\mathbf{S}}_i = \dot{\mathbf{R}}_i^-\mathbf{Y}_i$ where $\mathbf{S}^-$ and $\dot{\mathbf{R}}_i^-$ are the pseudo-inverses of $\mathbf{S}$ and $\dot{\mathbf{R}}_i$, respectively.

Main steps of IVA (see **Figure 1**).

(1) *Subject level PCA*: As in GICA, each subject's data matrix $(\mathbf{Y}_i)$ $[T \times V]$ is reduced in the time domain to compute $\mathbf{Y}_i^*$ $[C \times V]$, where C is the number of desired components.

(2) *Concatenation of subject data*: Unlike in GICA, in IVA subject data are concatenated along the third dimension to form the $\mathbf{X}$ matrix of dimension $[C \times V \times M]$.

(3) *Independent Vector Analysis (IVA)*: Perform IVA on the $\mathbf{X}$ matrix. In IVA, the decomposition is performed on the three-dimensional $\mathbf{X}$ matrix while keeping each subject's SMs and mixing matrices unmixed between subjects. The decomposition yields three dimensional matrices given by $\mathbf{X}_i = \mathbf{A}_i\mathbf{S}_i$, where $i = 1$ to M and denotes the i^{th} subject (in third dimension).

(4) *Subject Maps and time courses:* In IVA reconstruction of subject level SMs and TCs are straightforward as each subject's data is in its own space stacked along the third dimension of the matrices. Subject specific spatial map $\dot{\mathbf{S}}_i$ is given by $\dot{\mathbf{S}}_i = \mathbf{A}_i^{-1}\mathbf{X}_i$ and the subject specific timecourse is given by $\dot{\mathbf{R}}_i = \mathbf{Y}_i\dot{\mathbf{S}}_i^-$.

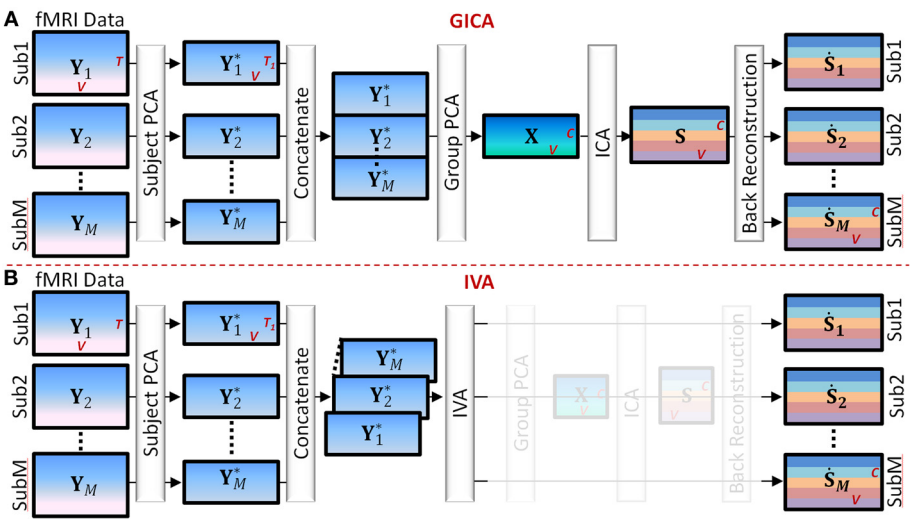

FIGURE 1 | Main Steps of GICA and IVA (see Section GICA vs. IVA for more details). (A) GICA: (i) subject level principal component analysis (PCA) on each subject's fMRI data $(\mathbf{Y_i})$ of size time points (T) by voxels (V) results in matrices $(\mathbf{Y_i^*})$ of size T_1 by V, T_1 is a user specified number, (ii) concatenate $\mathbf{Y_i^*}$ along the time domain, (iii) apply group PCA on the concatenated group matrix to get matrix $\mathbf{X}$ of size C by V, where C is a user specified number, (iv) apply independent component analysis (ICA) on $\mathbf{X}$ to obtain group level spatial maps (SMs) and time courses (TCs) and (v) apply a back reconstruction method to obtain subject specific SMs and TCs. **(B)** IVA: (i) same as GICA, (ii) concatenate $\mathbf{Y_i^*}$ along the 3rd dimension keeping each subject's data separate, (iii) apply IVA to obtain subject specific SMs and TCs.

SIMULATION SETUP

We used SimTB (Erhardt et al., 2012), a MATLAB toolbox available at (http://mialab.mrn.org/software/simtb/index.html), to simulate fMRI datasets. SimTB was designed to generate fMRI datasets under the assumption of spatiotemporal separability of the fMRI data. In other words it is assumed that the fMRI data can be given as a product of spatial and temporal processes (product of SMs and TCs). In SimTB the user defines the number of SMs and selects them from a predesigned set. The TCs of SMs were generated from a zero mean unit variance normal distribution. To create different types of fMRI datasets we changed the following: SM amplitude (or percentage signal change), baseline intensity, noise, spatial variability of SMs (translation, rotation, size) and varied TCs for each component and subject. The SMs were represented as 2D axial images of size 100×100 voxels. We reduced the number of voxels in the SMs (compared to real fMRI) to increase the speed of dataset generation, GICA/IVA decomposition and to reduce the hard disk space needed as a very large number of fMRI datasets were simulated in this study.

In order to better grasp the functionalities of the algorithms, for *Experiments 1–3*, we use a lower number of subjects and components with the following simulation parameters and for *Experiment 4* we use a larger number of subjects and components (*Experiment 4* numbers are presented below within parenthesis).

Number of subjects in the group, $M = 5$ (20)

Size of image slice = 100×100 voxels, number of in-brain voxels (V) = 7688

Number of time points, $T = 150$

Number of SMs in the data, $C = 6$ (15)

GND: Ground truth component

EST: Estimated or reconstructed component

Subi: *ith* Subject

SMj: *jth* SM

TCj: *jth* TC

Main Steps of data simulation, component estimation, and result comparison:

(1) *Simulate fMRI dataset:* In addition to the above parameters the following can be changed in SimTB: SM sources and their presence in subjects, SM translation in voxels, SM rotation in degrees, SM spread (size), baseline signal intensity, SM signal amplitude, and contrast to noise ratio (CNR). SimTB simulates fMRI datasets with the following main steps, for a detailed description of each of these steps refer to Erhardt et al. (2012)

   (i) TC *generation*: in our experiments, all TCs are generated as a random time series with an additional constraint of near zero correlation between the TCs of a subject. With this constraint we allow maximum variability in the time domain to make the evaluation of spatial variability as the main focus of our project.

   (ii) SM *generation*: SMs are generated as activation blobs defined by 2D Gaussian distributions with varying spatial characteristics (translations, rotations, size etc).

   (iii) *Make baseline intensity*: for each subject a variable baseline intensity map is computed, voxels outside the brain mask are set to zero.

   (iv) *Scale* SMs: SMs are scaled according to the percentage signal changes. Percentage signal changes are defined as the peak-to-peak signal change relative to the baseline. Varying percentage signal change values can be assigned to each component and subject.

   (v) *Mix* SMs *with* TCs: SMs and TCs are linearly combined as the matrix product and then each subject's baseline frame is added.

   (vi) *Add noise*: Rician noise is added to the data according to the CNR values assigned to each subject.

(2) *GICA/IVA Decomposition*: Simulated fMRI datasets of the M subjects are fed into the GICA and IVA algorithms separately to reconstruct SMs and TCs. We briefly describe the steps involved in the decomposition and the parameters used for estimation.

   (i) *Subject level PCA*: In this project, the actual number of components in the dataset are known and since the main focus is on analyzing the impact of subject variability, we reduce each subject's data to the actual number of components in the simulated data set, that is $T_1 = C$.

   (ii) *Group level PCA for ICA:* Here again we reduce the temporally concatenated group dataset to C number of principal components (except *Experiments 2h and 4c* where we perform overestimation). In real applications there are ways to estimate the number of components using methods such as minimum description length (Wax and Kailath, 1985; Li et al., 2007).

   (iii) *Component Estimation:* For ICA we feed the two dimensional $\mathbf{X}$ matrix (group level PCA reduced whitened matrix) to the *Infomax* algorithm (Bell and Sejnowski, 1995). For IVA we first feed in the three dimensional $\mathbf{X}$ matrix (subject level PCA reduced whitened matrix) to the second order IVA-GL algorithm (Anderson et al., 2010) to obtain a set of unmixing matrices. We re-run the data with the original IVA algorithm (Lee et al., 2007) where we initialize the unmixing matrix with the results obtained from IVA-GL. Default values set by the original GICA and IVA designers were used for parameters such as learning rate, maximum number of iterations and terminations threshold.

(3) *Component Scaling and Sorting*: In GICA and IVA decompositions have scaling and sign ambiguity (the amplitude and sign of the SMs and TCs can be scaled provided that the product of the scaling factors is unity). The amplitude or the sign of the components do not convey useful information by themselves. The signs of each SM and the corresponding TC were flipped based on the skewness of the SM. If the skewness of the SM was less than zero the signs of both SM and TC were flipped (multiplied by negative one). In an effort to display all recovered SMs in a consistent manner, we scaled all the SMs to values between negative one and positive one. TCs were z-scored, to have zero mean and unit variance.

Reconstructed components were matched with GND, based on the spatial cross correlation matrix between the GND and estimated (EST) SMs. Component pairing is made based on the descending order of the GND–EST correlations using a greedy algorithm where once an EST SM is paired with a GND SM, that SM is not selected again to pair up with another GND. The component sorting scheme used is an important step in the performance evaluation of the ICA/IVA algorithms. At higher subject variability, the EST SMs can be a mixture of GND SMs with significant correlations with more than one GND SM.

SIMULATION EXPERIMENT SETUP

To isolate the effect of spatial overlap, in most of our experiments SMs were chosen such that even after adding spatial variability there was no spatial overlap between SMs. For *Experiments 1–3* we simulated data for 5 subjects with 6 components each (SMs and TCs for Sub1 is shown in **Figure 2**). For *Experiment 4* 20 subjects with 15 components each (SMs are presented in Supplementary Figure 1) were simulated.

Experiment 1 (change in amplitude)

The spatial locations of the components are kept constant across subjects, but the amplitude of the components is varied across subjects. This experiment was designed to test whether subject variability in component amplitude introduces errors in the estimated SMs and TCs. We also checked if variability in component amplitude (Amp_{GND}) was preserved in the estimated components. The component amplitude of the estimated components (Amp_{EST}) were calculated as the product of the standard deviation of the TC (σ_{TC}) and the maximum intensity of SM (max_{SM}), a metric introduced by Allen et al. (2012). Amp_{EST} calculations were made before we scaled the SMs between negative and positive one.

Experiment 2 (spatial change in one component)

In this experiment, we introduce different types of inter-subject spatial variability in just one of the six SMs. We check how estimation errors change as spatial variability increases.

Experiment 2a (vertical translation of SM1)

We translate SM1 (see **Figure 2A**) in the vertical direction between zero and $\triangle d_{max}$ number of voxels. SM1 of Sub1 is shifted by zero voxels (no translation), in Sub5 SM1 is shifted by $\triangle d_{max}$ voxels and in Sub2–Sub4 SM1 is shifted by $\triangle d$ voxels relative to the previous subject, where $\triangle d = \triangle d_{max}/M$, $M = 5$ (number of subjects). We then repeat this test five times for incrementing values of $\triangle d_{max}$. The full width half max (FWHM) of SM1 is approximately equal to 10 voxels and $\triangle d_{max}$ was incremented as a multiple of the FWHM of SM1. In the first test $\triangle d_{max}$ was set to 5 voxels (or 0.5 FWHM) and for tests thereafter we incremented $\triangle d_{max}$ by 5 voxels.

Experiment 2b (spatial extent or size of SM2)

The size of SM1 was set to 0.1 for Sub1, $\triangle s_{max}$ for Sub5 and at increments of $\triangle s = \triangle s_{max}/M$ for Sub2–Sub4. This test was repeated five times at five different values of $\triangle s_{max}$, from 0.4 to 2.0 at intervals of 0.4. When $\triangle s$ is increased from 0.1 to 0.4 the size of SM2 is approximately doubled.

Experiment 2c: (Rotation of SM3)

In this sub-experiment we set the orientation of SM3 for Sub1 at 0°, Sub5 at $\triangle\theta_{max}$ and at increments of $\triangle\theta = \triangle\theta_{max}/M$ for Sub2–4. This test was repeated five times for five different values $\triangle\theta_{max}$ from 36 to 180° at intervals of 36°.

Experiment 2d (horizontal separation of SM5)

The horizontal separation between the two blobs of SM5 is varied. The FWHM of SM5 is approximately equal to 5 voxels and $\triangle d_{max}$ was incremented as a multiple of the FWHM of SM5 (from FWHM = 1 to 5).

Experiment 2e (component overlap)

The goal of this experiment is to check the effects of slight spatial overlap between SMs; this experiment is a continuation of *Experiment 2a*. Here we vertically translate SM1 across subjects. Here we set $\triangle d_{max}$ to 35 voxels. At this value of $\triangle d_{max}$, SM1 marginally overlaps with SM4 for Sub5 as shown in **Figure 4A**.

Experiment 2f (over estimation of model order)

In experiments 2a–2h the model order of the estimation was exactly matched with the actual number of components in the ground truth data. In this experiment, we test the effect of subject variability if the model order is over estimated. We repeat *Experiment 2a* (with $\triangle d_{max} = 25$ voxels and $C = 6$ ground truth components) with 9 estimated components.

Experiment 2g (missing components)

We perform this experiment in two parts: (i) all 5 subjects have all 6 components except Sub1 where SM1 is not present. (ii) SM1 is present in Sub1 but absent in all other subjects.

Experiment 3 (spatial change in two components)

The purpose of this set of experiments was to check how spatial variation in two components changed estimation accuracy.

Experiment 3a (vertical translation of SM1 and size change of SM2)

This experiment is essentially several experiments of *Experiment 2b* nested within *Experiment 2a.*

Experiment 3b (vertical translation of SM1 and rotation of SM3)

This experiment is essentially several experiments of *Experiment 2c* nested within *Experiment 2a.*

Experiment 3c (vertical translation of SM1 and horizontal separation of SM5)

This experiment is essentially several experiments of *Experiment 2d* nested within *Experiment 2a.*

Experiment 4 (spatial variability in all components)

For this experiment we increased the number of subjects to $M = 20$ and the number of components to $C = 15$. We made this to roughly replicate the application of GICA or IVA to a real fMRI study. Here all components in all subjects undergo all forms of spatial variations as introduced in *Experiment 2.*

Experiment 4a (spatial variability with uniform distribution)

In this sub-experiment the degree of variability is picked from a uniform distribution, $U(a, b)$, where a and b are varied depending on the type of spatial variability. For SM translations $a = -2k$ and $b = 2k$ (in voxels), for component rotation $a = -10k$ and $b = 10k$ (in degrees) and for component size $a = 1 - 0.2k$ and $b = 1 + 2k$, where k is an integer from 1 to 5. A higher k-value corresponds to increased subject variability.

Experiment 4b (spatial variability with normal distribution)

Exact repetition of *Experiment 4a*, with degree of variability drawn from a normal distribution, $N(\mu, \sigma)$ where μ and σ are the mean and standard deviation of the distribution. The mean values in all variability distributions were kept at zero except for size where the mean value was maintained at one. At each value of k the standard deviation of the spatial variability for this experiment and *4a* were kept constant.

Experiment 4c (model order over estimation)

We repeat *Experiment 4a* applying spatial variability using $k = 2$ and at each iteration we increase the model order by 5 components from $C = 15$ (actual number of components) to $C = 35$.

Experiment 4d (estimation at high noise level)

We repeat Experiment 4a for a range of *CNRs*; $CNR = 0.5$ to $CNR = 0.1$ at $k = 2$.

DEFINITION OF RESULT EVALUATION PARAMETERS

We use correlation as the primary metric to compare similarity between GND and EST. Let $\mathbf{R}_i^{\mathbf{G}}$, $\mathbf{R}_i^{\mathbf{C}}$, $\mathbf{R}_i^{\mathbf{V}}$ of size $[C \times C]$ be the GND–GND, GND–GICA, and GND–IVA correlation matrices respectively for the *ith* subject. There will be two types of correlation matrices: one from SM and the other from TC. Let $r_{i,l,m}^{C}$ be the correlation between the *lth* GND component and *mth* GICA component for the *ith* subject. Let $r_{i,l,m}^{V}$ be the same for IVA. We define the correlation error matrices as the absolute value of the difference between the GND–GND correlations and GND–EST correlations. For GICA let $\mathbf{E}_i^{\mathbf{C}} = abs\left(\mathbf{R}_i^{\mathbf{G}} - \mathbf{R}_i^{\mathbf{C}}\right)$ and for IVA $\mathbf{E}_i^{\mathbf{V}} = abs\left(\mathbf{R}_i^{\mathbf{G}} - \mathbf{R}_i^{\mathbf{V}}\right)$. We define $\overline{\mathbf{E}}^{\mathbf{C}}$ as the mean of $\mathbf{E}_i^{\mathbf{C}}$ across all subjects, similarly $\overline{\mathbf{E}}^{\mathbf{V}}$ for IVA. To get a better handle on the performance of the algorithms, we report the averages and standard deviations of the diagonal and the non-diagonal elements of the error matrices separately. Let $\mu_i^{d,C} = mean\left(diagonal\left(\mathbf{E}_i^{C}\right)\right)$ and $\mu_i^{n,C} = mean\left(nondiagonal\left(\mathbf{E}_i^{\mathbf{C}}\right)\right)$ be the *ith* subject's mean value of the diagonal and non-diagonal elements of $\mathbf{E}_i^{\mathbf{C}}$ and for $\mathbf{E}_i^{\mathbf{V}}$ as $\mu_i^{d,V}$ and $\mu_i^{n,V}$. Let the standard deviations of correlation errors be $\sigma_i^{d,C}$, $\sigma_i^{n,C}$, $\sigma_i^{d,V}$, and $\sigma_i^{n,V}$. In experiments where we check correlation errors across different degrees of spatial variability (*Experiment 2–4*), we report the overall mean correlation error across all subjects and all components and this we denote by $\mu_{all}^{d,C}$ and $\mu_{all}^{n,C}$ for mean diagonal and non-diagonal errors, respectively, across all subjects for GICA similarly by $\mu_{all}^{d,V}$ and $\mu_{all}^{n,V}$ for IVA. For standard deviations the following parameters will be used: $\sigma_{all}^{d,C}$, $\sigma_{all}^{n,C}$, $\sigma_{all}^{d,V}$, and $\sigma_{all}^{n,V}$.

RESULTS

EXPERIMENT 1: VARIATION IN COMPONENT AMPLITUDE

The simulation results of this experiment are presented in **Figure 2**: where Sub1's ground truth (GND) SMs is in 1st row, GICA SMs in 2nd row and IVA SMs in 3rd row. Both GICA and IVA performed near perfect reconstruction of all the SMs. In **Figure 2B**, the GND TC is presented in black ink and the errors between GND and GICA in blue and GND and IVA in red. TC error for Sub1 was close to zero in both GICA and IVA. All other subjects' SMs and TCs were very similar to Sub1's maps shown in **Figures 1A,B**; due to space limitations we do not present them here.

Correlation between GND SM and GICA SM were higher than 0.999 for all SMs and all subjects. TC correlations between GND and GICA reconstructions were upwards of 0.999 for all component TCs and subjects. Our results indicate that SMs (and TCs) were very well estimated irrespective of variability in their amplitude.

IVA estimates of SMs and TCs were also very close to GND, but the components were less clean than the GICA estimates. As seen in **Figure 2A** (3rd row) the IVA SMs had minor artifacts from other components. Correlations between the GND and IVA SMs were upwards of 0.991 for all components and subjects. Correlation between GND and IVA TCs were above 0.997.

In **Figure 2E**, we plot the product of the standard deviation of the TC (σ_{TC}) and the maximum intensity of SM (max_{SM}) vs. the component amplitude. Both methods' estimates had generally a linear association between GND amplitudes (Amp_{GND}) and estimated amplitudes (Amp_{EST}).

EXPERIMENT 2: SPATIAL VARIATION IN ONE COMPONENT

Results of this experiment are presented in **Figure 3**. The maximum degree of spatial variation ($\triangle d_{max}$, $\triangle s_{max}$, and $\triangle \theta_{max}$) are along the x-axis and the mean correlation error across all subjects and components ($\mu_{all}^{d,C}$, $\mu_{all}^{n,C}$, $\mu_{all}^{d,V}$, and $\mu_{all}^{n,V}$), are along y-axis The error bars correspond to the standard deviation of the errors ($\sigma_{all}^{d,C}$, $\sigma_{all}^{n,C}$, $\sigma_{all}^{d,V}$, and $\sigma_{all}^{n,V}$). Only the lower bounds of the error bars are presented to provide more resolution to smaller errors in the plot.

Experiment 2a (vertical translation of SM1, see Figure 3A)

All mean errors were less than 4.5×10^{-3} for both GICA and IVA. The mean error of the non-diagonal elements for both SM and TC gradually increased in GICA (from $\sim 2 \times 10^{-3}$ to $\sim 3 \times 10^{-3}$) with increase in $\triangle d_{max}$. In IVA, although the errors were higher than GICA, we did not observe this trend of gradual increase in error with an increase in $\triangle d_{max}$. The important observation from this experiment was that in both algorithms there was no clear break down of estimation accuracy as the amount of translation increased.

Experiment 2b (size of SM2, see Figure 3B)

Estimates of both GICA and IVA were close to the GND (all mean errors $< 5 \times 10^{-3}$). Here again, GICA errors were marginally less than IVA but there was a gradual increase in GICA non-diagonal mean correlation errors with an increase in the size variability of the component.

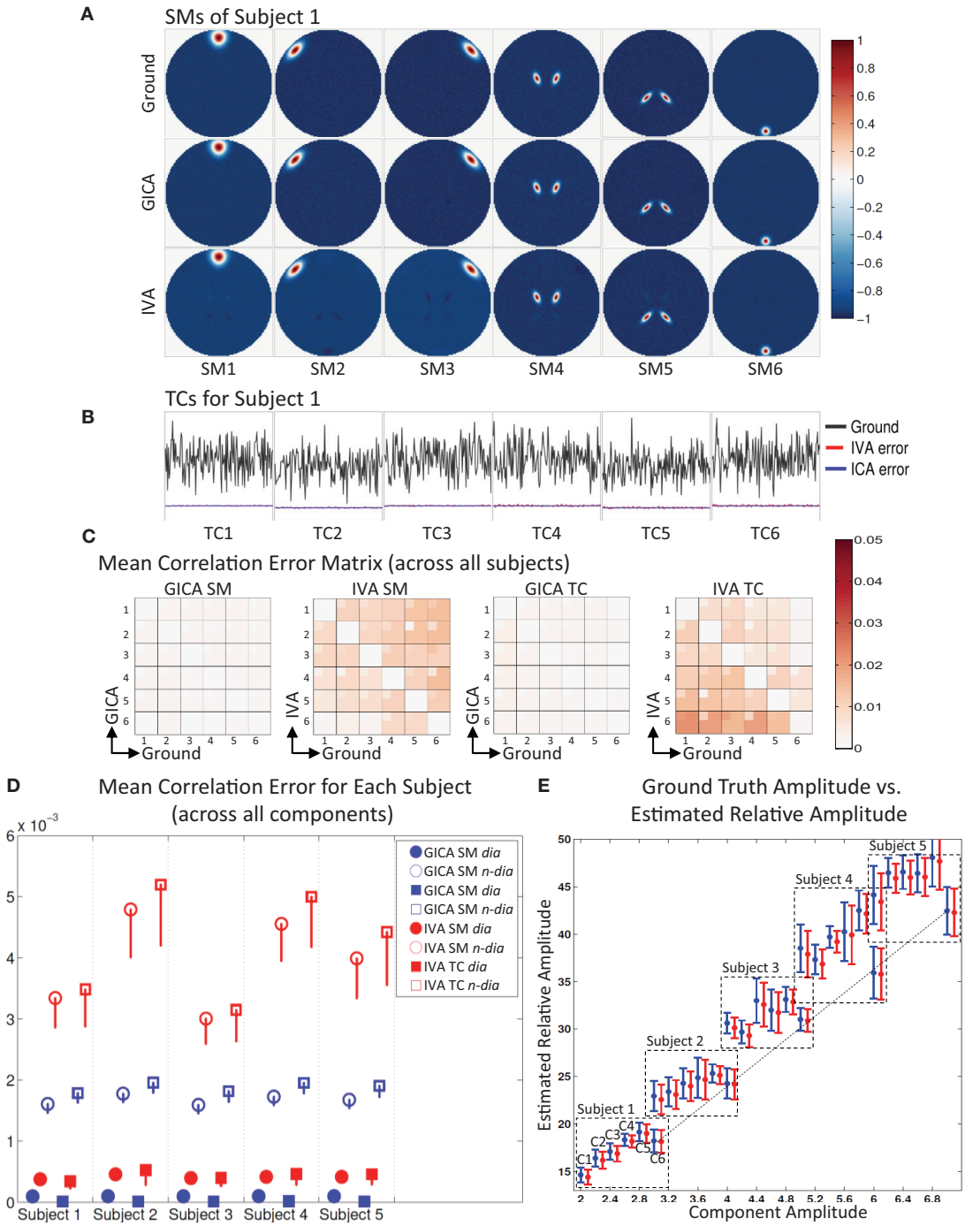

FIGURE 2 | Results of Experiment 1: Estimation accuracy with variation in only the Amplitude of SMs (no spatial variability of components). (A) Spatial Maps (SM) of subject 1: 6 Ground SMs, GICA SM estimates, and IVA SM estimates are respectively presented in different rows. All SMs are scaled between −1 and +1. SMs of Subjects 2–5 are very similar to Subject 1. SMs show that both GICA and IVA perform very good estimations (IVA estimations had minor artifacts). **(B)** Time Courses (TC) of Subject 1. TCs are normalized to zero mean unit variance. Under each TC the error (shifted for better representation, but scale unchanged) between the estimates and ground are presented in blue for GICA and red for IVA. Compared to ground TC, the relative magnitudes of the errors are very small. **(C)** Mean correlation error matrix between ground and estimates is calculated for all subjects and the mean and standard deviation (mini-cell inside each cell) is presented for GICA and IVA and SM and TC separately (see "Definition of Result Evaluation Parameters" section for their definitions). All mean errors are less than 0.05. **(D)** Mean correlation errors across all components, presented for each subject separately. Mean errors are in blue for GICA and in red for IVA. Diagonal elements of the correlation error matrix are in filled shapes and non-diagonal in unfilled shapes. SMs are presented in circles and TCs in squares. All errors are in the order of 10^{-3} indicating that variability in SM amplitude does not affect component reconstructions. **(E)** Ground truth vs. estimated amplitude. Changes in SM amplitude can be recovered in a relative sense.

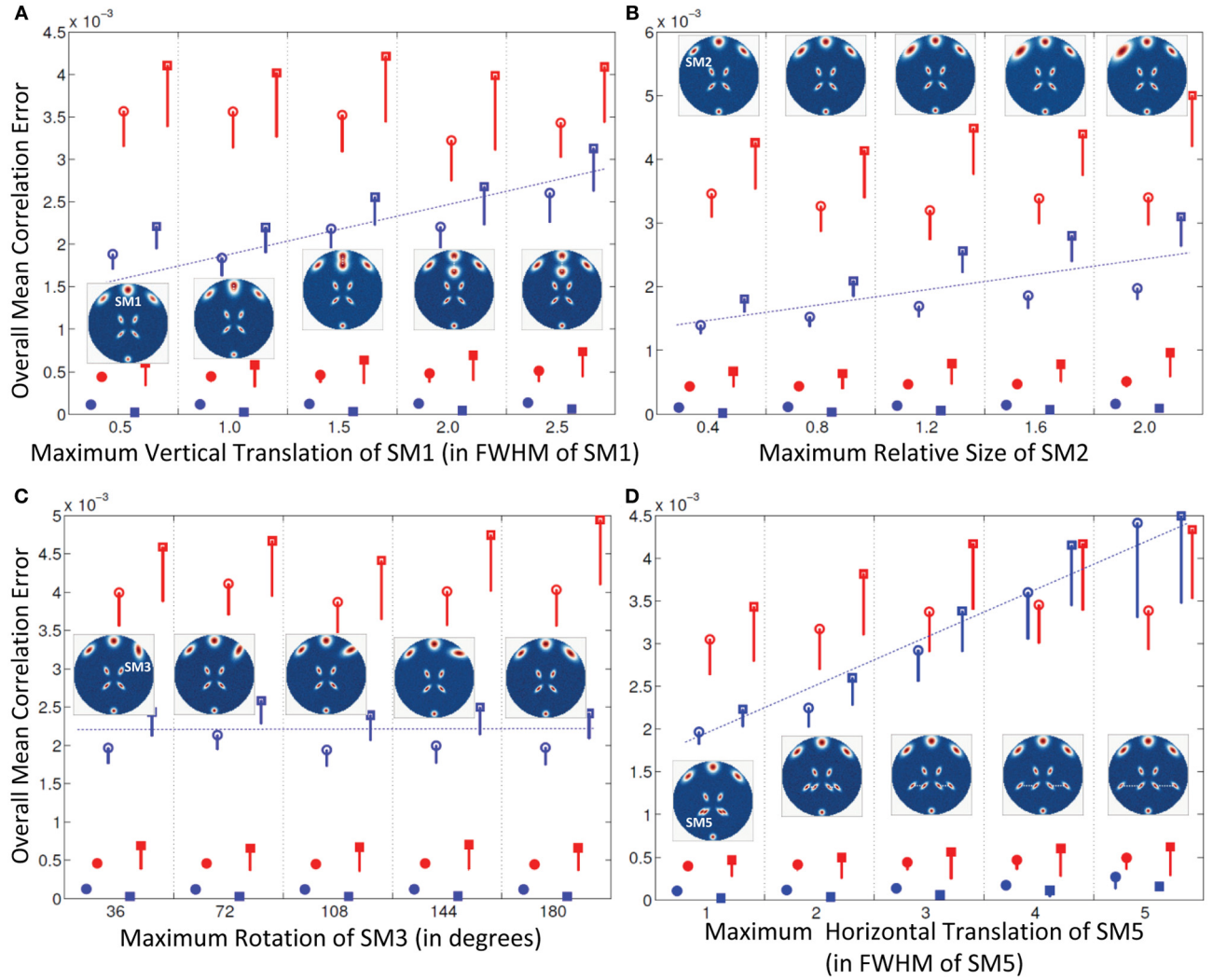

FIGURE 3 | Results of Experiment 2: Estimation accuracy when one spatial map (SM) is varied in subjects. Errors reported here are the overall mean correlation errors (across all components and subjects); see "Definition of Result Evaluation Parameters" section for definitions. Mean errors are in blue for GICA and in red for IVA. Diagonal elements of the correlation error matrix are in filled shapes and non-diagonal elements in unfilled shapes. SMs are presented in circles and TCs in squares. *X*-axis represents the maximum level of a single SM's variability between Subjects 1 and 5; other subjects' SMs are varied uniformly between Subjects 1 and 5 as illustrated by the SM maps presented within each plot. Minimal correlation errors ($<10^{-3}$) observed in both GICA and IVA, non-diagonal elements of GICA show an increasing trend at higher levels of variability. **(A)** Intersubject variability in the vertical translation of SM1, **(B)** Intersubject variability in the size of SM2; **(C)** Intersubject variability in the orientation (rotation) of SM3; **(D)** Intersubject variability in the horizontal translation of SM5.

Experiment 2c (rotation of SM3, see Figure 3C)

All mean correlation errors across subjects and components were less than $< 5 \times 10^{-3}$, with GICA marginally outperforming IVA. There was no increase in error with higher maximum rotation.

Experiment 2d (horizontal separation of SM5, see Figure 3D)

All mean errors were less than 4.5×10^{-3} for both GICA and IVA.

Experiment 2e (component overlap, see Figure 4)

In **Figure 4A**, we see that GND SM2 to SM5 are at the same location for all subjects and that SM1 was varied in all subjects. In addition, we see that in Sub5 SM1 slightly overlaps with SM4. In **Figure 4B**, we present the mean correlation error for all five subjects calculated across all the components. For subjects 1–4, for both SM and TC, $\mu_i^{d,C}$, and $\mu_i^{d,V}$ were near zero. In Sub5, where SM1 slightly overlapped with SM4, mean correlation errors were higher. The errors of Sub5 have higher standard deviation indicating that it may be as a result of just a few elements of the correlation error matrix. Upon closer inspection of the correlation error matrix of Sub5 (**Figure 4C**) we see that most of the elements have lower correlation errors except errors between GND SM4 and EST SM1 and GND TC1 and EST TC4. The correlation between GND SM1 and GND SM4 in Sub5 was equal to 0.13, and this was due to their slight spatial overlap. In

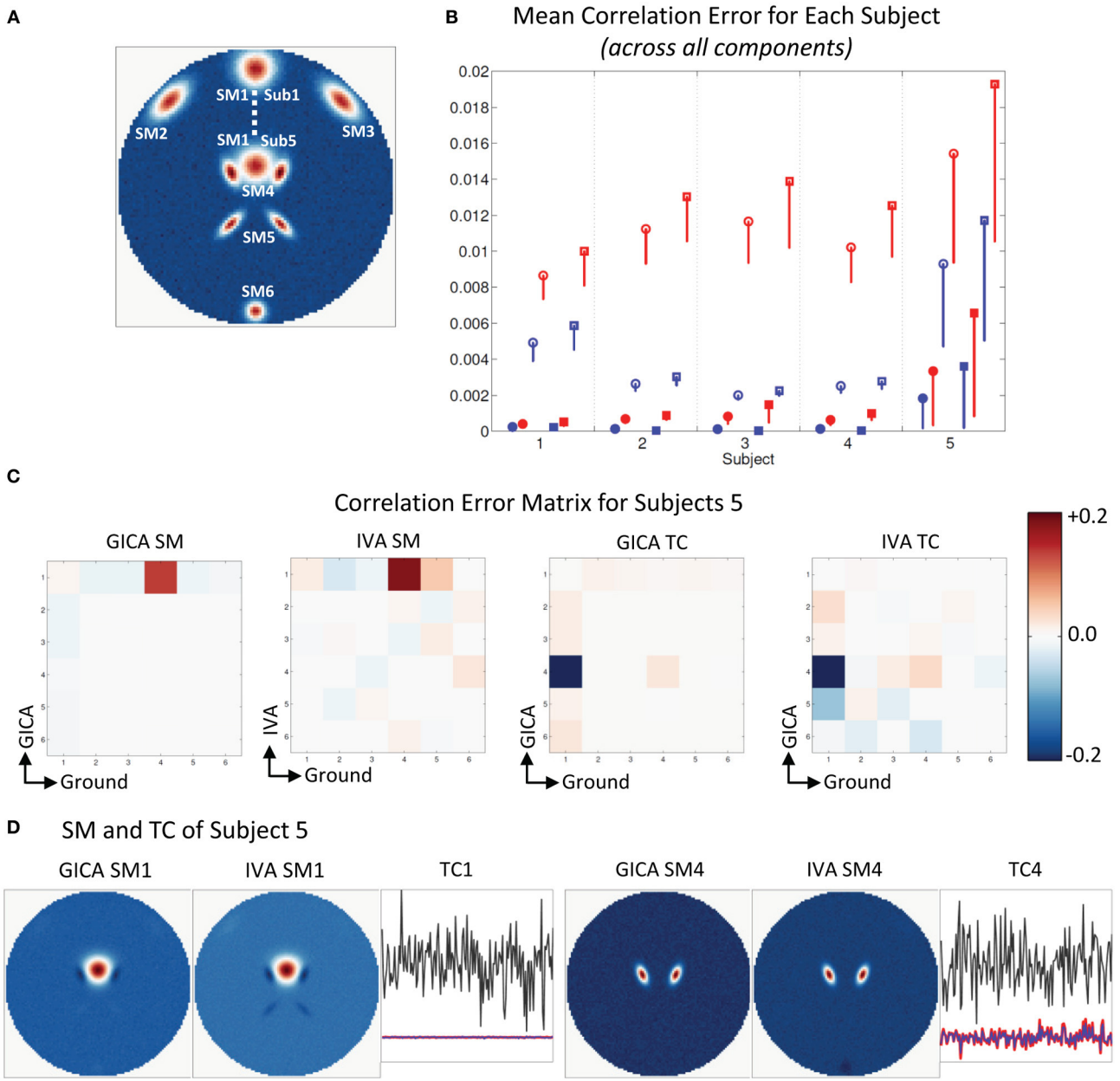

FIGURE 4 | Results of Experiment 2e: Estimation when components overlap spatially. (A) Ground truth SMs: SM2 to SM6 for all subjects are at the same location, SM1 of Subjects 1 and 5 are presented, SM1 for Subjects 2–4 are equally distributed between locations of Subjects 1 and 5. In Subject 5, SM1 slightly overlaps with SM4. **(B)** Mean correlation errors across all components, presented for each subject separately. Mean errors are in blue for GICA and in red for IVA. Diagonal elements of the correlation error matrix are in filled shapes and non-diagonal in unfilled shapes. SMs are presented in circles and TCs in squares (see "Definition of Result Evaluation Parameters" section for their definitions): correlation errors are small in Subjects 1–4, large errors in Subject 5 where SM1 and SM4 were overlapping. **(C)** Correlation error matrix for Subject 5 indicates that both GICA and IVA have removed the spatial correlation that existed (due to overlap) between SM1 and SM4 (diagonal element) and have introduced non-diagonal correlations between SM1 and SM4 and TC4 and TC1 that did not exist in the ground truth. Applying GICA/IVA can remove spatial correlations but will introduce artificial correlations in the temporal domain. **(D)** In both GICA and IVA estimates, we observe that SM1 has negative lobes in regions of overlap with SM4 and these negative lobes are causing the zero correlations between SM1 and SM4. SM4 is well reconstructed by both methods, but TC4 has high errors and has correlations with TC1.

the estimated components correlation between SM1 and SM4 in GICA and IVA was −0.003 and 0.05, respectively. In the time domain, the correlation between GND TC1 and GND TC4 in Sub5 was near zero (= −0.002). In the estimated TCs, correlation between TC1 and TC4 was equal to 0.2 in GICA and 0.26 in IVA. In **Figure 4D**, we see that the near zero correlation between the EST SM1 and EST SM4 is created by SM1 having negative lobes in the overlapping region with SM4 and due to this

same reason there is higher correlation between GND SM4 and EST SM1.

Experiment 2f (over estimation of number of components, see Figure 5)

Figure 5A shows that all SMs except SM1 has subject variability. In **Figure 5B**, $\mu_i^{d,C}$, $\mu_i^{d,V}$, $\mu_i^{n,C}$, and $\mu_i^{n,V}$ are presented for all five subjects. In all five subjects $\mu_i^{d,C}$ was between $0.03 - 0.14$ and $\mu_i^{d,V} < 10^{-3}$. GICA errors had a high standard deviation, indicating that outliers may be causing the error (again, only the lower bounds of the error bars are shown in the figure to illustrate higher resolution at lower error level). The non-diagonal elements of the SM correlation matrix show marginal error in both techniques with small standard deviation. The diagonal elements of the TC correlation error matrix show very low errors in both GICA ($< 10^{-3}$) and IVA ($< 10^{-2}$). In **Figure 5C**, we present the mean correlation error matrices and this time the averages are computed across subjects with standard errors represented by the mini-cell within each cell. The GND-GND matrix was of size $[6 \times 6]$ and due to overestimation the GND-EST correlation matrix was of size $[9 \times 6]$. The correlation error matrix indicates that the mean correlation error across subjects between GND SM1 and EST SM1 was equal to 0.4 in GICA and 0.001 in IVA. This was due to the poor reconstruction of SM1 by GICA. The worst performance of GICA was observed in Sub3 and in **Figure 5D** we present GICA and IVA SM1 and SM7 of Sub3. GICA SM1 and GND SM1 of Sub3 had a correlation of 0.16 and the same in IVA was 0.99. In both GICA and IVA the correlations between the extra components (SM7 to SM9), after the best pairs were matched, were all less than 0.006, except the correlation between GICA SM7 and GND SM1. In Sub3, GICA SM7 had a correlation of 0.16 with GND SM1. Overestimation in GICA essentially splits SM1, the component that was varied across subjects, into more than one estimate of SM1. The TCs of the extra GICA components showed significant correlation errors with GND TC1. The mean correlation between GICA TC7, TC8, and TC9 and GND TC1 were 0.999, 0.76, and 0.34 respectively. In IVA the same values were 0.103, 0.109, and 0.07. In **Figure 5E** we present a scatter plot of GND TC1 with GICA and IVA TC7, TC8, and TC9. It is clear that in GICA all TCs of the extra components have much higher correlation with GND TC1 than the extra components of IVA.

Experiment 2g (missing components)

In the first part of this experiment, where one SM was missing in just one subject, IVA reconstructed the SMs and TCs very close to the ground truth (correlation errors less than 0.06). In GICA SMs were closer to the ground truth but the TCs showed large errors. The TC of the component corresponding to the component that was not present in Sub1 showed high correlations errors (0.2–0.8). This was observed only in Sub1 and all other subject TCs were more accurately reconstructed in GICA. In the second part of the experiment where SM1 was present in Sub1 and missing in all other subjects, IVA continued to accurately estimate both SMs and TCs. GICA SM estimates were close to ground truth, but TC estimates of the missing component had high correlation errors with other components in some of the subjects.

EXPERIMENT 3: SPATIAL VARIATION IN TWO COMPONENTS

Experiment 3a (vertical translation of SM1 and size change of SM2, see Figure 6A)

In **Figure 6A**, we present the mean correlation errors across all subjects and components ($\mu_{all}^{d,C}$, $\mu_{all}^{d,V}$, $\mu_{all}^{n,C}$, and $\mu_{all}^{n,V}$) as images for each value of $\triangle d_{max}$ and $\triangle s_{max}$. The rows in **Figure 6A**, from top to bottom, represent increasing degrees of vertical translation of SM1 and columns, from left to right, represent increasing degrees of size change in SM2. Both GICA and IVA do an excellent job in component estimation. In **Figure 6A**, we present mean errors in diagonal SM, diagonal TC, non-diagonal SM, and non-diagonal TC. All mean correlation errors were less than 10^{-3} for both GICA and IVA. GICA errors were slightly less that ICA but the errors marginally increased in the diagonal direction, that is, errors were higher at higher variability.

Experiment 3b (vertical translation of SM1 and rotation of SM3, see Figure 6B)

Results were similar to that of the Experiment 3a.

Experiment 3c (vertical translation of SM1 and horizontal separation of SM5, see Figures 6C, 7)

Results indicate much better estimation accuracy in IVA. The mean values of the diagonal elements of the SM error correlation matrix indicate that up to $\triangle d_{max}$ translation of 1.5 FWHM of SM1 and 3 FWHM of SM5 GICA estimates are accurate. After this threshold there is a sudden increase in correlation error in the range of 0.1–0.2. For IVA, $\mu_{all}^{d,V}$ for both SM and TC correlation errors were less than 10^{-3}, and there was no clear jump in error with increasing level of variability.

In **Figure 7B**, we display the mean errors for each subject separately at SM1 $\triangle d_{max} = 20$ voxels and SM5 $\triangle d_{max} = 20$ voxels. This level of variability was selected as a representative example to further examine the nature of errors. The mean errors in SM and TC were much higher in GICA than IVA for diagonal and non-diagonal elements of the correlation error matrix.

Motivated by the large error bars, we further investigated the mean correlation error matrices (mean values were calculated across subjects). The mean correlation error images across subjects are presented in **Figure 7C**. In GICA there are large errors in the components that varied across subjects (Component 1 and 5) in both SM and TC. In IVA, all correlation errors across all subjects were less than 0.04. Mean correlation errors in TCs were high in GICA between GND TC5 and GICA TC5. Correlation error was also high in GICA between GND TC1 and GICA TC5. All TC correlation errors in IVA were less than 0.05.

In **Figures 7D,E**, we present the SMs and scatter plots of the TCs of components 1 and 5. Our first observation is that IVA SMs were well reconstructed with only minor artifacts. GICA SMs show extreme errors in SM1. In all Subjects the main lobe of SM1 appears less prominently than the artifact from SM5. In Sub3 the main blob of SM1 is hardly visible. SM5 in GICA was well estimated for all subjects with minor artifacts, but TC5 in GICA shows large errors. In **Figure 7E** (i), we present Sub3 scatter plots of the GND TC1 vs. GICA TC1 in blue filled circles, GND TC5 vs. GICA TC5 in blue unfilled circles and GND TC1 vs. GICA TC5

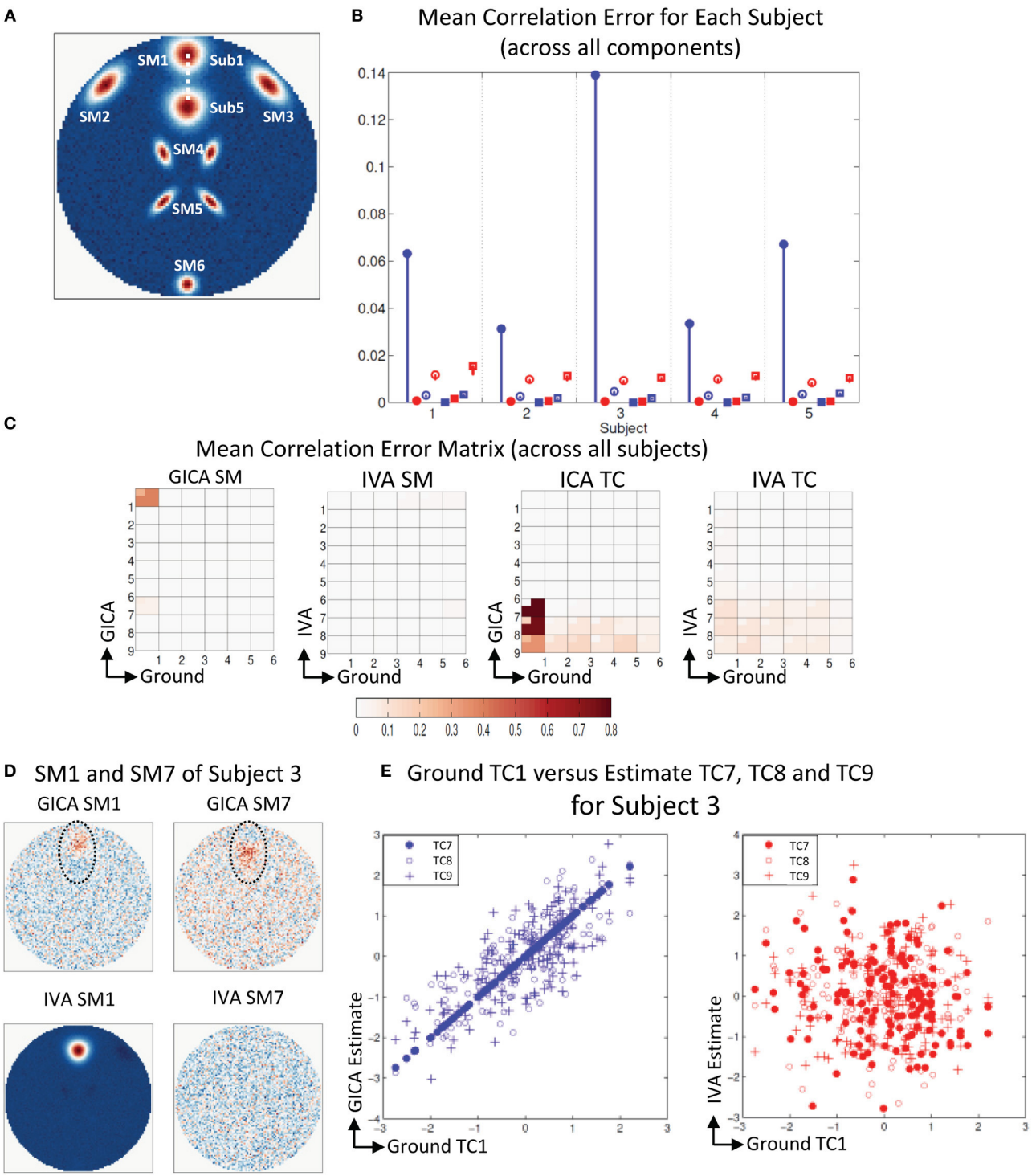

FIGURE 5 | Results of Experiment 2f: Over estimation of components (6 components are estimated with 9). (A) All SMs, except SM1, spatially overlap across subjects. SM1 is spatially varied for all subjects. Locations of SM1 for Subjects 1 and 5 are shown and SM1 for other subjects are equally spaced between those locations. **(B)** Mean correlation errors across all components, presented for each subject separately. Mean errors are in blue for GICA and in red for IVA. Diagonal elements of the correlation error matrix are in filled shapes and non-diagonal in unfilled shapes. SMs are presented in circles and TCs in squares (see "Definition of Result Evaluation Parameters" section for their definitions). GICA diagonal SM correlation error is high with a high error bar; Subject 3 has the largest mean error. **(C)** Mean correlation error matrix between ground and estimates is calculated for all subjects and the mean and standard deviation (mini-cell inside each cell) is presented for

(Continued)

FIGURE 5 | Continued
GICA and IVA for SM and TC separately. GICA produces errors in SM1 and SM7 and large errors in TC7, TC8, and TC9. **(D)** In Subject 3, SM1 shows noisy lobes (both positive and negative) at locations where SM1 was varied between subjects. The extra component (SM7) showed similar lobe patterns. In IVA SM1 is well reconstructed and the extra component (SM7) appears as a noisy frame. **(E)** Scatter plots of the Ground TC1 vs. GICA estimates of the extra components (TC7, TC8, and TC9) show significant correlation between them. In IVA TCs of extra components are not correlated with Ground TC1.

in black un-filled circles. Similar plots are presented for IVA in **Figure 7E** (ii). It is evident that GND TC1 and GICA TC1 have near perfect correlation, but GND TC5 and GICA TC5 have very weaker correlation. GICA TC5 has a much higher correlation with GND TC1. Sub3 had the poorest estimation of SM1 (correlation error = 0.96) and the poorest estimation of TC5 (correlation error = 0.96). In addition in Sub3 GICA SM1 had a high correlation with GND SM5 (correlation error = 0.98) and GICA TC5 had a high correlation with GND TC1 (correlation error = 0.98). IVA TCs were well reconstructed with appropriate correlations.

EXPERIMENT 4: SPATIAL VARIABILITY IN ALL COMPONENTS

Experiment 4a (uniform distribution of variability, see Figure 8A)

Mean errors across all subjects and components at increasing levels of variability (along x-axis). At $k = 1$, all mean correlation errors in both GICA and IVA were less than 0.02. At $k = 2$, GICA errors begin to become marginally higher than IVA. At $k = 3$, GICA diagonal errors begin to show much higher errors than IVA in both SM and TC components. Non-diagonal elements of the correlation error matrices are also higher in GICA than in IVA. At $k = 4$ and 5 GICA diagonal correlation errors increase rapidly compared to errors in IVA. In **Figure 8A** (ii), we present the SM with the highest correlation error of GICA along with the corresponding GND and IVA SMs. Similarly, in **Figure 8A** (iii) we present the SM with the highest correlation error of IVA along with the corresponding GND and GICA SMs. Correlations of these SMs between the GND and estimates are presented below the SMs.

Experiment 4b (normal distribution of variability, see Figure 8B)

Results of this experiment were very similar to results of *Experiment 4a*.

Experiment 4c (model order over estimation, see Figure 8C)

Mean correlation errors are presented in the y-axis and the number of estimated components are in the x-axis while the amount of spatial variability was kept at $k = 2$. At $C = 15$, the case where the number of components in the GND and the number of estimated components are equal, the performance of both methods were very similar. At $C = 20$ GICA SM diagonal errors begin to increase with. GICA SM correlation errors in the diagonal element continue to increase with higher number of estimated components. At $C = 25,\ 30,$ and 35 $\mu_{all}^{d,C}$ increased to 0.42, 0.52, and 0.57 respectively.

Experiment 4d (estimation at high noise level, see Figure 8D)

For this experiment we kept the degree of spatial variability at $k = 2$ and gradually increased the noise level. $\mu_{all}^{d,C}$ and $\mu_{all}^{d,V}$ increased with decrease in *CNR*.

DISCUSSION

In this simulation study, we evaluated the accuracy of component estimations of group independent component analysis (GICA) and independent vector analysis (IVA) under varying degrees of inter-subject spatial variability of components. By using a simulation toolbox (SimTB) to create sample fMRI data sets and a thorough set of experiments we were able to identify several interesting properties of GICA and IVA. We systematically changed the degree of subject variability and evaluated the performance of component estimation not only by measuring the changes in components that underwent spatial variability but also how this variability affected all other components' spatial maps (SMs) and time courses (TCs).

GICA vs. IVA: METHODOLOGICAL DIFFERENCES

As both GICA and IVA are extensions of ICA, inherent assumptions and limitations of ICA are common to both methods, but there are several methodological differences between GICA and IVA. The initial input data (**Y**) for both approaches are identical, but the **X** matrix in GICA and IVA algorithms is not the same. In GICA there are two levels of PCA reductions before arriving at **X**; first the subject level PCA and then the group level PCA. In IVA only a subject level PCA is performed. In GICA the group level PCA ensures that the common variances at the group level are well captured. Simulations from this study provide evidence that GICA can reconstruct individual subject variability but only up to a certain limit of subject variability. GICA maximizes the spatial independence of the components at the group level as it is applied on the two dimensional group level **X** matrix. IVA jointly maximizes two objectives on the three dimensional **X** matrix: (1) The spatial independence of within subject components and (2) dependence of "similar" components across subjects, by modeling the dependence structure of similar components.

IVA results are not limited or dependent upon the back-reconstruction methodology as back-reconstruction is not needed in IVA. In IVA, subject specific mixing coefficient matrices are kept separate from each other and the subject specific SMs and TCs are obtained by directly projecting them to their respective data. The initial SM outputs of GICA are representative of the whole group and extra steps are needed to construct the subject specific SMs and TCs using one of the back reconstruction methods. Based on the back-reconstruction methodology applied, the SMs and TCs can vary slightly, see Erhardt et al. (2011) for details.

In general, IVA seeks a decomposition of the multi-subject fMRI data to estimate sources that are independent within each dataset while also aligning the estimated sources (SMs) across subjects to maximize the dependency between the aligned sources. Thus, we can imagine an overlay of the same source

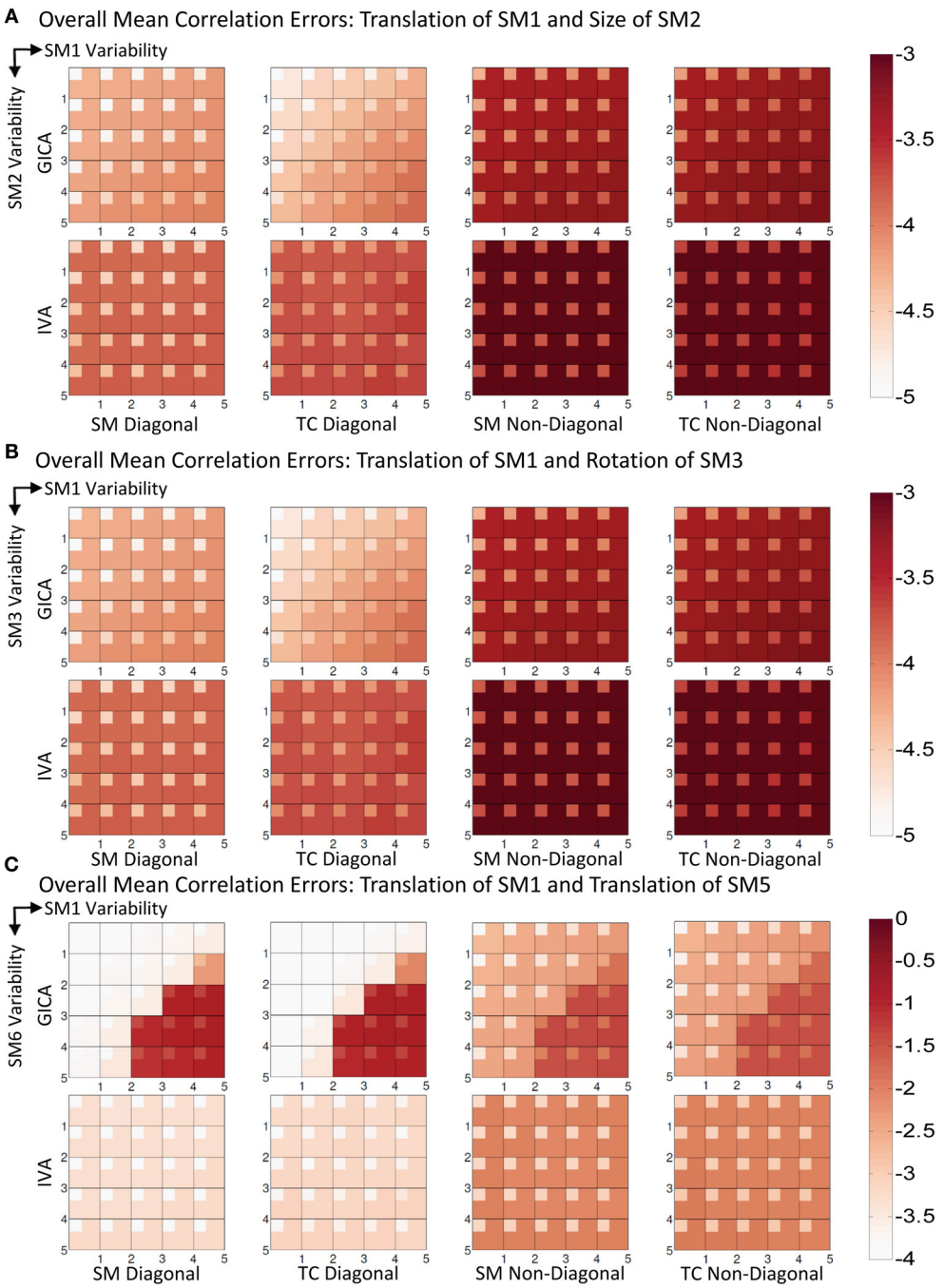

FIGURE 6 | Results of Experiment 3: Estimation when two components are varied across subjects. Overall mean correlation errors (across all subjects and components) are presented as images for diagonal and non-diagonal elements of for SM and TC separately. Increase in variability is from left to right of the image and from top to bottom. For details on the degree of variability at each step refer to the "Simulation Experiment Setup, Experiment 3" section. The errors are in log10 scale as indicated by the colorbar. **(A)** Translation of SM1 and size change of SM2. Both GICA and IVA errors are small, In GICA, errors are marginally increasing in the diagonal direction of the image. **(B)** Translation of SM1 and Rotation of SM3. Both GICA and IVA errors are small. In GICA errors are marginally increasing in the diagonal direction of the image. **(C)** Translation of SM1 and Translation of SM5. In IVA, errors still remain small across all levels of variability. In GICA, errors are small up to the third step, but thereafter give large errors. Note the change of colorbar values for this result, indicating higher levels of correlation errors.

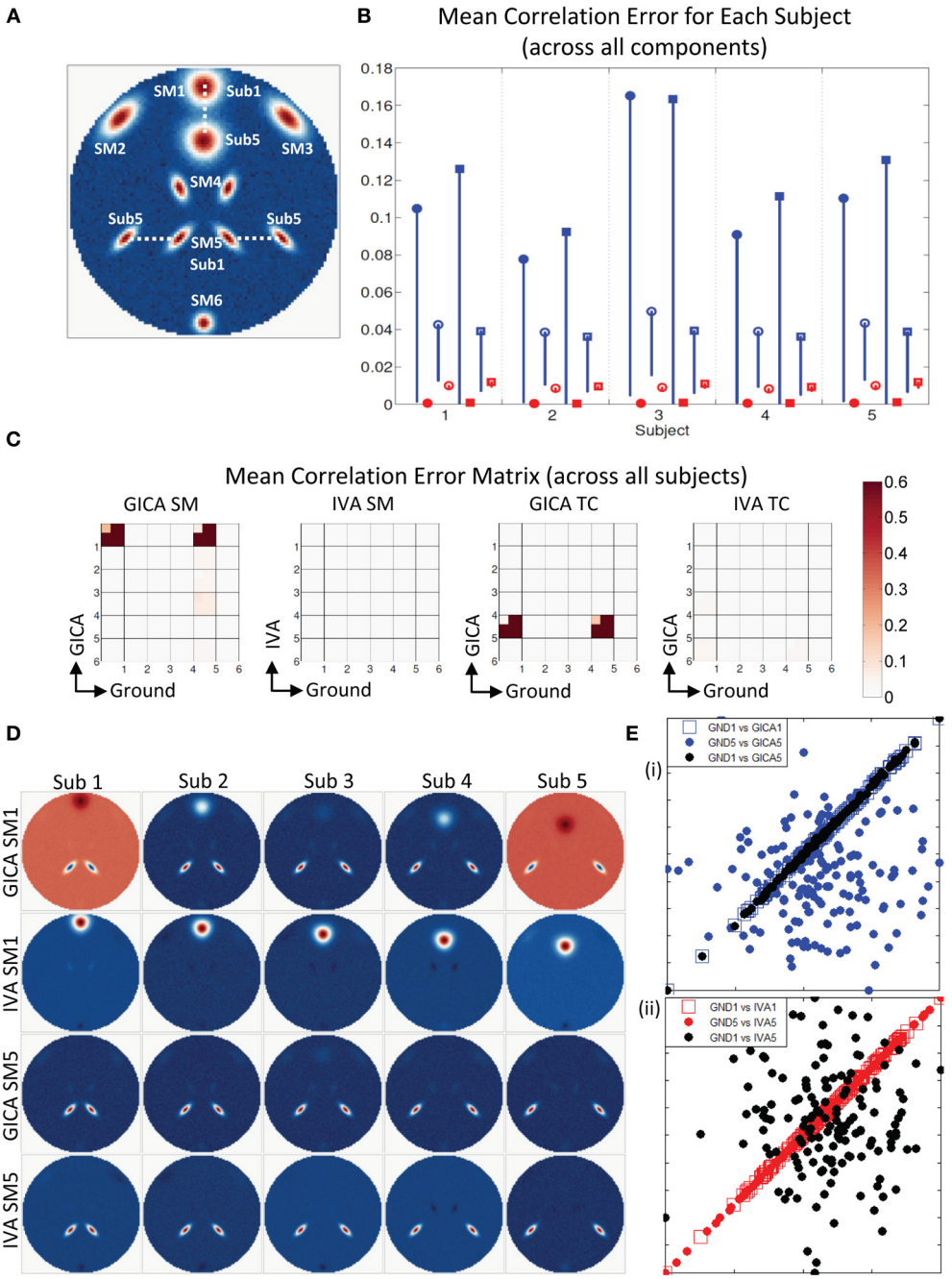

FIGURE 7 | Estimation when SM1 and SM5 are varied across subjects. (A) SM1 and SM5 are spatially varied for all subjects. Locations of SM1 for Subjects 1 and 5 are shown and SM1 for other subjects are equally spaced between those locations. **(B)** Mean correlation errors across all components, presented for each subject separately. Mean errors are in blue for GICA and in red for IVA. Diagonal elements of the correlation error matrix are in filled shapes and non-diagonal in unfilled shapes. SMs are presented in circles and TCs in squares (see "Definition of Result Evaluation Parameters" section for their definitions). All IVA mean correlation errors are less than 0.02. All GICA errors are much higher with large error bars. For clarity of lower error values, only the lower bounds of the error bar are presented. **(C)** Mean correlation error matrix between ground and estimates is calculated for all subjects and the mean and standard deviation (mini-cell inside each cell) is presented for SM and TC separately. GICA produces large errors in the components (SM1 and SM5) that were varied across subjects. **(D)** SM1 and SM5 across all subjects. IVA produces estimates SMs with little artifact. GICA SM1 has large artifacts from SM4 and the blob of SM1 appears weak; in Subject 3 it is hardly visible. GICA estimates of SM5 are close to ground truth. **(E)** Scatter plots of the Ground TC1 vs. GICA TC1 is in filled blue circle, Ground TC5 vs. GICA TC5 is in unfilled blue square and Ground TC1 vs. GICA TC5 in filled black circles; same for IVA are in red in the next plot. GICA TC1 is highly correlated with Ground TC1, but GICA TC5 is not correlated with Ground TC5 but has high correlation with ground TC1. GICA incorrectly assigns the TC of one spatially varying SM to another spatially varying SM. In IVA TC correlations are correctly estimated.

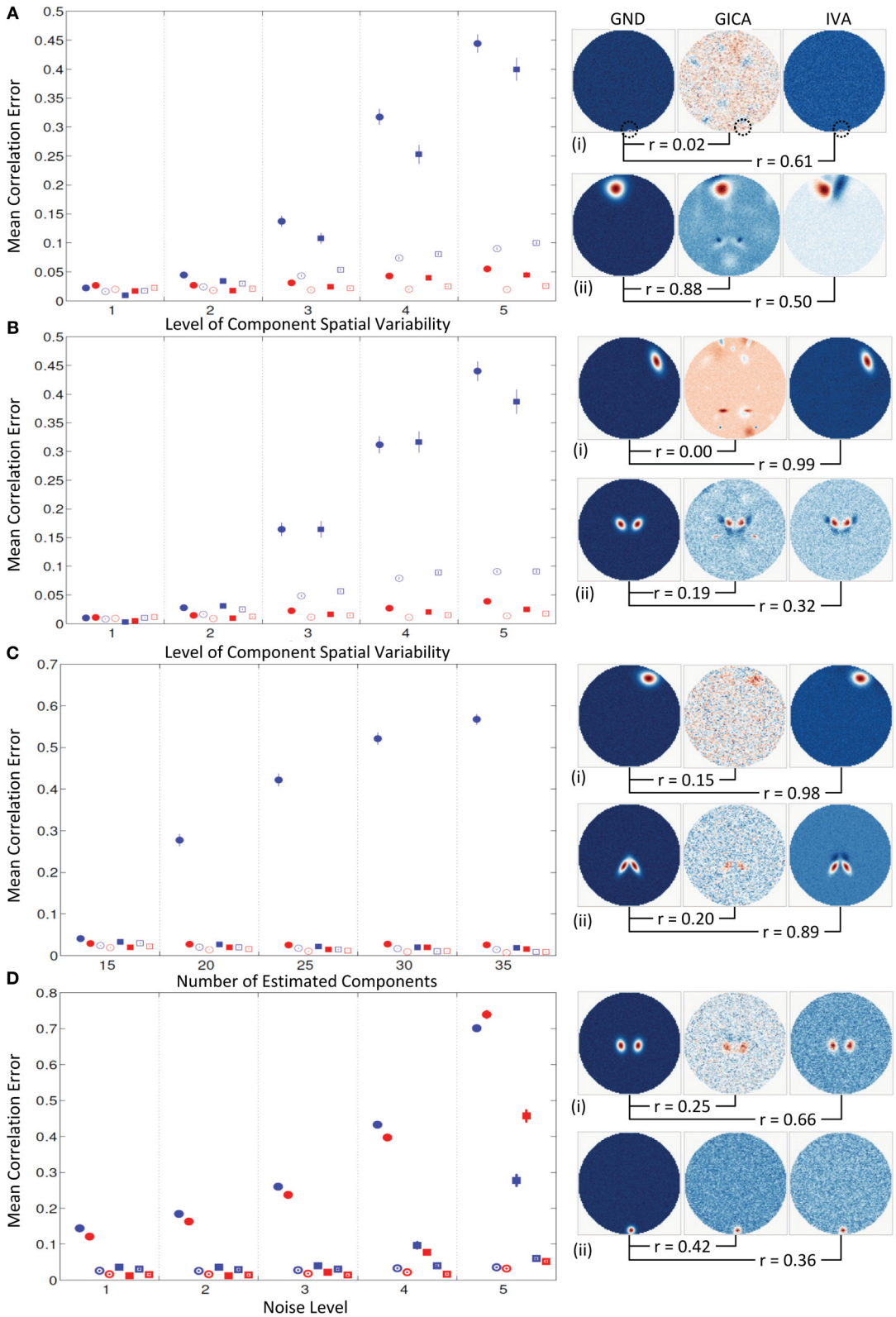

FIGURE 8 | Results of Experiment 4: Results from a larger dataset with higher number of subjects and components and with variability in all components. In this experiment all components of all subjects undergo a combination of variability. Correlation errors reported here are mean values across all subjects and components. Mean errors are in blue for GICA and in red for IVA. Diagonal elements of the correlation error matrix are in filled shapes and non-diagonal elements in unfilled shapes. SMs are presented in

(Continued)

FIGURE 8 | Continued
circles and TCs in squares (see "Definition of Result Evaluation Parameters" section for their definitions). Next to each error plot, are SMs with least correlation with ground, for GICA in (i), and IVA in (ii). These SMs are presented along with the corresponding SM from the other technique. **(A)** When variability is drawn from a uniform distribution. GICA and IVA errors are comparable at lower variability, but GICA errors increase with increase in the level of variability. **(B)** When variability is drawn from a Gaussian distribution; results are similar to that of uniform distribution. **(C)** When variability is drawn from mid-level variability, but the number of components is overestimated. At 15 components (actual number of components as in ground truth) GICA and IVA errors are comparable. With increase in number of estimated components, GICA SM diagonal errors increase, whereas IVA errors continue to be constant. **(D)** Performance with increase in noise level.

(SM) for multiple subjects, where the activation regions within each form a chain of slightly overlapped regions. For GICA, recovering such a source will be difficult because the averaging power will be diminished, while IVA can exploit the overlapping regions by maximizing dependency while preserving the subject variability.

INTERPRETATION OF RESULTS AND IMPLICATIONS

In order to better understand how inter-subject component spatial variability affected estimation accuracy, our study was broken into experiments with increasing complexity.

Estimations under variability in amplitude

Results indicate that both GICA and IVA approaches do an excellent estimation of both SM and TC components. Near zero elements in the cross-correlation error matrices (in both $\mathbf{E}_i^{\mathbf{C}}$ and $\mathbf{E}_i^{\mathbf{V}}$, for $i = 1$ to 5) indicate that correlations between both corresponding and other components were well estimated. Results of this experiment indicate that GICA estimates are marginally better than IVA, $max\left[diag\left(\left(\mathbf{E}_i^{\mathbf{C}} - \mathbf{E}_i^{\mathbf{V}}\right)\right)\right] < 10^{-3}$ (see **Figure 2E**). From a visual inspection of GICA and IVA SMs (see **Figure 2A**) it is evident that GICA SMs are slightly cleaner than IVA.

Spatial variability in one component

We investigated the effect of inter-subject variability of three types of spatial variability: component translation, component size and component rotation. One contrasting difference between GICA and IVA estimates is that, in IVA there was no clear indication of correlation errors increasing with the increase of variability. Whereas in GICA, increase in the degree of vertical and horizontal translations and size of the component resulted in an increase in correlation errors, as indicated by the positively sloped blue line in **Figure 3**.

Spatial overlap of components

We investigated the estimation accuracy while GND SMs were slightly overlapped. Our results indicate that both GICA and IVA spatially separate the overlapped components. By "spatially separate" we mean that the spatial correlation that existed between overlapping components was not present (zero correlation) in the estimated components. The estimated maps show negative lobes in the overlapping regions. There was no correlation between the ground TCs of the overlapping components, but the estimated TCs have higher correlation. In other words, both GICA and IVA remove or nullify the spatial correlation between SMs but introduce artificial correlation in the TCs of the same components (see **Figure 4C**). This fault in both algorithms needs to be carefully taken into consideration when the estimated components have high spatial overlap. *Experiment 2e* was a simple experiment that showed how slight spatial overlap of just two SMs in just one subject can cause errors in both SMs and TCs of that subject. In a real fMRI data application there may be multiple spatial intersections between the estimated SMs. Careful attention is needed in such cases, especially when performing functional network connectivity (FNC) analyses, as our simulation results indicate that spatial overlap between SMs can introduce non-existent artificial correlations in TCs.

Model order overestimation

One of the inherent issues of blind source separation techniques such as ICA and IVA is the absence of *a priori* knowledge of the actual number of independent sources (or SMs) present in the data. An approach that has gained popularity in the recent past is to estimate a large number of components. In *Experiment 2f* we estimated nine components on a dataset that had six original components. IVA produced SMs and TCs with very low correlation errors and the extra estimates (SM7 to SM9) were noise-like and were not correlated with the original GND components. GICA SM of the component with inter-subject variability had poorer correlation with the GND SM and had artifacts (negative lobes) at spatial locations of the SM in other subjects (see **Figure 5D**). Further the extra SMs in the estimates showed correlations with the original GND SM that had inter-subject variability. The extra TC estimates (TC7 to TC9) had significant correlations with the TC of the component that had spatial variability across subjects. The introduction of artificial TC correlations by GICA can pose potential inaccuracies in studies where FNCs are evaluated. Our results indicate that this problem is not present in IVA as the extra SMs look noise like, meaning no clear lobes of activation and the extra TCs do not have correlations with the varying component.

Spatial variability in two components

Our results of *Experiment 3* indicate that GICA performs well under combinations of translational, spatial and size variability. GICA performs well when both components undergo translational variability up to approximately around 1.5–3 FWHM of the component, but GICA fails beyond that maximum spatial variability. IVA performs significantly better than GICA at higher variability. GICA SM estimates resulted as a mixture of varying components (**Figure 7D**). GICA also incorrectly assigned the TC of one of the spatially varying SM to the other spatially varying SM (**Figure 7E**).

Missing Components: We checked the performance of GICA and IVA when components were completely missing from one or many subjects. Here again IVA continued perform well in both spatial and time domains of the estimations. GICA did well in estimating the SMs but the TCs of the missing components were not estimated accurately.

Spatial variability in all components

Both GICA and IVA performed well up to variability of $k = 2$ (component translations between -4 and $+4$ voxels, rotations between $-20°$ and $+20°$ and size between 0.6 and 1.4). At inter-subject variability greater than this simulated threshold GICA begins to show large errors for both uniform and Gaussian distributions. We expected that the errors of the Gaussian distribution would be less than that for uniform distribution as more subjects are centered at zero variability in a Gaussian distribution. Results indicate that GICA errors in both cases were similar (**Figures 8A,B**). In **Figure 8A**, we present the GICA SM with the largest error. The small activation or blob (indicated by green circle) appears very noisy with many other similar size artifacts from other components in GICA. IVA identifies this component distinctly in spite of its minute size. In general, at higher levels of spatial variability, GICA SMs were a combination of many GND components. In *Experiment 4c* we performed component overestimation and results show that when the number of components is higher than the number of components in the GND, GICA produces large errors in SMs. This experiment also showed that GICA components were noisy (see **Figure 8C**) and the extra components had remnants of activation from other GND components. IVA recovered the SMs and TCs well and the extra components appeared noisy (an ideal result).

GICA OR IVA

Both methods yield accurate component estimations at low levels of subject variability. Prior knowledge of the degree of subject variability in the fMRI data can help to decide which method to choose. A possible approach to find the degree of component variability is to apply individual ICA on real fMRI data for a few subjects, reconstruct the components, and evaluate the spatial dissimilarities. Spatial variability across subjects may be fMRI task dependent and possibly higher in resting state data. In this study, we showed that at low levels of subject variability, GICA SMs and TCs are much cleaner than IVA. IVA does very good estimations at low levels but there were minor artifacts from other components. At higher levels of subject spatial variability of components, GICA reconstructs the components that did not have inter-subject variability well, but performs poorly on the components with subject variability. In some cases GICA estimated the SMs well but introduced errors in the TC of the component. When the number of components was overestimated in the presence of subject variability, GICA estimates of varying components and the extra components had weak activations with high levels of noise; further the TCs of the varying and extra components were correlated.

If the goal of a certain project is to obtain group level maps, then GICA is preferred to IVA. GICA components are constructed after a second level PCA reduction across the whole group. This step identifies the common patterns of activation present in the data and the constructed components represent the components corresponding to the strongest variances across the whole group. As such variances due to noise or due to minor variability in one subject are minimized in GICA. If subject specific SMs are the main interest then GICA users need to select one of the many back-reconstruction techniques available and slight differences in the SMs and TCs can be present dependent on the technique chosen.

A few impediments do exist while applying IVA as currently implemented. One constraint is the need for large memory. In our simulations we used a 64 bit laptop with 4 GB RAM and clock speed of 2.67 GHz. To estimate 5 components with 8 k voxels from 5 subjects IVA takes 1.75 s and GICA 1.3 s. To estimate data from 25 subjects with 25 components IVA took more than 16 min while GICA performed the same in less than a minute. With real fMRI brain volumes usually of size 50–100 k voxels, computer memory needed for IVA is higher than GICA by a factor of number of subjects present in the data. As such applying IVA at its current state may not be feasible with typical desktop capacities if the number of subjects, number of components and number of voxels are very large. Additional optimizations to the IVA algorithm are needed to decrease computational burden.

LIMITATIONS AND FUTURE WORK

Verification with real fMRI data

Application of IVA to real fMRI data and its performance in terms of component fidelity, implication, and robustness were not checked in this study, but through a systematic simulation framework and thorough analyses of results we provide evidence that IVA may be a better approach to capture inter-subject variability. GICA is a well-tested and widely applied technique that has provided consistent results across many different types of fMRI data (different types of task related and resting state) and across many different studies. The level of inter-subject spatial variability of components present in real fMRI data is uncertain. Further studies are needed to evaluate the performance of GICA and IVA with respect to results from individual ICA. We intend to do that in our next project.

Limitations of our simulation setup

The simulated datasets used possess many realistic properties but unavoidably have many limitations. It should be noted that our simulations model the fMRI data as a weighted linear mixture of spatial SMs, where the weighting is determined by TCs, in other words that the fMRI data can be given as product of SMs and TCs and adheres to the assumptions of ICA. We assigned one single TC to represent the activation changes of all the voxels of a SM. This again is an extension of ICA assumptions. Further, the TCs in our simulations were randomly generated with close to zero correlation between different components of the same subject and similar components across different subjects. The ability of both IVA and GICA to construct good SM estimates when inter-subject TC correlations for similar components are near zero is encouraging and bodes well for the algorithms. Functional network studies have indicated that higher correlations can exist between components of the same subject. In this study we did not investigate how reconstruction accuracy may change at higher correlations between TCs or the correlation limit at which ICA would begin to cluster correlated components. In addition, our datasets did not include effects of subject motion and spatial smoothing. In summary, it should be noted that real fMRI datasets are much more complex than our simple datasets. There are several back reconstruction techniques

available to estimate subject specific components from group components and in our experiments we used spatio-temporal regression. We did not test other techniques for all our experiments, but in cases where there was high subject variability we checked the results with other back reconstruction techniques. Our preliminary results indicate that the errors in GICA were higher irrespective of the technique applied, but the nature of errors was different.

Future improvements

IVA has a high computation and memory burden compared to GICA. It should be noted that GICA has been highly optimized over many versions of the GIFT toolbox. In future work, we intend to improve these limitations of IVA. Further studies are also needed to examine if a joint framework of GICA and IVA can be developed to capture the advantages of both schemes.

ACKNOWLEDGMENTS

This project was primarily funded by NIH grant R01EB005846 and NIH NIGMS Center of Biomedical Research Excellent (COBRE) grant 5P20RR021938/P20GM103472 to Vince Calhoun (PI). We also thank Josselin Dea, **Figure 1** was adopted from her previous work.

SUPPLEMENTARY MATERIAL

The Supplementary Material for this article can be found online at: http://www.frontiersin.org/journal/10.3389/fnsys.2014.00106/abstract

REFERENCES

Allen, E. A., Erhardt, E. B., Damaraju, E., Gruner, W., Segall, J. M., Silva, R. F., et al. (2011). A baseline for the multivariate comparison of resting-state networks. *Front. Syst. Neurosci.* 5:2. doi: 10.3389/fnsys.2011.00002

Allen, E. A., Erhardt, E. B., Wei, Y., Eichele, T., and Calhoun, V. D. (2012). Capturing inter-subject variability with group independent component analysis of fMRI data: a simulation study. *Neuroimage* 59, 4141–4159. doi: 10.1016/j.neuroimage.2011.10.010

Anderson, M., Li, X.-L., and Adali, T. (2010). "Nonorthogonal independent vector analysis using multivariate Gaussian model," in *Latent Variable Analysis and Signal Separation, Proceedings of the 9th International Conference, LVA/ICA 2010* (St. Malo), 354–361. doi: 10.1007/978-3-642-15995-4_44

Bassett, D. S., and Bullmore, E. T. (2009). Human brain networks in health and disease. *Curr. Opin. Neurol.* 22, 340. doi: 10.1097/WCO.0b013e32832d93dd

Bell, A. J., and Sejnowski, T. J. (1995). An information maximisation approach to blind separation and blind deconvolution. *Neural Comput.* 7, 1129–1159. doi: 10.1162/neco.1995.7.6.1129

Calhoun, V., and Adali, T. (2012). Multi-subject independent component analysis of fMRI: a decade of intrinsic networks, default mode, and neurodiagnostic discovery. *IEEE Rev. Biomed. Eng.* 5, 60–73. doi: 10.1109/RBME.2012.2211076

Calhoun, V., Adali, T., Pearlson, G., and Pekar, J. (2001). A method for making group inferences from functional MRI data using independent component analysis. *Hum. Brain Mapp.* 14, 140–151. doi: 10.1002/hbm.1048

Calhoun, V. D., Eichele, T., and Pearlson, G. (2009). Functional brain networks in schizophrenia: a review. *Front. Hum. Neurosci.* 3:17. doi: 10.3389/neuro.09.017.2009

Cohen, A. L., Fair, D. A., Dosenbach, N. U., Miezin, F. M., Dierker, D., Van Essen, D. C., et al. (2008). Defining functional areas in individual human brains using resting functional connectivity MRI. *Neuroimage* 41, 45. doi: 10.1016/j.neuroimage.2008.01.066

Dea, J. T., Anderson, M., Allen, E., Calhoun, V. D., and Adali, T. (2011). "IVA for multi-subject FMRI analysis: a comparative study using a new simulation toolbox," in *Machine Learning for Signal Processing (MLSP), 2011 IEEE International Workshop on* (Beijing: IEEE), 1–6.

Erhardt, E. B., Allen, E. A., Wei, Y., Eichele, T., and Calhoun, V. D. (2012). SimTB, a simulation toolbox for fMRI data under a model of spatiotemporal separability. *Neuroimage* 59, 4160–4167. doi: 10.1016/j.neuroimage.2011.11.088

Erhardt, E. B., Rachakonda, S., Bedrick, E. J., Allen, E. A., Adali, T., and Calhoun, V. D. (2011). Comparison of multi−subject ICA methods for analysis of fMRI data. *Hum. Brain Mapp.* 32, 2075–2095. doi: 10.1002/hbm.21170

Garrity, A., Pearlson, G., McKiernan, K., Lloyd, D., Kiehl, K., and Calhoun, V. (2007). Aberrant "default mode" functional connectivity in schizophrenia. *Am. J. Psychiatry* 164, 450–457. doi: 10.1176/appi.ajp.164.3.450

Giedd, J. N., Blumenthal, J., Jeffries, N. O., Castellanos, F. X., Liu, H., Zijdenbos, A., et al. (1999). Brain development during childhood and adolescence: a longitudinal MRI study. *Nat. Neurosci.* 2, 861–863. doi: 10.1038/13158

Greicius, M. (2008). Resting-state functional connectivity in neuropsychiatric disorders. *Curr. Opin. Neurol.* 21, 424–430. doi: 10.1097/WCO.0b013e328306f2c5

Khullar, S., Michael, A. M., Cahill, N. D., Kiehl, K. A., Pearlson, G., Baum, S. A., et al. (2011). ICA-fNORM: spatial normalization of fMRI data using intrinsic group-ICA networks. *Front. Syst. Neurosci.* 5:93. doi: 10.3389/fnsys.2011.00093

Lee, I., Kim, T., and Lee, T.-W. (2007). Fast fixed-point independent vector analysis algorithms for convolutive blind source separation. *Signal Process.* 87, 1859–1871. doi: 10.1016/j.sigpro.2007.01.010

Lee, J.-H., Lee, T.-W., Jolesz, F. A., and Yoo, S.-S. (2008). Independent vector analysis (IVA): multivariate approach for fMRI group study. *Neuroimage* 40, 86. doi: 10.1016/j.neuroimage.2007.11.019

Li, X.-L., Adali, T., and Anderson, M. (2011). Joint blind source separation by generalized joint diagonalization of cumulant matrices. *Signal Process.* 91, 2314–2322. doi: 10.1016/j.sigpro.2011.04.016

Li, Y. O., Adali, T., and Calhoun, V. D. (2007). Estimating the number of independent components for functional magnetic resonance imaging data. *Hum. Brain Mapp.* 28, 1251–1266. doi: 10.1002/hbm.20359

Ma, S., Phlypo, R., Calhoun, V. D., and Adali, T. (2013). "Capturing group variability using IVA: a simulation study and graph-theoretical analysis," in *Processing IEEE International Conference on Acoustics, Speech and Signal Processing (ICASSP)* (Vancouver, BC: IEEE).

McKeown, M. J., Makeig, S., Brown, G. G., Jung, T. P., Kindermann, S. S., Bell, A. J., et al. (1998). Analysis of fMRI data by blind separation into independent spatial components. *Hum. Brain Mapp.* 6, 160–188. doi: 10.1002/(SICI)1097-0193(1998)6:3%3C160::AID-HBM5%3E3.3.CO;2-R

Sorg, C., Riedl, V., Mühlau, M., Calhoun, V. D., Eichele, T., Läer, L., et al. (2007). Selective changes of resting-state networks in individuals at risk for Alzheimer's disease. *Proc. Natl. Acad. Sci. U.S.A.* 104, 18760–18765. doi: 10.1073/pnas.0708803104

Wax, M., and Kailath, T. (1985). Detection of signals by information theoretic criteria. *Acoust. Speech Signal Process. IEEE Trans.* 33, 387–392. doi: 10.1109/TASSP.1985.1164557

Conflict of Interest Statement: The authors declare that the research was conducted in the absence of any commercial or financial relationships that could be construed as a potential conflict of interest.

Received: 01 January 2014; accepted: 15 May 2014; published online: 26 June 2014.
Citation: Michael AM, Anderson M, Miller RL, Adalı T and Calhoun VD (2014) Preserving subject variability in group fMRI analysis: performance evaluation of GICA vs. IVA. Front. Syst. Neurosci. ***8****:106. doi: 10.3389/fnsys.2014.00106*
This article was submitted to the journal Frontiers in Systems Neuroscience.

frontiers in
SYSTEMS NEUROSCIENCE

ORIGINAL RESEARCH ARTICLE
published: 09 October 2014
doi: 10.3389/fnsys.2014.00197

Electrophysiological monitoring of injury progression in the rat cerebellar cortex

Gokhan Ordek[1], Archana Proddutur[2], Vijayalakshmi Santhakumar[2], Bryan J. Pfister[1] and Mesut Sahin[1]*

[1] Department of Biomedical Engineering, New Jersey Institute of Technology, Newark, NJ, USA
[2] Department of Neurology and Neurosciences, Rutgers Biomedical and Health Sciences, Newark, NJ, USA

Edited by:
Richard Apps, University of Bristol, UK

Reviewed by:
Henrik Jörntell, Lund University, Sweden
Guy Cheron, Université Libre de Bruxelles (ULB), Belgium

***Correspondence:**
Mesut Sahin, Department of Biomedical Engineering, New Jersey Institute of Technology, 323 MLK Jr. Blvd., University Heights, Newark, NJ 07102, USA
e-mail: sahin@njit.edu

The changes of excitability in affected neural networks can be used as a marker to study the temporal course of traumatic brain injury (TBI). The cerebellum is an ideal platform to study brain injury mechanisms at the network level using the electrophysiological methods. Within its crystalline morphology, the cerebellar cortex contains highly organized topographical subunits that are defined by two main inputs, the climbing (CFs) and mossy fibers (MFs). Here we demonstrate the use of cerebellar evoked potentials (EPs) mediated through these afferent systems for monitoring the injury progression in a rat model of fluid percussion injury (FPI). A mechanical tap on the dorsal hand was used as a stimulus, and EPs were recorded from the paramedian lobule (PML) of the posterior cerebellum via multi-electrode arrays (MEAs). Post-injury evoked response amplitudes (EPAs) were analyzed on a daily basis for 1 week and compared with pre-injury values. We found a trend of consistently decreasing EPAs in all nine animals, losing as much as 72 ± 4% of baseline amplitudes measured before the injury. Notably, our results highlighted two particular time windows; the first 24 h of injury in the acute period and day-3 to day-7 in the delayed period where the largest drops (∼50% and 24%) were observed in the EPAs. In addition, cross-correlations of spontaneous signals between electrode pairs declined (from 0.47 ± 0.1 to 0.35 ± 0.04, $p < 0.001$) along with the EPAs throughout the week of injury. In support of the electrophysiological findings, immunohistochemical analysis at day-7 post-injury showed detectable Purkinje cell loss at low FPI pressures and more with the largest pressures used. Our results suggest that sensory evoked potentials (SEPs) recorded from the cerebellar surface can be a useful technique to monitor the course of cerebellar injury and identify the phases of injury progression even at mild levels.

Keywords: cerebellar evoked potentials, traumatic injury model, Purkinje cells, multi-electrode arrays, micro-ECoG

INTRODUCTION

Assessment of the injury progression in the neural circuits affected by brain trauma is crucial not only to understand the underlying pathophysiological mechanisms but also for designing new therapeutic interventions. However, there is currently no clinical method available to assess the severity of brain injuries acutely and monitor its progression over days following the injury. If certain milestones of injury progression can be identified, therapeutic interventions can be made at specific times targeting parts of the circuit under attack by the secondary mechanism of injury.

Traumatic brain injury (TBI) results from a direct or indirect force exerted on the head that quickly leads to a sequel of changes in the brain such as mechanical tissue deformation, hemorrhage, and an elevated level of intracranial pressure. Cerebellar related deficits were reported in individuals within weeks to years following head injury (Iwadate et al., 1989; Louis et al., 1996). Metabolic changes, which could be an indicator heralding a pathological sequel of head trauma, have also been reported in the cerebellar injuries (Kushner et al., 1987; Niimura et al., 1999; Hattori et al., 2003). Extensive cell death can be observed in different parts of the brain as early as 10 min and progresses over a month following injury (Conti et al., 1998; Sato et al., 2001; Ai et al., 2007). Ai et al. (2007) showed progressive Purkinje cells (PC) loss after direct injury to the rat cerebellum, which may also be correlated with electrophysiological changes within the cerebellar circuitry (Ai and Baker, 2002, 2004). While the initial injury is predominantly dependent on the severity of the impact, subsequent reactions, which may last days to months, involve a complex sequence of events (Thompson et al., 2005; Marklund et al., 2006; Bramlett and Dietrich, 2007). The latter is an emerging field of research, especially regarding under-diagnosed cases such as concussions since they present a broad window of cascaded injury events.

It has been suggested that progression of a brain injury involves molecular and cellular cascaded mechanisms, which may occur in minutes to months after trauma (Thompson et al., 2005; Marklund et al., 2006; Bramlett and Dietrich, 2007). Glutamate, the primary excitatory neurotransmitter in the CNS, is highly utilized in the cerebellum between different cell types; mossy fibers

(MFs)—granule cells (GCs), Parallel fibers—PCs and Climbing fibers (CFs)—PCs (Ito, 2001; Nishiyama and Linden, 2007). One of the proposed mechanisms of brain injury involves excessive release of glutamate that leads to excitotoxicity (Gross, 2006). Elevation in the glutamate transmission is likely to disrupt the synaptic communication in the cerebellar cortex and compromise the cerebellar function. Ai et al. documented presynaptic hyper-excitation at the parallel fibers and the amplitude increase in the MF potentials on the days after the injury in the rat cerebellum (Ai and Baker, 2002, 2004). In fluid percussion injury (FPI) rats 7 days after injury, the same investigators also reported an amplitude decrease in the complex spike activity, which typically occurs by direct activation of the CFs on the PCs. (Ai et al., 2007).

The lack of complete understanding of brain injury mechanisms, particularly the mild cases, motivates the search for novel methods of detection and their integration into clinical practice. Brainstem auditory (BAEP), visual (VEP) and somatosensory (SSEP) evoked potentials (EPs) recorded from various areas of the brain with EEG electrodes have been utilized to detect brain injuries in the acute phase (Lindsay et al., 1981; Narayan et al., 1981; Claassen and Hansen, 2001; Nuwer et al., 2005; Burghaus et al., 2013). Sensory evoked potentials (SEPs) are highly reproducible across individuals and they can detect subtle changes in the post-injury period. A typical EP analysis includes comparing peak-to-peak amplitudes and onset latencies of characteristic deflections (Lindsay et al., 1981; Claassen and Hansen, 2001), fluctuations in the power spectrum (Culic et al., 2005; Nuwer et al., 2005; Burghaus et al., 2013), and changes in the coherence spectrum (Thatcher et al., 1989).

Evoked potentials obtained from the cerebellar surface as a response to a stimulus in anesthetized animals have been analyzed to understand the neural signal flow in the cerebellar cortex (Eccles et al., 1967; Oscarsson, 1968; Armstrong and Drew, 1980; Atkins and Apps, 1997; Baker et al., 2001; Diwakar et al., 2011). Eccles et al. (1967) used the juxtafastigial stimulation to identify subsequent MF mediated evoked responses (i.e., P1, N1, P2, N2 and N3) with <5 ms onset latencies in anesthetized cats. Armstrong and Drew (1980) observed these potentials with similar onset latencies associated with MF activation to snout stimulation in surface recordings from the rat cerebellum. They also compared the evoked field potentials of the cerebellum by different depth measurements and stated that all MF-mediated signal components were detectable from the surface using micro-electrodes. In a more recent study, MF-potentials were clearly reported with the denoted onset latencies in ketamine-xylazine treated rats, despite the substantial depression in the evoked amplitudes (Bengtsson and Jörntell, 2007).

Also, due to the divergent connection of MFs on the sole output of the cerebellar cortex, the PCs, the activation of MFs can be detected at multiple levels of the neuronal circuitry. D'Angelo et al. (2001) showed ∼5 ms (N2 wave) onset latency for the MF—GC activation to intracerebellar electric stimulation, which was consistent with earlier reports. Adversely, the earliest evoked responses were recorded at ∼13 ms (T wave) in the granular layer to a tactile stimulation of the whisker pad. Investigators suggested that the N2 and T waves were directly comparable (Roggeri et al., 2008).

Climbing fibers; one of the two afferents to the cerebellum, contribute significantly to sensory processing, and their EPs can also be detected with surface recordings. In an earlier report, the CF related EPs to a forelimb nerve stimulation was detected at 14–22 ms after the stimulus in the cerebellar surface potentials (Larson et al., 1969). Armstrong et al. (1973) reported observable CF-activation with the onset latencies of 16–22 ms and 20–25 ms in the vermis and ipsilateral hemisphere of the rat cerebellum, respectively. Atkins and Apps conducted a detailed characterization of CF mediated EPs and concluded noticeable variations in the onset latencies of CF field potentials within the same lobule of the rat cerebellum. The local field potentials (LFPs) contained CF activations with 10–15 ms onset latencies to forelimb stimulation in the central area of the paramedian lobule (PML), while CF response delays spread over to 16–26 ms in the lateral side of the PML with forelimb stimulation (Atkins and Apps, 1997). All these reports agree that both MF- and CF-related EPs are detectable from surface recordings. Furthermore, it is convenient to be able to identify these two responses by their onset latencies where the MF-related EPs precede the CF-related responses.

In this study, we recorded SEPs using micro electrocorticography (ECoG) electrode arrays implanted on the rat cerebellar cortex. Detection of subtle changes in the EPs, which are indications of alterations in the underlying neural circuitry, can provide valuable information about the injury development at high spatio-temporal resolution.

MATERIALS AND METHODS

MULTI-ELECTRODE ARRAYS (MEAs) IMPLANTATION

Flexible multi-electrode arrays (MEAs) were chronically implanted in 15 (6-uninjured control for 21 days and 9-injured for 7 days) Sprague-Dawley rats (250–350 g) using sterile surgical techniques. All procedures were approved and performed in accordance to the guidelines of the Institutional Animal Care and Use Committee, Rutgers University, Newark, NJ. The rats were anesthetized with ketamine and xylazine mixture (100 mg/kg and 10 mg/kg respectively, IP), and additional doses were administered as needed during the surgical procedure. The skull over the PML of the cerebellum was removed. A custom-design 31-channel flexible substrate (thickness 12 μm) MEA (NeuroNexus, MI) was placed subdurally on the paramedian cortex (rectangle, **Figure 1**.), 0.5–1.0 mm lateral to the paravermal vein (**Figure 1**). Electrode contacts were 50 μm in diameter and at 300 μm from each other in a 4 × 8 configuration. Electrode impedances varied between 300–500 kΩ prior to implantation. Impedances measured between 700–800 kΩ immediately after implantation and stabilized around 500–600 kΩ in the survival period (7 or 21-days). The electrode array was fixed in place to the pia mater using very small amounts of octyl cyanoacrylate tissue adhesive (Nexaband, WPI, Inc., FL) applied on the edges of the array. A reference electrode was placed above the array after covering the dura with a piece of animal's own connective tissue. The Omnetics micro connector at the end of the ribbon

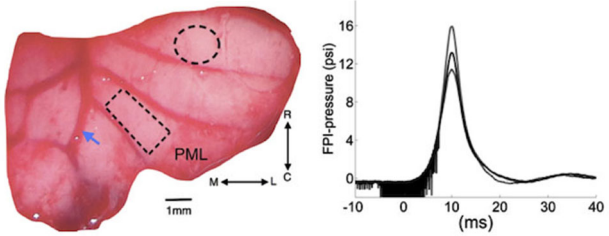

FIGURE 1 | Left: Position of cranial opening to induce FPI is shown as a dashed circle on the right cerebellar lobe rostral to the multi-electrode array (rectangle) implanted on the paramedian lobule (PML). Arrow shows the right paravermal vein. Right: the mean (solid trace) and lowest and highest (dash traces) of the FPI-pressure waves administered in all the rats of this study (n = 9). The noise seen before the rising phase is an artifact generated by forward motion of the voice coil. M-L: medio-lateral, R-C: rostro-caudal.

cable was fixed to the skull using dental acrylic and stainless steel screws. Detailed electrode implantation procedure was previously described (Ordek et al., 2013).

INJURY SITE CRANIOTOMY

A craniotomy of 1.8 mm diameter was opened to administer a pressure wave and injure the cerebellum at a distance of 2–2.5 mm from the edge of the implanted electrode (dashed circle, **Figure 1**). Once the dura was exposed, a plastic male Luer-loc port with a ∼1.7 mm inner diameter (cut from a 25G needle) was attached on the skull over the injury site with Nexaband adhesive. The port was filled with normal saline to check for leakage. Then, dental acrylic was applied to firmly attach the injury port to the skull.

FLUID PERCUSSION INJURY (FPI)

Nine of the 15 animals implanted with the MEAs were injured using the FPI method. The FPI device used in this study was a custom design voice-coil based system that could control the characteristics of the pressure waveform including the rise time, peak pressure and duration (Neuberger et al., 2014). A user specifies the displacement, velocity and acceleration of the voice coil that drives a hydraulic cylinder to generate the pressure wave when it hits the saline column in contact with the animal's brain. Integrated pressure transducer (Omega Inc.) and LabView program acquired the actual pressure waveform measured near the exit port for later analysis (right, **Figure 1**). A 2.3 mm-ID female Luer-loc fitting connects to the male Luer-loc cemented to the skull on the experimental animal. Animals were mildly anesthetized with a low dosage of ketamine and xylazine (50 mg/kg and 6 mg/kg respectively, IP). Prior to injury, the dura was visible through the port, which was then filled with 0.2 mL deionized water, free of air bubbles. Next, the animal was placed on a platform attached to the FPI device and a single pulse of pressure wave was released (∼15 psi, **Figure 1**). Only the animals that demonstrated overt signs of injury, i.e., a brief apnea (5–10 s), startling, and deferred-drowsiness (∼up to 3 h), were considered as successfully injured (n = 9 rats). No functional deficits, difficulty in walking or reaching, were observed in any of the FPI animals during the 7-day survival period.

ELECTROPHYSIOLOGY

Injured animals were removed from the FPI device and taken to the recording setup immediately (within 5 min) after the injury pulse to observe very early changes in the cerebellar signals. Recording sessions were kept relatively long on the day of injury (up to 1 h post-FPI) to observe the acute effects of injury. An additional dose of ketamine (30 mg/kg, IP) was administered for these sessions. Anesthesia regimen is very critical to obtain reproducible evoked potentials from the cerebellum and the cerebrum (Bengtsson and Jörntell, 2007; Ordek et al., 2013). Spontaneous and SEPs were collected each day for the next 7 days under anesthesia. The anesthesia dosage (ketamine/xylazine; 30 mg/kg and 2 mg/kg) and time of recording from anesthesia onset (∼5 min after) were standardized in order to minimize variations in anesthesia depth between recording sessions.

The recordings (both from injured and control animals) were performed in a large Faraday cage through a 34-channel headstage amplifier (Gain 800, Band-Pass; 0.8 Hz–3 kHz, Triangular Biosystems, NC) inserted into the micro connector on the rat's head. The multi-channel evoked and spontaneous signals were sampled at 16 kHz and collected in 20 s episodes into a desktop computer. In data analysis, raw signals were conditioned with an additional high-pass filter at 5 Hz and a low-pass at 400 Hz. Multiple trials were averaged to a 1 Hz stimulus in the 20 s window in order to reduce background activity against the evoked signals.

Sensory evoked potentials were elicited by a mechanical stimulation device, a tapered 1 mm cotton-tipped wood stick attached to the center of an audio speaker activated with a short pulse through a desktop computer. The mechanical stimuli were applied at a rate of one pulse per second throughout the 20 s recording episodes, bilaterally on the periphery, e.g., the left and right dorsal forearm, whiskers, face, and perioral areas. However, only ipsilateral (to injury and to the electrode implant side) dorsal hand EPs were included in this paper. All data analysis was performed in Matlab.

IMMUNOHISTOCHEMISTRY

Age matched naïve controls (n = 2) and 7 day post-FPI rats (n = 3) were anesthetized and perfused with 4% paraformaldehyde to harvest whole brains. The location of the FPI on the surface of cerebellum was marked with respect to the MEA implantation site, which was easily discernable after perfusion. The cerebellum was cut in half and then sliced in the lateral to medial direction in 50 μm parasagittal sections. The slices that contained the injury and electrode implantation regions were used for staining. Sliced sections were washed with 0.1 M phosphate buffered saline (PBS), and blocked using 10% normal goat serum in 0.3% triton in 0.1 M PBS. Then, sections were incubated overnight at room temperature with anti-CalbindinD28k antibody (MAB300, 1:1000, mouse monoclonal; Millipore) in 0.3% triton and 3% normal goat serum in PBS. Sections were reacted overnight at 4°C with Alexa 594-conjugated goat anti-mouse secondary antibody (1:500, Invitrogen) to reveal staining.

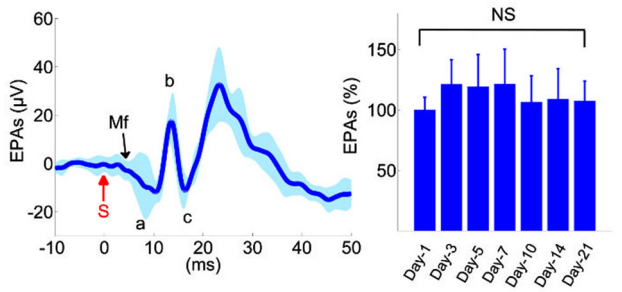

FIGURE 2 | Analysis of evoked potentials in the control animals ($n = 6$). Left: Evoked potential (EP) waveforms show sustained amplitudes over a 3-week period. Waveforms from 10 different recording days were superimposed from all animals. Evoked potential amplitudes (EPAs) of MF-mediated field potentials were calculated by averaging the triphasic potential amplitudes using the equation $\frac{|a-b|+|b-c|}{2}$. S: mechanical stimulus. Right: average MF response amplitudes from all six animals, normalized within each animal to the mean of the first day recording. None of the days were statistically different than the others ($F_{(6,59)} = 1.41$, rmANOVA, repeated measures of 6 rats,1–2 trials from each, 8–11 trials per day). Total number of trials is shown in parenthesis for each day. NS: not significant.

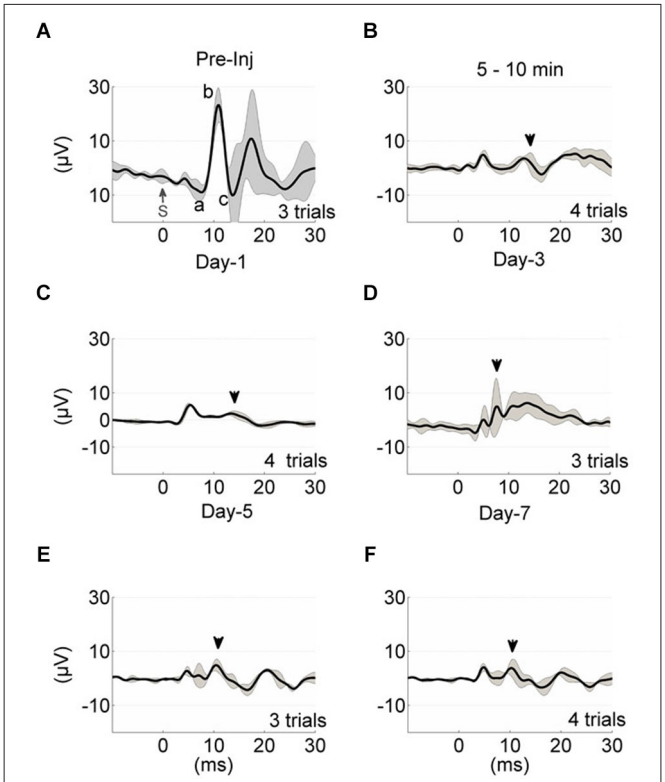

FIGURE 3 | Evoked potential waveform progression in a sample animal from the time of injury (A–F). Each trace represents the average of multiple trials (gray traces), and each trial is the stimulus (S, $t = 0$) trigger-average of 20 EPs. The black shade is the ± std. Mossy fiber-mediated potentials analyzed in **Figure 2** are marked in similar manner (**A**, a-c; **B–F**, arrowheads). The pre-injury recordings were obtained 5–10 min before the application of FPI **(A)**. Time of recording after anesthesia was ∼5 min **(A,C–F)** and 5–10 min after FPI induction **(B)**. All injury-day recordings showed great depression in the EP waveform and amplitudes. Day-3 EPs demonstrated larger amplitude variations; 5 ± 5 μV **(D)**.

Sections processed for CalbindinD28k staining were mounted on gelatin-coated slides to perform FluoroJade C staining for degenerating neurons (Neuberger et al., 2014). Sections were stained with 0.0001% FluoroJade C solution for 1 h at 4°C and cover slipped with DPX mounting media. Negative controls were routinely included in which primary antibody for CalbindinD28k was omitted. Representative images were obtained using Nikon A1R laser confocal microscope using 20× objective with identical camera settings.

RESULTS

EVOKED POTENTIALS

Evoked potentials showed reproducible waveforms in chronically implanted control animals (left plot, **Figure 2**), with peak-to-peak amplitudes ($V_{p\text{-}p}$) as high as 100 μV in individual channels, while the background level of neural activity was $V_{rms} = 2$ μV. A typical evoked response pattern demonstrated two or three distinct field potentials. The initial negative response arrived at ∼5 ms and usually measured in small amplitudes (∼5–10 $\mu V_{p\text{-}p}$). Conversely, subsequent evoked responses were larger positive deflections with ≥10 ms onset latencies. The first positive EP had a mean amplitude of ≥30 $\mu V_{p\text{-}p}$ in the control animals (a-b, **Figure 2**) and it was the most reproducible component across trials and animals. This EP was presumed to originate from the local MFs in the granular cell layer and it was followed by parallel fiber synaptic activations (c, **Figure 2**). The largest evoked field potential was usually detected with 13–17 ms onset latency, had a mean amplitude of ≥50 $\mu V_{p\text{-}p}$, and preceded a long-lasting (50–70 ms) refractory period. This potential was not included in the amplitude analysis because of high variability between the trials in the control animals.

In order to determine reproducibility of evoked amplitudes in the control animals, EPs were collected for MF-mediated potentials (a-c, **Figure 2**) during the 3-week survival period and analyzed in all animals at various time points (right panel, **Figure 2**, $n = 6$ rats, 8–11 trials per day). None of the days was statistically different in EP amplitudes in the recording period (Repeated measures of ANOVA, $F_{(6,59)} = 1.41$), though the largest variations were observed during the first few days, e.g., ∼21% on day-3 (Mann-Whitney; $n = 9$ trials, $p = 0.06$).

As a comparison, evoked potential waveforms are shown in an injured rat in 1-week period (**Figures 3A–F**). The amplitude of the MF-mediated responses declined drastically to 5 ± 2 μV (arrowhead, **Figure 3B**) within 10 min of injury induction from the baseline of 40 ± 5 μV (a-c, **Figure 3A**). There was no additional anesthesia injection at this period. Amplitude of MF-mediated EPs were diminished by ∼8 fold to a value barely above the background neural activity (2 μV_{rms}), while the arrival latency was preserved (10–11 ms) in these early acute responses. On the following day after injury (∼20 h), similar waveform characteristics were observed in the EP signals (**Figure 3C**). Multiple trials indicated detectable evoked potential amplitudes (EPAs) but reduced by 8–10 times from the baseline level. Three

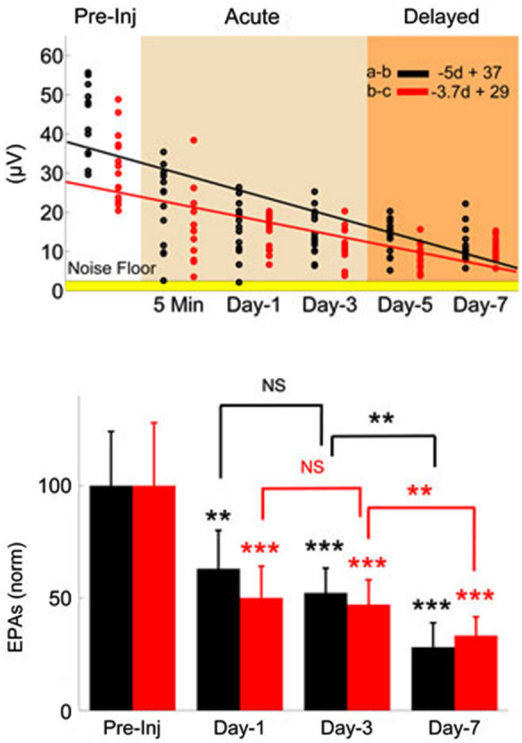

FIGURE 4 | Monitoring injury progression in EPAs of MF-mediated responses is presented on group data. Late MF-mediated potentials, a-b and b-c (shown in **Figure 3**) were analyzed individually. Top: All animals as a group demonstrated nearly a linear decreasing trend by the number of days (d) after the injury (R^2 = 0.47 and 0.43, respectively). Each dot in the scatter plot shows the mean of EPAs for subsequent a-b (black) and b-c potentials (red) in a different trial (n = 9 rats, 2–3 trials per animal on a given day). Bottom: Data shown are the mean ± std of normalized EPAs for the pre-injury and three selected days of the post-injury period. Same color representations in the scatter analysis are used here ($EPA_{(a-b)}$; black, $EPA_{(b-c)}$; red). All data were normalized to mean amplitude of the pre-injury recordings (n = 9 rats, 20 total trials). Amplitude loss reached as large as 75% at the end of the 7-day survival period. Other significances shown were calculated using repeated measures of ANOVA followed by Bonferroni correction. *$P < 0.05$, **$P < 0.005$, ***$P < 0.001$.

days post-injury, EPs were regressed to about ±10 μV range (gridlines, **Figure 3D**). Day-3 was noted as a recession point in the EPA trend, which was consistent across all injured animals (see **Figure 4**). At the end of the survival period, the EPA reductions were as large as 90% of the baseline, fluctuating around ±3–5 μV (**Figures 3E,F**).

The MF-mediated EPAs from all injured animals (n = 9) are analyzed for two characteristic amplitude measures (a-b and b-c, evoked potentials, **Figure 3**) in **Figure 4**. Each dot in the scatter plot is the mean amplitude calculated from 20 spike-trigger-averaged signals in 2–3 trials on the given day (top panel). There was a clear decline in the EPAs of both components as indicated by the negative slope; $V_{EPA(a-b)} = -5d + 37$ and $V_{EPA(b-c)} = -3.7d + 29$ (d; days, **Figure 4**). Amplitude drops in both characteristic measures were found to be significant for each day (Day 1, 3 and 7, bottom plot) of the post-injury period against the pre-injury values (14 trials per day, n = 9 rats, rmANOVA, $F_{(3,52)} = 20.52$; a-b and $F_{(3,52)} = 25.96$; b-c, $p < 0.001$). The sharpest drops (∼40%; a-b and ∼50%; b-c) were observed on day-1 of injury in both measures; (Paired t-test; a-b; $p = 0.0021$ and b-c; $p = 0.0007$). Relatively subtle amplitude changes were seen from day-1 to day-3 (NS; a-b; $p = 0.3282$, b-c; $p = 0.72$). The EPA losses were sustained at ∼50% of the baseline level on average on day-3. Prolonged recordings revealed that the greatest drops in EPAs occurred at the end of the survival period; Day-7 post-injury EPAs of a-b ∼28% of the pre-injury EPAs, while it was ∼33% for b-c (n = 9 animals; paired t-test, $p < 0.0001$). Statistical analysis suggested 80% power with a minimum sample size >7 animals to detect 50 ± 25% (mean ± std.) changes in normalized EPA ($\alpha = 0.05$, two-tail).

SPATIAL PATTERN OF INJURY

To determine whether there was a spatial variation in the altered EPs induced by injury, we analyzed the individual electrode channels by their orientation on the PML surface in one rat. Sample recordings of the pre-injury period (blue traces, **Figure 5**) showed different CF field potentials amplitudes (±10–20 μV) in response to the same peripheral stimulation. The spatial pattern of amplitude distribution was different after the induction of injury, i.e., each channel was affected by different amounts regardless of their initial amplitude (red traces). In some channels the amplitude decline was as large as 60–70 μV (paired t-test, $p < 0.005$), whereas in others as small as 5–10 μV (paired t-test, $p > 0.55$). Measurable changes clustered in both sagittally and transversely oriented electrode groups, however, the transverse group contained more contacts (center two rows; n = 11/16 channels). Interestingly, the amplitude reductions in this animal are less at the electrode sites closer to the injury point (∼2 mm in rostral direction) compared to the distant contacts.

SYNCHRONY

In order to evaluate the effect of injury on synchrony across the cerebellar cortex, we investigated cross-correlations between all contact pairs during evoked and spontaneous activity (not-evoked) before and after injury (**Figures 6A,B**). The EPs were large in amplitude and highly similar in waveform and timing across all 31-channels in the pre-injury trials (**Figure 6A**, top panel). Pearson correlation was as high as $r \geq 0.8$ between some channel pairs of EP waveforms, while it varied between $0.2 \leq r \leq 0.6$ during spontaneous oscillations (**Figure 6B**, top panel). After the injury, overall correlation for all channel pairs decreased by ∼2-fold (**Figure 6B**, bottom panel), i.e., to ∼0.2–0.3 and 0.3–0.4, respectively for spontaneous and evoked windows. Those channels that showed stronger correlations in the pre-injury trials (red squares in top panel) were also diminished to mean values of r = 0.3–0.4. Disruption of synchrony in evoked LFPs was clearly noticeable in the spike-trigger averaged plots of single channels (**Figure 6A**, bottom panel).

Correlation analysis was extended to all the animals at three time points after injury (n = 9 rats, **Figure 7**). Greatest reduction in mean correlation values for evoked and spontaneous recordings was noted at day-1 and day-7 of injury. At day-1 of injury,

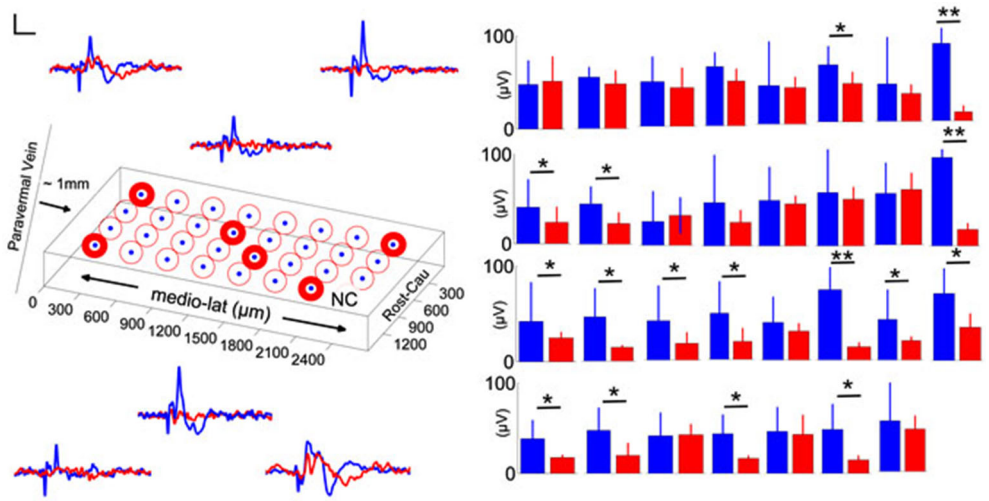

FIGURE 5 | Spatial distribution of pre-injury and day-7 (blue and red traces and bars, respectively) evoked potentials in a rat. Left: Orientation of the MEA on the PML and averaged recordings from six representative electrode contacts. Differential changes in EPAs with respect to the contact position were noted (n = 2–3 trials averaged for each day in one rat). NC: no channel, scale bar = 20 μV and 20 ms. Right: Pre- and post-injury, day-7 EPA changes are illustrated for all 31-contacts. While some of the channels did not indicate a significant amplitude drop with injury, in some others the changes were drastic (9–10 trials per day; error bars show one std; paired t-test; $*P < 0.05$; $**P < 0.005$).

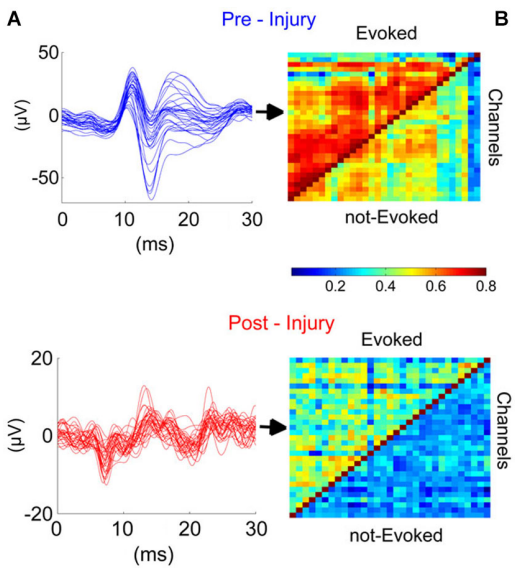

FIGURE 6 | Injury disrupted the synchrony across cerebellar cortex in the studied region (PML) during the evoked and not evoked (no stimulus) as demonstrated in this sample recording. **(A)** Traces (Blue and red; before and after injury, respectively) illustrate the EPs for all 31-channels. High synchronization (Top) was lost after the injury (7-day FPI; bottom). **(B)** Cross-correlations between all contact pairs for pre- and post-injury signals during EPs and nEPs periods. Prior to injury, inter-channel correlations varied within R = 0.5–0.8 and 0.3–0.6 during EPs and nEPs recordings, respectively (Top). Cross-correlation values diminished drastically in both EPs (R = 0.2–0.5) and nEPs periods (R = 0.2–0.4) by day-7 of injury (Bottom). EPs, evoked potentials; nEPs, not-evoked potentials.

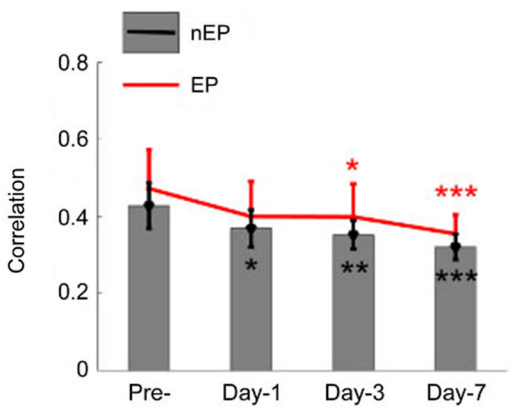

FIGURE 7 | Cross-correlations between all channel pairs were averaged in all animals and shown for the EP and not-evoked signals as in Figure 6. A declining trend was observed in this group data after the injury (n = 9 rats, 20 trials per day). By the end of the survival period, the mean and std of correlations were reduced to 0.35 ± 0.04 (from pre-inj. of 0.47 ± 0.12) and 0.32 ± 0.03 (from pre-inj. of 0.43 ± 0.06) for EP and nEP, respectively. Wilcoxon-signed rank test, $*P < 0.05$, $**P < 0.005$, $***P < 0.001$.

correlation value 'r' declined to 0.4 ± 0.09 from 0.47 ± 0.1 (EP-period, n = 9 rats; p = 0.055) and 0.37 ± 0.048 from 0.428 ± 0.06 (Spontaneous, n = 9 rats; p = 0.012). Correlation values exhibited greater deviations in the EP-period analysis due to existence of clustered electrode channels (see pre-injury results in **Figure 6**). Evoked potential correlations indicated that the first significant drops occurred at day-3 of injury, with only subtle differences from day-1 results (p = 0.044, r = 0.39 ± 0.08). Losses in averaged correlation values reached the greatest level at the end of the survival period in comparison to pre-injury values for both spontaneous and evoked period recordings. At day-7, averaged

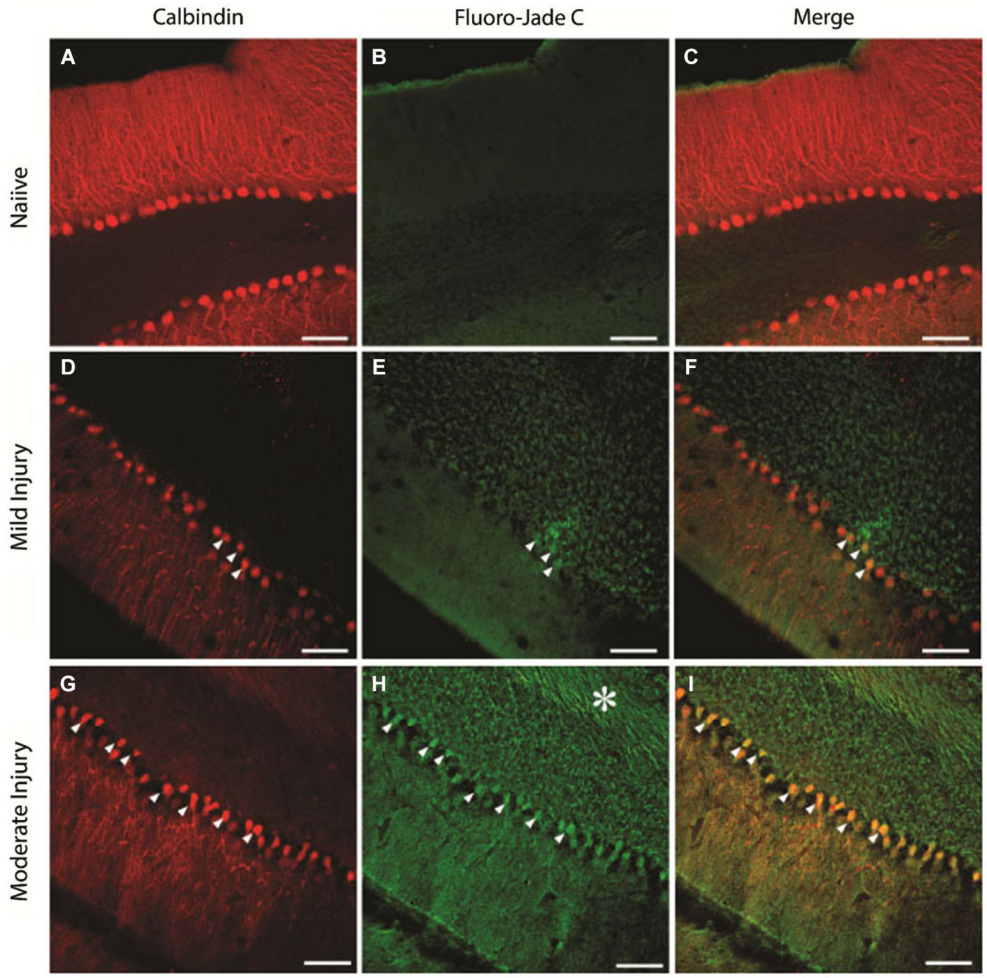

FIGURE 8 | Purkinje cell degeneration at mild and moderate levels of severity of cerebellar injury (15 psi and 25 psi). **(A–C)** Representative confocal images show CalbindinD28k labeled PCs **(A)** and the absence of FluoroJade C staining **(B)** in the same section from a naïve rat **(D–F)**. Images of a section from a rat 1 week after mild injury (15 psi) shows CalbindinD28k positive Purkinje cells **(D)** and the presence of a few FluoroJade C labeled cellular profiles (arrowheads in **E**). Merged image **(F)** shows that CalbindinD28k positive Purkinje cells are co-labeled with FluoroJade C (arrowheads) **(G–I)**. Representative section from a rat 1 week after moderate injury (25 psi) shows CalbindinD28k positive Purkinje cells **(G)** and extensive cellular (arrowheads) and axonal (asterisk) FluoroJade C labeling **(H)**. Merged image **(I)** shows numerous CalbindinD28k positive PCs labeled with FluoroJade C (arrowheads). Scale bar: 100 μm.

correlation was down to 0.35 ± 0.049 in the evoked-window and 0.32 ± 0.033 in the spontaneous recordings ($n = 9$ rats, 20 trials per analysis; $p < 0.001$).

IMMUNOHISTOLOGY

To determine the extent of cellular loss underlying the observed electrophysiological effects of injury, we performed double immunostaining of the cerebellar tissue extracted at the end of the physiological studies for expression of CalbindinD28k, a marker for PCs (Ishikawa et al., 1995) and FluoroJadeC. As expected, naïve animals showed a layer of CalbindinD28k-positive PCs (**Figures 8A–C**, $n = 15$ sections from three rats) with no FluoroJadeC labeling demonstrating the lack of neurodegeneration. There was a modest PC degeneration, as indicated by co-labeling of CalbindinD28k with FluoroJadeC labeled neuronal profiles in mildly injured rats (15 psi; **Figures 8D–F**, $n = 6$ sections from two rats). We found more CalbindinD28k expressing PCs co-labeled with FluoroJadeC in cerebellar sections from the rats injured at larger peak pressures, indicating more extensive PC degeneration (**Figures 8G–I**, $n = 6$ sections from one rat) than those with smaller peak pressure (**Figures 8D–F**). In addition to cell loss, sections from the rats subjected to injuries at higher peak pressures showed FluoroJadeC staining in the white matter tracks (asterisk in **Figure 8H**) suggesting the possibility of PC axonal degeneration. Remarkably, the domino-like alignment of PCs observed in naïve animals was degraded following injury at higher pressures (∼25 psi). The presence of FluorojadeC positive neurons in all FPI animals indicates ongoing neuronal degeneration at 1 week.

DISCUSSION

IDENTIFICATION OF EVOKED FIELD POTENTIALS

Evoked potentials have been investigated for assessment of severity in TBIs. Visual (Lachapelle et al., 2004), brainstem auditory (Soustiel et al., 1995), and sensory (Fossi et al., 2006; Amantini et al., 2009) EPs in EEG signals were proposed previously for detection of head injuries. The current study demonstrated prolonged reductions in the cerebellar EPs to hand stimulations during the 7-day period following the injury in a rat model of FPI. Characteristics (onset latencies and amplitudes) of MF- and CF-mediated cerebellar EPs were well documented by other investigators with highly reproducible results (Eccles et al., 1966a, 1967; Armstrong and Harvey, 1968; Armstrong and Drew, 1980; Atkins and Apps, 1997; Jörntell et al., 2000; Ordek et al., 2012). Our recordings in control animals (**Figure 1**) confirmed these reports with characteristic EPs containing mossy fiber (Brihaye et al., 1964; Eccles et al., 1967; Armstrong and Drew, 1980) and CF mediated responses (Eccles et al., 1967; Armstrong and Drew, 1980; Atkins and Apps, 1997) differentiated by their onset latencies.

Various components of surface recorded EPs were identified by the source localization in earlier reports (Eccles et al., 1967; Oscarsson, 1968; Armstrong and Drew, 1980; Atkins and Apps, 1997; Baker et al., 2001; Diwakar et al., 2011). Eccles et al. (1967) reported MF-mediated responses (MF— GCs—Parallel fibers—PCs) to have less than 5 ms onset latencies and denoted various deflections as P1, N1—N3, N4. Armstrong and Drew (1980) also identified similar MF-mediated field potentials within the same arrival latencies in response to peripheral electric stimulation in rats. In agreement to both, our control recordings indicated that the earliest noticeable evoked deflection was at ∼3–5 ms following the stimulus (**Figure 2**), which was relatively a weak response with a negative polarity and probably a direct recording from the MFs (P1-N1). The rising edge of the subsequent evoked response was detected at 8–11 ms in our recordings. This field potential was triphasic with a positive polarity, succeeded by excitation of parallel fibers (b-c, **Figure 2**), and it was attributed to MF activation in the granular layer (a-b, **Figure 2**). Evoked potentials (a-b and b-c) had in fact the most consistent and reproducible amplitudes among all evoked responses collected in the control animals, and thus we leveraged them for monitoring the injury progression (**Figures 3**, **4**). The onset latency of this MF field potential is slightly larger compared to the earlier reports. This may be explained by the stimulation paradigm, i.e., the location of the peripheral stimulation and the type of the stimulus. For instance, PC response latencies can increase from 6–8 ms to 7–10 ms by using tactile stimulation on the periphery instead of electrical stimulation of afferents (Bower and Woolston, 1983).

Conversely, CF-mediated potentials resembled late onset latencies (≥15 ms) in our results, which agreed with the previous reports. Pioneering studies on this subject showed that the CF activity arrives with ≥13 ms onset latencies in surface recordings (Eccles et al., 1966b; Armstrong and Drew, 1980). The delay varied between 13–19 ms in the contralateral hemisphere and between 16–22 ms in the contralateral vermis (Armstrong and Drew, 1980). Armstrong et al. (1973) also found evidence for increased PC activity with CF activation with 12–18 ms latencies compared to 4–10 ms latencies mediated by the MFs. More recently, Apps et al. demonstrated that CF response latencies to ipsilateral arm stimulation in anesthetized rats can vary between 16–26 ms when recorded from area 3 of the PML surface (Atkins and Apps, 1997). In addition to onset latencies, the CF-mediated responses can be identified by their amplitude and polarity. They are the largest positive deflections in the signals recorded from the cerebellar surface (Oscarsson, 1968; Armstrong et al., 1973) and distinguished by a refractory period up to 40 ms proceeding from the positive deflections (Armstrong and Harvey, 1968). Based on these features, we concluded that the latest EP in our recordings, which was detected at 15–20 ms in response to hand stimulation, was mediated through CF activation. The onset latency of the deflection was not the only evidence to support CF identification. The wave also resembled a strong and slow nature that succeeded a long-lasting (>50 ms) refractory period. Although the magnitude of this potential was the greatest in most of the trials, we did not include this deflection in amplitude analysis due to high variability across animals and trials. All evoked recordings presented in this particular work were obtained in anesthetized animals to avoid variations in the evoked responses due to changes in the cerebellar excitability across different awake states.

STABILITY OF EP RECORDINGS

Stability of EP amplitudes in the control animals clearly demonstrated that the tissue responses did not compromise the electrode array's ability to measure reproducibility of signals during 3-week implant period (**Figure 2**). Pre-injury recordings in the FPI animals also served as an additional confirmation on the feasibility of this recording method of EPs (**Figure 3A**). The depth of ketamine-xylazine anesthesia may alter the EP amplitudes (Bengtsson and Jörntell, 2007; Ordek et al., 2012). Jörntell et al. (2000) showed the anesthesia effects on both MF- and CF-mediated responses at varying doses of ketamine/xylazine injections (Bengtsson and Jörntell, 2007). In order to minimize the effect of anesthesia depth, the timing and duration of the recording sessions from the injection of anesthesia were carefully controlled (see Section Methods). After testing various peripheral sites (whisker, forelimb, hindlimb) of stimulation, we concluded that the late MF-related response to (ipsilateral) dorsal hand mechanical stimulation was the most reproducible as a pattern in the recordings of the investigated PML region.

FPI MODEL

The FPI model implemented in the current study produces a combination of focal and diffuse damages, and it is widely used as an animal model of TBI (Thompson et al., 2005). It was documented that FPI can induce structural and functional changes in the cerebellar cortex even at remote locations (Ai et al., 2007). This allowed us to apply the injury at a different location from the site of electrode implant without disturbing the electrode-tissue interface. Immunohistochemical analysis further

verified that the injury was spread to remote locations within the ipsilateral cerebellum.

PRIMARY VS. DELAYED INJURY PHASES

To investigate the relation between electrophysiological signals and the cerebellar insults, we demonstrated EPA changes as early as 5 min post-injury to 1 week in anesthetized rats, following FPI. Immediate recordings after trauma indicated substantial depression of the EP pattern as a whole; an effect that must be directly linked to initial impact of injury, e.g., tissue and/or blood vessel damage, and intracranial pressure elevation (Gaetz, 2004; Cernak, 2005). Interestingly, early arriving EP (<5 ms), presumably the direct MF activation, starts to increase in magnitude during the post-injury phase, which may be explained by hyper excitability of MFs as reported earlier (Ai and Baker, 2004). Monitoring the progression of injury-related changes at such detail can provide further insights about the course of the injury progression, which has been reported to present two main phases; primary and delayed-mechanisms (Doppenberg et al., 2004; Andriessen et al., 2010).

Progressive PC losses were documented in short (hours) as well as longitudinal (days—weeks) studies of immunohistology (Fukuda et al., 1996; Mautes et al., 1996). In support of this finding, MF and CF mediated EPAs of this study monotonously decreased in the post-injury period (**Figure 3**). At a closer evaluation, we quantified the EPA alteration in the late MF-mediated responses by analyzing in two separate EPs; a-b and b-c. Alterations in both response amplitudes were found to be very similar but not identical.

We determined that the largest drops were observed in the acute period for both amplitude measures between immediately after the injury to day-1. The EPA drops were more significant in the b-c segment (∼50%) compared to the a-b potential (∼37%) in this period. The second most drastic drop was noted from day-3 to day-7 (24% and 14%, respectively), which was termed as the delayed injury period in other reports (Sato et al., 2001). The two phases with distinct characteristics suggest two different injury mechanisms involved. Baker and colleagues concluded that day-3 is a critical time point in the course of injury (Ai and Baker, 2004; Ai et al., 2007). They found majority of cell deaths within the next 24 h after FPI, and the second wave of injury effect was delayed until day-3 (Ai et al., 2007).

SPATIAL DIFFERENTIATION

Fluid percussion injury induces a combination of focal and diffuse type of injuries (Potts et al., 2009). We found spatially varying degrees of EPA reduction across the PML surface covered by the electrode array (**Figure 5**). Somatotopy of the PML in the rat cerebellum was investigated in several reports including ours (Bower and Woolston, 1983; Atkins and Apps, 1997; Ordek et al., 2012), though there is no consensus regarding a single somatotopy in the cerebellum. In the animal shown in **Figure 5** (blue traces) the EP responses collected from the lateral side of the PML were relatively larger. Following FPI induction, EPAs were affected differentially across the PML surface without a certain directional preference. Interestingly, the smallest amplitude changes were observed on the most rostral contacts of the MEA closest to the injury site. This spatial differentiation supports our premise that the evoked amplitude changes are not due to some mechanical perturbation of the MEA by the fluid pressure wave at the time of impact, but because of damage to the underlying neural structures.

SYNCHRONY

Local field potentials emerge from the synchrony of a large population of neural components underneath the electrode contacts. Synchrony is observed at multiple levels of cerebellar cortex at various frequency bands. Low-frequency band (1–4 Hz) oscillations in the molecular layer were proposed to originate from the inferior olive and modulate the PC activity via the CF afferents (Lang et al., 2006). Whereas, theta and beta band oscillations are generated in the granular layer by MF activations (Hartmann and Bower, 1998; D'Angelo et al., 2001). In contrast to the deeper layers, the neurons in the molecular layer of the cerebellar cortex are capable of oscillating at higher frequencies, for instance at 30–80 Hz due to the interneuronal feedback mechanism in the molecular layer (Middleton et al., 2008) and 160–260 Hz in the Purkinje layer via axon collaterals (de Solages et al., 2008). Presumably, these oscillations originate from different neural structures, which have specific spatial alignments in the cerebellar cortex. For instance, it is possible to record sagittal synchrony in lower frequencies (1–4 Hz) that is mediated by the CFs (Lang et al., 2006) while the interneurons in the ML exhibit higher frequency oscillations (30–80 Hz) in the transverse plane (Middleton et al., 2008).Considering that the surface recordings with ball electrodes are able to detect even the deep MF related potentials, the subdural MEAs should be able to detect synchronous activities from various layers of the cerebellar cortex.

Although the synchrony in cerebellar cortex has been investigated for decades, there are just a few reports on the spatial aspect of these events. De Zeeuw et al. (2011) reviewed the spatiotemporal aspects of cerebellar oscillations in a recent report. They argued that complex spike synchrony can be observed between PCs that are separated up to ∼500 μm in the parasagittal zones and which is consistent throughout the cerebellar cortex. In contrast, simple spike synchrony doesn't indicate any particular directionality. In the flocculus, simple spike synchrony is in the same orientation of complex spike spatial pattern (parasagittal), whereas the synchrony is mainly oriented along the transverse plane in Crus 2 and in the PML. de Solages et al. (2008) showed the high-frequency oscillations (∼200 Hz) by using tetrode and multi-site recordings in both anesthetized and awake animals. They also showed that the synchrony at this frequency band extended as far as 375 μm across the electrodes aligned in the transversal orientation. Furthermore, their report suggested that there was a correlation between the oscillations obtained from different layers of cerebellar cortex, where molecular and Purkinje layer recordings displayed peak coherences. Similarly, Courtemanche et al. (2013) documented the ∼200 Hz oscillations in the Purkinje cell layer of anesthetized rats with metal electrodes separated by 500 μm.

In addition to *in vivo* studies, pathological findings also indicated the large scale synchrony in the cerebellar cortex.

In the experiments on cerebellar mutant mice, high-frequency synchrony (>150 Hz) was shown in the zones up to 1 mm (Servais and Cheron, 2005). Some of these oscillations were also noted in calretinin/calbindin mutant mice along the parallel fiber orientations ranging up to 2 mm (Servais et al., 2004; Cheron et al., 2008). These reports support the spatial synchrony that we observe in our recordings, although the area covered by our MEA was unprecedented in size (300 μm–2100 μm).

The effect of anesthesia on spontaneous recordings as well as EPs is a concern raised by a number of investigators in the past. Cheron and his colleague (Servais and Cheron, 2005) compared the differential effects of two different anesthesia regimens (ketamine and pentobarbitone) on LFPs. They found that ketamine, an NMDA antagonist, depresses the LFP oscillations with PC desynchronization, while pentobarbitone, which targets the $GABA_a$ receptors, caused slight changes in PC synchrony. In the cerebellum, excitatory networks such as the MF-GC-PFs pathway use the NMDA receptors, whereas inhibitory signaling is mediated by $GABA_a$ receptors through the PCs and molecular layer interneurons. Therefore, using different anesthesia regimens could have different effects on the neural activity by selectively targeting different synaptic mechanisms. Another critical factor in anesthesia is the time delay allowed before data collection. Jörntell and his colleague (Bengtsson and Jörntell, 2007) reported that ketamine-xylazine (20:1) depressed both MF and CF responses significantly for 10 min after the injection. Similarly, LFP oscillations in the cerebellum exhibited sustained depressions for 5–10 min after anesthetic injection (Servais and Cheron, 2005). Although the recovery time was dose dependent, we observed that the delay allowed between the injection and recordings can be used to control the anesthesia level in a reproducible manner, and thus obtain stable recordings.

Our findings suggested that there was a significant correlation loss in all electrode groups starting day-1 of injury. The correlation test applied to the EEG signals after head injuries is a diagnostic technique that has been used over decades. Thatcher et al. (1989) reported coherence changes across short-distance in different frequency bands after mild injuries. Our findings indicated progressive reductions in correlation values during spontaneous as well stimulated periods (**Figure 7**). Interestingly, correlation loss paralleled the decline in the EPAs. Both measures exhibited similar trends, i.e., greater losses at day-1 and then from day-5 to day- 7, but only subtle changes from day-1 to day-3. This suggests that the injury did not only affect the number of PCs that are firing in synch through MF or CF activations, hence the EPA loss, but also the connectivity between spatially distant zones (within 2 mm^2) was disrupted.

IMMUNOHISTOLOGY

We included immunohistological analysis into this study primarily for two reasons; first, to verify that an injury-related neuronal degeneration was produced by direct-FPI to the cerebellum. We used double immunostaining; CalbindinD28k and Fluoro-Jade C to determine the neuronal subtype that was injured. Fluoro-Jade markings showed irreversible cell deaths as delayed as 1 month of injury induction (molecular layer neurons and PCs) in the cerebellum by earlier reports (Sato et al., 2001). Hallam et al. (2004) also showed Fluoro-Jade C positive degenerating neurons at different time points (24 h, 48 h and 7-days) of the FPI in the rat cerebellum, which was correlated with motor behavioral deficits. Second, we aimed to evaluate the sensitivity of the electrophysiological parameters to detect neural damage due to FPI compared to immunostaining. Our results indicated that the subdural MEA recordings were able to glean valuable information about the injury at peak pressures as mild as 15 psi, an injury pressure that resulted in minimal neuronal degeneration by immunohistology (**Figures 8D–F**) and no overt behavioral deficits.

CONCLUSIONS

Here we presented data showing the feasibility of monitoring injury related changes in the cerebellar cortex using EPs recorded with subdurally implanted MEAs. Changes in peripherally evoked signal amplitudes were detected by 5-min post-injury recordings, and monitored periodically in the following 7 days. Our results also presented evidences showing that the decline of inter-contact correlations followed a similar trend to the evoked amplitudes in the 1 week post-injury period. Immunohistological results confirmed the cellular degenerations in the targeted cerebellar area as a result of injury. Overall, electrophysiological monitoring using MEAs is a promising technique to study the progression of neuronal degeneration in animal models of injury without the need of terminating experimental subjects at various time points in the study.

ACKNOWLEDGMENTS

We thank Luke Fritzky for the technical support on confocal images. We also acknowledge Mathew Long for calibrating the fluid percussion injury device prior to each injury. Study support: New Jersey Commission on Brain Injury Research, multi-investigator grant–CBIR11PJT003 to Bryan J. Pfister and Vijayalakshmi Santhakumar.

REFERENCES

Ai, J., and Baker, A. (2002). Presynaptic hyperexcitability at cerebellar synapses in traumatic injury rat. *Neurosci. Lett.* 332, 155–158. doi: 10.1016/s0304-3940(02)00945-x

Ai, J., and Baker, A. (2004). Presynaptic excitability as a potential target for the treatment of the traumatic cerebellum. *Pharmacology* 71, 192–198. doi: 10.1159/000078085

Ai, J., Liu, E., Park, E., and Baker, A. (2007). Structural and functional alterations of cerebellum following fluid percussion injury in rats. *Exp. Brain Res.* 177, 95–112. doi: 10.1007/s00221-006-0654-9

Amantini, A., Fossi, S., Grippo, A., Innocenti, P., Amadori, A., Bucciardini, L., et al. (2009). Continuous EEG-SEP monitoring in severe brain injury. *Neurophysiol. Clin.* 39, 85–93. doi: 10.1016/j.neucli.2009.01.006

Andriessen, T. M., Jacobs, B., and Vos, P. E. (2010). Clinical characteristics and pathophysiological mechanisms of focal and diffuse traumatic brain injury. *J. Cell. Mol. Med.* 14, 2381–2392. doi: 10.1111/j.1582-4934.2010.01164.x

Armstrong, D., and Drew, T. (1980). Responses in the posterior lobe of the rat cerebellum to electrical stimulation of cutaneous afferents to the snout. *J. Physiol.* 309, 357–374.

Armstrong, D. M., and Harvey, R. J. (1968). Responses to a spino-olivo-cerebellar pathway in the cat. *J. Physiol.* 194, 147–168.

Armstrong, D. M., Harvey, R. J., and Schild, R. F. (1973). Branching of inferior olivary axons to terminate in different folia, lobules or lobes of the cerebellum. *Brain Res.* 54, 365–371. doi: 10.1016/0006-8993(73)90062-0

Atkins, M. J., and Apps, R. (1997). Somatotopical organisation within the climbing fibre projection to the paramedian lobule and copula pyramidis of the rat cerebellum. *J. Comp. Neurol.* 389, 249–263. doi: 10.1002/(sici)1096-9861(19971215)389:2<249::aid-cne5>3.3.co;2-o

Baker, M. R., Javid, M., and Edgley, S. A. (2001). Activation of cerebellar climbing fibres to rat cerebellar posterior lobe from motor cortical output pathways. *J. Physiol.* 536, 825–839. doi: 10.1111/j.1469-7793.2001.00825.x

Bengtsson, F., and Jörntell, H. (2007). Ketamine and xylazine depress sensory-evoked parallel fiber and climbing fiber responses. *J. Neurophysiol.* 98, 1697–1705. doi: 10.1152/jn.00057.2007

Bower, J. M., and Woolston, D. C. (1983). Congruence of spatial organization of tactile projections to granule cell and Purkinje cell layers of cerebellar hemispheres of the albino rat: vertical organization of cerebellar cortex. *J. Neurophysiol.* 49, 745–766.

Bramlett, H. M., and Dietrich, W. D. (2007). Progressive damage after brain and spinal cord injury: pathomechanisms and treatment strategies. *Prog. Brain Res.* 161, 125–141. doi: 10.1016/s0079-6123(06)61009-1

Brihaye, J., Ectors, Y., Retif, J., Melot, G., and Gompel, C. (1964). Hemangiomas of the cervical vertebrae and repetition of spinal cord complications. Apropos of a 2d case. *Acta Chir. Belg.* 63, 299–307.

Burghaus, L., Liu, W. C., Dohmen, C., Haupt, W. F., Fink, G. R., and Eggers, C. (2013). Prognostic value of electroencephalography and evoked potentials in the early course of malignant middle cerebral artery infarction. *Neurol. Sci.* 34, 671–678. doi: 10.1007/s10072-012-1102-1

Cernak, I. (2005). Animal models of head trauma. *NeuroRx* 2, 410–422. doi: 10.1602/neurorx.2.3.410

Cheron, G., Servais, L., and Dan, B. (2008). Cerebellar network plasticity: from genes to fast oscillation. *Neuroscience* 153, 1–19. doi: 10.1016/j.neuroscience.2008.01.074

Claassen, J., and Hansen, H. C. (2001). Early recovery after closed traumatic head injury: somatosensory evoked potentials and clinical findings. *Crit. Care Med.* 29, 494–502. doi: 10.1097/00003246-200103000-00005

Conti, A. C., Raghupathi, R., Trojanowski, J. Q., and McIntosh, T. K. (1998). Experimental brain injury induces regionally distinct apoptosis during the acute and delayed post-traumatic period. *J. Neurosci.* 18, 5663–5672.

Courtemanche, R., Robinson, J. C., and Aponte, D. I. (2013). Linking oscillations in cerebellar circuits. *Front. Neural Circuits* 7:125. doi: 10.3389/fncir.2013.00125

Culic, M., Blanusa, L. M., Grbic, G., Spasic, S., Jankovic, B., and Kalauzi, A. (2005). Spectral analysis of cerebellar activity after acute brain injury in anesthetized rats. *Acta Neurobiol. Exp. (Wars)* 65, 11–17.

D'Angelo, E., Nieus, T., Maffei, A., Armano, S., Rossi, P., Taglietti, V., et al. (2001). Theta-frequency bursting and resonance in cerebellar granule cells: experimental evidence and modeling of a slow k+-dependent mechanism. *J. Neurosci.* 21, 759–770.

de Solages, C., Szapiro, G., Brunel, N., Hakim, V., Isope, P., Buisseret, P., et al. (2008). High-frequency organization and synchrony of activity in the purkinje cell layer of the cerebellum. *Neuron* 58, 775–788. doi: 10.1016/j.neuron.2008.05.008

De Zeeuw, C. I., Hoebeek, F. E., Bosman, L. W., Schonewille, M., Witter, L., and Koekkoek, S. K. (2011). Spatiotemporal firing patterns in the cerebellum. *Nat. Rev. Neurosci.* 12, 327–344. doi: 10.1038/nrn3011

Diwakar, S., Lombardo, P., Solinas, S., Naldi, G., and D'Angelo, E. (2011). Local field potential modeling predicts dense activation in cerebellar granule cells clusters under LTP and LTD control. *PLoS One* 6:e21928. doi: 10.1371/journal.pone.0021928

Doppenberg, E. M., Choi, S. C., and Bullock, R. (2004). Clinical trials in traumatic brain injury: lessons for the future. *J. Neurosurg. Anesthesiol.* 16, 87–94. doi: 10.1097/00008506-200401000-00019

Eccles, J. C., Llinás, R., and Sasaki, K. (1966a). Intracellularly recorded responses of the cerebellar Purkinje cells. *Exp. Brain Res.* 1, 161–183. doi: 10.1007/bf00236869

Eccles, J. C., Llináss, R., Sasaki, K., and Voorhoeve, P. E. (1966b). Interaction experiments on the responses evoked in Purkinje cells by climbing fibres. *J. Physiol.* 182, 297–315.

Eccles, J. C., Sasaki, K., and Strata, P. (1967). Interpretation of the potential fields generated in the cerebellar cortex by a mossy fibre volley. *Exp. Brain Res.* 3, 58–80. doi: 10.1007/bf00234470

Fossi, S., Amantini, A., Grippo, A., Innocenti, P., Amadori, A., Bucciardini, L., et al. (2006). Continuous EEG-SEP monitoring of severely brain injured patients in NICU: methods and feasibility. *Neurophysiol. Clin.* 36, 195–205. doi: 10.1016/j.neucli.2006.09.001

Fukuda, K., Aihara, N., Sagar, S. M., Sharp, F. R., Pitts, L. H., Honkaniemi, J., et al. (1996). Purkinje cell vulnerability to mild traumatic brain injury. *J. Neurotrauma* 13, 255–266. doi: 10.1089/neu.1996.13.255

Gaetz, M. (2004). The neurophysiology of brain injury. *Clin. Neurophysiol.* 115, 4–18. doi: 10.1016/s1388-2457(03)00258-x

Gross, L. (2006). "Supporting" players take the lead in protecting the overstimulated brain. *PLoS Biol.* 4:e371. doi: 10.1371/journal.pbio.0040371

Hallam, T. M., Floyd, C. L., Folkerts, M. M., Lee, L. L., Gong, Q. Z., Lyeth, B. G., et al. (2004). Comparison of behavioral deficits and acute neuronal degeneration in rat lateral fluid percussion and weight-drop brain injury models. *J. Neurotrauma* 21, 521–539. doi: 10.1089/089771504774129865

Hartmann, M. J., and Bower, J. M. (1998). Oscillatory activity in the cerebellar hemispheres of unrestrained rats. *J. Neurophysiol.* 80, 1598–1604.

Hattori, N., Huang, S. C., Wu, H. M., Yeh, E., Glenn, T. C., Vespa, P. M., et al. (2003). Correlation of regional metabolic rates of glucose with glasgow coma scale after traumatic brain injury. *J. Nucl. Med.* 44, 1709–1716.

Ishikawa, K., Mizusawa, H., Fujita, T., Ohkoshi, N., Doi, M., Komatsuzaki, Y., et al. (1995). Calbindin-D 28k immunoreactivity in the cerebellum of spinocerebellar degeneration. *J. Neurol. Sci.* 129, 179–185. doi: 10.1016/0022-510x(94)00279-w

Ito, M. (2001). Cerebellar long-term depression: characterization, signal transduction, and functional roles. *Physiol. Rev.* 81, 1143–1195.

Iwadate, Y., Saeki, N., Namba, H., Odaki, M., Oka, N., and Yamaura, A. (1989). Post-traumatic intention tremor–clinical features and CT findings. *Neurosurg. Rev.* 12(Suppl. 1), 500–507. doi: 10.1007/bf01790695

Jörntell, H., Ekerot, C., Garwicz, M., and Luo, X. L. (2000). Functional organization of climbing fibre projection to the cerebellar anterior lobe of the rat. *J. Physiol.* 522(Pt. 2), 297–309. doi: 10.1111/j.1469-7793.2000.00297.x

Kushner, M., Tobin, M., Alavi, A., Chawluk, J., Rosen, M., Fazekas, F., et al. (1987). Cerebellar glucose consumption in normal and pathologic states using fluorine-FDG and PET. *J. Nucl. Med.* 28, 1667–1670.

Lachapelle, J., Ouimet, C., Bach, M., Ptito, A., and Mckerral, M. (2004). Texture segregation in traumatic brain injury—a VEP study. *Vision Res.* 44, 2835–2842. doi: 10.1016/j.visres.2004.06.007

Lang, E. J., Llinas, R., and Sugihara, I. (2006). Isochrony in the olivocerebellar system underlies complex spike synchrony. *J. Physiol.* 573 (Pt. 1), 277–279. doi: 10.1113/jphysiol.2006.571101

Larson, B., Miller, S., and Oscarsson, O. (1969). Termination and functional organization of the dorsolateral spino-olivocerebellar path. *J. Physiol.* 203, 611–640.

Lindsay, K. W., Carlin, J., Kennedy, I., Fry, J., Mcinnes, A., and Teasdale, G. M. (1981). Evoked potentials in severe head injury—analysis and relation to outcome. *J. Neurol. Neurosurg. Psychiatry* 44, 796–802. doi: 10.1136/jnnp.44.9.796

Louis, E. D., Lynch, T., Ford, B., Greene, P., Bressman, S. B., and Fahn, S. (1996). Delayed-onset cerebellar syndrome. *Arch. Neurol.* 53, 450–454. doi: 10.1001/archneur.1996.00550050080027

Marklund, N., Bakshi, A., Castelbuono, D. J., Conte, V., and Mcintosh, T. K. (2006). Evaluation of pharmacological treatment strategies in traumatic brain injury. *Curr. Pharm. Des.* 12, 1645–1680. doi: 10.2174/138161206776843340

Mautes, A. E., Fukuda, K., and Noble, L. J. (1996). Cellular response in the cerebellum after midline traumatic brain injury in the rat. *Neurosci. Lett.* 214, 95–98. doi: 10.1016/0304-3940(96)12916-5

Middleton, S., Racca, C., Cunningham, M. O., Traub, R., Monyer, H., Knöpfel, T., et al. (2008). High-frequency network oscillations in cerebellar cortex. *Neuron* 58, 763–774. doi: 10.1016/j.neuron.2008.03.030

Narayan, R. K., Greenberg, R. P., Miller, J. D., Enas, G. G., Choi, S. C., Kishore, P. R., et al. (1981). Improved confidence of outcome prediction in severe head injury. A comparative analysis of the clinical examination, multimodality evoked potentials, CT scanning and intracranial pressure. *J. Neurosurg.* 54, 751–762. doi: 10.3171/jns.1981.54.6.0751

Neuberger, E. J., Abdul Wahab, R., Jayakumar, A., Pfister, B. J., and Santhakumar, V. (2014). Distinct effect of impact rise times on immediate and early neuropathology after brain injury in juvenile rats. *J. Neurosci. Res.* 92, 1350–1361. doi: 10.1002/jnr.23401

Niimura, K., Chugani, D. C., Muzik, O., and Chugani, H. T. (1999). Cerebellar reorganization following cortical injury in humans: effects of lesion size and age. *Neurology* 52, 792–797. doi: 10.1212/wnl.52.4.792

Nishiyama, H., and Linden, D. J. (2007). Pure spillover transmission between neurons. *Nat. Neurosci.* 10, 675–677. doi: 10.1038/nn0607-675

Nuwer, M., Hovda, D., Schrader, L., and Vespa, P. (2005). Routine and quantitative EEG in mild traumatic brain injury. *Clin. Neurophysiol.* 116, 2001–2025. doi: 10.1016/j.clinph.2005.05.008

Ordek, G., Groth, J. D., and Sahin, M. (2012). Effect of anesthesia on spontaneous activity and evoked potentials of the cerebellar cortex. *Conf. Proc. IEEE Eng. Med. Biol. Soc.* 2012, 835–838. doi: 10.1109/EMBC.2012.6346061

Ordek, G., Groth, J., and Sahin, M. (2013). Differential effects of ketamine/xylazine anesthesia on the cerebral and cerebellar cortical activities in the rat. *J. Neurophysiol.* 109, 1435–1443. doi: 10.1152/jn.00455.2012

Oscarsson, O. (1968). Termination and functional organization of the ventral spino-olivocerebellar path. *J. Physiol.* 196, 453–478.

Potts, M. B., Adwanikar, H., and Noble-Haeusslein, L. J. (2009). Models of traumatic cerebellar injury. *Cerebellum* 8, 211–221. doi: 10.1007/s12311-009-0114-8

Roggeri, L., Rivieccio, B., Rossi, P., and D'Angelo, E. (2008). Tactile stimulation evokes long-term synaptic plasticity in the granular layer of cerebellum. *J. Neurosci.* 28, 6354–6359. doi: 10.1523/JNEUROSCI.5709-07.2008

Sato, M., Chang, E., Igarashi, T., and Noble, L. (2001). Neuronal injury and loss after traumatic brain injury: time course and regional variability. *Brain Res.* 917, 45–54. doi: 10.1016/s0006-8993(01)02905-5

Servais, L., Bearzatto, B., Hourez, R., Dan, B., Schiffmann, S. N., and Cheron, G. (2004). Effect of simple spike firing mode on complex spike firing rate and waveform in cerebellar Purkinje cells in non-anesthetized mice. *Neurosci. Lett.* 367, 171–176. doi: 10.1016/j.neulet.2004.05.109

Servais, L., and Cheron, G. (2005). Purkinje cell rhythmicity and synchronicity during modulation of fast cerebellar oscillation. *Neuroscience* 134, 1247–1259. doi: 10.1016/j.neuroscience.2005.06.001

Soustiel, J. F., Hafner, H., Chistyakov, A. V., Barzilai, A., and Feinsod, M. (1995). Trigeminal and auditory evoked responses in minor head injuries and post-concussion syndrome. *Brain Inj.* 9, 805–813. doi: 10.3109/02699059509008236

Thatcher, R. W., Walker, R. A., Gerson, I., and Geisler, F. H. (1989). EEG discriminant analyses of mild head trauma. *Electroencephalogr. Clin. Neurophysiol.* 73, 94–106. doi: 10.1016/0013-4694(89)90188-0

Thompson, H. J., Lifshitz, J., Marklund, N., Grady, M. S., Graham, D. I., Hovda, D. A., et al. (2005). Lateral fluid percussion brain injury: a 15-year review and evaluation. *J. Neurotrauma* 22, 42–75. doi: 10.1089/neu.2005.22.42

Conflict of Interest Statement: The authors declare that the research was conducted in the absence of any commercial or financial relationships that could be construed as a potential conflict of interest.

Received: 20 June 2014; accepted: 23 September 2014; published online: 09 October 2014.

Citation: Ordek G, Proddutur A, Santhakumar V, Pfister BJ and Sahin M (2014) Electrophysiological monitoring of injury progression in the rat cerebellar cortex. Front. Syst. Neurosci. ***8****:197. doi: 10.3389/fnsys.2014.00197*

This article was submitted to the journal Frontiers in Systems Neuroscience.

frontiers in
SYSTEMS NEUROSCIENCE

REVIEW ARTICLE
published: 28 March 2014
doi: 10.3389/fnsys.2014.00041

Purkinje cell stripes and long-term depression at the parallel fiber-Purkinje cell synapse

Richard Hawkes*[1,2,3]

[1] Department of Cell Biology and Anatomy, University of Calgary, Calgary, AB, Canada
[2] Hotchkiss Brain Institute, University of Calgary, Calgary, AB, Canada
[3] Genes and Development Research Group, Faculty of Medicine, University of Calgary, Calgary, AB, Canada

Edited by:
Richard Apps, University of Bristol, UK

Reviewed by:
Egidio D'Angelo, University of Pavia, Italy
Izumi Sugihara, Tokyo Medical and Dental University, Japan

****Correspondence:***
Richard Hawkes, Department of Cell Biology and Anatomy, Hotchkiss Brain Institute, and Genes and Development Research Group, Faculty of Medicine, University of Calgary, 3330 Hospital Drive NW, Calgary, AB T2N 4N1, Canada
e-mail: rhawkes@ucalgary.ca

The cerebellar cortex comprises a stereotyped array of transverse zones and parasagittal stripes, built around multiple Purkinje cell subtypes, which is highly conserved across birds and mammals. This architecture is revealed in the restricted expression patterns of numerous molecules, in the terminal fields of the afferent projections, in the distribution of interneurons, and in the functional organization. This review provides an overview of cerebellar architecture with an emphasis on attempts to relate molecular architecture to the expression of long-term depression (LTD) at the parallel fiber-Purkinje cell (pf-PC) synapse.

Keywords: zebrin II, phospholipase Cβ4, Purkinje cell, stripes, long-term depression

The general hypothesis explored in this review is that the elaborate molecular architecture of the cerebellar cortex has its counterpart in the compartmentation of function. In particular, many forms of synaptic plasticity have been identified in the cerebellar cortex (e.g., Hansel et al., 2001)—a network property that De Zeeuw et al. have called "distributed synergistic plasticity" (Gao et al., 2012). Both long-term depression (LTD) and long-term potentiation (LTP) have been identified, and these are expressed at multiple synapses—parallel-fiber to Purkinje cell, mossy fiber to granule cell, inhibitory interneuron to Purkinje cell ("rebound potentiation": e.g., Tanaka et al., 2013) etc.

By way of example, the review focuses on LTD at the parallel fiber-Purkinje cell (pf-PC) synapse. A brief consideration of its opposite –LTP—is also included. Other forms of Purkinje synaptic plasticity in the cerebellum are not included since so little is known of their relationship to the stripe architecture. Therefore, to set the stage the review begins with a brief overview of the patterning of the main players—Purkinje cells, climbing and mossy fiber afferents, and granule cells.

OVERVIEW OF ZONE AND STRIPE ARCHITECTURE

PURKINJE CELLS

Several recent reviews have described the architecture of the adult cerebellar cortex (e.g., Apps and Garwicz, 2005; Apps and Hawkes, 2009; Ruigrok, 2011). In brief, a range of expression markers expressed in subsets of Purkinje cells have revealed an orthogonal matrix of transverse zones and parasagittal stripes (**Figure 1**). First, the cerebellar cortex is divided by transverse boundaries into transverse zones. These are most easily recognized in the vermis but appear to have their counterparts in the hemispheres as well. Each transverse zone is further subdivided into long narrow stripes that run parasagittally from rostral to caudal. The most-studied example is the expression pattern of zebrin II/aldolase C, which identifies a stereotyped array of zebrin II+ and zebrin II- stripes (e.g., Brochu et al., 1990; Hawkes and Gravel, 1991; Ahn et al., 1994; Hawkes and Herrup, 1995; **Figures 1A, B**). The combination of multiple such patterns adds up to a cerebellar cortex with several hundred distinct topographical units (e.g., Hawkes, 1997; Hawkes et al., 1997, 1999; Armstrong et al., 2000).

The Purkinje cell expression domains are reproducible between individuals to a remarkable level—individual stripes comprised of no more than 100 or so Purkinje cells are faithfully reproduced (e.g., the P4b+/P5a+ stripes in the hemispheres: Hawkes and Leclerc, 1987; **Figures 1A, B**). Indeed, although the size of a particular zone or stripe may be modified to suit the animal's mode of life a common ground plan is conserved across all mammals studied to date (∼30 species—Sillitoe et al., 2005; Marzban and Hawkes, 2011) and is also found in birds (Pakan et al., 2007; Iwanuik et al., 2009; Marzban et al., 2010).

AFFERENT PROJECTIONS

Stripes of Purkinje cells are targets of specific afferent subsets during development and restrict their terminal fields in the adult, with the result that specific afferent subsets terminate in stripes. Studies over the past 25 years or so have shown that afferent terminal fields are precisely aligned with Purkinje cell stripes. These studies have combined immunocytochemistry for stripe antigens with anterograde tracing to

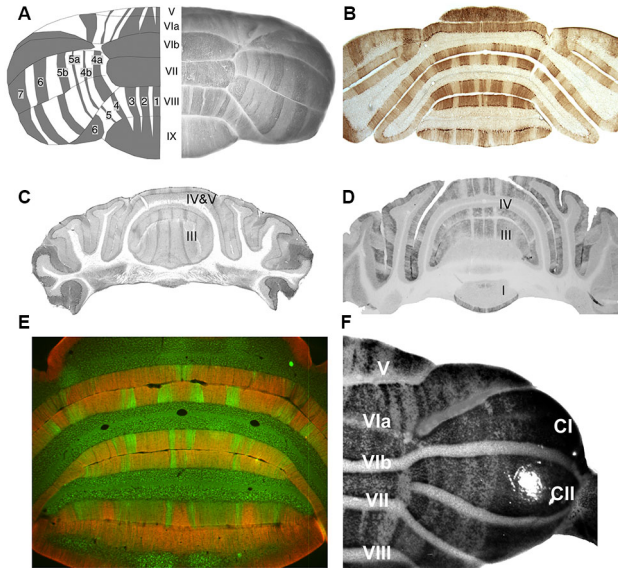

FIGURE 1 | Stripes in the adult mouse cerebellar cortex as revealed by various Purkinje cell subset markers. **(A)** On the right is a whole mount dorsal view of a hemicerebellum immunoperoxidase stained for zebrin II/aldolase C. On the left is a cartoon view: lobules are numbered with Roman numerals (V–IX); zebrin II+ stripes as 1–7 (Adapted from Furutama et al., 2010). **(B)** A transverse section through the posterior lobe immunoperoxidase stained by using anti-zebrin II (Adapted from Marzban et al., 2004). **(C)** A transverse section through the anterior lobe immunoperoxidase stained for phospholipase Cβ3 (PLCβ3) (Adapted from Sarna et al., 2006). **(D)** A transverse section taken close to that in panel C, immunoperoxidase stained for PLCβ4 (Adapted from Sarna et al., 2006). **(E)** Transverse section through the posterior lobe double immunofluorescence labeled for GABA type B receptors 2 ($GABA_BR2$) (red) and PLCβ4 (green) (Adapted from Chung et al., 2008). **(F)** A whole mount dorsal view of a hemicerebellum from an IP_3R1nls-lacZ transgenic mouse X-gal stained for transgene expression (Adapted from Furutama et al., 2010).

generate detailed topographical maps, in particular relating afferent terminal fields to zebrin II+/− stripes (e.g., climbing fibers—Gravel et al., 1987; Voogd et al., 2003; Sugihara and Shinoda, 2004; Voogd and Ruigrok, 2004; Sugihara and Quy, 2007 etc.; mossy fibers—Gravel and Hawkes, 1990; Akintunde and Eisenman, 1994; Ji and Hawkes, 1994; Armstrong et al., 2009; etc.). In some cases, molecular differences have also been demonstrated between afferent subsets. For example, mossy fibers that express somatostatin terminate on Purkinje cell stripes that express the small heat shock protein (HSP25; Armstrong et al., 2009), and climbing fibers immunoreactive for corticotropin-releasing factor (CRF) terminate selectively on zebrin II+ Purkinje cells (Sawada et al., 2008; see Section Corticotropin-releasing Factor).

Although striped patterns of Purkinje cell gene expression are aligned with stripes of afferent innervation, the formation and maintenance of stripes is not contingent upon afferent input: chemical or surgical afferent lesions do not alter the pattern (zebrin—Leclerc et al., 1988; Zagrebelsky et al., 1996, 1997; sphingosine kinase 1a—Terada et al., 2004; HSP25—Armstrong et al., 2001; L7/pcp2—Oberdick et al., 1993; etc.), and subtype phenotypes are expressed in slice and dissociated cerebellar cultures and after grafting the cerebellar anlage to an ectopic location (e.g., Wassef et al., 1990; Seil et al., 1995).

GRANULE CELLS

Purkinje cell stripe boundaries are also restriction boundaries for interneurons. Most prominent among these are the granule cells. First, the analysis of murine chimeras has identified a reproducible set of lineage boundaries within the granular layer that align with the transverse boundaries seen in the Purkinje cells (Hawkes et al., 1999). Multiple expression boundaries are also found at these locations in the adult and in the external granular layer during development (reviewed in Armstrong and Hawkes, 2000; Consalez and Hawkes, 2013). This strongly suggests that different granule cell lineages exploit the underlying Purkinje cell zonal architecture as the external granular layer spreads to cover the embryonic cerebellar anlage. Secondly, in the adult granular layer a complex array of patches and stripes can be revealed (e.g., nitric oxide (NO) synthase or its surrogate, reduced nicotinamide adenine dinucleotide phosphate (NADPH) diaphorase: Hawkes and Turner, 1994; Schilling et al., 1994; Ozol and Hawkes, 1997; Hawkes et al., 1998). These also align with the Purkinje cell architecture. It is difficult to credit that these represent cell autonomous properties of the granule cells, given the challenges such a model would present for the targeting of granule cell migration and settling, so it is more likely that the expression patterns are secondary to the local environment (e.g., Purkinje cells or mossy fibers).

FUNCTIONAL CORRELATES OF STRIPES

Given that pretty much everything in the anatomy of the cerebellar cortex is stripy, it should be unsurprising that similar compartmentation is seen by using functional mapping. First, parasagittal stripes are seen in electrophysiological recordings from the cerebellar cortex—the 12 A-D2 longitudinal zones and microzones (e.g., Oscarsson, 1979; for an account of the baroque terminology of cerebellar architecture, see Apps and Hawkes, 2009)—and these align with, and are likely the same thing as, the striped domains of differential gene expression. Similarly, optical imaging of the cerebellar cortex also reveals a parasagittally striped functional organization (e.g., Chen et al., 1996; Ebner et al., 2005, 2012; Gao et al., 2006). In contrast, recordings of tactile receptive fields in the hemispheres apparently reveal a somewhat different organization—a complex but reproducible array of functional patches responsive to different stimulus sites—vibrissae, lips, teeth etc., ("fractured somatotopy": reviewed in Welker, 1987). However, when the tactile receptive field boundaries and antigenic boundaries are compared, a reproducible alignment is found (e.g., Chockkan and Hawkes, 1994; Hallem et al., 1999) that is consistent with the evidence cited above that mossy fiber afferent terminal fields show stripe restriction.

Different Purkinje cell stripes receive climbing fibers from different sources. Consistent with this topography, Paukert et al. (2010) recently showed that climbing fibers that terminate on zebrin II+ Purkinje cells release more glutamate per action potential than do those terminating in zebrin II− stripes. As a result, climbing fiber-mediated excitatory postsynaptic potentials in

Purkinje cells decay more slowly in the zebrin II+ stripes, and thus longer-duration complex spikes are triggered. The implication is that prolonged climbing fiber-induced depolarization of Purkinje neurons in zebrin II+ stripes should preferentially enhance Ca^{2+} influx and thereby facilitate activity-dependent changes in the strength of both climbing and parallel fiber synapses (Hansel et al., 2001; Safo et al., 2006; Carey and Regehr, 2009; Mathy et al., 2009).

Finally, Wadiche and Jahr (2001, 2005) have shown that Purkinje cells in zebrin II+/− stripes express different complements of excitatory amino acid transporters (EAATs), some of which are more effective than others. As a result, regional differences in glutamate transporter expression affect the degree of metabotropic glutamate receptor (mGluR1) stimulation (see Section Glutamate Re-uptake).

MOLECULAR CORELATES OF LONG-TERM DEPRESSION AT THE PARALLEL FIBER-PURKINJE CELL SYNAPSE

The functional differences between stripes derive in two ways. On the one hand they reflect differences in connectivity (i.e., the striped organization of the olivocerebellar and mossy fiber projections). On the other hand—and central to what follows—different stripes display distinctly different intrinsic properties, notably a variety of different forms of synaptic plasticity (e.g., reviewed in Hansel et al., 2001). The hypothesis explored in this review is that the specificity of the afferent topography together with the molecular heterogeneity of the granule cells and Purkinje cells constitutes a substrate for multiple plastic adaptations of the pf-PC synapse. What follows focuses on LTD at the pf-PC synapse as an exemplar.

Purkinje cells receive 2 glutamatergic excitatory inputs, one from mossy fibers via pf-PC synapses on dendritic spines and another from climbing fibers onto the dendritic shafts. Conjunctive stimulation of the parallel fiber and climbing fiber pathways (1–4 Hz for 1–10 min) results in a long-lasting depression of transmission at the pf-PC synapse (e.g., recently reviewed in Vogt and Canepari, 2010; Finch et al., 2012; an excellent history is provided in Kano et al., 2008). LTD has often been evoked as a model of cerebellar motor learning, but recent studies cast doubt on this (Schonewille et al., 2011; Gao et al., 2012).

LTD at the pf-PC synapse is quantitatively different between stripes: it is easier to induce pf-PC synapse LTD in zebrin II- than in zebrin II+ Purkinje cells (Wadiche and Jahr, 2001). Little is known of the molecular basis for differences in LTD across stripes but it is striking that many molecules whose expression is in stripes are associated with the putative pathways leading to LTD (**Table 1**).

An influential model of the molecular basis of LTD at the pf-PC synapse, due to Ito (e.g., reviewed in Ito, 1984, 1989, 2002), is summarized in a simplified fashion in **Figure 2**. In brief, conjunctive glutamate release from parallel fiber and climbing fiber terminals acts through mGluR1 to activate several parallel intracellular signaling pathways—in particular, one via phospholipase C (PLC) and diacylglycerol (DAG) to protein kinase C (PKC), and another via inositol triphosphate (IP_3). The downstream consequence is the internalization of AMPA (α-amino-3-hydroxy-5-methyl-4-isoxazolepropionic acid)-sensitive glutamate receptors (AMPAR), and consequent synaptic desensitization. NO and CRF play supporting roles. It is instructive to examine the expression patterns of the different players in this pathway.

SYNAPTIC MARKERS

First of all a reproducible pattern of stripes is revealed in the molecular layer of the cerebellar cortex by using immunocytochemistry for the synaptic vesicle protein synaptophysin (Hawkes et al., 1985), with stripes of higher expression alternating with those of lower expression, both in the granular layer associated with mossy fiber synaptic glomeruli and in the molecular layer, associated primarily with pf-PC synapses (Hawkes et al., 1985; Leclerc et al., 1989). The interpretation of the observation is less obvious—does stronger staining reflect more antigen per vesicle, antibody access, more vesicles per synapse, a higher Purkinje cell spine density . . .? Appropriate comparisons with the expression patterns of other synaptic markers that might resolve this question have not been reported. A patchy/striped arrangement of mossy fiber terminals in the granular layer is reported with other presynaptic markers, but in these cases the expression in the molecular layer appears to be uniform (e.g., dysbindin—Sillitoe et al., 2003; neuronal nitric oxide synthase (nNOS); see Section Nitric Oxide). A uniform distribution in the molecular layer may be misleading in that differential expression of granule cell markers is easier to discern in the granular layer, where the somata are segregated into stripes and clusters, than in the molecular layer where the

Table 1 | A list of the synaptic molecules with striped expression patterns referred to in the text; whether they are preferentially expressed in zebrin II+ (zII+) or zebrin II− (zII−) stripes (or a mixture of both); and pertinent citations.

Molecule	Stripe preference	Citations
Synaptophysin	zII+/zII−	Hawkes et al. (1985); Leclerc et al. (1989)
Dysbindin	zII+/zII−	Sillitoe et al. (2003)
nNOS/NADPHd	zII+/zII−	Yan et al. (1993); Hawkes and Turner (1994); Schilling et al. (1994); Baader and Schilling (1996)
Neuroplastin	zII−	Marzban et al. (2003)
mGluR1b	zII−	Mateos et al. (2001)
EAAT4	zII+	Dehnes et al. (1998)
NMDA receptor ($NR2C^{nlacZ}$)	zII−	Karavanova et al. (2007)
CRF	zII+	Sawada et al. (2008)
PLCβ3	zII+	Sarna et al. (2006)
PLCβ4	zII−	Sarna et al. (2006)
IP_3R-nls-LacZ	zII+	Furutama et al. (2010)
PKCδ	zII+	Barmack et al. (2000)
$GABA_BR2$	zII+	Albin and Gilman (1989); Luján and Shigemoto (2006); Chung et al. (2008)
Neurogranin	zII−	Larouche et al. (2006)
PEP-19	?	Wassef et al. (1992)

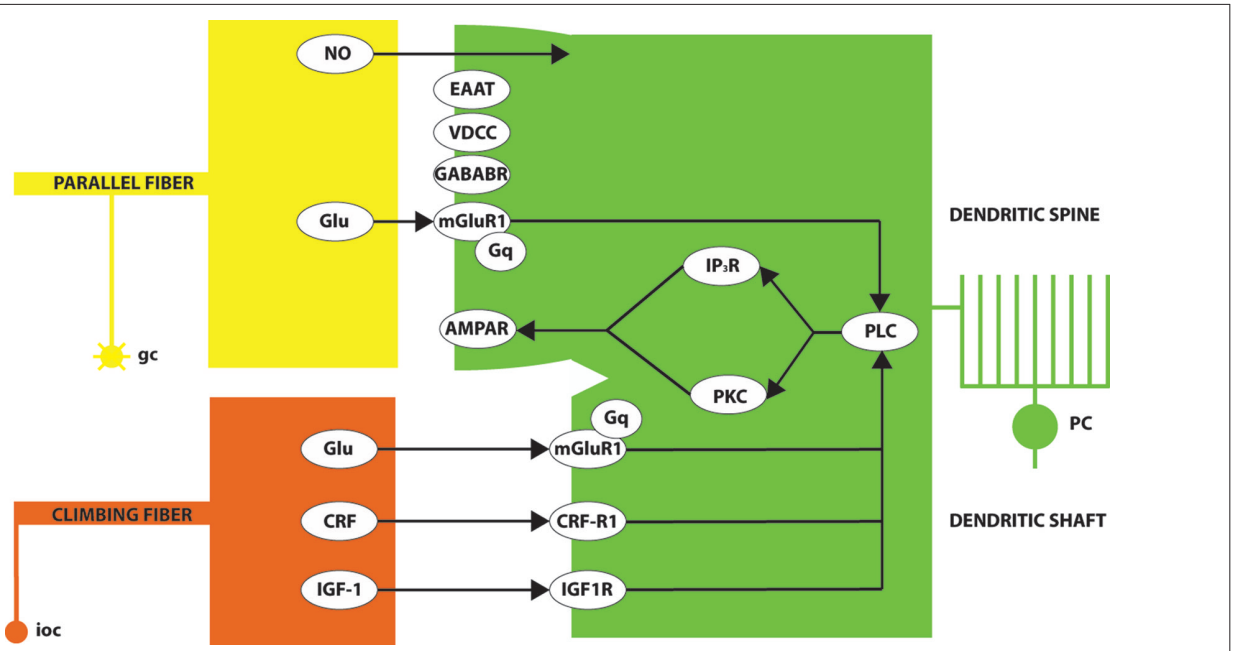

FIGURE 2 | A simplified model of some of the signaling pathways leading to LTD of the pf-PC synapse. Conjunctive glutamate (Glu) release at the granule cell (gc)/parallel fiber synapse on the Purkinje cell (PC) dendritic spine and the climbing fiber (from inferior olivary cells: ioc) synapses on the dendritic shaft activates the metabotropic glutamate receptor (mGluR1). Glutamate signaling across the synaptic cleft is modulated by excitatory amino acid transporters (EAAT). A signaling pathway via Gq proteins activates PLC. In turn, PLC signals via both the inositol triphosphate receptor (IP_3R) and protein kinase C (PKC). The upshot is the internalization of synaptic AMPA receptors and consequent LTD. The overall process is also modulated by various other signals including: presynaptic nitric oxide release (NO); the binding of corticotropin-releasing factor (CRF) to its receptor (CRF-R1) and insulin-like growth factor (IGF)-1 binding to its receptor (IGF-1R), both of which signal via PLC; signaling via postsynaptic $GABA_BR$; and calcium influx through voltage-dependent calcium channels (VDCCs).

long parallel fiber trajectories extensively overlap and smooth out different expression levels from different granule cell populations.

Structural synaptic proteins are also differentially expressed. For example, a prominent striped expression pattern is revealed by immunocytochemical staining for the postsynaptic membrane glycoprotein neuroplastin (Marzban et al., 2003; note—in the hippocampus, neuroplastin has been linked to the inhibition of LTP; Empson et al., 2006). High levels of neuroplastin expression are preferentially associated with the zebrin II- Purkinje cell stripes.

GLUTAMATE RECEPTORS

Glutamate released into the synaptic cleft at both the climbing fiber and the pf-PC synapse binds to three types of glutamate receptor in the postsynaptic membrane—metabotropic (mGluR), GluRδ2 and AMPAR. mGluRs are G protein-coupled receptors with 7 transmembrane segments that do not form ion channels but rather signal via intracellular chemical messenger systems. Eight genes coding for different subtypes of mGluRs have been identified, seven of which are expressed in the cerebellum. In particular, Purkinje cell mGluR1 is localized in the peri- and extra-synaptic membranes. It is functionally coupled to PLC through which it modulates the IP_3 (1,4,5)/Ca2+ signaling pathway and plays a key role in the induction of pf-PC LTD (reviewed in Knöpfel and Grandes, 2002).

There are at least 4 mGluR1 splice variants with differing subcellular and cellular distributions (mGluR1a-d: e.g., Conn and Pin, 1997). In the case of mGluR1b in the cerebellum, expression is striped in the molecular layer and co-located with zebrin II-stripe markers (Mateos et al., 2001). mGluR1a is also located in the Purkinje cell dendritic spine (e.g., Mateos et al., 2000) but whether or not there is an mGluR subtype restricted to the zebrin II+ Purkinje cell dendritic spines is not known.

GluRδ2 is also highly expressed in cerebellar Purkinje cells and is localized specifically to pf-PC synapses (Araki et al., 1993; reviewed in Hirano, 2006). GluRδ2 neither binds glutamate nor conducts current but rather regulates mGluR1-mediated synaptic transmission via PKCγ (e.g., Kato et al., 2012). Loss-of-function mutations in GluRδ2 result in multiple defects including impairment of LTD (Kashiwabuchi et al., 1995). There is no evidence that its expression is stripe-restricted (gain-of-function mutation of the GluRδ2 gene in the *lurcher* mouse ($Grid^{Lc}$/+) results in striped Purkinje cell degeneration (Zuo et al., 1997; reviewed in Armstrong et al., 2011) but this likely reflects differential sensitivity to the insult rather than selective GluRδ2 expression).

GLUTAMATE RE-UPTAKE

The time that glutamate resides in the synaptic cleft, and hence is available for receptor binding, is governed by EAAT. In particular, EAAT4 has been implicated at the pf-PC synapse. It is therefore striking that the expression of EAAT4 is different from stripe

to stripe with high levels associated with the zebrin II+ stripes (Dehnes et al., 1998). As a result, regional differences in glutamate transporter expression affect the degree of mGluR1 receptor stimulation, with the result that pf-PC LTD is dampened in Purkinje cells expressing high levels of EAAT4 (= zebrin II+; Wadiche and Jahr, 2005).

CALCIUM INFLUX

One consequence of mGluR1 activation is Ca^{2+} influx via VDCC in the postsynaptic dendritic membrane. There is no evidence that VDCCs are expressed differentially by Purkinje cell subsets (As for the *lurcher* mouse, it has been shown that a mutation of the VDCCα1a channel in the *tottering* mouse (*Cacna1a*^{tg}) results in the selective Purkinje cell death of the zebrin II- Purkinje cell subset, but again the evidence suggests that this is due to differential sensitivity to an abnormal Ca^{2+} influx rather than restricted expression of the α1a channel; Fletcher et al., 1996).

The downstream response to dendritic Ca^{2+} influx is modulated by calpacitins, notably the 2 Purkinje cell proteins PEP-19 and neurogranin/RC3. Sutcliffe and colleague have proposed that calpacitins regulate calmodulin availability in dendritic spines and thus regulates their ability to amplify the mobilization of Ca^{2+} in response to metabotropic glutamate receptor stimulation, releasing calmodulin rapidly in response to large influxes of Ca^{2+} and slowly in response to small increases. This action is inhibited by PKC-mediated phosphorylation (reviewed in Gerendasy and Sutcliffe, 1997; Díez-Guerra, 2010). α-Calmodulin kinase KII is also shown to be required for LTD at the pf-PC synapse (Hansel et al., 2006). Neurogranin knockout mice show deficits in the induction of hippocampal LTP (e.g., Pak et al., 2000) but no cerebellar phenotype is reported. On the other hand, the much more abundant PEP19 is directly implicated: in the PEP19 null mouse both motor learning and pf-PC LTD are impaired (Wei et al., 2011). During cerebellar development, both PEP19 (Wassef et al., 1992) and neurogranin (Larouche et al., 2006) expression is restricted to Purkinje cell subsets. However, in the adult PEP19 expression is uniformly expressed by all Purkinje cells (Mugnaini et al., 1987) whereas neurogranin has disappeared (Larouche et al., 2006), so any significance for patterned LTD at the adult pf-PC synapse is doubtful.

NITRIC OXIDE

In addition to releasing glutamate, parallel fibers also release NO. NO acts through inhibition of protein phosphatases in the Purkinje cell dendritic spine and thus enhance AMPAR phosphorylation. LTD is abolished in transgenic mice lacking nNOS (Lev-Ram et al., 1997). There is clear evidence of different stripes of nNOS in the granular layer of the cerebellar cortex (e.g., Yan et al., 1993; Hawkes and Turner, 1994; Schilling et al., 1994; Baader and Schilling, 1996). Similar striping is harder to discern in the molecular layer, perhaps obscured by the overlapping parallel fiber populations. The nNOS pathway is activated via N-methyl-D-aspartate (NMDA)-type glutamate receptors located at the pf-PC synapse (and/or located in the presynaptic terminals of inhibitory interneurons; Shin and Linden, 2005). Functional NMDA receptors are also expressed at climbing fiber-PC synapses, and channel blocking inhibits LTD (Piochon et al., 2010).

It is noteworthy that NMDA receptor expression, as revealed by an NRC2 subunit knock-in mouse (NR2C^{nlacZ}), reveals stripes of granule cells similar to those revealed by PLCβ4 expression (= zebrin II-; Karavanova et al., 2007). There is no evidence that Purkinje cell NMDA receptors are expressed in stripes.

CORTICOTROPIN-RELEASING FACTOR

Glutamate release and binding to mGluR1 is also the first step in signaling via the climbing fiber pathway. In parallel to glutamate release, climbing fibers also secrete CRF (Barmack and Young, 1990), which plays a permissive role in LTD that is probably mediated through PKC (Miyata et al., 1999). However, not all climbing fibers express CRF. Whole mount immunocytochemistry shows that CRF is restricted to (or is expressed at higher levels in) a striped subset of climbing fiber terminals that terminate in zebrin II+ Purkinje cell stripes (mouse—Sawada et al., 2008). However, the significance of this may not be straightforward as previous studies reported uniform CRF expression (e.g., cat—Cummings, 1989) or expression differences between lobules but not in the form of stripes (e.g., developing mouse—Overbeck and King, 1999). There is no evidence that G-protein coupled CRF receptor (CRFR1) expression is similarly striped (e.g., Allen Brain Atlas).

INSULIN-LIKE GROWTH FACTOR 1

As well as releasing CRF, climbing fiber synapses also store and release IGF-1 (Torres-Aleman et al., 1994). It is not known if IGF-1 or its receptor tyrosine kinase (IGF1R) is expressed in stripes in the adult cerebellum (in general in the brain IGF1R is broadly expressed—it is the ligands that show regional restriction: e.g., reviewed in D'Ercole et al., 1996). During early postnatal development, IGF-1 is also expressed in a zebrin II- Purkinje cell subset, where it acts to block apoptosis (Croci et al., 2011), but it is unclear whether selective expression is retained in the adult.

PHOSPHOLIPASE Cβ

mGluR1 signals via the Gq subclass of G-proteins to PLCβ (reviewed in Knöpfel and Grandes, 2002). There are four PLCβ isoforms, encoded by distinct genes (PLCβ1-4; Bahk et al., 1994). Strikingly, PLCβ3 and PLCβ4 are expressed by distinct, non-overlapping subsets of Purkinje cells. PLCβ3 is confined to the zebrin II+ Purkinje cell subset (**Figure 1C**) and PLCβ4 expression is coextensive with the zebrin II- Purkinje cell subset (**Figures 1D, E**; Sarna et al., 2006; Marzban et al., 2007) (Unexpectedly, a small subset of zebrin II+ Purkinje cell stripes in the nodular zone of the mouse cerebellum (∼ lobules IX and X)—those that express HSP25—is reproducibly immunonegative for both PLCβ3 and PLCβ4 (Sarna et al., 2006)—the implication of this is unclear).

PHOSPHOLIPASE A

Parallel to the PLCβ pathway, there is also a signaling pathway via phospholipase A (PLA)—in particular, the PLA2 isoform: e.g., Linden, 1995; Le et al., 2010), which acts to break down phospholipids into arachidonic acid, a potent activator of PK Cγ (e.g., Shearman et al., 1989). At least 20 PLA2 isoforms have been identified, three of which have been reported in Purkinje cells (cPLA2α, sPLA2IIA, and iPLA2; Shirai and Ito, 2004). There is

no evidence that any of these is restricted to a particular Purkinje cell subset.

INOSITOL (1,4,5) TRIPHOSPHATE RELEASE

Two signaling pathways leading to LTD lie downstream of PLC. The first involves IP_3 release from intracellular stores to bind to its receptor on the endoplasmic reticulum (IP_3R; e.g., Furuichi et al., 1989; Maeda et al., 1989). The cerebellar distribution of IP_3R has recently been reported in a transgenic mouse in which the IP_3R promoter was fused to a β-galactosidase reporter and a nuclear localization signal (IP_3R1nls-*lacZ*; Furutama et al., 1996, 2010; **Figure 1F**). Transgene expression in the heterozygote reveals a striking array of Purkinje cell stripes that can be traced continuously through embryogenesis through to adulthood. In general, IP_3R1nls-*lacZ* transgene expression is restricted to the zebrin II+ Purkinje cell subset. The extent to which this distribution reflects any feature of the true restriction of the receptor—perhaps developmentally—or is a transgene artifact (due to the transgene insertion, promoter truncation, enhancer trapping, etc.), is questionable. Immunocytochemistry with antibodies against IP_3R do not show Purkinje cell stripes (e.g., Mignery et al., 1989).

PROTEIN KINASE C (PKC)

An additional second-messenger signaling pathway between glutamate release and the induction of LTD goes via the generation of DAG by PLC, which in turn activates PKC (Crépel and Krupa, 1988; for a general review of PKC, see Newton, 1995). There are seven PKC subtypes—three (α, β and γ) activated in a Ca^{2+}/DAG-dependent manner and 4 (δ, ϵ, η and θ) Ca^{2+}-independent (reviewed in Tanaka and Nishizuka, 1994). Activation of Ca^{2+}-dependent PKC is necessary for induction of LTD at the pf-PC synapse (e.g., Ito, 1989, 2002; Daniel et al., 1998). LTD induction at the pf-PC synapse is blocked by the intracellular application of PKC inhibitors in Purkinje cells (Linden and Connor, 1991). De Zeeuw et al. (1998) constructed a transgenic mouse in which a Purkinje cell-specific promoter (pcp2-L7) was used to target the expression of a broad-spectrum PKC inhibitor (the pseudo-substrate PKC[19–31]) and thereby showed that PKC activation in the Purkinje cell is a prerequisite for the induction of LTD. None of the Ca^{2+}/DAG-dependent PKC isoforms is expressed selectively by a Purkinje cell subset (e.g., Barmack et al., 2000).

The role(s), if any, of the four Ca^{2+}-independent PKCs in LTD induction is unclear. However, they deserve attention here because while most PKC isoform distributions are uniform across the molecular layer the one exception is PKCδ, whose expression in the nodular zone of the rat reveals a reproducible striped expression pattern with higher levels in the zebrin II+ stripes (Barmack et al., 2000). Furthermore, experimental manipulation of the cerebellar afferent inputs by labyrinthectomy demonstrated an activity-dependent targeting of the PKCδ isoform to the pf-PC synapse (Barmack et al., 2001). PKCδ has been implicated in hippocampal LTP (e.g., Kim et al., 2013) but no specific role in cerebellar LTD is known.

$GABA_B$ RECEPTORS

LTD at the pf-PC synapse is also modulated by an unusual form of γ-aminobutyric acid (GABA) receptor signaling. In the adult cerebellum $GABA_BRs$ are predominantly located perisynaptically at the dendritic spines of Purkinje cells (e.g., Turgeon and Albin, 1993; Kaupmann et al., 1997; Bischoff et al., 1999; Kulik et al., 2002; Fritschy et al., 2004; Luján and Shigemoto, 2006). Both $GABA_A$ (reviewed in Fritschy and Panzanelli, 2006) and $GABA_B$ receptor classes are expressed in the cerebellum but only $GABA_BRs$ have been implicated in pf-PC LTD. $GABA_BRs$ are G-protein-coupled receptors formed as heteromers of 2 subunits ($GABA_BR1/2$; Marshall et al., 1999; Möhler and Fritschy, 1999). Postsynaptic $GABA_BR$ signaling enhances LTD (Tabata et al., 2004; Kamikubo et al., 2007), possibly as a Ca^{2+}-dependent cofactor of mGluR1 signaling. The role of $GABA_BRs$ in the modulation of LTD is unconventional in that it does not require GABA. Rather, extracellular Ca^{2+} binds to the $GABA_BR$ and constitutively increases the glutamate sensitivity of mGluR1 (Tabata et al., 2004). The role of $GABA_BR$ in LTD is relevant for the present discussion because immunocytochemistry for $GABA_BR2$ shows a strong restriction of receptor immunoreactivity to the zebrin II+ stripes (Albin and Gilman, 1989; Luján and Shigemoto, 2006; Chung et al., 2008; **Figure 1E**).

AMPA RECEPTORS

The ultimate downstream target of PLC signaling, via both PKC and IP_3R, is the phosphorylation (via both PKC and Src-family protein tyrosine kinases—e.g., Tsuruno et al., 2008) of postsynaptic AMPA receptors (AMPAR; Ito, 1984; Crépel and Krupa, 1988; Hirano, 1991; Linden et al., 1991; Matsuda et al., 2000; Tsuruno et al., 2008; etc.). AMPAR kinetics, agonist affinity and unitary conductances are unchanged by phosphorylation (Linden, 2001) but rather there results a reduction in AMPAR number due to enhanced endocytosis (Matsuda et al., 2000), which is dependent on phosphorylation at ser-880 in the AMPAR GluR2 subunit (Chung et al., 2003; reviewed in Shin and Linden, 2005). There is no evidence of selective expression of either Src kinases or AMPAR by Purkinje cell subsets.

MOLECULAR CORELATES OF LONG-TERM POTENTIATION AT THE PARALLEL FIBER-PURKINJE CELL SYNAPSE

The opposite process—LTP—countermands LTD at the pf-PC synapse. This endows the synapse with bidirectional plasticity (Lev-Ram et al., 2002; Coesmans et al., 2004). Postsynaptic LTP is induced by parallel fiber stimulation (1 Hz for 5 min: Lev-Ram et al., 2002, 2003). The signaling pathways implicated resemble those previously identified for hippocampal LTP (e.g., Jörntell and Hansel, 2006). Stimulation causes Ca^{2+} influx via voltage-sensitive channels, which activates several calmodulin-activated protein phosphatases (PP1, PP2A and PP2B; Lev-Ram et al., 2003; Coesmans et al., 2004; Belmeguenai and Hansel, 2005; Schonewille et al., 2010). In turn, this results in enhanced AMPA receptor insertion into the postsynaptic membrane (a process dependent upon NO—Huang et al., 2005; Kakegawa and Yuzaki, 2005). It is not known if this form of pf-PC LTD or the molecules in the downstream pathways are differentially expressed between Purkinje cell subsets.

In contrast, another apparent manifestation of pf-PC LTP has a close relationship to cerebellar stripes. This instance comes from the flavoprotein autofluorescence imaging of cerebellar activity

by Ebner and colleagues (e.g., Wang et al., 2009, 2011; Ebner et al., 2012). By stimulating mouse cerebellar cortex by using a paradigm that induces LTP at pf-PC synapses, an array of long-latency patches was revealed that aligns with the zebrin II+ Purkinje cell stripes and shows robust LTP. This form of LTP is mGluR1-dependent and blocked by application of PLCβ and ryanodine receptor inhibitors. This is pertinent because both mGluR1 receptor subtypes (Mateos et al., 2001; *III.ii* above) and PLCβ isoforms (Sarna et al., 2006; *III.vii.* above) are expressed in stripes. How this expression of LTP relates to that described above, is unclear.

CONCLUSIONS

In this review, LTD at the pf-PC synapse has been used as an example of a correlation between the molecular architecture of the cerebellar cortex and the specialization of cerebellar function. To recapitulate, the data show two things: first, LTD is manifested differently in different stripes; and secondly, some of the molecules implicated in the LTD signaling pathways also show expression patterns restricted to stripes, ranging from convincing (e.g., mGluR1b, EAAT4, PLCβ3, PLCβ3/4, $GABA_BR2$) to intriguing (e.g., nNOS, CRF), to being of marginal significance at best (e.g., IP_3R; IGF-1; PKCδ: **Table 1**). While this review has focused on one aspect of cerebellar function as an exemplar—LTD at the pf-PC synapse—it would be surprising if the molecular architecture were not similarly customized to serve other cerebellar functions. The evidence that LTP at the pf-PC synapse may also vary across stripes is also briefly reviewed. The conclusion is thus that cerebellar function has evolved to accommodate the different requirements of multiple, parallel afferent and efferent pathways, by customizing key molecular constituents. For example, on the afferent side Purkinje cell stripes receive mossy fiber pathway input from multiple sources and with very different firing patterns—have pf-PC synapses specialized to accommodate this? Likewise on the efferent side, do different cortical receiving areas require different LTD kinetics? Another consideration is that perhaps stripes work as zebrin II+/− pairs. One hint that this might be the case comes from the studies of optic flow in the pigeon cerebellum by Graham and Wylie (2012), which show that Purkinje cells in zebrin II+/− stripe pairs all respond best to the same pattern of optic flow. Given that climbing fibers onto zebrin II+ Purkinje cell stripes release more glutamate than those onto zebrin II- stripes (e.g., Paukert et al., 2010) it may be that both slow and fast adapting stripes work in concert as the fundamental functional unit in the cerebellar cortex.

REFERENCES

Ahn, A. H., Dziennis, S., Hawkes, R., and Herrup, K. (1994). The cloning of zebrin II reveals its identity with aldolase C. *Development* 120, 2081–2090.

Akintunde, A., and Eisenman, L. M. (1994). External cuneocerebellar projections and Purkinje cell zebrin II bands: a direct comparison of parasagittal banding in the mouse cerebellum. *J. Chem. Neuroanat.* 7, 75–86. doi: 10.1016/0891-0618(94)90009-4

Albin, R. L., and Gilman, S. (1989). Parasagittal zonation of GABA-B receptors in molecular layer of rat cerebellum. *Europ. J. Pharmacol.* 173, 113–114. doi: 10.1016/0014-2999(89)90014-9

Apps, R., and Garwicz, M. (2005). Anatomical and physiological foundations of cerebellar information processing. *Nat. Rev. Neurosci.* 6, 297–311. doi: 10.1038/nrn1646

Apps, R., and Hawkes, R. (2009). Cerebellar cortical organization: a one-map hypothesis. *Nat. Rev. Neurosci.* 10, 670–681. doi: 10.1038/nrn2698

Araki, K., Meguro, H., Kushiya, E., Takayama, C., Inoue, Y., and Mishina, M. (1993). Selective expression of the glutamate receptor channel delta 2 subunit in cerebellar Purkinje cells. *Biochem. Biophys. Res. Commun.* 3, 1267–1276. doi: 10.1006/bbrc.1993.2614

Armstrong, C. L., Chung, S. H., Armstrong, J. N., Hochgeschwender, U., Jeong, Y. G., and Hawkes, R. (2009). A novel somatostatin-immunoreactive mossy fiber pathway associated with HSP25-immunoreactive Purkinje cell stripes in the mouse cerebellum. *J. Comp. Neurol.* 517, 524–538. doi: 10.1002/cne.22167

Armstrong, C. L., Duffin, C. A., McFarland, R., and Vogel, M. W. (2011). Mechanisms of compartmental Purkinje cell death and survival in the lurcher mutant mouse. *Cerebellum* 10, 504–514. doi: 10.1007/s12311-010-0231-4

Armstrong, C. L., and Hawkes, R. (2000). Pattern formation in the cerebellar cortex. *Biochem. Cell Biol.* 78, 551–562. doi: 10.1139/o00-071

Armstrong, C. L., Krueger-Naug, A. M., Currie, R. W., and Hawkes, R. (2000). Constitutive expression of the 25kDa heat shock protein Hsp25 reveals novel parasagittal stripes of Purkinje cells in the adult mouse cerebellar cortex. *J. Comp. Neurol.* 416, 383–397. doi: 10.1002/(sici)1096-9861(20000117)416:3<383::aid-cne9>3.0.co;2-m

Armstrong, C. L., Krueger-Naug, A. M., Currie, R. W., and Hawkes, R. (2001). Expression of heat-shock protein Hsp25 in mouse Purkinje cells during development reveals novel features of cerebellar compartmentation. *J. Comp. Neurol.* 429, 7–21. doi: 10.1002/1096-9861(20000101)429:1<7::aid-cne2>3.0.co;2-q

Baader, S. L., and Schilling, K. (1996). Glutamate receptors mediate dynamic regulation of nitric oxide synthase expression in cerebellar granule cells. *J. Neurosci.* 16, 1440–1449.

Bahk, Y. Y., Lee, Y. H., Lee, T. G., Seo, J., Ryu, S. H., and Suh, P. G. (1994). Two forms of phospholipase C-beta 1 generated by alternative splicing. *J. Biol. Chem.* 269, 8240–8245.

Barmack, N. H., Qian, Z. Y., Kim, H. J., and Yoshimura, J. (2001). Activity-dependent distribution of protein kinase C-delta within rat cerebellar Purkinje cells following unilateral labyrinthectomy. *Exp. Brain Res.* 141, 6–20.

Barmack, N. H., Qian, Z., and Yoshimura, J. (2000). Regional and cellular distribution of protein kinase C in rat cerebellar Purkinje cells. *J. Comp. Neurol.* 427, 235–254. doi: 10.1002/1096-9861(20001113)427:2<235::aid-cne6>3.0.co;2-6

Barmack, N. H., and Young, W. S. (1990). Optokinetic stimulation increases corticotropin-releasing factor mRNA in inferior olivary neurons of rabbits. *J. Neurosci.* 10, 631–640.

Belmeguenai, A., and Hansel, C. (2005). A role for protein phosphatases 1, 2A and 2B in cerebellar long-term potentiation. *J. Neurosci.* 25, 10768–10772. doi: 10.1523/jneurosci.2876-05.2005

Bischoff, S., Leonhard, S., Reymann, N., Schuler, V., Shigemoto, R., Kaupmann, K., et al. (1999). Spatial distribution of $GABA_BR1$ receptor mRNA and binding sites in the rat brain. *J. Comp. Neurol.* 412, 1–16. doi: 10.1002/(sici)1096-9861(19990913)412:1<1::aid-cne1>3.3.co;2-4

Brochu, G., Maler, L., and Hawkes, R. (1990). Zebrin II: a polypeptide antigen expressed selectively by Purkinje cells reveals compartments in rat and fish cerebellum. *J. Comp. Neurol.* 291, 538–552. doi: 10.1002/cne.902910405

Carey, M. R., and Regehr, W. G. (2009). Noradrenergic control of associative synaptic plasticity by selective modulation of instructive signals. *Neuron* 62, 112–122. doi: 10.1016/j.neuron.2009.02.022

Chen, G., Hanson, C. L., and Ebner, T. J. (1996). Functional parasagittal compartments in the rat cerebellar cortex: an in vivo optical imaging study using neutral red. *J. Neurophysiol.* 76, 4169–4174.

Chockkan, V., and Hawkes, R. (1994). Functional and antigenic maps in the rat cerebellum: zebrin compartmentation and vibrissal receptive fields in lobule IXa. *J. Comp. Neurol.* 345, 33–45. doi: 10.1002/cne.903450103

Chung, S. H., Kim, C. T., and Hawkes, R. (2008). Compartmentation of GABA B receptor2 expression in the mouse cerebellar cortex. *Cerebellum* 7, 295–303. doi: 10.1007/s12311-008-0030-3

Chung, H. J., Steinberg, J. P., Huganir, R. L., and Linden, D. J. (2003). Requirement of AMPA receptor GluR2 phosphorylation for cerebellar long-term depression. *Science* 300, 1751–1755. doi: 10.1126/science.1082915

Coesmans, M., Weber, J. T., De Zeeuw, C. I., and Hansel, C. (2004). Bidirectional parallel fiber plasticity in the cerebellum under climbing fiber control. *Neuron* 44, 691–700. doi: 10.1016/j.neuron.2004.10.031

Conn, P. J., and Pin, J. P. (1997). Pharmacology and functions of metabotropic glutamate receptors. *Annu. Rev. Pharmacol. Toxicol.* 37, 205–237. doi: 10.1146/annurev.pharmtox.37.1.205

Consalez, G. G., and Hawkes, R. (2013). The compartmental restriction of cerebellar interneurons. *Front. Neural Circuits* 6:123. doi: 10.3389/fncir.2012.00123

Crépel, F., and Krupa, M. (1988). Activation of protein kinase C induces a long-term depression of glutamate sensitivity of cerebellar Purkinje cells. An in vitro study. *Brain Res.* 458, 397–401.

Croci, L., Barili, V., Chia, D., Massimino, L., van Vugt, R., Maserdotti, G., et al. (2011). Local insulin-like growth factor 1 expression is essential for Purkinje neuron survival at birth. *Cell Death Diff.* 18, 48–59. doi: 10.1038/cdd.2010.78

Cummings, S. L. (1989). Distribution of corticotropin-releasing factor in the cerebellum and precerebellar nuclei of the cat. *J. Comp. Neurol.* 289, 657–675. doi: 10.1002/cne.902890410

Daniel, H., Levenes, C., and Crépel, F. (1998). Cellular mechanisms of cerebellar LTD. *Trends Neurosci.* 21, 401–407. doi: 10.1016/s0166-2236(98)01304-6

Dehnes, Y., Chaudry, F. A., Ullensvang, K., Lehre, K. P., Storm-Mathisen, J., and Danbolt, N. C. (1998). The glutamate transporter EAAT4 in rat cerebellar Purkinje cells: a glutamate-gated chloride concentrated near the synapse in parts of the dendritic membrane facing astroglia. *J. Neurosci.* 18, 3606–3619.

D'Ercole, A. J., Ye, P., Calikoglu, A. S., and Gutierrez-Ospina, G. (1996). The role of the insulin-like growth factors in the central nervous system. *Mol. Neurobiol.* 13, 227–255. doi: 10.1007/BF02740625

De Zeeuw, C. I., Hansel, C., Bian, F., Koekkoek, S. K., van Alphen, A. M., Linden, D. J., et al. (1998). Expression of a protein kinase C inhibitor in Purkinje cells blocks cerebellar LTD and adaptation of the vestibulo-ocular reflex. *Neuron* 20, 495–508. doi: 10.1016/s0896-6273(00)80990-3

Díez-Guerra, F. J. (2010). Neurogranin, a link between calcium/calmodulin and protein kinase C signaling in synaptic plasticity. *IUBMB Life* 62, 597–606. doi: 10.1002/iub.357

Ebner, T. J., Chen, G., Gao, W., and Reinert, K. (2005). Optical imaging of cerebellar functional architectures: parallel fiber beams, parasagittal bands and spreading acidification. *Prog. Brain Res.* 148, 125–138. doi: 10.1016/s0079-6123(04)48011-x

Ebner, T. J., Wang, X., Gao, W., Cramer, S. W., and Chen, G. (2012). Parasagittal zones in the cerebellar cortex differ in excitability, information processing and synaptic plasticity. *Cerebellum* 11, 418–419. doi: 10.1007/s12311-011-0347-1

Empson, R. M., Buckby, L. E., Kraus, M., Bates, K. J., Crompton, M. R., Gundelfinger, E. D., et al. (2006). The cell adhesion molecule neuroplastin-65 inhibits hippocampal long-term potentiation via a mitogen-activated protein kinase p38-dependent reduction in surface expression of GluR1-containing glutamate receptors. *J. Neurochem.* 99, 850–860. doi: 10.1111/j.1471-4159.2006.04123.x

Finch, E. A., Tanaka, K., and Augustine, G. J. (2012). Calcium as a trigger for cerebellar long-term synaptic depression. *Cerebellum* 11, 706–717. doi: 10.1007/s12311-011-0314-x

Fletcher, C. F., Lutz, C. M., O'Sullivan, T. N., Shaughnessy, J. D. Jr., Hawkes, R., Frankel, W. N., et al. (1996). Absence epilepsy in tottering mutant mice is associated with calcium channel defects. *Cell* 87, 607–617. doi: 10.1016/s0092-8674(00)81381-1

Fritschy, J. M., and Panzanelli, P. (2006). Molecular and synaptic organization of GABAA receptors in the cerebellum: effects of targeted subunit gene deletions. *Cerebellum* 5, 275–285. doi: 10.1080/14734220600962805

Fritschy, J. M., Sidler, C., Parpan, F., Gassmann, M., Kaupmann, K., Bettler, B., et al. (2004). Independent maturation of the GABA (B) receptor subunits GABA (B1) and GABA (B2) during postnatal development in rodent brain. *J. Comp. Neurol.* 477, 235–252. doi: 10.1002/cne.20188

Furuichi, T., Yoshikawa, S., Miyawaki, A., Wada, K., Maeda, N., and Mikoshiba, K. (1989). Primary structure and functional expression of the inositol 1,4,5-trisphosphate-binding protein P400. *Nature* 342, 32–38. doi: 10.1038/342032a0

Furutama, D., Morita, N., Takano, R., Sekine, Y., Sadakata, T., Shinoda, Y., et al. (2010). Expression of the IP3R1 promoter-driven nls-lacZ transgene in Purkinje cell parasagittal arrays of developing mouse cerebellum. *J. Neurosci. Res.* 88, 2810–2825. doi: 10.1002/jnr.22451

Furutama, D., Shimoda, K., Yoshikawa, S., Miyawaki, A., Furuichi, T., and Mikoshiba, K. (1996). Functional expression of the type 1 inositol 1,4,5-trisphosphate receptor promoter-lacZ fusion genes in transgenic mice. *J. Neurochem.* 66, 1793–1801. doi: 10.1046/j.1471-4159.1996.66051793.x

Gao, W., Chen, G., Reinert, K. C., and Ebner, T. J. (2006). Cerebellar cortical molecular layer inhibition is organized in parasagittal zones. *J. Neurosci.* 26, 8377–8387. doi: 10.1523/jneurosci.2434-06.2006

Gao, Z., van Beugen, B. J., and De Zeeuw, C. I. (2012). Distributed synergistic plasticity and cerebellar learning. *Nat. Rev. Neurosci.* 13, 619–635. doi: 10.1038/nrn3312

Gerendasy, D. D., and Sutcliffe, J. G. (1997). RC3/neurogranin, a postsynaptic calpacitin for setting the response threshold to calcium influxes. *Mol. Neurobiol.* 15, 131–163. doi: 10.1007/bf02740632

Graham, D. J., and Wylie, D. R. (2012). Zebrin-immunopositive and -immunonegative stripe pairs represent functional units in the pigeon vestibulocerebellum. *J. Neurosci.* 32, 12769–12779. doi: 10.1523/JNEUROSCI.0197-12.2012

Gravel, C., Eisenman, L. E., Sasseville, R., and Hawkes, R. (1987). Parasagittal organization of the rat cerebellar cortex: a direct correlation between antigenic Purkinje cell bands revealed by mabQ73 and the organization of the olivocerebellar projection. *J. Comp. Neurol.* 265, 294–310. doi: 10.1002/cne.902650211

Gravel, C., and Hawkes, R. (1990). Parasagittal organization of the rat cerebellar cortex: direct comparison of Purkinje cell compartments and the organization of the spinocerebellar projection. *J. Comp. Neurol.* 291, 79–102. doi: 10.1002/cne.902910107

Hallem, J. S., Thompson, J., Gundappa-Sulur, G., Hawkes, R., Bjaalie, J. G., and Bower, J. M. (1999). Spatial correspondence between tactile projection patterns and the distribution of the antigenic Purkinje cell markers anti-zebrin I and anti-zebrin II in the cerebellar folium crus IIa of the rat. *Neuroscience* 93, 1083–1094. doi: 10.1016/s0306-4522(99)00144-x

Hansel, C., de Jeu, M., Belmeguenai, A., Houtman, S. H., Buitendijk, G. H., Andreev, D., et al. (2006). αCaMKII is essential for cerebellar LTD and motor learning. *Neuron* 51, 835–843. doi: 10.1016/j.neuron.2006.08.013

Hansel, C., Linden, D. J., and D'Angelo, E. (2001). Beyond parallel fiber LTD: the diversity of synaptic and non-synaptic plasticity in the cerebellum. *Nat. Neurosci.* 4, 467–475.

Hawkes, R., Gallagher, E., and Ozol, K. (1997). Blebs in the mouse cerebellar granular layer as a sign of structural inhomogeneity. I. Anterior lobe vermis. *Acta Anat. (Basel)* 158, 205–214. doi: 10.1159/000147931

Hawkes, R., and Turner, R. W. (1994). Compartmentation of NADPH-diaphorase activity in the mouse cerebellar cortex. *J. Comp. Neurol.* 346, 499–516. doi: 10.1002/cne.903460404

Hawkes, R. (1997). An anatomical model of cerebellar modules. *Prog. Brain Res.* 114, 39–52. doi: 10.1016/s0079-6123(08)63357-9

Hawkes, R., Beierbach, E., and Tan, S. S. (1999). Granule cell dispersion is restricted across transverse boundaries in mouse chimeras. *Eur. J. Neurosci.* 11, 3800–3808. doi: 10.1046/j.1460-9568.1999.00812.x

Hawkes, R., Colonnier, M., and Leclerc, N. (1985). Monoclonal antibodies reveal sagittal banding in the rodent cerebellar cortex. *Brain Res.* 333, 359–365. doi: 10.1016/0006-8993(85)91593-8

Hawkes, R., Gallagher, E., and Ozol, K. (1998). Blebs in the mouse cerebellar granular layer as a sign of structural inhomogeneity. II. Posterior lobe vermis. *Acta Anat. (Basel)* 163, 47–55. doi: 10.1159/000046445

Hawkes, R., and Gravel, C. (1991). The modular cerebellum. *Prog. Neurobiol.* 36, 309–327. doi: 10.1016/0301-0082(91)90004-k

Hawkes, R., and Herrup, K. (1995). Aldolase C/zebrin II and the regionalization of the cerebellum. *J. Mol. Neurosci.* 6, 147–158. doi: 10.1007/bf02736761

Hawkes, R., and Leclerc, N. (1987). Antigenic map of the rat cerebellar cortex: the distribution of parasagittal bands as revealed by a monoclonal anti-Purkinje cell antibody mabQ73. *J. Comp. Neurol.* 256, 29–41. doi: 10.1002/cne.902560104

Hirano, T. (1991). Differential pre- and postsynaptic mechanisms for synaptic potentiation and depression between a granule cell and a Purkinje cell in rat cerebellar culture. *Synapse* 7, 321–323. doi: 10.1002/syn.890070408

Hirano, T. (2006). Cerebellar regulation mechanisms learned from studies on GluRδ2. *Mol. Neurobiol.* 33, 1–16. doi: 10.1385/mn:33:1:001

Huang, Y., Man, H. Y., Sekine-Aizawa, Y., Han, Y., Juluri, K., Luo, H., et al. (2005). S-nitrosylation of N-ethylmaleimide sensitive factor mediates surface expression of AMPA receptors. *Neuron* 46, 533–540. doi: 10.1016/j.neuron.2005.03.028

Ito, M. (1984). *The Cerebellum and Neural Control.* New York: Raven Press.

Ito, M. (1989). Long-term depression. *Annu. Rev. Neurosci.* 12, 85–102. doi: 10.1146/annurev.ne.12.030189.000505

Ito, M. (2002). The molecular organization of cerebellar long-term depression. *Nat. Rev. Neurosci.* 3, 896–902. doi: 10.1038/nrn962

Iwanuik, A. N., Marzban, H., Pakan, J. M. P., Watanabe, M., Hawkes, R., and Wylie, D. R. W. (2009). Compartmentation of the cerebellar cortex of hummingbirds (Aves: Trochilidae) revealed by the expression of zebrin II and phospholipase Cβ4. *J. Chem. Neuroanat.* 37, 55–63. doi: 10.1016/j.jchemneu.2008.10.001

Jörntell, H., and Hansel, C. (2006). Synaptic memories upside down: bidirectional plasticity at cerebellar parallel fiber–Purkinje cell synapses. *Neuron* 52, 227–238. doi: 10.1016/j.neuron.2006.09.032

Ji, Z., and Hawkes, R. (1994). Topography of Purkinje cell compartments and mossy fiber terminal fields in lobules II and III of the rat cerebellar cortex: spinocerebellar and cuneocerebellar projections. *Neuroscience* 61, 935–954. doi: 10.1016/0306-4522(94)90414-6

Kakegawa, W., and Yuzaki, M. (2005). A mechanism underlying AMPA receptor trafficking during cerebellar long-term potentiation. *Proc. Natl. Acad. Sci. U S A* 102, 17846–17851. doi: 10.1073/pnas.0508910102

Kamikubo, Y., Tabata, T., Kakizawa, S., Kawakami, D., Watanabe, M., Ogura, A., et al. (2007). Postsynaptic $GABA_B$ receptor signalling enhances LTD in mouse cerebellar Purkinje cells. *J. Physiol.* 585, 549–563. doi: 10.1113/jphysiol.2007.141010

Kano, M., Hashimoto, K., and Tabata, T. (2008). Type-1 metabotropic glutamate receptor in cerebellar Purkinje cells: a key molecule responsible for long-term depression, endocannabinoid signalling and synapse elimination. *Philos. Trans. R. Soc. Lond. B Biol. Sci.* 363, 2173–2186. doi: 10.1098/rstb.2008.2270

Karavanova, I., Vasudevan, K., Cheng, J., and Buonanno, A. (2007). Novel regional and developmental NMDA receptor expression patterns uncovered in NR2C subunit-beta-galactosidase knock-in mice. *Mol. Cell Neurosci.* 34, 468–480. doi: 10.1016/j.mcn.2006.12.001

Kashiwabuchi, N., Ikeda, K., Araki, K., Hirano, T., Shibuki, K., Takayama, C., et al. (1995). Impairment of motor coordination, Purkinje cell synapse formation and cerebellar long-term depression in GluR delta 2 mutant mice. *Cell* 81, 245–252. doi: 10.1016/0092-8674(95)90334-8

Kato, A. S., Knierman, M. D., Siuda, E. R., Isaac, J. T., Nisenbaum, E. S., and Bredt, D. S. (2012). Glutamate receptor δ2 associates with metabotropic glutamate receptor 1 (mGluR1), protein kinase Cγ, and canonical transient receptor potential 3 and regulates mGluR1-mediated synaptic transmission in cerebellar Purkinje neurons. *J. Neurosci.* 32, 15296–15308. doi: 10.1523/JNEUROSCI.0705-12.2012.

Kaupmann, K., Huggel, K., Heid, J., Flor, P. J., Bischoff, S., Mickel, S. J., et al. (1997). Expression cloning of $GABA_B$ receptors uncovers similarity to metabotropic glutamate receptors. *Nature* 386, 239–246. doi: 10.1038/386239a0

Kim, E. C., Lee, M. J., Shin, S. Y., Seol, G. H., Han, S. H., Yee, J., et al. (2013). Phorbol 12-myristate 13-acetate enhances long-term potentiation in the hippocampus through activation of protein kinase Cδ and ϵ. *Korean J. Physiol. Pharmacol.* 17, 51–56. doi: 10.4196/kjpp.2013.17.1.51

Knöpfel, T., and Grandes, P. (2002). Metabotropic glutamate receptors in the cerebellum with a focus on their function in Purkinje cells. *Cerebellum* 1, 19–26. doi: 10.1007/bf02941886

Kulik, A., Nakadate, K., Nyíri, G., Notomi, T., Malitschek, B., Bettler, B., et al. (2002). Distinct localization of GABA(B) receptors relative to synaptic sites in the rat cerebellum and ventrobasal thalamus. *Eur. J. Neurosci.* 15, 291–307. doi: 10.1046/j.0953-816x.2001.01855.x

Larouche, M., Che, P. M., and Hawkes, R. (2006). Neurogranin expression identifies a novel array of Purkinje cell parasagittal stripes during mouse cerebellar development. *J. Comp. Neurol.* 494, 215–227. doi: 10.1002/cne.20791

Le, T. D., Shirai, Y., Okamoto, T., Tatsukawa, T., Nagao, S., Shimizu, T., et al. (2010). Lipid signaling in cytosolic phospholipase A2-alpha-cyclooxygenase-2 cascade mediates cerebellar long-term depression and motor learning. *Proc. Natl. Acad. Sci. U S A* 107, 3198–3203. doi: 10.1073/pnas.0915020107

Leclerc, N., Beesley, P. W., Brown, I., Colonnier, M., Gurd, J. W., Paladino, T., et al. (1989). Synaptophysin expression during synaptogenesis in the rat cerebellar cortex. *J. Comp. Neurol.* 280, 197–212. doi: 10.1002/cne.902800204

Leclerc, N., Gravel, C., and Hawkes, R. (1988). Development of parasagittal zonation in the rat cerebellar cortex. MabQ73 antigenic bands are created postnatally by the suppression of antigen expression in a subset of Purkinje cells. *J. Comp. Neurol.* 273, 399–420. doi: 10.1002/cne.902730310

Lev-Ram, V., Mehta, S. B., Kleinfeld, D., and Tsien, R. Y. (2003). Reversing cerebellar long-term depression. *Proc. Natl. Acad. Sci. U S A* 100, 15989–15993. doi: 10.1073/pnas.2636935100

Lev-Ram, V., Nebyelul, Z., Ellisman, M. H., Huang, P. L., and Tsien, R. Y. (1997). Absence of cerebellar long-term depression in mice lacking neuronal nitric oxide synthase. *Learn. Mem.* 4, 169–177. doi: 10.1101/lm.4.1.169

Lev-Ram, V., Wong, S. T., Storm, D. R., and Tsien, R. Y. (2002). A new form of cerebellar long-term potentiation is postsynaptic and depends on nitric oxide but not cAMP. *Proc. Natl. Acad. Sci. U S A* 99, 8389–8393. doi: 10.1073/pnas.122206399

Linden, D. J. (1995). Phospholipase A2 controls the induction of short-term versus long-term depression in the cerebellar Purkinje neuron in culture. *Neuron* 15, 1393–1401. doi: 10.1016/0896-6273(95)90017-9

Linden, D. J. (2001). The expression of cerebellar LTD in culture is not associated with changes in AMPA-receptor kinetics, agonist affinity, or unitary conductance. *Proc. Natl. Acad. Sci. U S A* 98, 14066–14071. doi: 10.1073/pnas.241384598

Linden, D. J., and Connor, J. A. (1991). Participation of postsynaptic PKC in cerebellar long-term depression in culture. *Science* 254, 1656–1659. doi: 10.1126/science.1721243

Linden, D. J., Dickinson, M. H., Smeyne, R., and Connor, J. A. (1991). A long-term depression of AMPA currents in cultured cerebellar Purkinje neurons. *Neuron* 7, 81–89. doi: 10.1016/0896-6273(91)90076-C

Luján, R., and Shigemoto, R. (2006). Localization of metabotropic GABA receptor subunits GABAB1 and GABAB2 relative to synaptic sites in the rat developing cerebellum. *Eur. J. Neurosci.* 23, 1479–1490. doi: 10.1111/j.1460-9568.2006.04669.x

Möhler, H., and Fritschy, J. M. (1999). GABAB receptors make it to the top - as dimers. *Trends Pharmacol. Sci.* 20, 87–89. doi: 10.1016/s0165-6147(99)01323-1

Maeda, N., Niinobe, M., Inoue, Y., and Mikoshiba, K. (1989). Developmental expression and intracellular location of P400 protein characteristic of Purkinje cells in the mouse cerebellum. *Dev. Biol.* 133, 67–76. doi: 10.1016/0012-1606(89)90297-2

Marshall, F. H., Jones, K. A., Kaupmann, K., and Bettler, B. (1999). $GABA_B$ receptors - the first 7TM heterodimers. *Trends Pharmacol. Sci.* 20, 396–399. doi: 10.1016/s0165-6147(99)01383-8

Marzban, H., Chung, S. H., Kheradpezhouh, M., Feirabend, H., Watanabe, M., Voogd, J., et al. (2010). Antigenic compartmentation of the cerebellar cortex in the chicken (*Gallus domesticus*). *J. Comp. Neurol.* 518, 2221–2239. doi: 10.1002/cne.22328

Marzban, H., Chung, S., Watanabe, M., and Hawkes, R. (2007). Phospholipase Cβ4 expression reveals the continuity of cerebellar topography through development. *J. Comp. Neurol.* 502, 857–871. doi: 10.1002/cne.21352

Marzban, H., and Hawkes, R. (2011). On the architecture of the posterior zone of the cerebellum. *Cerebellum* 10, 422–434. doi: 10.1007/s12311-010-0208-3

Marzban, H., Khanzada, U., Shabir, S., Hawkes, R., Langnaese, K., Smalla, K. H., et al. (2003). Expression of the immunoglobulin superfamily neuroplastin adhesion molecules in adult and developing mouse cerebellum and their localization to parasagittal stripes. *J. Comp. Neurol.* 462, 286–301. doi: 10.1002/cne.10719

Marzban, H., Sillitoe, R. V., Hoy, M., Chung, S. H., Rafuse, V. F., and Hawkes, R. (2004). Abnormal HNK-1 expression in the cerebellum of an N-CAM null mouse. *J. Neurocytol.* 33, 117–130. doi: 10.1023/b:neur.0000029652.96456.0d

Mateos, J. M., Benítez, R., Elezgarai, I., Azkue, J. J., Lázaro, E., Osorio, A., et al. (2000). Immunolocalization of the mGluR1b splice variant of the metabotropic glutamate receptor 1 at parallel fiber-Purkinje cell synapses in the rat cerebellar cortex. *J. Neurochem.* 74, 1301–1309. doi: 10.1046/j.1471-4159.2000.741301.x

Mateos, J. M., Osorio, A., Azkue, J. J., Benítez, R., Elezgarai, I., Bilbao, A., et al. (2001). Parasagittal compartmentalization of the metabotropic glutamate receptor mGluR1b in the cerebellar cortex. *Eur. J. Anat.* 5, 15–21.

Mathy, A., Ho, S. S., Davie, J. T., Duguid, I. C., Clark, B. A., and Häusser, M. (2009). Encoding of oscillations by axonal bursts in inferior olive neurons. *Neuron* 62, 388–399. doi: 10.1016/j.neuron.2009.03.023

Matsuda, S., Launey, T., Mikawa, S., and Hirai, H. (2000). Disruption of AMPA receptor GluR2 clusters following long-term depression induction in cerebellar Purkinje neurons. *EMBO J.* 19, 2765–2774. doi: 10.1093/emboj/19.12.2765

Mignery, G. A., Sudhof, T. C., Takei, K., and De Camilli, P. (1989). Putative receptor for inositol 1,4,5-triphosphate similar to ryanodine receptor. *Nature* 342, 192–195. doi: 10.1038/342192a0

Miyata, M., Okada, D., Hashimoto, K., Kano, M., and Ito, M. (1999). Corticotropin-releasing factor plays a permissive role in cerebellar long-term depression. *Neuron* 22, 763–775. doi: 10.1016/s0896-6273(00)80735-7

Mugnaini, E., Berrebi, A. S., Dahl, A. L., and Morgan, J. I. (1987). The polypeptide PEP-19 is a marker for Purkinje neurons in cerebellar cortex and cartwheel neurons in the dorsal cochlear nucleus. *Arch. Ital. Biol.* 126, 41–67.

Newton, A. C. (1995). Protein kinase C: structure, function, and regulation. *J. Biol. Chem.* 270, 28495–28498. doi: 10.1074/jbc.270.48.28495

Oberdick, J., Schilling, K., Smeyne, R. J., Corbin, J. G., Bocchiaro, C., and Morgan, J. I. (1993). Control of segment-like patterns of gene expression in the mouse cerebellum. *Neuron* 10, 1007–1018. doi: 10.1016/0896-6273(93)90050-2

Oscarsson, O. (1979). Functional units of the cerebellum- sagittal zones and microzones. *Trends Neurosci.* 2, 143–145. doi: 10.1016/0166-2236(79)90057-2

Overbeck, T. L., and King, J. S. (1999). Developmental expression of corticotropin-releasing factor in the postnatal murine cerebellum. *Brain Res. Dev. Brain Res.* 115, 145–159. doi: 10.1016/s0165-3806(99)00059-0

Ozol, K. O., and Hawkes, R. (1997). The compartmentation of the granular layer of the cerebellum. *Histol. Histopathol.* 12, 171–184.

Pak, J. H., Huang, F. L., Li, J., Balschun, D., Reymann, K. G., Chiang, C., et al. (2000). Involvement of neurogranin in the modulation of calcium/calmodulin-dependent protein kinase II, synaptic plasticity and spatial learning: a study with knockout mice. *Proc. Natl. Acad. Sci. U S A* 97, 11232–11237. doi: 10.1073/pnas.210184697

Pakan, J. M., Iwaniuk, A. N., Wylie, D. R., Hawkes, R., and Marzban, H. (2007). Purkinje cell compartmentation as revealed by zebrin II expression in the cerebellar cortex of pigeons (*Columba livia*). *J. Comp. Neurol.* 501, 619–630. doi: 10.1002/cne.21266

Paukert, M., Huang, Y. H., Tanaka, K., Rothstein, J. D., and Bergles, D. E. (2010). Zones of enhanced glutamate release from climbing fibers in the mammalian cerebellum. *J. Neurosci.* 30, 7290–7299. doi: 10.1523/jneurosci.5118-09.2010

Piochon, C., Levenes, C., Ohtsuki, G., and Hansel, C. (2010). Purkinje cell NMDA receptors assume a key role in synaptic gain control in the mature cerebellum. *J. Neurosci.* 30, 15330–15335. doi: 10.1523/jneurosci.4344-10.2010

Ruigrok, T. J. (2011). Ins and outs of cerebellar modules. *Cerebellum* 10, 464–474. doi: 10.1007/s12311-010-0164-y

Safo, P. K., Cravatt, B. F., and Regehr, W. G. (2006). Retrograde endocannabinoid signaling in the cerebellar cortex. *Cerebellum* 5, 134–145. doi: 10.1080/14734220600791477

Sarna, J. R., Marzban, H., Watanabe, M., and Hawkes, R. (2006). Complementary stripes of phospholipase Cβ3 and Cβ4 expression by Purkinje cell subsets in the mouse cerebellum. *J. Comp. Neurol.* 496, 303–313. doi: 10.1002/cne.20912

Sawada, K., Fukui, Y., and Hawkes, R. (2008). Spatial distribution of corticotropin-releasing factor immunopositive climbing fibers in the mouse cerebellum: analysis by whole mount immunocytochemistry. *Brain Res.* 1222, 106–117. doi: 10.1016/j.brainres.2008.05.029

Schilling, K., Schmidt, H. H., and Baader, S. L. (1994). Nitric oxide synthase expression reveals compartments of cerebellar granule cells and suggests a role for mossy fibers in their development. *Neuroscience* 59, 893–903. doi: 10.1016/0306-4522(94)90293-3

Schonewille, M., Belmeguenai, A., Koekkoek, S. K., Houtman, S. H., Boele, H. J., van Beugen, B. J., et al. (2010). Purkinje cell-specific knockout of the protein phosphatase PP2B impairs potentiation and cerebellar motor learning. *Neuron* 67, 618–628. doi: 10.1016/j.neuron.2010.07.009

Schonewille, M., Gao, Z., Boele, H. J., Veloz, M. F., Amerika, W. E., Simek, A. A., et al. (2011). Reevaluating the role of LTD in cerebellar motor learning. *Neuron* 70, 43–50. doi: 10.1016/j.neuron.2011.02.044

Seil, F. J., Johnson, M. L., and Hawkes, R. (1995). Molecular compartmentation expressed in cerebellar cultures in the absence of neuronal activity and neuron-glia interactions. *J. Comp. Neurol.* 356, 398–407. doi: 10.1002/cne.903560307

Shearman, M. S., Naor, Z., Sekiguchi, K., Kishimoto, A., and Nishizuka, Y. (1989). Selective activation of the γ-subspecies of protein kinase C from bovine cerebellum by arachidonic acid and its lipoxygenase metabolites. *FEBS Lett.* 243, 177–182. doi: 10.1016/0014-5793(89)80125-5

Shin, J. H., and Linden, D. J. (2005). An NMDA receptor/nitric oxide cascade is involved in cerebellar LTD but is not localized to the parallel fiber terminal. *J. Neurophysiol.* 94, 4281–4289. doi: 10.1152/jn.00661.2005

Shirai, Y., and Ito, M. (2004). Specific differential expression of phospholipase A2 subtypes in rat cerebellum. *J. Neurocytol.* 33, 297–307. doi: 10.1023/b:neur.0000044191.83858.f7

Sillitoe, R. V., Benson, M. A., Blake, D. J., and Hawkes, R. (2003). Abnormal dysbindin expression in cerebellar mossy fiber synapses in the *mdx* mouse model of Duchenne muscular dystrophy. *J. Neurosci.* 23, 6576–6585.

Sillitoe, R. V., Marzban, H., Larouche, M., Zahedi, S., Affanni, J., and Hawkes, R. (2005). Conservation of the architecture of the anterior lobe vermis of the cerebellum across mammalian species. *Prog. Brain Res.* 148, 283–297. doi: 10.1016/s0079-6123(04)48022-4

Sugihara, I., and Quy, P. N. (2007). Identification of aldolase C compartments in the mouse cerebellar cortex by olivocerebellar labeling. *J. Comp. Neurol.* 500, 1076–1092. doi: 10.1002/cne.21219

Sugihara, I., and Shinoda, Y. (2004). Molecular, topographic and functional organization of the cerebellar cortex: a study with combined aldolase C and olivocerebellar labeling. *J. Neurosci.* 24, 8771–8785. doi: 10.1523/jneurosci.1961-04.2004

Tabata, T., Araishi, K., Hashimoto, K., Hashimotodani, Y., van der Putten, H., Bettler, B., et al. (2004). Ca2+ activity at GABAB receptors constitutively promotes metabotropic glutamate signaling in the absence of GABA. *Proc. Natl. Acad. Sci. U S A* 101, 16952–16957. doi: 10.1073/pnas.0405387101

Tanaka, S., Kawaguchi, S. Y., Shioi, G., and Hirano, T. (2013). Long-term potentiation of inhibitory synaptic transmission onto cerebellar Purkinje neurons contributes to adaptation of vestibulo-ocular reflex. *J. Neurosci.* 33, 17209–17220. doi: 10.1523/jneurosci.0793-13.2013

Tanaka, C., and Nishizuka, Y. (1994). The protein kinase C family for neuronal signaling. *Annu. Rev. Neurosci.* 17, 551–567. doi: 10.1146/annurev.neuro.17.1.551

Terada, N., Banno, Y., Ohno, N., Fujii, Y., Murate, T., Sarna, J. R., et al. (2004). Compartmentation of the mouse cerebellar cortex by sphingosine kinase. *J. Comp. Neurol.* 469, 119–127. doi: 10.1002/cne.11002

Torres-Aleman, I., Pons, S., and Arévalo, M. A. (1994). The insulin-like growth factor I system in the rat cerebellum: developmental regulation and role in neuronal survival and differentiation. *J. Neurosci. Res.* 39, 117–126. doi: 10.1002/jnr.490390202

Tsuruno, S., Kawaguchi, S. Y., and Hirano, T. (2008). Src-family protein tyrosine kinase negatively regulates cerebellar long-term depression. *Neurosci. Res.* 61, 329–332. doi: 10.1016/j.neures.2008.03.004

Turgeon, S. M., and Albin, R. L. (1993). Pharmacology, distribution, cellular localisation and development of $GABA_B$ binding in rodent cerebellum. *Neuroscience* 55, 311–323. doi: 10.1016/0306-4522(93)90501-6

Vogt, K. E., and Canepari, M. (2010). On the induction of postsynaptic granule cell-Purkinje neuron LTP and LTD. *Cerebellum* 9, 284–290. doi: 10.1007/s12311-010-0174-9

Voogd, J., Pardoe, J., Ruigrok, T. J., and Apps, R. (2003). The distribution of climbing and mossy fiber collateral branches from the copula pyramidis and the paramedian lobule: congruence of climbing fiber cortical zones and the pattern of zebrin banding within the rat cerebellum. *J. Neurosci.* 23, 4645–4656.

Voogd, J., and Ruigrok, T. J. (2004). The organization of the corticonuclear and olivocerebellar climbing fiber projections to the rat cerebellar vermis: the congruence of projection zones and the zebrin pattern. *J. Neurocytol.* 33, 5–21. doi: 10.1023/b:neur.0000029645.72074.2b

Wadiche, J. I., and Jahr, C. E. (2001). Multivesicular release at climbing fiber-Purkinje cell synapses. *Neuron* 32, 301–313. doi: 10.1016/s0896-6273(01)00488-3

Wadiche, J. I., and Jahr, C. E. (2005). Patterned expression of Purkinje cell glutamate transporters controls synaptic plasticity. *Nat. Neurosci.* 8, 1329–1334. doi: 10.1038/nn1539

Wang, X., Chen, G., Gao, W., and Ebner, T. (2009). Long-term potentiation of the responses to parallel fiber stimulation in mouse cerebellar cortex in vivo. *Neuroscience* 162, 713–722. doi: 10.1016/j.neuroscience.2009.01.071

Wang, X., Chen, G., Gao, W., and Ebner, T. J. (2011). Parasagittally aligned, mGluR1-dependent patches are evoked at long latencies by parallel fiber stimulation in the mouse cerebellar cortex in vivo. *J. Neurophysiol.* 105, 1732–1746. doi: 10.1152/jn.00717.2010

Wassef, M., Cholley, B., Heizmann, C. W., and Sotelo, C. (1992). Development of the olivocerebellar projection in the rat: II. Matching of the developmental compartmentations of the cerebellum and inferior olive through the projection map. *J. Comp. Neurol.* 323, 537–550. doi: 10.1002/cne.903230406

Wassef, M., Sotelo, C., Thomasset, M., Granholm, A. C., Leclerc, N., Rafrafi, J., et al. (1990). Expression of compartmentation antigen zebrin I in cerebellar transplants. *J. Comp. Neurol.* 294, 223–234. doi: 10.1002/cne.902940207

Wei, P., Blundon, J. A., Rong, Y., Zakharenko, S. S., and Morgan, J. I. (2011). Impaired locomotor learning and altered cerebellar synaptic plasticity in pep-19/pcp4-null mice. *Mol. Cell. Biol.* 31, 2838–2844. doi: 10.1128/mcb.05208-11

Welker, W. (1987). "Spatial organization of somatosensory projections to granule cell cerebellar cortex: functional and connectional implications of fractured somatotopy (summary of Wisconsin studies)," in *New Concepts in Cerebellar Neurobiology*, ed J. S. King (New York: Alan R. Liss Inc.), 239–280.

Yan, X. X., Yen, L. S., and Garey, L. J. (1993). Parasagittal patches in the granular layer of the developing and adult rat cerebellum as demonstrated by NADPH-diaphorase histochemistry. *Neuroreport* 4, 1227–1230. doi: 10.1097/00001756-199309000-00004

Zagrebelsky, M., Rossi, F., Hawkes, R., and Strata, P. (1996). Topographically organised climbing fibre sprouting in the adult mammalian cerebellum. *Eur. J. Neurosci.* 8, 1051–1054. doi: 10.1111/j.1460-9568.1996.tb01591.x

Zagrebelsky, M., Rossi, F., Hawkes, R., and Strata, P. (1997). Reestablishment of the olivocerebellar projection map by compensatory transcommissural reinnervation following unilateral transection of the inferior cerebellar peduncle in the newborn rat. *J. Comp. Neurol.* 379, 283–299. doi: 10.1002/(sici)1096-9861(19970310)379:2<283::aid-cne9>3.0.co;2-#

Zuo, J., De Jager, P. L., Takahashi, K. A., Jiang, W., Linden, D. J., and Heintz, N. (1997). Neurodegeneration in *Lurcher* mice caused by mutation in δ2 glutamate receptor gene. *Nature* 388, 769–773. doi: 10.1038/42009

Conflict of Interest Statement: The author declares that the research was conducted in the absence of any commercial or financial relationships that could be construed as a potential conflict of interest.

Received: 13 December 2013; accepted: 07 March 2014; published online: 28 March 2014.

Citation: Hawkes R (2014) Purkinje cell stripes and long-term depression at the parallel fiber-Purkinje cell synapse. Front. Syst. Neurosci. ***8****:41. doi: 10.3389/fnsys.2014.00041*

This article was submitted to the journal Frontiers in Systems Neuroscience.

frontiers in
SYSTEMS NEUROSCIENCE

ORIGINAL RESEARCH ARTICLE
published: 30 October 2014
doi: 10.3389/fnsys.2014.00210

Modulation of Purkinje cell complex spike waveform by synchrony levels in the olivocerebellar system

Eric J. Lang[1]*, Tianyu Tang[1], Colleen Y. Suh[1], Jianqiang Xiao[1], Yuriy Kotsurovskyy[1], Timothy A. Blenkinsop[1], Sarah P. Marshall[1] and Izumi Sugihara[2,3]

[1] Department of Neuroscience and Physiology, New York University School of Medicine, New York, NY, USA
[2] Department of Systems Neurophysiology, Graduate School of Medical and Dental Sciences, Tokyo Medical and Dental University, Tokyo, Japan
[3] Center for Brain Integration Research, Tokyo Medical and Dental University, Tokyo, Japan

Edited by:
Richard Apps, University of Bristol, UK

Reviewed by:
Matthew Nolan, The University of Edinburgh, UK
Rafael Gutierrez, Centro de Investigación y Estudios Avanzados del IPN, Mexico

***Correspondence:**
Eric J. Lang, Department of Neuroscience and Physiology, New York University School of Medicine, 550 First Avenue, New York, NY 10016, USA
e-mail: eric.lang@nyumc.org

Purkinje cells (PCs) generate complex spikes (CSs) when activated by the olivocerebellar system. Unlike most spikes, the CS waveform is highly variable, with the number, amplitude, and timing of the spikelets that comprise it varying with each occurrence. This variability suggests that CS waveform could be an important control parameter of olivocerebellar activity. The origin of this variation is not well known. Thus, we obtained extracellular recordings of CSs to investigate the possibility that the electrical coupling state of the inferior olive (IO) affects the CS waveform. Using multielectrode recordings from arrays of PCs we showed that the variance in the recording signal during the period when the spikelets occur is correlated with CS synchrony levels in local groups of PCs. The correlation was demonstrated under both ketamine and urethane, indicating that it is robust. Moreover, climbing fiber reflex evoked CSs showed an analogous positive correlation between spikelet-related variance and the number of cells that responded to a stimulus. Intra-IO injections of GABA-A receptor antagonists or the gap junction blocker carbenoxolone produced correlated changes in the variance and synchrony levels, indicating the presence of a causal relationship. Control experiments showed that changes in variance with synchrony were primarily due to changes in the CS waveform, as opposed to changes in the strength of field potentials from surrounding cells. Direct counts of spikelets showed that their number increased with synchronization of CS activity. In sum, these results provide evidence of a causal link between two of the distinguishing characteristics of the olivocerebellar system, its ability to generate synchronous activity and the waveform of the CS.

Keywords: inferior olive, complex spike, zebrin, synchrony, spikelets, gap junctions

INTRODUCTION

The Purkinje cell (PC) of the cerebellum displays two types of action potentials: simple spikes, which are generated intrinsically and in response to excitation by the mossy fiber/parallel fiber system (Llinas and Sugimori, 1980; Häusser and Clark, 1997; Raman and Bean, 1999; Cerminara and Rawson, 2004), and complex spikes (CSs), which are evoked by the olivocerebellar system (Eccles et al., 1966a). Unlike simple spikes, which are essentially standard action potentials, the CS has a distinctive and variable waveform consisting of an initial spike followed by small spikelets that vary in number and amplitude. This distinctive waveform has led to hypotheses about the function of CS activity, and the spikelets, in particular, have been postulated to be an important functional parameter of CS activity. For example, the number of spikelets in a CS has been hypothesized to be a readout of the state of the PC at the time of the CS (Eccles et al., 1966a, 1967), and has been correlated with the type and strength of synaptic plasticity (LTD or LTP) induced by climbing fiber activity (Mathy et al., 2009).

What makes the CS waveform a particularly attractive possibility for being a functional parameter of olivocerebellar activity is that it is variable, and thus potentially subject to modulation. However, the causes underlying this variation have received relatively little attention, perhaps because the CS has often been incorrectly thought of as an all-or-none event (reviewed in Najafi and Medina, 2013) when it is probably best conceived of as a composite of many all-or-none events (Llinas and Nicholson, 1971).

Potential causes of CS waveform variation can be broadly split into those related to the state of the cerebellar cortex, the PC in particular, and those related to the state of the inferior olive (IO). Although this division is almost certainly not absolute, because of the closed loop nature of the circuits connecting the IO and the cerebellum (Ruigrok, 1997; Marshall and Lang, 2009; Chaumont et al., 2013), it provides a useful experimental and conceptual framework. For example, evidence that cerebellar cortical activity can modulate the CS waveform includes classic results, such as that when a CS is conditioned by the activation of molecular layer interneurons it has a reduced number

of spikelets (Eccles et al., 1966b), and more recent ones, such as the demonstration of a negative correlation between glutamate transporter EAAT4 expression levels in PCs and spikelet number under *in vitro* conditions (Paukert et al., 2010).

The possibility that the state of the IO plays a significant role in determining the CS waveform is raised by the ability of IO neurons to discharge high frequency bursts of spikes rather than individual action potentials (Armstrong and Harvey, 1966, 1968; Crill, 1970), and by the fact that the size of these bursts is correlated with number of spikelets in the resulting CS (Mathy et al., 2009). Thus, factors that modulate the size of the IO bursts would likely also modify the CS waveform; and indeed, several such factors relating to the subthreshold oscillation displayed by IO neurons, including its amplitude, have been identified experimentally (Maruta et al., 2007; Mathy et al., 2009; Bazzigaluppi et al., 2012; De Gruijl et al., 2012). Moreover, modeling results predict that the amplitude of the subthreshold oscillation should be inversely related to the degree of electrical coupling between IO neurons (De Gruijl et al., 2012), suggesting that the latter should also influence the CS waveform.

Here we used multiple electrode recording of CS activity to investigate whether the CS waveform is in fact affected by the state of coupling among IO neurons. These recordings allowed us not only to measure the CS waveform, but also to monitor the state of the IO, because of the one-to-one relationship between CSs and IO discharges, and the fact that synchronous CS activity reflects the effective electrical coupling pattern among IO neurons (Lang et al., 1996; Lang, 2001, 2002; Long et al., 2002; Blenkinsop and Lang, 2006; Marshall et al., 2007; Onizuka et al., 2013). The present results indicate that the level of CS synchrony is causally linked to the CS waveform, and thus provide evidence that the state of electrical coupling among IO neurons is a mechanism by which this waveform may be modulated.

METHODS

Experiments were performed in accordance with the NIH's *Guide for the Care and Use of Laboratory Animals*. Experimental protocols were approved by the Institutional Animal Care and Use Committee of New York University School of Medicine.

GENERAL SURGICAL AND RECORDING PROCEDURES

In most experiments, female Sprague-Dawley rats (225–300 g) were initially anesthetized with ketamine (100 mg/kg) and xylazine (8 mg/kg) intraperitoneally. Supplemental anesthetic was given via a femoral catheter to maintain a constant depth of anesthesia. In some experiments, urethane was used as the anesthetic with an initial dose of 1.5 g/kg followed by supplemental doses of 0.3 g/kg as needed, all given intraperitoneally. In all experiments, the depth of anesthesia was assessed by a paw pinch and the absence of spontaneous movements. Rectal temperature was maintained at 37°C using a heating pad connected to a temperature control system. To gain access to the cerebellum, animals were placed in a stereotaxic frame, and a craniotomy was performed to expose the posterior lobe of the cerebellum. The dura mater was then removed, and the cortical surface was stabilized and protected by covering it with a platform constructed from an electron microscope grid that was pre-embedded in a thin sheet of silicone rubber and supported by tungsten rods. The platform was cemented to the skull of the animal. For further details on the platform construction, see Sasaki et al. (1989).

Extracellular recordings of CS activity were made using single and multiple electrode techniques. In both cases, recording electrodes were implanted by driving them through the rubber and into the apex of the folium using a micromanipulator. Most recordings were from crus IIa except where specified in the Results, in which cases recordings were from vermis lobule VIII.

Single electrode recordings were made with glass micropipettes containing 2 M NaCl solution and were used to obtain high signal-to-noise recordings of CS activity, usually at the PC somatic level (typically 250–300 μm below the cortical surface). The presence of simple spikes and the initial positivity of the CS waveform were used as indicators that these recordings were made at, or close to, the PC soma.

A multiple electrode technique was used to obtain recordings from arrays of PCs simultaneously. In this case, electrodes were typically implanted 75–150 μm below the surface. At these depths simple spike activity is not observed, and thus CSs can be easily recorded in isolation from the PC dendrites. For these recordings the electrode solution was a 50/50 mixture of 2 M NaCl solution and glycerol. Electrodes were implanted sequentially, with each electrode being released from the manipulator upon isolation of CS activity, and then held in place by the rubber platform. Recordings were made following completion of the electrode array. For further details on the electrode implantation procedure, see Sasaki et al. (1989).

All neuronal activity was recorded using a multichannel recording system (MultiChannel Systems, Germany) with a 25 kHz/channel sampling rate, gain of 1000x, and band pass filters set at 0.1 or 0.2–8.0 kHz (somatic level recordings, low cutoff of 0.1 kHz; dendritic level recordings 0.2 kHz). For the multielectrode recordings, CS activity could be discriminated using a single voltage level threshold, as simple spike activity was not detected because of the superficial placement of the electrodes. Recordings obtained at the PC somatic level contained both simple spikes and CSs, and therefore the entire record was spike-sorted offline to separate the two spike types.

ZEBRIN EXPERIMENTS

Zebrin band location was used for grouping PCs, because PCs located in the same band receive input from the same region of the IO, and thus will likely have functionally related CS activity. The multielectrode recordings of CS activity used here were used in a previous study that described the relationship between the zebrin bands and the patterns of CS synchrony, and details about the localization of PCs to specific zebrin bands can be found there (Sugihara et al., 2007). In brief, spontaneous crus IIa CS activity was recorded from arrays of PCs. Following the recording session (20 min), alcian blue dye was injected into the cerebellar cortex at the corners of the array to mark their locations, the animal was perfused, and the cerebellum was then stained for zebrin. The locations of the PCs in the array were then plotted on zebrin maps of the cortex using the dye marks as fiduciary points.

CEREBELLAR NUCLEAR CELL RECORDINGS

Convergence onto the same nuclear cell was used as the criterion for grouping PCs. In these experiments a multielectrode array was implanted on crus IIa and a single microelectrode was used to search for cerebellar nuclear neurons once the array was completed. Upon good isolation of a nuclear cell, the activity of all cells was typically recorded for 20 min. The subset of PCs in the recording array that synapse with the nuclear cell was then identified using cross-correlation analyses. The detailed recording methods and analyses related to establishing synaptic connectivity have been published previously (Blenkinsop and Lang, 2011). In brief, a significant negative deflection in the CS-triggered correlogram that occurred at a latency of 1–5 ms after the CS onset was taken as evidence for a synaptic connection between the PC and cerebellar nuclear cell being recorded.

CLIMBING FIBER REFLEX EXPERIMENTS

Cerebellar white matter stimulation elicits both a direct CS response in PCs, due to orthodromically conducted action potentials along the olivocerebellar axons from the stimulation site, and a longer latency reflex response, mediated by the antidromic spikes that travel back to the IO and cause electrotonic spread of current, via gap junctions, to other IO neurons, that in turn generate spikes that travel back to the cerebellum to evoke the reflex CSs (Eccles et al., 1966a; Llinás et al., 1974; Sotelo et al., 1974; Blenkinsop and Lang, 2006; Marshall et al., 2007). Here we will analyze the waveforms of the reflex responses that were recorded for a previous study in which the response distribution and its dependence on gap junction coupling of IO cells were reported (Blenkinsop and Lang, 2006). Details of the methods can be found in that report. However, essentially, the multielectrode array was implanted on crus IIa as described earlier, and a bipolar stimulus electrode was lowered through lobule crus I to a depth of 1–2 mm into the cerebellar white matter. Approximately 300 current pulses (100–200 μs, 50–500 μA) were given in each experiment to evoke CS responses.

INTRA-IO INJECTION EXPERIMENTS

Picrotoxin (1–2 mg/ml), gabazine (1 mM), or carbenoxolone (500 μM) dissolved in 0.9% saline or Ringers solutions was injected into the IO to manipulate CS synchrony levels (Lang et al., 1996; Lang, 2002). In these experiments, a multielectrode array was used to record CS activity. After baseline CS activity was recorded for one or more 20-min control periods, an electrode was lowered from the dorsal surface of the medulla to the region of the IO, guided by stereotaxic coordinates (Paxinos and Watson, 1998). When IO multi- or single-unit activity was observed through the electrode, a short (5 min) recording period was obtained, and a correlogram of the IO activity with the CSs was generated for each PC in the array. A clear peak in at least some of the correlograms was used as the criterion for identifying the desired injection site within the IO (i.e., the part of the IO that projects to crus IIa being recorded). The electrode was then removed and an injection pipette was lowered to the same coordinates. An injection of approximately 1 μL of drug solution was then made over 5 min [for example, see Figure 1C of Blenkinsop and Lang (2006)]. CS activity was then recorded for 20-min periods.

DATA ANALYSIS

Variance analysis

Because spikelets are not always unambiguously distinguishable from baseline noise fluctuations, we developed a method for characterizing their parameters indirectly by using the variance associated with the CS waveform. Recordings where the 0.1 kHz lower limit of the bandpass filter was used (somatic recordings) were first high pass filtered using the FIR filter in Igor Pro (Wavemetrics) with a Hanning window with the transition band frequency limits set to 400 and 500 Hz. This was done for the recordings in the cerebellar nuclear recording, climbing fiber reflex, and urethane experiments. The recordings for the zebrin and pharmacological experiments were not refiltered. Variance, σ^2, of the recording signal for a specified time window containing n sample points is defined in the usual manner:

$$\sigma^2 = \frac{1}{n-1}\sum_{i=1}^{n}(y_i - \bar{y})^2 \quad (1)$$

where y_i is the value of the recording at time point i, and $\bar{y}$ is the average value of the y_i for the window.

We define several time windows for which variance measurements will be made (**Figure 1A**). The first is the total spikelet window (T), which is a fixed duration window that starts at the termination of the initial spike, and lasts long enough so that all (or nearly all) spikelets from any CS from the recorded PC will occur within it. The duration was chosen by first visually inspecting an overlay of all CSs and/or an average of all CSs from a PC to determine the approximate times of appropriate start and end points for that PC. The difference in these points set the duration of the T window. The exact duration used was not critical (similar results were obtained when the duration was varied by several milliseconds in test cases). However, if a PC had a few very long outlier CSs, they were excluded from the analysis in order to avoid making the T window excessively long, as that decreased its sensitivity for distinguishing between the vast majority of CSs.

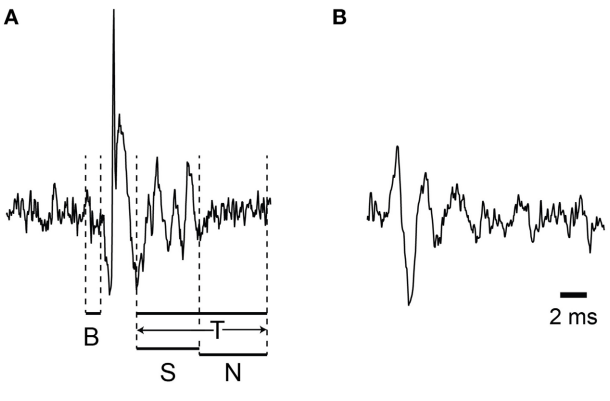

FIGURE 1 | Demonstration of the windows used for variance measurements. The windows used to measure signal variance are illustrated: B (baseline), S (spikelet), N (non-spikelet), and T (total). **(A,B)** each present a sample CS waveform recorded from PC soma and dendrite.

For most CSs the T window can be divided into two successive portions, spikelet (S) and non-spikelet (N), where the dividing line is the time of the peak of the last spikelet plus half an inter-spikelet interval. This division point varies from CS to CS, and thus the S and N windows are variable, but their sum is fixed and equal to the time of the T window. Finally, we define baseline periods as those from times surrounding the CSs when no spike activity is present (i.e., either a time period before the CS starts or a period that starts later than end of the T window).

Depending on the analysis window there are several potential contributions to the overall variance in the recording. For the S window two signals contribute to the overall variance, the spikelet and the baseline noise signals. We assume that these are independent, and since the variances of two independent signals sum (Wonnacott and Wonnacott, 1977), $\sigma_S^2 = \sigma_{spikelet}^2 + \sigma_{base}^2$. By definition, $\sigma_{spikelet}^2$ is that due to only the spikelets themselves. The σ_{base}^2 includes all other signals, including the background noise of the electronics and any physiologically-generated electric activity not due to the spikelets. For the N period the variance is simply σ_{base}^2.

The signal during the T period is a combination of the signals during the S and N periods, and so, in general, its variance, σ_T^2, depends on σ_S^2 and σ_N^2 as well as the mean values of the S and N signals according to Equation (2) (Frühwirth-Schnatter, 2006):

$$\sigma_T^2 = \sum_i f_i(\sigma_i^2 + (\mu_i - \mu_T)^2) \tag{2}$$

where $i =$ S and N, μ_T is the mean of the signal over T, μ_i is the mean of the signal over period i, and f_i is the fraction of T that corresponds to period i. However, note that if the baseline noise and spikelet signals have the same mean amplitude, the overall variance is simply the weighted sum of the variances of the individual S and N periods.

Finally, we define a modified total variance, σ_{T*}^2, where the contribution due to the difference in the means of the S and N periods is subtracted, by Equation (3).

$$\sigma_{T*}^2 = \sigma_T^2 - \sum_i f_i(\mu_i - \mu_T)^2 = \sum_i f_i\sigma_i^2 \tag{3}$$

Testing goodness of linear fits to variance plots

In many of the analyses the variance of each of the time windows defined above was plotted against particular variables, such as spikelet number or synchrony level. Least squares regression lines were then fit to these scatterplots to assess the relationship between the variables. A linear model was chosen, in part, because of the linear summation properties of the variances. The goodness of the regression model was tested by comparing the mean sum of squares related to within group or pure error (PE) and the error due to deviation from linearity or lack of fit (LOF), as defined according to Equations (4) and (5) (Brook and Arnold, 1985; Zar, 1999). The sum of the squares (SS) of the PE is:

$$SS_{PE} = \sum_{i=1}^{k}\sum_{j=1}^{n_i}(y_{ij} - \bar{y}_i)^2 \tag{4}$$

where there are n_i observations at the ith value of the independent variable, k different values of that variable, and where $\bar{y}_i$ is the average of the y_{ij} at the ith value of that variable. The SS_{LOF} is then obtained by subtracting the PE from the total error:

$$SS_{LOF} = \sum_{i=1}^{N}(y_i - \widehat{y_i})^2 - SS_{PE} \tag{5}$$

where the total error is the sum of the squares of the residuals about the regression line, $\widehat{y_i}$ is the predicted value of y_i from the regression equation, and N is total number of observations. The mean SS (MSS) for PE and LOF are then obtained by dividing them by their respective degrees of freedom: $MSS_{PE} = SS_{PE}/(k-2)$ and $MSS_{LOF} = SS_{LOF}/(N-k)$, and the ratio MSS_{LOF}/MSS_{PE}, provides an F-statistic that can then be used to test the goodness of fit of the model (Brook and Arnold, 1985; Zar, 1999).

Counting spikelets

Spikelets were counted mainly in recordings with high signal-to-noise ratios in which separation of spikelets from noise fluctuations in individual traces was possible. To count spikelet numbers, all CS waveforms were first automatically processed by a custom-written procedure in Igor Pro (Wavemetrics, Portland, OR), which detected all deflections with a peak-to-trough level exceeding a pre-defined threshold. The counts were then manually verified, and only a small portion was adjusted with necessary deletions and/or additions (median percentage: 8%).

Synchrony analysis

In all analyses of synchrony, the time of the CS was defined as its onset. For a number of the analyses the level of synchronous CS activity was analyzed spike by spike. This was done by taking the time of the reference CS and determining whether CSs occurred in the other PCs in its group within a specified time window surrounding that time. The time windows for defining synchrony were either 1 or 5 ms depending on the experiment. The 1 ms window was used except when too few highly synchronous events (i.e., synchronous CSs among a large percentage of the group members) occurred for the analyses to be performed. In several instances we ran the analyses using both definitions, and similar results were obtained.

For some analyses, it was necessary to define the average level of synchrony that a PC had with other cells over an entire recording session. In these cases, we quantified the level of synchronous activity using a cross-correlation coefficient, $C(0)$, as described previously (Gerstein and Kiang, 1960; Sasaki et al., 1989). The spike train of a cell was represented by $X(i)$, where i represents the time step ($i = 1, 2, \ldots,$ N). $X(i) = 1$ if a CS onset occurs in the ith time bin, otherwise $X(i) = 0$. $Y(i)$ was the same as $X(i)$, but for the reference cell. $C(0)$ was then calculated as:

$$C(0) = [\sum_{i=1}^{N} V(i) * W(i)] / \sqrt{\sum_{i=1}^{N} V(i)^2 * \sum_{i=1}^{N} W(i)^2}$$

where $V(i)$ and $W(i)$ are

$$V(i) = X(i) - \sum_{j=1}^{N} \frac{X(j)}{N}, \; W(i) = Y(i) - \sum_{j=1}^{N} \frac{Y(j)}{N}$$

Unless otherwise stated, population statistics are given as mean $\pm SD$. The regression lines in this and all subsequent figures were fit using least squares.

RESULTS

For investigating the relationship between CS waveform (in particular, the number of spikelets) and synchrony with extracellular recordings, the relatively small and variable amplitude of the spikelets presents an obstacle. CSs recorded from near the PC layer are shown in **Figure 1A**. Here the initial spike amplitude is approximately 10 times the baseline, but the larger spikelets are only about 2 times the baseline noise, and what may be smaller spikelets fall within the range of the baseline noise fluctuations. As a result, not all spikelets can be unambiguously identified in most recordings, even with recordings that have high signal-to-noise ratios. The issue is more problematic for multielectrode recordings from the molecular layer, where the single to noise ratio of most spikes is usually less than what it is when a single electrode, which can be continually repositioned, is used for recording (**Figure 1B**). As a result, although isolation of CSs is not an issue, distinguishing spikelets from noise fluctuations is often difficult and time consuming, and generally cannot be done with absolute certainty from the multielectrode recordings needed to measure population activity.

Thus, we used the variance of the recording signal during various time windows during the CS as an indirect way to detect changes in the CS waveform. Below we will first present results showing that the variance in the T window (**Figure 1A**), which corresponds to the time when spikelets may be present, is modulated by the level of CS synchrony. The rationale for using the T window is that the variance in it will increase linearly with the number of spikelets contained within it (assuming that spikelet shape doesn't also vary with number, i.e., that σ_S^2 is constant). This follows from Equation (2), that $\sigma_S^2 > \sigma_N^2$, and that an increase in the number of spikelets is reflected as an increase in f_S. However, other factors may influence the variance during the T window, such as fields generated by synchronously active nearby neurons, and other assumptions may not hold. For example, the shape of the spikelets could, in fact, vary systematically with the total number of spikelets. These possibilities will also be addressed below. Lastly, direct evidence for changes in spikelet number with synchrony will be presented.

SPIKELET-RELATED VARIANCE IS CORRELATED WITH CS SYNCHRONY LEVELS WITHIN A ZEBRIN COMPARTMENT

To test the relationship between CS synchrony and CS waveform, we analyzed multielectrode recordings of CS activity from crus IIa PCs whose locations had been mapped onto zebrin II stained brains in a previous study (Sugihara et al., 2007). PCs located in the same zebrin band receive their climbing fibers from the same small region of the IO (Voogd et al., 2003; Sugihara and Shinoda, 2004; Voogd and Ruigrok, 2004). Thus, CS synchrony among PCs in the same zebrin band should reflect the coupling state of the local region of the IO that projects to that band.

We analyzed data from three such multielectrode experiments. In total, seven groups of three PCs, where all of the PCs were located within the same zebrin band, were analyzed ($n = 21$ PCs). According to the nomenclature of Sugihara and Shinoda (2004), the PC groups were located in bands 4−, 4b−, 5−, 5+, 6−, and 6+. The plotting of PCs onto a zebrin map for one experiment is shown in **Figure 2A**. The two groups of PCs from this experiment that were analyzed are enclosed by ellipses.

To analyze the relationship between CS waveform and synchrony among the PCs in a zebrin band group, each CS was classified according to the level of synchrony in its group at its time of occurrence; i.e., according to how many other PCs (zero, one, or two) in the group also fired a CS within 5 ms of its onset. Spikelet-related variance (T window) and baseline (from a period just following the T window) variances were measured for each CS.

Averages of baseline and spikelet-related (T window) variances were computed for each cell at every available synchrony level. Plots of average spikelet-related variance as a function of synchrony level showed a positive relationship for almost all PCs, as shown for two PCs from two groups in one experiment (**Figure 2B**). Because only two or three levels of synchrony existed for any given PC, we tested whether there was a difference in average spikelet-related variance levels between the lowest and highest synchrony groups rather than doing regression analyses. In 81% of PCs (17/21) the spikelet-related variance of the highest synchrony level was significantly different, all greater, than that of the lowest synchrony level ($p < 0.05$). Of the other four PCs, three showed no significant difference and one had significantly larger variance in the lower synchrony group. In contrast, for baseline variance, either no statistical difference in baseline variance between the highest and lowest synchrony groups (20/21, $p > 0.05$, two-sided t-test) or a small negative relationship (1/21, $p = 0.004$) was found.

On a population level, the distributions of average spikelet-related variance for the highest and lowest synchrony levels were also different, whereas the distributions of baseline variances were not (spikelet-related, $p = 0.0027$; baseline, $p = 0.33$; **Figure 2C**). In sum, synchronous CSs were associated with higher spikelet-related variance.

SPIKELET-RELATED VARIANCE CORRELATES WITH SYNCHRONY AMONG PCs THAT PROJECT TO THE SAME CEREBELLAR NUCLEAR CELL

To investigate the correlation between spikelet-related variance and CS synchrony with more resolution in terms of synchrony levels, we used experiments from a data set in which CSs were recorded from PCs that all projected to the same cerebellar nuclear neuron (Blenkinsop and Lang, 2011). This criterion was used because cerebellar nuclear cells tend to receive input from PCs that are located within the same zebrin compartment (Chung et al., 2009; Sugihara, 2011), and thus can be used as a surrogate for zebrin in identifying PCs that receive climbing fiber input from the same region of the IO.

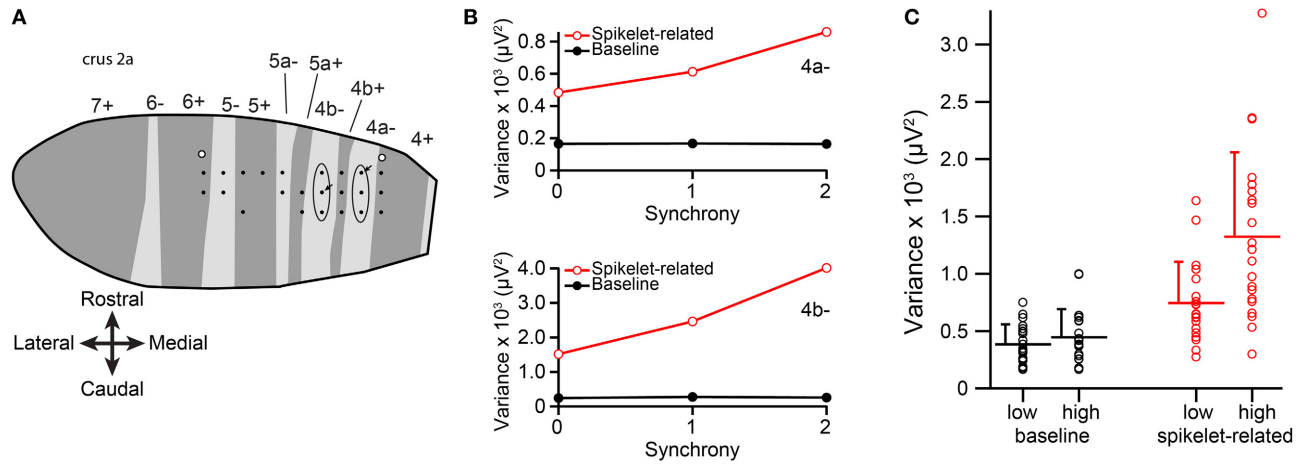

FIGURE 2 | Spikelet-related variance increases with CS synchrony among PCs within a single zebrin band. (A) Plotting of electrode array from one experiment onto the zebrin map of crus IIa. Each black dot represents the position of an electrode in the array. Ellipses indicate the two PC groups whose CS activity was analyzed from this experiment. White-filled circles indicate locations of dye injections that were used to align the recording array with the zebrin map. **(B)** Plots of average variance as a function of group synchrony for the two PCs indicated by arrows in **(A)**. **(C)** Average variance for the lowest and highest synchrony levels for the population. Each circles represents data from one PC, bars indicate population averages, and error bars are one *SD*.

CS-triggered correlograms of nuclear cell activity were used to identify PCs that were synaptically connected to the nuclear cell, with the criterion being a sharp-onset inhibition of nuclear cell activity starting several milliseconds after the onset of the CS (**Figure 3A**, time lag = 0 ms, dashed line). This precisely timed inhibition, combined with the anatomy of the circuits, provides strong evidence of a direct synaptic connection between the PC and nuclear cell that were being recorded. For further details, including statistical tests of the significance of the inhibitory effect, see Blenkinsop and Lang (2011).

The CSs from six groups of crus IIa PCs so identified were analyzed, with the groups ranging in size from 4 to 9 PCs (mean 7.2 ± 1.7 PCs; $n = 42$ PCs total; $n = 5$ animals; note four PCs were part of two groups because two nuclear cells that were recorded in the same animal had partially overlapping PC groups). **Figure 3B** illustrates the arrangement of the PCs for one typical group, where the black circles indicate PCs that projected to the same cerebellar nuclear neuron and gray circles show the positions of the remaining PCs in the array.

For each PC, all of its CS were classified according to the level of synchrony in the group at the time of their occurrence using a 1-ms time window. The spikelet-related (T window) variance was also measured for each CS (defined in Methods). CSs were distributed over a range of 4–9 synchrony levels, depending on the PC. Although there was considerable scatter, a clear relationship between spikelet-related variance and synchrony could almost always be observed by plotting the average variance level as a function of synchrony within the group (**Figure 3C**, red circles).

To test the significance of the relationship between spikelet-related variance and synchrony, a scatterplot of these parameters was constructed from the CSs of each PC. Such plots showed a significant and positive correlation with synchrony for spikelet-related variance for 41/42 PCs ($p < 0.02$). The overall distribution of r-values is shown in **Figure 3D** ($r = 0.26 \pm 0.089$, $n = 42$). Tests for linearity showed a good fit for most cells (MSS_{LOF}/MSS_{PE}; $p > 0.05$, $n = 25/41$ PCs). For the other PCs no dominant pattern to the deviation from linearity was found, with some cells showing supralinear increases at the highest synchrony levels, and some having curves that plateaued.

Next, to look for evidence of field effects that might contribute to the variance signal, we measured the baseline variance in the millisecond just prior to the onset of the CS. If fields due to synchronized activity from nearby cells were contributing to the signal, they should be present in the milliseconds preceding the CSs in the recorded cell, because "synchronized" CSs occur over a time window that spans at least several milliseconds (see Discussion for details).

Overall, the r values for the baseline (0.030 ± 0.062, $n = 42$) were much smaller than those for the T window. However, although the r value for the baseline was either not different from zero or negative for the majority of PCs (**Figures 3C,D**, black circles; $p > 0.05$, $n = 20$; $r < 0$ and $p < 0.05$, $n = 3$), for many PCs, a small but significant correlation was found ($r > 0$ and $p < 0.05$, $n = 19$). Thus, in at least some cells, fields may be contributing to the observed correlation between synchrony and the signal variance. However, for the 41 PCs with significant positive correlations for spikelet-related (T window) variance, the baseline r value was smaller than that for the T window. Moreover, we compared the slopes of the regression lines, and the line for the baseline variance was less steep than that for the T window for 37 of 41 PCs, with the difference being significant in 26 cases. Overall, excluding one outlier, the slope for the T window variance was on average 4–5 times greater than that for the baseline (T window: mean, 19.76 ± 35.62, median, 13.59; baseline: 4.43 ± 7.42, median, 2.18 μV^2/synchrony level).

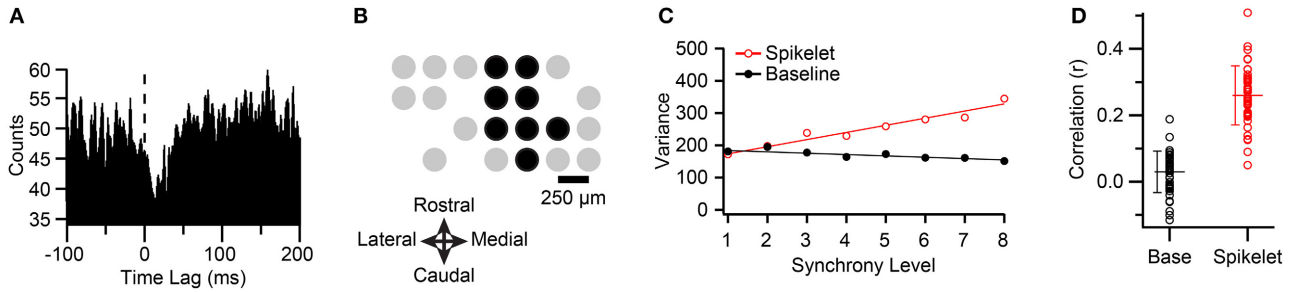

FIGURE 3 | Synchronous CSs among PCs projecting to the same cerebellar nuclear cell have higher spikelet-related variance. (A) CS triggered histogram of cerebellar nuclear cell activity. Note the sharp reduction in activity just after the occurrence of the CS (time lag = 0 ms). Histogram was constructed using 1-ms bins, and smoothing by averaging each bin with its neighbors. **(B)** Schematic showing recording array arrangement. Each circle represents the relative position of an electrode on crus IIa. Black circles indicate PCs that projected to the cerebellar nuclear cell being recorded. **(C)** Plot of average spikelet-related (red) and baseline (black) variances as a function of synchrony level among the PCs indicated by black circles in **(B)** for one cell in the group (cell corresponding to the fifth circle of top row in **(B)**. A synchrony level (x-axis) of zero means that the CS occurred in the absence of CSs in any other PC in the group. Regression lines are fits to the entire data set for that cell. **(D)** Distribution of correlation (*r*) values between synchrony and variances for all PCs (circles). Population means indicated by horizontal lines, and error bars indicate the *SD*.

SPIKELET-RELATED VARIANCE IS CORRELATED WITH THE NUMBER OF PCs RESPONDING TO THE CLIMBING FIBER REFLEX

We next investigated whether we could see the same relationship between variance and synchrony for CSs that were evoked using the climbing fiber reflex. The timing of such evoked CSs should occur randomly with respect to the ongoing state of the cerebellar cortex, and therefore should be evoked independent of direct effects of the state of the cerebellar cortex on the PC. Thus, the evoked CS waveforms should reflect factors related to the IO state, and not cortical activity directly. An indirect effect is still possible, as the cortical state can influence the state of the IO (Marshall and Lang, 2009; Chaumont et al., 2013), but the effect of changes in the IO state are what we are trying to demonstrate.

In each experiment, an array of electrodes was implanted into crus IIa to record CS activity ($n = 51$ PCs, 3 animals evoked via the climbing fiber reflex). The reflex was triggered by electrical stimuli ($n = 300$) delivered to the cerebellar white matter via a bipolar electrode implanted into crus I. Nine PCs were chosen for analysis because their reflex responses allowed individual spikelets to be counted (see later Section "Spikelet Count Correlates with CS Synchrony"). The average response rate among these nine cells was 24.6 ± 7.9% (range, 15–38%).

Figure 4A shows the responses of a crus IIA PC to five electrical stimuli applied to the white matter core of crus I. In each case the stimulus evoked a short-latency direct CS response (**Figure 4A**, indicated by "∗") that is due to purely axonal conduction along the branches of the olivary axons. In most cases (bottom four traces), the direct response was followed by a climbing fiber reflex response (indicated by arrow and arrowheads) whose reflex arc involves spread of current among IO neurons via gap junctions, and thus, whose spatial distribution reflects the state of electrical coupling among IO neurons (Llinás et al., 1974; Sotelo et al., 1974; Blenkinsop and Lang, 2006; Marshall et al., 2007).

The direct response was relatively constant, and in this cell, usually consisted of a single negative deflection with one or two surrounding positive peaks. In contrast, the waveform of the reflex CS contained varying numbers of spikelets whose shape and timing could also vary. However, note that the initial spike of the reflex response was relatively constant, as can be seen by aligning the traces to its onset (**Figure 4A**, traces in upper right corner).

To investigate whether variation in the spikelet portion of the reflex response waveform was related to the electrical coupling state of the IO, T window variance was measured. Scatter plots were then constructed to compare the variance of each reflex response of a PC to the number of PCs in the array showing a response to the corresponding stimulus (**Figure 4B**, red circles). Almost all PCs ($n = 8/9$) showed a significant positive correlation between spikelet-related variance of a reflex CS and the number of PCs responding to the same stimulus ($p < 0.05$). In contrast, for the baseline variance, which was measured during the time just preceding the electrical stimuli, no significant correlation was found ($n = 0/9$; **Figure 4B**, black circles). Overall, the average correlation of spikelet-related variance with the number of cells responding was significantly different from zero, whereas that of the baseline value was not (**Figure 4C**; spikelet-related, $r = 0.39 \pm 0.20$, $n = 9$, $p = 0.0004$; baseline, $r = 0.01 \pm 0.15$, $n = 9$, $p = 0.84$). Moreover, the average spikelet-related correlation was significantly higher than that of the baseline ($p = 0.0018$, paired *t*-test).

SPIKELET-RELATED VARIANCE AND CS SYNCHRONY ARE CORRELATED UNDER URETHANE ANESTHESIA

The above results demonstrating a correlation between spikelet-related variance and CS synchrony were all obtained in ketamine/xylazine anesthetized animals. To rule out the possibility that this relationship is specific to the ketamine/xylazine state, we analyzed data from urethane anesthetized animals ($n = 21$ PCs, 2 animals). Multielectrode recordings of spontaneous CS activity were obtained for 20-min periods. In these experiments we did not have zebrin stained tissue or simultaneous recordings of cerebellar nuclear cells, and so cell groups were formed as a localized cluster of PCs that had synchronized CS activity. The spatial distribution of synchrony under urethane is similar to that found under ketamine; that is, synchronous activity is most common among PCs aligned in the same rostrocaudal strip of cortex (Blenkinsop and Lang, unpublished results), and

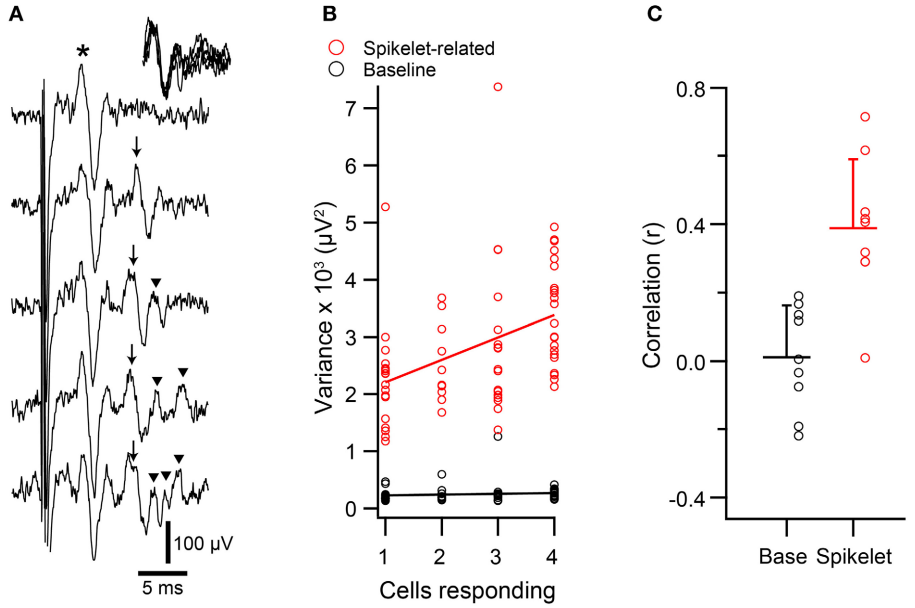

FIGURE 4 | Spikelet-related variance in climbing fiber reflex evoked CSs is correlated with size of responding population. (A) Extracellular recordings of evoked responses, which showed both an initial direct response (∗) and a reflex response (arrows). In the top trace only a direct response is present, whereas the remaining traces have both responses. Note the variable number of spikelets in the reflex responses (initial spike and each spikelet indicated by an arrow). Inset at upper right: overlapping of reflex response from bottom four traces, aligned to the initial spike in the reflex response. **(B)** Scatterplot of baseline (black) and spikelet-related (red) variance vs. the number of PCs that responded to the reflex for a representative PC. In this experiment the data were analyzed from four PCs, all of which showed significant reflex response percentages (17, 22, 23, and 29%). Circles represent the data from trials in which a response was evoked for this PC (one cell responding means that a response was evoked in only this PC). **(C)** Average correlation values for the relationship between variance and number of responding cells for baseline (black) and spikelet-related (red) variance. Each circle represents the data from one cell. Horizontal bars indicate mean of population. Error bars show 1*SD*.

this rostrocaudal pattern aligns with the zebrin banding and PC-nuclear cell projection patterns (Sugihara et al., 2007; Sugihara, 2011). Therefore, these groups should be quite similar to those formed by the other two criteria. An example of the synchrony distribution with respect to one cell (cell M) of the recording array is shown in the bubble plot of **Figure 5A**, where the area of each circle represents the synchrony between the CSs of cell M and those of the PC at the location of the circle. Because synchrony levels in the urethane experiments were somewhat lower than those in the ketamine ones, a 5-ms window was used to define synchrony in order to obtain enough synchronous events that included a large percentage of PCs in the group.

In total, the CS activity from four groups of 5–6 PCs (two groups from each animal) were analyzed for the relationship between spikelet-related (T window) variance and synchrony levels. As was observed in the experiments where ketamine/xylazine anesthesia was used, a clear correlation between spikelet-related variance and the level of synchrony among group members was found. This is illustrated in **Figure 5B** for two cells from a PC group (the group comprises cell M and those PCs indicated by black circles in **Figure 5A**). For both PCs, the average spikelet-related variance (red circles) rises with synchrony level, whereas baseline variance (black circles) remains essentially constant. In these experiments the baseline was measured for a 4-ms period starting 10 ms after the onset of the CS, shortly after the end of the T window, because the activity preceding the CS onset was not recorded.

Almost all PCs showed a significant positive correlation between spikelet-related variance and synchrony level (**Figure 5C**, red circles; $p < 0.05$, $n = 21/22$; note, the activity from one PC was analyzed as part of two groups, giving a total n of 22). In contrast, for baseline variance, 7/22 PCs showed no significant correlation ($p > 0.05$), and while the remaining 15 PCs did show a statistically significant correlation, the values were small in comparison with those of spikelet-related variance (**Figure 5C**, black circles; baseline all cells: $r = 0.072 \pm 0.042$, $n = 22$, baseline cells with significant r: $r = 0.076 \pm 0.045$, $n = 15$; spikelet-related, all cells, 0.31 ± 0.077, $n = 22$). Furthermore, in those cases where a significant positive correlation of baseline variance occurred, the correlation of synchrony with spikelet-related variance was always greater than that with baseline variance ($n = 15/15$). In sum, the results were obtained under urethane and ketamine/xylazine anesthesia were quite similar.

PHARMACOLOGICAL MANIPULATIONS OF CS SYNCHRONY PRODUCE CORRESPONDING CHANGES IN SPIKELET-RELATED VARIANCE

To test whether the correlation between synchrony and spikelet-related variance reflects a direct causal relationship, we first manipulated CS synchrony levels by injecting a GABA-A receptor antagonist (either picrotoxin or gabazine) into the IO. Such injections have been shown to increase CS synchrony *in vivo* (Lang et al., 1996; Lang, 2002) and to increase synchronization of IO activity in brainstem slices (Leznik et al., 2002), effects that are likely due to increased electrical

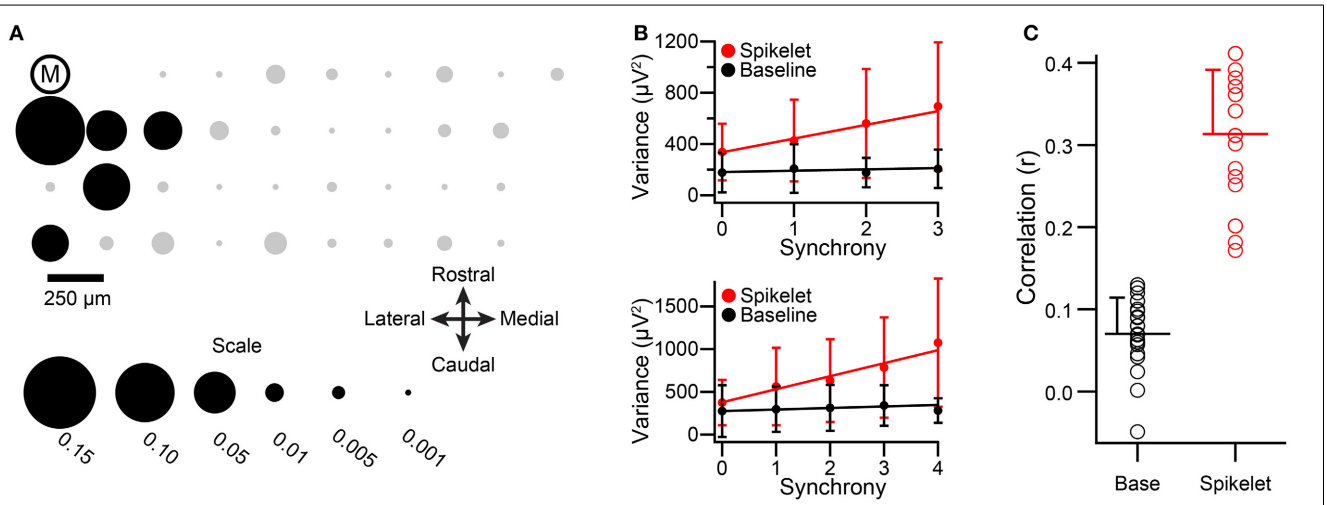

FIGURE 5 | Relationship between spikelet-related variance and CS synchrony holds under urethane anesthesia. (A) Bubble plot representing the synchrony distribution with respect to cell M. The relative positions of the recorded PCs in the array are indicated by circles, and the encircled "M." The areas of the circles are proportional to the synchrony between CSs of cell M and the other PCs in the array. Note that cell M's activity is strongly correlated mainly with neighboring cells. Black circles along with cell M comprise the cell group that was analyzed. **(B)** Plots of average variances during the CSs and the baseline periods as a function of CS synchrony among group members. Top graph is for cell M. Bottom graph is for another group member (indicated by black circle in third row, second column of the array). Regression lines are fits to the entire set of CSs for each cell, not the average points that are plotted. Error bars are one *SD*. Synchrony defined using a 5 ms bin. **(C)** Distribution of correlation values for the relationship between synchrony and variance for spikelet-related and baseline periods. Circles indicate individual cell *r* values, horizontal lines show distribution means, and error bars indicate the *SD*.

coupling within the IO (Onizuka et al., 2013; Lefler et al., 2014).

Data were analyzed from three multielectrode experiments in which crus IIa CS activity was recorded. In two experiments ketamine/xylazine anesthesia was used ($n = 50$ PCs), and in the other urethane was used ($n = 23$ PCs). The spatial arrangements of the electrode arrays from two of these experiments are shown in **Figures 6A1,B1**. In all three experiments, injection of picrotoxin or gabazine into the IO increased CS synchrony (1 ms time bin) when measured across all PC pairs in the array (ketamine/xylazine: 70 and 40%; urethane: 88.6%). The average spikelet-related (T window) variance was calculated for the CS activity of each PC in control and after injection of a GABA-A antagonist, and then these variances were plotted against each other (**Figures 6A2,B2**). Across all three experiments, 68/73 cells showed an increase in variance. For the experiments in **Figures 6A2,B2**, the consistency of the effect is shown by almost all the data points being above the y = x line in the plots. The change in variance was significant in all three experiments (ketamine/xylazine, $p = 0.0002$, both experiments; urethane, $p = 2.7 \times 10^{-5}$, paired *t*-tests).

To test the relationship between spikelet-related variance and synchrony further, we calculated the percent change in both synchrony level and spikelet-related variance from the control to the drug condition for each PC. For all three experiments a significant correlation existed between the change in synchrony and the change in variance levels (ketamine/xylazine: $r = 0.48$ and 0.54, $p = 0.013$ and 0.02; urethane: $r = 0.70$, $p = 0.0003$). Scatterplots from two of the experiments are shown in **Figures 6A3,B3** to illustrate the relationship.

We next tested whether spikelet-related variance decreased when CS synchrony was reduced by injection of carbenoxolone, a gap junction blocker, into the IO in two experiments from a previous study (Blenkinsop and Lang, 2006). The recording arrays are shown in **Figures 7A1,B1**. Overall, the induced changes in synchrony and variance were highly correlated. In the first experiment the intra-IO injection produced a $-72.5 \pm 11.0\%$ change in synchrony, with all PCs showing a reduction ($n = 14$ PCs; $p = 6.4 \times 10^{-5}$, paired *t*-test). Correspondingly, variance was reduced from control levels in every PC ($-28.2 \pm 12.7\%$; $p = 1.5 \times 10^{-5}$, paired *t*-test; **Figure 7A2**, all circles below y = x line). However, a scatterplot of the percent changes in synchrony and variance showed only a relatively weak correlation that was not significant ($r = 0.37$, $p = 0.187$; **Figure 7A3**).

The weakness of the correlation may be attributable to the strong and consistent reduction in synchrony caused by carbenoxolone in the experiment shown in **Figure 7A**, leading to both a floor effect and a relatively narrow range of synchrony changes over which to evaluate variance levels. This possibility is supported by the results of the second experiment ($n = 23$ PCs), in which carbenoxolone produced a more variable effect on CS synchrony, as was often the case (Blenkinsop and Lang, 2006). In this experiment, carbenoxolone reduced synchrony in most PCs ($n = 18/23$ PCs; **Figure 7B1**, red circles), but the magnitude of the reduction ranged widely, from just a few percent to almost 80% (**Figure 7B3**, red circles). Moreover, a minority of PCs had somewhat higher synchrony levels in the carbenoxolone condition ($n = 5$; **Figures 7B1,B3**, black circles). Note that these latter PCs were clustered on the medial edge of the recording array and likely received input from a different region of

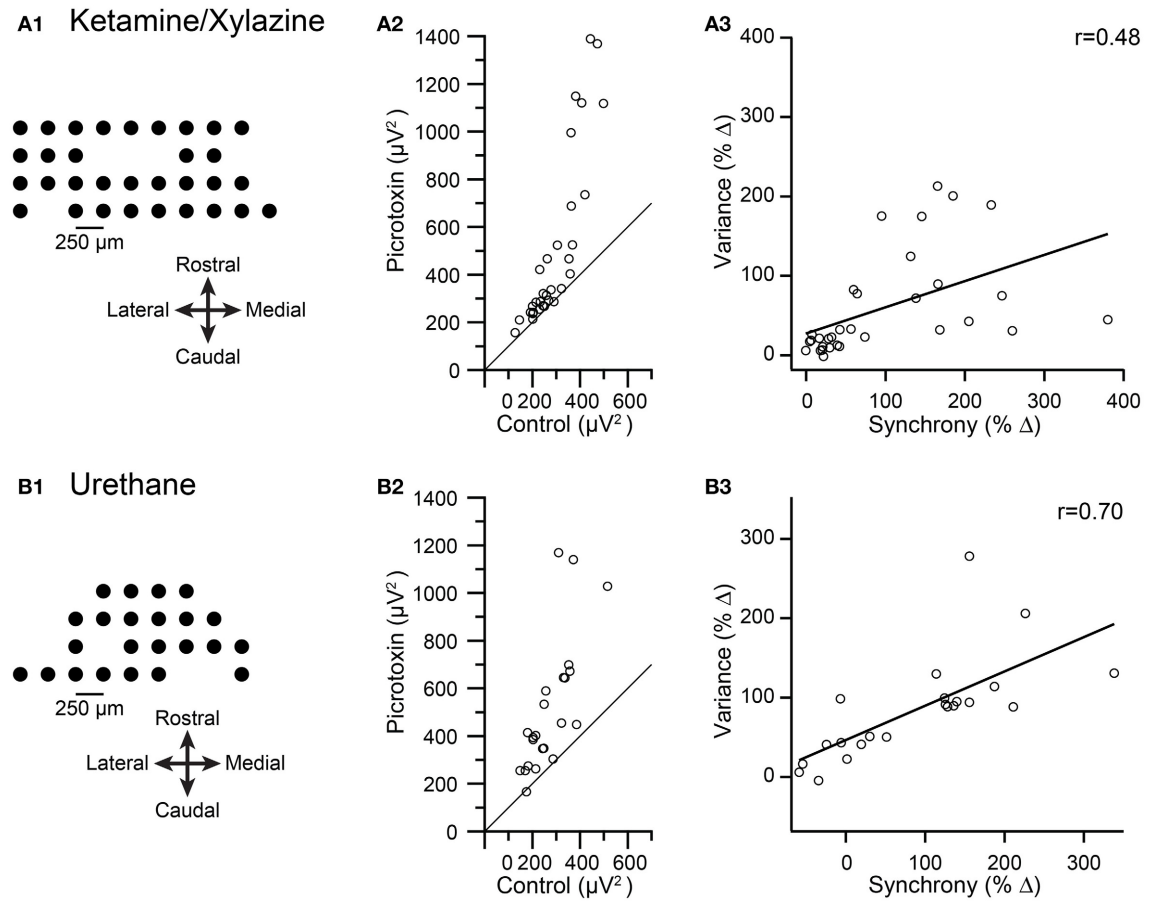

FIGURE 6 | Pharmacologically-induced increases in CS synchrony also increase spikelet-related variance. Results from recordings made under ketamine/xylazine **(A)** and urethane **(B)** are shown. **(A1,B1)** Schematics showing recording arrays. **(A2,B2)** Plot of average spikelet-related variance in control (x-axis) vs. following an injection of picrotoxin into the IO (y-axis). Each circle represents the data from one PC in the array. Diagonal line in each plot is the line y = x. **(A3,B3)** Plots of percent change in variance between control and picrotoxin conditions vs. the percent change in synchrony between these conditions for each PC. Regression lines are plotted and *r* values are indicated.

the IO than the remainder of the PCs, explaining the failure of the injection to reduce the synchrony level of their CS activity (Blenkinsop and Lang, 2006). Comparison of variance in the two conditions in the second experiment revealed that most PCs showing a reduction in synchrony also had a reduction in variance (**Figure 7B2**, red circles; note that most are below the y = x line), whereas all PCs showing an increase in synchrony also had an increase in variance (black circles). For the PCs that showed a reduction in synchrony, a modest but significant reduction in variance was found ($-10.48 \pm 34.1\%$; $p = 0.029$). However, in contrast to the first experiment, here the magnitude of the effect on variance varied widely, particularly when the PCs experiencing an increase in synchrony were included (**Figure 7B3**), and a strong correlation was found between the change in synchrony and variance in this case ($r = 0.76$; $p = 2.8 \times 10^{-5}$). Finally, when the PCs from both carbenoxolone experiments are combined, it can be seen that a clear correlation ($r = 0.80$; $p = 2.8 \times 10^{-9}$) between synchrony and variance is present for an extended range of synchrony changes (**Figure 7C**).

In sum, the results of the IO injection experiments show that manipulations that increase and decrease the electrical coupling of IO neurons lead to corresponding changes in spikelet-related variance.

MEASUREMENT OF FIELD EFFECTS DURING THE TIME OF THE SPIKELETS

Comparison of the baseline and T window variance correlations with synchrony suggests that the T window variance correlation is largely due to changes in the CS waveform, as opposed to field effects from synchronized activity of neighboring cells. However, the baseline measurements were made just before or after the time of the spikelets, whereas, ideally, one would want to measure the baseline during the spikelet period itself. This is not possible when the PC being recorded is firing; however, it is possible to measure the contribution of these fields selectively by identifying synchronous CS events among neighboring cells during which the PC itself is not spiking (either CSs or SSs).

We did this in two multielectrode experiments (one group from each experiment, $n = 9$ PCs/group) using urethane

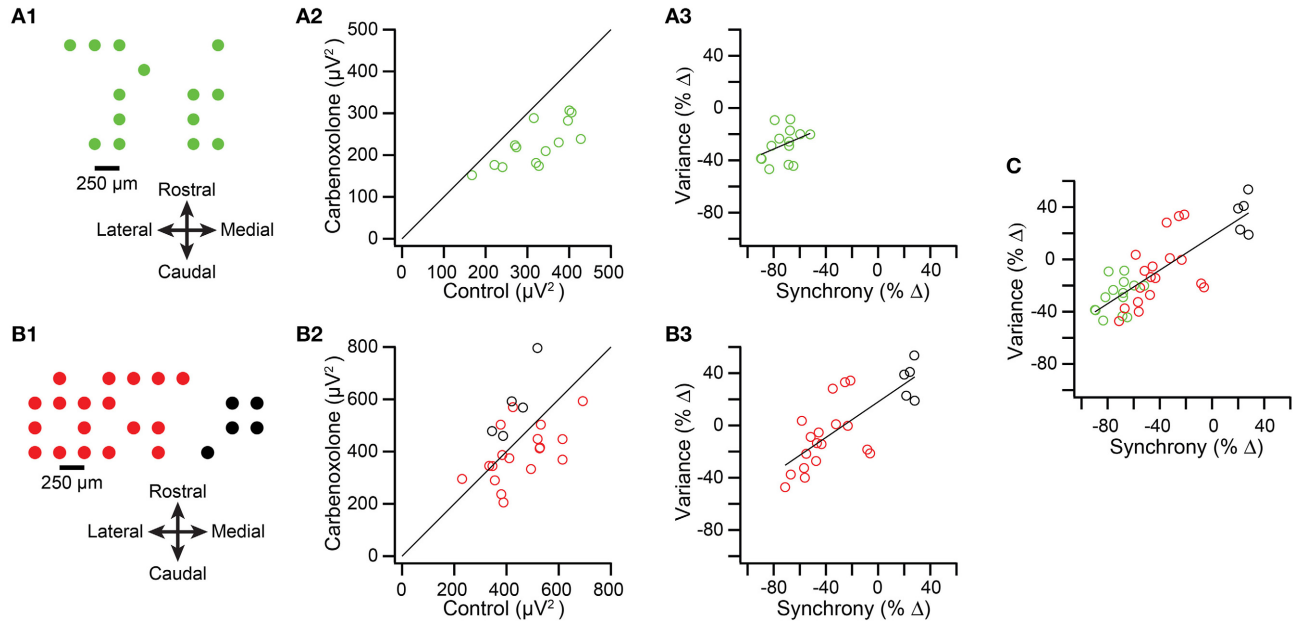

FIGURE 7 | Intra-IO injection of carbenoxolone reduces spikelet-related variance. (A1,B1) Schematics showing layout of multielectrode recording arrays from two experiments. In the second experiment **(B1)** the red circles represent PCs whose CSs became less synchronous after carbenoxolone and the black circles represent PCs whose CSs became more synchronous. **(A2,B2)** scatter plot of spikelet-related variance in control vs. carbenoxolone condition. **(A3,B3)** Scatter plot of percent change in synchrony vs. percent change in variance between control and carbenoxolone conditions. **(C)** Data from plots **(A3,B3)** combined.

anesthesia. As was described above, the CSs for each cell in the group were classified according to the synchrony level at the time of their occurrence (5-ms window). Then one focal PC (the one with the highest signal-to-noise ratio) was selected for analysis. Next, segments of this PC's recording corresponding to the times of the CSs (from 10 ms prior to 10 ms after the onset) in each of the other cells in the group were made. Thus, for each synchrony level, a set of traces of the focal PC's activity were obtained, all aligned on the CSs of the other PCs (time $t = 0$ ms in **Figure 8A**). One such set is shown in **Figure 8A1**. In most traces the selected PC had spike activity (**Figure 8A2**), as shown by the denseness of the spikes when the traces are overlapped. To exclude spike-related activity from the selected PC, all traces with simple spikes between $t = -5$ and 10 ms or CSs between $t = -10$ and 10 ms were removed (the differing times reflects an attempt to preserve as many traces as possible for analysis while also avoiding contamination of the 0–10 ms period with spike-related activity). The remaining traces were then analyzed for their variance between $t = 0$ and 10 ms (**Figure 8A3**). The spikelet-related variance was also measured for the focal PC using a T window in order to compare it with that from the field only traces.

In both experiments the correlation between CS synchrony and the actual spikelet-related variance was significant, and in the range reported for the other experiments (Experiment 1: $r = 0.11$, $n = 587$ CSs, $p = 0.007$; Experiment 2: $r = 0.19$, $n = 639$ CSs, $p = 1.7 \times 10^{-6}$). The correlation for the field-only traces was smaller in each case, and only significantly different from zero in one experiment (Experiment 1: $r = 0.017$, $n = 964$ traces, $p = 0.60$; Experiment 2: $r = 0.134$, $n = 809$ traces, $p = 0.00013$). Thus, the fields can sometimes contribute to the correlation observed, consistent with the earlier baseline results. To test whether the correlation due to the fields could fully explain the one observed for the spikelets, we performed a regression analysis and compared the slopes of the two lines (**Figures 8B–E**). In both experiments the slope of the spikelet-related regression line is significantly steeper than that of the field-only regression line. This difference is most easily observed when the vertical displacement of the two lines is eliminated at their starts (**Figures 8C,E**), which shows that the spikelet-related lines were 10–11 and 3 times steeper than their field-related counterparts for the two experiments. Thus, only about 10 and 33%, respectively, of the effect of synchrony on the variance signal was explained by the contribution from the fields in these experiments.

The above results indicate that spikelet-related variance increases with synchrony. The potential causes underlying this relationship may relate to modulation of basic spikelet parameters. Thus, we now describe results related to how changes in these parameters affect spikelet-related variance.

SPIKELET-RELATED VARIANCE IS CORRELATED WITH THE NUMBER OF SPIKELETS IN SPONTANEOUS CSs

To investigate how spikelet-related variance is influenced by spikelet number, we used a single electrode approach to make recordings of CS activity with high signal-to-noise ratios ($n = 28$ PCs total; 10 animals; crus IIa, $n = 26$; vermis lobule VIII, $n = 2$). These recordings were made at or near the level of the PC soma, as determined by the presence of simple spike activity and the predominantly positive polarity of the SSs and the initial spike

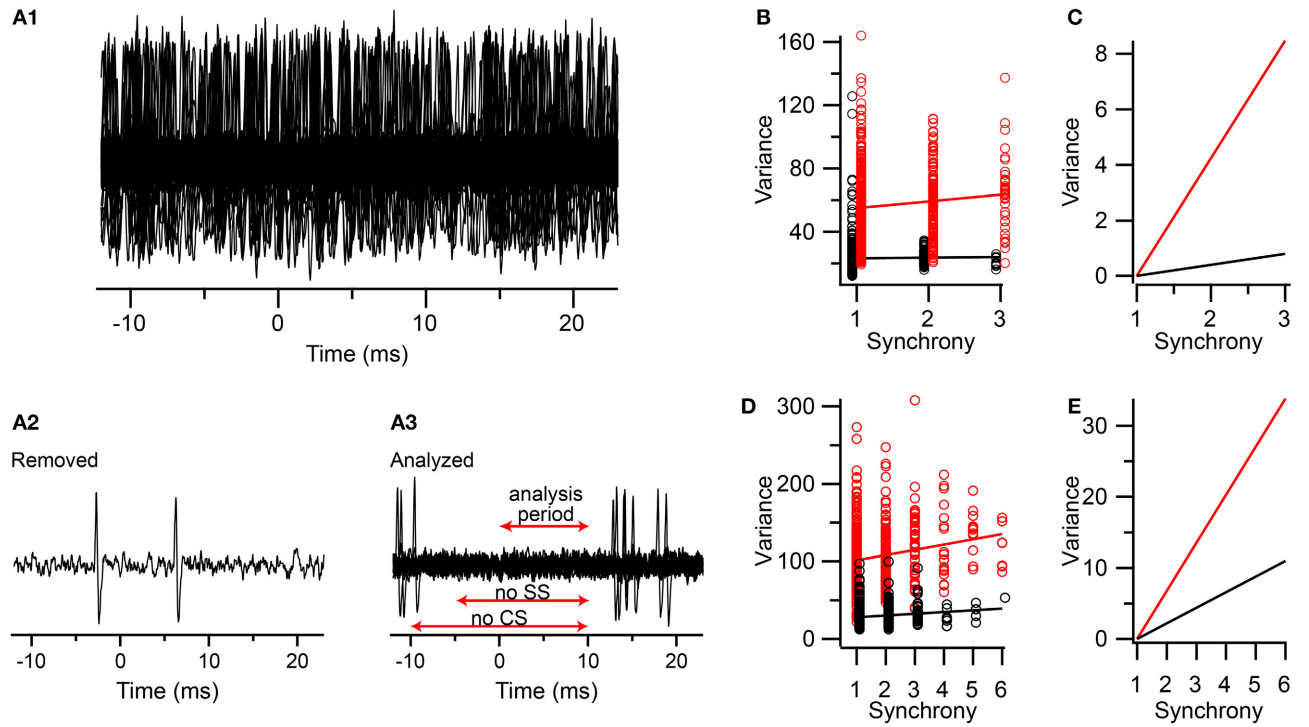

FIGURE 8 | Comparison of contributions of spikelets and fields from neighboring neurons to the correlation of synchrony and spikelet-related variance. (A1) Segments of an extracellular recording from a PC all aligned to the times of the CSs in other PCs in a group of PCs whose CSs are synchronized. **(A2)** Example of one trace that was removed from set shown in **(A1)** because of simple spikes being present just before and during the analysis period **(A3)** The set of traces selected from those in **(A1)** in which no CSs or simple spikes were present during the time windows indicated (SS = simple spikes). **(B)** Plot of variance vs. CS synchrony among PCs in the group. Variance measurements during the 0–10 ms period in the traces with no spikes indicated by black circles. T window variance for the CSs for the PC whose traces were analyzed for fields indicated by red circles. **(C)** Replotting of regression lines shown in **(B)** after vertically aligning their left-most points. **(D,E)** Same as **(B,C)** respectively, but for a second experiment. Data markers in **(B,D)** are slightly offset along the x-axis for clarity.

of the CSs (**Figure 9A**). The high signal-to-noise ratio allowed semi-automated counting of spikelets with only minor manual corrections (see Methods).

For each PC, spikelet-related variance, σ_T^2, was measured using a fixed time window, the T window. For 93% of the PCs, a significant correlation was found between the variance and spikelet count ($r = 0.42 \pm 0.15$; $p < 0.05$, $n = 26/28$; **Figure 9B**, uncorrected). A scatterplot was then constructed from the data of each PC, and a least squares regression line was fit to the data (**Figure 9C**). We tested for evidence of non-linearity by using the residuals to compare the pure error to the error due to the lack of fit of the linear model (Brook and Arnold, 1985; Zar, 1999). For 24 PCs having a significant correlation (two of the 26 such PCs were not analyzed because their spikelet number only varied between two values), no evidence for a non-linear dependency of variance on spikelet number was found in most cases (MSS_{LOF}/MSS_{PE}; $p > 0.05$, $n = 19/24$). The non-linear plots ($n = 5/24$; $p < 0.05$) were examined visually, and the deviation from linearity appeared to be due to a plateauing of the variance curve with increasing spikelet number.

CHANGES IN SPIKELET SHAPE WITH NUMBER OF SPIKELETS IN A CS

The linearity of the relationship found for most PCs between spikelet number and σ_T^2 suggests that shape of the individual spikelets (at least as measured by variance) doesn't generally co-vary with the number of spikelets. In contrast, the plateauing relationship observed in the remaining PCs suggests that in a minority of cases, spikelet size tends to vary inversely with number. That is, when more spikelets are present, their average size is smaller, resulting in progressively smaller increases in σ_T^2 with each additional spikelet.

To investigate this issue further, we assessed the dependence of spikelet shape on the number of spikelets in a CS by measuring variance using a variable time window whose duration was matched to that of the individual CS, the S window (**Figure 1A**). In contrast to σ_T^2, which is explicitly a function of both the shape and number of the spikelets, S window variance, σ_S^2, essentially depends on just the shape of the spikelets, because spikelets are present throughout the S window (i.e., the variance of the S window is approximately the average variance of the individual spikelets, and thus is independent of the number of spikelets). For the S window, the correlation of variance with spikelet number was positive in a few cases ($n = 4$, $r > 0$ and $p < 0.05$), but for the large majority of PCs, it was either not statistically different from zero ($n = 13$, $p > 0.05$) or negative ($n = 11$, $r < 0$ and $p < 0.05$) (**Figures 9D,E**). The median correlation coefficient was -0.35 for the 15 cells with significant correlation between the σ_S^2 and the spikelet number, and 0.03 for the 13 cells without

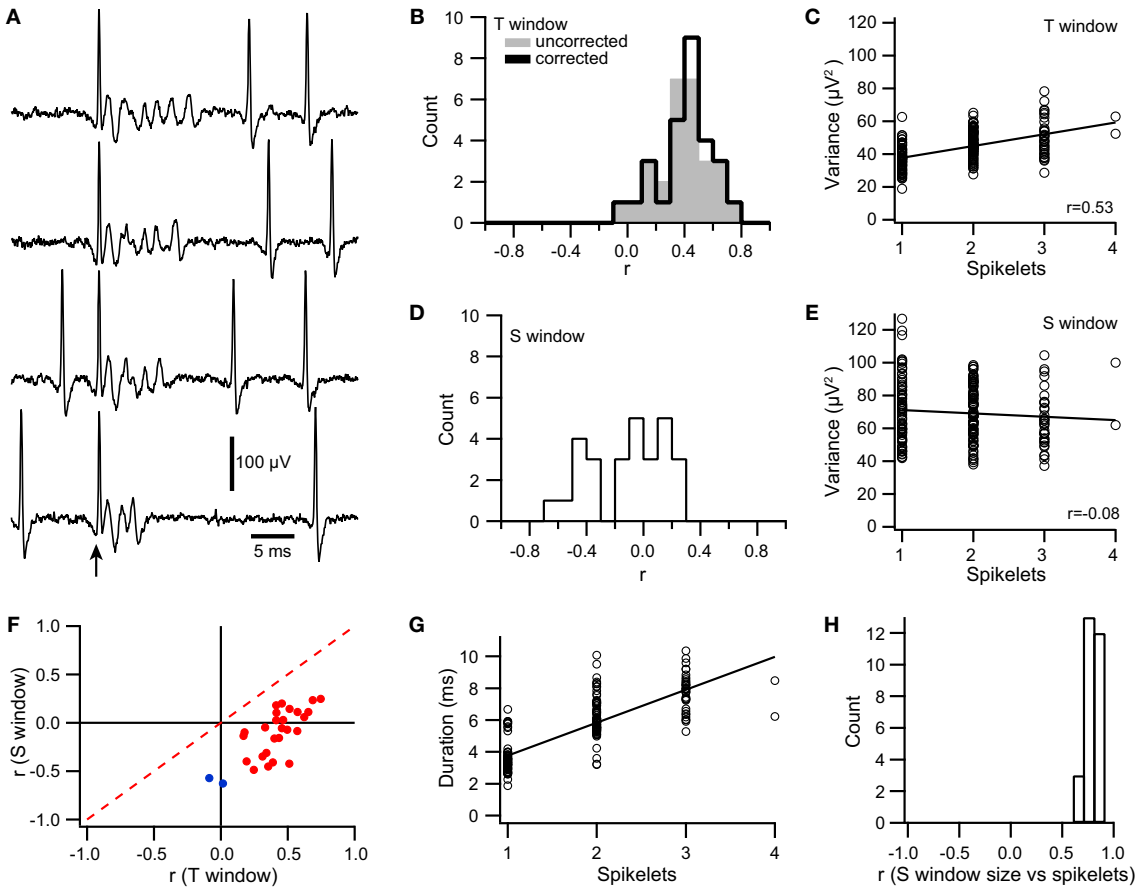

FIGURE 9 | Signal variance is correlated with the number of spikelets in a CS. (A) Extracellular traces of a PC recorded near its soma. Traces are aligned to the onset of the CS (arrow). The number of spikelets varies between CSs. Simple spikes are also present before and after the CS depending on the trace. **(B)** Histograms showing distribution of correlation coefficient values (*r*) between the number of spikelets and spikelet-related variance (T window) using σ_T^2 (gray fill) and σ_{T*}^2 (black line). **(C)** Scatterplot of signal variance during the T window vs. spikelet count for a PC. Each circle represents the values for one CS. **(D,E)** Same as **(B,C)**, respectively except that the S window was used to measure variance. **(F)** Scatter plot of *r* values obtained by correlating spikelet number with variance for the S window and the T window. Significant *r* values for the T window are in red, those that are not are shown in blue. **(G)** Scatter plot of CS duration vs. number of spikelets for a typical cell, which generated CSs containing between 1 and 4 spikelets. **(H)** Histogram of *r* value between CS duration and number of spikelets for the somatically-recorded PC population.

significant correlation, whereas the overall median correlation coefficient was −0.09 ($n = 28$).

We then compared the correlation of spikelet number with σ_T^2 and σ_S^2. In all cases σ_T^2 showed a more positive (in one case less negative) correlation with spikelet number than did σ_S^2 (**Figure 9F**, all points are right of the dashed red y = x line). Furthermore, when r for σ_T^2 was large, r for σ_S^2 was close to zero, whereas as r for σ_T^2 moved toward zero, r for σ_S^2 became negative. Indeed, the two cells for which r for σ_T^2 was not significant had the two most negative *r* values for σ_S^2 (**Figure 9F**, blue points).

For cells showing a linear relationship between σ_T^2 and spikelet count, the correlation of σ_S^2 with spikelet count was close to zero (-0.03 ± 0.23; median = 0.03; $n = 19$). In contrast, for the cells having a plateau type curve with σ_T^2, the correlation with σ_S^2 tended to be negative (-0.22 ± 0.17; median = −0.11; $n = 5$). Although the correspondence is not absolute, it is consistent with the plateauing relationship between σ_T^2 and spikelet count observed for some PCs being due to a decrease in average spikelet amplitude as the number of spikelets increases.

The duration of the S window was then compared to the number of spikelets in order to assess whether spikelet duration varied with the number of spikelets. A strong linear relationship was found in all cases ($r = 0.795 \pm 0.065$, $n = 28$, **Figures 9G,H**), indicating that average individual spikelet duration does not co-vary with spikelet number.

In sum, these results indicate that there is no consistent trend in average spikelet width and amplitude correlated with the number of spikelets for most PCs, but that for a significant minority of PCs, a tendency for spikelet amplitude to decrease with increasing spikelet numbers exists.

SPIKELET PERIOD HAS A DISTINCT BASELINE VARIANCE

To test whether baseline variance is altered during the CS, we used the regression lines fit to the somatic recording data (**Figure 9C**).

These regression lines describe spikelet-related variance, σ_T^2, as a function of spikelet number, and so extrapolating to zero spikelets gives a prediction of the baseline variance. We compared this predicted value with that measured directly from times just after the end of the T window in a subset of 15 PCs with a linear relationship between spikelet number and σ_T^2 (MSS_{LOF}/MSS_{PE} ratio, $p > 0.05$) and the highest correlation coefficient values in the dataset (all $r > 0.35$). In all cases the predicted value was higher than the measured baseline ($p < 0.001$, paired t-test). This is shown in **Figure 10A**, where the predicted values (blue circles) all fall above the corresponding measured baseline values.

To understand the cause of this discrepancy, we first considered the possibility that the mean signal during the period when spikelets actually occurred (S window) was different from the mean for the later part of the T window, the N window, within which the spikelets were absent, as such a difference would increase the overall spikelet-related variance, σ_T^2, and thereby over-predict the baseline variance (see Equation 2). To test this possibility, we computed a corrected variance, σ_{T*}^2, for each CS using Equation (3), and carried out the above analyses with this new value. Correlation of σ_{T*}^2 with spikelet number produced similar, though slightly higher, r values (0.44 ± 0.15; **Figure 9B**, compare corrected and uncorrected histograms). Extrapolation of regression lines based on the relationship of σ_{T*}^2 to spikelet number to zero spikelets gave lower estimates of baseline variance (**Figure 10A**, red circles; $p < 0.001$, paired Wilcoxon signed rank test), but ones that were still well above the measured values from the surrounding times.

These results suggest that the baseline variance (estimated via extrapolation) is, indeed, different during the CS than at times when there is no CS activity. Thus, we next assessed whether this change occurs throughout the T window or whether it is limited to the S window. During the S window both baseline and spikelet signals are present, making it impossible to measure the baseline signal. Instead, we measured the variance for the N window, σ_N^2, to test whether it was different from the general baseline. For this analysis it was critical not to have any spikelet-related activity in the N window, so here the N window was defined as starting one interspikelet interval after the peak of the last counted spikelet (rather than half of an interspikelet interval). This delay prevented contamination from the trough of the last spikelet and its recovery. σ_N^2 was found to be statistically the same as the general baseline for almost all cells (14/15, $p > 0.05$; Wilcoxon rank sum tests). However, even though σ_N^2 was not statistically significant for individual cells, viewing the population data (**Figure 10B**) suggests that σ_N^2 has a slight tendency to fall below the baseline variance line, and indeed on a population level, this difference was significant ($p = 0.0074$, $n = 15$; paired t-test), indicating a small depression of variance immediately following each CS. Nevertheless, the match of σ_N^2 and the general baseline variances suggests that the change in the baseline variance during the T window occurs during the S window, that is, during the time when spikelets are actually occurring.

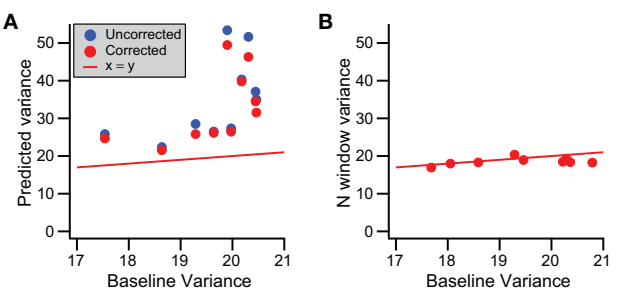

FIGURE 10 | Prediction of baseline variance during CS. (A) Scatter plot of predicted baseline variance, obtained by extrapolating the regression line between number of spikelets and the spikelet-related variance to zero spikelet, vs. baseline variance measured from times surrounding the CS (outside the T window). The predictions were made from regression lines with either σ_T^2 (uncorrected, blue) or σ_{T*}^2 (corrected, red circles) vs. spikelet number. **(B)** Scatter plot of σ_N^2 vs. measured baseline variance. Red line indicates y = x in both **(A,B)**.

SPIKELET COUNT CORRELATES WITH CS SYNCHRONY

The above results provide evidence that CS waveform varies with CS synchrony, and are consistent with the change in waveform being due to changes in spikelet number with synchrony. However, they do not rule out the possibility that changes in spikelet size are responsible. Thus, to provide direct evidence for spikelet number varying with synchrony, we have examined both CF reflex evoked and spontaneous CSs in a few PCs recorded with a multielectrode array and where the spikelets were relatively large, making direct counting of spikelets possible.

Spikelets were counted for the climbing fiber reflex responses of 9 PCs. These were the same PCs as described in **Figure 4**, so that the correlation of both measures of the CS waveform (variance and spikelet count) to the size of the reflex response could be directly compared. Correlation of spikelet count with the number of PCs responding yielded significant correlations in all cases ($p < 0.05$). The correlation values obtained using spikelet counts ($r = 0.33 \pm 0.17$) were not statistically different from those obtained with variance measurements ($p = 0.25$, paired t-test; **Figure 11A**), and were well matched to each other across the population (**Figure 11B**).

The spikelets of spontaneous CSs were counted for three cells from two multielectrode experiments (**Figure 12**, each row shows the data from one cell). For each cell, the level of synchrony, C(0), was calculated for all cell pairs it formed with other PCs in the recording array, and the distribution of synchrony for each cell was examined. The three PCs were chosen because they showed synchronous activity with a defined group of neighboring PCs and had relatively large spikelets. The recording arrays and the cell groups are shown in **Figure 12A**. The spikelet counts were done blindly with respect to knowledge of the synchronization of the individual CSs. Once the counts were completed, the CSs were sorted according to their level of synchronization with CSs from other PCs in the group. For each cell the correlation between synchrony level among group members and spikelet number was determined, and a regression line was fit to the data ($n = 1135$, 1014, and 680 CSs). The correlation of the spikelet counts to the synchrony level was significant in each case ($r = 0.23$, 0.36, and 0.25; $p < 1 \times 10^{-10}$). Moreover, plots of the average spikelet number at each level of synchrony (number of other

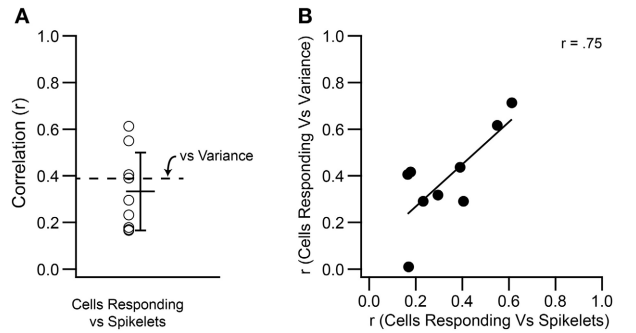

FIGURE 11 | Variance and spikelet number are correlated to the number of PCs showing climbing fiber reflex evoked CSs. (A) Each circle shows, for a PC, the *r* value for the correlation between number of spikelets in an evoked CS and number of cells showing a reflex response to the same stimulus. Mean and *SD* are shown. The mean *r* value for the correlation between T window variance and number of responding cells is replotted from **Figure 4** for comparison (dashed line). **(B)** Scatter plot showing the correspondence between the *r* values for correlation of variance and spikelets with the number of PCs responding to a stimulus.

PCs firing synchronously with the reference cell) show a nearly perfect correlation ($r = 0.97$, 0.99, and 0.998), and the regression lines (fit to the entire dataset from each PC) show no systematic deviation from the averages. This suggests a linear relationship between synchrony and spikelet number (**Figure 12B**), which was confirmed statistically (MSS_{LOF}/MSS_{PE} ratio, $p > 0.05$). In sum, these results directly demonstrate that spikelet number increases with synchrony, albeit for a limited sample of PCs.

For comparison, the correlation between the spikelet-related (T-window) variance and the synchrony for these PCs was tested, and were consistent with the results of using spikelet number ($r = 0.44$, 0.45, and 0.32; **Figure 12C**), although, interestingly, the *r* values were somewhat higher than those for direct spikelet counts. Correlation of average variance with synchrony produced near perfect correlations (0.97, 0.995, and 0.97), and tests for goodness of fit indicated a linear relationship (MSS_{LOF}/MSS_{PE} ratio, $p > 0.05$) for two of three PCs. Lastly, we compared spikelet number and variance to each other directly. Once again, significant correlations were found (**Figure 12D**; all data: $r = 0.46$, 0.58, 0.56; averages: $r = 0.97$, 0.996, 0.998).

DISCUSSION

The major findings of this paper indicate that a causal relationship exists between CS synchrony and the variance of the recording signal during the spikelet portion of the CS. This variance was shown to reflect the shape and number of spikelets comprising the CS, suggesting that CS synchrony may be a parameter related to the characteristics of the spikelets themselves. Spikelet size and number have been linked to the axonal output of the PC (Ito and Simpson, 1971; Khaliq and Raman, 2005; Monsivais et al., 2005), and to the degree and type of plasticity induced by CS activity (Mathy et al., 2009). Thus, the results raise the possibility that synchrony is an important control parameter for both the motor coordination and motor learning functions that have been proposed for the olivocerebellar system.

The validity of these conclusions, however, rests, in the first place, upon whether the changes in the measured variance with synchrony actually reflect changes in the CS waveform of a PC, as opposed to changes in the electric fields generated by synchronized activity among cells that surround the PC. Thus, we first discuss whether such field effects can fully explain the observed correlation or whether changes in the variance can, at least partly, be ascribed to changes in the CS waveform.

IS THE CORRELATION OF SPIKELET-RELATED VARIANCE AND CS SYNCHRONY DUE TO FIELDS FROM SURROUNDING CELLS?

The CS recordings were made with extracellular microelectrodes. Local field potentials, due to the summed activity of simultaneously active nearby cells, may also be recorded along with the single unit activity by such electrodes. However, the contribution of such fields was minimized by using high pass filters with cutoff frequencies in the 300–400 Hz range. Such filtering, in particular, should strongly attenuate fields associated with relatively long lasting events, such as synaptic potentials, which are usually the major sources of fields.

Nevertheless, the geometrical arrangement of the PCs, and the ability of the olivocerebellar system to activate PCs synchronously, provide the potential substrate for substantial fields to be generated by faster events, namely CSs. Indeed, a significant field is produced in the molecular layer following electrical stimulation of the IO, and likely reflects both synaptic and spike activity (Eccles et al., 1966a). While electrical stimuli evoke precisely synchronized CSs in greater numbers of PCs than would normally occur with spontaneous activity, the fields associated with spontaneous CS activity, although smaller in absolute size, should still correlate with the level of synchrony, and thus might lead to a correlation between the variance we measured during the T window and synchrony.

A number of the results (i.e., the baseline and N window variance measurements) address this issue. Overall, they indicate that, although fields were detected by our electrodes along with the single unit activity, and sometimes contributed significantly to the increase in variance measured during the spikelet period, their contribution generally only accounted for at most a small fraction of the observed change in spikelet-related variance (T window) with synchrony level.

The precision of CS synchrony is important for drawing conclusions from these measurements. Specifically, the central peak in cross-correlograms of CS activity between two PCs often has a width of 5–20 ms (Bell and Kawasaki, 1972; Sasaki et al., 1989). Moreover, the CS itself lasts on the order of 10 ms. Thus, if fields from the CS activity of surrounding cells were to have a significant effect on the signal being recorded by a particular electrode, such an effect should be present for a significant time period surrounding the CSs recorded by the electrode. Such an effect was searched for using the N window, but the variance during this window was essentially identical to the general baseline, from which we conclude that fields from the spontaneous CS activity of surrounding PCs do not generally make significant contributions to the variance of the CS signal.

However, it is still possible that during highly synchronous events, detectable effects of the fields on the variance might occur,

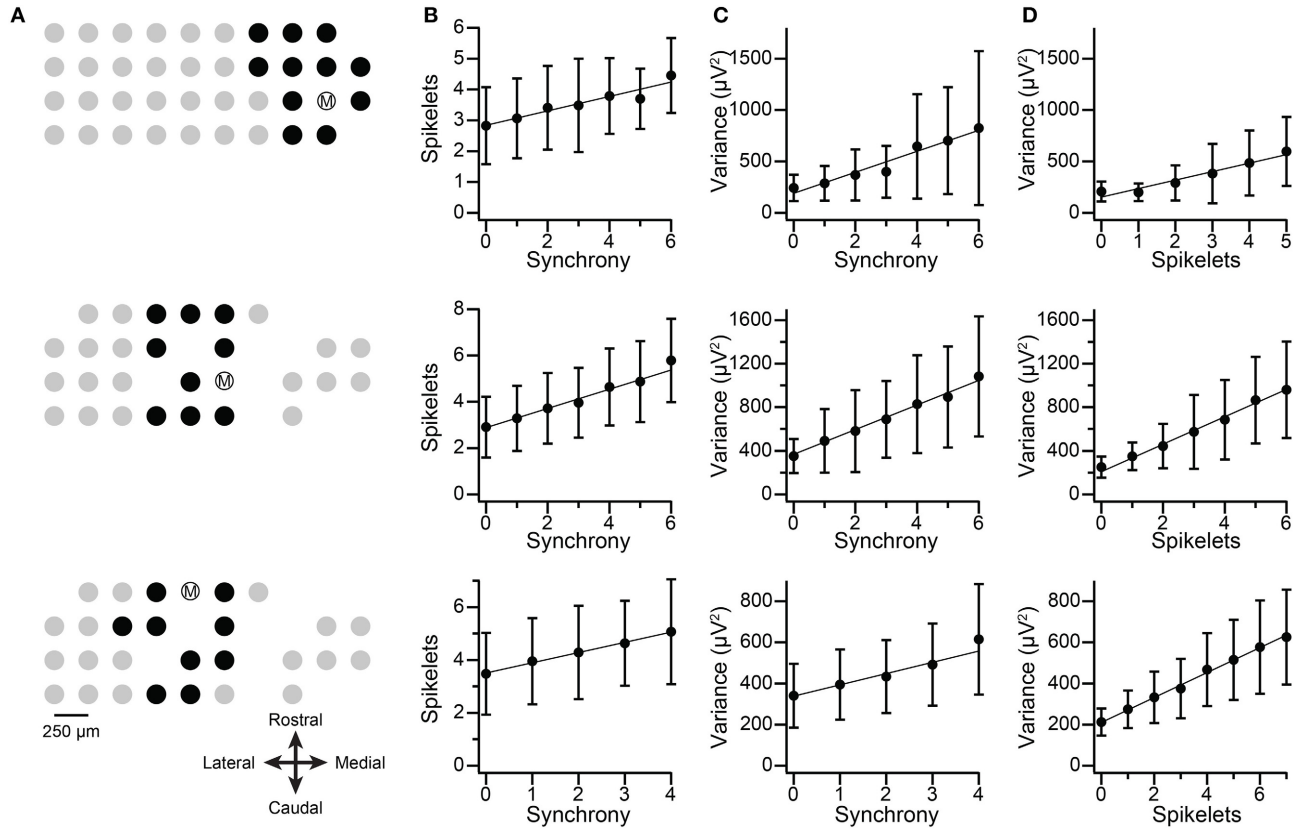

FIGURE 12 | Synchronous CSs show increased number of spikelets and spikelet-related variance. Each row in figure shows data from one PC. (A) Recording electrode arrays on crus IIa. Dots show relative positions of electrodes. Encircled M indicates the PC being analyzed. Black dots indicate PCs chosen to be part of the group with cell M for the purpose of the synchrony analysis. **(B)** Plots of the average number of spikelets as a function of synchrony. Synchrony values are the number of PCs in the group that fired synchronously with cell M. **(C)** Plots of the average spikelet-related (T–window) variance as a function of synchrony. **(D)** Plots of spikelet-related variance as a function of spikelet number. In **(B–D)** the data points shown are the mean $\pm SD$ at each *x*-value. The regression lines are fits to the entire data set for each cell (top, middle, bottom row: $n = 1135$, 1014, and 680 CSs). Middle and bottom row PCs are from the same experiment and had largely overlapping groups.

leading to a correlation. Measurements of the baseline just preceding the CS indicates that this does not usually happen, as a significant correlation between synchrony and the baseline variance was not found in the majority of cells. Even for the remaining PCs, where evidence for a significant effect was detected, comparison of the slope of the regression lines indicated that the increase in variance due to the fields accounted for a relatively small fraction (20–25%) of the total increase that was observed, in most cases. One caveat should be noted. Even when the baseline variance was measured from the 1-ms period just before the CS onset, the level of synchronization might be less, and thus the fields smaller, at that point relative to during the CS itself. However, given the typical width (5–20 ms) of the central peak in the CS cross-correlograms it seems unlikely that the fields would be diminished so significantly in such a short interval. Moreover, the analysis of the fields-only traces also showed a similarly weak correlation with shallow regression line slopes, and in this case the variance was measured during what should be the time when the T window variance is measured when a CS is present.

In sum, these results indicate that although fields from surrounding cells may contribute to the measured signal variance during the spikelet portion of the CS, this contribution cannot fully explain the relationship of the variance with synchrony levels. Thus, we conclude that much of the correlation between the T window variance and synchrony is due to changes in the waveform of the CS itself.

IS THE CORRELATION BETWEEN SPIKELET-RELATED VARIANCE AND CS SYNCHRONY DUE TO INCREASED SPIKELET NUMBER OR CHANGES IN THEIR SHAPE?

The increase in T window variance of synchronous CSs could indicate greater numbers of spikelets and/or a change in the shape of individual spikelets, such as increased amplitude or width (duration); however, actual counts of spikelets in several PCs provide direct evidence that synchronous CSs tend to have larger numbers of CSs. Whether they also show increased amplitudes or duration needs to be determined; however, the variance data can address the question of whether both factors co-vary with synchrony. For the majority of PCs, a linear relationship existed between synchrony and variance, which strongly suggests that spikelet number and shape do not simultaneously co-vary with the synchrony level, because a non-linear

relationship would likely result if they did. This is consistent with the linear relationship of T window variance and spikelet number shown by the majority of PCs. For PCs with non-linear relationships between synchrony and variance, no consistent pattern was found, with some curves showing a plateau and others showing a supralinear trend (data not shown). The plateau relationship is consistent with the negative correlation of the S window variance with spikelet number shown by a minority of PCs. The supralinear curves do not correspond to either of the patterns observed when looking at the general relationship between spikelets and variance levels, which suggests that certain types of changes in the spikelet character driven by synchrony may not follow the standard relationships between spikelet number and shape.

FUNCTIONAL CONSEQUENCES OF MODULATING CS WAVEFORM

The olivocerebellar system has been proposed to have roles in both motor coordination (Llinás, 1991) and motor learning (Ito, 2001). For its motor coordination role, the focus is on how the CS activity can alter the axonal output of the PC and how that influences cerebellar nuclear activity. In contrast, for motor learning, the focus is not on the CS's contribution to PC output, but rather on how the CS gates changes in the strength of the parallel fiber-PC synapse. In both cases, the number of spikelets is a potential way for allowing the CS to make a contribution that is distinguishable from that from simple spikes. Indeed, the type of plasticity induced, LTP or LTD, by a CS has been related to its number of spikelets (Mathy et al., 2009). In contrast, for affecting nuclear cell activity, the direct effect of synchronous activity among PCs that converge on the same cell is the usual mechanism thought to be involved, and a number of results are consistent with this interpretation (Llinás and Mühlethaler, 1988; Bengtsson et al., 2011; Blenkinsop and Lang, 2011; Lang and Blenkinsop, 2011). An increase of spikelets with synchrony (as the present suggest should happen) would amplify the effect of convergence, and further help distinguish CS signals from the tonic simple spike activity, because at least some spikelets are transmitted down the PC axon at short intervals (Ito and Simpson, 1971; Khaliq and Raman, 2005; Monsivais et al., 2005).

Finally, we recently proposed that the olivocerebellar system may participate in both motor control and motor learning processes (Schweighofer et al., 2013). Having a dual function raises the issue of whether and how the olivocerebellar system can selectively act in one capacity, as it would seem problematic to initiate significant changes in connectivity with every motor command and vice versa. Thus, it was further proposed that synchrony level could act as a switching mechanism, such that at lower synchrony levels CSs would gate plasticity but would not cause significant changes in ongoing cerebellar output, and that highly synchronized activity would affect ongoing cerebellar output directly (Schweighofer et al., 2013). The increase in spikelets with high synchrony described here could be a mechanism to further enhance the difference between high and low levels of synchronous CS activity, and thereby help limit motor commands to the high synchrony realm.

ACKNOWLEDGMENTS

This work was supported by grants to Eric J. Lang from the NSF (IOS-1051858) and NIH (NS-37028) and to Izumi Sugihara from the Japan Society for the Promotion of Science (JSPS) (Grants-in-Aid for Scientific Research-KAKENHI, 25430032).

REFERENCES

Armstrong, D. M., and Harvey, R. J. (1966). Responses in the inferior olive to stimulation of the cerebellar and cerebral cortices in the cat. *J. Physiol.* 187, 553–574.

Armstrong, D. M., and Harvey, R. J. (1968). Responses to a spino-olivo-cerebellar pathway in the cat. *J. Physiol.* 194, 147–168.

Bazzigaluppi, P., De Gruijl, J. R., Van Der Giessen, R. S., Khosrovani, S., De Zeeuw, C. I., and De Jeu, M. T. (2012). Olivary subthreshold oscillations and burst activity revisited. *Front. Neural Circuits* 6:91. doi: 10.3389/fncir.2012.00091

Bell, C. C., and Kawasaki, T. (1972). Relations among climbing fiber responses of nearby Purkinje cells. *J. Neurophysiol.* 35, 155–169.

Bengtsson, F., Ekerot, C. F., and Jorntell, H. (2011). *In vivo* analysis of inhibitory synaptic inputs and rebounds in deep cerebellar nuclear neurons. *PLoS ONE* 6:e18822. doi: 10.1371/journal.pone.0018822

Blenkinsop, T. A., and Lang, E. J. (2006). Block of inferior olive gap junctional coupling decreases Purkinje cell complex spike synchrony and rhythmicity. *J. Neurosci.* 26, 1739–1748. doi: 10.1523/JNEUROSCI.3677-05.2006

Blenkinsop, T. A., and Lang, E. J. (2011). Synaptic action of the olivocerebellar system on cerebellar nuclear spike activity. *J. Neurosci.* 31, 14708–14720. doi: 10.1523/JNEUROSCI.3323-11.2011

Brook, R. J., and Arnold, G. C. (1985). *Applied Regression Analysis and Experimental Design.* New York, NY: Marcel Dekker, Inc.

Cerminara, N. L., and Rawson, J. A. (2004). Evidence that climbing fibers control an intrinsic spike generator in cerebellar Purkinje cells. *J. Neurosci.* 24, 4510–4517. doi: 10.1523/JNEUROSCI.4530-03.2004

Chaumont, J., Guyon, N., Valera, A. M., Dugue, G. P., Popa, D., Marcaggi, P., et al. (2013). Clusters of cerebellar Purkinje cells control their afferent climbing fiber discharge. *Proc. Natl. Acad. Sci. U.S.A.* 110, 16223–16228. doi: 10.1073/pnas.1302310110

Chung, S. H., Marzban, H., and Hawkes, R. (2009). Compartmentation of the cerebellar nuclei of the mouse. *Neuroscience* 161, 123–138. doi: 10.1016/j.neuroscience.2009.03.037

Crill, W. E. (1970). Unitary multiple-spiked responses in cat inferior olive nucleus. *J. Neurophysiol.* 33, 199–209.

De Gruijl, J. R., Bazzigaluppi, P., De Jeu, M. T., and De Zeeuw, C. I. (2012). Climbing fiber burst size and olivary sub-threshold oscillations in a network setting. *PLoS Comput. Biol.* 8:e1002814. doi: 10.1371/journal.pcbi.1002814

Eccles, J. C., Ito, M., and Szentágothai, J. (1967). *The Cerebellum as a Neuronal Machine*. Berlin: Springer-Verlag. doi: 10.1007/978-3-662-13147-3

Eccles, J. C., Llinas, R., and Sasaki, K. (1966a). The excitatory synaptic action of climbing fibres on the Purkinje cells of the cerebellum. *J. Physiol.* 182, 268–296.

Eccles, J. C., Llinás, R., Sasaki, K., and Voorhoeve, P. E. (1966b). Interaction experiments on the responses evoked in Purkinje cells by climbing fibres. *J. Physiol.* 182, 297–315.

Frühwirth-Schnatter, S. (2006). *Finite Mixture and Markov Switching Models*. New York, NY: Springer.

Gerstein, G. L., and Kiang, W. Y. (1960). An approach to the quantitative analysis of equations of electrophysiological data from single neurons. *Biophys. J.* 1, 15–28. doi: 10.1016/S0006-3495(60)86872-5

Häusser, M., and Clark, B. A. (1997). Tonic synaptic inhibition modulates neuronal output pattern and spatiotemporal synaptic integration. *Neuron* 19, 665–678. doi: 10.1016/S0896-6273(00)80379-7

Ito, M. (2001). Cerebellar long-term depression: characterization, signal transduction, and functional roles. *Physiol. Rev.* 81, 1143–1195. Available online at: http://physrev.physiology.org/content/81/3/1143

Ito, M., and Simpson, J. I. (1971). Discharges in Purkinje cell axons during climbing fiber activation. *Brain Res.* 31, 215–219. doi: 10.1016/0006-8993(71)90648-2

Khaliq, Z. M., and Raman, I. M. (2005). Axonal propagation of simple and complex spikes in cerebellar Purkinje neurons. *J. Neurosci.* 25, 454–463. doi: 10.1523/JNEUROSCI.3045-04.2005

Lang, E. J. (2001). Organization of olivocerebellar activity in the absence of excitatory glutamatergic input. *J. Neurosci.* 21, 1663–1675. Available online at: http://www.jneurosci.org/content/21/5/1663.long

Lang, E. J. (2002). GABAergic and glutamatergic modulation of spontaneous and motor-cortex-evoked complex spike activity. *J. Neurophysiol.* 87, 1993–2008. Available online at: http://jn.physiology.org/content/87/4/1993.long

Lang, E. J., and Blenkinsop, T. A. (2011). Control of cerebellar nuclear cells: a direct role for complex spikes? *Cerebellum* 10, 694–701. doi: 10.1007/s12311-011-0261-6

Lang, E. J., Sugihara, I., and Llinás, R. (1996). GABAergic modulation of complex spike activity by the cerebellar nucleoolivary pathway in rat. *J. Neurophysiol.* 76, 255–275.

Lefler, Y., Yarom, Y., and Uusisaari, M. Y. (2014). Cerebellar inhibitory input to the inferior olive decreases electrical coupling and blocks subthreshold oscillations. *Neuron* 81, 1389–1400. doi: 10.1016/j.neuron.2014.02.032

Leznik, E., Makarenko, V., and Llinas, R. (2002). Electrotonically mediated oscillatory patterns in neuronal ensembles: an *in vitro* voltage-dependent dye-imaging study in the inferior olive. *J. Neurosci.* 22, 2804–2815. Available online at: http://www.jneurosci.org/content/22/7/2804.long

Llinás, R. (1991). "The noncontinuous nature of movement execution," in *Motor Control: Concepts and Issues*, eds D.R. Humphrey and H.-J. Freund (New York, NY: John Wiley & Sons), 223–242.

Llinás, R., Baker, R., and Sotelo, C. (1974). Electrotonic coupling between neurons in cat inferior olive. *J. Neurophysiol.* 37, 560–571.

Llinás, R., and Mühlethaler, M. (1988). Electrophysiology of guinea-pig cerebellar nuclear cells in the *in vitro* brain stem-cerebellar preparation. *J. Physiol.* 404, 241–258.

Llinas, R., and Nicholson, C. (1971). Electrophysiological properties of dendrites and somata in alligator Purkinje cells. *J. Neurophysiol.* 34, 532–551.

Llinas, R., and Sugimori, M. (1980). Electrophysiological properties of *in vitro* Purkinje cell somata in mammalian cerebellar slices. *J. Physiol.* 305, 171–195.

Long, M. A., Deans, M. R., Paul, D. L., and Connors, B. W. (2002). Rhythmicity without synchrony in the electrically uncoupled inferior olive. *J. Neurosci.* 22, 10898–10905. Available online at: http://www.jneurosci.org/content/22/24/10898.long

Marshall, S. P., and Lang, E. J. (2009). Local changes in the excitability of the cerebellar cortex produce spatially restricted changes in complex spike synchrony. *J. Neurosci.* 29, 14352–14362. doi: 10.1523/JNEUROSCI.3498-09.2009

Marshall, S. P., Van Der Giessen, R. S., De Zeeuw, C. I., and Lang, E. J. (2007). Altered olivocerebellar activity patterns in the connexin36 knockout mouse. *Cerebellum* 6, 287–299. doi: 10.1080/14734220601100801

Maruta, J., Hensbroek, R. A., and Simpson, J. I. (2007). Intraburst and interburst signaling by climbing fibers. *J. Neurosci.* 27, 11263–11270. doi: 10.1523/JNEUROSCI.2559-07.2007

Mathy, A., Ho, S. S., Davie, J. T., Duguid, I. C., Clark, B. A., and Hausser, M. (2009). Encoding of oscillations by axonal bursts in inferior olive neurons. *Neuron* 62, 388–399. doi: 10.1016/j.neuron.2009.03.023

Monsivais, P., Clark, B. A., Roth, A., and Häusser, M. (2005). Determinants of action potential propagation in cerebellar Purkinje cell axons. *J. Neurosci.* 25, 464–472. doi: 10.1523/JNEUROSCI.3871-04.2005

Najafi, F., and Medina, J. F. (2013). Beyond "all-or-nothing" climbing fibers: graded representation of teaching signals in Purkinje cells. *Front. Neural Circuits* 7:115. doi: 10.3389/fncir.2013.00115

Onizuka, M., Hoang, H., Kawato, M., Tokuda, I. T., Schweighofer, N., Katori, Y., et al. (2013). Solution to the inverse problem of estimating gap-junctional and inhibitory conductance in inferior olive neurons from spike trains by network model simulation. *Neural Netw.* 47, 51–63. doi: 10.1016/j.neunet.2013.01.006

Paukert, M., Huang, Y. H., Tanaka, K., Rothstein, J. D., and Bergles, D. E. (2010). Zones of enhanced glutamate release from climbing fibers in the mammalian cerebellum. *J. Neurosci.* 30, 7290–7299. doi: 10.1523/JNEUROSCI.5118-09.2010

Paxinos, G., and Watson, C. (1998). *The Rat Brain in Stereotaxic Coordinates*. 4th Edn. Sydney, NSW: Academic Press.

Raman, I. M., and Bean, B. P. (1999). Ionic currents underlying spontaneous action potentials in isolated cerebellar Purkinje neurons. *J. Neurosci.* 19, 1663–1674.

Ruigrok, T. J. (1997). Cerebellar nuclei: the olivary connection. *Prog. Brain Res.* 114, 167–192. doi: 10.1016/S0079-6123(08)63364-6

Sasaki, K., Bower, J. M., and Llinas, R. (1989). Multiple Purkinje cell recording in rodent cerebellar cortex. *Eur. J. Neurosci.* 1, 572–586. doi: 10.1111/j.1460-9568.1989.tb00364.x

Schweighofer, N., Lang, E. J., and Kawato, M. (2013). Role of the olivo-cerebellar complex in motor learning and control. *Front. Neural Circuits* 7:94. doi: 10.3389/fncir.2013.00094

Sotelo, C., Llinás, R., and Baker, R. (1974). Structural study of inferior olivary nucleus of the cat: morphological correlates of electrotonic coupling. *J. Neurophysiol.* 37, 541–559.

Sugihara, I. (2011). Compartmentalization of the deep cerebellar nuclei based on afferent projections and aldolase C expression. *Cerebellum* 10, 449–463. doi: 10.1007/s12311-010-0226-1

Sugihara, I., Marshall, S. P., and Lang, E. J. (2007). Relationship of complex spike synchrony to the lobular and longitudinal aldolase C compartments in crus IIA of the cerebellar cortex. *J. Comp. Neurol.* 501, 13–29. doi: 10.1002/cne.21223

Sugihara, I., and Shinoda, Y. (2004). Molecular, topographic, and functional organization of the cerebellar cortex: a study with combined aldolase C and olivocerebellar tracing. *J. Neurosci.* 24, 8771–8785. doi: 10.1523/JNEUROSCI.1961-04.2004

Voogd, J., Pardoe, J., Ruigrok, T. J. H., and Apps, R. (2003). The distribution of climbing and mossy fiber collateral branches from the copula pyramidis and the paramedian lobule: congruence of climbing fiber cortical zones and the pattern of zebrin banding within the rat cerebellum. *J. Neurosci.* 23, 4645–4656. Available online at: http://www.jneurosci.org/content/23/11/4645.long

Voogd, J., and Ruigrok, T. J. (2004). The organization of the corticonuclear and olivocerebellar climbing fiber projections to the rat cerebellar vermis: the congruence of projection zones and the zebrin pattern. *J. Neurocytol.* 33, 5–21. doi: 10.1023/B:NEUR.0000029645.72074.2b

Wonnacott, T. H., and Wonnacott, R. J. (1977). *Introductory Statistics, 3rd Edn.* New York, NY: John Wiley & Sons.

Zar, J. H. (1999). *Biostatistical Analysis, 4th Edn*. Upper Saddle River, NJ: Pearson Education.

Conflict of Interest Statement: The authors declare that the research was conducted in the absence of any commercial or financial relationships that could be construed as a potential conflict of interest.

*Received: 06 June 2014; accepted: 06 October 2014; published online: 30 October 2014. Citation: Lang EJ, Tang T, Suh CY, Xiao J, Kotsurovskyy Y, Blenkinsop TA, Marshall SP and Sugihara I (2014) Modulation of Purkinje cell complex spike waveform by synchrony levels in the olivocerebellar system. Front. Syst. Neurosci. **8**:210. doi: 10.3389/fnsys.2014.00210*

This article was submitted to the journal Frontiers in Systems Neuroscience.

frontiers in
SYSTEMS NEUROSCIENCE

REVIEW ARTICLE
published: 04 November 2014
doi: 10.3389/fnsys.2014.00205

How the cerebellum may monitor sensory information for spatial representation

***Laure Rondi-Reig*[1,2,3]*, *Anne-Lise Paradis*[1,2,3], *Julie M. Lefort*[1,2,3], *Benedicte M. Babayan*[1,2,3] and *Christine Tobin*[1,2,3]**

[1] *Sorbonne Universités, UPMC Univ Paris 06, UMR-S 8246/UM 119, Neuroscience Paris Seine, Cerebellum, Navigation and Memory Team, Paris, France*
[2] *Institut National de la Santé et de la Recherche Médicale 1130, Neuroscience Paris Seine, Cerebellum, Navigation and Memory Team, Paris, France*
[3] *Centre National de la Recherche Scientifique, UMR 8246, Neuroscience Paris Seine, Cerebellum, Navigation and Memory Team, Paris, France*

Edited by:
Matthew Jones, University of Bristol, UK

Reviewed by:
Jeffrey S. Taube, Dartmouth College, USA
Laura Petrosini, University Sapienza of Rome, Italy

****Correspondence:***
Laure Rondi-Reig, IBPS-Neurosciences, UPMC, CeZaMe Team, 9 Quai Saint Bernard, 5e étage, 75005 Paris, France
e-mail: laure.rondi-reig@upmc.fr

The cerebellum has already been shown to participate in the navigation function. We propose here that this structure is involved in maintaining a sense of direction and location during self-motion by monitoring sensory information and interacting with navigation circuits to update the mental representation of space. To better understand the processing performed by the cerebellum in the navigation function, we have reviewed: the anatomical pathways that convey self-motion information to the cerebellum; the computational algorithm(s) thought to be performed by the cerebellum from these multi-source inputs; the cerebellar outputs directed toward navigation circuits and the influence of self-motion information on space-modulated cells receiving cerebellar outputs. This review highlights that the cerebellum is adequately wired to combine the diversity of sensory signals to be monitored during self-motion and fuel the navigation circuits. The direct anatomical projections of the cerebellum toward the head-direction cell system and the parietal cortex make those structures possible relays of the cerebellum influence on the hippocampal spatial map. We describe computational models of the cerebellar function showing that the cerebellum can filter out the components of the sensory signals that are predictable, and provides a novelty output. We finally speculate that this novelty output is taken into account by the navigation structures, which implement an update over time of position and stabilize perception during navigation.

Keywords: cerebellum, self-motion, navigation, place cells, head direction cells, parietal cortex, sensory processing, hippocampus

INTRODUCTION

The ability to maintain a sense of direction and location while moving in one's environment is a fundamental cognitive function. Humans and more generally animals rely on a spatial cognitive process in complex environments for obtaining food, avoiding dangers and finding their nest/home. The cerebellum has been shown to participate in this spatial cognitive process (see review in Petrosini et al., 1998; Schmahmann and Sherman, 1998; Rondi-Reig et al., 2002; Rondi-Reig and Burguière, 2005). However, the computational processes supported by the cerebellum in that function and its anatomo-functional links with more traditional navigation structures are still debated.

Neuronal navigation circuits have been described in various behaviors ranging from exploration to goal-directed navigation. Those circuits underlie the acquisition of knowledge about the environment through different elementary processes we can exemplify by imagining the following situation. When one arrives in a new city, one may wander around, gathering and memorizing information about salient and/or recognizable landmarks, either proximal (this red house, the hairdresser…) or visible from a distance (distal; a tower, a church, a hill…). One can then use this information to get to a place by either moving toward a distantly visible monument or by trying to remember the succession of direction changes performed from the departure point, possibly at the recognizable landmarks. When the city becomes well-known, other elementary processes may take place and allow the navigator to use the knowledge previously acquired. Indeed, Spiers and Maguire (2006) have shown that after initially planning the route to our destination, we set up expectations, waiting to see a particular landmark to check if we are on the right route, we occasionally inspect the city around us as we travel through it ("this building has been cleaned"), and we may also see an opportunity to adjust our route if necessary. If driving, we also continuously monitor the surrounding traffic to achieve safe passage to our destination and plan actions, such as changing lanes.

This detailed description reveals the complexity of navigation and the multiplicity of sub-processes that can vary in time depending on the amount of knowledge one has of one's environment and the given navigational constraints.

Interestingly, all these sub-processes of navigation rely on sensory processing to provide the navigator with information about their position and orientation in the environment. Much of the information about where we are is known to come from

external or allothetic cues. However, navigation also generates self-motion—also called idiothetic—information when one is moving in this environment. Monitoring such self-motion information is essential to estimate one's movement in space to update one's position and orientation.

The continuous monitoring of this self-motion information may subserve the mental handling of spatial knowledge. This review will focus on the engagement of the cerebellum in this continuous process.

To this end, we will first review the sensory inputs to the cerebellum and the cerebellar outputs directed toward navigation circuits. We will then discuss the computational algorithm(s) thought to be performed by the cerebellum in this context. Finally, we will review how self-motion signals influence information coded in these navigation circuits. Recent literature now provides anatomo-functional descriptions of the cerebellum at the micro-circuit level, revealing microcomplexes depending on the zebrin-histochemical status of the Purkinje cells, longitudinal zones and microzones of the cerebellar cortex (Hawkes and Herrup, 1995; Pijpers et al., 2006; Cerminara et al., 2013) and subdivision of the inferior olivary and deep cerebellar nuclei (Garwicz et al., 1998; Sugihara and Shinoda, 2004; Pijpers et al., 2005, see also Apps and Watson, 2013 for a review). However, the present literature describing cerebellar links with forebrain areas is much less detailed. The functional links proposed in this review will therefore be described at a macroscopic level.

MONITORING SELF-MOTION INFORMATION FOR NAVIGATION

The importance of monitoring self-motion information during navigation was first revealed by Mittelstaedt and Mittelstaedt (1980) who studied the ability to navigate without external cues. They tested the ability of gerbils to retrieve their pups from within a circular arena and then return to their nest at the arena border. After using sometimes convoluted paths to initially find their pups, the gerbils then returned to their nests using direct paths, even in darkness. This behavior suggested that gerbils could integrate their movements to calculate a direct vector toward their departure. When the gerbils were slowly rotated on a platform (with an angular acceleration below the vestibular threshold, and hence not detected by the animals) while picking up a pup, they returned "home" in a direction that deviated from the nest by the amount they had been rotated. In other words, they homed using an internal (and in this case disrupted) sense of direction rather than external references. This ability was called path integration (Mittelstaedt and Mittelstaedt, 1980).

It is noteworthy that animals can rely on self-motion even when external information is available. This was highlighted by studies showing that an animal can find its goal in the darkness after learning it with a landmark or inducing a conflict between external and self-motion cues (Etienne and Jeffery, 2004; Rochefort et al., 2011). Therefore, self-motion information appears to be constantly available and effectively used whatever the navigation constraints.

Self-motion cues are provided by several systems: vestibular (translational and rotational accelerations) (Stackman and Herbert, 2002; Zheng et al., 2007), proprioceptive (feedback information from muscles, tendons, and joints), visual in the presence of light (linear and radial optic flow) (Etienne and Jeffery, 2004), acoustic (Valjamae, 2009) and even tactile (tactile flow) (Bremmer, 2011; Schroeder and Hartmann, 2012). It has also been suggested that during an active movement, while the motor cortex sends a motor command to the periphery, a copy of this command (called an efference copy) is also generated and sent to the cerebellum where it could be used to generate a prediction of the sensory consequences of the intended movement (Holst and Mittelstaedt, 1950).

In the following section we propose a schematic description of the anatomical pathways that convey self-motion information to the cerebellum. We will specify the intermediate relay nuclei from sensors to cerebellum and the main lobules receiving this multisource information. The anatomical description is restricted to rodents and rabbits, with inputs from primates which provide extensive electrophysiological functional data.

SENSORY INPUTS TO THE CEREBELLUM

The principal inputs to the cerebellar cortex are mossy fibers and climbing fibers. Mossy fibers originate from the spinal cord and from a wide range of nuclei in the brain stem, namely the pontine, vestibular, trigeminal and dorsal column nuclei. These mossy fibers convey information to the cerebellum from peripheral sensors located on body and head, and from cerebral cortices (see for review Ruigrok, 2004).

Sensory information entering the cerebellar cortex via mossy fibers is then distributed to, and integrated by, granule cells in the granular layer, which in turn excite the principle output of the cerebellar cortex, Purkinje cells, as well as interneurons within the molecular layer (stellate cells and basket cells).

The climbing fibers constitute the other main afferent to the cerebellar cortex. They arise exclusively from the inferior olive, a well defined nucleus in the ventral part of the brainstem. The axon of an olivary neuron divides into several branches that terminate in the molecular layer where they wrap around the dendritic tree of a Purkinje cell and make numerous synaptic contacts. Remarkably, in adults rats, each Purkinje cell is contacted by only one climbing fiber but each climbing fiber contacts seven Purkinje cell on average (Armstrong and Schild, 1970). The inferior olive receives information from many sources, including the dorsal column nuclei, the prepositus hypoglossi nucleus (PrH) (McCrea and Horn, 2006), the spinal trigeminal nuclei (Van Ham and Yeo, 1992; Yatim et al., 1996), the superior colliculus (May, 2006) and the cerebral cortex, mainly the sensori-motor cortex (Baker et al., 2001; Azizi, 2007; Watson et al., 2013).

In the following we briefly detail anatomical projections of visuo-vestibular and neck proprioception signals which are well documented in terms of pathway and computational combination in optokinetic and vestibulo-ocular reflexes. We also describe whisker signal afferences, the processing of which is usually considered independently from that of visual and vestibular signals. We will question whether a convergence may exist between those signals within the context of navigation, and whether the efference copy signal, which targets the cerebellum and circuits engaged in self motion information process, may also be integrated with sensory signals in the cerebellum. The

cerebro-cerebellar pathway which transmits already processed information, in particular from the sensory and associative cerebral cortices (Morissette and Bower, 1996) will not be described here. We will focus our description on the inputs to the vestibulocerebellum lobules IX, X (**Figure 1**), to the flocculus and paraflocculus, as well as the posterior lobules (VII, Crus I, Crus II) of the cerebellar cortex, which are often associated with the involvement of the cerebellum in cognitive functions (see Buckner, 2013 for a review). **Figures 2**, **3** illustrate the anatomical projections of these sensory inputs to the cerebellar cortex in rodents and rabbits.

VESTIBULAR PROJECTIONS

Vestibular inputs to the cerebellar cortex have two main origins. A small projection from the vestibular sensors, called the primary afferents, directly reach the ipsilateral uvula-nodulus. A larger projection, called the secondary afferents, pass through the vestibular nuclei before reaching different cerebellar lobules.

In rabbits, most of the mossy fibers directly originating from the vestibular sensors reach the uvula-nodulus (Barmack et al., 1993). The uvula-nodulus also receives indirect vestibular signals though the prepositus hypoglossi nucleus (PrH), which also sends ascending projection to the flocculus (Thunnissen et al., 1989).

In rodents, vestibular signals relayed by various vestibular nuclei not only project to the uvula-nodulus but also project to the flocculus, paraflocculus and lobule VII via the PrH (Päällysaho et al., 1991; Ruigrok, 2003).

Vestibular climbing fibers originate from two subnuclei of the inferior olive, the β-nucleus and the dorsomedial cell column. The outputs of these olivary nuclei terminate in the contralateral uvula-nodulus (See review in Barmack, 2003) and in the flocculus (Schonewille et al., 2006). The inferior olive receives vestibular inputs from the vestibular nuclei as well as the PrH (Gerrits et al., 1985). Indeed, the PrH nucleus does not belong to the vestibular complex, it does however receive numerous vestibular afferents from the vestibular nuclei (Baker and Berthoz, 1975; McCrea and Horn, 2006).

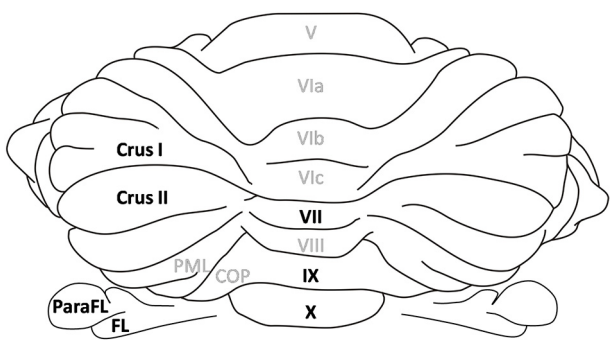

FIGURE 1 | Cerebellar lobules. Dorsal view of the rat cerebellum. Lobules in the vermis are numbered according to Larsell's schema (Larsell, 1952). The lobules discussed in the review are highlighted in black. The flocculus and paraflocculus correspond to the hemispheric part of the flocculo-nodular lobe whereas lobules IX and X refer to its vermal part. Similarly Crus I and II are hemispheric regions in the posterior lobe whereas lobule VII is the corresponding vermal lobule. ParaFL, paraflocculus; FL, flocculus; PML, paramedian lobe; COP, copula pyramidis.

VISUAL PROJECTIONS

Visual inputs are received by two areas of the posterior cerebellar cortex, lobule VII and the dorsal paraflocculus (see review Kralj-Hans et al., 2007).

In monkey, the basilar pontine nuclei (BPN), which receive inputs from cortices involved in eye movements (e.g., the frontal eye fields) and the perception of visual motion, sends mossy fiber projections to the dorsal paraflocculus (Giolli et al., 2001) and to lobule VII. Some projections to lobule VII also come from the nucleus reticularis tegmenti pontis (NRTP). Both the basilar pontine nuclei and the NRTP receive visual and oculomotor inputs from the cerebral cortex via the superior colliculus (see review Voogd and Barmack, 2006).

More visual information also reaches the cerebellum through mossy fibers from PrH. This structure, known to be involved in eye velocity and gaze signals, receives ascending projections from the Accessory Optic System (AOS). AOS is known to receive retinal signals related to the speed and direction of movement of large, textured visual patterns (AOS) (Soodak and Simpson, 1988) and is proposed to be dedicated to the processing of "optic flow fields" (Wylie et al., 1999). It has been shown to detect self-motion rather than the motion of external objects (Simpson et al., 1988). In sum, mossy fibers conveying visual information mainly arise from the BPN, the NRTP, and the PrH.

Climbing fibers projecting to the dorsal paraflocculus and lobule VII originate from different sub-parts of the inferior olive. Major projections to the dorsal paraflocculus arise from the rostral medial accessory olive (MAO) and the ventral lamella of the principal olive (PO) while projections from the lobule VII arise from the caudal MAO (Apps and Hawkes, 2009).

TACTILE SIGNALS FROM WHISKERS

Both anatomical and electrophysiological studies indicate that the cerebellum receives tactile whisker information and is involved in its processing. In particular, stimulation of the whiskers induces simple and/or complex spikes electrophysiological activity in Crus I and Crus II (see review by Bosman et al., 2010, 2011).

Sensory inputs from the whiskers enter the trigeminal nuclei (TGN) (Stuttgen et al., 2008; Schroeder and Hartmann, 2012) and reach the cerebellar cortex via different pathways. Mossy fibers from the trigeminal nuclei project to lobule VII, as well as Crus I, Crus II, lobules IX, X, and to a lesser extent to the flocculus and paraflocculus (Yatim et al., 1996). The trigeminal nuclei also projects to the superior colliculus, which sends afferents to the pontine nuclei (NRTP) and the inferior olive (see **Figure 3** and Bosman et al., 2010). The basilar pontine nuclei (BPN) receive whisker inputs both from direct TGN projections, and from the whisker sensory and motor cortices (S1 and S2, M1). The BPN also receive projections from other structures conveying whisker-related information such as motor and sensory whisker cortices as well as the superior colliculus, (Burne et al., 1981; Diamond et al., 2008), which receives inputs from TGN (May, 2006).

Concerning the climbing fiber projections, the three main nuclei of the inferior olive (i.e., MAO, DAO, and PO) receive inputs from TGN (Yatim et al., 1996). Tracing (Swenson et al., 1989) and electrophysiological studies in rats show that they

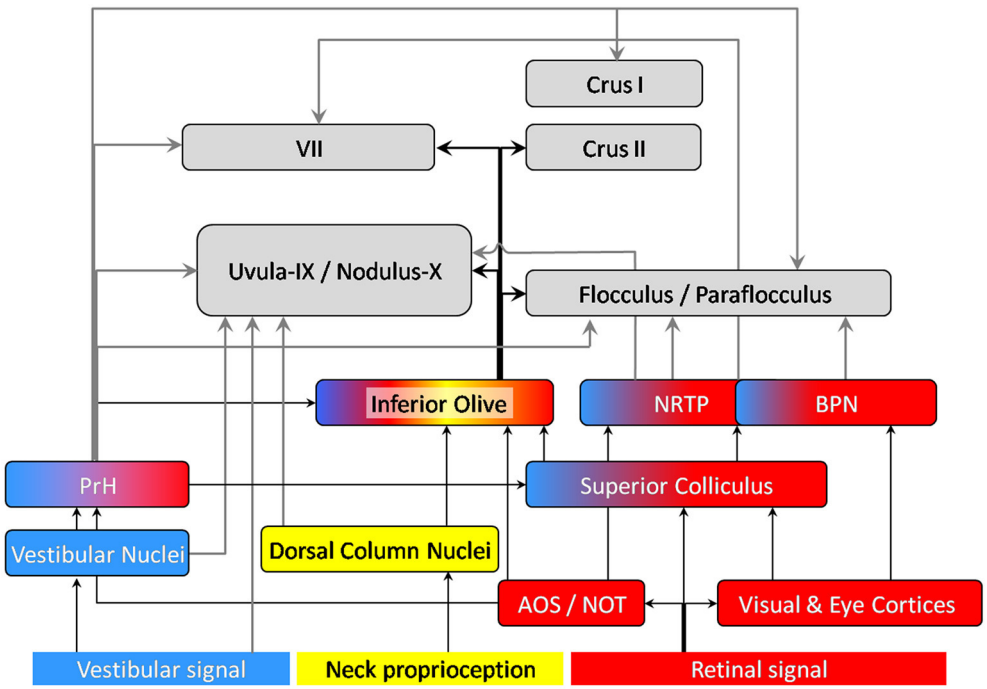

FIGURE 2 | Anatomical projections of visual (red), vestibular (blue) and neck proprioception (yellow) inputs to the cerebellar cortex. The displayed connections were found in rodents and/or rabbits. Arrows connecting the cerebellum are highlighted in bold: gray arrows correspond to mossy fibers, black ones to climbing fibers. AOS, Accessory Optic System; NOT, Nucleus of the Optic Tract; BPN, Basilar Pontine Nuclei; NRTP, Nucleus Reticularis Tegmenti pontis; PrH, Prepositus Hypoglossi Nucleus. Note that the vermal regions of the cerebellar cortex (lobule VII, Uvula-Nodulus) are represented on the left whereas the hemispheric regions are represented on the right (Crus I, II, flocculus-paraflocculus).

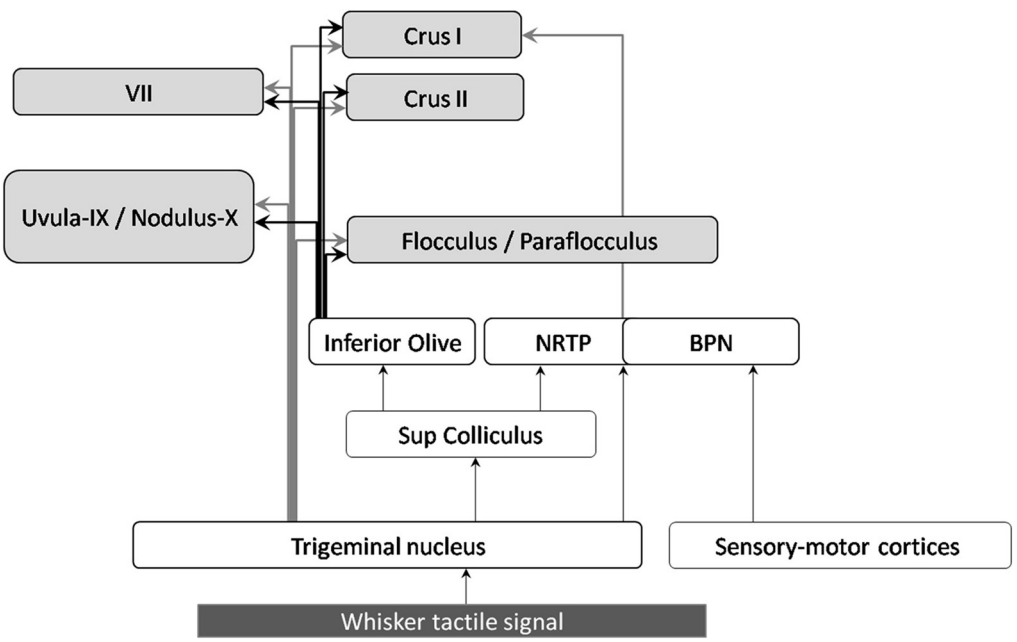

FIGURE 3 | Anatomical projections of whisker tactile inputs to the cerebellar cortex. The displayed connections were found in rodents and/or rabbits. Arrows connecting the cerebellum are highlighted in bold: gray arrows correspond to mossy fibers, black ones to climbing fibers.

also receive inputs from the whisker sensory cortex (Brown and Bower, 2002).

PROPRIOCEPTIVE SIGNAL

Cerebellum plays a crucial role in proprioception (Bhanpuri et al., 2013). Proprioceptive information from the limbs are conveyed through spino-cerebellar pathways which are not going to be described here except for neck and shoulder proprioception that can be integrated with visuo-vestibular signals to account for possible head vs. body movement during navigation (Gdowski and McCrea, 2000; Bove et al., 2004; Brooks and Cullen, 2009). Proprioceptive information is conveyed by both mossy and climbing fibers (Murphy et al., 1973; Swenson and Castro, 1983). Mossy fiber information from neck and shoulder is relayed in the ECuN, a subnucleus of the dorsal column nuclei (DoCN) and projects mainly to lobule IX (Quy et al., 2011), lobule VII, Crus I, Crus II, paraflocculus and paramedian lobule (Huang et al., 2013). It has been shown that climbing fibers conveying this proprioceptive information reach the same zones as those innervated by mossy fiber at least in the anterior cerebellum (Murphy et al., 1973).

MULTIMODAL INFORMATION INTEGRATION

The description above reveals that multiple sources of self-motion information converge at different anatomical locations en-route to the cerebellum.

The superior colliculus has been described as a multi-sensory integrator (see for example Meredith and Stein, 1983, 1986; review in DeAngelis and Angelaki, 2012). It receives visual inputs from the retina and cortices. It is likely to receive visuo-vestibular information through its connection with PrH (**Figure 2**). It also receives whisker signals through the TGN (**Figure 2**).

The prepositus hypoglossi nucleus (PrH)

Besides the superior colliculus, the PrH appears to be an important precerebellar nucleus that sends multimodal information to the cerebellum (McCrea and Horn, 2006). It receives inputs from both vestibular nuclei and AOS. The efferent connections of the AOS not only convey visual-oculomotor signal but also contribute to visuo-vestibular interaction (Giolli et al., 2006).

It has extensive projection to the uvula-nodulus, the flocculus and paraflocculus, the oculomotor cerebellum (Lobule VII) and Crus I (Barmack, 2003; Ruigrok, 2003; McCrea and Horn, 2006; Voogd and Barmack, 2006) as well as Crus II in primates (Belknap and McCrea, 1988). Therefore, the PrH belongs to a network involved in visual, oculomotor, vestibular, and proprioceptive information integration.

The cerebellar cortex

As the caudal medial accessory olive receives afferents from the superior colliculus (receiving retinal and tactile signals) and the dorsal column nuclei (neck proprioception), climbing fiber inputs to lobule VII are modulated by multi-source signals (Azizi, 2007). Interestingly, whisker inputs also reach lobule VII (Bower and Kassel, 1990). Whisking movements are closely coordinated with head movements and such coordination is essential during navigation. The integration of whisker and head movements could be mediated by lobule VII (Hartmann, 2011).

Lobule IX and X receive vestibular inputs (Barmack, 2003) and proprioceptive neck signals related to body-head-position via the external cuneate nucleus which is part of the Dorsal Column Nuclei (Quy et al., 2011).

Purkinje cells of the cerebellar cortex receive convergent inputs of the same multi-sensorial information both from mossy and climbing fiber inputs. Brown and Bower described a convergence of mossy fibers and climbing fibers at the level of the Purkinje cells in the lateral hemispheres of the rats (Crus IIa) after peripherical tactile stimulation (Brown and Bower, 2001). This multisensory information is also conveyed directly from collaterals of these two inputs to the cerebellar nuclei (Sugihara et al., 1999).

Integration of the sensory and efference copy signals

When a motor command is sent to an effector, a copy of that command called "efference copy" is sent to the cerebellar cortex via the pontine nuclei (Angel, 1976; Miall and Wolpert, 1996). It is classically proposed that the cerebellar processing of the efference copy provides an expected sensory outcome or "corollary discharge," which can be compared to the actual sensory consequences of the motor command (Miall and Wolpert, 1996; Blakemore et al., 2001; see review by Stock et al., 2013). Recently Huang et al. (2013) reported that the same granule cells receive both upper body proprioceptive information from ECuN and cortical afferents from an area associated with upper body motor control via the BPN. This convergence is observed in several cerebellar lobules, especially in paramedian lobule, paraflocculus and Crus II. By showing that granule cells of those lobules receive in parallel efference copy and sensory information originating from the same part of the body, those results provide a neural basis for the integration of the two types of information. Besides results in rabbits suggest that efference copy and sensory signal could also terminate on the same Purkinje cells. Indeed, Winkelman and Frens (2006) showed that climbing fibers reaching the flocculus, and previously reported as encoding the retinal slip only, also receive an oculomotor component. Those data thus suggest two levels of convergence of the sensory and motor efference inputs at the granule cells on one hand and via the climbing fiber pathway on the other hand.

In conclusion, the cerebellum appears to be in a position to combine and weight multi-sensory signals originating from various sources. Interestingly, this multisource signal is conveyed redundantly by the MF and the CF inputs. In the following sections, we will question how such multi-source self-motion information arriving in the cerebellum might be processed and then conveyed to spatially modulated cells well described in navigation circuits.

WHAT COMPUTATIONS ARE PERFORMED IN THE CEREBELLUM DURING SELF-MOTION?

To build a unified representation of the body in space, the brain needs to compare and integrate signals coming from different sensors and from the motor cortex (the efference copy). However, information coming from each modality is intrinsically ambiguous: first, it is generated by sensors located in different parts of

the body (e.g., head, neck, limbs), it is therefore measured in relation with the organ and does not give direct access to whole body motion in space; second, each sensory signal can be insufficient to distinguish self-motion from external information by itself (e.g., linear acceleration vs. gravity in the vestibular information; optic flow generated by self-motion vs. the motion of a large object in the environment). Such ambiguities may only be resolved by combining several signals arising from different sensory modalities. The convergence of multi-source signals in the cerebellum described above is likely to contribute to this disambiguation, and provide the navigation structures with reliable self-motion information. That is what we describe in the following.

REFERENCE FRAME CONVERSIONS

Locating oneself is only meaningful relative to a spatial reference frame, i.e., a coordinate system into which spatial information is coded. It is defined by the origin on which it is centered, i.e., the point in space relative to which positions are measured, and by a set of axes corresponding to the three directions of space. A reference frame can be centered on the subject (egocentric reference frame) and more precisely on different parts of the subject (e.g., head vs. trunc-centered reference frame) or on the external world (allocentric reference frame).

Sensory information generated by sensors located in different parts of the body (e.g., head, neck, limbs) are initially encoded in the respective reference frames of its sensors. For example, as vestibular organs are located in the head, vestibular signal is detected in head coordinates. To allow the combination and/or comparison of different sensory signals, those must be expressed in a common reference frame. For example, to compute the movement of the whole body in space, vestibular information needs to be integrated relative to the body (taking into account the relative position of the head and the body given by the neck curvature) and also to the world (taking into account gravity).

Converting the signal initially in head-fixed coordinates into a signal in body-frame and world-frame coordinates are not necessarily successive computations. Several recent studies showed that these two reference frame transformations may occur (in parallel) in different cerebellar subregions (see review in Rochefort et al., 2013). Indeed, signals related to head-to-body frame transformation have been detected in the cerebellar fastigial nucleus (Kleine et al., 2004; Shaikh et al., 2004; Brooks and Cullen, 2009), and Purkinje cell activity has been shown to be modulated by head-to-body position, a signal required for such a transformation, in the cerebellar anterior lobules IV and V of decerebrate cats (Manzoni et al., 1999). On the other hand, the head-to-world reference frame conversion has been proposed to occur in the lobules IX and X of the cerebellar cortex (Yakusheva et al., 2007; Angelaki et al., 2010). We have already proposed that, once adequately transformed, the vestibular information fuels the neuronal circuits of navigation, in particular the hippocampus (Rochefort et al., 2013).

THE CEREBELLUM AS AN ADAPTIVE FILTER

In parallel with functional and experimental descriptions seen above, computational models of cerebellar function have also been proposed (Marr, 1969; Albus, 1971; Ito, 2002). Recent descriptions of the cerebellar micro-circuit features (Cerminara et al., 2013) led to the proposal of an updated and more generalistic model of the cerebellar function as an adaptive filter (Dean and Porrill, 2010).

A filter transforms an input signal into an output signal. In the context of the cerebellar microcircuits, the input signal comes from the mossy fibers (MF) and is distributed onto different granule cells (GC), each one extracting a component of this signal. Interestingly, a GC combines the signal from up to four MF in average (Albus, 1971) and therefore not only analyzes the input signal but also combines several ones (see Section Integration of the sensory and efference copy signals in this paper). Those components of the signal are transmitted through parallel fibers (PF) to dendrites of Purkinje cells (PC) via PF-PC synapses. One Purkinje cell therefore receives the signal from different parallel fibers which are weighted at the PF-PC synapse and recombined to form the filter output (PC simple spike).

The filter is adaptive because the weight at the PF-PC synapses, corresponding to the synapse efficiency, can be modified through bi-directional plasticity (LTP and LTD). In Dean and Porrill's model, these plasticities are under the control of a teaching or error signal coming from the climbing fibers input. The weight adjustment follows the covariance rule: a PF signal that is positively correlated with an error signal has its weight reduced (through LTD), whereas a signal that is negatively correlated with an error signal has its weight increased (through LTP). The climbing fiber signal is thus considered to implement a supervised learning. Interestingly, LTP at the PF-PC synapses can be induced by PF activity alone (Belmeguenai and Hansel, 2005). In this condition, the increase of the filter weights would not be exclusively under the control of the climbing fibers, and could occur through monosynaptic plasticity/LTP at the PF-PC synapse, which could implement a non-supervised learning. It is still unclear which specific role each type of learning could play and how these two could combine in the same model. The extensive literature on the manipulation of cerebellar LTP and/or LTD in genetically modified mice (Gao et al., 2012) could help to tackle this question.

SENSORIMOTOR PREDICTION

With the present model, Dean and Porrill propose possible neural implementations of forward model architectures for taking into account self-induced signals and detecting novelty in particular in the rat whisker system (Anderson et al., 2012; Porrill et al., 2013). This model accounts for the known competence of the cerebellum in sensorimotor prediction (Blakemore et al., 2001) and fits with the recent findings that the primate cerebellum encodes unexpected self-motion (Brooks and Cullen, 2013). Recording from monkeys during voluntary and externally applied self-motion, Brooks and Cullen (2013) demonstrated that the cerebellum can distinguish unexpected self-motion resulting from external factors and self-motion generated by voluntary actions by making predictions about the expected sensory state. Cullen et al. (2011) propose the possible production of a cancelation signal to suppress self-generated vestibular stimulation due to active movements. This computation implies using the efferent copy of the motor command to model a sensory prediction (expected sensory

feedback) then comparing this expected feedback to the actual sensory signal (Roy and Cullen, 2004). This cerebellar internal model could be responsible for the error prediction necessary to finely tune motor movements, as well as to perceive oneself in space correctly.

In line with this hypothesis, Bhanpuri et al. (2013) and Bhanpuri et al. (2012) showed that cerebellar patients have proprioceptive deficits compared with controls during active movement, but not when the arm is moved passively. They also find that similar deficits can be reproduced in healthy subjects by making them moving in a force field with unpredictable dynamics. The authors propose that it is the predictability of self-generated movement rather than muscle activity alone which is important to enhance proprioception, and conclude that the proprioceptive deficit of cerebellar patients in active conditions is consistent with disrupted movement prediction. Christensen et al. (2014) also found that cerebellar patients had no beneficial influence of action execution on perception compared with healthy controls. Cerebellum is thus proposed to be crucial to take into account self-generated movement to enhance somato-sensory perception related to those movements.

The adaptive filter not only accounts for those results but also extend their conclusions from the mere cancelation of the auto-generated signal to the possible detection of an external novelty signal. Here, we discuss the possible generalization of this model to the detection of new features of the external environment in the context of navigation, whatever the sensory modality.

NOVELTY DETECTION

Whether we consider vestibular, acoustic, visual or whisker tactile signal, we can consider sensory information received by the cerebellum as two-dimensional: that which is internally generated by voluntary self-motion and that which is externally generated (for instance passive self-motion due to unexpected external events). In externally generated self-motion, we can further dissociate sensory inputs which already occurred and are thus predictable from newly occurring features (novelty). The sensory prediction performed by the cerebellum takes into account both the motor efference and the current sensory state of the navigator. With this double input it is possible to predict the future sensory inputs due to internally generated self-motion by "adding" to the current sensory state the evolution of this current state expected from the intended movement (see Miall and Wolpert, 1996). It might also be possible to predict the expected future sensory state due to the navigation context already encountered (Anderson et al., 2012). In a non-navigational context, the cerebellum (lobule VII Crus I) was found engaged in predicting the position change over time of an occluded target based on its visual speed before occlusion (O'Reilly et al., 2008). The comparison between the actual sensory state and the predicted sensory signal will then provide the novelty information. Accordingly, Naatanen and Michie (1979) proposed that the cerebellum detects "discordances between the input from the deviant event and the sensory memory representation of the regular aspects of the preceding stimulation." Thus, cerebellar patients were impaired in the cortical processing of deviant somatosensory inputs presented in a regular context (Restuccia et al., 2007), suggesting that the cerebellum could be the site where novelty is extracted by comparing actual stimuli with predictable ones.

This comparison has been proposed to be performed by the superior colliculus (Porrill et al., 2013). We propose this could also occur in the deep cerebellar nuclei as those receive adequate projections to perform this comparison: on one hand from Purkinje cells conveying sensory prediction to inhibitory synapses; on the other hand, from mossy fibers conveying sensory inputs to excitatory synapses. Interestingly, the inferior olive could also have a role of comparator since it receives on one hand inhibitory inputs from the deep cerebellar nuclei (Angaut and Sotelo, 1989), which could convey sensory prediction, and on the other hand actual sensory signals (see **Figure 4**).

The new sensory inputs containing (1) actively generated, (2) passively generated, and (3) external information, novelty can arise from any of those three sources, e.g., (1) internal modification of the muscle strength, (2) obstacle modifying/blocking unexpectedly the trajectory of a limb, (3) new object in the navigator environment inducing tactile stimulation and therefore influence space modulated cells.

FROM CEREBELLUM TO SPATIAL KNOWLEDGE

We saw previously that, once adequately transformed in the cerebellum, the sensory information may provide the neuronal circuits of navigation, in particular the hippocampus, with reliable self-motion information or novelty information. We now describe how this information may influence navigation-related cells.

To our knowledge, only one study has reported the consequence of cerebellar impairment on the activity of navigation-related cells (Rochefort et al., 2011). In this study, hippocampal place cells (review by O'Keefe, 1979) were recorded in freely exploring L7-PKCI mice, which lack PKC dependent LTD at the parallel fiber—purkinje cell synapses (De Zeeuw et al., 1998). The results revealed an implication of cerebellar LTD in maintaining the hippocampal spatial map when the mice had to rely on self-motion information. This finding first raised the question of how such self-motion information, processed by the cerebellum, may influence place field properties.

INFLUENCE OF SELF-MOTION INFORMATION ON PLACE CELL FIRING

The role of self-motion information in the control of place fields has originally been demonstrated from the observation that place fields were maintained in the dark if the animal stayed in the arena when the light was switched off (Quirk et al., 1990). If the animal was placed in the arena directly in the dark, i.e., in the absence of any visual information, the place field appeared at a random location. This suggested that self-motion information was used to maintain the location specific firing of place cells previously recorded in the light (Quirk et al., 1990). Among the different self-motion inputs, vestibular information was shown to be important for hippocampal spatial representation since a temporary inactivation of the vestibular system by tympanic injection of tetrodotoxin (TTX) dramatically altered the activity pattern of place cells (Stackman et al., 2002; see review in Smith and Zheng, 2013).

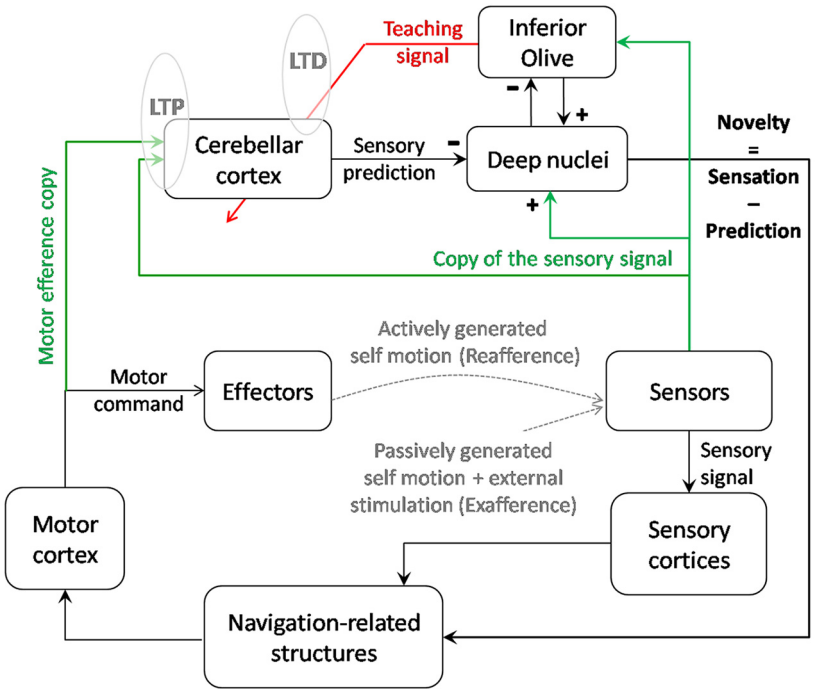

FIGURE 4 | Contribution of cerebellar computation to navigation. Cerebellar cortex as an adaptive filter could transform an input signal consisting of self-motion sensory signals and a motor efference copy into a prediction of the sensory signal expected from voluntary movements and the previous sensory state. By comparing the sensory prediction with the actual sensory signal, the cerebellar output helps the system to detect novelty in the environment. Thanks to a parallel output sent to the inferior olive, this novelty signal is modified into a teaching signal which, if repeated in correlation with the sensory inputs, could contribute to modify the cerebellar model of prediction through LTD. Reciprocally, repeated inputs to the cerebellum may trigger LTP at the synapses gating those inputs and act as an unsupervised learning of the most relevant inputs. Depending on the type of signal (vestibular, tactile. . .) and possibly on the targeted lobules (IX-X vs. VII, crus I, and II), the output of the cerebellar computation could cancel the signal induced by voluntary self-motion and allow detection of novelty. This computation could have a double role: stabilizing perception during voluntary navigation and informing the navigator about the necessity to update his/her relative position in the context.

Recently, the development of recording techniques for head-fixed mice navigating in virtual environments has given the opportunity to further dissect the contribution of non-vestibular self-motion signals to place cell firing (Chen et al., 2013; Ravassard et al., 2013). In such an experimental setup, head-fixed mice are trained to run on an air-cushioned ball surrounded by a screen showing a first-person perspective view of a virtual linear track or maze. The movement of the viewpoint corresponds to the movement of the ball, and the mouse receives visual and other non-vestibular self-motion cues such as proprioceptive and efference copy inputs. Despite the absence of vestibular motion signals, normal place cell firing was found. Amongst these place cells, visual information alone was sufficient to sustain location-specific firing in 25% of place cells and additional movement-related information was required for normally localized firing by the remaining 75% of place cells (Chen et al., 2013). Comparing the hippocampus spatiotemporal selectivity in virtual reality and similar real world navigation tasks, Ravassard et al., reported that distal visual and non-vestibular self-motion cues are sufficient to generate a cognitive map but that vestibular and other sensory cues present in the real world, such as tactile and olfactory cues, are necessary to fully activate the place cell population (Ravassard et al., 2013).

The importance of tactile whisker signals in navigation processes has also been described. Hippocampal CA1 neurons have been shown to encode tactile stimuli in conjunction with the location in which they appeared (Itskov et al., 2011). Diamond et al. showed that a representation of the surrounding world is built through a whisker-mediated sense of touch (Diamond et al., 2008).

Therefore, self-motion signals can clearly influence space hippocampal coding. Nevertheless, as no direct pathway has been anatomically described between the cerebellum and the hippocampus (see review in Rochefort et al., 2013), we propose two potential pathways that could provide a neuro-anatomical substrate allowing for cerebellar interactions with navigation-related cells (see **Figure 5**):

- The projection of the lobule IX-X-floculus and parafloculus to vestibular nuclei and PrH which directly feed the head-direction (HD) cells system (Shinder and Taube, 2010);
- The projection of posterior cerebellar lobules (including VII, Crus I, and Crus II), through the deep cerebellar nuclei and ventro and centro-lateral thalamus (Giannetti and Molinari, 2002), to the parietal cortex which contains "movement cells" (Whitlock et al., 2012) as well as "path cells" (Nitz, 2006, 2012).

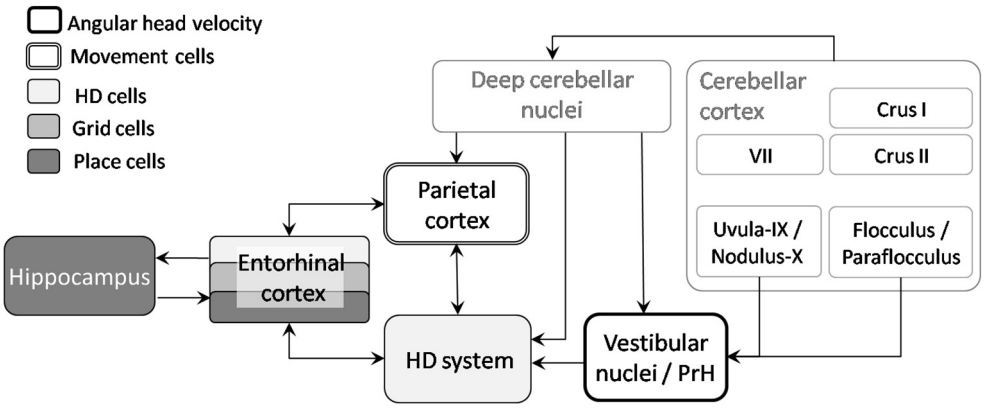

FIGURE 5 | From cerebellum to navigation-related structures. Two pathways could sustain the influence of the cerebellum on place cells activity: the projection of lobule IX-X-floculus-paraflocculus through vestibular nuclei to the head direction cells system and projection of other cerebellar lobules via deep cerebellar nuclei to the parietal cortex and HD system. AHV, Angular head velocity; HD, Head direction; PrH, Prepositus Hypoglossi Nucleus.

INFLUENCE OF SELF-MOTION INFORMATION ON HD FIRING

Head direction (HD) cells fire when a rat's head is facing a specific direction relative to the environment, irrespective of its location or whether it is moving or still (Taube et al., 1990a,b). These cells were first discovered in the dorsal portion of the rat presubiculum, often referred to as the post subiculum (PoS) (Ranck, 1984), but have since been found in multiple structures which are anatomically interconnected: anterior dorsal thalamic nucleus (Taube, 1995), lateral mammillary nuclei (Stackman and Taube, 1998), lateral dorsal thalamus (Mizumori and Williams, 1993), retrosplenial cortex (Chen et al., 1994; Cho and Sharp, 2001), entorhinal cortex (Sargolini et al., 2006) and even striatum (6% of HD) (Mizumori and Williams, 1993; Wiener, 1993). Lesion and electrophysiological studies have shown that the head-direction signal travels from the dorsal tegmental nucleus, to the hippocampus, through the hypothalamus (mammillary nucleus), the antero-dorsal thalamus and the retrosplenial, subicular and entorhinal cortices (Taube, 2007). The dorsal tegmental nucleus receives indirect inputs from vestibular nuclei via the supragenual nucleus (Clark et al., 2012) and the Nucleus prepositus hypoglossi (McCrea and Horn, 2006; Clark et al., 2012). It is important to note that most of the connections between these structures are bidirectional and that the transfer of head direction information is not necessarily unidirectional.

Despite the strong reliance of the HD system on landmark cues (Goodridge and Taube, 1995), removing all the visual cues or turning off the light does not strongly affect HD cell firing in the post subiculum and thalamus (Taube et al., 1990b; Mizumori and Williams, 1993; Goodridge et al., 1998). Using Fischer albino rats, Knierim et al. (1998) found that self-motion inputs could predominate over the visual landmarks when a conflict was created between both types of information and the mismatch was larger than 45°. This suggests that self-motion information can maintain HD signals to some extent in the absence of reliable visual information. Numerous rodent studies have demonstrated that vestibular signals influence landmark navigation (see review Yoder and Taube, 2014). The PrH is one of the two main nuclei that provide multimodal information to the HD cell circuit through connections with the dorsal tegmental nucleus, which is considered as a putative location of head direction signal generation (Yoder and Taube, 2014). Consistently, vestibular lesions abolished the directional firing properties of HD cells, demonstrating that the HD signal critically depends on vestibular information (Stackman and Taube, 1997; Stackman and Herbert, 2002). The importance of proprioceptive (and motor command) information was shown by recording HD cells in the antero-dorsal thalamus in two environments connected by a passageway. In the dark, if the animal actively walked from one environment to the other, HD cells could partly retain their preferred direction between the two environments. However, this was no longer the case if animals were passively transported in the dark from one environment to another, conditions in which only the available information was the vestibular signals (Yoder et al., 2011). This showed the requirement to combine different types of self-motion information (vestibular and proprioceptive) to maintain HD signals in the absence of visual information. Head direction cell were recently shown to be sensitive to optic flow information as well. Rats were freely moving in an arena where the repetitive background (not usable as a landmark) of the cylinder wall was slowly rotated, thus providing a continuously drifting optic flow. Recordings in the antero-dorsal thalamus showed that HD cells exhibit a significant drift in the same direction as the rotating background (Arleo et al., 2013).

MOTION-RELATED CELLS IN THE PARIETAL CORTEX

Interestingly, in the parietal cortex which constitutes the second possible pathway from the cerebellum, at least two types of cells have recently been discovered to be modulated by the displacement of the animal. The first type, which we will call "movement cells" fires whenever the animal moves in a specific direction, irrespective of its location and heading, for example forward or rightward (McNaughton et al., 1994; Whitlock et al., 2012). These cells fire independently from context since their activity pattern is preserved in different environments and seems to depend on self-motion information. When the animals perform a specific sequence of movements (in a hairpin maze), these cells can

acquire new movement specificity (from leftward to backward for example). This last finding led the authors to propose that the activity of these cells is determined by the organization of actions. The second type, which we will call "path cells," has been identified by Nitz (2006) as encoding the state of progression through a route. Recording parietal neurons while rats traversed squared spiral tracks, he further dissected this finding by showing that those neurons simultaneously encoded the rat's position in several coexistent reference frames: linear segments, square loops and full route (Nitz, 2012). Such encoding may contribute to relate different parts of a route by taking into account the motion of the animal in the maze.

SELF-MOTION INFORMATION INFLUENCE ON GRID CELL FIRING

Finally, the entorhinal cortex receives convergent inputs from both the parietal cortex and the retrosplenial cortex, the latter being part of the HD system (Taube, 2007). Grid cells were first discovered in the dorsal medial entorhinal cortex (Fyhn et al., 2004; Hafting et al., 2005), but have also been found in the pre- and parasubiculum (Boccara et al., 2010). Each grid cell fires in several locations in an environment, with the locations forming a regular pattern as though they were nodes on a triangular grid (Fyhn et al., 2004; Hafting et al., 2005). They are most abundant in layers II and III of the medial entorhinal cortex (Sargolini et al., 2006), which receive convergent inputs from the retrosplenial and the parietal cortices and sends major projections to the hippocampus, but are also found in the layers V/VI, which receive inputs from the hippocampus.

Several observations indicate that grid cell firing depends primarily on self-motion information (Hafting et al., 2005). First, a grid cell fires in all environments (in contrast to the hippocampus where an environment is encoded by a subset of active cells), and the spacing of a grid cell is independent of the context. Second, grid fields appear relatively independent of specific landmarks since they can be observed immediately as an animal starts to explore an environment, and the grid pattern does not change drastically in the dark. Grid cell are thus proposed to encode a metric system for spatial navigation, whereby the animal can update its own location using self-motion information (path integration) (Jeffery and Burgess, 2006; Moser and Moser, 2008). This is also consistent with the finding that entorhinal cortex lesions alter self-motion based navigation (Parron and Save, 2004).

In conclusion, different types of navigation-related cells display modifications of firing in response to the manipulation or suppression of different modalities of self-motion cues. The direct anatomical projections of the cerebellum toward the HD system and the parietal cortex make HD cells and movement cells likely candidates for potential influence of the cerebellum on the hippocampal spatial representation. Studies manipulating sensory signals from different modalities reveal the diversity of information that is taken into account to build mental maps. They also illustrate the necessity to process multi-source information to extract the signal appropriate to shape the firing characteristics of the spatially modulated cells. We speculate that what will arise in the navigation structures from the cerebellum will convey the novelty signal necessary to implement an update over time of position in the context of navigation and allow stabilization of perception during voluntary navigation.

ACKNOWLEDGMENTS

This work was supported by the Agence Nationale de la Recherche and the Fondation pour la Recherche Médicale (France). The group of Laure Rondi-Reig is member of the Bio-Psy Labex and the ENP foundation.

REFERENCES

Albus, J. S. (1971). A theory of cerebellar function. *Math. Biosci.* 10, 25–61. doi: 10.1016/0025-5564(71)90051-4

Anderson, S. R., Porrill, J., Pearson, M. J., Pipe, A. G., Prescott, T. J., and Dean, P. (2012). An internal model architecture for novelty detection: implications for cerebellar and collicular roles in sensory processing. *PLoS ONE* 7:e44560. doi: 10.1371/journal.pone.0044560

Angaut, P., and Sotelo, C. (1989). Synaptology of the cerebello-olivary pathway. Double labelling with anterograde axonal tracing and GABA immunocytochemistry in the rat. *Brain Res.* 479, 361–365. doi: 10.1016/0006-8993(89)91641-7

Angel, R. W. (1976). Efference copy in the control of movement. *Neurology* 26, 1164–1168. doi: 10.1212/WNL.26.12.1164

Angelaki, D. E., Yakusheva, T. A., Green, A. M., Dickman, J. D., and Blazquez, P. M. (2010). Computation of egomotion in the macaque cerebellar vermis. *Cerebellum* 9, 174–182. doi: 10.1007/s12311-009-0147-z

Apps, R., and Hawkes, R. (2009). Cerebellar cortical organization: a one-map hypothesis. *Nat. Rev. Neurosci.* 10, 670–681. doi: 10.1038/nrn2698

Apps, R., and Watson, T. C. (2013). "Cerebro-cerebellar connections," in *Handbook of the Cerebellum and Cerebellar Disorders*, eds M. Manto, J. D. Schmahmann, F. Rossi, D. L. Gruol, and N. Koibuchi (Dordrecht: Springer), 1131–1153. doi: 10.1007/978-94-007-1333-8_48

Arleo, A., Déjean, C., Allegraud, P., Khamassi, M., Zugaro, M. B., and Wiener, S. I. (2013). Optic flow stimuli update anterodorsal thalamus head direction neuronal activity in rats. *J. Neurosci.* 33, 16790–16795. doi: 10.1523/JNEUROSCI.2698-13.2013

Armstrong, D. M., and Schild, R. F. (1970). A quantitative study of the Purkinje cells in the cerebellum of the albino rat. *J. Comp. Neurol.* 139, 449–456. doi: 10.1002/cne.901390405

Azizi, A. S. (2007). And the olive said to the cerebellum: organization and functional significance of the olivo-cerebellar system. *Neuroscientist* 13, 616–625. doi: 10.1177/1073858407299286

Baker, M. R., Javid, M., and Edgley, S. A. (2001). Activation of cerebellar climbing fibres to rat cerebellar posterior lobe from motor cortical output pathways. *J. Physiol.* 536(Pt 3), 825–839. doi: 10.1111/j.1469-7793.2001.00825.x

Baker, R., and Berthoz, A. (1975). Is the prepositus hypoglossi nucleus the source of another vestibulo-ocular pathway? *Brain Res.* 86, 121–127. doi: 10.1016/0006-8993(75)90643-5

Barmack, N. H. (2003). Central vestibular system: vestibular nuclei and posterior cerebellum. *Brain Res. Bull.* 60, 511–541. doi: 10.1016/S0361-9230(03)00055-8

Barmack, N. H., Baughman, R., Errico, P., and Shojaku, H. (1993). Vestibular primary afferent projection to the cerebellum of the rabbit. *J. Comp. Neurol.* 327, 521–534. doi: 10.1002/cne.903270405

Belknap, D. B., and McCrea, R. A. (1988). Anatomical connections of the prepositus and abducens nuclei in the squirrel monkey. *J. Comp. Neurol.* 268, 13–28. doi: 10.1002/cne.902680103

Belmeguenai, A., and Hansel, C. (2005). A role for protein phosphatases 1, 2A, and 2B in cerebellar long-term potentiation. *J. Neurosci.* 25, 10768–10772. doi: 10.1523/JNEUROSCI.2876-05.2005

Bhanpuri, N. H., Okamura, A. M., and Bastian, A. J. (2012). Active force perception depends on cerebellar function. *J. Neurophysiol.* 107, 1612–1620. doi: 10.1152/jn.00983.2011

Bhanpuri, N. H., Okamura, A. M., and Bastian, A. J. (2013). Predictive modeling by the cerebellum improves proprioception. *J. Neurosci.* 33, 14301–14306. doi: 10.1523/JNEUROSCI.0784-13.2013

Blakemore, S. J., Frith, C. D., and Wolpert, D. M. (2001). The cerebellum is involved in predicting the sensory consequences of action. *Neuroreport* 12, 1879–1884. doi: 10.1097/00001756-200107030-00023

Boccara, C. N., Sargolini, F., Thoresen, V. H., Solstad, T., Witter, M. P., Moser, E. I., et al. (2010). Grid cells in pre-and parasubiculum. *Nat. Neurosci.* 13, 987–994. doi: 10.1038/nn.2602

Bosman, L. W., Houweling, A. R., Owens, C. B., Tanke, N., Shevchouk, O. T., Rahmati, N., et al. (2011). Anatomical pathways involved in generating and sensing rhythmic whisker movements. *Front. Integr. Neurosci.* 5:53. doi: 10.3389/fnint.2011.00053

Bosman, L. W., Koekkoek, S. K., Shapiro, J., Rijken, B. F., Zandstra, F., van der Ende, B., et al. (2010). Encoding of whisker input by cerebellar Purkinje cells. *J. Physiol.* 588, 3757–3783. doi: 10.1113/jphysiol.2010.195180

Bove, M., Brichetto, G., Abbruzzese, G., Marchese, R., and Schieppati, M. (2004). Neck proprioception and spatial orientation in cervical dystonia. *Brain* 127(Pt 12), 2764–2778. doi: 10.1093/brain/awh291

Bower, J. M., and Kassel, J. (1990). Variability in tactile projection patterns to cerebellar folia crus IIA of the Norway rat. *J. Comp. Neurol.* 302, 768–778. doi: 10.1002/cne.903020409

Bremmer, F. (2011). Multisensory space: from eye−movements to self−motion. *J. Physiol.* 589, 815–823. doi: 10.1113/jphysiol.2010.195537

Brooks, J. X., and Cullen, K. E. (2009). Multimodal integration in rostral fastigial nucleus provides an estimate of body movement. *J. Neurosci.* 29, 10499–10511. doi: 10.1523/JNEUROSCI.1937-09.2009

Brooks, J. X., and Cullen, K. E. (2013). The primate cerebellum selectively encodes unexpected self-motion. *Curr. Biol.* 23, 947–955. doi: 10.1016/j.cub.2013.04.029

Brown, I. E., and Bower, J. M. (2001). Congruence of mossy fiber and climbing fiber tactile projections in the lateral hemispheres of the rat cerebellum. *J. Comp. Neurol.* 429, 59–70. doi: 10.1002/1096-9861(20000101)429:1<59::AID-CNE5>3.0.CO;2-3

Brown, I. E., and Bower, J. M. (2002). The influence of somatosensory cortex on climbing fiber responses in the lateral hemispheres of the rat cerebellum after peripheral tactile stimulation. *J. Neurosci.* 22, 6819–6829. Available online at: http://www.jneurosci.org/content/22/15/6819.long

Buckner, R. L. (2013). The cerebellum and cognitive function: 25 years of insight from anatomy and neuroimaging. *Neuron* 80, 807–815. doi: 10.1016/j.neuron.2013.10.044

Burne, R., Azizi, S., Mihailoff, G., and Woodward, D. (1981). The tectopontine projection in the rat with comments on visual pathways to the basilar pons. *J. Comp. Neurol.* 202, 287–307. doi: 10.1002/cne.902020212

Cerminara, N. L., Aoki, H., Loft, M., Sugihara, I., and Apps, R. (2013). Structural basis of cerebellar microcircuits in the rat. *J. Neurosci.* 33, 16427–16442. doi: 10.1523/JNEUROSCI.0861-13.2013

Chen, G., King, J. A., Burgess, N., and O'Keefe, J. (2013). How vision and movement combine in the hippocampal place code. *Proc. Natl. Acad. Sci. U.S.A.* 110, 378–383. doi: 10.1073/pnas.1215834110

Chen, L. L., Lin, L. H., Green, E. J., Barnes, C. A., and McNaughton, B. L. (1994). Head-direction cells in the rat posterior cortex. I. Anatomical distribution and behavioral modulation. *Exp. Brain Res.* 101, 8–23. doi: 10.1007/BF00243212

Cho, J., and Sharp, P. E. (2001). Head direction, place, and movement correlates for cells in the rat retrosplenial cortex. *Behav. Neurosci.* 115, 3–25. doi: 10.1037/0735-7044.115.1.3

Christensen, A., Giese, M. A., Sultan, F., Mueller, O. M., Goericke, S. L., Ilg, W., et al. (2014). An intact action-perception coupling depends on the integrity of the cerebellum. *J. Neurosci.* 34, 6707–6716. doi: 10.1523/JNEUROSCI.3276-13.2014

Clark, B. J., Brown, J. E., and Taube, J. S. (2012). Head direction cell activity in the anterodorsal thalamus requires intact supragenual nuclei. *J. Neurophysiol.* 108, 2767–2784. doi: 10.1152/jn.00295.2012

Cullen, K. E., Brooks, J. X., Jamali, M., Carriot, J., and Massot, C. (2011). Internal models of self-motion: computations that suppress vestibular reafference in early vestibular processing. *Exp. Brain Res.* 210, 377–388. doi: 10.1007/s00221-011-2555-9

Dean, P., and Porrill, J. (2010). The cerebellum as an adaptive filter: a general model? *Funct. Neurol.* 25, 173–180.

DeAngelis, G. C., and Angelaki, D. E. (2012). "Visual–vestibular integration for self-motion perception," in *Neural Bases of Multisensory Processes*, Chapter 31, eds M. M. Murray and M. T. Wallace (Boca Raton, FL: CRC Press). Available online at: http://www.ncbi.nlm.nih.gov/books/NBK92839/

De Zeeuw, C. I., Hansel, C., Bian, F., Koekkoek, S. K., van Alphen, A. M., Linden, D. J., et al. (1998). Expression of a protein kinase C inhibitor in Purkinje cells blocks cerebellar LTD and adaptation of the vestibulo-ocular reflex. *Neuron* 20, 495–508. doi: 10.1016/S0896-6273(00)80990-3

Diamond, M. E., von Heimendahl, M., Knutsen, P. M., Kleinfeld, D., and Ahissar, E. (2008). 'Where' and 'what' in the whisker sensorimotor system. *Nat. Rev. Neurosci.* 9, 601–612. doi: 10.1038/nrn2411

Etienne, A. S., and Jeffery, K. J. (2004). Path integration in mammals. *Hippocampus* 14, 180–192. doi: 10.1002/hipo.10173

Fyhn, M., Molden, S., Witter, M. P., Moser, E. I., and Moser, M. B. (2004). Spatial representation in the entorhinal cortex. *Science* 305, 1258–1264. doi: 10.1126/science.1099901

Gao, Z., van Beugen, B. J., and De Zeeuw, C. I. (2012). Distributed synergistic plasticity and cerebellar learning. *Nat. Rev. Neurosci.* 13, 619–635. doi: 10.1038/nrn3312

Garwicz, M., Ekerot, C. F., and Jorntell, H. (1998). Organizational principles of cerebellar neuronal circuitry. *News Physiol. Sci.* 13, 26–32.

Gdowski, G. T., and McCrea, R. A. (2000). Neck proprioceptive inputs to primate vestibular nucleus neurons. *Exp. Brain Res.* 135, 511–526. doi: 10.1007/s002210000542

Gerrits, N. M., Voogd, J., and Magras, I. N. (1985). Vestibular afferents of the inferior olive and the vestibulo-olivo-cerebellar climbing fiber pathway to the flocculus in the cat. *Brain Res.* 332, 325–336. doi: 10.1016/0006-8993(85)90601-8

Giannetti, S., and Molinari, M. (2002). Cerebellar input to the posterior parietal cortex in the rat. *Brain Res. Bull.* 58, 481–489. doi: 10.1016/S0361-9230(02)00815-8

Giolli, R. A., Blanks, R. H., and Lui, F. (2006). The accessory optic system: basic organization with an update on connectivity, neurochemistry, and function. *Prog. Brain Res.* 151, 407–440. doi: 10.1016/S0079-6123(05)51013-6

Giolli, R. A., Gregory, K. M., Suzuki, D. A., Blanks, R. H., Lui, F., and Betelak, K. F. (2001). Cortical and subcortical afferents to the nucleus reticularis tegmenti pontis and basal pontine nuclei in the macaque monkey. *Vis. Neurosci.* 18, 725–740. doi: 10.1017/S0952523801185068

Goodridge, J. P., Dudchenko, P. A., Worboys, K. A., Golob, E. J., and Taube, J. S. (1998). Cue control and head direction cells. *Behav. Neurosci.* 112:749. doi: 10.1037/0735-7044.112.4.749

Goodridge, J. P., and Taube, J. S. (1995). Preferential use of the landmark navigational system by head direction cells in rats. *Behav. Neurosci.* 109, 49–61. doi: 10.1037/0735-7044.109.1.49

Hafting, T., Fyhn, M., Molden, S., Moser, M. B., and Moser, E. I. (2005). Microstructure of a spatial map in the entorhinal cortex. *Nature* 436, 801–806. doi: 10.1038/nature03721

Hartmann, M. J. (2011). A night in the life of a rat: vibrissal mechanics and tactile exploration. *Ann. N.Y. Acad. Sci.* 1225, 110–118. doi: 10.1111/j.1749-6632.2011.06007.x

Hawkes, R., and Herrup, K. (1995). Aldolase C/zebrin II and the regionalization of the cerebellum. *J. Mol. Neurosci.* 6, 147–158. doi: 10.1007/BF02736761

Holst, E., and Mittelstaedt, H. (1950). Das reafferenzprinzip. *Naturwissenschaften* 37, 464–476. doi: 10.1007/BF00622503

Huang, C. C., Sugino, K., Shima, Y., Guo, C., Bai, S., Mensh, B. D., et al. (2013). Convergence of pontine and proprioceptive streams onto multimodal cerebellar granule cells. *Elife* 2:e00400. doi: 10.7554/eLife.00400

Ito, M. (2002). Historical review of the significance of the cerebellum and the role of Purkinje cells in motor learning. *Ann. N.Y. Acad. Sci.* 978, 273–288. doi: 10.1111/j.1749-6632.2002.tb07574.x

Itskov, P. M., Vinnik, E., and Diamond, M. E. (2011). Hippocampal representation of touch-guided behavior in rats: persistent and independent traces of stimulus and reward location. *PLoS ONE* 6:e16462. doi: 10.1371/journal.pone.0016462

Jeffery, K. J., and Burgess, N. (2006). A metric for the cognitive map: found at last? *Trends Cogn. Sci.* 10, 1–3. doi: 10.1016/j.tics.2005.11.002

Kleine, J., Guan, Y., Kipiani, E., Glonti, L., Hoshi, M., and Büttner, U. (2004). Trunk position influences vestibular responses of fastigial nucleus neurons in the alert monkey. *J. Neurophysiol.* 91, 2090–2100. doi: 10.1152/jn.00849.2003

Knierim, J. J., Kudrimoti, H. S., and McNaughton, B. L. (1998). Interactions between idiothetic cues and external landmarks in the control of place cells and head direction cells. *J. Neurophysiol.* 80, 425–446.

Kralj-Hans, I., Baizer, J. S., Swales, C., and Glickstein, M. (2007). Independent roles for the dorsal paraflocculus and vermal lobule VII of the cerebellum in visuomotor coordination. *Exp. Brain Res.* 177, 209–222. doi: 10.1007/s00221-006-0661-x

Larsell, O. (1952). The morphogenesis and adult pattern of the lobules and fissures of the cerebellum of the white rat. *J. Comp. Neurol.* 97, 281–356. doi: 10.1002/cne.900970204

Manzoni, D., Pompeiano, O., Bruschini, L., and Andre, P. (1999). Neck input modifies the reference frame for coding labyrinthine signals in the cerebellar vermis: a cellular analysis. *Neuroscience* 93, 1095–1107. doi: 10.1016/S0306-4522(99)00275-4

Marr, D. (1969). A theory of cerebellar cortex. *J. Physiol.* 202, 437–470.

May, P. J. (2006). The mammalian superior colliculus: laminar structure and connections. *Prog. Brain Res.* 151, 321–378. doi: 10.1016/S0079-6123(05)51011-2

McCrea, R. A., and Horn, A. K. (2006). Nucleus prepositus. *Prog. Brain Res.* 151, 205–230. doi: 10.1016/S0079-6123(05)51007-0

McNaughton, B. L., Mizumori, S. J., Barnes, C. A., Leonard, B. J., Marquis, M., and Green, E. J. (1994). Cortical representation of motion during unrestrained spatial navigation in the rat. *Cereb. Cortex* 4, 27–39. doi: 10.1093/cercor/4.1.27

Meredith, M. A., and Stein, B. E. (1983). Interactions among converging sensory inputs in the superior colliculus. *Science* 221, 389–391. doi: 10.1126/science.6867718

Meredith, M. A., and Stein, B. E. (1986). Visual, auditory, and somatosensory convergence on cells in superior colliculus results in multisensory integration. *J. Neurophysiol.* 56, 640–662.

Miall, R. C., and Wolpert, D. M. (1996). Forward models for physiological motor control. *Neural Netw.* 9, 1265–1279. doi: 10.1016/S0893-6080(96)00035-4

Mittelstaedt, M.-L., and Mittelstaedt, H. (1980). Homing by path integration in a mammal. *Naturwissenschaften* 67, 566–567. doi: 10.1007/BF00450672

Mizumori, S. J., and Williams, J. D. (1993). Directionally selective mnemonic properties of neurons in the lateral dorsal nucleus of the thalamus of rats. *J. Neurosci.* 13, 4015–4028.

Morissette, J., and Bower, J. M. (1996). Contribution of somatosensory cortex to responses in the rat cerebellar granule cell layer following peripheral tactile stimulation. *Exp. Brain Res.* 109, 240–250. doi: 10.1007/BF00231784

Moser, E. I., and Moser, M. B. (2008). A metric for space. *Hippocampus* 18, 1142–1156. doi: 10.1002/hipo.20483

Murphy, J. T., MacKay, W. A., and Johnson, F. (1973). Differences between cerebellar mossy and climbing fibre responses to natural stimulation of forelimb muscle proprioceptors. *Brain Res.* 55, 263–289. doi: 10.1016/0006-8993(73)90295-3

Naatanen, R., and Michie, P. T. (1979). Early selective-attention effects on the evoked potential: a critical review and reinterpretation. *Biol. Psychol.* 8, 81–136. doi: 10.1016/0301-0511(79)90053-X

Nitz, D. A. (2006). Tracking route progression in the posterior parietal cortex. *Neuron* 49, 747–756. doi: 10.1016/j.neuron.2006.01.037

Nitz, D. A. (2012). Spaces within spaces: rat parietal cortex neurons register position across three reference frames. *Nat. Neurosci.* 15, 1365–1367. doi: 10.1038/nn.3213

O'Keefe, J. (1979). A review of the hippocampal place cells. *Prog. Neurobiol.* 13, 419–439. doi: 10.1016/0301-0082(79)90005-4

O'Reilly, J. X., Mesulam, M. M., and Nobre, A. C. (2008). The cerebellum predicts the timing of perceptual events. *J. Neurosci.* 28, 2252–2260. doi: 10.1523/JNEUROSCI.2742-07.2008

Päällysaho, J., Sugita, S., and Noda, H. (1991). Brainstem mossy fiber projections to lobules VIa, VIb, c, VII, and VIII of the cerebellar vermis in the rat. *Neurosci. Res.* 12, 217–231. doi: 10.1016/0168-0102(91)90112-C

Parron, C., and Save, E. (2004). Evidence for entorhinal and parietal cortices involvement in path integration in the rat. *Exp. Brain Res.* 159, 349–359. doi: 10.1007/s00221-004-1960-8

Petrosini, L., Leggio, M. G., and Molinari, M. (1998). The cerebellum in the spatial problem solving: a co-star or a guest star? *Prog. Neurobiol.* 56, 191–210. doi: 10.1016/S0301-0082(98)00036-7

Pijpers, A., Apps, R., Pardoe, J., Voogd, J., and Ruigrok, T. J. (2006). Precise spatial relationships between mossy fibers and climbing fibers in rat cerebellar cortical zones. *J. Neurosci.* 26, 12067–12080. doi: 10.1523/JNEUROSCI.2905-06.2006

Pijpers, A., Voogd, J., and Ruigrok, T. J. (2005). Topography of olivo-corticonuclear modules in the intermediate cerebellum of the rat. *J. Comp. Neurol.* 492, 193–213. doi: 10.1002/cne.20707

Porrill, J., Dean, P., and Anderson, S. R. (2013). Adaptive filters and internal models: multilevel description of cerebellar function. *Neural Netw.* 47, 134–149. doi: 10.1016/j.neunet.2012.12.005

Quirk, G. J., Muller, R. U., and Kubie, J. L. (1990). The firing of hippocampal place cells in the dark depends on the rat's recent experience. *J. Neurosci.* 10, 2008–2017.

Quy, P. N., Fujita, H., Sakamoto, Y., Na, J., and Sugihara, I. (2011). Projection patterns of single mossy fiber axons originating from the dorsal column nuclei mapped on the aldolase C compartments in the rat cerebellar cortex. *J. Comp. Neurol.* 519, 874–899. doi: 10.1002/cne.22555

Ranck, J. B. Jr. (1984). Head direction cells in the deep cell layer of dorsal presubiculum in freely moving rats. *Soc. Neurosci. Abstr.* 10, 599.

Ravassard, P., Kees, A., Willers, B., Ho, D., Aharoni, D., Cushman, J., et al. (2013). Multisensory control of hippocampal spatiotemporal selectivity. *Science* 340, 1342–1346. doi: 10.1126/science.1232655

Restuccia, D., Della Marca, G., Valeriani, M., Leggio, M. G., and Molinari, M. (2007). Cerebellar damage impairs detection of somatosensory input changes. A somatosensory mismatch-negativity study. *Brain* 130(Pt 1), 276–287. doi: 10.1093/brain/awl236

Rochefort, C., Arabo, A., André, M., Poucet, B., Save, E., and Rondi-Reig, L. (2011). Cerebellum shapes hippocampal spatial code. *Science* 334, 385–389. doi: 10.1126/science.1207403

Rochefort, C., Lefort, J., and Rondi-Reig, L. (2013). The cerebellum: a new key structure in the navigation system. *Front. Neural Circuits* 7:35. doi: 10.3389/fncir.2013.00035

Rondi-Reig, L., and Burguière, E. (2005). Is the cerebellum ready for navigation? *Prog. Brain Res.* 148, 199–212. doi: 10.1016/S0079-6123(04)48017-0

Rondi-Reig, L., Le Marec, N., Caston, J., and Mariani, J. (2002). The role of climbing and parallel fibers inputs to cerebellar cortex in navigation. *Behav. Brain Res.* 132, 11–18. doi: 10.1016/S0166-4328(01)00381-3

Roy, J. E., and Cullen, K. E. (2004). Dissociating self-generated from passively applied head motion: neural mechanisms in the vestibular nuclei. *J. Neurosci.* 24, 2102–2111. doi: 10.1523/JNEUROSCI.3988-03.2004

Ruigrok, T. J. (2003). Collateralization of climbing and mossy fibers projecting to the nodulus and flocculus of the rat cerebellum. *J. Comp. Neurol.* 466, 278–298. doi: 10.1002/cne.10889

Ruigrok, T. J. H. (2004). "Precerebellar nuclei and red nucleus," in *The Rat Nervous System*, ed G. Paxinos (San Diego, CA: Elsevier Academic Press), 167–204.

Sargolini, F., Fyhn, M., Hafting, T., McNaughton, B. L., Witter, M. P., Moser, M. B., et al. (2006). Conjunctive representation of position, direction, and velocity in entorhinal cortex. *Science* 312, 758–762. doi: 10.1126/science.1125572

Schmahmann, J. D., and Sherman, J. C. (1998). The cerebellar cognitive affective syndrome. *Brain* 121(Pt 4), 561–579. doi: 10.1093/brain/121.4.561

Schonewille, M., Luo, C., Ruigrok, T. J., Voogd, J., Schmolesky, M. T., Rutteman, M., et al. (2006). Zonal organization of the mouse flocculus: physiology, input, and output. *J. Comp. Neurol.* 497, 670–682. doi: 10.1002/cne.21036

Schroeder, C. L., and Hartmann, M. J. (2012). Sensory prediction on a whiskered robot: a tactile analogy to "optical flow". *Front. Neurorobot.* 6:9. doi: 10.3389/fnbot.2012.00009

Shaikh, A. G., Meng, H., and Angelaki, D. E. (2004). Multiple reference frames for motion in the primate cerebellum. *J. Neurosci.* 24, 4491–4497. doi: 10.1523/JNEUROSCI.0109-04.2004

Shinder, M. E., and Taube, J. S. (2010). Differentiating ascending vestibular pathways to the cortex involved in spatial cognition. *J. Vestib. Res.* 20, 3–23. doi: 10.3233/VES-2010-0344

Simpson, J. I., Leonard, C. S., and Soodak, R. E. (1988). The accessory optic system of rabbit. II. Spatial organization of direction selectivity. *J. Neurophysiol.* 60, 2055–2072.

Smith, P. F., and Zheng, Y. (2013). From ear to uncertainty: vestibular contributions to cognitive function. *Front. Integr. Neurosci.* 7:84. doi: 10.3389/fnint.2013.00084

Soodak, R. E., and Simpson, J. I. (1988). The accessory optic system of rabbit. I. Basic visual response properties. *J. Neurophysiol.* 60, 2037–2054.

Spiers, H. J., and Maguire, E. A. (2006). Thoughts, behaviour, and brain dynamics during navigation in the real world. *Neuroimage* 31, 1826–1840. doi: 10.1016/j.neuroimage.2006.01.037

Stackman, R. W., Clark, A. S., and Taube, J. S. (2002). Hippocampal spatial representations require vestibular input. *Hippocampus* 12, 291–303. doi: 10.1002/hipo.1112

Stackman, R. W., and Herbert, A. M. (2002). Rats with lesions of the vestibular system require a visual landmark for spatial navigation. *Behav. Brain Res.* 128, 27–40. doi: 10.1016/S0166-4328(01)00270-4

Stackman, R. W., and Taube, J. S. (1997). Firing properties of head direction cells in the rat anterior thalamic nucleus: dependence on vestibular input. *J. Neurosci.* 17, 4349–4358.

Stackman, R. W., and Taube, J. S. (1998). Firing properties of rat lateral mammillary single units: head direction, head pitch, and angular head velocity. *J. Neurosci.* 18, 9020–9037.

Stock, A. K., Wascher, E., and Beste, C. (2013). Differential effects of motor efference copies and proprioceptive information on response evaluation processes. *PLoS ONE* 8:e62335. doi: 10.1371/journal.pone.0062335

Stuttgen, M. C., Kullmann, S., and Schwarz, C. (2008). Responses of rat trigeminal ganglion neurons to longitudinal whisker stimulation. *J. Neurophysiol.* 100, 1879–1884. doi: 10.1152/jn.90511.2008

Sugihara, I., and Shinoda, Y. (2004). Molecular, topographic, and functional organization of the cerebellar cortex: a study with combined aldolase C and olivocerebellar labeling. *J. Neurosci.* 24, 8771–8785. doi: 10.1523/JNEUROSCI.1961-04.2004

Sugihara, I., Wu, H., and Shinoda, Y. (1999). Morphology of single olivocerebellar axons labeled with biotinylated dextran amine in the rat. *J. Comp. Neurol.* 414, 131–148.

Swenson, R. S., and Castro, A. J. (1983). The afferent connections of the inferior olivary complex in rats: a study using the retrograde transport of horseradish peroxidase. *Am. J. Anat.* 166, 329–341. doi: 10.1002/aja.1001660307

Swenson, R., Sievert, C., Terreberry, R., Neafsey, E., and Castro, A. (1989). Organization of cerebral cortico-olivary projections in the rat. *Neurosci. Res.* 7, 43–54. doi: 10.1016/0168-0102(89)90036-9

Taube, J. S. (1995). Head direction cells recorded in the anterior thalamic nuclei of freely moving rats. *J. Neurosci.* 15(1 Pt 1), 70–86.

Taube, J. S. (2007). The head direction signal: origins and sensory-motor integration. *Annu. Rev. Neurosci.* 30, 181–207. doi: 10.1146/annurev.neuro.29.051605.112854

Taube, J. S., Muller, R. U., and Ranck, J. (1990a). Head-direction cells recorded from the postsubiculum in freely moving rats. I. Description and quantitative analysis. *J. Neurosci.* 10, 420–435.

Taube, J. S., Muller, R. U., and Ranck, J. B. (1990b). Head-direction cells recorded from the postsubiculum in freely moving rats. II. Effects of environmental manipulations. *J. Neurosci.* 10, 436–447.

Thunnissen, I., Epema, A., and Gerrits, N. (1989). Secondary vestibulocerebellar mossy fiber projection to the caudal vermis in the rabbit. *J. Comp. Neurol.* 290, 262–277. doi: 10.1002/cne.902900207

Valjamae, A. (2009). Auditorily-induced illusory self-motion: a review. *Brain Res. Rev.* 61, 240–255. doi: 10.1016/j.brainresrev.2009.07.001

Van Ham, J. J., and Yeo, C. H. (1992). Somatosensory trigeminal projections to the inferior olive, cerebellum and other precerebellar nuclei in rabbits. *Eur. J. Neurosci.* 4, 302–317. doi: 10.1111/j.1460-9568.1992.tb00878.x

Voogd, J., and Barmack, N. H. (2006). Oculomotor cerebellum. *Prog. Brain Res.* 151: 231–268. doi: 10.1016/S0079-6123(05)51008-2

Watson, T. C., Koutsikou, S., Cerminara, N. L., Flavell, C. R., Crook, J. J., Lumb, B. M., et al. (2013). The olivo-cerebellar system and its relationship to survival circuits. *Front. Neural Circuits* 7:72. doi: 10.3389/fncir.2013.00072

Whitlock, J. R., Pfuhl, G., Dagslott, N., Moser, M. B., and Moser, E. I. (2012). Functional split between parietal and entorhinal cortices in the rat. *Neuron* 73, 789–802. doi: 10.1016/j.neuron.2011.12.028

Wiener, S. I. (1993). Spatial and behavioral correlates of striatal neurons in rats performing a self-initiated navigation task. *J. Neurosci.* 13, 3802–3817.

Winkelman, B., and Frens, M. (2006). Motor coding in floccular climbing fibers. *J. Neurophysiol.* 95, 2342–2351. doi: 10.1152/jn.01191.2005

Wylie, D. R., Glover, R. G., and Aitchison, J. D. (1999). Optic flow input to the hippocampal formation from the accessory optic system. *J. Neurosci.* 19, 5514–5527.

Yakusheva, T. A., Shaikh, A. G., Green, A. M., Blazquez, P. M., Dickman, J. D., and Angelaki, D. E. (2007). Purkinje cells in posterior cerebellar vermis encode motion in an inertial reference frame. *Neuron* 54, 973–985. doi: 10.1016/j.neuron.2007.06.003

Yatim, N., Billig, I., Compoint, C., Buisseret, P., and Buisseret-Delmas, C. (1996). Trigeminocerebellar and trigemino-olivary projections in rats. *Neurosci. Res.* 25, 267–283. doi: 10.1016/0168-0102(96)01061-9

Yoder, R. M., Clark, B. J., Brown, J. E., Lamia, M. V., Valerio, S., Shinder, M. E., et al. (2011). Both visual and idiothetic cues contribute to head direction cell stability during navigation along complex routes. *J. Neurophysiol.* 105, 2989–3001. doi: 10.1152/jn.01041.2010

Yoder, R. M., and Taube, J. S. (2014). The vestibular contribution to the head direction signal and navigation. *Front. Integr. Neurosci.* 8:32. doi: 10.3389/fnint.2014.00032

Zheng, Y., Goddard, M., Darlington, C. L., and Smith, P. F. (2007). Bilateral vestibular deafferentation impairs performance in a spatial forced alternation task in rats. *Hippocampus* 17, 253–256. doi: 10.1002/hipo.20266

Conflict of Interest Statement: The authors declare that the research was conducted in the absence of any commercial or financial relationships that could be construed as a potential conflict of interest.

Received: 17 June 2014; paper pending published: 07 August 2014; accepted: 01 October 2014; published online: 04 November 2014.
*Citation: Rondi-Reig L, Paradis A-L, Lefort JM, Babayan BM and Tobin C (2014) How the cerebellum may monitor sensory information for spatial representation. Front. Syst. Neurosci. **8**:205. doi: 10.3389/fnsys.2014.00205*
This article was submitted to the journal Frontiers in Systems Neuroscience.

frontiers in
SYSTEMS NEUROSCIENCE

REVIEW ARTICLE
published: 17 June 2014
doi: 10.3389/fnsys.2014.00113

The cerebellum for jocks and nerds alike

Laurentiu S. Popa, Angela L. Hewitt and Timothy J. Ebner*

Department of Neuroscience, University of Minnesota, Minneapolis, MN, USA

Edited by:
Richard Apps, University of Bristol, UK

Reviewed by:
Yosef Yarom, Hebrew University, Israel
Henrik Jörntell, Lund University, Sweden

****Correspondence:***
Timothy J. Ebner, Department of Neuroscience, University of Minnesota, Lions Research Building, Room 421, 2001 Sixth Street S.E., Minneapolis, MN 55455, USA
e-mail: ebner001@umn.edu

Historically the cerebellum has been implicated in the control of movement. However, the cerebellum's role in non-motor functions, including cognitive and emotional processes, has also received increasing attention. Starting from the premise that the uniform architecture of the cerebellum underlies a common mode of information processing, this review examines recent electrophysiological findings on the motor signals encoded in the cerebellar cortex and then relates these signals to observations in the non-motor domain. Simple spike firing of individual Purkinje cells encodes performance errors, both predicting upcoming errors as well as providing feedback about those errors. Further, this dual temporal encoding of prediction and feedback involves a change in the sign of the simple spike modulation. Therefore, Purkinje cell simple spike firing both predicts and responds to feedback about a specific parameter, consistent with computing sensory prediction errors in which the predictions about the consequences of a motor command are compared with the feedback resulting from the motor command execution. These new findings are in contrast with the historical view that complex spikes encode errors. Evaluation of the kinematic coding in the simple spike discharge shows the same dual temporal encoding, suggesting this is a common mode of signal processing in the cerebellar cortex. Decoding analyses show the considerable accuracy of the predictions provided by Purkinje cells across a range of times. Further, individual Purkinje cells encode linearly and independently a multitude of signals, both kinematic and performance errors. Therefore, the cerebellar cortex's capacity to make associations across different sensory, motor and non-motor signals is large. The results from studying how Purkinje cells encode movement signals suggest that the cerebellar cortex circuitry can support associative learning, sequencing, working memory, and forward internal models in non-motor domains.

Keywords: performance errors, sensory prediction errors, internal models, Purkinje cells, cognition

INTRODUCTION

The role of the cerebellum in the nervous system remains controversial. Traditionally, cerebellar function has been viewed in the context of motor control, given the well-established fact that cerebellar insults result in movement deficits. Different aspects of the cerebellum's involvement in motor control have generated multiple hypotheses regarding cerebellar function including movement timing (Braitenberg and Atwood, 1958; Keele and Ivry, 1990; Welsh et al., 1995; O'Reilly et al., 2008), error detection and correction (Oscarsson, 1980), motor learning (Marr, 1969; Albus, 1971; Gilbert and Thach, 1977; Ito, 2002), and providing internal models (Wolpert et al., 1998; Kawato, 1999; Imamizu et al., 2000; Morton and Bastian, 2006; Shadmehr et al., 2010).

More recently, evidence for cerebellar involvement in non-motor processes such as cognition, emotions and social interaction has accumulated at a rapid pace. The findings include the rapid expansion of the cerebellar hemispheres in primates (Leiner et al., 1986, 1989) with development of projections between the cerebellum and non-motor cortical areas (Schmahmann and Pandya, 1989, 1991, 1997; Middleton and Strick, 1994, 2001; Kelly and Strick, 2003), cerebellar activation related to cognitive behaviors (Petersen et al., 1988; Kim et al., 1994; Hayter et al., 2007), cognitive and emotional dysfunction associated with cerebellar lesions/disease (Fiez et al., 1992; Schmahmann, 2004; Burk, 2007), and the influence on cognitive processes by manipulating cerebellar excitability (Ferrucci et al., 2008; Pope and Miall, 2012; Boehringer et al., 2013). These contributions to non-motor behaviors raise the question of whether the cerebellum performs specific computations/functions in different domains or performs a common process across all domains. Based on its stereotypical architecture, a plausible and parsimonious hypothesis is that the cerebellum performs a uniform process in both motor and non-motor processes (Schmahmann, 2000, 2010; Ramnani, 2006; Thach, 2007; Ito, 2008). An important implication of this hypothesis is that understanding cerebellar information processing in the motor domain can illuminate the contributions of the cerebellum in non-motor domains.

Working from the common processing viewpoint, this review argues that the present state of our understanding of the cerebellum's role in motor behavior can shed light on non-motor functions. Several authors have taken a similar perspective (Ito, 2008; Imamizu and Kawato, 2009; Pezzulo, 2011; Pezzulo et al., 2012). An advantage of applying a motor control view to non-motor processing is that subjects, including non-human primates, can be

required to perform extremely demanding motoric tasks in highly controlled environments. Despite task complexity, motor behavior can be described and quantified by well-defined measures, allowing intimate and unambiguous access to cerebellar signals. Therefore, this review evaluates the motor signals encoded by cerebellar neurons, including the existence of a new class of signals in Purkinje cell simple spike activity related to performance errors, as well as a dual encoding mechanism for motor parameters (Hewitt et al., 2011; Popa et al., 2012). Together, these signals could provide the neural substrate for computing sensory prediction errors postulated by internal model hypotheses (Wolpert and Ghahramani, 2000; Mazzoni and Krakauer, 2006; Shadmehr et al., 2010). We suggest these new findings regarding simple spike signaling in motor behaviors provide insights into cerebellar function that could help understanding cerebellar involvement in non-motor domains.

CEREBELLUM AND MOTOR DOMAIN

KINEMATIC SIGNALS

Numerous studies have documented that simple spike activity encodes kinematic variables, including position, velocity, speed and acceleration that describe body part motions without consideration of their causes such as forces or joint torques. This common encoding of kinematics is true for different effectors and motor behaviors. In the intermediate zone and its neighboring lateral zones surrounding the primary fissure, Purkinje cells encode position, direction, amplitude, velocity and speed of arm movements (Thach, 1970; Harvey et al., 1977; Mano and Yamamoto, 1980; Marple-Horvat and Stein, 1987; Fortier et al., 1989; Fu et al., 1997; Coltz et al., 1999; Roitman et al., 2005; Pasalar et al., 2006). These regions in the monkey are analogous to the regions in the human cerebellum engaged during limb movements (Stoodley and Schmahmann, 2009; Timmann et al., 2009). In the floccular complex, Purkinje cells encode eye position, velocity and acceleration during smooth pursuit and ocular following (Stone and Lisberger, 1990; Shidara et al., 1993; Gomi et al., 1998; Medina and Lisberger, 2009). In the posterior vermis, similar kinematic encoding of the eye movements is present for saccades and smooth pursuit (Thier et al., 2002; Dash et al., 2013). An important issue in interpreting these results is the possible confound between effector kinematics and kinetics (Shidara et al., 1993; Ebner et al., 2011). However, a study designed to eliminate this confound demonstrated that Purkinje cells do not encode kinetics or muscle activity during manual tracking (Pasalar et al., 2006). We conclude that the representations of kinematics in the simple spike activity are unambiguous and ubiquitous, suggesting that the cerebellar cortex performs common processing for very different movements and effectors.

However, other confounds present in some experimental paradigms have introduced ambiguity in the results. For example, saccadic eye movements, circular tracking, and center-out reach all introduce high degrees of correlation among kinematic parameters (Paninski et al., 2004; Hewitt et al., 2011). Further, most paradigms do not provide a uniform or complete coverage of the work space of kinematic variables. Another confound in assessing if cell firing leads kinematics, required of forward internal hypotheses (Miall and Wolpert, 1996; Bastian, 2006; Shadmehr et al., 2010), is the predictability found in many tasks. Task predictability introduces the possibility that leading simple spike activity could be due to expectations related to upcoming trials rather than predicting the consequences of the motor command.

A random tracking task, briefly described in **Figures 1A,B,** eliminates or reduces these experimental problems and allows for a more systematic evaluation of how arm kinematics are encoded (Paninski et al., 2004). Therefore, we evaluated Purkinje cell firing during random tracking and verified that position, velocity and speed of the limb (denoted in **Figure 1B** by the C subscripted variables) were statistically independent (Hewitt et al., 2011). For a large majority of Purkinje cells, simple spike firing is modulated in relation to these kinematic parameters. The firing of individual Purkinje cells was characterized using lagged linear regressions of the simple spike firing with kinematics, identifying significant correlations and the timing of the strongest correlations (lead and/or lag). A similar approach has been used by a number of cerebellar investigators (Shidara et al., 1993; Gomi et al., 1998; Medina and Lisberger, 2009). Comparing the regression results based on individual parameters with those based on multiple parameters shows that signals encoding single parameters are mutually independent. Velocity is the dominant parameter, followed by position and then speed (Hewitt et al., 2011; Popa et al., 2012). The lead/lag values, the time intervals by which the neural activity leads (negative values) or lags (positive values) motor behavior, show a negative bias in which the simple spike firing tends to lead motor behavior, as observed in other studies (Marple-Horvat and Stein, 1987; Coltz et al., 1999; Roitman et al., 2005; Medina and Lisberger, 2009). Given the unpredictability of random tracking, this observation strongly supports the assumption that a majority of Purkinje cells predict the kinematic consequences of motor commands. However, the wide distribution of leads and lags, including both negative and positive values, also suggests the presence of both predictive and feedback signals (Marple-Horvat and Stein, 1987; Fu et al., 1997; Roitman et al., 2005). Remarkably, using the coefficients determined during random tracking allowed an accurate reconstruction of the simple spike activity recorded during different tasks, including circular tracking and center-out reach (Hewitt et al., 2011), strongly suggesting that the representations of arm kinematics are task-independent. This implies that a single global limb model is used widely as opposed to requiring large numbers of internal models for specific movements (Wolpert and Kawato, 1998; Imamizu et al., 2003, 2007).

It is possible that the temporal relationships between cerebellar signals and motor behavior reflect hard-wired circuitry properties like synaptic delays and conduction times in which the distribution of lead/lag populations would be normal, centered on well-defined time values. However, the distribution of the lead/lag values of the cerebellar signals during random tracking is extremely broad and quasi-uniform (Hewitt et al., 2011). This observation suggests that the temporal properties of the cerebellar signals are the results of computational processes reflecting the temporal constrains and requirements necessary to execute motor behaviors. For example, as internal model predictions are expected in various motor sequences involved in implementation of motor behavior, the predictions need to be "broadcasted" over

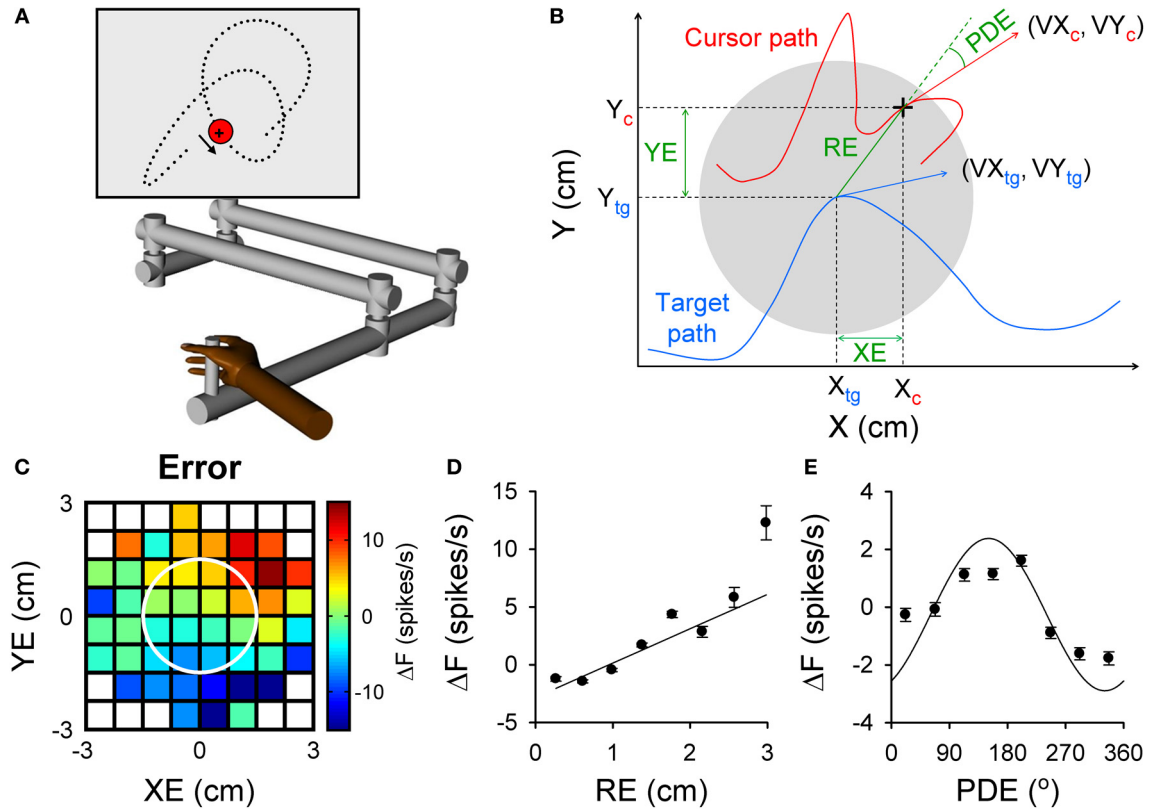

FIGURE 1 | Purkinje cell simple spike modulation in relation to task errors and hand kinematics during random tracking. (A) Using a robot manipulandum, moving in an horizontal plane, monkeys track a randomly moving target on a vertical screen, by keeping the cross-shaped cursor within the target (3 cm in diameter). Excursions of the cursor outside target area longer than 500 ms result in trial abort. **(B)** Geometry of the motor parameters. Target (gray circle) moves on a random trajectory (blue trace). Cursor (black cross) maps the hand movement (red trace). Hand kinematic parameters are position (X_c and Y_c), velocity (VX_c and VY_c) and speed (magnitude of the hand velocity vector). Performance error parameters are position error (XE and YE) and RE (magnitude of the position error vector) and position director error (PDE—the difference between the direction of the position error vector and direction of hand movement). **(C–E)** Simple spike modulation for an example Purkinje cell is plotted in relation to performance errors: XE and YE **(C)**, RE **(D)**, and PDE **(E)**. In **(C)** the firing rate is color coded relative to overall mean firing and in relation to the target (white circle). Plots of the simple spike firing with each error parameter based on the optimal τ obtained from the lagged regressions. **(A)** is reproduced from Hewitt et al. (2011) and **(B–E)** from Popa et al. (2012) with permission.

a wide range of time intervals. The temporal properties of the kinematic representation are specific to different structures and regions. For example, in the primary motor cortex the distribution of the kinematic leads/lags during a continuous spiral tracing experiment is uni-modal and centered around a 100 ms lead, as determined from signals conveying very accurate representations of the trajectory, while premotor cortex leads/lags are distributed bi-modally around 250 and 0 ms (Moran and Schwartz, 1999). Also, the timing of the signals in the motor cortices are dependent on trajectory curvature (Moran and Schwartz, 1999), while the cerebellar representations are independent of the curvature (Hewitt et al., 2011). These findings highlight fundamental functional differences in kinematic signaling in the cerebellum vs. the motor cortical areas.

ERROR PROCESSING IN THE CEREBELLUM—COMPLEX SPIKES OR SIMPLE SPIKES?

Error processing has been a long-standing hypothesis of cerebellar function, (Oscarsson, 1980) and there is a long history of studies focused on identifying error-related signals in cerebellar activity. The dominant hypothesis is that the error signals are encoded by the complex spike discharge of Purkinje cells (Oscarsson, 1980; Ito, 2000). An error encoding role of complex spikes has been proposed, not only in the motor domain, but also in the cerebellum's role in non-motor behaviors (Ito, 2008; Schmahmann, 2010; Koziol et al., 2012; Yamazaki and Nagao, 2012). Observations favoring this hypothesis in the motor domain are the complex spike modulation occurring with retinal-slip (Graf et al., 1988; Barmack and Shojaku, 1995; Kobayashi et al., 1998) and induced saccadic errors during eye movements (Soetedjo et al., 2008). Also, complex spike discharge modulates with reach end point errors (Kitazawa et al., 1998), learning a predictable target redirection during smooth pursuit (Medina and Lisberger, 2008), redirection of reaching (Kim et al., 1987), responding to unexpected loads (Gilbert and Thach, 1977), and adaptation to visuomotor transformations (Ojakangas and Ebner, 1994). However, many other experiments found no clear relationship between motor errors and complex spike discharge. Complex spike modulation

could not be related to direction or speed errors during center-out reaching (Ebner et al., 2002) nor with eye movement errors during saccade and smooth pursuit learning (Catz et al., 2005; Dash et al., 2010). Also, perturbations and performance errors during reaching in cats failed to evoke responses in inferior olive neurons, the origin of the climbing fiber projection (Horn et al., 1996). An intriguing observation is that complex spike modulation in the oculomotor vermis occurs late in eye movement adaptation and persists after learning has stabilized (Catz et al., 2005; Dash et al., 2010; Prsa and Thier, 2011), which is inconsistent with the traditional error signal hypothesis. Additionally, complex spike error signals occur in a small fraction of trials and are evident only after extensive averaging (Ojakangas and Ebner, 1994; Kitazawa et al., 1998). Also, the very low complex spike firing frequency provides a limited bandwidth to encode the continuous error signals that occur during movements (Ebner et al., 2011).

An open question is whether simple spike discharge encodes errors. Until recently there was limited information on the presence of error signals in the simple spike discharge. In a reaching task, the simple spike activity was modulated with trial success or failure (Greger and Norris, 2005). During manual tracking, simple spike discharge was correlated with direction and speed errors (Roitman et al., 2009), however, the interpretation was confounded because the error parameters were not statistically independent from the kinematics. Instructive signals in the simple spike firing contribute to cerebellar-dependent learning in the vestibulo-ocular reflex (Ke et al., 2009), also suggesting the presence of error signals.

The random tracking paradigm has numerous advantages for addressing these questions about simple spike error encoding. Random tracking involves a high degree of difficulty and the monkeys make frequent excursions outside the target area that require correction in 500 ms to avoid a trial abort (Hewitt et al., 2011). As a result, the task requires continuous evaluation of motor performance and implementing corrective movements to compensate for errors. Performance errors, defined as the divergence between the current movement goal and the consequence of the motor commands, were characterized based on the relative movement between the target center and the hand-controlled cursor. The performance errors evaluated included the cursor position relative to the target center (XE and YE), the distance between cursor and target center (RE) and angular distance from the direction necessary to move from the current position to the target center (PDE) (Popa et al., 2012). These defined performance errors, depicted in **Figure 1B**, assume that the target center is the current movement goal. Accordingly, the probability density functions of the kinematics and performance measures show the animals strive to keep the cursor in the center of the target and prefer to move toward the target center. It is interesting to note that the error parameters, although related to arm movement, are independent of the kinematic variables, thus forming a novel, non-kinematic class of motor variables related to task execution.

We found that simple spike firing robustly modulates with all four error parameters. As shown for an example Purkinje cell in **Figure 1**, the simple spike activity increases with both XE and YE, resulting in a planar pattern characterized by increased firing in the upper right quadrant and decreased firing in the lower left quadrant of the circular target (**Figure 1C**). Firing increases linearly with RE (**Figure 1D**) and modulates with PDE (**Figure 1E**), demonstrating that individual Purkinje cells can simultaneously encode a complex representation of performance errors. The frequency of significant error-related modulation was extremely high, with over 90% of Purkinje cells modulated with respect to XE, YE, and RE and over 80% with PDE. In contrast with the view that error coding is relegated to the complex spike discharge, simple spike firing carries a wealth of information about performance errors.

DUAL TEMPORAL ENCODING OF ERRORS

An intriguing aspect of the simple spike modulation with these error parameters is the temporal properties. A natural assumption would be that Purkinje cell firing either leads or lags the behavior by a single, constant time interval at which the firing pattern best correlates with the behavioral parameter. However, examination of the simple spike modulation at different leads and lags reveals a different story. In the example shown in **Figure 2**, maps of the simple spike firing relative to XE and YE show a modulation pattern characterized by high firing in the lower right quadrant at −480 to −400 ms (i.e., leading the position error) that fades as the time shift approaches 0 ms. Therefore, firing precedes the position errors by 400 ms and suggests simple spike encoding predicts the sensory consequences of the motor command. However, a new modulation pattern emerges at a lag of approximately 100 ms, with high firing at the target edge, except for the lower right quadrant of the error space. This new modulation pattern then fades as the lags approach 500 ms. Therefore, the simple spike firing also lags position error by 100 ms suggesting that firing is modulated by sensory feedback. Interestingly, the modulation patterns at different leads and lags are complementary: the region of high firing at lead time (−400 ms) coincides with the region of low firing at lag time (100 ms). This example shows that encoding of error parameters by individual cells can include both a prediction of the sensory consequences of motor commands as well as sensory feedback.

The analyses designed to quantify and characterize the encoding of the error variables across the population of Purkinje cells had to clear two hurdles. The first was to capture the complex temporal properties described above. To accomplish this, we used repeated linear regressions of the instantaneous firing against the error parameters at all lags to characterize the temporal relationships between Purkinje cell firing and behavioral variables. The second hurdle was to ensure that the encoding is not due to interactions with other variables, such as kinematics. Here we used linear regressions for each error parameter based on residual firing that was obtained by eliminating the firing variability associated with known variables such as kinematics and the other error parameters (Popa et al., 2012). These analyses yield, as functions of the lead or lag (τ), measures of the goodness of fit [the coefficient of determination (R^2)] and firing sensitivity [the regression coefficients (β)] for each parameter. **Figure 3** exemplifies the R^2 and β profiles computed only for XE (A,B, respectively) and YE (D,E, respectively) although the cell (the same as in **Figure 1**) significantly encodes all errors (XE, YE, RE, and PDE). Both R^2 profiles are bi-modal (**Figures 3A,D**), with

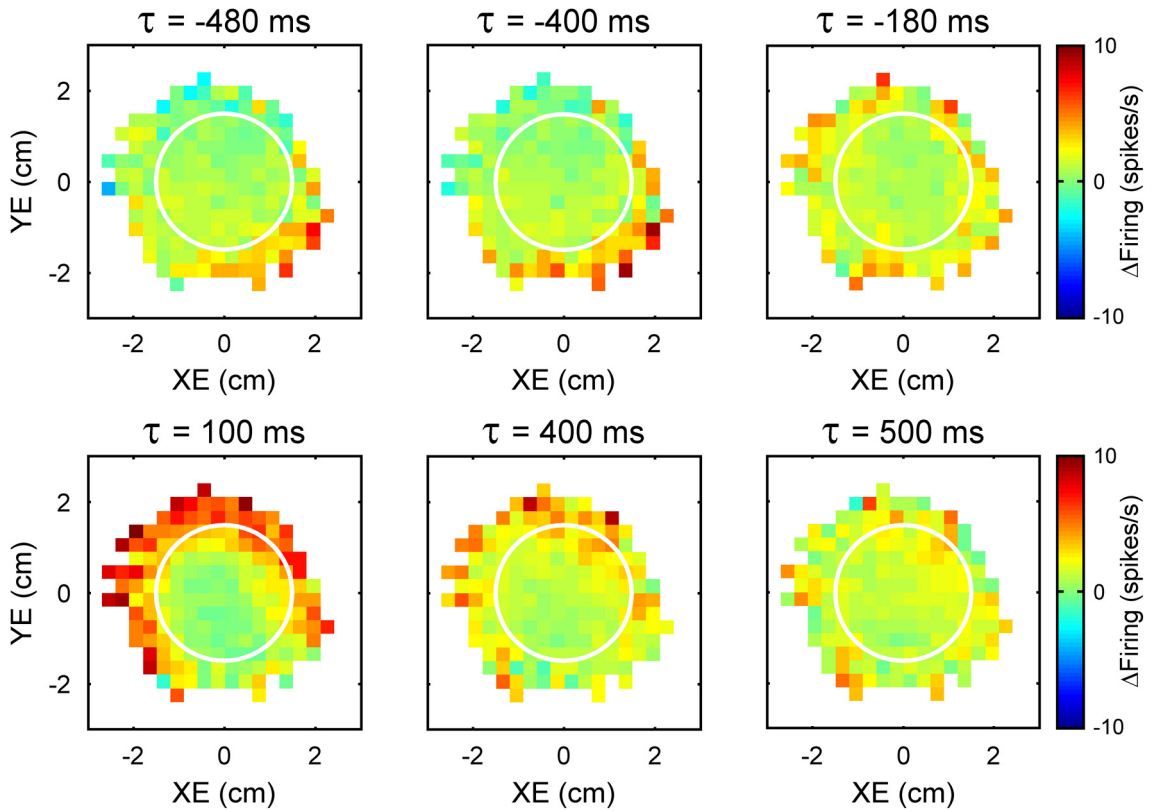

FIGURE 2 | Time course of the simple spike modulation with performance errors. Each plot is the simple spike firing in relation to XE and YE as a function of time (τ) from an example Purkinje cell. Negative τ represents the firing leading the error signals. As in **Figure 1**, simple spike firing rate is color coded relative to overall mean firing and in relation to the target (white circle).

two local maxima. Each R^2 profile has a peak at negative time values (XE at −400 ms and YE at −300 ms) and a peak at positive time values (XE at 200 ms and YE at 250 ms). Our interpretation of these observations is that XE and YE are dually encoded by predictive and feedback-related signals in the simple spike discharge of a single cell. Importantly, the discharge sensitivity changes sign for both β profiles, with negative values for the predictive representations and positive values for the feedback representations (**Figures 3B,E**), showing opposing modulations for the predictive and feedback signals encoding the same behavioral parameter. Dual temporal encoding is common. It was observed in 72% of Purkinje cells and 74% of dually encoded parameters show opposing modulations between predictive and feedback signals (Popa et al., 2012). Interestingly, a similar dual encoding mechanism was discovered when monkeys perform a rule processing task where the signals between prefrontal and parietal cortices exhibit dual timing at 50 and 150 ms with anti-correlated modulation (Crowe et al., 2013).

The presence and ubiquity of the dual error signal representations can be interpreted in the context of internal models. Many researchers have postulated that the cerebellum acts as a forward internal model that predicts the sensory consequences of a motor command (Robinson, 1975; Miall and Wolpert, 1996; Wolpert and Ghahramani, 2000; Bastian, 2006; Shadmehr et al., 2010). Integral to implementing a forward internal model is comparing the prediction of the sensory consequences with the actual sensory feedback to compute sensory prediction errors. Sensory prediction errors are the critical signals that drive adaptation of both eye and limb movements (Wallman and Fuchs, 1998; Noto and Robinson, 2001; Mazzoni and Krakauer, 2006; Shadmehr et al., 2010). Functional imaging and patient studies suggest the cerebellum is involved in error processing, including sensory prediction errors (Diedrichsen et al., 2005; Morton and Bastian, 2006; Tseng et al., 2007; Xu-Wilson et al., 2009; Izawa et al., 2012).

Decoding analysis allows one to test whether the simple spike error signals in a population of Purkinje cells contain sufficient information to understand the behavior. **Figure 3C,F** show the results for decoding the predictions for XE and YE, respectively. Decoded values have highly linear correlations with the observed values for all error variables. Moreover, for XE, YE, and PDE the slope is very close to unity, showing that the Purkinje cell population provides a remarkably accurate prediction of the upcoming errors. As we have noted (Popa et al., 2012), there is some degradation of the decoding accuracy toward the boundaries of the error space that reflects either the relative scarcity of data points or that the predictions are confined to the space relevant for successfully performing the task.

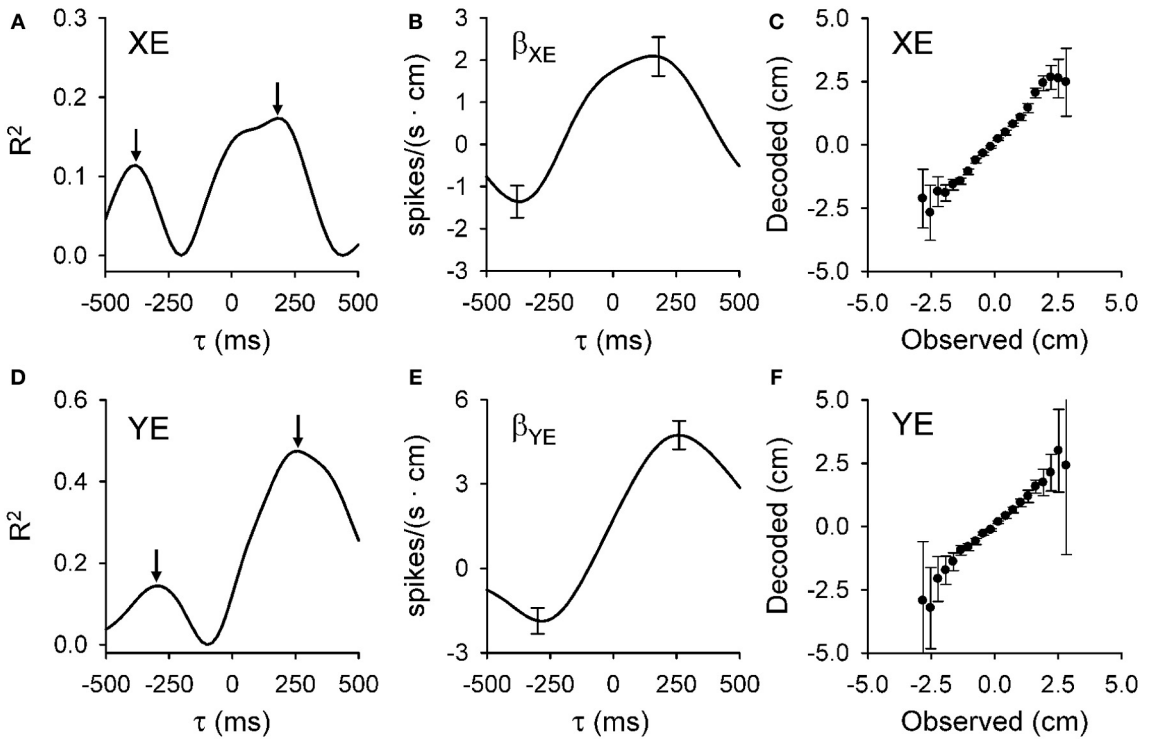

FIGURE 3 | Dual temporal encoding of error signals. (A,D) R^2 as a function of lead/lag (τ) for position error parameters (XE and YE, respectively) from the Purkinje cell shown in **Figure 1**. **(B,E)** Regression coefficients for XE (β_{XE}) and YE (β_{YE}) as a function of τ. Arrows denote the times of the significant R^2 peaks and error bars the confidence intervals of β_{XE} and β_{YE} at the times of the R^2 maxima [arrows in **(A,D)**, respectively]. Note change in the sign of regression coefficient showing the reversal in the firing sensitivity at predictive versus feedback timing. **(C,F)** Plot of the decoded upcoming XE and YE (mean ± *SD*) versus observed based on the population of Purkinje cells. Slope of decoded estimate versus the observed is 0.99 ($\rho = 0.95$, $p < 0.001$) for XE and 0.98 ($\rho = 0.83$, $p < 0.001$) for YE showing the accuracy of the prediction. Decoding estimates were from 25 repetitions of the off-line decoding algorithm (see Popa et al., 2012). Plots are reproduced from Popa et al. (2012) with permission.

We hypothesized that the dual encoding of performance errors provides the neural substrate needed to generate sensory prediction errors. For the majority of Purkinje cells, the prediction and feedback error signals have opposing effects on simple spike modulations, precisely as required to compute the difference between the predicted and the actual feedback. Dual encoding could result in reduced simple spike sensitivity to self-generated sensory information whereby the presence of both the predicted consequences of the motor commands and sensory feedback signals act to cancel each other. Consistent with this interpretation, Purkinje cells show greater sensitivity to passive self-motion, driven by sensory feedback than to active, self-generated motion driven by both sensory and internal feedback (Brooks and Cullen, 2013). Also, the long term decrease in sensitivity to motor errors observed with PET imaging during adaptation to constant force fields (Nezafat et al., 2001) could be due to an improving match between internally generated predictions and sensory feedback. A similar reduction in the cerebellar BOLD response occurs during a cognitive task in which subjects learn first-order rules (Balsters and Ramnani, 2011), presumably due to a comparison in the cerebellar cortex between the predicted and perceptual consequences of mental manipulations. A study of fear conditioning found that cerebellar activation decreased during the conditioning phase while either unexpected application or omission of the noxious stimuli resulted in increased cerebellar activation (Ploghaus et al., 2000). This result is consistent with acquiring a dual representation of the stimulus application, resulting in cancellation of predictive and feedback signals when the prediction is correct and increased activity when there is prediction error. Furthermore, cerebellar activation during a letter manipulation task is consistent with encoding task execution errors in a non-motor task (Marvel and Desmond, 2012). Although the hypothesis that individual Purkinje cells compute directly sensory prediction errors by subtracting the predictive and feedback signals is very seductive, the fact that the two signals are separated in time requires further investigation. It is possible that this computation is performed downstream, for example, in the cerebellar nuclei. It is also possible that for relatively slow changing signals the dual encoding could approximate the sensory prediction error.

Similar cancellation of self-generated sensory signals occurs in cerebellum-like structures (Bell et al., 2008; Sawtell and Bell, 2008; Requarth and Sawtell, 2011). This suppression is due to anti-Hebbian plasticity at the parallel fiber-principle neuron synapse that sculpts the response to the efferent copy into a negative image of the response to the sensory input (Bell et al., 1997; Han et al., 2000; Requarth and Sawtell, 2011). This mechanism is predicated

on the appropriate convergence of sensory inputs and an efference copy of the motor command on the principal neurons (Sawtell, 2010). A comparable convergence of proprioceptive and corticopontine inputs has been reported in the mouse cerebellar cortex (Huang et al., 2013).

To test whether dual encoding is a general principle of cerebellar representations, we re-examined the simple spike firing relationship with kinematics using the analytical methods described above, regressing the appropriate residuals in which variability associated with all other motor parameters was removed against individual kinematic variables (Popa, 2013). Similar to the error parameters described earlier, a majority of Purkinje cells also encode kinematics with dual signals, one related to an internal prediction and one related to sensory feedback. There is increasing evidence that the time delays required to create opposing signals might be generated by the mossy fiber-granule cell circuitry in the mammalian cerebellum. Long term plasticity at the mossy fiber—granule cell synapse can delay incoming signals for up to 100 ms, or even longer when larger sections of the circuitry are entrained (D'Angelo, 2011). Similar delays are generated in cerebellar-like structures involving the mossy fibers, granule cells and unipolar brush cells (Kennedy et al., 2014). Together, these findings suggest that the leads/lags found for performance errors and kinematic signals are determined, at least in part, by computations occurring in the cerebellar cortex, resulting in specific temporal alignments of cerebellar signals. We hypothesize that dual temporal encoding is a general property of cerebellar cortical information processing and also likely plays a central role in non-motor cerebellar functions.

Both motor coordination and motor sequences require interactions between different components (e.g., effectors, muscles, etc.) activated at different times and, therefore, controlling the individual components requires motor predictions across a spectrum of leads. Successful population decoding of the error predictions combines individual Purkinje cell signals at all possible lead times, with values between -500 and 0 ms. In other words, the cerebellar cortex unfurls the predictions throughout a long time window. Similarly, the simple spike signals that lag kinematics or errors occur across this rather protracted time course. One possible interpretation is that this provides a mechanism for the cerebellum's role in coordination among effectors (Thach et al., 1992; van Donkelaar and Lee, 1994; Bastian et al., 1996; Serrien and Wiesendanger, 2000; Miall et al., 2001) and in movement sequences (Braitenberg et al., 1997; Doyon et al., 1997; Molinari and Petrosini, 1997; Molinari et al., 1997, 2008; Nixon and Passingham, 2000). Under this assumption, cerebellar cortical output integrates the predicted motor command outcomes at specific lead times with appropriately matched feedback signals to generate the required coordination among effectors needed to accomplish the movement goal while simultaneously updating the motor controller so that the next motor command can be generated. It has been hypothesized that the cerebellum fulfills a similar function in detecting sequences in the verbal, spatial and cognitive domains (Molinari et al., 2008). The long and quasi-uniform lead and lag times found in the simple spike discharge provides a neural substrate for monitoring and controlling sequences. For example, cerebellar damage impairs sequencing of cards depicting brief stories regardless of whether verbal, spatial, or behavioral strategies are used (Leggio et al., 2008). An imaging study based on letter manipulations showed an interesting difference in cerebellar activation depending on the cognitive process engaged (Marvel and Desmond, 2012). The presentation of a sequence of letters, without processing requirements, induces a fast, transient activation, consistent with the response to tightly packed input signals. However, when processing instructions are added, the activation becomes sustained over a longer time interval. This temporal expansion is consistent with the temporal unfurling of the cerebellar representations observed during random tracking.

Another interesting implication for the capacity of Purkinje cells to provide predictions and feedback at a wide range of times is in working memory. Numerous functional imaging studies demonstrate cerebellar activation associated with the working memory system (Chen and Desmond, 2005; Hautzel et al., 2009; Marvel and Desmond, 2010). Given that the storage capacity of working memory is limited to between four and seven items (Miller, 1956; Luck and Vogel, 1997), the changes in its content associated with shifting attention focus occurs every 200–500 ms (Muller et al., 1998; Woodman and Luck, 1999). Having both prediction and feedback signals over comparable time horizons, the cerebellar cortex may facilitate novel associations between past and current working memory content and among different classes of information.

LINEAR INTEGRATION OF KINEMATICS AND ERROR SIGNALS

The presence of both error and kinematic signals in the Purkinje cell simple spike discharge raises the question of whether the cells are functionally segregated into populations that preferentially encode one class of signals over the other. Using multi-linear models that included (1) all variables from each class, (2) position, velocity, and speed kinematics, and (3) position, radial, and direction errors, we showed that the average R^2 for kinematics and error models are comparable. As detailed above, accurate decoding of the upcoming behavior can be achieved for both errors and kinematics. Therefore, encoding of these two classes of variables is equally robust. For single cells, the distribution of R^2 values reveals a strong linear positive correlation between errors and kinematics and there is no evidence of segregation into subpopulations. The representations of single parameters are additive, as the sum of the R^2 profiles for the individual parameters closely matches the R^2 profile of both error and kinematic multi-linear models (Popa et al., 2012; Popa, 2013). These observations reinforce the concept of signal independence and supports the hypothesis that Purkinje cells linearly integrate parallel fiber input (Walter and Khodakhah, 2006, 2009). Therefore, kinematic and error signals are highly integrated at the single neuron and population levels.

The integration of the kinematic and error signals strongly suggests that Purkinje cells favor complexity. There are approximately 200,000 parallel fiber-Purkinje cell synapses (Napper and Harvey, 1988), while less than 200 active synapses are required to drive simple spike discharge (Isope and Barbour, 2002), suggesting a very high theoretical bandwidth. During random tracking, we evaluated nine behavioral parameters, five kinematic and four

error signals. Each parameter could be dually encoded, resulting in 18 independent signals in the simple spike discharge. Out of these 18 possible signals, on average, individual Purkinje cells encode 10 different signals simultaneously (Popa, 2013). Therefore, each Purkinje cell carries a very rich representation of the motor behavior suggesting that an important aspect of cerebellar function is associating different signals, possibly of different modalities.

The number of signals identified in individual cell simple spike discharges is small in comparison to the theoretical bandwidth, suggesting the possibility that the same cell could encode diverse representations in different contexts. For example, one cell could use a common representation of an effector with multiple performance error signals that differ across tasks. As reviewed above, functional imaging studies show that the cerebellum encodes errors as well as kinematics. Although clearly not at the level of single cells, imaging suggests the cerebellum is activated in relation to non-motor functions including language, spatial processing, working memory, executive function, and emotional processing (for review see Stoodley, 2012). These activations particularly engaged the postero-lateral regions and are consistent with the integration of many classes of signals within the same areas. Association of information across modalities has been central to several theories of the cerebellum's role in cognition (Drepper et al., 1999; Timmann et al., 2002, 2010; Molinari et al., 2008).

The high number of independent signals present in each Purkinje cell discharge and the additive property of these signals suggest that the cerebellar function includes an associative aspect. As others have proposed, it is possible that Purkinje cells use plasticity mechanisms to select only the relevant signals from the high number of possible parallel fiber inputs to each neuron, and these relevant signals maintain consistent relationships to form a representation of the motor behavior (Marr, 1969; Albus, 1971). Associative learning in the cerebellum is not restricted to the motor domain (for review see Timmann et al., 2010). For example, the cerebellum is implicated in fear learning (Sacchetti et al., 2004) and cognitive associative learning (Drepper et al., 1999; Timmann et al., 2002). Making the required association between the relevant afferent signals would utilize the Purkinje cell's capacity to integrate large numbers of signals. Interestingly, the cerebellum appears to acquire an internal model related to the application of noxious stimuli but fails to respond when innocuous stimuli are applied (Ploghaus et al., 2000), suggesting that the cerebellum evaluates the relevance of inputs and disregards the irrelevant ones.

IMPLICATIONS FOR INTERNAL MODELS OF COGNITIVE PROCESSES

Understanding cerebellar involvement in non-motor domains faces numerous challenges ranging from imprecise definitions and imperfect models of cognitive behavior to indirect investigation methods (Koziol et al., 2012; Buckner, 2013). Fortunately, the remarkable uniformity of the cerebellar cortex architecture (Eccles et al., 1967; Ito, 1984; Ramnani, 2006) suggests that the cerebellum should perform the same signal processing across motor and non-motor domains (Ramnani, 2006; Thach, 2007; Ito, 2008; Schmahmann, 2010). Under this hypothesis, insights into cerebellar processes provided by single cell studies of motor behavior in well controlled experimental conditions and within a rigorous theoretical framework may help illuminate non-motor aspects of cerebellar function.

Throughout this review we have noted how the information processing properties of cerebellar neurons might contribute to non-motor functions. In this final section we explore more fully the concept of internal models in motor and non-motor functions of the cerebellum. Several investigators have proposed that the internal model hypotheses can be used to understand cerebellar involvement in non-motor domains (Ito, 2008; Imamizu and Kawato, 2009; Koziol et al., 2012). In support of the hypothesis that forward internal model processes are common across function domains is the observation that the information provided by an internal model of the hand during visually guided tracking is used in a visual discrimination task (Stanley and Miall, 2009) showing that signals involved in motor control are used in non-motor behaviors. It also been hypothesized that forward internal models acquired in the motor domain, interacting with the mirror system in the cerebral cortex, facilitate action understanding (Caligiore et al., 2013), the capability to asses mental states such as goals and intentions underlying actions performed by different subjects. Several functional imaging studies found specific cerebellar activation in response to noun-verb associations (Petersen et al., 1988) or to word completion tasks (Desmond and Fiez, 1998), suggesting activation of a forward internal model that provides lexical predictions. Strongly supporting this hypothesis is the observation that disruption of cerebellar function by repeated transcranial magnetic stimulation reduces language predictive performance (Lesage et al., 2012). Under the assumption that cerebellar processing in the motor domain translates to non-motor functions, we consider the implications of our random tracking results to understanding the cerebellar contribution to cognitive processes in the context of forward internal models. The classical version of the forward internal model assumes that the cerebellum provides a model of the effector that predicts the sensory consequences of the motor commands (Robinson, 1975; Miall and Wolpert, 1996; Bastian, 2006; Shadmehr et al., 2010). In this framework, the internal model updating is driven by the motor error signals, more specifically sensory prediction errors (Morton and Bastian, 2006; Tseng et al., 2007; Xu-Wilson et al., 2009; Shadmehr et al., 2010; Izawa et al., 2012). As detailed above, the historical emphasis has been that the error signals are conveyed solely by the climbing fibers and complex spikes. Likewise, it has been assumed that complex spikes provide error signals in non-motor behaviors (Ito, 2008; Schmahmann, 2010; Koziol et al., 2012; Yamazaki and Nagao, 2012). It has also been proposed that the cerebellum uses the same processes performed by a forward internal model on copies of the mental models encoded in the parietal cortex which are then manipulated by the commands issued by the prefrontal cortex, while the inferior olive encodes the cognitive errors (Ito, 2008). Recently described projections between the cerebral cortex and cerebellum provide the required pathways to support the hypothesis that the cerebellar cortex acquires and manipulates copies of the mental models (Schmahmann and Pandya, 1989, 1991, 1997; Middleton and

Strick, 1994, 2001; Kelly and Strick, 2003). However, the existence of pathways necessary to support the hypothesis that the inferior olive encodes cognitive error signals remain tentative at best (Ito, 2008). For example, principal olive, the subdivision of the inferior olive that provides the climbing fiber projections to cerebellar cortical regions connected to associative areas of the cerebral cortex, does not receive projections from the cerebral cortex (Schmahmann, 2010). Further, as discussed above, the validity of the concept that complex spikes signal motor errors is being questioned.

Our recent findings describing performance error signals in the simple spike activity show that the signals required by the forward internal model theories are conveyed by parallel fiber inputs, thus eliminating the idea that climbing fibers are the sole pathway for conveying error signals (Ito, 2008). This would strengthen the hypothesis that forward internal model processes could be replicated in the cognitive domain by emphasizing the established projections between cerebellum and prefrontal and parietal cortices and reducing the relevance on inferior olive input. However, this would also require a reassessment of the role of complex spikes in the cerebellar function. For example, recent optogenetic experiments show that simple spike activation induces a complex spike response (Chaumont et al., 2013; Witter et al., 2013). This suggests that the complex spike activity, modulated by the response of Purkinje cells to parallel fiber inputs, engage specific plasticity mechanisms (Ito et al., 1982; Marquez-Ruiz and Cheron, 2012) that refine suboptimal outputs of the cerebellar cortex.

Complex goal-directed behavior, such as visually guided, random tracking, raises the question of how a motor command is selected and implemented under very stringent temporal constraints as the monkey has only 500 ms to recover from excursions outside the target. Within such a tight temporal budget it is unlikely that a classical process of error perception and action selection, which requires ∼400 ms, can be implemented (Madl et al., 2011). One accepted solution to this problem is that the cerebellum acts as a forward internal model that predicts the future state of the effector (Ito, 2008; Shadmehr and Krakauer, 2008). Nevertheless, the selection of the motor command cannot be completed based only on effector state predictions, as the action selection is also dependent on performance information. This information is presumably processed in the classical sequence of perception-selection-execution. However, our demonstration of the integration of kinematic and performance error predictions shows that the cerebellar cortex provides predictions of the consequences of the motor command both in terms of future states of the effector and the usefulness toward meeting the current movement goal. We suggest that the cerebellar cortex predictions provide the information needed to complete action selection with little reliance on sensory feedback.

First, it is interesting to explore the implications of cerebellar prediction of both kinematic and performance states for the process of action selection that involves interactions among widely distributed cortical areas and also subcortical structures including the cerebellum and basal ganglia (Cisek and Kalaska, 2010). Action selection appears to be heavily dependent on perception (Ledberg et al., 2007) and therefore, may be too slow for the implementation and control of fast, ongoing behaviors, such as random tracking. Decision making may be adequate to control the slower components of the behavior, such as the decision to start a new trial or to abandon an ongoing trial. However, once the decision to engage in a trial is made, the selection and implementation of the on-going movements required to complete the behavior needs to be controlled by faster mechanisms (Shadmehr et al., 2010). Faster control could be achieved by acquiring a forward internal model of the behavior that combines signals describing the effector response and the task-specific performance and then learning to predict the consequences of the specified actions. Therefore, action bias might be viewed as a staged process in which a slower, perception-driven component are under prefrontal and basal ganglia control, while the cerebellum controls a faster, experience-dependent and perception-independent component.

Second, it is interesting to examine the cerebellar internal model of thought process hypothesis (Ito, 2008) in an expanded version of the forward internal model framework. It had been suggested that when the cerebellum acquires a forward internal model of a cognitive problem, by performing the manipulations required to solve the problem on cerebellar copies of the mental models eliminates the perception of thinking about the problem, thus generating an "intuition" (Ito, 2008). However, this model leaves unanswered the problem of recognizing the solution. It is possible to perform the evaluation of the intermediate results under conscious control, which would eliminate the "unexpected" quality associated with intuition. An internal model that includes not only copies of the mental models manipulated in the process, but also copies of cognitive error representations, could allow the evaluation of the results under cerebellar control.

Extending the internal forward model hypothesis to both predictions about the effectors and performance could have another implication. Presumably, experience-driven internal models are acquired by consistently activating and associating specific cerebellar inputs and the required plasticity mechanisms. Under normal conditions the consistency of inputs would be only related to repeated consideration of the same problem and, therefore, the resulting internal models could be refined to provide an optimal solution. However, if unrelated inputs are consistently activated, for example in pathological conditions, this could bias the internal forward model. In this condition, the subject would perceive a suboptimal result as the correct solution.

NEXT STEPS

Extending cerebellar function into non-motor processing has raised a host of intriguing questions about the computations performed by the cerebellar circuitry and how these computations support processes such as cognition, working memory, and language processing. While patient studies, non-invasive stimulation techniques and functional imaging in human subjects are powerful tools to test hypotheses on the role of the cerebellum in non-motor functions and have already provided considerable insights, single unit electrophysiological studies are clearly needed to gain a greater understanding of how the cerebellum participates in and contributes to higher cortical functions at the neuronal level. Electrophysiological studies would use

non-human primates because these subjects are capable of the types of complex, non-motor behaviors needed to address these questions. Furthermore, non-human primates have the required cerebellar-cortical connectivity that underpins the cerebellum's role in non-motor behaviors. Finally, single cell recordings are the only present day technique that can answer the question central to this review, which is "Are the computations performed by the cerebellar cortex similar in the motor and non-motor domains?"

AUTHOR CONTRIBUTIONS

Angela L. Hewitt, Laurentiu S. Popa, and Timothy J. Ebner all contributed to the design, analysis, and interpretation of the work. Angela L. Hewitt had primary responsibility for data acquisition. All authors contributed to the drafting, giving final approval and agreeing to be held accountable for all aspects of the work.

ACKNOWLEDGMENTS

We wish to thank Michael McPhee for generating graphics and Kris Bettin and Lauren Skalicky for preparation of the manuscript. Supported in part by NIH grants R01 NS18338, R01 F31 NS071686, and T32 GM008244.

REFERENCES

Albus, J. S. (1971). A theory of cerebellar function. *Math. Biosci.* 10, 25–61. doi: 10.1016/0025-5564(71)90051-4

Balsters, J. H., and Ramnani, N. (2011). Cerebellar plasticity and the automation of first-order rules. *J. Neurosci.* 31, 2305–2312. doi: 10.1523/JNEUROSCI.4358-10.2011

Barmack, N. H., and Shojaku, H. (1995). Vestibular and visual climbing fiber signals evoked in the uvula-nodulus of the rabbit cerebellum by natural stimulation. *J. Neurophysiol.* 74, 2573–2589.

Bastian, A. J. (2006). Learning to predict the future: the cerebellum adapts feedforward movement control. *Curr. Opin. Neurobiol.* 16, 645–649. doi: 10.1016/j.conb.2006.08.016

Bastian, A. J., Martin, T. A., Keating, J. G., and Thach, W. T. (1996). Cerebellar ataxia: abnormal control of interaction torques across multiple joints. *J. Neurophysiol.* 76, 492–509.

Bell, C. C., Han, V., and Sawtell, N. B. (2008). Cerebellum-like structures and their implications for cerebellar function. *Annu. Rev. Neurosci.* 31, 1–24. doi: 10.1146/annurev.neuro.30.051606.094225

Bell, C. C., Han, V. Z., Sugawara, Y., and Grant, K. (1997). Synaptic plasticity in a cerebellum-like structure depends on temporal order. *Nature* 387, 278–281. doi: 10.1038/387278a0

Boehringer, A., Macher, K., Dukart, J., Villringer, A., and Pleger, B. (2013). Cerebellar transcranial direct current stimulation modulates verbal working memory. *Brain Stimul.* 6, 649–653. doi: 10.1016/j.brs.2012.10.001

Braitenberg, V., and Atwood, R. P. (1958). Morphological observations on the cerebellar cortex. *J. Comp. Neurol.* 109, 1–33. doi: 10.1002/cne.901090102

Braitenberg, V., Heck, D., and Sultan, F. (1997). The detection and generation of sequences as a key to cerebellar function: experiments and theory. *Behav. Brain Sci.* 20, 229–245. doi: 10.1017/S0140525X9700143X

Brooks, J. X., and Cullen, K. E. (2013). The primate cerebellum selectively encodes unexpected self-motion. *Curr. Biol.* 23, 947–955. doi: 10.1016/j.cub.2013.04.029

Buckner, R. L. (2013). The cerebellum and cognitive function: 25 years of insight from anatomy and neuroimaging. *Neuron* 80, 807–815. doi: 10.1016/j.neuron.2013.10.044

Burk, K. (2007). Cognition in hereditary ataxia. *Cerebellum* 6, 280–286. doi: 10.1080/14734220601115924

Caligiore, D., Pezzulo, G., Miall, R. C., and Baldassarre, G. (2013). The contribution of brain sub-cortical loops in the expression and acquisition of action understanding abilities. *Neurosci. Biobehav. Rev.* 37, 2504–2515. doi: 10.1016/j.neubiorev.2013.07.016

Catz, N., Dicke, P. W., and Thier, P. (2005). Cerebellar complex spike firing is suitable to induce as well as to stabilize motor learning. *Curr. Biol.* 15, 2179–2189. doi: 10.1016/j.cub.2005.11.037

Chaumont, J., Guyon, N., Valera, A. M., Dugue, G. P., Popa, D., Marcaggi, P., et al. (2013). Clusters of cerebellar Purkinje cells control their afferent climbing fiber discharge. *Proc. Natl. Acad. Sci. U.S.A.* 110, 16223–16228. doi: 10.1073/pnas.1302310110

Chen, S. H., and Desmond, J. E. (2005). Cerebrocerebellar networks during articulatory rehearsal and verbal working memory tasks. *Neuroimage* 24, 332–338. doi: 10.1016/j.neuroimage.2004.08.032

Cisek, P., and Kalaska, J. F. (2010). Neural mechanisms for interacting with a world full of action choices. *Annu. Rev. Neurosci.* 33, 269–298. doi: 10.1146/annurev.neuro.051508.135409

Coltz, J. D., Johnson, M. T., and Ebner, T. J. (1999). Cerebellar Purkinje cell simple spike discharge encodes movement velocity in primates during visuomotor arm tracking. *J. Neurosci.* 19, 1782–1803.

Crowe, D. A., Goodwin, S. J., Blackman, R. K., Sakellaridi, S., Sponheim, S. R., MacDonald, A. W. 3rd., et al. (2013). Prefrontal neurons transmit signals to parietal neurons that reflect executive control of cognition. *Nat. Neurosci.* 16, 1484–1491. doi: 10.1038/nn.3509

D'Angelo, E. (2011). Neural circuits of the cerebellum: hypothesis for function. *J. Integr. Neurosci.* 10, 317–352. doi: 10.1142/S0219635211002762

Dash, S., Catz, N., Dicke, P. W., and Thier, P. (2010). Specific vermal complex spike responses build up during the course of smooth-pursuit adaptation, paralleling the decrease of performance error. *Exp. Brain Res.* 205, 41–55. doi: 10.1007/s00221-010-2331-2

Dash, S., Dicke, P. W., and Thier, P. (2013). A vermal Purkinje cell simple spike population response encodes the changes in eye movement kinematics due to smooth pursuit adaptation. *Front. Syst. Neurosci.* 7:3. doi: 10.3389/fnsys.2013.00003

Desmond, J. E., and Fiez, J. A. (1998). Neuroimaging studies of the cerebellum: language, learning and memory. *Trends Cogn. Sci.* 2, 355–362. doi: 10.1016/S1364-6613(98)01211-X

Diedrichsen, J., Hashambhoy, Y., Rane, T., and Shadmehr, R. (2005). Neural correlates of reach errors. *J. Neurosci.* 25, 9919–9931. doi: 10.1523/JNEUROSCI.1874-05.2005

Doyon, J., Gaudreau, D., Laforce, R. Jr., Castonguay, M., Bedard, P. J., Bedard, F., et al. (1997). Role of the striatum, cerebellum, and frontal lobes in the learning of a visuomotor sequence. *Brain Cogn.* 34, 218–245. doi: 10.1006/brcg.1997.0899

Drepper, J., Timmann, D., Kolb, F. P., and Diener, H. C. (1999). Non-motor associative learning in patients with isolated degenerative cerebellar disease. *Brain* 122(Pt 1), 87–97. doi: 10.1093/brain/122.1.87

Ebner, T. J., Hewitt, A., and Popa, L. S. (2011). What features of movements are encoded in the discharge of cerebellar neurons during limb movements? *Cerebellum* 10, 683–693. doi: 10.1007/s12311-010-0243-0

Ebner, T. J., Johnson, M. T., Roitman, A., and Fu, Q. (2002). What do complex spikes signal about limb movements? *Ann. N.Y. Acad. Sci.* 978, 205–218. doi: 10.1111/j.1749-6632.2002.tb07568.x

Eccles, J. C., Ito, M., and Szentagothai, J. (1967). *The Cerebellum as a Neuronal Machine*. Berlin: Springer-Verlag.

Ferrucci, R., Marceglia, S., Vergari, M., Cogiamanian, F., Mrakic-Sposta, S., Mameli, F., et al. (2008). Cerebellar transcranial direct current stimulation impairs the practice-dependent proficiency increase in working memory. *J. Cogn. Neurosci.* 20, 1687–1697. doi: 10.1162/jocn.2008.20112

Fiez, J. A., Petersen, S. E., Cheney, M. K., and Raichle, M. E. (1992). Impaired nonmotor learning and error detection associated with cerebellar damage. A single case study. *Brain* 115(Pt 1), 155–178. doi: 10.1093/brain/115.1.155

Fortier, P. A., Kalaska, J. F., and Smith, A. M. (1989). Cerebellar neuronal activity related to whole-arm reaching movements in the monkey. *J. Neurophysiol.* 62, 198–211.

Fu, Q. G., Flament, D., Coltz, J. D., and Ebner, T. J. (1997). Relationship of cerebellar Purkinje cell simple spike discharge to movement kinematics in the monkey. *J. Neurophysiol.* 78, 478–491.

Gilbert, P. F., and Thach, W. T. (1977). Purkinje cell activity during motor learning. *Brain Res.* 128, 309–328. doi: 10.1016/0006-8993(77)90997-0

Gomi, H., Shidara, M., Takemura, A., Inoue, Y., Kawano, K., and Kawato, M. (1998). Temporal firing patterns of Purkinje cells in the cerebellar ventral

paraflocculus during ocular following responses in monkeys I. Simple spikes. *J. Neurophysiol.* 80, 818–831.

Graf, W., Simpson, J. I., and Leonard, C. S. (1988). Spatial organization of visual messages of the rabbit's cerebellar flocculus. II. Complex and simple spike responses of Purkinje cells. *J. Neurophysiol.* 60, 2091–2121.

Greger, B., and Norris, S. (2005). Simple spike firing in the posterior lateral cerebellar cortex of Macaque Mulatta was correlated with success-failure during a visually guided reaching task. *Exp. Brain Res.* 167, 660–665. doi: 10.1007/s00221-005-0155-2

Han, V. Z., Grant, K., and Bell, C. C. (2000). Reversible associative depression and nonassociative potentiation at a parallel fiber synapse. *Neuron* 27, 611–622. doi: 10.1016/S0896-6273(00)00070-2

Harvey, R. J., Porter, R., and Rawson, J. A. (1977). The natural discharges of Purkinje cells in paravermal regions of lobules V and VI of the monkey's cerebellum. *J. Physiol.* 271, 515–536.

Hautzel, H., Mottaghy, F. M., Specht, K., Muller, H. W., and Krause, B. J. (2009). Evidence of a modality-dependent role of the cerebellum in working memory? An fMRI study comparing verbal and abstract n-back tasks. *Neuroimage* 47, 2073–2082. doi: 10.1016/j.neuroimage.2009.06.005

Hayter, A. L., Langdon, D. W., and Ramnani, N. (2007). Cerebellar contributions to working memory. *Neuroimage* 36, 943–954. doi: 10.1016/j.neuroimage.2007.03.011

Hewitt, A., Popa, L. S., Pasalar, S., Hendrix, C. M., and Ebner, T. J. (2011). Representation of limb kinematics in Purkinje cell simple spike discharge is conserved across multiple tasks. *J. Neurophysiol.* 106, 2232–2247. doi: 10.1152/jn.00886.2010

Horn, K. M., van Kan, P. L., and Gibson, A. R. (1996). Reduction of rostral dorsal accessory olive responses during reaching. *J. Neurophysiol.* 76, 4140–4151.

Huang, C. C., Sugino, K., Shima, Y., Guo, C., Bai, S., Mensh, B. D., et al. (2013). Convergence of pontine and proprioceptive streams onto multimodal cerebellar granule cells. *Elife* 2:e00400. doi: 10.7554/eLife.00400

Imamizu, H., Higuchi, S., Toda, A., and Kawato, M. (2007). Reorganization of brain activity for multiple internal models after short but intensive training. *Cortex* 43, 338–349. doi: 10.1016/S0010-9452(08)70459-3

Imamizu, H., and Kawato, M. (2009). Brain mechanisms for predictive control by switching internal models: implications for higher-order cognitive functions. *Psychol. Res.* 73, 527–544. doi: 10.1007/s00426-009-0235-1

Imamizu, H., Kuroda, T., Miyauchi, S., Yoshioka, T., and Kawato, M. (2003). Modular organization of internal models of tools in the human cerebellum. *Proc. Natl. Acad. Sci. U.S.A.* 100, 5461–5466. doi: 10.1073/pnas.0835746100

Imamizu, H., Miyauchi, S., Tamada, T., Sasaki, Y., Takino, R., Putz, B., et al. (2000). Human cerebellar activity reflecting an acquired internal model of a new tool. *Nature* 403, 192–195. doi: 10.1038/35003194

Isope, P., and Barbour, B. (2002). Properties of unitary granule cell–>Purkinje cell synapses in adult rat cerebellar slices. *J. Neurosci.* 22, 9668–9678.

Ito, M. (1984). *The Cerebellum and Neural Control*. New York, NY: Raven Press.

Ito, M. (2000). Mechanisms of motor learning in the cerebellum. *Brain Res.* 886, 237–245. doi: 10.1016/S0006-8993(00)03142-5

Ito, M. (2002). Historical review of the significance of the cerebellum and the role of Purkinje cells in motor learning. *Ann. N.Y. Acad. Sci.* 978, 273–288. doi: 10.1111/j.1749-6632.2002.tb07574.x

Ito, M. (2008). Control of mental activities by internal models in the cerebellum. *Nat. Rev. Neurosci.* 9, 304–313. doi: 10.1038/nrn2332

Ito, M., Sakurai, M., and Tongroach, P. (1982). Climbing fibre induced depression of both mossy fibre responsiveness and glutamate sensitivity of cerebellar Purkinje cells. *J. Physiol.* 324, 113–134.

Izawa, J., Criscimagna-Hemminger, S. E., and Shadmehr, R. (2012). Cerebellar contributions to reach adaptation and learning sensory consequences of action. *J. Neurosci.* 32, 4230–4239. doi: 10.1523/JNEUROSCI.6353-11.2012

Kawato, M. (1999). Internal models for motor control and trajectory planning. *Curr. Opin. Neurobiol.* 9, 718–727. doi: 10.1016/S0959-4388(99)00028-8

Ke, M. C., Guo, C. C., and Raymond, J. L. (2009). Elimination of climbing fiber instructive signals during motor learning. *Nat. Neurosci.* 12, 1171–1179. doi: 10.1038/nn.2366

Keele, S. W., and Ivry, R. (1990). Does the cerebellum provide a common computation for diverse tasks? A timing hypothesis. *Ann. N.Y. Acad. Sci.* 608, 179–207. doi: 10.1111/j.1749-6632.1990.tb48897.x

Kelly, R. M., and Strick, P. L. (2003). Cerebellar loops with motor cortex and prefrontal cortex of a nonhuman primate. *J. Neurosci.* 23, 8432–8444.

Kennedy, A., Wayne, G., Kaifosh, P., Alvina, K., Abbott, L. F., and Sawtell, N. B. (2014). A temporal basis for predicting the sensory consequences of motor commands in an electric fish. *Nat. Neurosci.* 17, 416–422. doi: 10.1038/nn.3650

Kim, J. H., Wang, J. J., and Ebner, T. J. (1987). Climbing fiber afferent modulation during treadmill locomotion in the cat. *J. Neurophysiol.* 57, 787–802.

Kim, S. G., Ugurbil, K., and Strick, P. L. (1994). Activation of a cerebellar output nucleus during cognitive processing. *Science* 265, 949–951. doi: 10.1126/science.8052851

Kitazawa, S., Kimura, T., and Yin, P. B. (1998). Cerebellar complex spikes encode both destinations and errors in arm movements. *Nature* 392, 494–497. doi: 10.1038/33141

Kobayashi, Y., Kawano, K., Takemura, A., Inoue, Y., Kitama, T., Gomi, H., et al. (1998). Temporal firing patterns of Purkinje cells in the cerebellar ventral paraflocculus during ocular following responses in monkeys II. Complex spikes. *J. Neurophysiol.* 80, 832–848.

Koziol, L. F., Budding, D. E., and Chidekel, D. (2012). From movement to thought: executive function, embodied cognition, and the cerebellum. *Cerebellum* 11, 505–525. doi: 10.1007/s12311-011-0321-y

Ledberg, A., Bressler, S. L., Ding, M., Coppola, R., and Nakamura, R. (2007). Large-scale visuomotor integration in the cerebral cortex. *Cereb. Cortex* 17, 44–62. doi: 10.1093/cercor/bhj123

Leggio, M. G., Tedesco, A. M., Chiricozzi, F. R., Clausi, S., Orsini, A., and Molinari, M. (2008). Cognitive sequencing impairment in patients with focal or atrophic cerebellar damage. *Brain* 131, 1332–1343. doi: 10.1093/brain/awn040

Leiner, H. C., Leiner, A. L., and Dow, R. S. (1986). Does the cerebellum contribute to mental skills? *Behav. Neurosci.* 100, 443–454. doi: 10.1037/0735-7044.100.4.443

Leiner, H. C., Leiner, A. L., and Dow, R. S. (1989). Reappraising the cerebellum: what does the hindbrain contribute to the forebrain? *Behav. Neurosci.* 103, 998–1008. doi: 10.1037/0735-7044.103.5.998

Lesage, E., Morgan, B. E., Olson, A. C., Meyer, A. S., and Miall, R. C. (2012). Cerebellar rTMS disrupts predictive language processing. *Curr. Biol.* 22, R794–R795. doi: 10.1016/j.cub.2012.07.006

Luck, S. J., and Vogel, E. K. (1997). The capacity of visual working memory for features and conjunctions. *Nature* 390, 279–281. doi: 10.1038/36846

Madl, T., Baars, B. J., and Franklin, S. (2011). The timing of the cognitive cycle. *PLoS ONE* 6:e14803. doi: 10.1371/journal.pone.0014803

Mano, N., and Yamamoto, K. (1980). Simple-spike activity of cerebellar Purkinje cells related to visually guided wrist tracking movement in the monkey. *J. Neurophysiol.* 43, 713–728.

Marple-Horvat, D. E., and Stein, J. F. (1987). Cerebellar neuronal activity related to arm movements in trained rhesus monkeys. *J. Physiol.* 394, 351–366.

Marquez-Ruiz, J., and Cheron, G. (2012). Sensory stimulation-dependent plasticity in the cerebellar cortex of alert mice. *PLoS ONE* 7:e36184. doi: 10.1371/journal.pone.0036184

Marr, D. (1969). A theory of cerebellar cortex. *J. Physiol.* 202, 437–470.

Marvel, C. L., and Desmond, J. E. (2010). Functional topography of the cerebellum in verbal working memory. *Neuropsychol. Rev.* 20, 271–279. doi: 10.1007/s11065-010-9137-7

Marvel, C. L., and Desmond, J. E. (2012). From storage to manipulation: how the neural correlates of verbal working memory reflect varying demands on inner speech. *Brain Lang.* 120, 42–51. doi: 10.1016/j.bandl.2011.08.005

Mazzoni, P., and Krakauer, J. W. (2006). An implicit plan overrides an explicit strategy during visuomotor adaptation. *J. Neurosci.* 26, 3642–3645. doi: 10.1523/JNEUROSCI.5317-05.2006

Medina, J. F., and Lisberger, S. G. (2008). Links from complex spikes to local plasticity and motor learning in the cerebellum of awake-behaving monkeys. *Nat. Neurosci.* 11, 1185–1192. doi: 10.1038/nn.2197

Medina, J. F., and Lisberger, S. G. (2009). Encoding and decoding of learned smooth pursuit eye movements in the floccular complex of the monkey cerebellum. *J. Neurophysiol.* 102, 2039–2054. doi: 10.1152/jn.00075.2009

Miall, R. C., Reckess, G. Z., and Imamizu, H. (2001). The cerebellum coordinates eye and hand tracking movements. *Nat. Neurosci.* 4, 638–644. doi: 10.1038/88465

Miall, R. C., and Wolpert, D. M. (1996). Forward models for physiological motor control. *Neural Netw.* 9, 1265–1279. doi: 10.1016/S0893-6080(96)00035-4

Middleton, F. A., and Strick, P. L. (1994). Anatomical evidence for cerebellar and basal ganglia involvement in higher cognitive function. *Science* 266, 458–461. doi: 10.1126/science.7939688

Middleton, F. A., and Strick, P. L. (2001). Cerebellar projections to the prefrontal cortex of the primate. *J. Neurosci.* 21, 700–712.

Miller, G. A. (1956). The magical number seven plus or minus two: some limits on our capacity for processing information. *Psychol. Rev.* 63, 81–97. doi: 10.1037/h0043158

Molinari, M., Chiricozzi, F. R., Clausi, S., Tedesco, A. M., De, L. M., and Leggio, M. G. (2008). Cerebellum and detection of sequences, from perception to cognition. *Cerebellum* 7, 611–615. doi: 10.1007/s12311-008-0060-x

Molinari, M., Leggio, M. G., Solida, A., Ciorra, R., Misciagna, S., Silveri, M. C., et al. (1997). Cerebellum and procedural learning: evidence from focal cerebellar lesions. *Brain* 120(Pt 10), 1753–1762. doi: 10.1093/brain/120.10.1753

Molinari, M., and Petrosini, L. (1997). Is sequence in/sequence out a cerebellar mode of operation in cognition too? *Behav. Brain Sci.* 20, 259–260. doi: 10.1017/S0140525X97391432

Moran, D. W., and Schwartz, A. B. (1999). Motor cortical activity during drawing movements: population representation during spiral tracing. *J. Neurophysiol.* 82, 2693–2704.

Morton, S. M., and Bastian, A. J. (2006). Cerebellar contributions to locomotor adaptations during splitbelt treadmill walking. *J. Neurosci.* 26, 9107–9116. doi: 10.1523/JNEUROSCI.2622-06.2006

Muller, M. M., Teder-Salejarvi, W., and Hillyard, S. A. (1998). The time course of cortical facilitation during cued shifts of spatial attention. *Nat. Neurosci.* 1, 631–634. doi: 10.1038/2865

Napper, R. M., and Harvey, R. J. (1988). Number of parallel fiber synapses on an individual Purkinje cell in the cerebellum of the rat. *J. Comp. Neurol.* 274, 168–177. doi: 10.1002/cne.902740204

Nezafat, R., Shadmehr, R., and Holcomb, H. H. (2001). Long-term adaptation to dynamics of reaching movements: a PET study. *Exp. Brain Res.* 140, 66–76. doi: 10.1007/s002210100787

Nixon, P. D., and Passingham, R. E. (2000). The cerebellum and cognition: cerebellar lesions impair sequence learning but not conditional visuomotor learning in monkeys. *Neuropsychologia* 38, 1054–1072. doi: 10.1016/S0028-3932(99)00138-4

Noto, C. T., and Robinson, F. R. (2001). Visual error is the stimulus for saccade gain adaptation. *Brain Res. Cogn. Brain Res.* 12, 301–305. doi: 10.1016/S0926-6410(01)00062-3

Ojakangas, C. L., and Ebner, T. J. (1994). Purkinje cell complex spike activity during voluntary motor learning: relationship to kinematics. *J. Neurophysiol.* 72, 2617–2630.

O'Reilly, J. X., Mesulam, M. M., and Nobre, A. C. (2008). The cerebellum predicts the timing of perceptual events. *J. Neurosci.* 28, 2252–2260. doi: 10.1523/JNEUROSCI.2742-07.2008

Oscarsson, O. (1980). "Functional organization of olivary projection to the cerebellar anterior lobe," in *The Inferior Olivary Nucleus: Anatomy and Physiology*, ed J. Courville (New York, NY: Raven), 279–290.

Paninski, L., Fellows, M. R., Hatsopoulos, N. G., and Donoghue, J. P. (2004). Spatiotemporal tuning of motor cortical neurons for hand position and velocity. *J. Neurophysiol.* 91, 515–532. doi: 10.1152/jn.00587.2002

Pasalar, S., Roitman, A. V., Durfee, W. K., and Ebner, T. J. (2006). Force field effects on cerebellar Purkinje cell discharge with implications for internal models. *Nat. Neurosci.* 9, 1404–1411. doi: 10.1038/nn1783

Petersen, S. E., Fox, P. T., Posner, M. I., Mintun, M., and Raichle, M. E. (1988). Positron emission tomographic studies of the processing of single words. *J. Cogn. Neurosci.* 1, 154–170.

Pezzulo, G. (2011). Grounding procedural and declarative knowledge in sensorimotor anticipation. *Mind Lang.* 26, 78–114. doi: 10.1111/j.1468-0017.2010.01411.x

Pezzulo, G., Barsalou, L. W., Cangelosi, A., Fischer, M. H., McRae, K., and Spivey, M. J. (2012). Computational grounded cognition: a new alliance between grounded cognition and computational modeling. *Front. Psychol.* 3:612. doi: 10.3389/fpsyg.2012.00612

Ploghaus, A., Tracey, I., Clare, S., Gati, J. S., Rawlins, J. N., and Matthews, P. M. (2000). Learning about pain: the neural substrate of the prediction error for aversive events. *Proc. Natl. Acad. Sci. U.S.A.* 97, 9281–9286. doi: 10.1073/pnas.160266497

Popa, L. S. (2013). *Computational Studies of Cerebellar Cortical Circuitry*. Minneapolis, MN: University of Minnesota.

Popa, L. S., Hewitt, A. L., and Ebner, T. J. (2012). Predictive and feedback performance errors are signaled in the simple spike discharge of individual Purkinje cells. *J. Neurosci.* 32, 15345–15358. doi: 10.1523/JNEUROSCI.2151-12.2012

Pope, P. A., and Miall, R. C. (2012). Task-specific facilitation of cognition by cathodal transcranial direct current stimulation of the cerebellum. *Brain Stimul.* 5, 84–94. doi: 10.1016/j.brs.2012.03.006

Prsa, M., and Thier, P. (2011). The role of the cerebellum in saccadic adaptation as a window into neural mechanisms of motor learning. *Eur. J. Neurosci.* 33, 2114–2128. doi: 10.1111/j.1460-9568.2011.07693.x

Ramnani, N. (2006). The primate cortico-cerebellar system: anatomy and function. *Nat. Rev. Neurosci.* 7, 511–522. doi: 10.1038/nrn1953

Requarth, T., and Sawtell, N. B. (2011). Neural mechanisms for filtering self-generated sensory signals in cerebellum-like circuits. *Curr. Opin. Neurobiol.* 21, 602–608. doi: 10.1016/j.conb.2011.05.031

Robinson, D. A. (1975). "Oculomotor control signals," in *Basic Mechanisms of Ocular Motility and their Clinical Implications*, eds P. Bachyrita and G. Lennerstrand (Oxford: Pergamon), 337–374.

Roitman, A. V., Pasalar, S., and Ebner, T. J. (2009). Single trial coupling of Purkinje cell activity to speed and error signals during circular manual tracking. *Exp. Brain Res.* 192, 241–251. doi: 10.1007/s00221-008-1580-9

Roitman, A. V., Pasalar, S., Johnson, M. T., and Ebner, T. J. (2005). Position, direction of movement, and speed tuning of cerebellar Purkinje cells during circular manual tracking in monkey. *J. Neurosci.* 25, 9244–9257. doi: 10.1523/JNEUROSCI.1886-05.2005

Sacchetti, B., Scelfo, B., Tempia, F., and Strata, P. (2004). Long-term synaptic changes induced in the cerebellar cortex by fear conditioning. *Neuron* 42, 973–982. doi: 10.1016/j.neuron.2004.05.012

Sawtell, N. B. (2010). Multimodal integration in granule cells as a basis for associative plasticity and sensory prediction in a cerebellum-like circuit. *Neuron* 66, 573–584. doi: 10.1016/j.neuron.2010.04.018

Sawtell, N. B., and Bell, C. C. (2008). Adaptive processing in electrosensory systems: links to cerebellar plasticity and learning. *J. Physiol. Paris* 102, 223–232. doi: 10.1016/j.jphysparis.2008.10.009

Schmahmann, J. D. (2000). The role of the cerebellum in affect and psychosis. *J. Neurolinguistics* 13, 189–214. doi: 10.1016/S0911-6044(00)00011-7

Schmahmann, J. D. (2004). Disorders of the cerebellum: ataxia, dysmetria of thought, and the cerebellar cognitive affective syndrome. *J. Neuropsychiatry Clin. Neurosci.* 16, 367–378. doi: 10.1176/appi.neuropsych.16.3.367

Schmahmann, J. D. (2010). The role of the cerebellum in cognition and emotion: personal reflections since 1982 on the dysmetria of thought hypothesis, and its historical evolution from theory to therapy. *Neuropsychol. Rev.* 20, 236–260. doi: 10.1007/s11065-010-9142-x

Schmahmann, J. D., and Pandya, D. N. (1989). Anatomical investigation of projections to the basis pontis from posterior parietal association cortices in rhesus monkey. *J. Comp. Neurol.* 289, 53–73. doi: 10.1002/cne.902890105

Schmahmann, J. D., and Pandya, D. N. (1991). Projections to the basis pontis from the superior temporal sulcus and superior temporal region in the rhesus monkey. *J. Comp. Neurol.* 308, 224–248. doi: 10.1002/cne.903080209

Schmahmann, J. D., and Pandya, D. N. (1997). Anatomic organization of the basilar pontine projections from prefrontal cortices in rhesus monkey. *J. Neurosci.* 17, 438–458.

Serrien, D. J., and Wiesendanger, M. (2000). Temporal control of a bimanual task in patients with cerebellar dysfunction. *Neuropsychologia* 38, 558–565. doi: 10.1016/S0028-3932(99)00116-5

Shadmehr, R., and Krakauer, J. W. (2008). A computational neuroanatomy for motor control. *Exp. Brain Res.* 185, 359–381. doi: 10.1007/s00221-008-1280-5

Shadmehr, R., Smith, M. A., and Krakauer, J. W. (2010). Error correction, sensory prediction, and adaptation in motor control. *Annu. Rev. Neurosci.* 33, 89–108. doi: 10.1146/annurev-neuro-060909-153135

Shidara, M., Kawano, K., Gomi, H., and Kawato, M. (1993). Inverse-dynamics model eye movement control by Purkinje cells in the cerebellum. *Nature* 365, 50–52. doi: 10.1038/365050a0

Soetedjo, R., Kojima, Y., and Fuchs, A. F. (2008). Complex spike activity in the oculomotor vermis of the cerebellum: a vectorial error signal for saccade motor learning? *J. Neurophysiol.* 100, 1949–1966. doi: 10.1152/jn.90526.2008

Stanley, J., and Miall, R. C. (2009). Using predictive motor control processes in a cognitive task: behavioral and neuroanatomical perspectives. *Adv. Exp. Med. Biol.* 629, 337–354. doi: 10.1007/978-0-387-77064-2_17

Stone, L. S., and Lisberger, S. G. (1990). Visual responses of Purkinje cells in the cerebellar flocculus during smooth-pursuit eye movements in monkeys. I. Simple spikes. *J. Neurophysiol.* 63, 1241–1261.

Stoodley, C. J. (2012). The cerebellum and cognition: evidence from functional imaging studies. *Cerebellum* 11, 352–365. doi: 10.1007/s12311-011-0260-7

Stoodley, C. J., and Schmahmann, J. D. (2009). Functional topography in the human cerebellum: a meta-analysis of neuroimaging studies. *Neuroimage* 44, 489–501. doi: 10.1016/j.neuroimage.2008.08.039

Thach, W. T. (1970). Discharge of cerebellar neurons related to two maintained postures and two prompt movements. II. Purkinje cell output and input. *J. Neurophysiol.* 33, 537–547.

Thach, W. T. (2007). On the mechanism of cerebellar contributions to cognition. *Cerebellum* 6, 163–167. doi: 10.1080/14734220701373530

Thach, W. T., Goodkin, H. P., and Keating, J. G. (1992). The cerebellum and the adaptive coordination of movement. *Annu. Rev. Neurosci.* 15, 403–442. doi: 10.1146/annurev.ne.15.030192.002155

Thier, P., Dicke, P. W., Haas, R., Thielert, C. D., and Catz, N. (2002). The role of the oculomotor vermis in the control of saccadic eye movements. *Ann. N.Y. Acad. Sci.* 978, 50–62. doi: 10.1111/j.1749-6632.2002.tb07555.x

Timmann, D., Drepper, J., Frings, M., Maschke, M., Richter, S., Gerwig, M., et al. (2010). The human cerebellum contributes to motor, emotional and cognitive associative learning. A review. *Cortex* 46, 845–857. doi: 10.1016/j.cortex.2009.06.009

Timmann, D., Drepper, J., Maschke, M., Kolb, F. P., Boring, D., Thilmann, A. F., et al. (2002). Motor deficits cannot explain impaired cognitive associative learning in cerebellar patients. *Neuropsychologia* 40, 788–800. doi: 10.1016/S0028-3932(01)00181-6

Timmann, D., Konczak, J., Ilg, W., Donchin, O., Hermsdorfer, J., Gizewski, E. R., et al. (2009). Current advances in lesion-symptom mapping of the human cerebellum. *Neuroscience* 162, 836–851. doi: 10.1016/j.neuroscience.2009.01.040

Tseng, Y. W., Diedrichsen, J., Krakauer, J. W., Shadmehr, R., and Bastian, A. J. (2007). Sensory prediction errors drive cerebellum-dependent adaptation of reaching. *J. Neurophysiol.* 98, 54–62. doi: 10.1152/jn.00266.2007

van Donkelaar, P., and Lee, R. G. (1994). Interactions between the eye and hand motor systems: disruptions due to cerebellar dysfunction. *J. Neurophysiol.* 72, 1674–1685.

Wallman, J., and Fuchs, A. F. (1998). Saccadic gain modification: visual error drives motor adaptation. *J. Neurophysiol.* 80, 2405–2416.

Walter, J. T., and Khodakhah, K. (2006). The linear computational algorithm of cerebellar Purkinje cells. *J. Neurosci.* 26, 12861–12872. doi: 10.1523/JNEUROSCI.4507-05.2006

Walter, J. T., and Khodakhah, K. (2009). The advantages of linear information processing for cerebellar computation. *Proc. Natl. Acad. Sci. U.S.A.* 106, 4471–4476. doi: 10.1073/pnas.0812348106

Welsh, J. P., Lang, E. J., Suglhara, I., and Llinas, R. (1995). Dynamic organization of motor control within the olivocerebellar system. *Nature* 374, 453–457. doi: 10.1038/374453a0

Witter, L., Canto, C. B., Hoogland, T. M., de Gruijl, J. R., and De Zeeuw, C. I. (2013). Strength and timing of motor responses mediated by rebound firing in the cerebellar nuclei after Purkinje cell activation. *Front. Neural Circuits* 7:133. doi: 10.3389/fncir.2013.00133

Wolpert, D. M., and Ghahramani, Z. (2000). Computational principles of movement neuroscience. *Nat. Neurosci.* 3(Suppl.), 1212–1217. doi: 10.1038/81497

Wolpert, D. M., and Kawato, M. (1998). Multiple paired forward and inverse models for motor control. *Neural Netw.* 11, 1317–1329. doi: 10.1016/S0893-6080(98)00066-5

Wolpert, D. M., Miall, R. C., and Kawato, M. (1998). Internal models in the cerebellum. *Trends Cogn. Sci.* 2, 338–347. doi: 10.1016/S1364-6613(98)01221-2

Woodman, G. F., and Luck, S. J. (1999). Electrophysiological measurement of rapid shifts of attention during visual search. *Nature* 400, 867–869. doi: 10.1038/23698

Xu-Wilson, M., Chen-Harris, H., Zee, D. S., and Shadmehr, R. (2009). Cerebellar contributions to adaptive control of saccades in humans. *J. Neurosci.* 29, 12930–12939. doi: 10.1523/JNEUROSCI.3115-09.2009

Yamazaki, T., and Nagao, S. (2012). A computational mechanism for unified gain and timing control in the cerebellum. *PLoS ONE* 7:e33319. doi: 10.1371/journal.pone.0033319

Conflict of Interest Statement: The authors declare that the research was conducted in the absence of any commercial or financial relationships that could be construed as a potential conflict of interest.

Received: 28 February 2014; accepted: 27 May 2014; published online: 17 June 2014.
Citation: Popa LS, Hewitt AL and Ebner TJ (2014) The cerebellum for jocks and nerds alike. Front. Syst. Neurosci. ***8****:113. doi: 10.3389/fnsys.2014.00113*
This article was submitted to the journal Frontiers in Systems Neuroscience.

frontiers in
SYSTEMS NEUROSCIENCE

HYPOTHESIS AND THEORY ARTICLE
published: 19 November 2014
doi: 10.3389/fnsys.2014.00221

Disruption of the LTD dialogue between the cerebellum and the cortex in Angelman syndrome model: a timing hypothesis

Guy Cheron[1,2]*, Javier Márquez-Ruiz[3], Tatsuya Kishino[4] and Bernard Dan[5]

[1] *Laboratory of Electrophysiology, Université de Mons, Mons, Belgium*
[2] *Laboratory of Neurophysiology and Movement Biomechanics, ULB Neuroscience Institut, Université Libre de Bruxelles, Brussels, Belgium*
[3] *División de Neurociencias, Universidad Pablo de Olavide, Sevilla, Spain*
[4] *Division of Functional Genomics, Center for Frontier Life Sciences, Nagasaki University, Nagasaki, Japan*
[5] *Department of Neurology, Hôpital Universitaire des Enfants Reine Fabiola, Université Libre de Bruxelles, Brussels, Belgium*

Edited by:
Thomas C. Watson, University of Bristol, UK

Reviewed by:
Christian Hansel, Erasmus Medical Center, Netherlands
Freek Hoebeek, Erasmus Medical Center, Netherlands

****Correspondence:***
Guy Cheron, Laboratory of Neurophysiology and Movement Biomechanics, ULB Neuroscience Institut, Université Libre de Bruxelles, Route de Lennik, Bâtiment N, CP601, 1070 Brussels, Belgium
e-mail: gcheron@ulb.ac.be

Angelman syndrome (AS) is a genetic neurodevelopmental disorder in which cerebellar functioning impairment has been documented despite the absence of gross structural abnormalities. Characteristically, a spontaneous 160 Hz oscillation emerges in the Purkinje cells network of the *Ube3a*$^{m-/p+}$ Angelman mouse model. This abnormal oscillation is induced by enhanced Purkinje cell rhythmicity and hypersynchrony along the parallel fiber beam. We present a pathophysiological hypothesis for the neurophysiology underlying major aspects of the clinical phenotype of AS, including cognitive, language and motor deficits, involving long-range connection between the cerebellar and the cortical networks. This hypothesis states that the alteration of the cerebellar rhythmic activity impinges cerebellar long-term depression (LTD) plasticity, which in turn alters the LTD plasticity in the cerebral cortex. This hypothesis was based on preliminary experiments using electrical stimulation of the whiskers pad performed in alert mice showing that after a 8 Hz LTD-inducing protocol, the cerebellar LTD accompanied by a delayed response in the wild type (WT) mice is missing in *Ube3a*$^{m-/p+}$ mice and that the LTD induced in the barrel cortex following the same peripheral stimulation in wild mice is reversed into a LTP in the *Ube3a*$^{m-/p+}$ mice. The control exerted by the cerebellum on the excitation vs. inhibition balance in the cerebral cortex and possible role played by the timing plasticity of the Purkinje cell LTD on the spike–timing dependent plasticity (STDP) of the pyramidal neurons are discussed in the context of the present hypothesis.

Keywords: plasticity, cerebellum, somatosensory cortex, LTD, LTP, STDP, Purkinje cells

INTRODUCTION

ANGELMAN SYNDROME

Angelman syndrome (AS) is a genetic neurodevelopmental condition characterized by intellectual and learning disability, motor dysfunction including ataxia, speech impairment, epilepsy and typical behavioral manifestations including exuberance and easily provoked laughter. It is caused by lack of expression of the maternally inherited *UBE3A* gene, an imprinted gene located on chromosome 15Q10–Q12 (Kishino et al., 1997). Cerebellar dysfunction was suggested since the original clinical description of the syndrome (Angelman, 1965). It has been confirmed by motor studies (Dan et al., 2001; Dan and Cheron, 2004) and functional imaging (Holopainen et al., 2001; Peters et al., 2011; Tiwari et al., 2012). Mouse models with knockout maternal *Ube3a* (*Ube3a*$^{m-/p+}$) show no morphologic cerebellar abnormalities (Jiang et al., 1998; Miura et al., 2002). However, lack of *Ube3a* expression was specifically demonstrated in the Purkinje cell layer (Miura et al., 2002; Daily et al., 2012). These mice showed ataxia (Jiang et al., 1998; Miura et al., 2002; Heck et al., 2008; Mulherkar and Jana, 2010; Jana, 2012). We previously reported the emergence of fast (160 Hz) oscillation in the cerebellum of the *Ube3a*$^{m-/p+}$ mice (Dan et al., 2004; Cheron et al., 2005). This local field potential oscillation (LFPO) is maximum at the level the Purkinje cell layer. It is related to an increase in Purkinje cell simple spike firing and rhythmicity. The 160 Hz LFPO is highly synchronized along the parallel fiber beam. It is inhibited by gabazine and carbenoxolone (Cheron et al., 2005). In sum, it appears to be physiologically similar to that described in calcium-binding proteins knockout mice, including calretinin, calbindin and parvalbumin (Cheron et al., 2004; Servais et al., 2005). However, immunocytochemical staining demonstrated normal calbindin expression in the Purkinje cell of *Ube3a*$^{m-/p+}$ mice (Jiang et al., 1998), this might suggest other factors than calcium signaling in the emergence of the LFPO. More recently, Egawa et al. (2012) showed that tonic inhibition is specifically decreased in cerebellar granule cells in slice recordings obtained in *Ube3a*$^{m-/p+}$ mice. This was due related to Ube3a implication in the degradation of GABA(A) transporter 1 (GAT1) with

lack of Ube3a expression inducing excess GAT1 in *Ube3a*$^{m-/p+}$ mice resulting in a decrease of GABA(A) concentration in the extrasynaptic space (Egawa et al., 2012). This default in tonic inhibition of the granule cells may increase their excitatory input onto the Purkinje cell, which is a recognized mechanism in the emergence of the 160 Hz LFPO (Bearzatto et al., 2006). In addition, a dysfunction in tonic GABA(A) conductance may explain a number of phenotypic features encountered in neurodevelopmental disorders like AS (Egawa and Fukuda, 2013).

NEURONAL PLASTICITY

Given the cardinal learning impairments and cerebellar dysfunction in AS, the role of cerebellar plasticity has attracted increasing attention. The specific relationship between cerebellar cortex and inferior olive has recently been suggested to provide an informative avenue for integrating the evidences of neuronal plasticity in a translational perspective (Cheron et al., 2013). The Purkinje cells plastic properties are specifically controlled by input from climbing fibers, allowing processing through both feed-forward and feedback loops inside the cerebellar cortex. In addition, bidirectional connections with the basal ganglia and multiple cerebral cortex areas extend the cerebellar dynamic function toward a wide range of behaviors. More specifically, reversible inactivation of the somatosensory cortex in the rat results in a lengthening of the latency of the climbing fiber in response to a peripheral stimulus (Brown and Bower, 2002). Interestingly, it was recently demonstrated (Najafi et al., 2014) in awake mice that the climbing fiber-triggered calcium signals are enhanced when it was elicited by a sensory event allowing a strong modulation of cerebellar plasticity. The majority of brain operations necessitate the cerebellum assistance to provide exact timing of multiple signals coming from the sensory systems (Bower, 1997) and their integration in the cerebral cortex. This multidimensional computation would also require a timing plasticity allowing motor sequence ordering, detection of error and sensory prediction (D'Angelo and De Zeeuw, 2009; De Zeeuw et al., 2011; Heiney et al., 2014). Very recently, it was demonstrated that the L7-PP2B mice presenting impaired PC intrinsic plasticity were severely impaired in learning of an object localization task requiring a precise timing (Rahmati et al., 2014). This is of particular interest considering that the ability to produce adequate responses to sensory stimuli was preserved in this mutant. Based on these findings, these authors suggested an important role of cerebellum-cerebrum interaction in cognitive task necessitating a strict temporal tuning.

As *Ube3a* expression is present in all brain regions in principal neurons as well as GABAergic interneurons there is a great probability that a number of neuronal processes such as neuronal plasticity are compromised in AS (Gustin et al., 2010). Deficit in learning and plasticity in *Ube3a*$^{m-/p+}$ mice have been mainly reported in hippocampal slice. Recently, following contextual fear conditioning *Ube3a*$^{m-/p+}$ mice, Filonova et al. (2014) demonstrated a deficit in the activity-dependent increases in ERK1/2 phosphorylation, which corroborates previously reported alteration in synaptic plasticity and cognitive function in AS mice (Jiang et al., 1998; van Woerden et al., 2007; Huang et al., 2013). In particular, an abnormal LTP was demonstrated in hippocampal slice of AS mice (van Woerden et al., 2007), where following the conditioning stimuli a short time long-term depression (LTD) was recorded in place of an LTP. Moreover, these authors demonstrated that this abnormal plasticity can be rescued by introducing an additional mutation at the inhibitory phosphorylation site of alpha CaMKII. To our knowledge there is no available data about LTP or LTD in the cerebellum of the *Ube3a*$^{m-/p+}$ mice.

RESULTS

HYPOTHESIS

Here we propose a pathophysiological hypothesis stating that the cerebellar abnormal rhythmic activity recorded as fast LFPO in AS mouse model impairs cerebellar LTD plasticity, which in turn alters the LTD plasticity in the cerebral cortex. This would provide a new understanding for a range of phenotypic abnormalities seen in AS and have implications for targeted management of patients with this condition. Long range bidirectional communications as those reported between the cerebellum, the basal ganglia and the cortex highlight the importance of the precise timing operating at the different loci. Interestingly, the LTD reported in cerebellar slice (Roggeri et al., 2008) and in our recent experiments in the cerebellum of alert mice (Márquez and Cheron, 2012) were accompanied by a short delay (**Figure 1B**). The cerebellar LTD may influence all the chain of neuronal targets from the deep cerebellar nucleus (DCN) to the cerebral cortex via the thalamus. In order to study such possible cooperation between the cerebellar and cortical plasticity a same sensory input and a same inductor of plasticity must be used. This sensory input is in our case represented by an electrical pulse given on the whisker pad and the inductor of plasticity consists in an 8 Hz electrical stimulus given during 10 min on the whisker pad (**Figure 1A**). As previously reported by Han et al. (2014) such lower frequency rate (5 Hz in this case) induced also an LTD in the barrel cortex of the anesthetized rat. It seems a priori that the LTD in the barrel cortex was not accompanied by a timing plasticity as the one present in the cerebellum. How the cerebellar LTD may or not contribute to the LTD in the barrel cortex is the central question of the present hypothesis.

CEREBELLAR AND CEREBRAL LTD

This hypothesis stems from a series of results obtained using a novel LTD-inducing protocol in which 8 Hz electrical stimulation is applied on the whisker pad in the alert mouse during 10 min (Márquez-Ruiz and Cheron, 2012). A single electrical stimulus given on the whisker pad activates the afferent fibers of the trigeminal ganglion and reaches different modules of the cerebellum by the mossy fibers originating from the trigeminal nucleus (Tn) in the brainstem. From this nucleus the sensory input also reaches the inferior olive activating the climbing fiber input to the cerebellum. We have recently shown that the basic prerequisite for producing the classical LTD at the parallel fiber-Purkinje cell synapse (conjunctive stimulation of the mossy and climbing fibers; Ito and Kano, 1982; Ito, 2001) is encountered in awake mouse when single electrical stimulation was applied on the whisker pad (Márquez-Ruiz and Cheron, 2012). Indeed, this

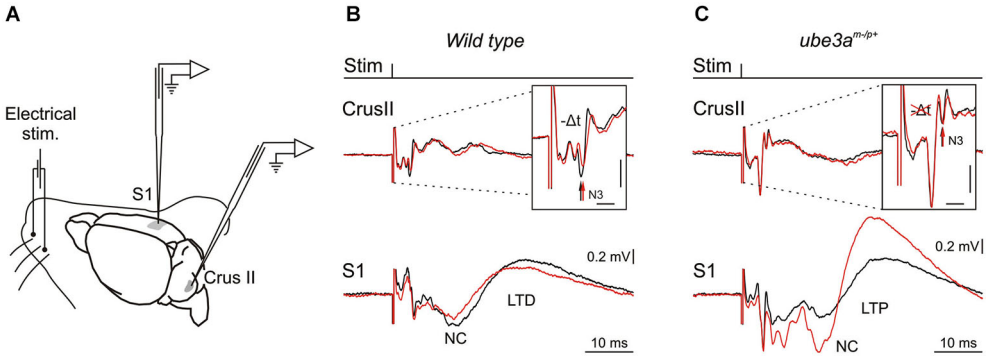

FIGURE 1 | Experimental design and electrophysiological responses to electrical stimulation of mouse whiskers during 8 Hz inducing-LTD. **(A)** Animals were prepared for chronic recordings of local field potentials (LFP) and unitary extracellular activity in the Purkinje cell layer of the Crus I/II area and in S1 cortical area. Facial dermatomes of the whisker region were electrically stimulated with a pair of needles under the skin (Stim). **(B)** In the upper part, LFP recorded in the Crus II in response of a single electrical pulse before (black trace) and after 10 min of the 8 Hz LTD-inducing protocol in wild type (WT) mouse (red trace). Note the delayed and reduced N3 component (vertical arrows) after the 8 Hz LTD-inducing protocol. In the lower part, LFP recorded in the somatosensory cortex (S1) before (black trace) and after the same 8 Hz LTD-inducing protocol (red trace). Note the reduced negative component (NC) indexing a cortical LTD in WT mouse. **(C)** The same type of LFP components as in B but recorded in a *Ube3a*$^{m-/p+}$ mouse. Note the absence of cerebellar LTD indexed by the absence of amplitude and timing change in N3 component after the 8 Hz LTD-inducing protocol (red trace) in upper part, and the reversal of the NC LTD into a NC LTP recorded in S1 (lower part). Horizontal and vertical scales in **(B)** and **(C)** correspond to 2 ms and 0.2 mV, respectively.

stimulation produced a first simple spike response (excitation-inhibition) shortly followed by a complex spike response (Bosman et al., 2010). This peripheral stimulus evoked a series of components in the local field of the cerebellar cortex (Márquez-Ruiz and Cheron, 2012; **Figure 1B**, *upper part*). Among these, the N3 component is directly related to the postsynaptic activity of the parallel fiber-Purkinje cell synapse. During the 8 Hz LTD-inducing stimulus both the simple and complex spike firing were significantly increased. Ten minutes after the 8 Hz stimulation, the amplitude of N3 peak is decreased and its latency delayed during at least 30 min (**Figure 1B**, *upper part*). These effects have been reproduced in the littermate wild type (WT) of the *Ube3a*$^{m-/p+}$ mice (**Figure 2A**). The N3 amplitude was significantly decreased (from 0.39 ± 0.02 mV before the 8 Hz stimulation to 0.22 ± 0.04 ($p < 0.01$) 15 min after and 0.24 ± 0.03 ($p < 0.01$) 30 min after ($p < 0.05$; $n = 4$; **Figure 2A**). A cerebellar LTD is thus recorded in alert WT mouse. During the same time, from the Tn via the ventro-posterior medial (VPM) nucleus of the thalamus, the same electrical stimulation reaches the primary somatosensory area of the cerebral cortex (Bosman et al., 2011), where it induces a number of evoked components (**Figure 1B**, *lower part*). Among these, a large NC peaks around 15 ms. This NC represents compound postsynaptic activity of the pyramidal neurons. The lower part of the **Figure 1B** illustrates that the 8 Hz LTD-inducing stimulus specifically reduced the amplitude of the NC (from 0.16 ± 0.04 to 0.09 ± 0.03 ($p < 0.03$) 15 min after and 0.09 ± 0.04 ($p < 0.03$) 30 min after; **Figure 2B**). This effect thus corresponds to specific LTD of the NC evoked response. A similar evoked NC component occurring at the latency of 13–15 ms has been recently demonstrated by Han et al. (2014) in the barrel cortex of the anesthetized rat by using air puff stimulation of the whisker. These authors also demonstrated a long-lasting increase (LTP up to 60 min) of this NC after a 100 Hz conditioning stimulus and a long-lasting decrease (LTD) after a 5 Hz conditioning stimulus. This latter evidence corroborates the present cortical LTD recorded in the

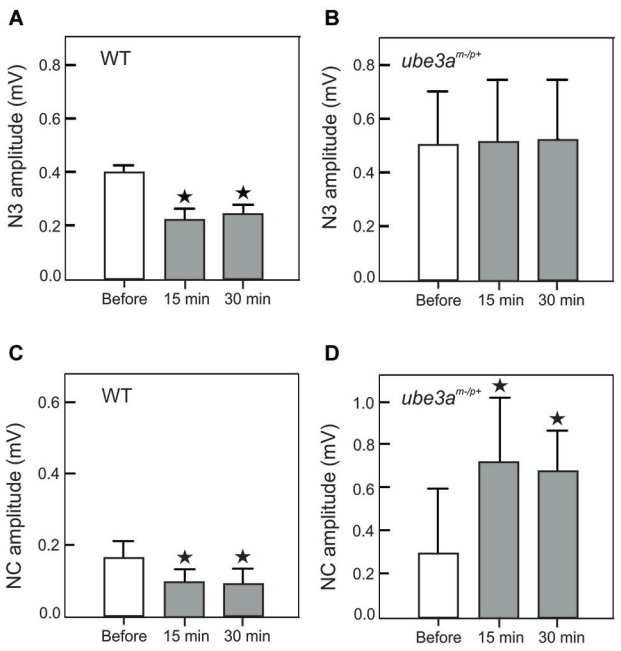

FIGURE 2 | Amplitude histogram of cerebellar N3 LFP component (A, B) and the negative component (NC) of the S1 cortical area (C, D). These components were recorded before, 15 and 30 min after the 8 Hz LTD-inducing protocol in WT **(A, C)** and in *Ube3a*$^{m-/p+}$ mice **(B, D)**. Note the presence of a LTD of N3 and NC in WT mice **(A, C)** and the absence of modification of N3 **(B)** and the presence of a LTP in *Ube3a*$^{m-/p+}$ mice. The asterisks correspond to $p < 0.05$.

alert mice after 8 Hz electrical stimulus. In addition, microinjection of APV in the barrel cortex demonstrated that both LTP and LTD of the NC component are NMDA dependent (Han et al., 2014).

In *Ube3a*$^{m-/p+}$ mice (AS mouse model), our preliminary results showed that the Purkinje cell LTD (in particular the N3 component) was absent (Dan et al., 2010), both the latency (**Figure 1C**, upper part) and the amplitude (**Figure 2C**) remained the same before and after the 8 Hz stimulation period ($p = 0.99$) In addition, we show here that a LTP of the NC was obtained in the cerebral cortex of *Ube3a*$^{m-/p+}$ mice instead of the physiological LTD (**Figure 1C**, *lower part*). The NC amplitude increased from 0.30 ± 0.11 mV to 0.72 ± 0.32 ($p < 0.05$) and 0.67 ± 0.18 ($p < 0.05$) 15 and 30 min after the 8 Hz stimulation period, respectively (**Figure 2D**). In accordance with our hypothesis, the absence of Purkinje cell LTD is accompanied by a LTD to LTP reversal in the barrel cortex following the same peripheral stimulation and 8 Hz LTD-inducing stimulus as applied in WT controls (**Figure 1B**).

EXCITATION VS. INHIBITION BALANCE AND SPIKE–TIMING DEPENDENT PLASTICITY

In order to account for these findings, two main mechanisms could be implicated. One concerns the control exerted by the cerebellum on the excitation vs. inhibition balance in the cerebral cortex; the other the influence of the timing of the cerebellar input on to the cerebral cortex. In terms of the excitation-inhibition balance mechanism, we hypothesize the action of the cerebellum in the control of the balance between excitatory and inhibitory neural activities within the cerebral cortex of the *Ube3a*$^{m-/p+}$ mice may be disrupted. On the other hand, the timing plasticity of the Purkinje cell LTD may influence the spike–timing dependent plasticity (STDP) of the pyramidal neurons (**Figure 3**). These two possible mechanisms are not mutually exclusive but could cooperate allowing the distant action of the Purkinje cell LTD on the plasticity of the cerebral cortex.

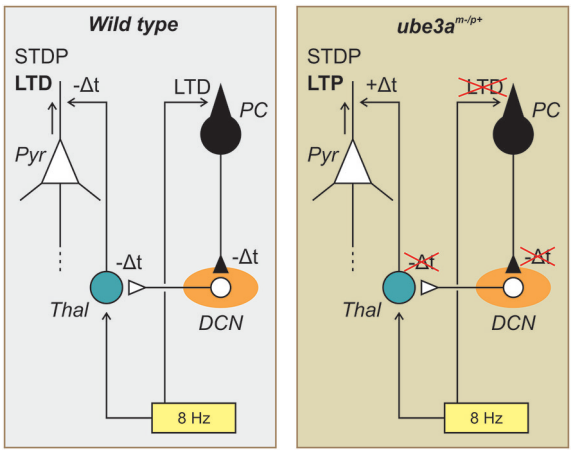

FIGURE 3 | Schematic drawing of the possible role played by the timing plasticity of the Purkinje cell LTD on the spike–timing dependent plasticity (STDP) of the pyramidal neurons. In the WT mouse (left side), the 8 Hz LTD-inducing protocol (yellow rectangle) produce both a cerebellar LTD (at the parallel fiber-Purkinje cell (*PC*) synapse, black symbol) and a cortical LTD (in the Pyramidal cell (*Pyr*), white symbol). The PC-LTD signals is transmitted to the deep cerebellar nucleus (*DCN*, orange elipse) and via the thalamus (*Thal*, blue circle) to the somatosensory cortex. Following the present hypothesis the delayed signals ($-\Delta t$) accompanying the cerebellar LTD is transmitted to the cerebral cortex where thanks to the SDTP mechanism a LTD is favored. In the *Ube3a*$^{m-/p+}$ mouse (right side) the same diagram is represented but in this case because the cerebellar LTD is missing the delayed signals is not transmitted to the cerebral cortex resulting in $+\Delta t$ inducing by the SDTP mechanism a LTP (see text for more details).

DISCUSSION

ANATOMICAL PATHWAYS SUPPORTIVE OF THE HYPOTHESIS

The present hypothesis focused on early evoked responses both in the cerebellar Crus I-II and in the somatosensory cortex (S1). Indeed, electrical stimulation applied on the whisker pad as used in the present paradigm mainly concerned the afferent inputs conveyed by myelinated sensory fibers whose cell bodies are located either in the trigeminal ganglion or in the mesencephalic nucleus (see Bosman et al., 2011, for a review). From there the sensory input reaches the somatosensory cortex via the thalamus, and the sensory volley reaches the cerebellum by a direct path (i.e., mossy fibers) and an indirect path via the inferior olive (Cook and Wiesendanger, 1976). After integration in the cerebellar cortex and subsequently in the cerebellar module (Cerminara and Apps, 2011; Ruigrok, 2011; Llinás, 2014) the sensory message is sent back to the thalamus via the deep cerebellar nuclei. The cerebellar inputs pass through the ventral lateral (VL) complex (Asanuma et al., 1983; Aumann et al., 1994, 1996; Teune et al., 2000; Ruigrok and Teune, 2014) and the central medial nucleus of the intralaminar complex of the thalamus (Allen and Tsukara, 1974; Molinari et al., 2002) before reaching the cortex. In the rat the caudal region of the central medial nucleus projects more specifically to the sensorimotor cortex (Vertes et al., 2012).

The trigeminal input conveyed by the lemniscal and paralemniscal pathways arrives in the somatosensory (barrel) cortex mainly via the VPM and posterior medial (POM) thalamus, respectively (Viaene et al., 2011). The thalamocortical neurons of the VPM organized in "barreloids" (Lefort et al., 2009; Aronoff et al., 2010) provide about 90% of excitatory connections within layer IV and layers II/III of the cortex and convey sensory input with short latency (Killackey and Ebner, 1973; Lübke et al., 2000; Cruikshank et al., 2009; Bosman et al., 2011), In contrast, the thalamocortical POM neurons are not organized in "barreloids". They project to layers I and V and convey sensory input with longer latency. As the present hypothesis concerns plasticity exerted on short latency responses, only the VPM contribution may be considered here.

Recent studies (Kuramoto et al., 2009) demonstrated segregation of basal ganglia and cerebellum inputs in the rat motor thalamic nuclei. The ventral anterior (VA) region mainly receives basal ganglia afferents while the VL region receives the cerebellar afferent. In addition, these regions contain two different types of thalamocortical neurons, the IZ and EZ neurons, respectively. The IZ neurons are under the inhibitory control of the internal segment of the globus pallidus and the substantia nigra pars reticulata and selectively project on the superficial cortical layer

(I), whereas the EZ neurons are under the excitatory control of the deep cerebellar nuclei and selectively project to cortical layers II-V. Although, these thalamic inputs mainly concern the motor cortex (M1) they also project to the somatosensory cortex (S1; see, neurons EZ in Figure 8 of Kuramoto et al., 2009).

In addition, S1 is reciprocally connected to M1 (Ferezou et al., 2007; Mao et al., 2011). This cortico-cortical coupling between sensory and motor signals might mediate active tactile sensory perception (Ferezou et al., 2006, 2007), sensorimotor integration and motor learning (Mao et al., 2011). In addition, electrical stimulations of M1 and S1 evoked autofluorescence responses with similar time courses and amplitudes in the cerebellar cortex (Crus I; Proville et al., 2014), corroborating the well-defined corticopontine projections to the cerebellum (Leergaard et al., 2000; Suzuki et al., 2012). In this context, it was demonstrated (Popa et al., 2013) that inactivation of the cerebellum by the injection of GABAergic agonist muscimol in the cerebellar nuclei maintained a normal whisking behavior but disrupted the coherence of the gamma-band local field potentials between S1 and M1 cortices. This evidence is particularly important and in line with the present hypothesis because it demonstrates that the cerebellum may coordinate the rhythmic activities of the sensorimotor cortex.

The intracortical network is composed (1) in layer IV by the excitatory spiny stellates neurons (regular spiking) of layer IV, which are the primary targets for thalamic afferents surrounded by inhibitory basket and non-basket interneurons (fast spiking; Feldmeyer et al., 1999); and (2) in layer II/III by the excitatory pyramidal regular-spiking neurons, the fast-spiking basket and the low-threshold spiking non-basket inhibitory interneurons (McCormick et al., 1985; Gibson et al., 1999).

EFFECTS OF CEREBELLAR STIMULATION ON THE CEREBRAL CORTEX

Cerebellar stimulation studies are in accordance with the first mechanism implicating the excitation vs. inhibition balance of the cerebral cortex. As it was demonstrated that the cerebellum may influence both inhibitory and excitatory neurons of the motor cortex in the cat (Noda and Yamamoto, 1984), monkey (Holdefer et al., 2000) and human (Daskalakis et al., 2004), we may reasonably expect that this possibility is also present in the somatosensory cortex. Cerebellar stimulation (electrical, Ugawa et al., 1991, 1994; or magnetic, Ugawa et al., 1995) applied on the lateral part of the cerebellum 5–7 ms before transcranial magnetic stimulation (TMS) of the motor cortex induces an inhibition of the motor-evoked potential. This inhibition may be provided through cortical inhibitory interneurons (Na et al., 1997) or by inhibition of thalamocortical neurons at the thalamic level (Ando et al., 1995). Interestingly, magnetic cerebellar stimulation decreases the short-interval intracortical inhibition and increases the intracortical facilitation (Daskalakis et al., 2004; Koch et al., 2008). When the inhibitory action of the Purkinje cell on the DCN is depressed, as during LTD of the Purkinje cell, the DCN could be able to activate the short-interval intracortical inhibition and to decrease the intracortical facilitation which may in turn facilitate the expression of a cortical LTD as reported after 5 Hz (Han et al., 2014) or 8 Hz (Márquez-Ruiz and Cheron, 2012) LTD-inducing protocol. Conversely, when the Purkinje cell LTD is missing, as in *Ube3a*$^{m-/p+}$ mice, DCN output is expected to be depressed and not to be able to favor cortical LTD. On the contrary, it would activate the intracortical facilitation inducing a LTP (**Figure 3**).

THE STDP AS A CENTRAL MECHANISM

We propose that the reversal of the cerebral LTD into a LTP is a consequence of the disruption of the timing message controlled by the Purkinje cell LTD that could be crucial for the STDP of the pyramidal neurons of the cortex (**Figure 3**). The STDP is a central mechanism which occurs in the neocortex (Markram et al., 2011). It allows revisiting the LTP and LTD mechanisms at this level by highlighting the importance of a precise timing between the input and the output signals of the neocortex. The STDP was initially demonstrated by dual whole-cell voltage recordings from pyramidal neurons (Markram et al., 1997) and was independently supported by the theoretical work of Gerstner et al. (1996). It follows from this major discovery that the coincidence of the back propagation of the postsynaptic action potential and the excitatory postsynaptic potentials (EPSPs) are crucial for the induction of up or down regulation of the active synapses. Thus, we may summarize the STDP by the fact that synapses are reinforced if presynaptic spikes repeatedly occur before postsynaptic spikes within a few tens of milliseconds or less, whereas the opposite temporal order elicits synaptic weakening. In accordance with STDP mechanism we hypothesize that the delay imposed by the Purkinje cell LTD on the DCN disinhibition is transmitted to the barrel cortex where it facilitated a delayed control of the pyramidal synapse in favor of a cortical LTD. On contrary, the absence of this delayed timing in the *Ube3a*$^{m-/p+}$ mice induces reversal plasticity toward a cortical LTP (**Figure 3**).

By linking output-input activities of a neuron by a strong timing constraint for plasticity, when considering the STDP, it is important to take into account all the interacting neuronal loops involved in a single behavioral plasticity. As reverberating activity (Lorente de Nó, 1938) inside of closed loop circuits and re-entrant paths are central for the understanding of Hebbian plasticity (Hebb, 1949), a local plasticity occurring in one part of the cortex (LTP or LTD) probably depends on all the input-output relationships of this part of the cortex and of the other local plasticity (LTD or LTP) occurring in other communicant networks, as for example the cerebellum. In this context, it was recently proposed that although Purkinje cells lack backpropagating Na(+) spikes, the relative timing between the climbing and parallel fibers could played a STDP at the level of the parallel fiber-Purkinje cell synapse controlling the LTP/LTD switch (Piochon et al., 2013).

The present hypothesis is supported by multiple lines of evidences supporting the existence of STDP in the somatosensory cortex (Feldman, 2000; Allen et al., 2003; Banerjee et al., 2014). Spike-timing dependent plasticity occurring at vertical layer IV and horizontal layer II/III inputs onto postsynaptic layer II/III neurons in the mouse barrel cortex has been studied and compared (Banerjee et al., 2014). They demonstrated that STDP is present for both vertical and horizontal inputs but that LTD induction at vertical inputs necessitates

presynaptic NMDA supporting presynaptic LTD whereas LTD at the horizontal inputs is postsynaptic and require postsynaptic NMDA receptors. These data support the present hypothesis that cerebellar inputs could play a role in these STDP in the barrel cortex. In addition, a large scale model of the barrel cortex (Phoka et al., 2012) demonstrated that STDP can induce long-term synaptic modifications in the network encoding the dynamic features of the sensory inputs. This model corroborates the present hypothesis by the fact that via the synaptic weights modification the sensory experience reverberates into the spontaneous state dynamics which would logically integrate the presence or the absence of cerebellar plasticity.

PLASTICITY IN THE THALAMUS

The segregation and relative independence of the lemniscal and cerebellar input at the thalamic level (Aumann et al., 1994, 1996) may simplify the further studies of the present hypothesis based on the interaction between cerebellar and cortical plasticity. However, we may consider the possibility that the 8 Hz stimulation of the whisker produces long-term synaptic modification at the thalamic level independently from cortical and cerebellar plasticity.

The fact that during whisker plucking, the receptive field modifications occur first in LII/III and only later or not at all in LIV layer, the site of arrival of the VPM projection, indicates that such type of plasticity occur primarily in the cortex and not in the VPM (Fox, 1994; Glazewski and Fox, 1996; Wallace and Fox, 1999).

However, this does not preclude that in case of subcutaneous block of peripheral trigeminal nerve fibers (with lidocaine), immediate plasticity occurs in the VPM, independently from the potent influence of the cortical feedback (Krupa et al., 1999). It has been proposed that the contribution of thalamic vs. cortical plasticity largely depends on the nature of factors at the origin of plasticity (Fox et al., 2000). When plasticity is induced by nerve block or lesions, thalamic plasticity is the norm (Krupa et al., 1999). Interestingly, when the nucleus gracilis of the dorsal column is destroyed, thalamic plasticity occurs but this plasticity is prevented if the cortex is ablated before inducing plasticity (Parker and Dostrovsky, 1999). In contrast, when whisker experiences are the inducing factor of plasticity, the cortical plasticity is not accompanied by measurable thalamic plasticity (Fox, 1994; Glazewski and Fox, 1996; Wallace and Fox, 1999). As the present hypothesis and related data concern whisker experience and not lesion, we may reasonably suppose that no major subcortical plasticity is concerned and that the cerebellar input remains generally unaltered when reaching the cortex. This would facilitate the further testing of the present hypothesis.

Whatever the exact role played by the olivo-cerebellar modules (motor learning vs. motor timing, Llinás, 2011), the phase locking of the PC complex spike on the 160 Hz LFP oscillation in knockout mice for genes encoding calcium binding proteins (Cheron et al., 2004) and in the *Ube3a*$^{m-/p+}$ mice (Cheron et al., 2005) indicates that the inferior olive is influenced by the 160 Hz oscillation. This would greatly disturb the operation of the olivo-cerebellar modules and the related DCN outputs to the thalamus and the cerebral cortex. In addition, the increased PC synchrony along the parallel fiber beam recorded in the *Ube3a*$^{m-/p+}$ mice may also influence the DCN neurons which are very sensitive to the degree of PC synchrony (Person and Raman, 2011, 2012). The presence of the cerebellar 160 Hz oscillation in *Ube3a*$^{m-/p+}$ mice may thus be viewed as a strong pathological factor explaining the absence of cerebellar LTD and the reversal of the cerebral LTD into LTP. However, if the presence of 160 Hz LFP oscillations in the PC layer of the *Ube3a*$^{m-/p+}$ may explain the impaired cerebellar LTD, we never recorded similar high frequency LFP oscillation in the S1 cortex of these mice (unpublished communication).

These lines of evidence seem to provide a robust avenue for testing cerebellar contribution to a number of manifestations of abnormal brain functions. In human patients with AS, several cardinal features have been related to abnormal cortical function/plasticity, including learning disability, cognitive disorder, behavioral abnormality, speech impairment and epilepsy. When testing the present hypothesis in the mouse model, there may be a case for specifically addressing the impact of high frequency oscillation on thalamo-cortical networks, and that of aberrant cerebellar LTD on cerebral plasticity. In this context, other neurophysiological abnormalities which are not specific to the cerebellum may also play a role. For example, excitatory/inhibitory imbalance has been demonstrated at both cellular and network levels in the visual cortex of *Ube3a*$^{m-/p+}$ mice (Wallace et al., 2012). In our experimental paradigm the conjunction of cerebellar and cortical LTD would logically influence the reverberating activity inside the closed loop in a way that is greatly dependent of the synaptic sign and the precise timing throughout the different loop stations. If the cortical output is depressed by a local LTD it may in turn depress the excitatory input of the cerebellar input and reinforces the LTD at the level of the Purkinje cell and thus increases the delayed disinhibition of the DCN which in turn facilitates an increase of the cerebellar input to the cerebral cortex. If this acting loop is directed to the inhibitory interneurons of the barrel cortex (Na et al., 1997; Daskalakis et al., 2004; Koch et al., 2008) it must logically facilitate the presence of the LTD in the pyramidal cell of the barrel cortex, where in the same time the delayed cerebellar excitatory input also reinforce the LTD plasticity.

The present hypothesis is also in line with the recent proposal (Watson et al., 2013) that the cerebellum may be involved in the selective relaying of "teaching signals" in order to coordinate survival and emotional behaviors through the selective relaying of "teaching signals" arising from higher centers associated with emotional behaviors.

Very recently, Proville et al. (2014) developed a new experimental paradigm using optogenetic mapping of the cerebello-cortical connections in anesthetized mice and their effect on the whisking movement in awake mice. This study elegantly demonstrates the bidirectional functional links between M1-S1 and the Crus I. On the one hand the electrical stimulation applied on S1 and or M1 induced excitatory response of PC and Golgi cells at latencies compatible with a disynaptic cortico-ponto-cerebellar connection. On the other hand, optogenetic

activation of PC induced a clear switch-off of the DCN activity directly followed by excitatory responses in the thalamus and the cortex. Interestingly, during whisking the optogenetic stimulation of the PC (Crus I) triggered a backward shift of the whisking set point at about 25 ms and induced perturbation in touch control demonstrating the involvement of the cerebello-cortical loop in vibrissa-guided behavior. This timing of the PC related motor action is compatible with the present evoked field triggered by whisker at about 5 ms in the cerebellar cortex and 15 ms in S1 cortex. The latter experimental evidences are in accordance with the present hypothesis and pave the way for further investigation of plasticity dialogue along the cerebello-cortical loops.

ACKNOWLEDGMENTS

The authors thank T. D'Angelo, M. Dufief, E. Hortmanns, M. Petieau and E. Toussaint for expert technical assistance. This work was funded by the Belgian Federal Science Policy Office, the European Space Agency (AO-2004, 118), the Belgian National Fund for Scientific Research (FNRS), and the Research Funds of the Université Libre de Bruxelles and the Université de Mons (Belgium). This work was also supported by SAM'sWALK and AFSA and by the Ministerio de Educación y Ciencia Programa Nacional de Movilidad de Recursos Humanos del Plan Nacional de I-D+I 2008–2011 of the Spanish Government.

REFERENCES

Allen, C. B., Celikel, T., and Feldman, D. E. (2003). Long-term depression induced by sensory deprivation during cortical map plasticity in vivo. *Nat. Neurosci.* 6, 291–299. doi: 10.1038/nn1012

Allen, G. I., and Tsukara, N. (1974). Cerebrocerebellar communication systems. *Physiol. Rev.* 54, 957–1006.

Ando, N., Izawa, Y., and Shinoda, Y. (1995). Relative contributions of thalamic reticular nucleus neurons and intrinsic interneurons to inhibition of thalamic neurons projecting to the motor cortex. *J. Neurophysiol.* 73, 2470–2485.

Angelman, H. (1965). 'Puppet' children. A report of three cases. *Dev. Med. Child Neurol.* 7, 681–688. doi: 10.1111/j.1469-8749.1965.tb07844.x

Aronoff, R., Matyas, F., Mateo, C., Ciron, C., Schneider, B., and Petersen, C. C. (2010). Long-range connectivity of mouse primary somatosensory barrel cortex. *Eur. J. Neurosci.* 31, 2221–2233. doi: 10.1111/j.1460-9568.2010.07264.x

Asanuma, C., Thach, W. T., and Jones, E. G. (1983). Distribution of cerebellar terminations and their relation to other afferent terminations in the ventral lateral thalamic region of the monkey. *Brain Res.* 286, 237–265. doi: 10.1016/0165-0173(83)90015-2

Aumann, T. D., Rawson, J. A., Finkelstein, D. I., and Horne, M. K. (1994). Projections from the lateral and interposed cerebellar nuclei to the thalamus of the rat: a light and electron microscopic study using single and double anterograde labelling. *J. Comp. Neurol.* 349, 165–181. doi: 10.1002/cne.903490202

Aumann, T. D., Rawson, J. A., Pichitpornchai, C., and Horne, M. K. (1996). Projections from the cerebellar interposed and dorsal column nuclei to the thalamus in the rat: a double anterograde labelling study. *J. Comp. Neurol.* 368, 608–619. doi: 10.1002/(sici)1096-9861(19960513)368:4<608::aid-cne11>3.0.co;2-d

Banerjee, A., González-Rueda, A., Sampaio-Baptista, C., Paulsen, O., and Rodríguez-Moreno, A. (2014). Distinct mechanisms of spike timing-dependent LTD at vertical and horizontal inputs onto L2/3 pyramidal neurons in mouse barrel cortex. *Physiol. Rep.* 2:e00271. doi: 10.1002/phy2.271

Bearzatto, B., Servais, L., Roussel, C., Gall, D., Baba-Aïssa, F., Schurmans, S., et al. (2006). Targeted calretinin expression in granule cells of calretinin-null mice restores normal cerebellar functions. *FASEB J.* 20, 380–382. doi: 10.1096/fj.05-3785fje

Bosman, L. W., Houweling, A. R., Owens, C. B., Tanke, N., Shevchouk, O. T., Rahmati, N., et al. (2011). Anatomical pathways involved in generating and sensing rhythmic whisker movements. *Front. Integr. Neurosci.* 5:53. doi: 10.3389/fnint.2011.00053

Bosman, L. W., Koekkoek, S. K., Shapiro, J., Rijken, B. F., Zandstra, F., van der Ende, B., et al. (2010). Encoding of whisker input by cerebellar Purkinje cells. *J. Physiol.* 588, 3757–3783. doi: 10.1113/jphysiol.2010.195180

Bower, J. M. (1997). Control of sensory data acquisition. *Int. Rev. Neurobiol.* 41, 489–513. doi: 10.1016/s0074-7742(08)60367-0

Brown, I. E., and Bower, J. M. (2002). The influence of somatosensory cortex on climbing fiber responses in the lateral hemispheres of the rat cerebellum after peripheral tactile stimulation. *J. Neurosci.* 22, 6819–6829.

Cerminara, N. L., and Apps, R. (2011). Behavioural significance of cerebellar modules. *Cerebellum* 10, 484–494. doi: 10.1007/s12311-010-0209-2

Cheron, G., Dan, B., and Márquez-Ruiz, J. (2013). Translational approach to behavioral learning: lessons from cerebellar plasticity. *Neural Plast* 2013:853654. doi: 10.1155/2013/853654

Cheron, G., Gall, D., Servais, L., Dan, B., Maex, R., and Schiffmann, S. N. (2004). Inactivation of calcium-binding protein genes induces 160 Hz oscillations in the cerebellar cortex of alert mice. *J. Neurosci.* 24, 434–441. doi: 10.1523/JNEUROSCI.3197-03.2004

Cheron, G., Servais, L., Wagstaff, J., and Dan, B. (2005). Fast cerebellar oscillation associated with ataxia in a mouse model of Angelman syndrome. *Neuroscience* 130, 631–637. doi: 10.1016/j.neuroscience.2004.09.013

Cook, J. R., and Wiesendanger, M. (1976). Input from trigeminal cutaneous afferents to neurones of the inferior olive in rats. *Exp. Brain Res.* 26, 193–202. doi: 10.1007/bf00238283

Cruikshank, S. J., Urabe, H., Nurmikko, A. V., and Connors, B. W. (2009). Pathway-specific feedforward circuits between thalamus and neocortex revealed by selective optical stimulation of axons. *Neuron* 65, 230–245. doi: 10.1016/j.neuron.2009.12.025

Daily, J., Smith, A. G., and Weeber, E. J. (2012). Spatial and temporal silencing of the human maternal UBE3A gene. *Eur. J. Paediatr. Neurol.* 16, 587–5891. doi: 10.1016/j.ejpn.2012.03.006

Dan, B., Bouillot, E., Bengoetxea, A., Boyd, S. G., and Cheron, G. (2001). Distinct multi-joint control strategies in spastic diplegia associated with prematurity or Angelman syndrome. *Clin. Neurophysiol.* 112, 1618–1625. doi: 10.1016/s1388-2457(01)00618-6

Dan, B., and Cheron, G. (2004). Postural rhythmic muscle bursting activity in Angelman syndrome. *Brain Dev.* 26, 389–393. doi: 10.1016/j.braindev.2003.12.002

Dan, B., Prigogine, C., Márquez-Ruiz, J., Kishino, T., and Cheron, G. (2010). Study of plasticity in cerebellar cortex in a mouse model of Angelman syndrome. *Dev. Med. Child. Neurol.* 52(Suppl. 4), 64.

Dan, B., Servais, L., Boyd, S. G., Wagstaff, J., and Cheron, G. (2004). From electrophysiology to chromatin: a bottom-up approach to Angelman syndrome. *Ann. N. Y. Acad. Sci.* 1030, 599–611. doi: 10.1196/annals.1329.070

D'Angelo, E., and De Zeeuw, C. I. (2009). Timing and plasticity in the cerebellum: focus on the granular layer. *Trends Neurosci.* 32, 30–40. doi: 10.1016/j.tins.2008.09.007

Daskalakis, Z. J., Paradiso, G. O., Christensen, B. K., Fitzgerald, P. B., Gunraj, C., and Chen, R. (2004). Exploring the connectivity between the cerebellum and motor cortex in humans. *J. Physiol.* 557, 689–700. doi: 10.1113/jphysiol.2003.059808

De Zeeuw, C. I., Hoebeek, F. E., Bosman, L. W., Schonewille, M., Witter, L., and Koekkoek, S. K. (2011). Spatiotemporal firing patterns in the cerebellum. *Nat. Rev. Neurosci.* 12, 327–344. doi: 10.1038/nrn3011

Egawa, K., and Fukuda, A. (2013). Pathophysiological power of improper tonic GABA(A) conductances in mature and immature models. *Front. Neural. Circuits* 7:170. doi: 10.3389/fncir.2013.00170

Egawa, K., Kitagawa, K., Inoue, K., Takayama, M., Takayama, C., Saitoh, S., et al. (2012). Decreased tonic inhibition in cerebellar granule cells causes motor dysfunction in a mouse model of Angelman syndrome. *Sci. Transl. Med.* 4:163ra157. doi: 10.1126/scitranslmed.3004655

Feldman, D. E. (2000). Timing-based LTP and LTD at vertical inputs to layer II/III pyramidal cells in rat barrel cortex. *Neuron* 27, 45–56. doi: 10.1016/s0896-6273(00)00008-8

Feldmeyer, D., Egger, V., Lubke, J., and Sakmann, B. (1999). Reliable synaptic connections between pairs of excitatory layer 4 neurones within a single 'barrel' of developing rat somatosensory cortex. *J. Physiol.* 521, 169–190. doi: 10.1111/j.1469-7793.1999.00169.x

Ferezou, I., Bolea, S., and Petersen, C. C. (2006). Visualizing the cortical representation of whisker touch: voltage-sensitive dye imaging in freely moving mice. *Neuron* 50, 617–629. doi: 10.1016/j.neuron.2006.03.043

Ferezou, I., Haiss, F., Gentet, L. J., Aronoff, R., Weber, B., and Petersen, C. C. (2007). Spatiotemporal dynamics of cortical sensorimotor integration in behaving mice. *Neuron* 56, 907–923. doi: 10.1016/j.neuron.2007.10.007

Filonova, I., Trotter, J. H., Banko, J. L., and Weeber, E. J. (2014). Activity-dependent changes in MAPK activation in the Angelman syndrome mouse model. *Learn. Mem.* 21, 98–104. doi: 10.1101/lm.032375.113

Fox, K. (1994). The cortical component of experience-dependent synaptic plasticity in the barrel cortex. *J. Neurosci.* 14, 7665–7679.

Fox, K., Glazewski, S., and Schulze, S. (2000). Plasticity and stability of somatosensory maps in thalamus and cortex. *Curr. Opin. Neurobiol.* 10, 494–497. doi: 10.1016/s0959-4388(00)00112-4

Gerstner, W., Kempter, R., van Hemmen, J. L., and Wagner, H. (1996). A neuronal learning rule for sub-millisecond temporal coding. *Nature* 383, 76–81. doi: 10.1038/383076a0

Gibson, J. R., Beierlein, M., and Connors, B. W. (1999). Two networks of electrically coupled inhibitory neurons in neocortex. *Nature* 402, 75–79. doi: 10.1038/47035

Glazewski, S., and Fox, K. (1996). Time course of experience-dependent synaptic potentiation and depression in barrel cortex of adolescent rats. *J. Neurophysiol.* 75, 1714–1729.

Gustin, R. M., Bichell, T. J., Bubser, M., Daily, J., Filonova, I., Mrelashvili, D., et al. (2010). Tissue-specific variation of Ube3a protein expression in rodents and in a mouse model of Angelman syndrome. *Neurobiol. Dis.* 39, 283–291. doi: 10.1016/j.nbd.2010.04.012

Han, Y., Huang, M. D., Sun, M. L., Duan, S., and Yu, Y. Q. (2014). Long-term synaptic plasticity in rat barrel cortex. *Cereb. Cortex* doi: 10.1093/cercor/bhu071. [Epub ahead of print].

Hebb, D. O. (1949). *The Organization of Behavior.* New York: Wiley.

Heck, D. H., Zhao, Y., Roy, S., LeDoux, M. S., and Reiter, L. T. (2008). Analysis of cerebellar function in Ube3a-deficient mice reveals novel genotype-specific behaviors. *Hum. Mol. Genet.* 17, 2181–2189. doi: 10.1093/hmg/ddn117

Heiney, S. A., Kim, J., Augustine, G. J., and Medina, J. F. (2014). Precise control of movement kinematics by optogenetic inhibition of Purkinje cell activity. *J. Neurosci.* 34, 2321–2330. doi: 10.1523/jneurosci.4547-13.2014

Holdefer, R. N., Miller, L. E., Chen, L. L., and Houk, J. C. (2000). Functional connectivity between cerebellum and primary motor cortex in the awake monkey. *J. Neurophysiol.* 84, 585–590.

Holopainen, I. E., Metsähonkala, E. L., Kokkonen, H., Parkkola, R. K., Manner, T. E., Någren, K., et al. (2001). Decreased binding of [11C] flumazenil in Angelman syndrome patients with GABA(A) receptor beta3 subunit deletions. *Ann. Neurol.* 49, 110–113. doi: 10.1002/1531-8249(200101)49:1<110::aid-ana17>3.0.co;2-t

Huang, H. S., Burns, A. J., Nonneman, R. J., Baker, L. K., Riddick, N. V., Nikolova, V. D., et al. (2013). Behavioral deficits in an Angelman syndrome model: effects of genetic background and age. *Behav. Brain Res.* 243, 79–90. doi: 10.1016/j.bbr.2012.12.052

Ito, M. (2001). Cerebellar long-term depression: characterization, signal transduction and functional roles. *Physiol. Rev.* 81, 1143–1195.

Ito, M., and Kano, M. (1982). Long-lasting depression of parallel fiber-Purkinje cell transmission induced by conjunctive stimulation of parallel fibers and climbing fibers in the cerebellar cortex. *Neurosci. Lett.* 33, 253–258. doi: 10.1016/0304-3940(82)90380-9

Jana, N. R. (2012). Understanding the pathogenesis of Angelman syndrome through animal models. *Neural Plast.* 2012:710943. doi: 10.1155/2012/710943

Jiang, Y., Armstrong, D., Albrecht, U., Atkins, C. M., Noebels, J. L., Eichele, G., et al. (1998). Mutation of the Angelman ubiquitin ligase in mice causes increased cytoplasmic p53 and deficits of contextual learning and long-term potentiation. *Neuron* 21, 799–811. doi: 10.1016/s0896-6273(00)80596-6

Killackey, H. P., and Ebner, F. (1973). Convergent projection of three separate thalamic nuclei on to a single cortical area. *Science* 179, 283–285. doi: 10.1126/science.179.4070.283

Kishino, T., Lalande, M., and Wagstaff, J. (1997). UBE3A/E6-AP mutations cause Angelman syndrome. *Nat. Genet* 15, 70–73. doi: 10.1038/ng0197-70

Koch, G., Mori, F., Marconi, B., Codecà, C., Pecchioli, C., Salerno, S., et al. (2008). Changes in intracortical circuits of the human motor cortex following theta burst stimulation of the lateral cerebellum. *Clin. Neurophysiol.* 119, 2559–2569. doi: 10.1016/j.clinph.2008.08.008

Krupa, D. J., Ghazanfar, A. A., and Nicolelis, M. A. (1999). Immediate thalamic sensory plasticity depends on corticothalamic feedback. *Proc. Natl. Acad. Sci. U S A* 96, 8200–8205. doi: 10.1073/pnas.96.14.8200

Kuramoto, E., Furuta, T., Nakamura, K. C., Unzai, T., Hioki, H., and Kaneko, T. (2009). Two types of thalamocortical projections from the motor thalamic nuclei of the rat: a single neuron-tracing study using viral vectors. *Cereb. Cortex* 19, 2065–2077. doi: 10.1093/cercor/bhn231

Leergaard, T. B., Alloway, K. D., Mutic, J. J., and Bjaalie, J. G. (2000). Three-dimensional topography of corticopontine projections from rat barrel cortex: correla-tions with corticostriatal organization. *J. Neurosci.* 20, 8474–8484.

Lefort, S., Tomm, C., Floyd Sarria, J. C., and Petersen, C. C. (2009). The excitatory neuronal network of the C2 barrel column in mouse primary somatosensory cortex. *Neuron* 61, 301–316. doi: 10.1016/j.neuron.2008.12.020

Llinás, R. R. (2011). Cerebellar motor learning versus cerebellar motor timing: the climbing fibre story. *J. Physiol.* 589, 3423–3432. doi: 10.1113/jphysiol.2011.207464

Llinás, R. R. (2014). The olivo-cerebellar system: a key to understanding the functional significance of intrinsic oscillatory brain properties. *Front. Neural Circuits* 7:96. doi: 10.3389/fncir.2013.00096

Lorente de Nó, R. (1938). Analysis of the activity of the chains of internuncial neurons. *J. Neurophysiol.* 1, 207–244.

Lübke, J., Egge, V., Sakmann, B., and Feldmeyer, D. (2000). Columnar organization of dendrites and axons of single and synaptically coupled excitatory spiny neurons in layer 4 of the rat barrel cortex. *J. Neurosci.* 20, 5300–5311.

Mao, T., Kusefoglu, D., Hooks, B. M., Huber, D., Petreanu, L., and Svoboda, K. (2011). Long-range neuronal circuits underlying the interaction between sensory and motor cortex. *Neuron* 72, 111–123. doi: 10.1016/j.neuron.2011.07.029

Markram, H., Gerstner, W., and Sjöström, P. J. (2011). A history of spike-timing-dependent plasticity. *Front. Synaptic. Neurosci.* 3:4. doi: 10.3389/fnsyn.2011.00004

Markram, H., Lübke, J., Frotscher, M., and Sakmann, B. (1997). Regulation of synaptic efficacy by coincidence of postsynaptic APs and EPSPs. *Science* 275, 213–215. doi: 10.1126/science.275.5297.213

Márquez-Ruiz, J., and Cheron, G. (2012). Sensory stimulation-dependent plasticity in the cerebellar cortex of alert mice. *PLoS One.* 7:e36184. doi: 10.1371/journal.pone.0036184

McCormick, D. A., Connors, B. W., Lighthall, J. W., and Prince, D. A. (1985). Comparative electrophysiology of pyramidal and sparsely spiny neurons of the neocortex. *J. Neurophysiol.* 54, 782–806.

Miura, K., Kishino, T., Li, E., Webber, H., Dikkes, P., Holmes, G. L., et al. (2002). Neurobehavioral and electroencephalographic abnormalities in Ube3a maternal-deficient mice. *Neurobiol. Dis* 9, 149–159. doi: 10.1006/nbdi.2001.0463

Molinari, M., Filippini, V., and Leggio, M. G. (2002). Neuronal plasticity of interrelated cerebellar and cortical networks. *Neuroscience* 111, 863–870. doi: 10.1016/s0306-4522(02)00024-6

Mulherkar, S. A., and Jana, N. R. (2010). Loss of dopaminergic neurons and resulting behavioural deficits in mouse model of Angelman syndrome. *Neurobiol. Dis.* 40, 586–592. doi: 10.1016/j.nbd.2010.08.002

Na, J., Kakei, S., and Shinoda, Y. (1997). Cerebellar input to corticothalamic neurons in layers V and VI in the motor cortex. *Neurosci. Res.* 28, 77–91. doi: 10.1016/s0168-0102(97)00031-x

Najafi, F., Giovannucci, A., Wang, S. S., and Medina, J. F. (2014). Sensory-driven enhancement of calcium signals in individual Purkinje cell dendrites of awake mice. *Cell Rep.* 6, 792–798. doi: 10.1016/j.celrep.2014.02.001

Noda, T., and Yamamoto, T. (1984). Response properties and morphological identification of neurons in the cat motor cortex. *Brain Res.* 306, 197–206. doi: 10.1016/0006-8993(84)90369-x

Parker, J. L., and Dostrovsky, J. O. (1999). Cortical involvement in the induction, but not expression, of thalamic plasticity. *J. Neurosci.* 19, 8623–8629.

Person, A. L., and Raman, I. M. (2011). Purkinje neuron synchrony elicits time-locked spiking in the cerebellar nuclei. *Nature* 481, 502–505. doi: 10.1038/nature10732

Person, A. L., and Raman, I. M. (2012). Synchrony and neural coding in cerebellar circuits. *Front. Neural Circuits* 6:97. doi: 10.3389/fncir.2012.00097

Peters, S. U., Kaufmann, W. E., Bacino, C. A., Anderson, A. W., Adapa, P., Chu, Z., et al. (2011). Alterations in white matter pathways in Angelman syndrome. *Dev. Med. Child Neurol.* 53, 361–367. doi: 10.1111/j.1469-8749.2010.03838.x

Phoka, E., Wildie, M., Schultz, S. R., and Barahona, M. (2012). Sensory experience modifies spontaneous state dynamics in a large-scale barrel cortical model. *J. Comput. Neurosci.* 33, 323–339. doi: 10.1007/s10827-012-0388-6

Piochon, C., Kruskal, P., Maclean, J., and Hansel, C. (2013). Non-Hebbian spike-timing-dependent plasticity in cerebellar circuits. *Front Neural Circuits* 6:124. doi: 10.3389/fncir.2012.00124

Popa, D., Spolidoro, M., Proville, R. D., Guyon, N., Belliveau, L., and Léna, C. (2013). Functional role of the cerebellum in gamma-band synchronization of the sensory and motor cortices. *J. Neurosci.* 33, 6552–6556. doi: 10.1523/jneurosci.5521-12.2013

Proville, R. D., Spolidoro, M., Guyon, N., Dugué, G. P., Selimi, F., Isope, P., et al. (2014). Cerebellum involvement in cortical sensorimotor circuits for the control of voluntary movements. *Nat. Neurosci.* 17, 1233–1239. doi: 10.1038/nn.3773

Rahmati, N., Owens, C. B., Bosman, L. W., Spanke, J. K., and Lindeman, S. (2014). Cerebellar potentiation and learning a whisker-based object localization task with a time response window. *J. Neurosci.* 34, 1949–1962. doi: 10.1523/jneurosci.2966-13.2014

Roggeri, L., Rivieccio, B., Rossi, P., and D'Angelo, E. (2008). Tactile stimulation evokes long-term synaptic plasticity in the granular layer of cerebellum. *J. Neurosci.* 28, 6354–6359. doi: 10.1523/jneurosci.5709-07.2008

Ruigrok, T. J. (2011). Ins and outs of cerebellar modules. *Cerebellum* 10, 464–474. doi: 10.1007/s12311-010-0164-y

Ruigrok, T. J., and Teune, T. M. (2014). Collateralization of cerebellar output to functionally distinct brainstem areas. A retrograde, non-fluorescent tracing study in the rat. *Front. Syst. Neurosci* 8:23. doi: 10.3389/fnsys.2014.00023

Servais, L., Bearzatto, B., Schwaller, B., Dumont, M., De Saedeleer, C., Dan, B., et al. (2005). Mono- and dual-frequency fast cerebellar oscillation in mice lacking parvalbumin and/or calbindin D-28k. *Eur. J. Neurosci.* 22, 861–870. doi: 10.1111/j.1460-9568.2005.04275.x

Suzuki, L., Coulon, P., Sabel-Goedknegt, E. H., and Ruigrok, T. J. (2012). Organization of cerebral projections to identified cerebellar zones in the posterior cerebellum of the rat. *J. Neurosci.* 32, 10854–10869. doi: 10.1523/jneurosci.0857-12.2012

Teune, T. M., van der Burg, J., van der Moer, J., Voogd, J., and Ruigrok, T. J. H. (2000). "Topography of cerebellar nuclear projections to the brainstem in the rat," in *Cerebellar Modules: Molecules, Morphology and Function*, eds N. M. Gerrits T. J. H. Ruigrok, and C. I. DeZeeuw (Amsterdam: Elsevier Science B.V.), 141–172.

Tiwari, V. N., Jeong, J. W., Wilson, B. J., Behen, M. E., Chugani, H. T., and Sundaram, S. K. (2012). Relationship between aberrant brain connectivity and clinical features in Angelman Syndrome: a new method using tract based spatial statistics of DTI color-coded orientation maps. *Neuroimage* 59, 349–355. doi: 10.1016/j.neuroimage.2011.07.067

Ugawa, Y., Day, B. L., Rothwell, J. C., Thompson, P. D., Merton, P. A., and Marsden, C. D. (1991). Modulation of motor cortical excitability by electrical stimulation over the cerebellum in man. *J. Physiol.* 441, 57–72.

Ugawa, Y., Genba-Shimizu, K., Rothwell, J. C., Iwata, M., and Kanazawa, I. (1994). Suppression of motor cortical excitability by electrical stimulation over the cerebellum in ataxia. *Ann. Neurol.* 36, 90–96. doi: 10.1002/ana.410360117

Ugawa, Y., Uesaka, Y., Terao, Y., Hanajima, R., and Kanazawa, I. (1995). Magnetic stimulation over the cerebellum in humans. *Ann. Neurol.* 37, 703–713. doi: 10.1002/ana.410370603

van Woerden, G. M., Harris, K. D., Hojjati, M. R., Gustin, R. M., Qiu, S., de Avila Freire, R., et al. (2007). Rescue of neurological deficits in a mouse model for Angelman syndrome by reduction of alphaCaMKII inhibitory phosphorylation. *Nat. Neurosci.* 10, 280–282. doi: 10.1038/nn1845

Vertes, R. P., Hoover, W. B., and Rodriguez, J. J. (2012). Projections of the central medial nucleus of the thalamus in the rat: node in cortical, striatal and limbic forebrain circuitry. *Neuroscience* 219, 120–136. doi: 10.1016/j.neuroscience.2012.04.067

Viaene, A. N., Petrof, I., and Sherman, S. M. (2011). Properties of the thalamic projection from the posterior medial nucleus to primary and secondary somatosensory cortices in the mouse. *Proc. Natl. Acad. Sci. U S A* 108, 18156–18161. doi: 10.1073/pnas.1114828108

Wallace, M. L., Burette, A. C., Weinberg, R. J., and Philpot, B. D. (2012). Maternal loss of Ube3a produces an excitatory/inhibitory imbalance through neuron type-specific synaptic defects. *Neuron* 74, 793–800. doi: 10.1016/j.neuron.2012.03.036

Wallace, H., and Fox, K. (1999). Local cortical interactions determine the form of cortical plasticity. *J. Neurobiol.* 41, 58–63. doi: 10.1002/(SICI)1097-4695(199910)41:1<58::AID-NEU8>3.3.CO;2-6

Watson, T. C., Koutsikou, S., Cerminara, N. L., Flavell, C. R., Crook, J. J., Lumb, B. M., et al. (2013). The olivo-cerebellar system and its relationship to survival circuits. *Front. Neural Circuits* 7:72. doi: 10.3389/fncir.2013.00072

Conflict of Interest Statement: The authors declare that the research was conducted in the absence of any commercial or financial relationships that could be construed as a potential conflict of interest.

Received: 31 July 2014; accepted: 25 October 2014; published online: 19 November 2014.

*Citation: Cheron G, Márquez-Ruiz J, Kishino T and Dan B (2014) Disruption of the LTD dialogue between the cerebellum and the cortex in Angelman syndrome model: a timing hypothesis. Front. Syst. Neurosci. **8**:221. doi: 10.3389/fnsys.2014.00221*

This article was submitted to the journal Frontiers in Systems Neuroscience.

frontiers in
SYSTEMS NEUROSCIENCE

ORIGINAL RESEARCH ARTICLE
published: 30 January 2014
doi: 10.3389/fnsys.2014.00009

Marked reduction of cerebellar deficits in upper limbs following transcranial cerebello-cerebral DC stimulation: tremor reduction and re-programming of the timing of antagonist commands

Giuliana Grimaldi[1], Nordeyn Oulad Ben Taib[1,2], Mario Manto[1,3]* and Florian Bodranghien[1]

[1] *Unité d'Etude du Mouvement, ULB Neurologie, Bruxelles, Belgium*
[2] *Service de Neurochirurgie, CHU Saint-Pierre, Bruxelles, Belgium*
[3] *Fonds de la Recherche Scientifique-ULB, Bruxelles, Belgium*

Edited by:
Richard Apps, University of Bristol, UK

Reviewed by:
José M. Delgado-García, University Pablo de Olavide, Spain
Huo Lu, Philadelphia College of Osteopathic Medicine, USA

****Correspondence:***
Mario Manto, Unité d'Etude du Mouvement, FNRS – ULB, 808 Route de Lennik, 1070 Bruxelles, Belgium
e-mail: mmanto@ulb.ac.be

Cerebellar ataxias represent a very heterogeneous group of disabling disorders for which we lack effective symptomatic therapies in most cases. There is currently an intense interest in the use of non-invasive transcranial DC stimulation (tDCS) to modulate the activity of the cerebellum in ataxic disorders. We performed a detailed laboratory assessment of the effects of transcranial cerebello-cerebral DC stimulation (tCCDCS, including a sham procedure) on upper limb tremor and dysmetria in 2 patients presenting a dominant spinocerebellar ataxia (SCA) type 2, one of the most common SCAs encountered during practice. Both patients had a very similar triplet expansion size in the ATXN2 gene (respectively, 39 and 40 triplets). tCCDCS reduced both postural tremor and action tremor, as confirmed by spectral analysis. Quadratical PSD (power spectral density) of postural tremor dropped to 38.63 and 41.42% of baseline values in patient 1 and 2, respectively. The integral of the subband 4–20 Hz dropped to 46.9 and 62.3% of baseline values, respectively. Remarkably, tCCDCS canceled hypermetria and reduced dramatically the onset latency of the antagonist EMG activity associated with fast goal-directed movements toward 3 aimed targets (0.2, 0.3, and 0.4 rad). Following tCCDCS, the latency dropped from 108–98 to 63–57 ms in patient 1, and from 74–87 to 41–46 ms in patient 2 (mean control values ± *SD*: 36 ± 8 to 45 ± 11 ms), corresponding to a major drop of z scores for the 2 patients from 7.12 ± 0.69 to 1.28 ± 1.27 (sham procedure: 6.79 ± 0.71). This is the first demonstration that tCCDCS improves upper limb tremor and hypermetria in SCA type 2. In particular, this is the first report of a favorable effect on the onset latency of the antagonist EMG activity, a neurophysiological marker of the defect in programming of *timing* of motor commands. Our results indicate that tCCDCS should be considered in the symptomatic management of upper limb motor deficits in cerebellar ataxias. Future studies addressing a tDCS-based neuromodulation to improve motor control of upper limbs are required (a) in a large group of cerebellar disorders, and (b) in different subgroups of ataxic patients. The anatomical location of the cerebellum below the skull is particularly well suited for such studies.

Keywords: DC stimulation, cerebellum, ataxia, tremor, hypermetria, antagonist, EMG, timing

INTRODUCTION

Cerebellar ataxias represent a very heterogeneous group of sporadic and genetic disabling diseases (Manto and Marmolino, 2009). Voluntary movement of the limbs is typically jerky (Holmes, 1917). Tremor and dysmetria are two main clinical manifestations which contribute to disability during daily life (Saute et al., 2012). Although the number of defined cerebellar ataxias is growing thanks to genetic discoveries, we still lack efficient symptomatic therapies for the majority of them, hence the current intense research effort to identify novel strategies aiming to reduce the motor deficits, to promote learning and to increase the effects of rehabilitation (Hamada et al., 2012; Grimaldi and Manto, 2013).

There is a growing interest in using transcranial DC stimulation (tDCS) to modulate cerebellar functions (Galea et al., 2009; Pope and Miall, 2012; Ferrucci and Priori, 2014). This non-invasive technique is based on the application of a steady current of small intensity (usually between 0.5 and 2 mAmp; anodal or cathodal) between 2 large electrodes fixed on the scalp (Tomlinson et al., 2013). The current, administered either in a continuous or in an intermittent mode, causes a polarity-dependent modulation of brain activity which is site-specific

(Nitsche et al., 2003). tDCS of the cerebellum is particularly attractive also because of the anatomical location of the cerebellar cortex immediately below the skull. It has been shown that anodal tDCS of the cerebellum increases the excitability of the cerebellar cortex in human, thus reinforcing the inhibitory effect exerted by the cerebellar cortex over cerebellar nuclei (Galea et al., 2009). These latter project to the contralateral motor cortex mainly via the cerebello-thalamo-cortical pathway. Hypoexcitability of the motor cortex with enhanced intra-cortical inhibition is a major defect commonly observed in cerebellar ataxias and contributes to the deficits of motor skills (Wessel et al., 1996; Tamburin et al., 2004). Therefore, one therapeutic possibility to reduce cerebellar ataxia could be the neuromodulation of the excitability of the cerebello-thalamo-cortical pathway by acting on the cerebellar cortex and/or the contralateral motor cortex. In a recent report including a sham procedure, Pozzi et al. have shown that anodal tDCS of the primary motor cortex improves gait asymmetry in sporadic ataxia or in the dominant SCA type 6 (Pozzi et al., 2013). The combination of tDCS of the cerebellum with tDCS of the contralateral motor/premotor cortex appears as an interesting option (Grimaldi and Manto, 2013). Indeed, experimental studies in rodents show that (1) anodal tDCS of the motor cortex restores the excitability of the motor cortex in case of extensive damage of the contralateral cerebellar hemisphere (Oulad Ben Taib and Manto, 2009), (2) epidural DCS of the cerebellum reshapes the corticomotor maps of couples of agonist/antagonist muscles in limbs, enhances the spinocerebellar evoked potentials associated with peripheral electrical stimulation and augments cerebellar blood flow both at the level of cerebellar cortex and cerebellar nuclei likely by acting on the neurovascular coupling (Grimaldi and Manto, 2013; Oulad Ben Taib and Manto, 2013); Oulad Ben Taib and Manto, in preparation), (3) epidural DCS of the cerebellum followed by tDCS of the contralateral motor cortex is very efficient to modulate the corticomotor output which is normally associated with repetitive electrical stimulation of the sciatic nerve (Grimaldi and Manto, 2013; Oulad Ben Taib and Manto, 2013), and (4) the sequence epidural DCS of the cerebellum followed by epidural DCS of the contralateral motor cortex is more efficient than the reverse when attempting to restore the adaptation of the corticomotor responses to peripheral repetitive stimulation in the model of high frequency electrical stimulation of the interpositus nucleus (Oulad Ben Taib et al., 2005a,b; Oulad Ben Taib and Manto, in preparation). Based on findings in rodents and on the work of Pozzi et al., we tested the hypothesis that tDCS applied over the cerebellum immediately followed by tDCS applied over the contralateral motor cortex (tCCDCS: transcranial cerebello-cerebral DC stimulation) could antagonize upper limb tremor and dysmetria in patients with a commonly encountered SCA and who exhibited a predominant cerebellar syndrome.

METHODS

PATIENTS

Patient 1: This right-handed 49-year-old right-handed woman had a 5 years history of gait difficulties, in a context of familial dominant ataxia. In addition to cerebellar signs (see ataxia rating score in the Results section), neurological examination showed impaired horizontal saccades (decreased velocities; very suggestive of the disorder) and decreased tendon reflexes in 4 limbs. Detailed sensory examination (position sense, vibration, tactile sensation) and evaluation of motor strength (5/5 on MRC scale) were normal in upper limbs. Hoffmann's reflex was negative.

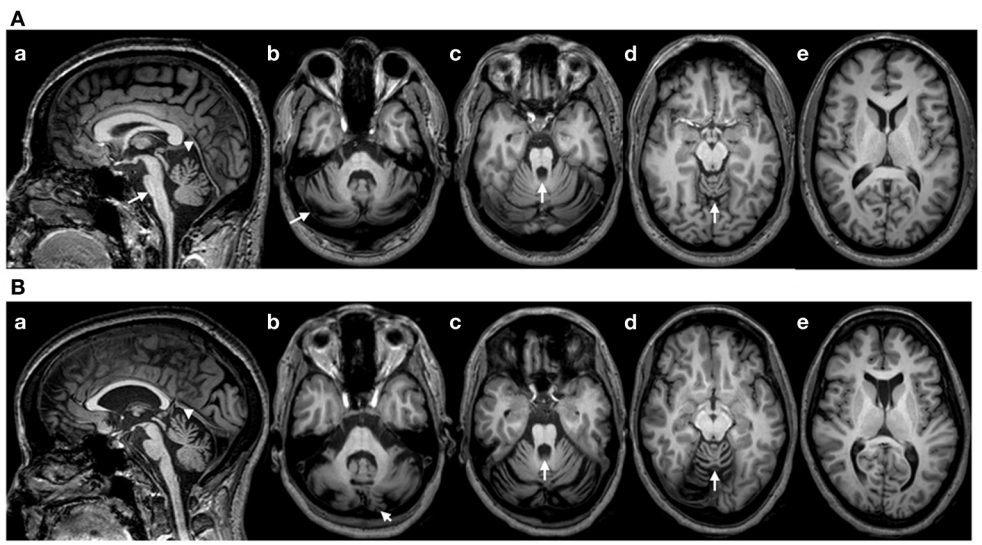

FIGURE 1 | (A) Brain MRI (T1-weighted images) in patient 1. (a): sagittal image showing a flattening of the pons (arrow), atrophy of the upper vermis (arrowhead) and a thin spinal cord in upper cervical segments; (b–d): axial sections showing atrophy of the cerebellum at the level of the middle cerebellar peduncle (b; arrow: atrophy of the cerebellar cortex), the upper pons with enlargement of the 4th ventricle (c; arrow) and the upper vermis (d; arrow). (e): Normal appearance of the cerebral cortex (axial slice at the level of the head of caudate nucleus). **(B)** Brain MRI in patient 2 (T1-weighted images). Flattening of the pons is less severe as compared to patient 1 (a), whereas the degree of cerebellar atrophy is relatively similar (b–e). Note the presence of a cavum of the septum pellucidum in patient 2.

Brain MRI showed atrophy of the cerebellum and brainstem, extending to the cervical segments of the spinal cord (**Figure 1A**). We did not apply voxel-based morphometry (VBM) or 3D-based volumetry to quantify the atrophy. Genetic study for SCA type 2 (ATXN2 gene; chromosome 12q23-24.1) showed 22 and 39 CAG triplets ($N < 32$) (Gispert et al., 1993). *Patient 2*: this right-handed 43-year-old right-handed man had a 14 years history of loss of balance, in a context of familial dominant ataxia. In addition to cerebellar signs, neurological examination showed slowing of horizontal saccades and decreased tendon reflexes in 4 limbs. Detailed sensory examination and evaluation of motor strength were normal in upper limbs. Hoffmann's reflex was negative. Brain MRI showed atrophy of the cerebellum and brainstem (**Figure 1B**; no VBM or 3D-based volumetry performed). Genetic study for SCA type 2 showed 22 and 40 triplets.

We selected these patients because (a) they both presented deficits of motor control in upper limbs characterized by a postural/action tremor steady in amplitude and dysmetria (these are clinical features commonly observed in SCA2), (b) they both exhibited a delayed onset latency of the antagonist EMG activity associated with fast goal-directed movements (this delay is insensitive to practice trials), and (c) the size of the triplet expansion was very similar.

The study was approved by the local ethical committee of ULB and both patients signed a written informed consent following full explanation of the experimental procedures.

tCCDCS

Data were collected on right upper limb in 3 experimental conditions: (1) at baseline, (2) after a sham stimulation (20 min of sham stimulation over the cerebellum, immediately followed by sham stimulation over the contralateral motor cortex—see below), and (3) after tCCDCS (20 min of anodal stimulation over the cerebellum, immediately followed by anodal stimulation over the contralateral motor cortex). The rationale for this design baseline-sham-tDCS in cerebellar disorders has been explained elsewhere (Grimaldi and Manto, 2013). We did not observe any effect on upper limb movements by the sole anodal tDCS of the cerebellum in a previous study. We applied an "off-line" methodology for the recordings of tremor and fast goal-directed movements (assessment within 45 min after application of sham or tCCDCS; we attempted to avoid the occurrence of fatigue which occurs typically when recordings sessions last more than 3 h in cerebellar patients). This off-line approach is commonly applied in tDCS studies.

For sham and anodal stimulation of the cerebellum, the anode—a sponge electrode; size: 50 × 40 mm—was positioned at the level of the posterior fossa on the right side with the center of the sponge at about 3 cm to the right of the inion, in order to target the right cerebellar hemisphere, given the lateralized cerebellar functions for upper limbs (Galea et al., 2009). The second sponge electrode—the cathode; same size than anode—was applied over the contralateral supra-orbital area. Electrodes were soaked (with a solution of NaCl 0.9%). The period of stimulation lasted 20 min both for sham stimulation and anodal stimulation. Subsequently, the anode was positioned over the hand representation of left primary motor cortex, with the cathode placed over the right supra-orbital area (this selection is based on our experience in rodents). A second period of stimulation of 20 min for both conditions (sham and active stimulation) was used. Current delivered was 1 mAmp (portable stimulator with a 9 V battery; CES, Canada). Current was increased gradually from 0 to 1 mAmp over 30 s, as confirmed by the analysis of the current using a Fluke PM3384A Comb scope. For sham stimulation, once the current reached the plateau, it was gradually decreased to zero over a period of about 1 min, so that patients were blinded as to whether they were receiving sham stimulation or anodal tDCS.

Upper limb tremor (postural and action) and dysmetria were studied at baseline, post-sham and post-tCCDCS. We did not assess kinetic tremor because it was more variable in our patients as compared to postural and action tremor which were both steady.

CLINICAL EVALUATION

An ataxia rating scale (SARA; scale designed for dominant ataxias—higher values correspond to a lower performance) was applied at baseline, immediately after sham and immediately after tCCDCS.

UPPER LIMB TREMOR

Postural tremor

Patients were comfortably seated in an armchair, and equipped with 2 triaxial accelerometers, located at the right index finger and at the right metacarpal region (see Grimaldi et al., 2013). They were asked to maintain the upper limbs motionless horizontally in front of them and parallel to the floor. Three recordings of 15 s were performed at baseline, after sham and post-tCCDCS. The sampling rate was 512 Hz per axis for each accelerometer. For signal processing of accelerometry signals, we computed the Root Mean Square (RMS) and the total traveled distance (expressed in mm). We performed the spectral analysis using Fast Fourier Transform (FFT) as recommended, using Matlab (MathWorks, USA) (Grimaldi and Manto, 2010; McNames, 2013). The 15 s time-series were segmented in 5 segments. Auto-spectra of 5 sequential 3 s data epochs were averaged to produce smoothed autospectra, with mean removal and a windowing (Hamming) for each data segment (Grimaldi and Manto, 2010). The following spectral parameters were extracted and means were computed for the 3 experimental conditions (baseline, post-sham and post-tCCDCS): maximal PSD (maxPSD), peak frequency of power spectra (PFr), crest factor in the 4–20 Hz frequency band (CF = the ratio of maximal PSD divided by the integral of the 4–20 Hz frequency sub-band), center frequency (median value of the area below the power spectrum) (Grimaldi and Manto, 2008; Grimaldi et al., 2013). Composite data (square root of the sum of the accelerations squared for all three axis) were processed as reported earlier (Grimaldi et al., 2013; Shaikh et al., 2008). Data presented in the results section are mean ± standard deviation (*SD*) of the 3 recordings performed in each experimental condition.

Action tremor

Patients were asked to maintain the manipulandum of a mechatronic myohaptic device specifically designed and built for

wrist motion analysis (see also next section). Patients were asked to keep the manipulandum motionless during 16 s. The manipulandum exerted a constant extensor torque of 0.5 Nm from the neutral position, thus eliciting an action tremor. Patients were allowed to perform 5 practice trials before recordings. This number of practice trials is based on our experience with ataxic patients (patients are familiar with the test after 2–3 trials). Sampling rate for position signal was 2048 Hz. We extracted the short-time Fourier transform (STFT) using Igor Pro 6.01 software (Wavemetrics, USA). The 16 s time-series were filtered (IIR high-pass 2 Hz) and segmented in 8 segments. Auto-spectra of 8 sequential data epochs of 2 s were averaged. We computed maxPSD, PFr, CF in the 4–20 Hz frequency sub-band, integrals of frequency sub-bands (2–4, 4–8, 8–12, 12–16, 4–20 Hz). Because cerebellar action tremor is often more severe at the frequency of 3 Hz, we also extracted the tremor data in the sub-band 2.5–3.5 Hz by applying a corresponding band-pass IIR filter of order 4. The RMS was also computed on the filtered data.

Relative entropy of postural and action tremor

Cerebellum is well known to contribute to timing of motor commands and is considered as a "clock" in the brain (Braitenberg, 1967; Ivry and Spencer, 2004). Therefore, in order to measure the possible effectiveness of tCCDCS on the randomness of spectral data, we computed the Kullback-Leibler entropy, a method used to measure the degree of similarity between 2 spectrograms (Freeman and Quian Quiroga, 2013). The relative entropy was computed using the basal state as the reference (post-sham condition vs. basal condition, and post-tCCDCS vs. basal condition). The following formula was used (Freeman and Quian Quiroga, 2013):

$$K(p|q) = \sum_k p_k \log_2 \frac{p_k}{q_k}$$

where:

p_k is the frequency probability of the post-sham (or post-tCCDCS) signal.

q_k is the frequency probability of baseline signal.

DYSMETRIA

We investigated fast goal-directed pointing single-joint movements with the haptic technology as reported earlier (Manto et al., 2010). The range of motion was constrained mechanically from −1 rad to +1 rad. Movements were studied in the free mode of the manipulandum at a sampling rate of 2048 Hz. The 2 patients performed sets of 10 fast pointing movements over 3 distances (targets displayed on a computer screen in front of the patient; 3 targets: 0.2, 0.3, 0.4 rad) following 3–4 practice trials. Subjects were comfortably seated, with the shoulder relaxed and the upper arm perpendicular to the forearm. The hand and forearm were affixed with straps. The wrist joint was carefully aligned with the motor axis. Movements were performed in the horizontal plane. We recorded the surface EMG activities of the flexor carpi radialis (FCR; agonist) and extensor carpi radialis (ECR; antagonist) muscles. Surface EMG activities were amplified (× 1000) and full-wave rectified (filter settings: 20–500 Hz; Delsys surface electrodes, USA; electrodes fixed on the skin with tape). We averaged each set of 10 movements, both for wrist angle data and EMG data. Individual records were aligned to the onset of the agonist EMG burst according to a method reported earlier (Gottlieb, 1998). Kinematic and EMG data were compared with those obtained previously in a control group using identical experimental conditions ($n = 8$ right-handed healthy subjects, mean age ± *SD*: 34.8 ± 10.2 years; 3 women—values of this control group were used to compute z scores in the 3 experimental conditions) (see Manto et al., 2010).

STATISTICAL ANALYSIS

For both postural and action tremor, parameters in the post-sham and post-tCCDCS conditions were expressed as percentages of baseline values. For postural tremor, we computed the *z* scores as compared to patients' basal values. A *z* score between 1.959 *SD* above mean and 1.959 *SD* below mean corresponds to the 95% confidence interval (a *z* score between 2.576 *SD* above mean and 2.576 *SD* below mean corresponds to the 99% confidence interval). For fast goal-directed movements in the 3 conditions (basal, post-sham and post-tCCDCS), mean movement amplitudes and onset latencies of antagonist EMG activities were compared to data obtained in a control group reported earlier (see previous section) and expressed as *z* scores (Manto et al., 2010). To compare the relative entropy (sham/basal vs. tCCDCS/basal, bor both action tremor and postural tremor), we first applied the Shapiro-Wilk test to assess the normality. We subsequently used the Mann-Whitney rank sum test. Values were expressed as median ± *SD*. Statistical significance was set at 0.05.

RESULTS

CLINICAL EVALUATION

In patient 1, the SARA rating score was:

-*at baseline*: Gait (G) 3, Stance (St) 2, Sitting (Si) 4, Speech (Sp) 3, Finger chase (Fc): right 2 and left 2 (mean 2), Nose-finger test (Nf): right 1 and left 1 (mean 1), Fast alternating movements (Fa): right 1 and left 1 (mean 1), Heel-shin slide (Hs) right 2 and left 2 (mean 2). *Total*: 18;

-*after sham*: G3, St2, Si2, Sp3, Fc: right 2 and left 2 (mean 2), Nf: right 1 and left 1 (mean 1), Fa: right 1 and left 1 (mean 1), Hs: right 2 and left 2 (mean 2). *Total*: 16;

-*after tCCDCS*: G3, St2, Si2, Sp3, Fc: right 1 and left 2 (mean 1.5), Nf: right 1 and left 1 (mean 1), Fa: right 0 and left 1 (mean 0.5), Hs: right 2 and left 2 (mean 2). *Total*: 15.

In patient 2, the SARA rating score was:

-*at baseline*: G3, St2, Si1, Sp3, Fc: right 1 and left 1 (mean 1), Nf: right 1 and left 1 (mean 1), Fa: right 1 and left 1 (mean 1), Hs: right 1 and left 1 (mean 1). *Total*: 13;

-*after sham*: G2, St2, Si2, Sp3, Fc: right 1 and left 1 (mean 1), Nf: right 1 and left 1 (mean 1), Fa: right 1 and left 1 (mean 1), Hs: right 1 and left 1 (mean 1). Total: 13;

-*after tCCDCS*: G2, St1, Si1, Sp3, Fc: right 0 and left 1 (mean 0.5), Nf: right 1 and left 1 (mean 1), Fa: right 0 and left 0 (mean 0), Hs: right 1 and left 1 (mean 1). Total: 9.5.

UPPER LIMB TREMOR

Postural tremor

Figure 2A illustrates a representative recording of the postural tremor at the level of the index (accelerometer 1—gravity axis: axis with most intense oscillations in this task) in patient 1 in the 3 conditions (baseline, post-sham, post-tCCDCS). tCCDCS induced a major reduction of the amplitudes of the oscillations, unlike the sham procedure which did not modify tremor. PFr shifted from 7.1 Hz at baseline (post-sham: 7.2 Hz) to 8.3 Hz post-tCCDCS (z score: 2.97 as compared to baseline). The analysis

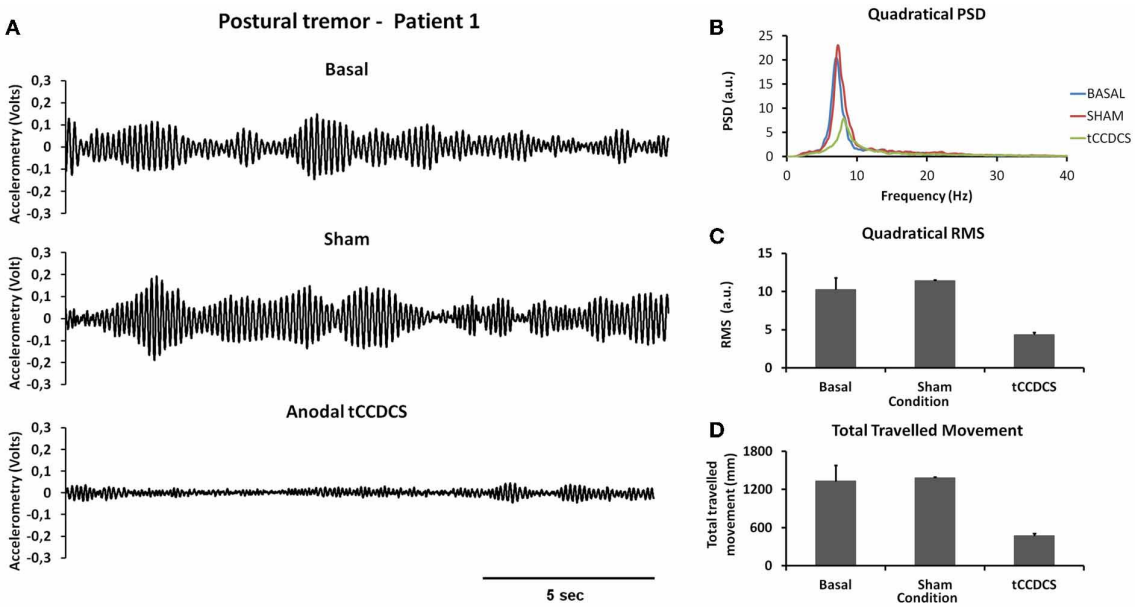

FIGURE 2 | Postural tremor in patient 1. (A) Tremor recorded at the level of right index in the 3 experimental conditions (from top to bottom: baseline, post-sham and post-tCCDCS) for the gravity axis (dominant axis in this task). Calibration value: 1.55 mV = 100 mm/s^2. **(B)** Mean quadratical power spectral density (PSD) of all epochs of postural tremor, showing a marked reduction of peak PSD following tCCDCS (blue line: baseline; red line: post-sham; green line: post-tCCDCS). Quadratical PSD is expressed in arbitrary units (a.u.). **(C)** Quadratical RMS (expressed in a.u.) of all epochs of postural tremor. (D) Total traveled movement (expressed in mm). Values in **(C)** and **(D)** are mean (±*SD*) of all epochs.

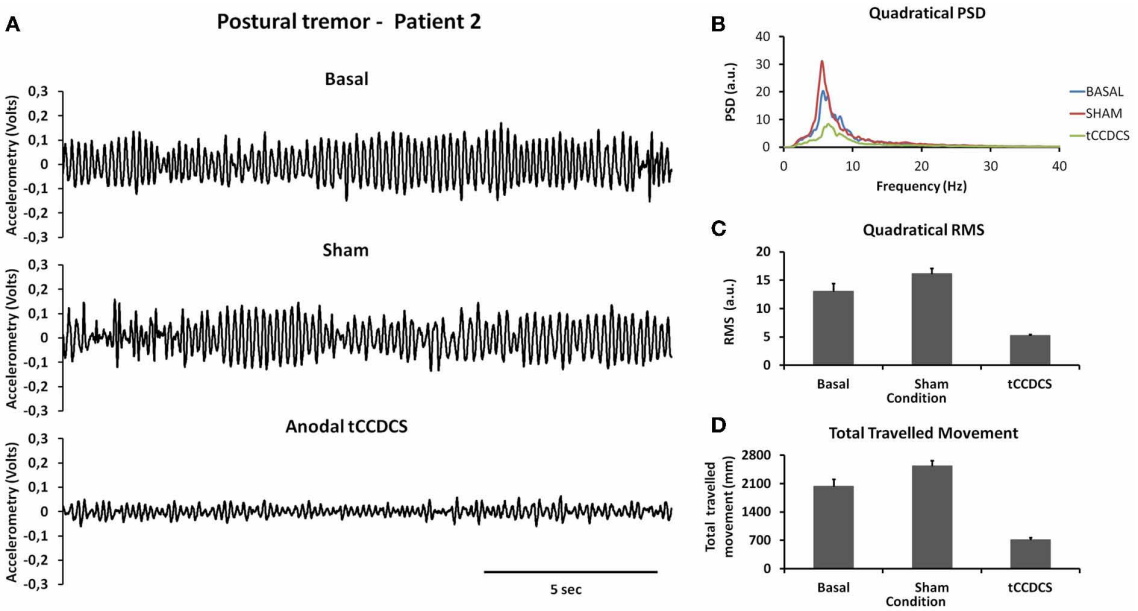

FIGURE 3 | Postural tremor in patient 2 (recordings at the right index; representative trace for the dominant axis in the gravity axis). (A) Tremor in the 3 experimental conditions. **(B)** Quadratical PSD. **(C)** Quadratical RMS. **(D)** Total traveled movement. See also legend of **Figure 2** for details.

of quadratical PSD of all epochs showed a drop of the peak PSD from 20.4 a.u. at baseline (post-sham: 23.0 a.u.) to 7.9 a.u. in the condition post-tCCDCS (38.63% of baseline values; see **Figure 2B**). The integral of the sub-band 4–20 Hz changed from 54.39 ± 7.26 a.u. (basal) to 60.52 ± 6.01 a.u. (post-sham; *z* score: 1.11 as compared to baseline) and to 29.23 ± 3.92 a.u. post-tCCDCS (*z* score: −3.46 as compared to baseline; drop to 53.74% of baseline values). CF decreased from 0.47 ± 0.04 to 0.39 ± 0.06 (post-sham; *z* score: −2 as compared to baseline), and to 0.28 ± 0.1 a.u. post-tCCDCS (z score: −3.71 as compared to baseline). Center frequency showed a trend to increase from 7.39 Hz (basal) to 8.6 Hz (post-tCCDCS) (*z* score: 2.36 as compared to baseline). Quadratical RMS changed from 10.36 ± 2.65 a.u. (basal) to 11.38 ± 0.27 a.u. (post-sham; *z* score: 0.42 as compared to baseline) and to 4.34 ± 0.48 a.u. post-tCCDCS (*z* score: −2.22 as compared to baseline) (see **Figure 2C**). Values for the total traveled movement are illustrated in **Figure 2D**. Very similar results were obtained for accelerometer 2 (data not shown).

Similar observations were made for patient 2 (see **Figure 3**). Quadratical PSD showed a drop of the peak PSD from 20.3 a.u. at baseline (post-sham: 31.1) to 8.4 a.u. post-tCCDCS (41.42% of baseline values). The integral of the sub-band 4–20 Hz changed from 81.09 ± 11.97 a.u. (basal) to 96.65 ± 10.08 a.u. post-sham (*z* score: 1.29 as compared to baseline) and to 37.08 ± 4.94 a.u. post-tCCDCS (*z* score: −3.68 as compared to baseline). PFr, CF, and center frequency showed no significant changes in patient 2. Quadratical RMS changed from 13.0 ± 2.40 a.u. (basal) to 16.10 ± 1.75 a.u. post-sham (*z* score: 1.28 as compared to baseline) and to 5.19 ± 0.44 a.u. post-tCCDCS (*z* score: −3.25 as compared to baseline) (see **Figure 3B**).

Action tremor

For patient 1, the action tremor had a PFr of 7, 7.5, and 6.5 Hz, respectively, at baseline, post-sham and post-tCCDCS. The integral in the subband 4–20 Hz changed from 0.00769 a.u.

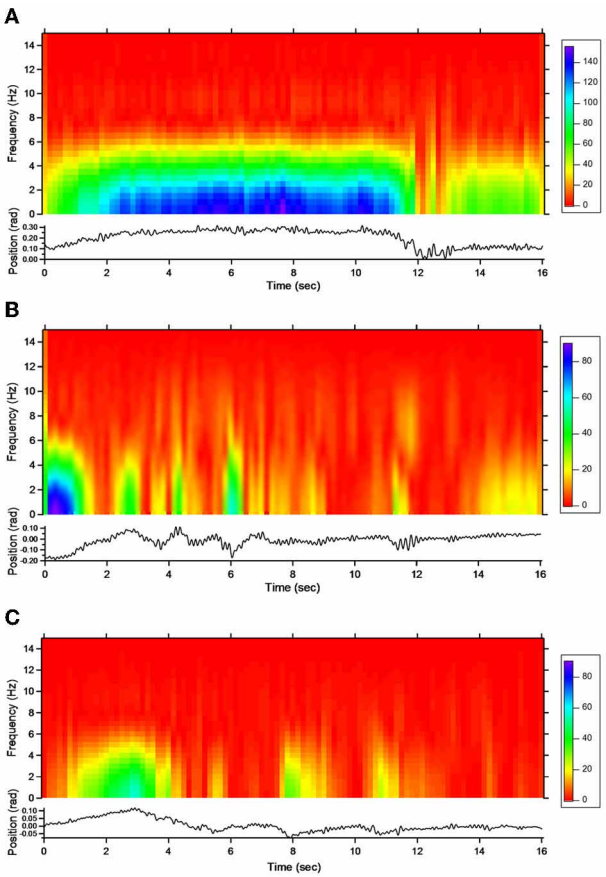

FIGURE 4 | Short-term Fourier transform (STFT) representation of action tremor in patient 1. In each of the 3 panels (**A,B** and **C**), frequency (in Hz, upper) and position of the manipulandum (in rad, bottom) are illustrated as a function of time. **(A)** Baseline, **(B)** post-sham, **(C)** post-tCCDCS. Note that the color scale of the Y axis is larger in **(A)** as compared to **(B)** and **(C)**.

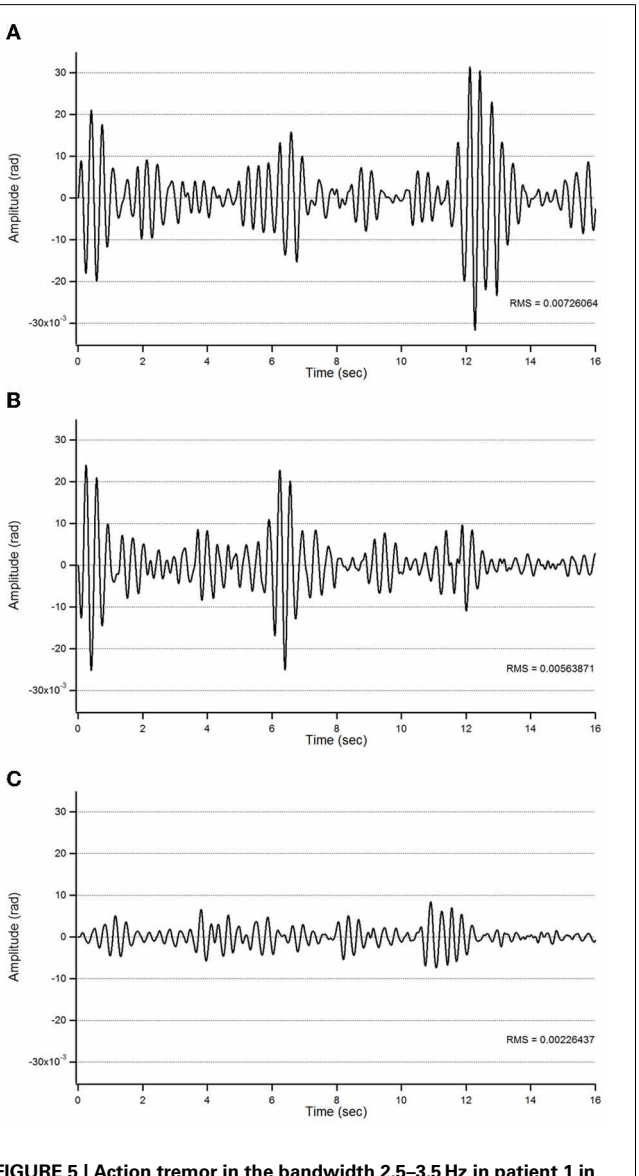

FIGURE 5 | Action tremor in the bandwidth 2.5–3.5 Hz in patient 1 in the 3 experimental conditions (A: basal; B: post-sham; C: post-tCCDCS) as a function of time (expressed in s).

(baseline) to 0.00695 a.u. (post-sham: 90.3% as compared to baseline) and to 0.00361 a.u. (post-tCCDCS: 46.9% as compared to baseline). At baseline, the STFT study showed that the oscillations were predominantly found below 5 Hz (**Figure 4A**). Although the sham procedure had a favorable effect on the magnitude of these low-frequency oscillations (**Figure 4B**), the effects were dramatic after tCCDCS (**Figure 4C**). These observations were confirmed by the analysis of tremor using a band-pass filter of 2.5–3.5 Hz (**Figure 5**). RMS decreased from 2.06 (basal; post-sham: 2.19) to 0.86 post-tCCDCS.

For patient 2, the action tremor had a PFr of 7, 7.05, and 1 Hz, respectively, at baseline, after sham and after tCCDCS. The integral in the subband 4–20 Hz changed from 0.01024 a.u. (baseline) to 0.01349 a.u. post-sham (131.7% as compared to baseline) and to 0.00638 a.u. post-tCCDCS (62.3% as compared to baseline). The STFT study also confirmed a favorable effect of tCCDCS on frequencies below 5 Hz, although at a lower extent as compared to patient 1 (**Figure 6**). These observations were confirmed by the analysis of tremor using a band-pass of 2.5–3.5 Hz (**Figure 7**). RMS decreased from 1.79 (basal; 2.84 post-sham) to 1.19 post-tCCDCS.

HYPERMETRIA

In both patients, fast goal-directed movements were markedly hypermetric at baseline and following application of the sham procedure (see **Table 1**). In both patients, hypermetria was associated with a delayed onset latency of the antagonist EMG activity. After application of tCCDCS, a dramatic effect on hypermetria was observed, with a clear reduction of the onset latency of the antagonist EMG activity. This is illustrated in **Figure 8** in patient 1 for the aimed target of 0.3 rad. **Figure 9** illustrates similar observations in patient 2 (aimed target of 0.3 rad). Considering the 3 aimed amplitudes and the 2 patients, the *z* scores for the values of the onset latency of the antagonist activity were (mean ± *SD*): 7.12 ± 0.69 at baseline, 6.79 ± 0.71 post-sham (95.5% as compared to baseline), and 1.28 ± 1.27 post-tCCDCS (18.8% as compared to baseline).

RELATIVE ENTROPY

In both patients, we found a strong overlap in terms of relative entropy of tremor (**Figure 10**). However, a statistically significant increase in relative entropy was found for postural tremor

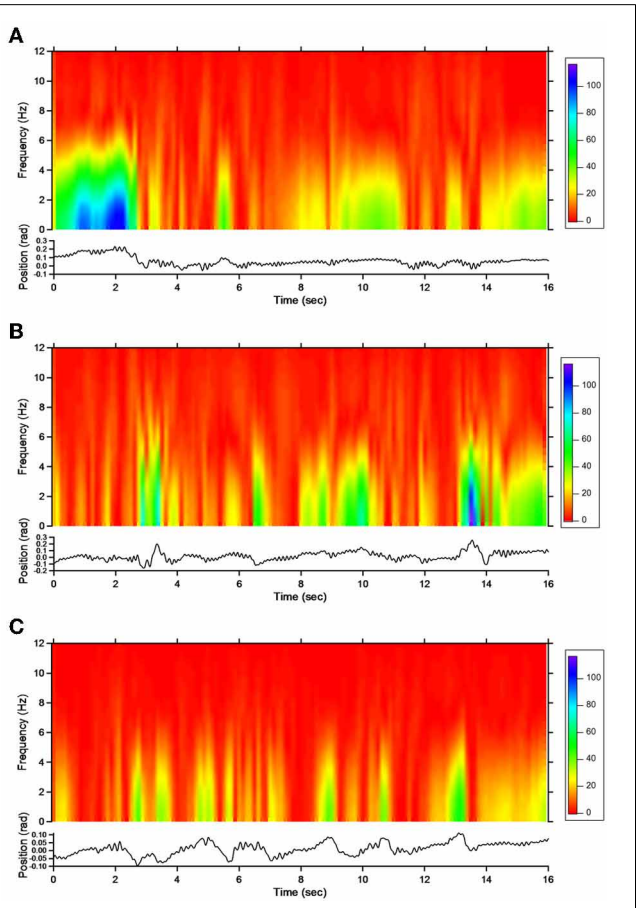

FIGURE 6 | STFT representation of action tremor in patient 2. (A) Baseline, **(B)** post-sham, **(C)** post-tCCDCS. See also legend of **Figure 4**.

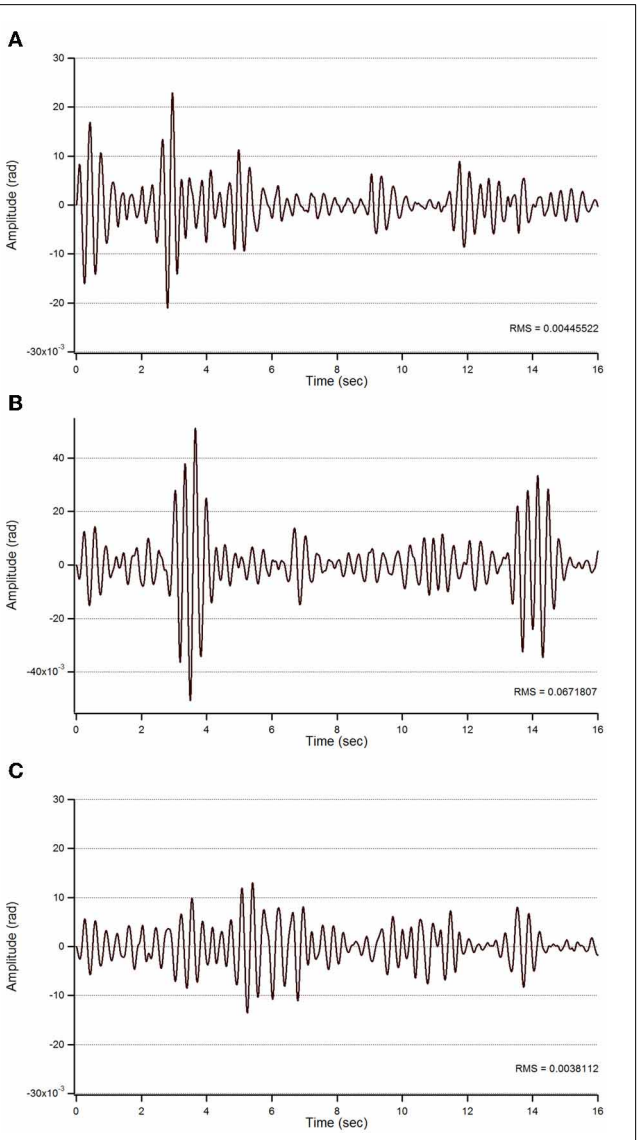

FIGURE 7 | Action tremor in the bandwidth 2.5–3.5 Hz in patient 2. See also legend of **Figure 5**.

Table 1 | Kinematic and EMG parameters associated with fast goal-directed movements in the 2 patients.

Kinematic and EMG parameter	Condition	Target: 0.2 rad		Target: 0.3 rad		Target: 0.4 rad	
		Patient 1 (*z* score)*,#	Patient 2 (*z* score)*,#	Patient 1 (*z* score)*,#	Patient 2 (*z* score)*,#	Patient 1 (*z* score)*,#	Patient 2 (*z* score)*,#
Mean movement Amplitude (rad)[a]	Basal	0.2948 ± 0.0512 (7.53)#	0.2601 ± 0.035 (4.79)#	0.3679 ± 0.0254 (4.76)#	0.3633 ± 0.0241 (4.43)#	0.4720 ± 0.018 (5.43)#	0.4678 ± 0.0268 (5.12)#
	Sham	0.2985 ± 0.0480 (7.82)#	0.2519 ± 0.0292 (4.10)#	0.3788 ± 0.0288 (5.53)#	0.3527 ± 0.0231 (3.68)#	0.4630 ± 0.025 (4.76)#	0.4557 ± 0.0233 (4.21)#
	tCCDCS	0.2191 ± 0.0193 (1.48)	0.2108 ± 0.021 (0.81)	0.3222 ± 0.0156 (1.53)	0.3023 ± 0.0185 (0.12)	0.4118 ± 0.016 (0.94)	0.4118 ± 0.0162 (0.94)
Onset latency of antagonist EMG activity (ms)[b]	Basal	98 (7.75)#	87 (6.38)#	105 (7.22)#	78 (4.22)#	108 (5.73)#	74 (2.64)#
	Sham	95 (7.38)#	84 (6.0)#	103 (7.0)#	77 (4.11)#	101 (5.09)#	72 (2.45)
	tCCDCS	63 (3.38)#	43 (0.88)	59 (2.11)	41 (0.11)	57 (1.09)	46 (0.09)

**As compared to values obtained in a control group (n = 8 subjects; see also Methods).*

 # Values are outside the 99% confidence interval of control values.

[a] Control values: target at 0.2 rad: 0.2006 ± 0.01251 rad; target at 0.3 rad: 0.3006 ± 0.01451; target at 0.4 rad: 0.3992± 0.01341.

[b] Control values: target at 0.2 rad: 36 ± 8 ms; target at 0.3 rad: 40 ± 9 ms; target at 0.4 rad: 45 ± 11 ms.

in patient 1 (median ± *SD*: 0.085 ± 0.061 vs. 0.131 ± 0.052; $p = 0.031$). Still, no difference was found for action tremor: median values (±*SD*) were 0.153 (±0.279) and 0.066 (±0.28) in sham/basal vs. tCCDCS/basal, respectively ($p = 0.059$). For patient 2, relative entropies were similar for postural tremor (0.129 ± 0.069 vs. 0.125 ± 0.048; $p = 0.988$) and for action tremor (0.086 ± 0.183 vs. 0.077 ± 0.213; $p = 0.593$).

DISCUSSION

Our observation highlights a novel way to modulate cerebellar motor functions in a neurological disorder manifesting with a predominant cerebellar syndrome. This is the first demonstration that tCCDCS could be considered as a symptomatic therapeutic strategy of upper limb deficits in a disabling cerebellar ataxia. In our 2 patients, tCCDCS improved clinically the voluntary movements of the upper limbs, without affecting oculomotor disturbances, dysarthria and ataxia of stance/gait as confirmed by the ataxia rating scale. Interestingly, both patients reported a feeling of motor improvement after tCCDCS.

The excitability of the cerebellar circuitry is impaired in numerous cerebellar disorders, as a result of the degenerative process occurring in the cerebellum and its afferences (Wessel et al., 1996). In SCAs, the degenerative process even extends beyond cerebellar circuits. The sole application of tDCS at the level of the cerebellum in ataxic patients has not shown functional effects so far. Although anodal tDCS of the cerebellum reduces the magnitudes of long-latency stretch reflexes (LLSR) in sporadic cerebellar atrophy or in dominant ataxias (Grimaldi and Manto, 2013), it does not improve coordination in upper limbs or postural ataxia. The enhanced LLSR in ataxic patients are explained by a disinhibition of cerebellar nuclei as a result of a damage of the cerebellar cortex (Diener et al., 1984). Anodal tDCS of the cerebellum reinforces the inhibitory tone exerted by the cerebellar cortex over cerebellar nuclei, but these effects alone seem insufficient to improve cerebellar ataxia. Effects on brainstem nuclei are unlikely since cerebellar tDCS does not modify the excitability of vestibular or trigeminal nuclei (Galea et al., 2011; Jayaram et al., 2012). Modeling studies show that the diffusion of electric field outside the cerebellum is small (Parazzini et al., 2013). We have suggested that anodal tDCS of the cerebellum does not improve functional tests because these tasks depend on the integrity of diffuse cerebello-cerebral networks whose activity is not modified substantially by anodal tDCS applied over the cerebellum in a spatially-restricted manner, as used here (Grimaldi and Manto, 2013). The combination of tDCS of the cerebellum with tDCS of the motor/premotor cortex is thus emerging as a possible novel approach in the field of cerebellar neuromodulation.

The delayed onset latency of the antagonist EMG activity associated with fast goal-directed movements is a major finding in patients with a cerebellar disorder (Hore et al., 1991; Manto et al., 1994). The parameter is robust for the follow-up of cerebellar patients and is correlated with the clinical deficits (Manto et al., 1995). The variability of the onset latency of antagonist EMG activity is less than 7% when fast goal-directed movements are performed at the same peak velocities. It is assumed that the delayed onset of the braking action of the antagonist activity results in the hypermetria, a cardinal feature of genuine cerebellar diseases. So far, attempts to improve this key-parameter of the timing of antagonist commands to voluntary muscles with the use of drugs have failed. Cooling the dentate nucleus in

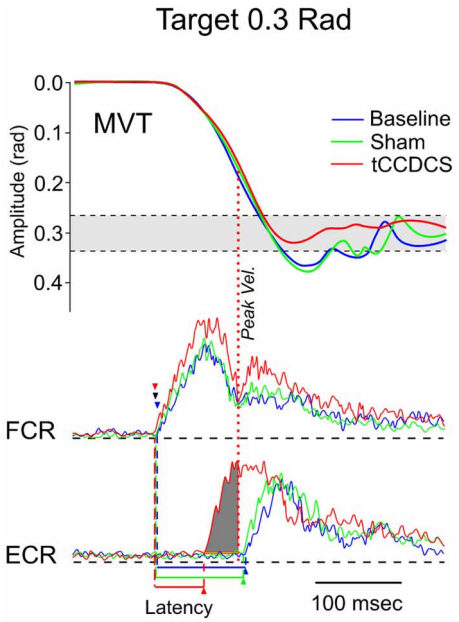

FIGURE 8 | Fast goal-directed wrist flexion movements in patient 1. Target located at 0.3 rad from the start position. **Top part**: mean movement (MVT; averages of sets of 10 movements) in the 3 experimental conditions (blue line: basal condition, green line: sham, red line: post-tCCDCS); gray area corresponds to the mean ± 2.5 *SD* of position values obtained in a control group. **Middle** and **bottom part**: FCR and ECR correspond to averages (for the 10 movements) of full-wave rectified surface EMG activities of the flexor carpi radialis muscle (agonist muscle) and extensor carpi radialis muscle (antagonist muscle), respectively (blue lines: basal condition, green lines: sham, red lines: post-tCCDCS). Arrowheads indicate the onset of EMG activities (blue: baseline; green: post-sham; red: post-tCCDCS). Note that the burst of antagonist EMG activity starts earlier after tCCDCS, demonstrating an effect of tCCDCS on the timing of antagonist EMG activity. The dark gray area below the ECR trace corresponds to the portion of EMG activity occurring *before* the peak velocity (illustrated by a red dotted line, whereas the peak velocity for the baseline and post-sham condition occurred *before* the onset latency of the antagonist EMG activity), and thus having an efficient braking action to avoid the overshoot of the target.

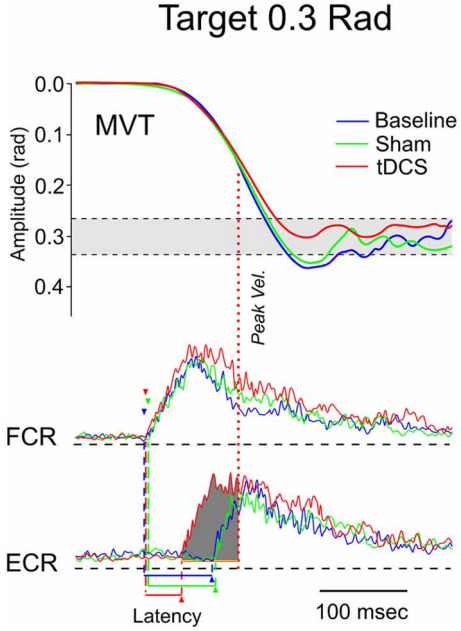

FIGURE 9 | Fast goal-directed wrist flexion movements in patient 2 (target: 0.3 rad from the start position). Top part: mean movement (MVT) in the 3 experimental conditions (blue line: basal condition, green line: sham, red line: post-tCCDCS). **Middle** and **bottom part:** FCR and ECR correspond to surface EMG activities of the flexor carpi radialis muscle and extensor carpi radialis muscle, respectively (blue lines: basal condition, green lines: sham, red lines: post-tCCDCS). Note the reduction of the onset latency of the antagonist EMG activity following tCCDCS. See also legend of **Figure 8** for details.

monkeys induces hypermetria (Flament and Hore, 1986). The overshoot is associated with a delay in the generation of the antagonist muscle activity *and* abnormal neuronal discharges in the contralateral motor cortex (Hore and Flament, 1988). This distorted timing of muscle discharges is considered as a signature of a cerebellar lesion involving the cerebello-thalamo-cortical pathway. We suggest that tCCDCS restores this property of the cerebello-thalamo-cortical pathway. The internal representation of temporal information would be modified by tCCDCS (Ivry and Spencer, 2004). Consequently, predictions of body states would be improved (Molinari et al., 2009).

At a first glance, a strong overlap was found between sham and tCCDCS in terms of entropy. Still, the relative entropy was increased in one patient following tCCDCS in the postural condition. However, this is an avenue for future studies. Indeed, subsequent works are required to assess whether tCCDCS really impacts on the randomness of neurological tremor. The study of relative entropy parameter has not been exploited so far in the field of ataxic disorders, despite (a) the critical roles of the cerebellum in the programming of timing and sequencing of motor operations, and (b) the major contributions of cerebellar circuits in the so-called Guillain-Mollaret triangle implicated in tremor genesis (Vidailhet et al., 1998; Molinari et al., 2009).

A severe postural tremor highly responsive to subthalamic-thalamic deep brain stimulation (DBS) has been reported in a patient with SCA2 (Freund et al., 2007). However, DBS is usually not considered as a primary option in the management of tremor in SCA2, especially because the disease is progressive and the surgical procedure carries several risks. Nevertheless, the previously reported excellent response to DBS also underlines that cerebellar efferences are critical to cause limb oscillations.

Although our results are very encouraging, there are limitations to our study: our number of patients is small, we did not address the pathogenesis of other cerebellar deficits such as gait deficits and we did not investigate specifically the dynamics of the duration of the after-effects. Future studies should be performed in larger groups of ataxic patients not only to confirm our findings in the numerous forms of cerebellar ataxias, but also to identify the categories of ataxic patients which can be considered as potential responders. tDCS is non-invasive and more extensive electrodes covering the skull over the posterior fossa can be

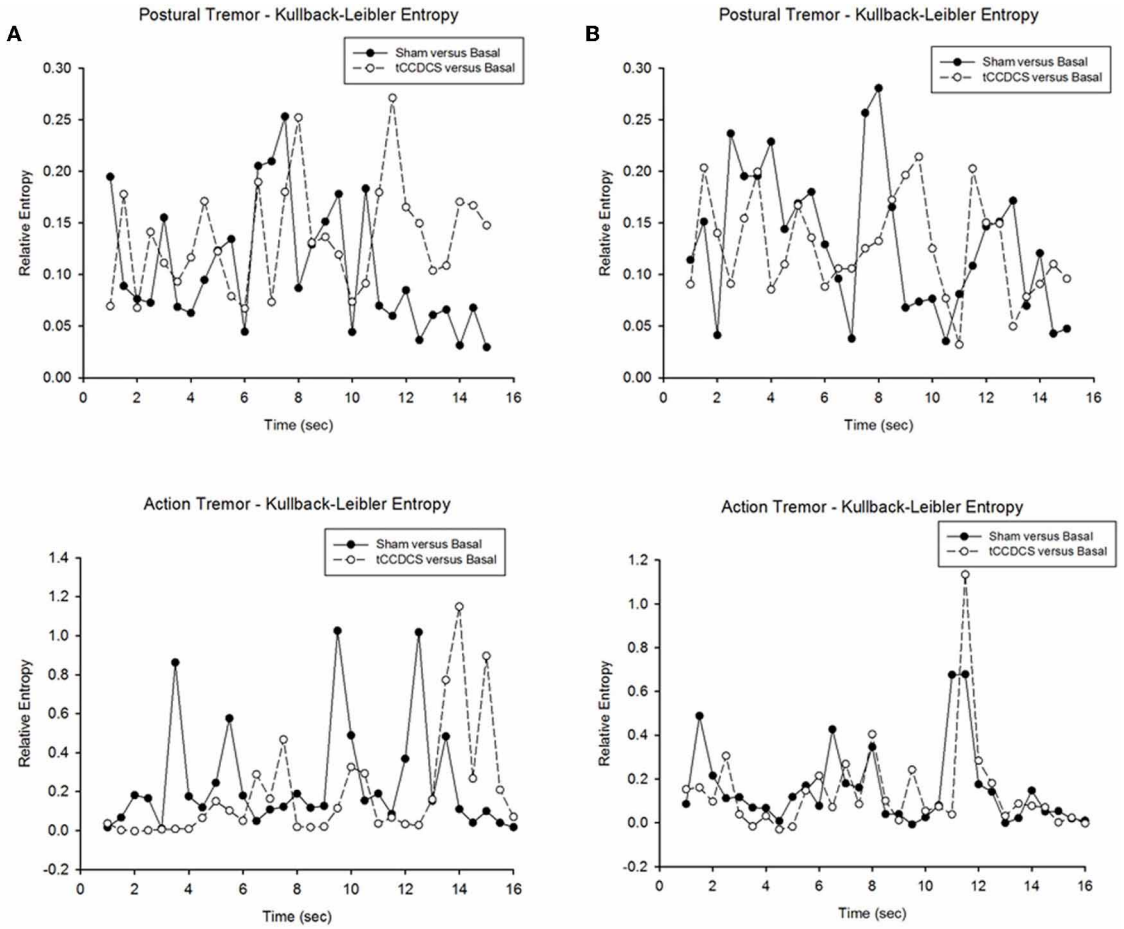

FIGURE 10 | Relative entropy in patient 1 (A) and patient 2 (B). Upper panels correspond to the relative entropy for postural tremor in the condition sham vs. basal (filled circles) and tCCDCS vs. basal (open circles—dotted lines). Bottom panels correspond to the relative entropy for action tremor in the condition sham vs. basal (filled circles) and tCCDCS vs. basal (open circles—dotted lines).

envisioned. These electrodes might have the advantage of modulating the entire cerebellar cortex and could be characterized by a spatial map allowing a dynamic application of currents, with the intensity of currents being adapted to the region of the cerebellum targeted by tDCS as well as to the task. Future studies are required to validate this "*whole cerebellum DCS*" strategy in cerebellar ataxias. The mechanisms and duration of the after-effects deserve attention (Márquez-Ruiz et al., 2012). At the cerebral cortex level of behaving rabbits, tDCS modifies thalamo-cortical synapses by acting principally at presynaptic sites and cathodal tDCS appears more effective than the anodal tDCS in terms of duration of the after-effects (Márquez-Ruiz et al., 2012). In healthy subjects, cathodal tDCS of the cerebellum lasts up to 30 min after the cessation of stimulation in a paradigm of cerebellum-brain inhibition (CBI) evaluated with transcranial magnetic stimulation (TMS) (Galea et al., 2009). Other studies point out that anodal tDCS induces significant and long-lasting effects (more than 24 h) in models of pain related to peripheral inflammation in rats (Laste et al., 2012). Both immediate effects and after-effects are influenced by stimulus parameters (pulse shape, intensity, duration, and frequency of stimuli) and electrodes (location, size, and orientation). The non-linear relationships between stimuli and physiological responses should be taken into account (Paulus et al., 2013). The region of the brain which is stimulated is another factor. For instance, the cerebellum has a distinct electrical conductivity and permittivity—a measure of how an electric field influences a dielectric medium—as compared to the brainstem or cerebrum (Nightingale et al., 1983). The question of the use of repeated administration of tDCS in chronic disorders of the brain remains open at this stage. In particular, it is difficult to anticipate whether tDCS will become a technique applicable repeatedly to patients with chronic cerebellar atrophy. Safety studies as well as efficacy studies are needed. In terms of safety, several studies addressing the effects of tDCS on cerebellar function have typically used a current intensity of 2 mA, which is often the intensity associated with prickling sensations at the skin or a mild discomfort (Tomlinson et al., 2013). Recent works in chronic aphasic patients underline that tDCS potentiates the recovery of clinical deficits, but long-term studies with repeated sessions of stimulation are still missing (Marangolo et al., 2014).

Cerebellum is part of a distributed cognitive network and its neuromodulation influences the contribution of cerebellar

circuits, especially for linguistic processes, working memory tasks and processing of emotions (Ferrucci et al., 2008; Argyropoulos et al., 2011; Pope and Miall, 2012). This extends strongly the potential applications. The impacts of using non-invasive neurostimulation such as tDCS techniques over the cerebellum in cognitive and psychiatric rehabilitation strategies, as well as the long-term neural consequences need to be clarified in rigorous large scale trials (Grimaldi et al., 2014).

AUTHOR CONTRIBUTIONS

Overall study design and protocol development: Giuliana Grimaldi, Nordeyn Oulad Ben Taib, Mario Manto. Data analysis: Giuliana Grimaldi, Mario Manto, Florian Bodranghien. Writing of manuscript: Giuliana Grimaldi, Nordeyn Oulad Ben Taib, Mario Manto, Florian Bodranghien. Final version reviewed and approved by all the authors.

ACKNOWLEDGMENTS

Mario Manto is supported by the FNRS-Belgium.

REFERENCES

Argyropoulos, G. P., Kimiskidis, V., and Papagiannopoulos, S. (2011). Theta-burst stimulation of the right neocerebellar vermis selectively disrupts the practice-induced acceleration of lexical decisions. *Behav. Neurosci*. 125, 724–734. doi: 10.1037/a0025134

Braitenberg, V. (1967). Is the cerebellar cortex a biological clock in the millisecond range? *Prog. Brain Res*. 25, 334–346. doi: 10.1016/S0079-6123(08)60971-1

Diener, H. C., Dichgans, J., Bacher, M., and Guschlbauer, B. (1984). Characteristic alterations of long-loop reflexes in patients with Friedreich's disease and late atrophy of the cerebellar anterior lobe. *J. Neurol. Neurosurg. Psychiatry* 47, 679–685. doi: 10.1136/jnnp.47.7.679

Ferrucci, R., Marceglia, S., Vergari, M., Cogiamanian, F., Mrakic-Sposta, S., Mameli, F., et al. (2008). Cerebellar transcranial direct current stimulation impairs the practice-dependent proficiency increase in working memory. *J. Cogn. Neurosci*. 20, 1687–1697. doi: 10.1162/jocn.2008.20112

Ferrucci, R., and Priori, A. (2014). Transcranial cerebellar direct current stimulation (tcDCS): motor control, cognition, learning and emotions. *Neuroimage* 85, 918–923. doi: 10.1016/j.neuroimage.2013.04.122

Flament, D., and Hore, J. (1986). Movement and electromyographic disorders associated with cerebellar dysmetria. *J. Neurophysiol*. 55, 1221–33.

Freeman, W. J., and Quian Quiroga, R. (2013). *Imaging Brain Function With EEG. Advanced Temporal and Spatial Analysis of Electroencephalographic Signals*. New York, NY: Springer. doi: 10.1007/978-1-4614-4984-3

Freund, H. J., Barnikol, U. B., Nolte, D., Treuer, H., Auburger, G., Tass, P. A., et al. (2007). Subthalamic-thalamic DBS in a case with spinocerebellar ataxia type 2 and severe tremor—a unusual clinical benefit. *Mov. Disord*. 22, 732–735. doi: 10.1002/mds.21338

Galea, J. M., Jayaram, G., Ajagbe, L., and Celnik, P. (2009). Modulation of cerebellar excitability by polarity-specific noninvasive direct current stimulation. *J. Neurosci*. 29, 9115–9122. doi: 10.1523/JNEUROSCI.2184-09.2009

Galea, J. M., Vazquez, A., Pasricha, N., de Xivry, J. J., and Celnik, P. (2011). Dissociating the roles of the cerebellum and motor cortex during adaptive learning: the motor cortex retains what the cerebellum learns. *Cereb. Cortex* 21, 1761–1770. doi: 10.1093/cercor/bhq246

Gispert, S., Twells, R., Orozco, G., Brice, A., Weber, J., Heredero, L., et al. (1993). Chromosomal assignment of the second locus for autosomal dominant cerebellar ataxia (SCA2) to chromosome 12q23-24.1. *Nat. Genet*. 4, 295–299. doi: 10.1038/ng0793-295

Gottlieb, G. L. (1998). Muscle activation patterns during two types of voluntary single-joint movement. *J. Neurophysiol*. 80, 1860–1867.

Grimaldi, G., Argyropoulos, G. P., Boehringer, A., Celnik, P., Edwards, M. J., Ferrucci, R., et al. (2014). Non-invasive cerebellar stimulation-a consensus paper. *Cerebellum* 13, 121–138. doi: 10.1007/s12311-013-0514-7

Grimaldi, G., Fernandez, A., and Manto, M. (2013). Augmented visual feedback counteracts the effects of surface muscular functional electrical stimulation on physiological tremor. *J. Neuroeng. Rehabil*. 10, 100. doi: 10.1186/1743-0003-10-100

Grimaldi, G., and Manto, M. (2008). *Tremor: From Pathogenesis to Treatment*. San Rafael, CA: Morgan & Claypool Publishers. doi: 10.2200/S00129ED1V01Y200807BME020

Grimaldi, G., and Manto, M. (2010). Neurological tremor: sensors, signal processing and emerging applications. *Sensors* 10, 1399–1422. doi: 10.3390/s100201399

Grimaldi, G., and Manto, M. (2013). Anodal transcranial direct current stimulation (tDCS) decreases the amplitudes of long-latency stretch reflexes in cerebellar ataxia. *Ann. Biomed. Eng.* 41, 2437–2447. doi: 10.1007/s10439-013-0846-y

Hamada, M., Strigaro, G., Murase, N., Sadnicka, A., Galea, J. M., Edwards, M. J., et al. (2012). Cerebellar modulation of human associative plasticity. *J. Physiol. (Lond.)* 590, 2365–2374. doi: 10.1113/jphysiol.2012.230540

Holmes, G. (1917). The symptoms of acute cerebellar injuries due to gunshot injuries. *Brain* 40, 461–535. doi: 10.1093/brain/40.4.461

Hore, J., and Flament, D. (1988). Changes in motor cortex neural discharge associated with the development of cerebellar limb ataxia. *J. Neurophysiol*. 60, 1285–302.

Hore, J., Wild, B., and Diener, H. C. (1991). Cerebellar dysmetria at the elbow, wrist, and fingers. *J. Neurophysiol.* 65, 563–571.

Ivry, R. B., and Spencer, R. M. (2004). The neural representation of time. *Curr. Opin. Neurobiol*. 14, 225–232. doi: 10.1016/j.conb.2004.03.013

Jayaram, G., Tang, B., Pallegadda, R., Vasudevan, E. V., Celnik, P., and Bastian, A. (2012). Modulating locomotor adaptation with cerebellar stimulation. *J. Neurophysiol*. 107, 2950–2957. doi: 10.1152/jn.00645.2011

Laste, G., Caumo, W., Adachi, L. N., Rozisky, J. R., de Macedo, I. C., Filho, P. R., et al. (2012). After-effects of consecutive sessions of transcranial direct current stimulation (tDCS) in a rat model of chronic inflammation. *Exp. Brain Res*. 221, 75–83. doi: 10.1007/s00221-012-3149-x

Manto, M., Godaux, E., and Jacquy, J. (1994). Cerebellar hypermetria is larger when the inertial load is artificially increased. *Ann. Neurol*. 35, 45–52. doi: 10.1002/ana.410350108

Manto, M., Jacquy, J., Hildebrand, J., and Godaux, E. (1995). Recovery of hypermetria after a cerebellar stroke occurs as a multistage process. *Ann. Neurol*. 38, 437–445. doi: 10.1002/ana.410380314

Manto, M., and Marmolino, D. (2009). Cerebellar ataxias. *Curr. Opin. Neurol*. 22, 419–429. doi: 10.1097/WCO.0b013e32832b9897

Manto, M., Van Den Braber, N., Grimaldi, G., and Lammertse, P. (2010). A new myohaptic instrument to assess wrist motion dynamically. *Sensors* 10, 3180–3194. doi: 10.3390/s100403180

Marangolo, P., Fiori, V., Gelfo, F., Shofany, J., Razzano, C., Caltagirone, C., et al. (2014). Bihemispheric tDCS enhances language recovery but does not alter BDNF levels in chronic aphasic patients. *Restor. Neurol. Neurosci.* doi: 10.3233/RNN-130323. [Epub ahead of print].

Márquez-Ruiz, J., Leal-Campanario, R., Sánchez-Campusano, R., Molaee-Ardekani, B., Wendling, F., Miranda, P. C., et al. (2012). Transcranial direct-current stimulation modulates synaptic mechanisms involved in associative learning in behaving rabbits. *Proc. Natl. Acad. Sci. U.S.A*. 109, 6710–6715. doi: 10.1073/pnas.1121147109

McNames, J. (2013). "Signal processing," in *Mechanisms and Emerging Therapies in Tremor Disorders*, eds G. Grimaldi and M. Manto (New York, NY: Springer), 371–389. doi: 10.1007/978-1-4614-4027-7_20

Molinari, M., Restuccia, D., and Leggio, M. G. (2009). State estimation, response prediction, and cerebellar sensory processing for behavioral control. *Cerebellum*. 8, 399–402. doi: 10.1007/s12311-009-0112-x

Nightingale, N. R., Goodridge, V. D., Sheppard, R. J., and Christie, J. L. (1983). The dielectric properties of the cerebellum, cerebrum and brain stem of mouse brain at radiowave and microwave frequencies. *Phys. Med. Biol.* 28, 897–903. doi: 10.1088/0031-9155/28/8/002

Nitsche, M. A., Schauenburg, A., Lang, N., Liebetanz, D., Exner, C., Paulus, W., et al. (2003). Facilitation of implicit motor learning by weak transcranial direct current stimulation of the primary motor cortex in the human. *J. Cogn. Neurosci*. 15, 619–626. doi: 10.1162/089892903321662994

Oulad Ben Taib, N., and Manto, M. (2009). Trains of transcranial direct current stimulation antagonize motor cortex hypoexcitability induced by acute hemicerebellectomy. *J. Neurosurg*. 111, 796–806. doi: 10.3171/2008.2.17679

Oulad Ben Taib, N., and Manto, M. (2013). Trains of epidural DC stimulation of the cerebellum tune corticomotor excitability. *Neural. Plast*. 2013:613197. doi: 10.1155/2013/613197

Oulad Ben Taib, N., Manto, M., Laute, M. A., and Brotchi, J. (2005a). The cerebellum modulates rodent cortical motor output after repetitive somatosensory stimulation. *Neurosurgery*. 56, 811–820. doi: 10.1227/01.NEU.0000156616.94446.00

Oulad Ben Taib, N., Manto, M., Pandolfo, M., and Brotchi, J. (2005b). Hemicerebellectomy blocks the enhancement of cortical motor output associated with repetitive somatosensory stimulation in the rat. *J. Physiol. (Lond.)* 567, 293–300. doi: 10.1113/jphysiol.2005.088229

Parazzini, M., Rossi, E., Ferrucci, R., Liorni, I., Priori, A., and Ravazzani, P. (2013). Modelling the electric field and the current density generated by cerebellar transcranial DC stimulation in humans. *Clin. Neurophysiol*. doi: 10.1016/j.clinph.2013.09.039. [Epub ahead of print].

Paulus, W., Peterchev, A. V., and Ridding, M. (2013). Transcranial electric and magnetic stimulation: technique and paradigms. *Handb. Clin. Neurol*. 116, 329–342. doi: 10.1016/B978-0-444-53497-2.00027-9

Pope, P. A., and Miall, R. C. (2012). Task-specific facilitation of cognition by cathodal transcranial direct current stimulation of the cerebellum. *Brain Stimul.* 5, 84–94. doi: 10.1016/j.brs.2012.03.006

Pozzi, N. G., Minafra, B., Zangaglia, R., De Marzi, R., Sandrini, G., Priori, A., et al. (2013). Transcranial direct current stimulation (tDCS) of the cortical motor areas in three cases of cerebellar ataxia. *Cerebellum*. doi: 10.1007/s12311-013-0524-5. [Epub ahead of print].

Saute, J. A., Donis, K. C., Serrano-Munuera, C., Genis, D., Ramirez, L. T., Mazzetti, P., et al. (2012). Iberoamerican multidisciplinary network for the study of movement disorders (RIBERMOV) study group. Ataxia rating scales-psychometric profiles, natural history and their application in clinical trials. *Cerebellum* 11, 488–504. doi: 10.1007/s12311-011-0316-8

Shaikh, A. G., Jinnah, H. A., Tripp, R. M., Optican, L. M., Ramat, S., Lenz, F. A., et al. (2008). Irregularity distinguishes limb tremor in cervical dystonia from essential tremor. *J. Neurol. Neurosurg. Psychiatry* 79, 187–189. doi: 10.1136/jnnp.2007.131110

Tamburin, S., Fiaschi, A., Marani, S., Andreoli, A., Manganotti, P., and Zanette, G. (2004). Enhanced intracortical inhibition in cerebellar patients. *J. Neurol. Sci*. 217, 205–210. doi: 10.1016/j.jns.2003.10.011

Tomlinson, S., Davis, N., and Bracewell, R. (2013). Brain stimulation studies of non-motor cerebellar function: a systematic review. *Neurosci. Biobehav. Rev.* 37, 766–789. doi: 10.1016/j.neubiorev.2013.03.001

Vidailhet, M., Jedynak, C. P., Pollak, P., and Agid, Y. (1998). Pathology of symptomatic tremors. *Mov. Disord*. 13, 49–54. doi: 10.1002/mds.870131309

Wessel, K., Tegenthoff, M., Vorgerd, M., Otto, V., Nitschke, M. F., and Malin, J. P. (1996). Enhancement of inhibitory mechanisms in the motor cortex of patients with cerebellar degeneration: a study with transcranial magnetic brain stimulation. *Electroencephalogr. Clin. Neurophysiol*. 101, 273–280. doi: 10.1016/0924-980X(96)95531-9

Conflict of Interest Statement: The authors declare that the research was conducted in the absence of any commercial or financial relationships that could be construed as a potential conflict of interest.

Received: 10 December 2013; paper pending published: 09 January 2014; accepted: 14 January 2014; published online: 30 January 2014.

Citation: Grimaldi G, Oulad Ben Taib N, Manto M and Bodranghien F (2014) Marked reduction of cerebellar deficits in upper limbs following transcranial cerebellocerebral DC stimulation: tremor reduction and re-programming of the timing of antagonist commands. Front. Syst. Neurosci. ***8****:9. doi: 10.3389/fnsys.2014.00009*

This article was submitted to the journal Frontiers in Systems Neuroscience.